

ARMY RESEARCH LABORATORY



Research in Close-In Blast Loading From High Explosives

James E. Drotleff
Coye T. Vincent
Scott A. Mullin
James D. Walker
Bruce L. Morris

ARL-CR-308

September 1996

prepared by

FMC Corporation
Ground Systems Division
2830 De La Cruz Blvd
P.O. Box 58123
Santa Clara, CA 95052

under contract

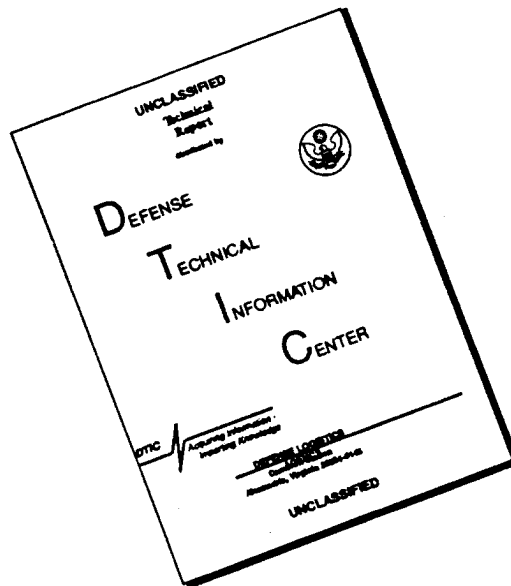
DAAA15-89-C-0037

APPROVED FOR PUBLIC RELEASE; DISTRIBUTION IS UNLIMITED.

19961028 032

DTC QUALITY INSPECTED 1

DISCLAIMER NOTICE



THIS DOCUMENT IS BEST QUALITY AVAILABLE. THE COPY FURNISHED TO DTIC CONTAINED A SIGNIFICANT NUMBER OF PAGES WHICH DO NOT REPRODUCE LEGIBLY.

NOTICES

Destroy this report when it is no longer needed. DO NOT return it to the originator.

Additional copies of this report may be obtained from the National Technical Information Service, U.S. Department of Commerce, 5285 Port Royal Road, Springfield, VA 22161.

The findings of this report are not to be construed as an official Department of the Army position, unless so designated by other authorized documents.

The use of trade names or manufacturers' names in this report does not constitute indorsement of any commercial product.

REPORT DOCUMENTATION PAGE			Form Approved OMB No. 0704-0188	
<small>Public reporting burden for this collection of information is estimated to average 1 hour per response, including the time for reviewing instructions, searching existing data sources, gathering and maintaining the data needed, and completing and reviewing the collection of information. Send comments regarding this burden estimate or any other aspect of this collection of information, including suggestions for reducing this burden, to Washington Headquarters Services, Directorate for Information Operations and Reports, 1215 Jefferson Davis Highway, Suite 1204, Arlington, VA 22202-4302, and to the Office of Management and Budget, Paperwork Reduction Project(0704-0188), Washington, DC 20503.</small>				
1. AGENCY USE ONLY (Leave blank)		2. REPORT DATE September 1996		3. REPORT TYPE AND DATES COVERED Final, Sep 89 - Feb 92
4. TITLE AND SUBTITLE Research in Close-In Blast Loading From High Explosives			5. FUNDING NUMBERS C: DAAA15-89-C-0037	
6. AUTHOR(S) James E. Drotleff, Coye T. Vincent, Scott A. Mullin, James D. Walker, and Bruce L. Morris				
7. PERFORMING ORGANIZATION NAME(S) AND ADDRESS(ES) FMC Corporation / Ground Systems Division 2830 De La Cruz Blvd P.O. Box 58123 Santa Clara, CA 95052			8. PERFORMING ORGANIZATION REPORT NUMBER	
9. SPONSORING/MONITORING AGENCY NAMES(S) AND ADDRESS(ES) U.S. Army Research Laboratory ATTN: AMSRL-WT-TB Aberdeen Proving Ground, MD 21005-5066			10. SPONSORING/MONITORING AGENCY REPORT NUMBER ARL-CR-308	
11. SUPPLEMENTARY NOTES Contracting Officer's Representative for this project is Richard Lottero, U.S. Army Research Laboratory.				
12a. DISTRIBUTION/AVAILABILITY STATEMENT Approved for public release; distribution is unlimited.			12b. DISTRIBUTION CODE	
13. ABSTRACT (Maximum 200 words) <p>This work was performed under contract to the U.S. Army Ballistic Research Laboratory (now the U.S. Army Research Laboratory) by FMC Corporation. It involved the use of experimental and theoretical means to study blast loading caused by the detonation of high explosive (HE) at close-in ranges. Close-in blast loading from HE is generally defined as explosive products interacting with a target during the time that the HE has expanded between 3 and 50 times its original volume. The impulse generated from close-in blast loading can cause gross structural damage to light armored vehicles, and is a serious threat to the vehicle and its crew. Precision, right circular cylindrical, top-detonated HE charges with a nominal mass of one kilogram were used for all experiments. Pressure measurements were taken on the surface of a nonresponding flat plate using a variety of gages. Predictions of the blast loading on the plate were made with a hydrodynamic computer code. Very good repeatability was experienced with some gage types, while others did not work well or had too low a signal relative to noise to be fully effective. The frequency response of the gages was also addressed. Firings against a ballistic pendulum were conducted using bare explosive charges, as well as charges with different casing thickness to quantify the effect of casing thickness on total integrated impulse. A full set of all data taken is included in the appendices to serve as documentation of the work.</p>				
14. SUBJECT TERMS detonations; impulse loading; close-in blast			15. NUMBER OF PAGES 286	
			16. PRICE CODE	
17. SECURITY CLASSIFICATION OF REPORT UNCLASSIFIED	18. SECURITY CLASSIFICATION OF THIS PAGE UNCLASSIFIED	19. SECURITY CLASSIFICATION OF ABSTRACT UNCLASSIFIED	20. LIMITATION OF ABSTRACT UL	

INTENTIONALLY LEFT BLANK.

TABLE OF CONTENTS

	<u>Page</u>
LIST OF FIGURES	v
LIST OF TABLES	ix
SUMMARY	xi
ACKNOWLEDGMENTS	xv
PREFACE	xvii
1. INTRODUCTION	1
1.1 Problem	1
1.2 Objectives	1
1.3 Approach	2
1.4 Background	3
2. ANALYTICAL AND EXPERIMENTAL TECHNIQUES	5
2.1 Overall Methods	5
2.2 Computational Methodology	5
2.2.1 Preliminary Computations	7
2.2.2 Final Computations	13
2.3 Baseplate Measurements	16
2.3.1 Experimental Design	16
2.3.2 Explosive Charge	18
2.3.2.1 Charge Placement for Firing	18
2.3.3 Instrumentation	19
2.3.3.1 Piezoresistive Pressure Gages	20
2.3.3.2 Pressure Bars	28
2.3.3.3 Impulse Plugs	30
2.3.3.4 Airblast Pressure (Freefield)	30
2.3.4 Signal Conditioning	30
2.3.4.1 Airblast Pressure	32
2.3.4.2 Pulse Power Supplies	32
2.3.4.3 Strain Gage Completion and Power Supply	33
2.3.4.4 Photodiodes	33
2.3.4.5 Electronic Detonation Unit Zero Time	33
2.3.4.6 Data Acquisition and Reporting	33
2.4 Ballistic Pendulum	33
2.4.1 Design of Pendulum	34
2.4.2 Explosives	37
2.4.3 Instrumentation and Data Acquisition	42
2.4.4 Data Analysis	46

3.	RESULTS	50
3.1	Computational Analysis of Bare Explosives	50
3.2	Baseplate Measurements	57
3.2.1	Results of Individual Gage Types	57
3.2.1.1	Ytterbium Gages	63
3.2.1.2	Manganin Gages	64
3.2.1.3	Pressure Bar Gages	64
3.2.1.4	Impulse Plug Gages	66
3.2.1.5	Airblast Gages	66
3.2.2	Baseplate Tests, Comp B at 15-cm HOB	66
3.2.3	Baseplate Tests, Comp B at 20-cm HOB	70
3.2.4	Baseplate Tests, Pentolite at 15-cm HOB	73
3.2.5	Baseplate Tests, Pentolite at 20-cm HOB	75
3.3	Ballistic Pendulum Measurements	80
3.4	Comparison of Computational and Experimental Results	91
4.	CONCLUSIONS	109
5.	RECOMMENDATIONS	110
6.	REFERENCES	113
	APPENDIX A: STRESS AND IMPULSE HISTORIES FROM YTTERBIUM AND MANGANIN ELEMENTS, BASEPLATE TESTS 2A.1-2A.12 ..	115
	APPENDIX B: STRESS AND IMPULSE HISTORIES FROM BAR GAGES, BASEPLATE TESTS 2A.1-2A.12	211
	APPENDIX C: COMPUTED STRESS HISTORIES, BASEPLATE TESTS 2A.1-2A.12	249
	APPENDIX D: DATA REDUCTION PROCEDURES FOR BASEPLATE INSTRUMENTATION	263

LIST OF FIGURES

<u>Figure</u>	<u>Page</u>
1. Effect of Predetonation Pressure Value on Explosive Burn Pressure	9
2. Effect of Initiation Criteria on Explosive Burn Pressure	10
3. Computer Gridding Description (All Units in Centimeters)	14
4. Test Fixture Used for Baseplate Tests 2A.1–2A.12	17
5. Schematic Diagram of Foam Holder Used to Position Explosive Charges	20
6. Photograph of Explosive Charge Foam Holder	21
7. Baseplate Instrumentation, Tests 2A.1–2A.4	24
8. Baseplate Instrumentation, Tests 2A.5–2A.12	25
9. Detail of Piezoresistant Stress Transducer	26
10a. Photograph of Test Fixture With Baseplate in Place	27
10b. Photograph of Test Fixture With Explosive Charge and Lead Shielding in Place	27
11. Impulse and Bar Gage Setup, Baseplate Instrumentation	29
12. Impulse Plug Used for Baseplate Instrumentation	31
13. Airblast Gage Used for Baseplate Instrumentation	32
14. Ballistic Pendulum	35
15. Side View of the Ballistic Pendulum Fixture	36
16. Front View of Ballistic Pendulum	38
17. View of Pendulum and Fragment Capture Matting	39
18. Photograph of the Ballistic Pendulum Fixture, Showing the Coverplate	39
19. Photograph of the Ballistic Pendulum Fixture, Showing the Rails Used to Interpret Pendulum Swing	40
20. Photograph of the Ballistic Pendulum Fixture	40

<u>Figure</u>	<u>Page</u>
21. Closeup Photo of the Pendulum Pivot Axle	41
22. Explosive Configuration for Pendulum Tests	41
23. Explosive Charge Holder Device Without Coverplate	44
24. Charge Holder Device for a Test With the Coverplate	44
25. Peak Pressure vs. Location From Comp B Simulations at 15- and 20-cm HOB	55
26. Peak Pressure vs. Location From Pentolite Simulations at 15- and 20-cm HOB	55
27. Specific Impulse vs. Location From Comp B Simulations at 15- and 20-cm HOB	56
28. Specific Impulse vs. Location From Pentolite Simulations at 15- and 20-cm HOB	56
29. Pressure-Time Traces From Simulation of Comp B at 20-cm HOB	58
30. Pressure-Time Traces From Simulation of Comp B at 15-cm HOB	58
31. Pressure-Time Traces From Simulation of Pentolite at 15-cm HOB	59
32. Pressure-Time Traces From Simulation of Pentolite at 20-cm HOB	59
33. Individual and Combined Stress-Time Records From Two Pressure Bar Strain Elements	65
34. Representative Stress-Time Records From Comp B Tests at 15-cm HOB	67
35. Impulse-Time Records, Comp B at 15-cm HOB, Ytterbium, 2.5-cm Range	69
36. Impulse-Time Records, Comp B at 15-cm HOB, Ytterbium, 5.0-cm Range	69
37. Representative Stress-Time Records, Comp B at 20-cm HOB	71
38. Impulse-Time Records, Comp B at 20-cm HOB, Ytterbium, 2.5-cm Range	72
39. Impulse-Time Records, Comp B at 20-cm HOB, Ytterbium, 5.0-cm Range	72
40. Representative Stress-Time Records, Pentolite at 15-cm HOB	74
41. Impulse-Time Records, Pentolite at 15-cm HOB, Ytterbium, 2.5-cm Range . . .	76

<u>Figure</u>	<u>Page</u>
42. Impulse-Time Records, Pentolite at 15-cm HOB, Ytterbium, 5.0-cm Range . . .	76
43. Representative Stress-Time Records, Pentolite at 20-cm HOB	78
44. Impulse-Time Records, Pentolite at 20-cm HOB, Ytterbium, 2.5-cm Range . . .	79
45. Impulse-Time Records, Pentolite at 20-cm HOB, Ytterbium, 5.0-cm Range . . .	79
46. RVDT Record, One Swing, Test 2 (Bare Charge - 15-cm HOB)	84
47. RVDT Record, Two Swings, Test 2 (Bare Charge - 15-cm HOB)	84
48. RVDT Record, Four Swings, Test 2 (Bare Charge - 15-cm HOB)	85
49. RVDT Record, Eight Swings, Test 2 (Bare Charge - 15-cm HOB)	85
50. RVDT Record, One Swing, Test 3 (Bare Charge - 15-cm HOB)	86
51. RVDT Record, Two Swings, Test 3 (Bare Charge - 15-cm HOB)	86
52. RVDT Record A, Two Swings, Test 4 (Bare Charge - 20-cm HOB)	87
53. RVDT Record B, Two Swings, Test 4 (Bare Charge - 20-cm HOB)	87
54. RVDT Record, Two Swings, Test 5 (Bare Charge - 20-cm HOB)	88
55. RVDT Record, Two Swings, Test 6 (6.35-mm Cased Charge - 15-cm HOB) . .	88
56. RVDT Record, Two Swings, Test 13 (9.53-mm Cased Charge - 20-cm HOB) .	89
57. Averaged Pendulum Swing Angles for All Tests	90
58. Calculated Impulse for All Tests	91
59. Computation (Dashed Line) vs. Experimental Record (Solid Line), Comp B at 15-cm HOB, 2.5-cm Range	93
60. Computation (Dashed Line) vs. Experimental Record (Solid Line), Comp B at 20-cm HOB, 2.5-cm Range	94
61. Computation (Dashed Line) vs. Experimental Record (Solid Line), Pentolite at 15-cm HOB, 2.5-cm Range	95
62. Computation (Dashed Line) vs. Experimental Record (Solid Line), Pentolite at 20-cm HOB, 2.5-cm Range	96

<u>Figure</u>	<u>Page</u>
63. Computation (Dashed Line) vs. Experimental Record (Solid Line), Comp B at 15-cm HOB, 2.5-cm Range	97
64. Computation (Dashed Line) vs. Experimental Record (Solid Line), Comp B at 20-cm HOB, 2.5-cm Range	98
65. Computation (Dashed Line) vs. Experimental Record (Solid Line), Pentolite at 15-cm HOB, 2.5-cm Range	99
66. Computation (Dashed Line) vs. Experimental Record (Solid Line), Pentolite at 20-cm HOB, 2.5-cm Range	100
67. Computation (Dashed Line) vs. Experimental Record (Solid Line), Comp B at 15-cm HOB, 5.0-cm Range	101
68. Computation (Dashed Line) vs. Experimental Record (Solid Line), Comp B at 20-cm HOB, 5.0-cm Range	102
69. Computation (Dashed Line) vs. Experimental Record (Solid Line), Pentolite at 15-cm HOB, 5.0-cm Range	103
70. Computation (Dashed Line) vs. Experimental Record (Solid Line), Pentolite at 20-cm HOB, 5.0-cm Range	104
71. Computation (Dashed Line) vs. Experimental Record (Solid Line), Comp B at 15-cm HOB, 5.0-cm Range	105
72. Computation (Dashed Line) vs. Experimental Record (Solid Line), Comp B at 20-cm HOB, 5.0-cm Range	106
73. Computation (Dashed Line) vs. Experimental Record (Solid Line), Pentolite at 15-cm HOB, 5.0-cm Range	107
74. Computation (Dashed Line) vs. Experimental Record (Solid Line), Pentolite at 20-cm HOB, 5.0-cm Range	108

LIST OF TABLES

<u>Table</u>	<u>Page</u>
1. Convergence Study Results, Pressure and Impulse on Baseplate at Ground Zero	11
2. Baseplate Explosive Charges (Using RP-80 Detonator and CH-6 Booster; Test Site Was HTS No. 2)	18
3. Baseplate Shot Geometry (Cylindrical Charges, Top Center Initiation)	19
4. Gage Locations	22
5. Gage Position and Type	23
6. Baseplate Shot Conditions	34
7. Ballistic Pendulum Explosive Charges	43
8. Ballistic Pendulum Period Calculations	49
9. Ballistic Pendulum Properties	50
10. Computational Data at Baseplate, Comp B at 20-cm HOB	51
11. Computational Data at Baseplate, Comp B at 15-cm HOB	52
12. Computational Data at Baseplate, Pentolite at 20-cm HOB	53
13. Computational Data at Baseplate, Pentolite at 15-cm HOB	54
14. TOA, Peak Stress and Specific Impulse from Piezoresistant Gages, Baseplate Tests 2A.1–2A.12	60
15. Impulse Plug Data, Tests 2A.1–2A.8	63
16. Ballistic Pendulum Explosive Charges	80
17. Ballistic Pendulum Shot Geometry	81
18. Ballistic Pendulum Shot Conditions	81
19. Pendulum Swing Results (Degrees at Peak)	82
20. Impulse and Natural Period	90

INTENTIONALLY LEFT BLANK.

SUMMARY

Problem. The work presented in this report was completed under contract DAAA15-89-C-0037 for the U.S. Army Ballistic Research Laboratory (BRL). It involves the use of experimental and theoretical means to study blast loading caused by the detonation of high explosives (HE) at close-in ranges. Close-in blast loading from HE is generally defined as explosive products interacting with a target during the time that the HE has expanded to between 3 and 50 times its original volume. The impulse generated from blast loading can cause gross structural damage to light armored vehicles and is a serious threat to the vehicle and its crew; therefore, its study is of particular importance to the Army.

In addition to studying bare explosives, FMC sought to quantify the contribution made by fragments or flyplates to the overall impulsive loading produced by a close-in blast from a "cased" explosive. Conditions exist where an accelerated mass can contribute significantly to the overall structural deformation of a vehicle and can exceed the contribution made by the explosive overpressure. Other conditions exist where the loading from the explosive overpressure far exceeds the contribution from an accelerated mass.

Limited quantitative experimental information exists of the loading profiles, in space and time, produced by close-in blast loads. The lack of such information precludes the development of a validated theoretical model.

Objectives. The overall objective of this contract was to develop an experimentally validated theoretical model capable of predicting the loading in space and time of military explosives detonated at close-in ranges over a nonresponding (nonexplosive) plate. The specific objectives were to:

- Provide computational analysis of stress-time and impulse-time loading curves from bare charge explosives on a nonresponding baseplate at two heights of burst (HOB) and compare these calculations with empirical measurements.

- Provide empirical measurements of stress and impulse histories resulting from the detonation of condensed military bare charges over a nonresponding baseplate at two HOBs to compare with the analytical model developed.
- Experimentally measure the total impulse imparted from a condensed military bare charge at two close-in ranges and empirically determine the contribution two thicknesses of steel casing on the total impulse.

Approach. This contract was divided into three distinct areas to satisfy the above objectives:

- Southwest Research Institute (SwRI), as a subcontractor to FMC, provided a theoretical analysis of loadings produced on a nonresponding plate by bare charge explosives at close-in ranges.
- FMC designed, fabricated and tested experimental instrumentation capable of measuring the stress and specific impulse histories resulting from the detonation of bare military cylindrical explosives at two close-in blast ranges. A test fixture was modified to accept a nonresponding steel plate that was outfitted with various types of gage instrumentation, including piezoresistant stress transducers, Hopkinson bar gages and impulse plugs.
- SwRI also designed, fabricated and tested a ballistic pendulum capable of measuring the total impulsive load produced by cased and uncased military explosives at close-in ranges.

Results and Conclusions. Under this contract, FMC developed an analytical model capable of generating stress and impulse histories produced from bare charge explosives at close-in ranges that compare favorably to experimentally measured loading curves produced from actual military bare charges at close-in ranges (0.15 and 0.20 m). Reproducible peak stresses ranging from 0.8 to 2.0 GPa were measured using ytterbium gage instrumentation. These records are the first known repeatable measurements of stress and impulse histories at close-in ranges. In addition, the use of a ballistic pendulum showed an increase in total impulse delivered when a steel casing is placed around a bare military charge.

Specifically, the following results and conclusions were drawn:

- Ytterbium elements returned the highest quality and quantity of data.
- Calculated stress and impulse histories were generally higher than measured at 0- and 2.5-cm ranges from ground zero (GZ) and lower at 5.0-cm ranges from GZ.
- The differences observed between analytical and empirical measurements might be attributable to the different initiation schemes used.
- Records obtained from bar gages generally had fair signal-to-noise (S/N) ratios and long durations but did not yield detailed stress waveforms, reproducible peak stresses or accurate times of arrival (TOAs), and were deemed unreliable.
- Manganin elements did not return any usable stress or impulse data because the pressures present in these experiments were not within the effective range for manganin.
- Repeatable ytterbium measurements were not obtained at the 0.0-cm range from GZ.
- Reproducible impulse plug measurements were obtained from the initial eight tests. However, data obtained from this gage type is in the form of a single total specific impulse, which made it difficult to ascertain measurement accuracy.
- The baffle constructed to house the airblast gages was not properly designed to withstand the severe environment produced in a close-in blast environment.
- The ballistic pendulum proved reliable, repeatable and relatively easy to use for measuring total impulse imparted by a charge at close-in ranges.
- A coverplate is needed surrounding the face of the pendulum to prevent blastwave wraparound.
- The total impulse delivered increased sharply as the steel casing thickness was increased from 0 to 6.35 mm. However, an increase in casing thickness to 9.53 mm produced only a marginal increase in total impulse.

Recommendations. Based on the results of this program, the following recommendations are provided for continuing research in the area of close-in blast:

- A computer simulation should be run with a single-point initiation at the top center of a bare charge. This analysis could determine if the multipoint initiation used in this program focused the charge and led to the higher peak stresses and specific impulses seen in the computations. The setup for such a run would essentially be the same as that described in this report and would require about 6 Cray hours to complete.
- Additional baseplate tests, using different explosive geometries, should be performed using the successful experimental techniques developed in this program. Such measurements would provide a more complete database and should include actual military ordnance such as TOW missiles. Further baseplate tests should include a focused effort to determine stress-time profiles directly under the charge as well as outside of the charge diameter.
- In conjunction with additional baseplate tests, the analytical model developed in this program should be used to simulate the loadings produced by actual military ordnance.
- Ytterbium elements should be used exclusively for any future experiments conducted in this regime.
- A smaller, more robust airblast baffle should be designed for any future tests.
- Impulse plug gages should either not be used or the impulse plug photodiode housing should be redesigned for any future tests.

ACKNOWLEDGMENTS

This work was sponsored by BRL and the authors would like to thank the technical contract monitor, Rich Lottero, for his guidance, ideas and support of this program. In addition, we would like to acknowledge the following persons whose contributions were essential to the successful completion of this program: Darwin Henley, for guidance in the design and fabrication of the stress transducers and baseplates; Carolyn Krebs for the initiation and development of the overall program; Al Hall and High Hanna for their careful handling of explosives; and Ed Stenerson for his help in debugging the instrumentation.

INTENTIONALLY LEFT BLANK.

PREFACE

The U.S. Army Ballistic Research Laboratory was deactivated on 30 September 1992 and subsequently became a part of the U.S. Army Research Laboratory (ARL) on 1 October 1992.

INTENTIONALLY LEFT BLANK.

1. INTRODUCTION

1.1 Problem. The work presented in this report was completed under contract DAAA15-89-C-0037 for the U.S. Army Ballistic Research Laboratory (BRL). It involves the use of experimental and theoretical means to study blast loading caused by the detonation of high explosives (HE) at close-in ranges. Close-in-blast loading from HE is generally defined as explosive products interacting with a target during the time that the HE has expanded to between 3 and 50 times its original volume. The impulse generated from blast loading can cause gross structural damage to light armored vehicles and is a serious threat to the vehicle and its crew; therefore, its study is of particular importance to the Army.

In addition to studying bare explosives, FMC sought to quantify the contribution made by fragments or flyplates to the overall impulsive loading produced by a close-in blast from a "cased" explosive. Conditions exist where an accelerated mass can contribute significantly to the overall structural deformation of a vehicle and can exceed the contribution made by the explosive overpressure itself. Other conditions exist where the loading from the explosive overpressure far exceeds the contribution from an accelerated mass.

Limited quantitative experimental information exists of the loading profile, in space and time, produced by close-in blast loads. The lack of such information precludes the development of a validated theoretical model.

1.2 Objectives. The overall objective of this contract was to develop an experimentally validated theoretical model capable of predicting the loading in space and time from military explosives detonated at close-in ranges over a nonresponding (nonexplosive, nondeforming) plate. The specific objectives were to:

- Provide computational analysis of stress-time and impulse-time loading curves from bare charge explosives on a nonresponding baseplate at two heights of burst (HOB) and compare these calculations with empirical measurements.

- Provide empirical measurements of stress and impulse histories resulting from the detonation of condensed military bare charges over a nonresponding baseplate at two HOBs to compare with the analytical model developed.
- Experimentally measure the total impulse imparted from a condensed military bare charge at several close-in ranges and empirically determine the contribution that two different thicknesses of steel casing have on the total impulse.

1.3 Approach. This contract was divided into three distinct areas to satisfy the above objectives:

- Southwest Research Institute (SwRI), as a subcontractor to FMC, provided a theoretical analysis of loadings produced on a nonresponding plate by bare charge explosives at close-in ranges.
- FMC designed, fabricated and tested experimental instrumentation capable of measuring the stress and specific impulse histories resulting from the detonation of bare military cylindrical explosives at two close-in blast ranges. A test fixture was modified to accept a nonresponding steel plate that was outfitted with various types of gage instrumentation, including piezoresistant stress transducers, Hopkinson bar gages and impulse plugs.
- SwRI also designed, fabricated and tested a ballistic pendulum capable of measuring the total impulsive load produced by cased and uncased military explosives at close-in ranges.

This report will:

- Describe the overall methods used by FMC and SwRI to perform the tasks described above
- Describe the specific procedures used to perform calculations
- Describe the experimental procedures developed for the baseplate test series, including test setup, gage fabrication and data acquisition techniques

- Describe the experimental procedures developed for the ballistic pendulum tests, including pendulum design and fabrication, data acquisition techniques and experimental setup
- Compare the analytical results obtained by SwRI with experimental results obtained by FMC
- Present the analytical results of stress and impulse histories produced by close-in blast loading
- Present the experimentally obtained pressure and impulse histories from instrumentation fielded in the baseplate test series
- Present the experimentally obtained total impulse measurements for cased and bare charges in the ballistic pendulum tests
- Discuss the results of all data obtained and the lessons learned in fielding and acquiring data in a close in blast environment
- Provide recommendations for future work in the close-in blast regime and discuss how analytical and empirical techniques could be improved

1.4 Background. One way to obtain information on the effects of loading on a given target is by controlled laboratory testing. This helps determine the practical extent of a given problem and indicates whether further study is needed. Frequently, experiments can be iterated until a successful design is found. While certainly useful, this approach often lacks an in-depth phenomenological understanding of the underlying processes involved. Without such understanding, each major variation of a given system may require extensive iterative testing before a satisfactory design is achieved.

Even if this approach is successful, it is unclear that optimized designs can be reliably reached, especially in situations where maximum structural strength at a minimized weight is required. This is a typical requirement of tactical military systems, where weight is often critical. One part of a structure may be over-designed, while another part may be near failure

and yet the overall structural design could appear successful. An understanding of the physical processes is needed to shift excess strength, and hence weight, to a location where it is needed to produce a balanced design. In addition to experimental studies, BRL has also been conducting theoretical and computational studies of close-in blast loading. The computational studies have been performed using theoretical hydrodynamic computer codes (hereinafter referred to as "hydrocodes") that provide simultaneous numerical solutions of the time-dependent equations of mass, momentum and energy conservation. Also solved are the equation for the absolute pressure, or equation of state (EOS), of each material; the sound speed equation of each material; and the relations governing the propagation of detonation waves in explosives. The inherent limitations in the approximations to the mass, momentum and energy equations are relatively well known.

Recent work [1] has demonstrated that existing EOSs for explosive products are not adequate for close-in blast loading. Much effort has been successfully put into developing EOSs for explosives in contact with structures (and up to two explosive volume expansions [2]), and for farfield explosive effects. Two hydrocodes used extensively at BRL are the HULL [3] hydrocode by Orlando Technology, Inc., and previously, the airblast HULL [4] version (now rewritten and renamed "SHARC") supported by S-Cubed.

The most commonly used explosive product EOS in HULL is the Jones-Wilkins-Lee [2,5] (JWL) EOS. Explosive product models such as the JWL EOS, in conjunction with chemically nonreacting material (e.g., air, steel) simulated in computer codes, can produce calculations of pressure and dynamic response in agreement with experiment in which the explosive and material are in either direct contact or close proximity. However, the JWL EOS does not appear adequate for predicting the blast pressures and, hence, the response of materials and structures at distances that include a standoff length or air gap such that the explosive products undergo significantly more than a twofold expansion from the original undetonated volume. In fact, the principal purpose of the JWL EOS is its use in predicting the ability of an explosive to accelerate metal plates [2].

The problems with predicting the loading at standoff distances typical of close-in blast loading have been documented by BRL in comparisons of available experimental results to computations. An additional difficulty in determining the accuracy of a given EOS for close-in

blast loading is that the pressures are typically so high (e.g., 0.3 - 2.0 GPa, or 43,500 - 290,000 lb/in²) and thermal effects and debris fields are so intense that pressure measurement gages either do not survive or produce records that are not repeatable enough to accept with confidence [6]. Thus, reliable data against which an EOS can be calibrated are lacking.

What is needed to solve the problem of close-in blast loading is an in-depth phenomenological understanding of the underlying processes involved. By developing a model that has a sufficient experimental footing, one can design a given system without the expensive iterations involved in an empirically derived design.

2. ANALYTICAL AND EXPERIMENTAL TECHNIQUES

2.1 Overall Methods. FMC used a combination of empirical and analytical analyses to increase computational capabilities to a level where these models can successfully be applied to a diverse range of applications involving close-in blast loading. Discrete analytical nodes of information were tailored to match the experimental measurement locations, explosive types and test configurations used in both the baseplate and ballistic pendulum tests. By so doing, comparisons between empirical and analytical results could easily be made and a strong footing could be established for validating the computer models generated in this program with reproducible, independently validated experimental methods.

2.2 Computational Methodology. Two of the more common gridding schemes in hydrocode calculations are the Lagrangian and the Eulerian. In Lagrangian calculations, the grid motion follows the material motion. This means that a computational node will remain at the same place in the material during the whole deformation. Thus, computational cells are required only where there is material; however, large deformations lead to small computational cells and therefore small time steps. This approach is usually taken for computational simulations of structural deformation. In a Eulerian calculation, the grid remains fixed, and the material moves through it. Here, a computational node remains at the same point in space, regardless of where the material goes. Thus, cell size never changes (so time steps do not become very small) but a large region of space must be included in the computational grid to follow large displacements.

The code chosen for this project was CSQIII, a state-of-the-art (at that time), two-dimensional Eulerian finite difference computer program code originated at Sandia National Laboratories. A Eulerian code such as CSQIII is well suited to model the detonation of solid explosives and the propagation of the detonation products and shockwave. CSQIII employs second-order advection schemes to distribute the state variables within a computational cell, a scheme that is more accurate than the first-order scheme employed in codes such as HULL.

CSQIII has existing JWL EOS values for Comp B and Pentolite, but has no complete EOS for air. Several sources were searched to obtain a real gas model for air. The most complete and most convenient to implement was a tabular EOS provided by Michael McGlaun of Sandia National Laboratories (the developer of CSQ). This EOS was implemented into the CSQIII input decks.

FMC and BRL initially agreed to explore a multipoint initiation scheme for the detonation of the explosive. The scheme detonated the explosive charge at the top centerpoint, and at six equally spaced points along a circle which is 2.2 cm from the top centerpoint of the explosive. CSQIII simulated the multipoint initiation by detonating the charge simultaneously at the center and along a continuous circle 2.2 cm from center. The continuous circle results from the cylinder symmetry of the two-dimensional model. It should be noted that the computer simulations used this scheme, but when the experiments were conducted, this initiation scheme was abandoned and a single point initiation at the center was employed.

The output of interest from the code includes the pressure as a function of time and location along a rigid baseplate surface below the charge bottom:

P (r) vs. time

and the specific impulse at selected radial locations:

$$i(r) = \int_0^T P(r) dt$$

where T is the total time of blast loading. The total impulse can also be computed over a given surface area of the rigid surface defined by a radial distance R :

$$I = 2\pi \int_0^R i(r) dr$$

Several internal lines of code were added in CSQIII to output pressure and specific impulse at various locations on the baseplate. The locations decided upon were the center (axis of symmetry), and 1.0, 2.0, 2.5, 3.0, 4.0, 5.0, 6.0, 7.0, 10.0, 13.0, and 16.0 cm radial distance from center. Also, freefield locations 25.0 and 35.0 cm from the axis of symmetry at the HOB were flagged to provide output. To provide the total impulse, lines of code were added to integrate the specific impulse out to a radial distance of 50 cm on the baseplate. These modifications were implemented and verified.

2.2.1 Preliminary Computations. Several preliminary runs involved the selection of the burn criteria (program burn vs compression burn), the choice of the predetonation value for the compression burn model, the initiation methodology used, and convergence studies aimed at selection of grid size.

CSQIII employed a program burn model which uses the explosive detonation velocity and the time from initiation to determine which cells "detonate." The detonation model known as compression burn allows pressure to build up in a cell until a critical value is achieved, from whence detonation occurs. This model can achieve the Chapman-Jouget (C-J) pressure without resorting to very fine grid spacing usually necessary with the program burn model. For this reason, the compression burn model was added to CSQIII and used in this program.

Preliminary CSQIII calculations used a one-dimensional strip geometry to simplify the results and reduce run time. The one-dimensional strip was three zones wide, constrained on one edge by the axis of symmetry and on the other edge by a rigid boundary. Actually, due to axisymmetry, the strip represented a solid tube of explosive. When the top edge was detonated across all three zones, the burn proceeded in one direction down through the strip

in a planar manner. In other words, the pressure across all three zones was constant, and did not show a radial variation.

The initial variable investigated using the strip was the value of the predetonation pressure used by the compression burn routine. The predetonation pressure is that value which the code requires to detonate the zone. Through many trial and error calculations it was determined that the strip achieved steady-state burn using a predetonation value of one-tenth the C-J pressure for Comp B (C-J pressure for Comp B equals 29.5 GPa). For values higher than 6.57 GPa, the detonation pressure in the steady-state region oscillated at values 10% higher than the C-J pressure, which is not a realistic burn situation. Lower values of the predetonation pressure (less than 1.83 GPa) caused a similar behavior, except that the oscillations were about a pressure value approximately 80% of the C-J pressure. Using the optimal predetonation pressure value, the runs achieved a steady-state pressure at the detonation front of 26.8 GPa.

This value seems reasonable for burn situations that are not truly one-dimensional, because the C-J value is actually an ideal one-dimensional approximation of real explosive behavior. This behavior is displayed graphically in Figure 1, which shows the burn behavior when the normal initiation scheme is employed to start the detonation. The normal scheme involves flagging those zones that are to start the detonation; the code then releases the energy in those zones and employs the JWL EOS to determine pressures. The explosive front propagates by pressurizing adjacent zones until they detonate. Figure 1 shows that approximately 20 computational zones are required for the pressure to build to a steady value. In the one-dimensional simulation modeled, the attainment of the steady-state implies proper numerical detonation behavior. It should be noted that employing the compression burn logic offers a significant advantage over the program burn logic with respect to attainment of the steady-state burn condition. A similar computation using the program burn logic required over 140 zones to achieve a steady-state pressure at the detonation front.

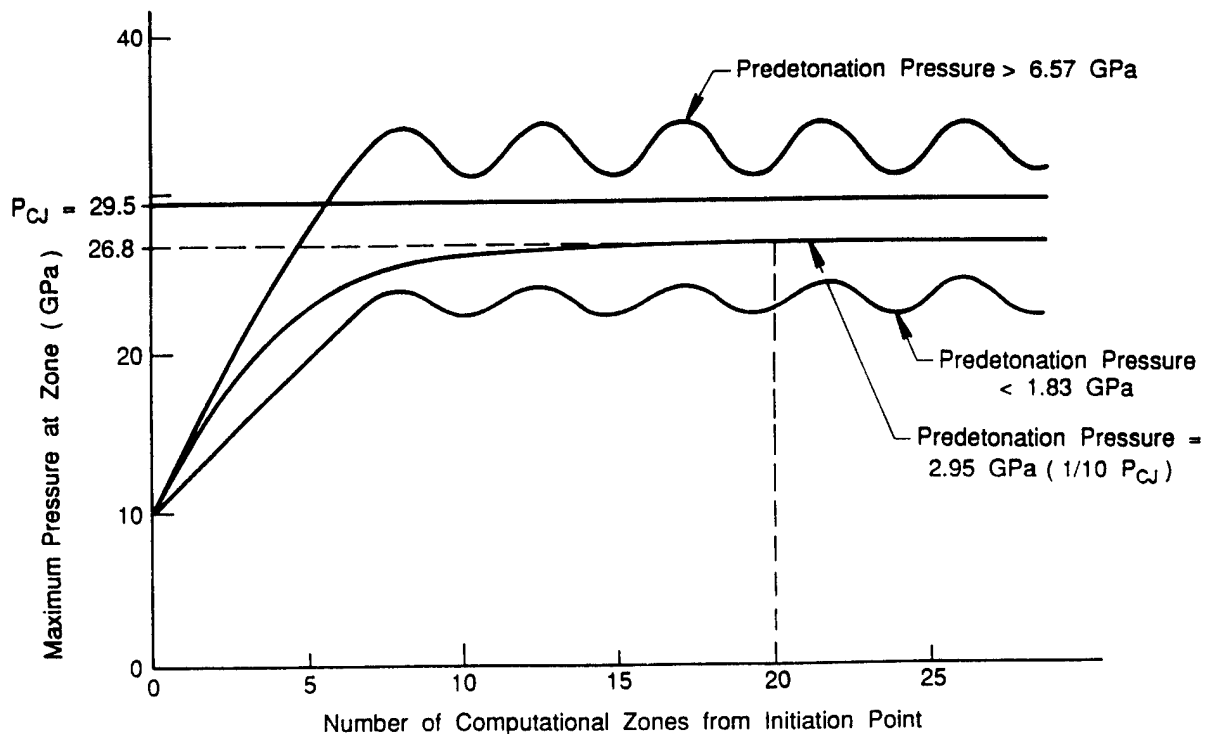


Figure 1. Effect of Predetonation Pressure Value on Explosive Burn Pressure.

Another method of initiating detonation was investigated to apply an initial boundary pressure equal to the P_{CJ} at the initiation zones. This approach was felt to be more similar to the geometry used in the baseplate tests. Figure 2 depicts the effect of both initiation criteria on the detonation pressure front. It can be seen that applying an initial pressure caused the net pressure in the first zone to overshoot the P_{CJ} a little. As the burn progressed through the explosive, it tended to oscillate about the value of 26.8 GPa, then smoothed to a steady state with no oscillations. The pressure initiation criteria had the advantage of having the pressure approach 26.8 GPa in only eight zones, sooner than the normal initiation criteria, and was therefore employed in all subsequent models.

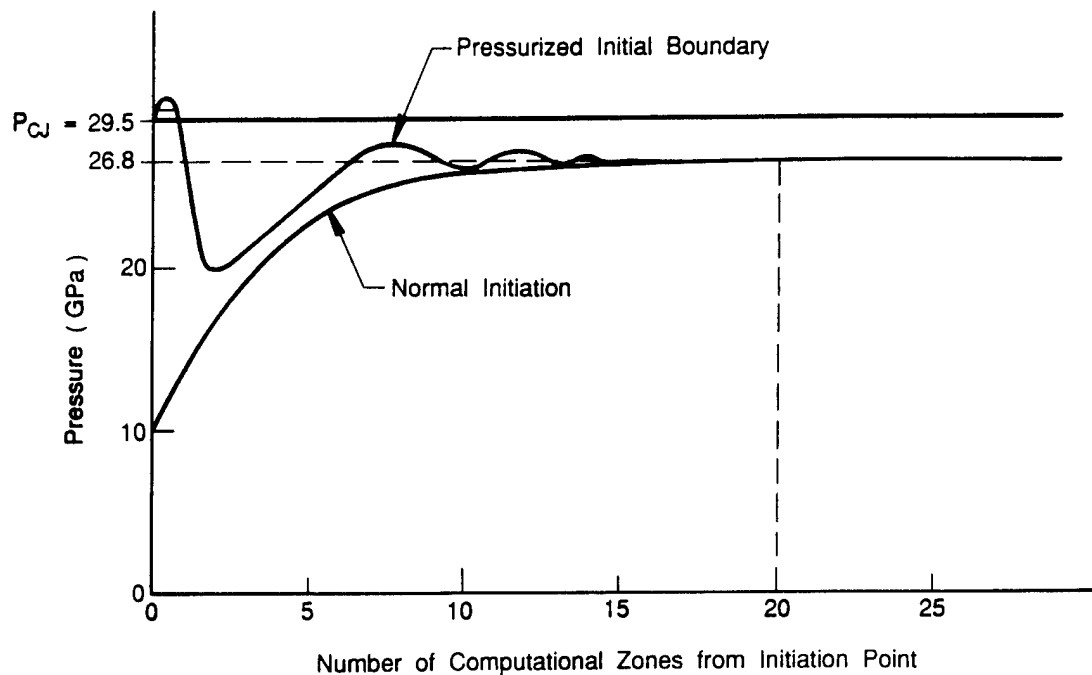


Figure 2. Effect of Initiation Criteria on Explosive Burn Pressure.

The effect of grid size on the achievement of a steady-state pressure at the detonation front was investigated next. The strip model was run using grid sizes of 10.0, 5.0, and 1.0 mm. It was discovered that the pressure rose in the explosive to a value close to 26.8 GPa in about eight zones, and steadied at that value in 20 zones, regardless of the size of the zones.

CSQIII has an option to (roughly) spread the burn front over a set number of zones. Trial and error runs showed that the best results were achieved when the number of zones in the burn front was one. When additional zones were used, the burn front was unstable.

The one-dimensional strip model described above originally used a rigid boundary across the initiation zone; however, subsequent runs modeled a free surface at that location. As a result, more zones (approximately 80) were required to achieve the steady-state pressures of 26.8 GPa. This result indicated that the build up to pressure occurs more slowly when the top

of the charge is free to expand into air. It may be necessary to have at least 80 zones in the two-dimensional cylindrical model to allow for numerical buildup of pressure.

Several two-dimensional simulations were performed to determine the effect of grid size on the convergence of pressure and impulse values on the baseplate. These runs modeled the Comp B explosive, which had a length of 8.8 cm and a radius of 4.4 cm. The charge was initiated on the top surface at the axis of symmetry and in a ring at a radius 2.2 cm from the axis of symmetry. For these convergence studies, the pressure and impulse values reported were recorded at a rigid baseplate 20 cm below the charge center (20-cm HOB).

The dimensions of the square grid were varied: 10, 4, 2, and 1 mm. For comparison purposes, peak pressure and specific impulse are reported for the point on the baseplate which lies on the axis of symmetry. Total impulse is also reported; this value was obtained by integrating the specific impulse out to a radius of 50 cm (for 400 μ sec run time). The results, shown in Table 1, are discussed in the following paragraphs.

Table 1. Convergence Study Results, Pressure and Impulse on Baseplate at Ground Zero

Grid Size (mm)	Peak Pressure (GPa)	Specific Impulse (MPa-sec)	Total Impulse (N-sec)	CPU Time (hours)
10	0.21	0.008	793	0.14
4	1.27	0.027	1100	0.50
2	1.65	0.036	1120	3.50
1	1.97	N/A	N/A	3.10
1 -> 2	1.91	0.039	1030	4.60

Results of the 10-, 4-, and 2-mm grids suggest that the grid was not small enough to indicate convergence of peak pressure and specific impulse. If the numerical simulations had "converged," these values would not have changed as grid size decreased. Table 1 indicates the run time in CPU hours on the BRL Cray X-MP. As can be seen the 2-mm grid requires a significant amount of CPU time. It was desirable to run a simulation with a 1-mm square grid throughout, but this would require an estimated 30 CPU hours—an amount of time far beyond

the scope of this effort. However, to obtain another datapoint from which to judge the convergence of the pressure and specific impulse, a simulation with a 1-mm grid was performed utilizing a smaller portion of the normal grid extent (10 x 30 cm, compared to 50 x 70 cm for the other runs). Additionally, the 1-mm grid was only run for 59.6 μ sec compared to 400 μ sec in a complete run. Using the smaller size and shorter time, we obtained results in about 3.1 CPU hours. Due to the reduced size and run time, only peak pressure at the axis of symmetry on the baseplate could be obtained, as shown in Table 1.

Total impulse appeared to converge at a grid size of approximately 4-mm—an encouraging result because peak pressure and specific impulse convergence may not even occur with 1-mm grid resolution. However, it should be noted that the one-dimensional strip simulations reported earlier showed that 80 zones were required to achieve a steady-state burn condition. The 1-mm grid size simulation achieves this zone requirement in the explosive (8.8 cm divided into 1-mm grids equals 88 zones). It is possible that the results with the 1-mm grid are "converged"; the only way to verify this would be to run a simulation with a smaller grid. Unfortunately, any such run was beyond the time and funding constraints of this project.

To take advantage of the 1-mm grid size in the explosive, yet prevent excessive run time, it was decided to perform simulations where a mapping to a coarser grid occurred in midcalculation. These runs zoned the explosive and a portion of air around the explosive with 1-mm square zones. The simulation was allowed to run until the explosive had completely burned, and the detonation front had propagated up to the air. The simulation was then stopped, and the values of energy, pressure, density, and velocity from the 1-mm zones were mapped into a grid composed of 2-mm-square zones. The 2-mm grids covered the area in a normal run. The mapping technique can sometimes smear pressure spikes due to the averaging involved when values are transferred to larger grids.

The 1- to 2-mm simulations provided pressure results consistent with the 1-mm run, and did not incur significant CPU time penalties. As shown in Table 1, the peak pressure was maintained but the total impulse in the 1- to 2-mm runs was 8% lower than with the 2-mm grid. When the explosive burn portion of the Comp B 1-mm run was mapped into the 2-mm grid, some explosive energy was lost through the upper and right-hand transmitting

boundaries of the high resolution grid. Comparisons to results of the 2-mm run proved that this loss would have minimal effect upon the pressure at the gage points on the baseplate due to the small magnitude and direction of the energy. However, the energy loss may have contributed to long-term effects, causing the total impulse to be slightly lower in the 1- to 2-mm run. Also, the slightly lower value may be within the differences to be expected in performing similar but slightly different computational experiments.

2.2.2 Final Computations. Figure 3 depicts the four main computer runs completed for the two explosives (Comp B and Pentolite) at the two HOBs (15 and 20 cm as measured from the center of the charge). Each computer run was preceded by a run to model the explosive detonation with a 1-mm-square zoning, and after some 20 μ sec the data were transferred to a coarser (2-mm) grid, which covered the whole problem region.

The following paragraphs first describe the explosive detonation, then detail the continuation of the simulation on the coarser grid. For each explosive type, the same explosive burn could be used for each HOB calculation because the detonation of the explosive with surrounding air on the fine grid was terminated before any interaction with the plate occurred. In all cases, the explosive had a radius of 4.4 cm and a height of 8.8 cm. Figure 3 depicts the overall dimensions used to define the computational grid for the numerical simulations.

Case 009: Comp B explosive was modeled as an axisymmetric cylinder by using a grid having a radius of 10 cm and a height of 30 cm with 1-mm square zones (area A on Figure 3). This represented a total grid of 30,000 (100 by 300 zones). The center of the explosive was 15 cm from the lower boundary. The explosive was surrounded by air and detonated by "pressurizing" three zones on the top of the explosive: the zone by the axis of symmetry, and the two zones surrounding the 2.20-cm radial location. The JWL EOS was used for the Comp B explosive products, and the detonation propagated according to pressure criteria. The run took some 5000 CPU seconds. The restart file used to start the two continuations was written at 21.837 μ sec. It was later realized that a small amount of detonation product had "leaked off" the side of the grid and so was lost. The extent of the detonation products at 21.837 μ sec is shown as the bold line on Figure 3. The loss is felt to be rather small since it is directed

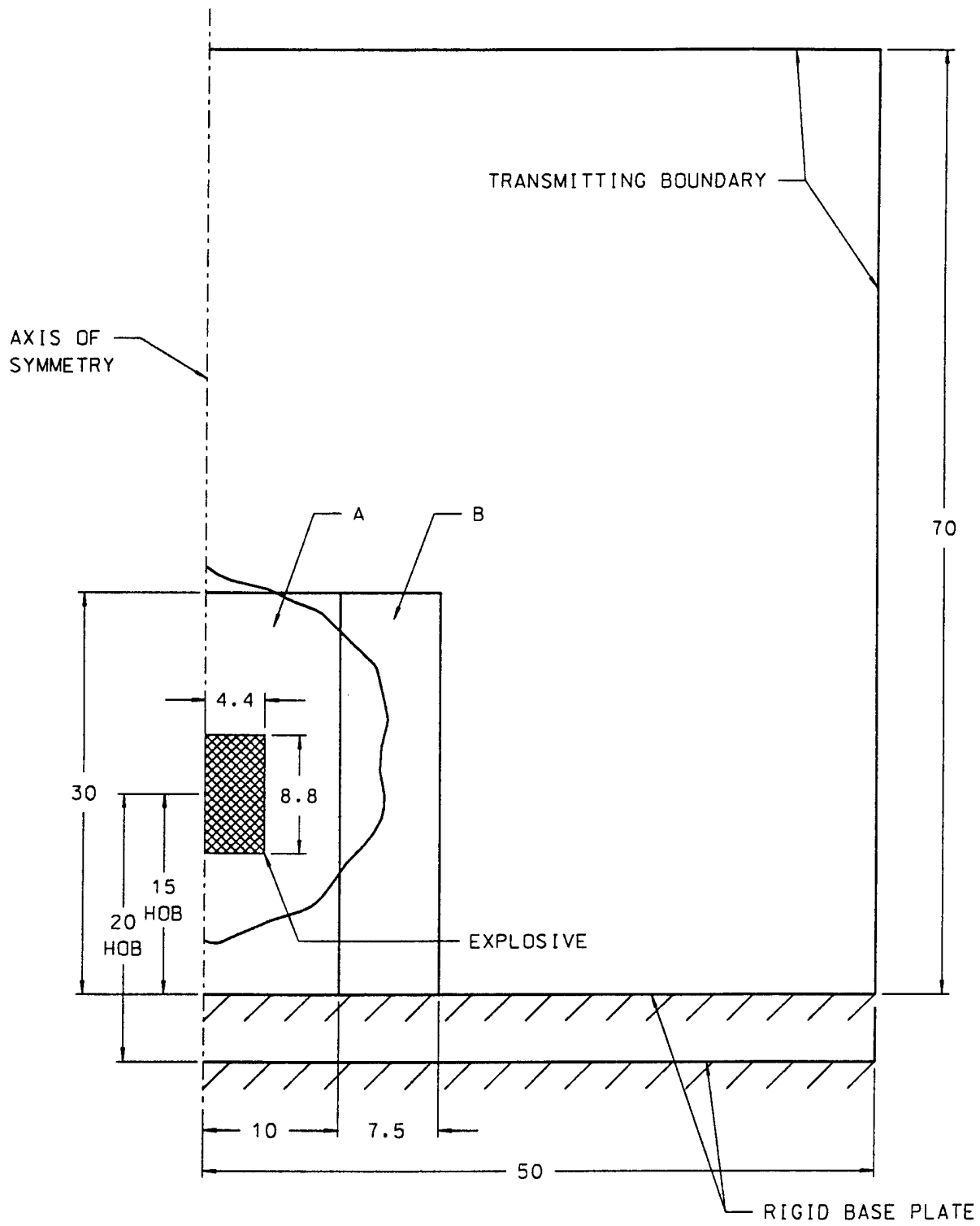


Figure 3. Computer Gridding Description (All Units in Centimeters).

parallel to the baseplate. Blast products were also lost off the top (the near boundary) of the grid, but it is thought that this loss would also have minimal effect on the pressures experienced at the plate.

Case 009A: This computation is a continuation of the Comp B run at a 20-cm HOB. The problem setup size was 50 x 70 cm. A cylinder with a 10-mm radius and a 30-mm height was zoned with 2-mm square zones, for a total grid of 50 x 150 zones. The zoning then continued geometrically in the radial direction and in height until the boundary was reached. The geometric zoning had a 2% increase over 80 zones, leading to a 1-cm zone of height, or an aspect ratio of 5:1 at two opposite corners of the grid. A total of 130 x 230 zones was thus used to describe the complete problem. Each of the ensuing runs used this same zoning.

To map the 1-mm grid results to the 2-mm grid took about 100 CPU seconds. From there, it took 3.2 CPU hours to run to 400 μ sec.

Case 009B: This computation was the continuation of the Comp B explosive blast, but with a 15-cm HOB. This was accomplished by removing the bottom 5 cm of the zoning described above, so that the total grid had 130 x 205 zones, and the problem dimensions were 50 cm x 65 cm. This run took 2.38 CPU hours to go to 400 μ sec.

Case 14: The detonation of the 50/50 Pentolite explosive was modeled in the case 14 series of computer runs. Experience with the Comp B detonation suggested some changes in the zoning of this problem. The center of Pentolite charge was placed in the middle of the 10-cm x 30-cm cylinder which had 1-mm square zoning. To remove the problem of explosive products and pressure wave being lost out the side of the grid, a larger radial region was included in the problem. A radial extension of 7.5 cm was added (area B on Figure 3), giving 35 zones with geometric zoning increasing at a rate of 4% and reaching a size of 0.39 cm on the far right. This gave a total problem region of 17.5 cm x 30 cm, with the total grid giving 135 x 300 zones. Pentolite was modeled with the JWL equation of state. Detonation and early expansion was modeled to 20 μ sec; this took 3433 CPU seconds, or about 1 CPU hour. The front of the explosive products traveled 7.5 cm. No explosive products or any of the pressure wave were lost out the side of the cylinder, and a minimal amount was lost off the top.

Case 14A: This was the continuation of the case 14 run to 400 μ sec for the 15-cm HOB after mapping the 1-mm grid results onto a 2-mm grid. The rezone took 94 CPU seconds and the run itself took 2.5 CPU hours. The same zoning as in case 009B was used.

Case 14B: This was the continuation of the run to 400 μ sec for the 20-cm HOB. Again, the rezone took 94 CPU seconds, and the run itself took 3.2 CPU hours. The same zoning as case 009A was used.

2.3 Baseplate Measurements.

2.3.1 Experimental Design. Twelve baseplate tests were completed using a top-detonated, right circular cylinder composed of two types of explosives (Comp B and Pentolite) detonated at two HOBs over a nonresponding steel plate. Each unique configuration was tested three times.

The test fixture (Figure 4) consisted of a 1.5-m x 1.5-m steel support table positioned on 1.2-m legs. A 0.15-m-thick rigid steel plate (herein called the backing plate) was placed on the support table. Steel plates, 0.3-m square and 2.5-cm thick (herein called baseplates) were bolted to this rigid plate to protect the backing plate and accept instrumentation. Gage designations were consistently maintained throughout the test series: Mn for manganin elements, Yb for ytterbium elements, Pb for pressure bar gages, Imp for impulse plugs and AB for airblast gages.

The initial four tests used three distinct measurement systems for reflected pressure (piezoresistant stress transducers, Hopkinson bar gages and impulse plugs) and one measurement system for airblast pressures (piezoelectric quartz sensor). Piezoresistant elements and Hopkinson bar gages were fielded and maintained a high rate of data return for all tests. Impulse plug gages were fielded for the initial eight tests. Cumulative damage to the photodiode sensors, however, precluded use of these gages in the final four tests. Airblast gages were not fielded after the first two baseplate tests due to low data return and damage to the airblast fixtures in the first two tests.

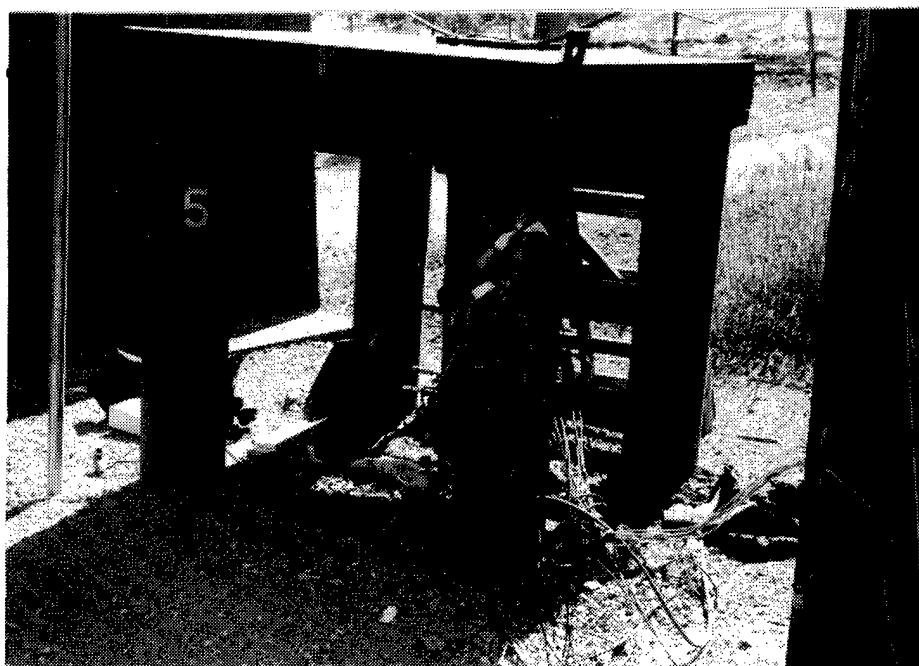
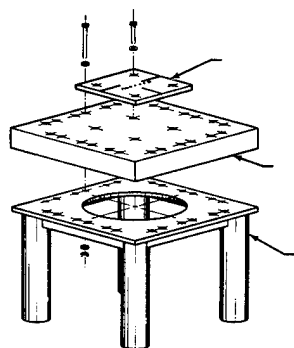


Figure 4. Test Fixture Used for Baseplate Tests 2A.1–2A.12.

2.3.2 Explosive Charge. All of the Comp B and Pentolite charges were furnished GFE to Hollister Test Site (HTS). The charges were right circular cylinders with a geometry such that the charge radius (nominally 4.4 cm) equaled one half the charge axial length and had a nominal mass of 1.0 kg. The charges were made without a detonator well and were initiated on the top surface with a Reynolds RP-80 detonator and a cylindrical booster charge 1.27 cm in diameter and 1.27 cm in height. Tables 2 and 3 describe the physical characteristics of each explosive and booster charge used.

Table 2. Baseplate Explosive Charges (Using RP-80 Detonator and CH-6 Booster; Test Site Was HTS No. 2)

Charge Number	Main Charge Explosive Type	Main Charge Mass (g)	Booster Mass (mg)
2A.1	Comp B	906.6	3,002
2A.2	Comp B	906.8	3,003
2A.3	Pentolite	888.9	3,000
2A.4	Pentolite	880.2	2,998
2A.5	Comp B	904.0	2,999
2A.6	Comp B	906.0	3,003
2A.7	Pentolite	885.0	3,004
2A.8	Pentolite	886.0	3,000
2A.9	Comp B	906.0	2,999
2A.10	Comp B	906.0	3,002
2A.11	Pentolite	886.0	3,000
2A.12	Pentolite	886.0	2,998

2.3.2.1 Charge Placement for Firing. All charges were placed such that the axis of symmetry of the charge was perpendicular to the baseplate surface being loaded. The HOB was measured from the center of volume of the charge to the baseplate surface containing the instrumentation.

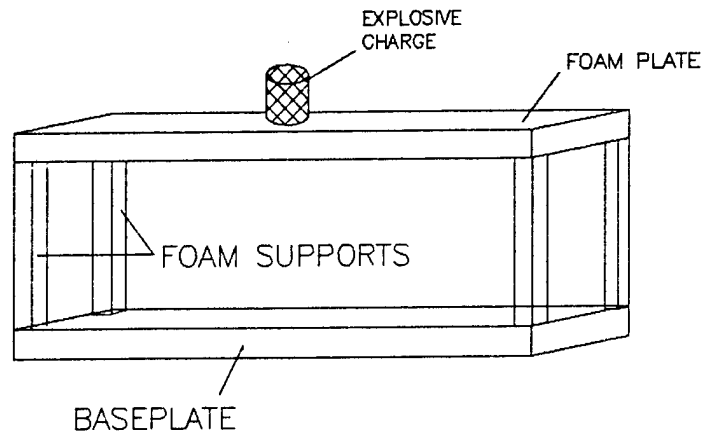
Table 3. Baseplate Shot Geometry (Cylindrical Charges, Top Center Initiation)

Charge Number	HOB (m)	Charge Radius (CM)	Charge Axial Length (cm)
2A.1	0.15	4.392	8.797
2A.2	0.20	4.389	8.822
2A.3	0.15	4.404	8.784
2A.4	0.20	4.397	8.776
2A.5	0.15	4.395	8.840
2A.6	0.20	4.390	8.800
2A.7	0.15	4.391	8.880
2A.8	0.20	4.387	8.805
2A.9	0.15	4.400	8.800
2A.10	0.20	4.395	8.802
2A.11	0.15	4.390	8.795
2A.12	0.20	4.400	8.790

The cylindrical explosive charges of Comp B and Pentolite used in this program were precisely positioned above the test fixture with accurately cut foam holders (Figures 5 and 6). These holders kept the charges in place under variable wind conditions and allowed for easy and accurate leveling and HOB adjustment.

2.3.3 Instrumentation. The instrumentation consisted of gages or transducers, power supplies, signal conditioners, and data acquisition systems. Gage type and location in axial and radial position for all tests are given in Tables 4 and 5. Gages measuring reflected pressures were contained within a disposable baseplate (Figures 7 and 8) that was machined to accept this instrumentation. Gages are described in paragraphs 2.3.3.1 - 2.3.3.3. Airblast gages were used to measure the freefield static pressure of the explosives and are described in paragraph 2.2.3.4.

a - Perspective view



b - Cross-section

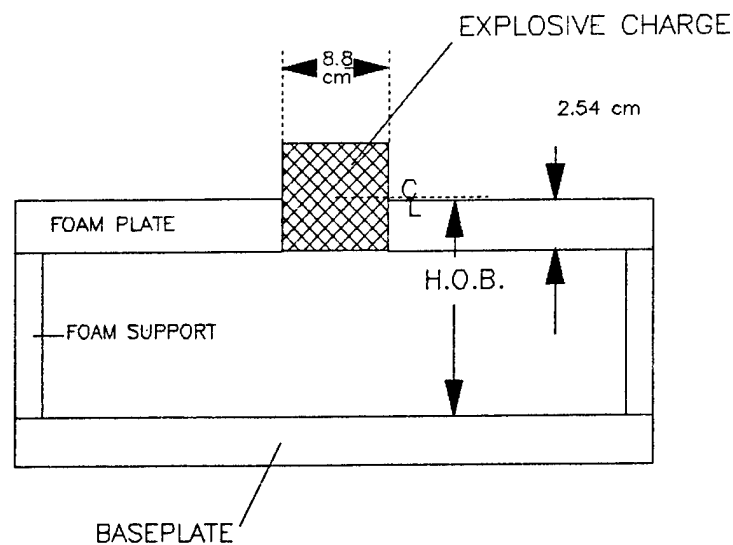


Figure 5. Schematic Diagram of Foam Holder Used to Position Explosive Charges.

2.3.3.1 Piezoresistive Pressure Gages. The dynamic reflected pressures incident on the baseplate were measured with piezoresistive transducers. These elements are electrically insulated, placed within a grooved area of the baseplate and covered with a 0.16-cm-thick



Figure 6. Photograph of Explosive Charge Foam Holder.

stainless steel strip, as shown in Figures 7, 8 and 9. The first four shots contained four piezoresistive elements (two ytterbium and two manganin) with dimensions of 1.52 x 1.52 x 0.10 cm thick. Copper leads were soldered to tabs on the stress transducers. The leads were protected by the steel strips and were connected to RG-58 cables using BNC connectors. These connections were protected using lead sheets as shown in Figures 10a and 10b. The final eight shots contained five piezoresistant elements (all ytterbium) with the same dimensions as the first four tests. As described in paragraph 2.1, ytterbium elements Yb.1 and Yb.2 in test 2A.9 were encapsulated with glycerol to provide a hydrostatic environment.

Table 4. Gage Locations

Gage Position Number	Axial Position Z (cm)	Radial Position X (cm), Y (cm)
SHOT 2A.1		
Yb.1	0	0,5
Mn.2	0	0,2.5
Yb.3	0	0,-2.5
Mn.4	0	0,-5.0
PB.5	0	0,0
PB.6	0	2.5,0
PB.7	0	5.0,0.0
IMP.8	0	-2.5,0.0
IMP.9	0	-5.0,0.0
AB.10	25	-17.7,17.7
AB.11	25	17.7,-17.7
SHOTS 2A.2 - 2A.4		
Yb.1	0	0,5
Mn.2	0	0,2.5
Yb.3	0	0,-2.5
Mn.4	0	0,-5.0
PB.5	0	0,0
PB.6	0	2.5,0
PB.7	0	5.0,0.0
IMP.8	0	-2.5,0.0
IMP.9	0	-5.0,0.0
SHOTS 2A.5 -2A.12		
Yb.1	0	0,5
Yb.2	0	0,2.5
Yb.3	0	0,-2.5
YB.4	0	0,-5.0
Yb.5	0	0,0
PB.6	0	2.5,0
PB.7	0	5.0,0.0
IMP.8	0	-2.5,0.0
IMP.9	0	-5.0,0.0

Table 5. Gage Position and Type

Charge	Gage Position Number										
	1	2	3	4	5	6	7	8	9	10	11
2A.1	Yb	Mn	Yb	Mn	PB	PB	PB	IMP	IMP	AB	AB
2A.2	Yb	Mn	Yb	Mn	PB	PB	PB	IMP	IMP		
2A.3	Yb	Mn	Yb	Mn	PB	PB	PB	IMP	IMP		
2A.4	Yb	Mn	Yb	Mn	PB	PB	PB	IMP	IMP		
2A.5	Yb	Yb	Yb	Yb	Yb	PB	PB	IMP	IMP		
2A.6	Yb	Yb	Yb	Yb	Yb	PB	PB	IMP	IMP		
2A.7	Yb	Yb	Yb	Yb	Yb	PB	PB	IMP	IMP		
2A.8	Yb	Yb	Yb	Yb	Yb	PB	PB	IMP	IMP		
2A.9	Yb	Yb	Yb	Yb	Yb	PB	PB	IMP	IMP		
2A.10	Yb	Yb	Yb	Yb	Yb	PB	PB	IMP	IMP		
2A.11	Yb	Yb	Yb	Yb	Yb	PB	PB	IMP	IMP		
2A.12	Yb	Yb	Yb	Yb	Yb	PB	PB	IMP	IMP		

The piezoresistant stress transducers in the first four tests were comprised of both ytterbium and manganin elements. Results from these tests indicated that the peak pressures recorded were below 0.20 GPa and therefore were in the effective range of ytterbium piezoresistant elements. The manganin elements were less sensitive and did not produce adequate signal-to-noise (S/N) ratios at the described pressures. Therefore, the second and third series of four tests were completed using ytterbium only as the piezoresistant gage. These tests produced records that had high S/N ratios, long durations (over 100 μ sec), and were reproducible when comparing gage records at similar ranges both between and within tests. In addition, lessons learned regarding the fielding of both the impulse plug and Hopkinson bar gages in the first series resulted in acquisition of good quality data from both gage types in subsequent test series.

Calibration and interpretation of piezoresistant elements are best achieved if the elements are loaded uniaxially. If the loading is not planar, in-plane strains can have an additive effect

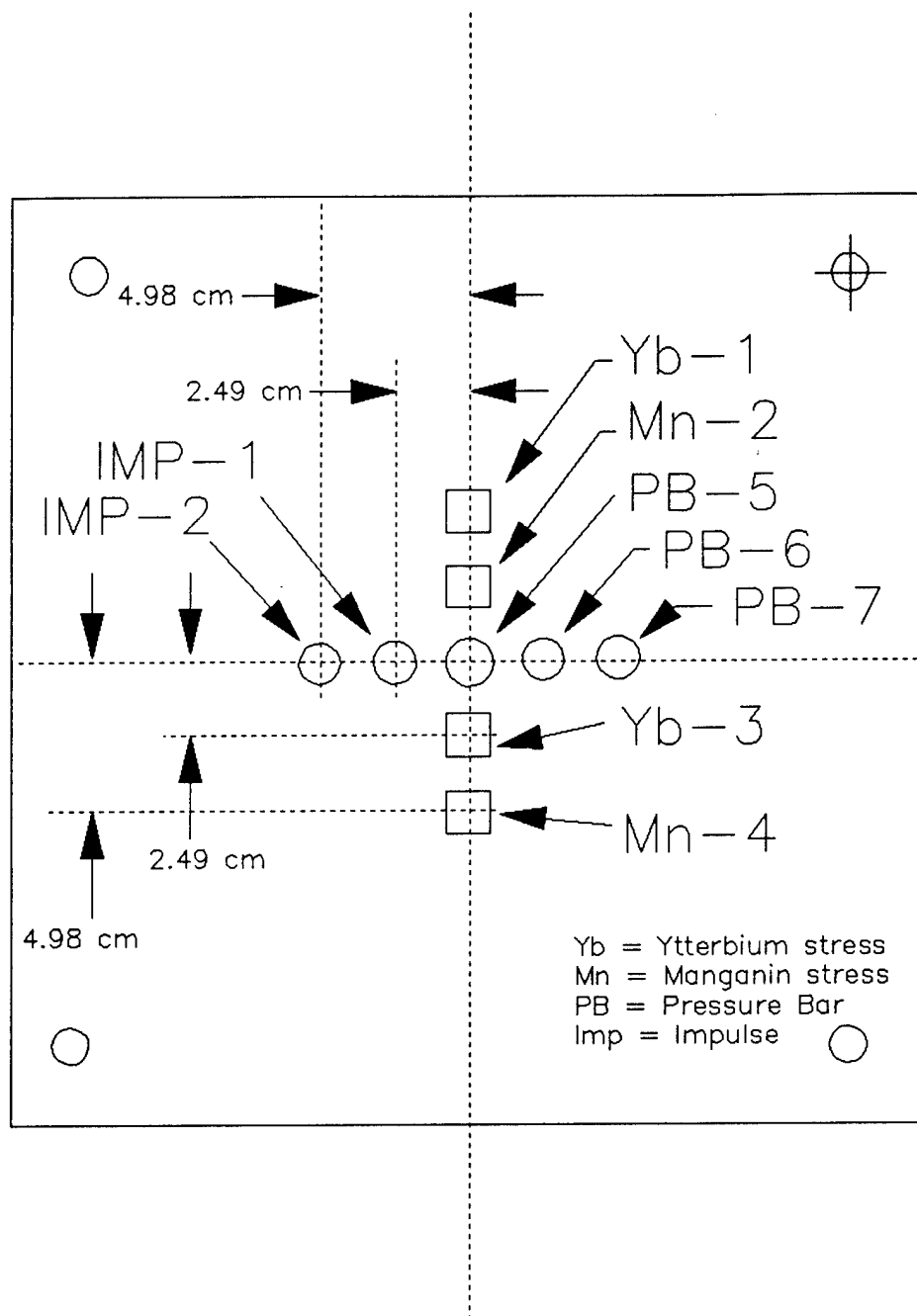


Figure 7. Baseplate Instrumentation, Tests 2A.1-2A.4.

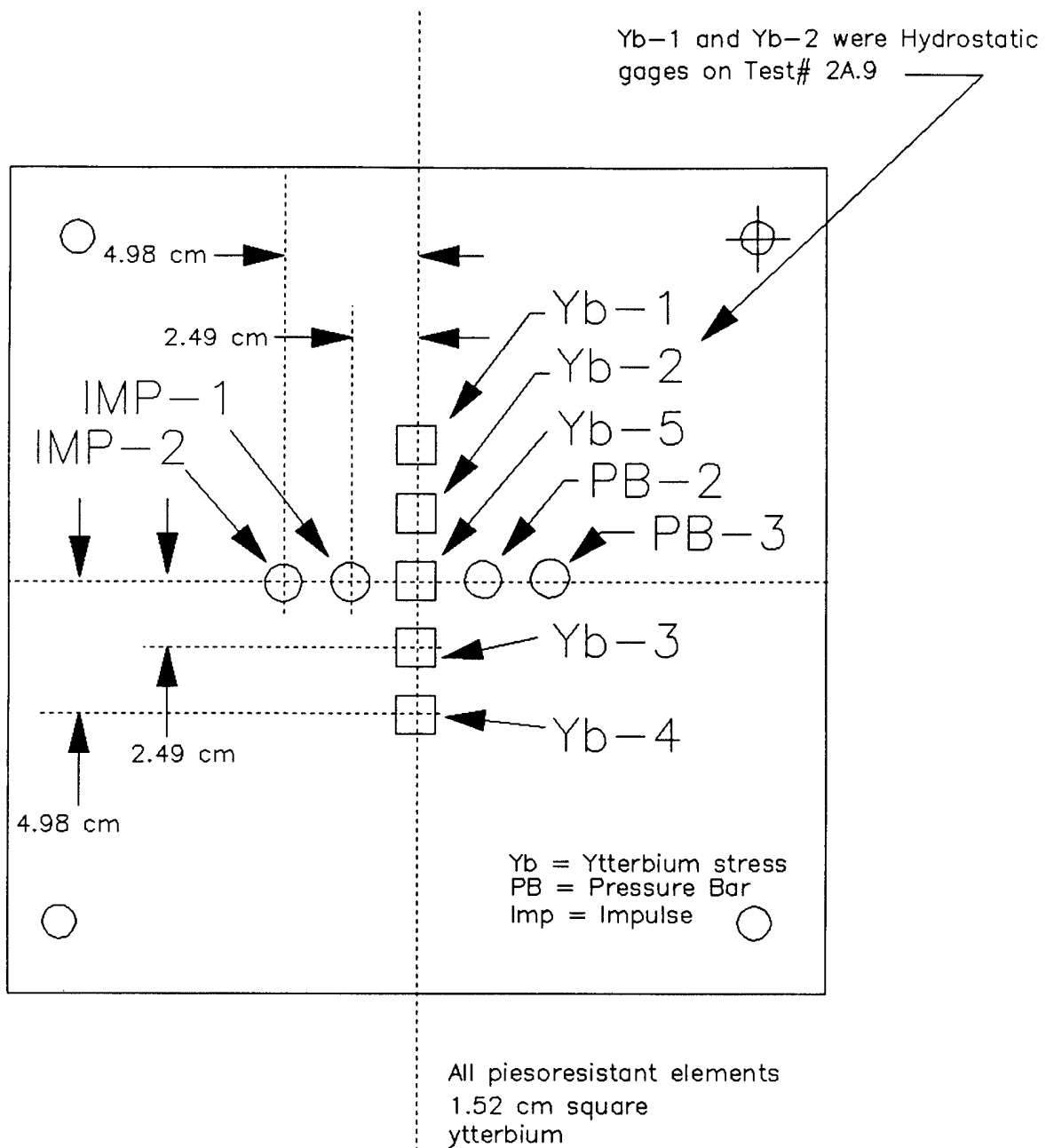
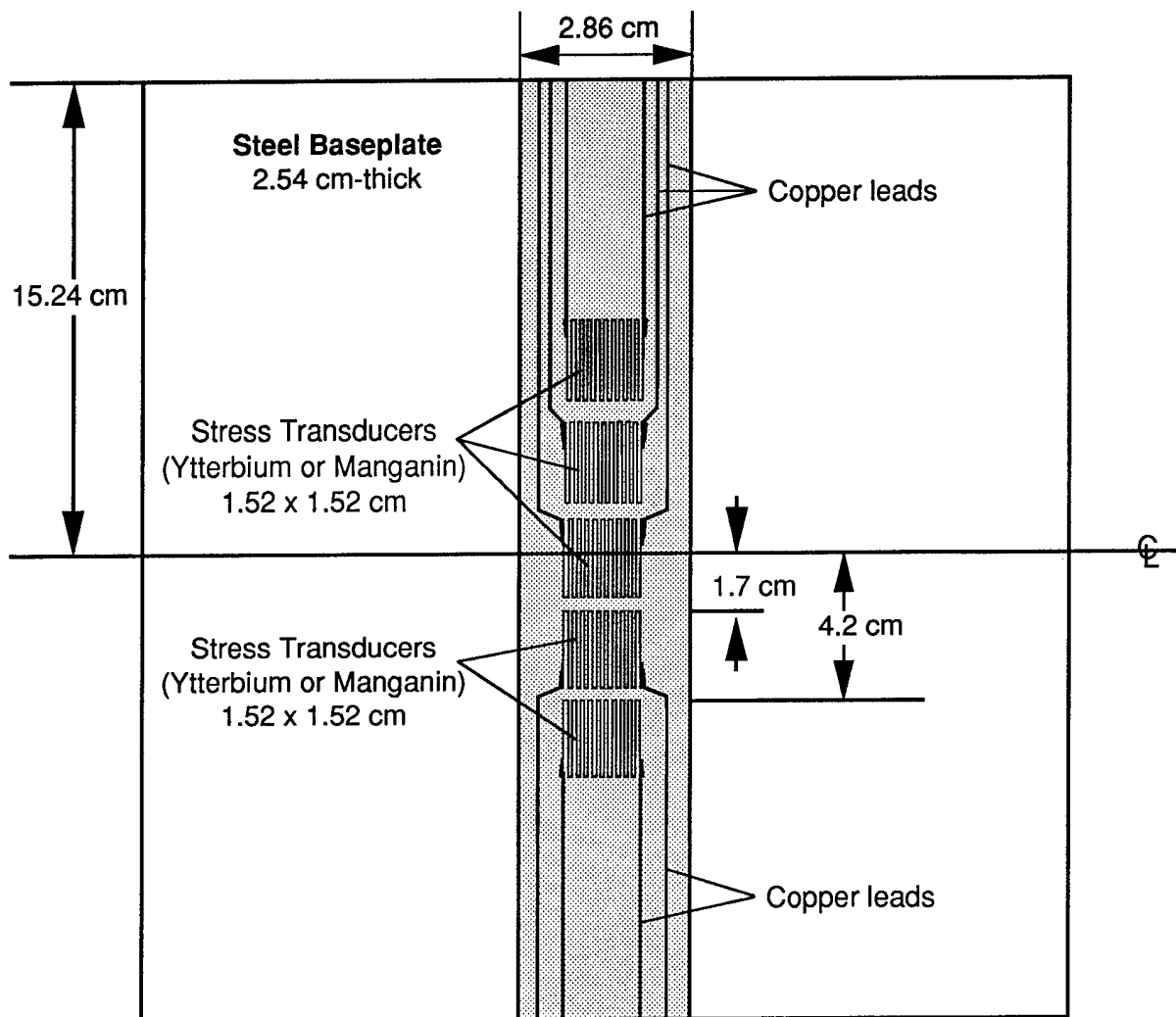
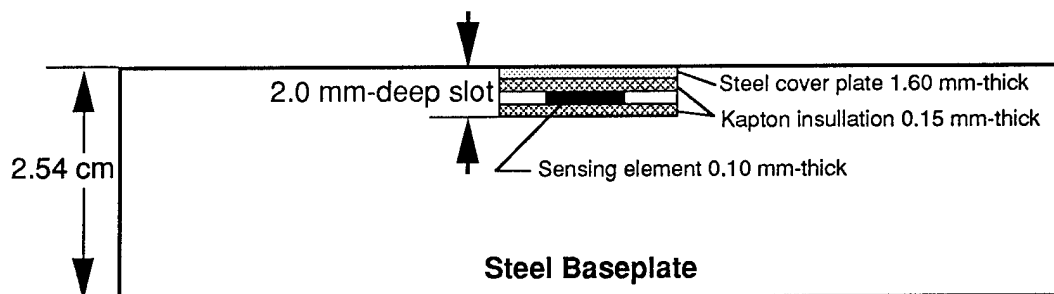


Figure 8. Baseplate Instrumentation, Tests 2A.5-2A.12.



a. Plan View



b. Cross Section

Figure 9. Detail of Piezoresistant Stress Transducer.

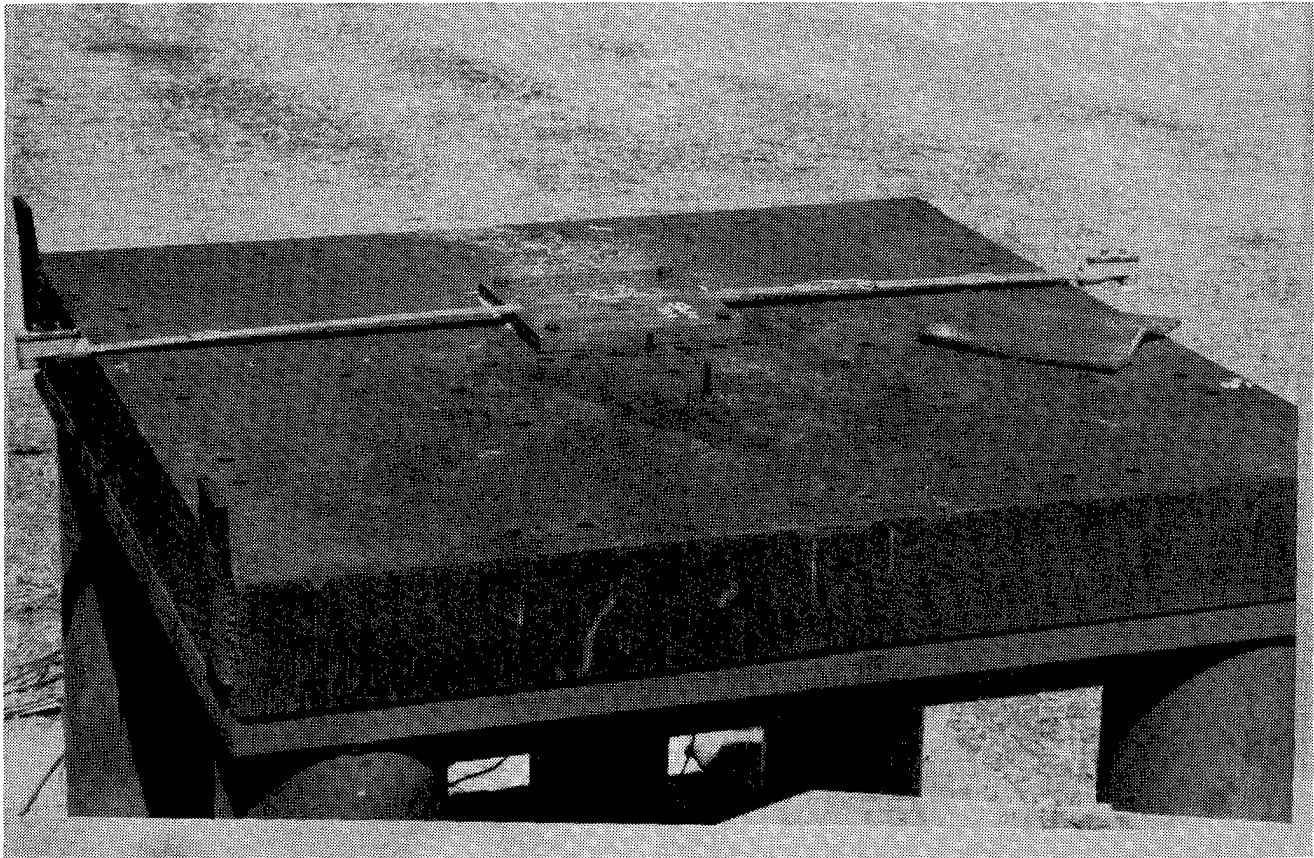


Figure 10a. Photograph of Test Fixture With Baseplate in Place.

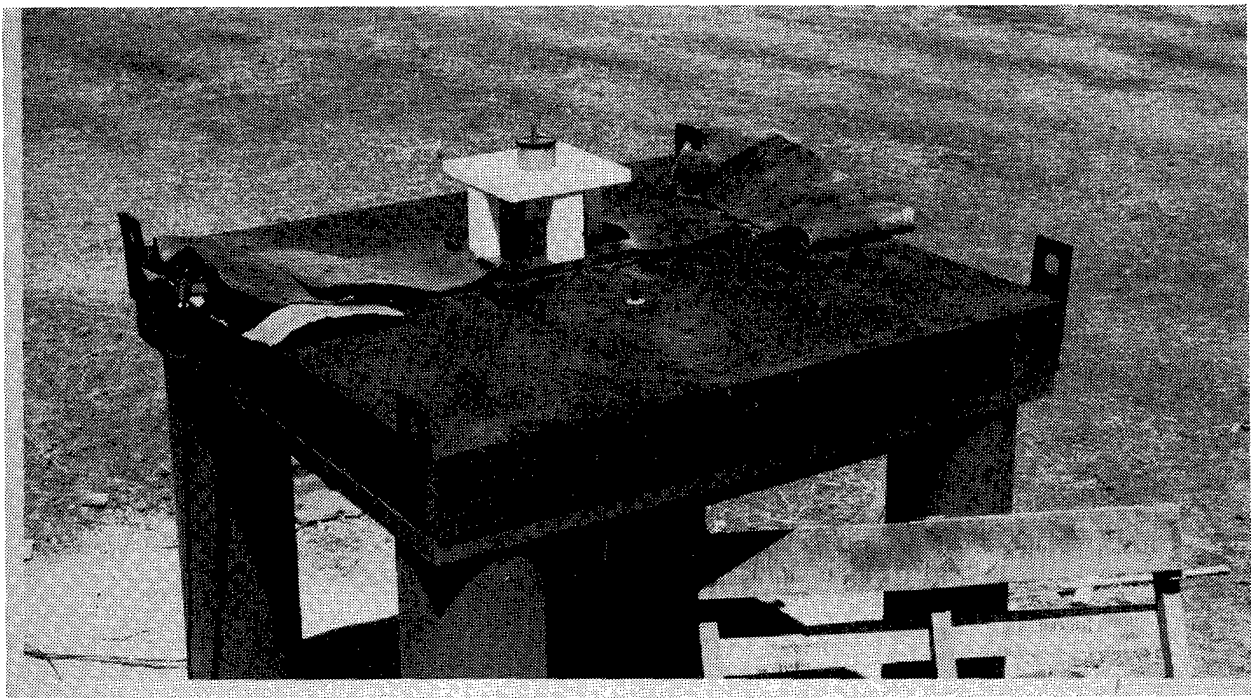


Figure 10b. Photograph of Test Fixture With Explosive Charge and Lead Shielding in Place.

on the resistance changes produced by the piezoresistive effect. One method for determining if in-plane strains are impacting stress measurements is to encapsulate the element in a fluid. In so doing, the gage operates in a hydrostatic environment and cannot support in-plane strains.

The reproducibility of gage records between and within tests from the initial eight experiments suggests that in-plane strains are not currently a problem. Gage elements were not fielded outside of the projected area of the explosive charge because it was felt that in-plane strains would render the gage records interpretable. Future work could depend on acquiring more reliable records in nonplanar environments.

In an attempt to validate the hydrostatic gage concept in a near-uniaxial condition, two ytterbium elements were encapsulated in glycerol so that a direct comparison could be made with other gage records produced in identical conditions. Tests 2A.1 and 2A.5 provided the highest data return for any of the conditions tested in the initial eight shots. Therefore, shot 2A.9 was selected to test this modification.

2.3.3.2 Pressure Bars. The pressure bars used for these tests were a variation of the Hopkinson bar method. In this application the blast pressure induced by the explosive acts as the striker bar, which produces an elastic wave down the bar. The resultant compressive strain is sensed by two strain elements positioned in symmetric locations on the side of the bar. (Two strain elements are used so that any strain generated by a bending mode could be removed). An insulating material is needed both to isolate the bar from the backing and baseplates and to protect the elements from the explosive products.

The pressure bars were made of Vasomax 350 steel bars 1.27 cm in diameter and 1 m long. They were instrumented with two Micromeritics 350-ohm strain gages, 0.32 cm long, positioned symmetrically 20.3 cm from the top of the bar (Figure 11). The bars were inserted through both the backing plate and the baseplate so that the surface of the bar was flush with the baseplate surface. The hole in the baseplate allowed for a 0.25-mm gap between the bar and the baseplate. Initially, water was used to insulate the bar from the baseplate and the explosive products. Significant electrical noise and difficulty in sealing the waterjacket around the bar during the first four tests led us to change the insulating material.

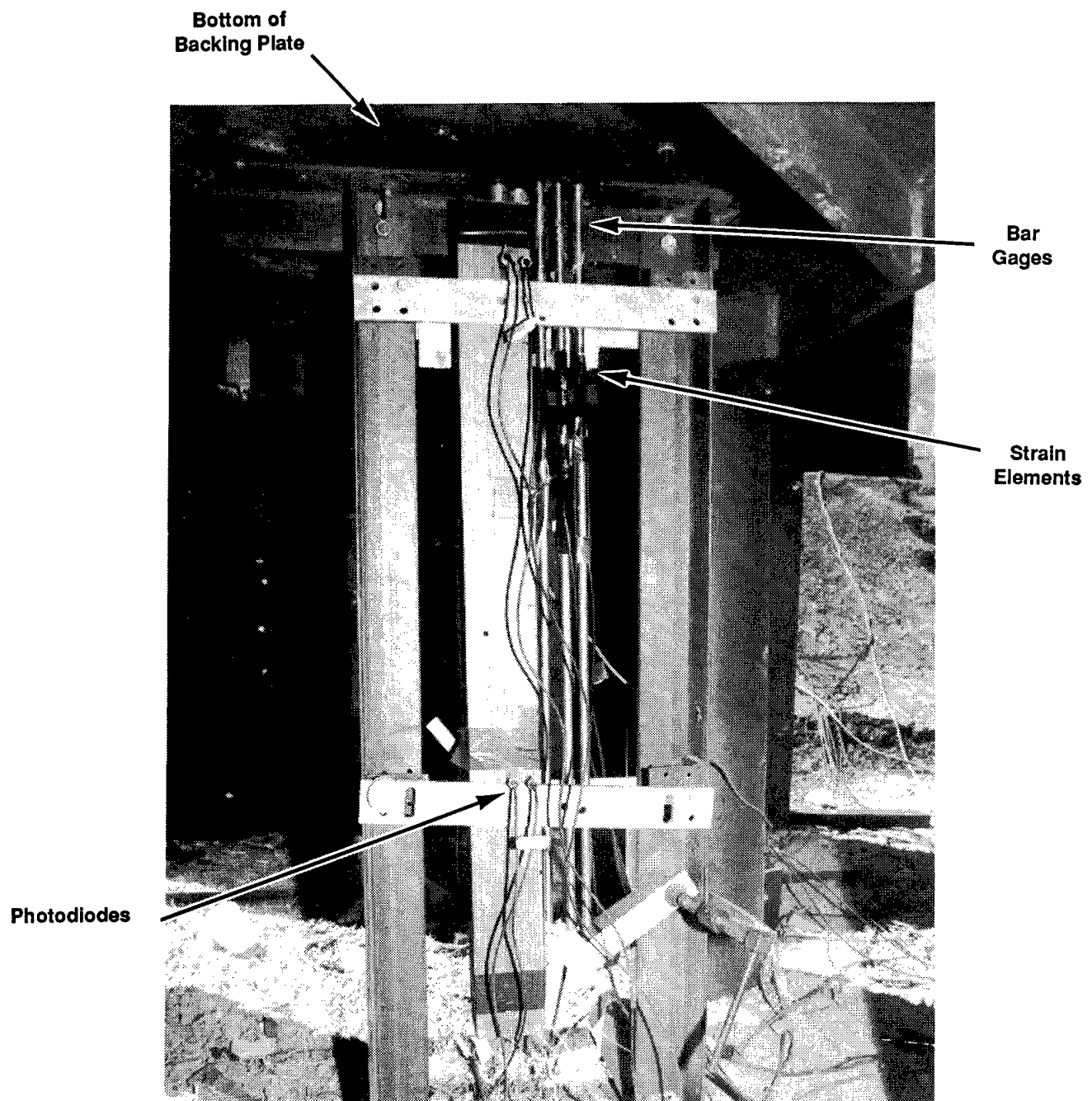


Figure 11. Impulse and Bar Gage Setup, Baseplate Instrumentation.

Silicone lubricant was used for the remaining eight tests. It provided easy installation and eliminated the majority of the electrical noise seen in the initial tests.

The position of the strain elements was based on two factors: the estimated time it takes for explosive products to push through the insulating material and reach the strain elements and the estimated time it takes for the elastic wave induced in the bar to reflect off the bottom of the bar and pass by the strain element a second time. After estimating the shock velocity in water and steel, we determined that the optimum position of the strain gage elements was 20.3 cm (ref. *Handbook of Chemistry and Physics*).

2.3.3.3 Impulse Plugs. Impulse plug measurements are based on the assumption that the incident blast pressure applied to one end of a bar or plug can be considered to be an impulsive load. Therefore, the acceleration to a constant velocity of the plug can be assumed to be instantaneous. This allows the velocity of the plug to be measured anywhere along its flight path. Using the well-known equation $F = ma$, and applying the measured velocity and mass of the plug, we can determine the impulse imparted to the end of the plug.

The impulse plugs used in these experiments were made of Vasomax 350 steel bars, 1.27 cm in diameter and 7.6 cm long. The plugs, placed in holes through the baseplate with a 0.14-mm radial clearance, were suspended with a noninterfering thin rod of graphite (Figures 11 and 12). Two photodiode sensors for each plug were placed in aluminum tubes beneath the backing plate. As the plug passed by the photodiode sensors, the voltage signal dropped. The velocity of the plug was determined by dividing the distance traveled by the time of arrival.

2.3.3.4 Airblast Pressure (Freefield). The freefield static pressures were measured with two piezoelectric quartz pressure transducers (model PCB 109A02). This high-pressure, acceleration-compensated quartz transducer is designed for explosive applications in environments up to 700 MPa. A baffleplate was designed to protect the transducer. The airblast shockwave sweeps across this plate to allow a static (side-on) measure of the explosive pressures. The gages were placed at the HOB and 25 cm from the vertical centerline of the explosive with the sensing element parallel to the plane that bisects the explosive (Figure 13).

2.3.4 Signal Conditioning. Signals from transducers are rarely in a form that can easily be recorded. In most cases, they must first be "conditioned." The following paragraphs describe the type of signal conditioning used for each gage system.

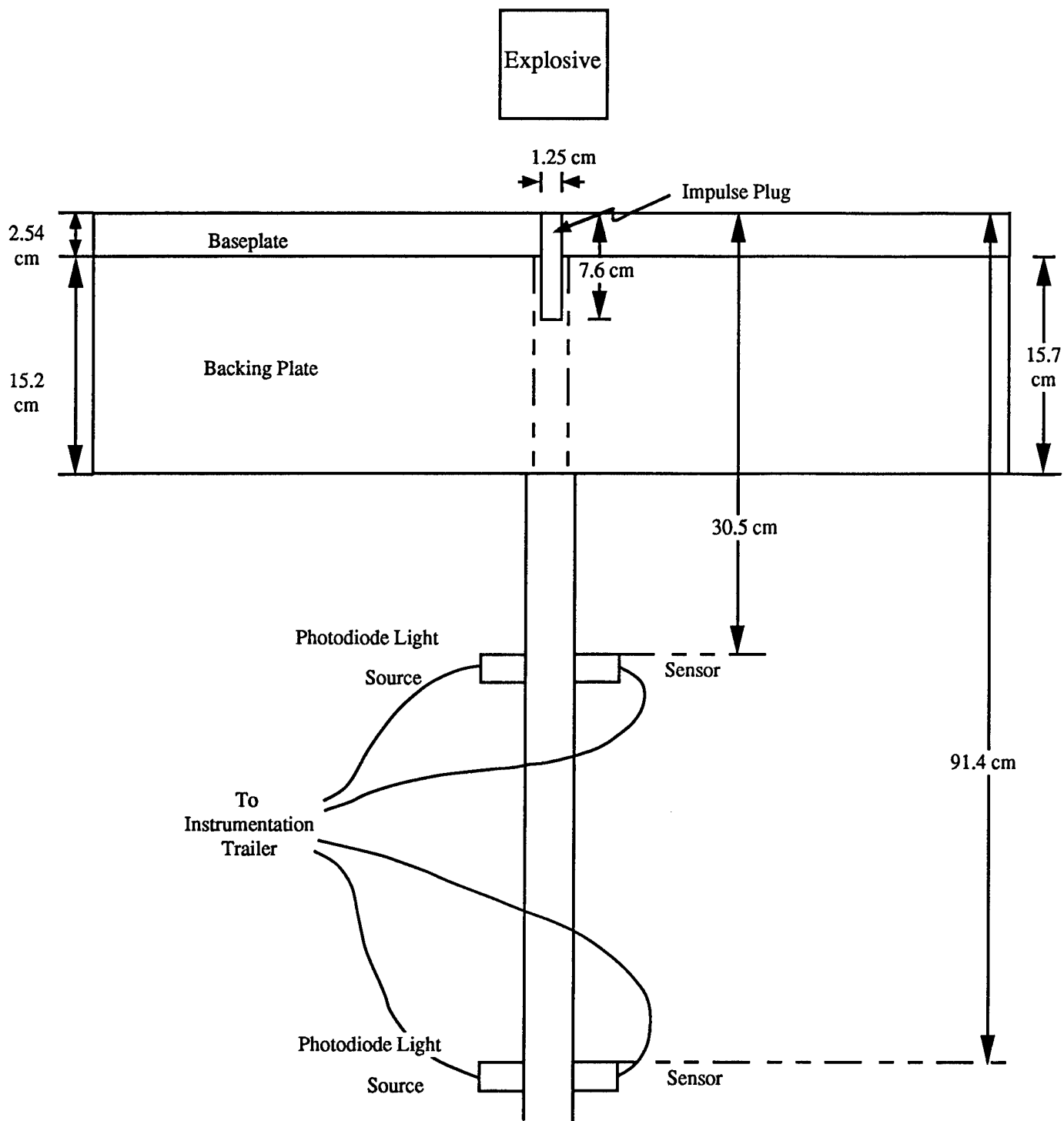


Figure 12. Impulse Plug Used for Baseplate Instrumentation.

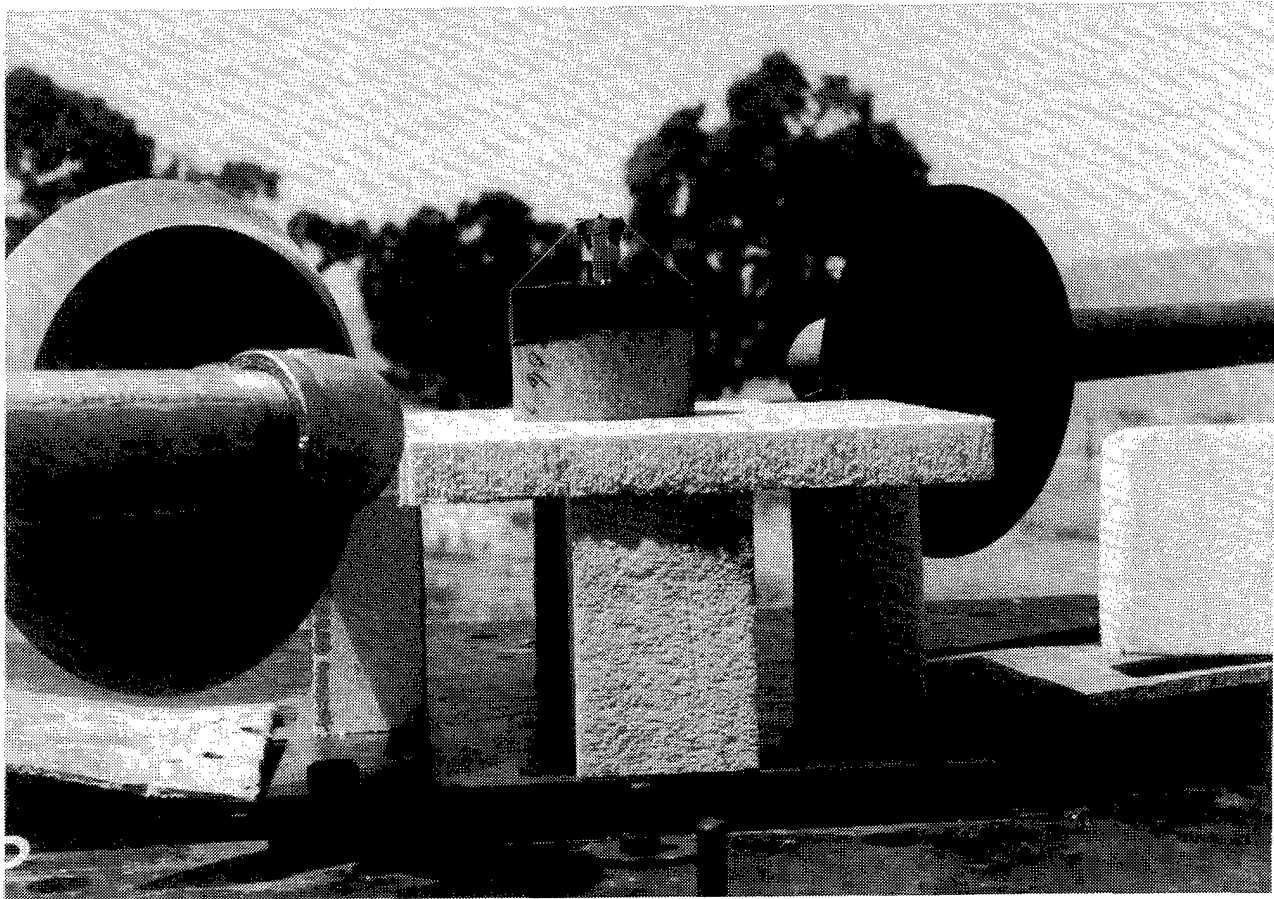


Figure 13. Airblast Gage Used for Baseplate Instrumentation.

2.3.4.1 Airblast Pressure. The outputs of the freefield pressure gages (PCB 109A02) were passed through PCB 480B02 power units, which provided proper coupling to the recorder and also supplied power to the gage. The output from this conditioner was sent to the recorder using RG/58 coaxial cable.

2.3.4.2 Pulse Power Supplies. SAIC Model SG-133A two-channel power supplies were used to condition the output of the flatpack gages. A Wheatstone bridge circuit (which includes the gage element) was contained in this unit, which provided completion and calibration resistors as well as bridge balancing functions. In addition, these units supplied a 100-V pulse, 1 msec long, to the Wheatstone bridge. The output of this unit was fed directly to the recorder using RG/58 coaxial cable.

2.3.4.3 Strain Gage Completion and Power Supply. The strain gages on the pressure bars were completed with two noninductive resistors attached close to the bar. The bridge was connected to the recorder and power supply in the shelter with a two-pair shielded strain gage cable. Power to the bridge was supplied by a laboratory-precision stable power supply.

2.3.4.4 Photodiodes. As the impulse plugs passed downward at an assumed constant velocity from the incident pressure pulse, their passage was detected by photodiodes at two locations. The output from the photodiodes was connected directly to the Nicolet digital oscilloscopes. Two photodiodes, placed 30 and 90 cm down from the top of the baseplate, were used to sense the time of arrival and departure of each plug.

2.3.4.5 Electronic Detonation Unit Zero Time. In all records obtained, the zero time fiducial correlated to 0 μ sec. The time of arrivals (TOAs) were measured from this point. This zero time was when the electronic detonation unit (EDU) was initiated. SwRI's computational zero time was the initiation at the top of the explosive and therefore does not include the time to bridge the detonator and booster charges or the short pulse duration between the EDU and detonator.

2.3.4.6 Data Acquisition and Reporting. The active data generated on this project was recorded from the signal conditioners on an eight-channel Tektronix digital data acquisition system and on Nicolet 4570 digital recording oscilloscopes. Polaroid photographs were taken of records on the Nicolet scopes and then transferred to floppy disks for further data reduction. A complete set of stress-time and impulse-time records from all ytterbium and pressure bar gages deemed reliable were recorded onto 360-kb floppy disks and submitted to the government.

Ambient temperature and pressure were recorded prior to each shot (Table 6).

2.4 Ballistic Pendulum. The third phase of this project was concerned with the empirical measurement of total impulse provided by bare military explosives at close-in distances and the contributions of two different thicknesses of steel casings around the bare charge to the total impulse. The nominal charge size shapes and masses used in these tests were the same as used in the baseplate experiments and the computational simulations. Testing was

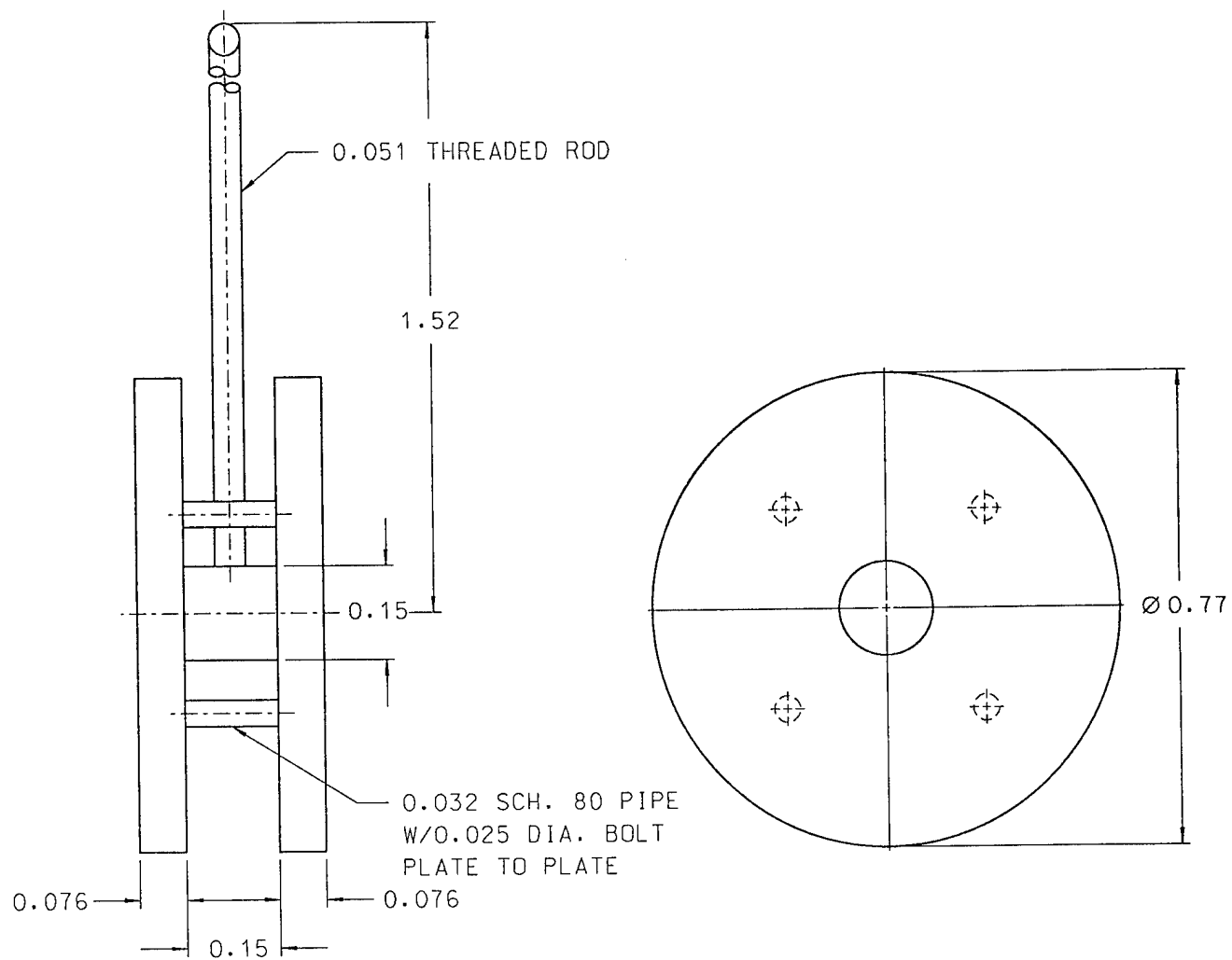
Table 6. Baseplate Shot Conditions

Charge Number	Date	Ambient Pressure (kPa)	Ambient Temp (K)
2A.1	08/16/90	104.48	300.9
2A.2	08/16/90	104.34	310.1
2A.3	08/23/90	103.77	296.5
2A.4	08/23/90	103.69	300.9
2A.5	09/12/90	104.35	296.5
2A.6	09/13/90	104.17	291.5
2A.7	09/13/90	103.98	302.0
2A.8	09/14/90	104.87	296.5
2A.9	07/11/91	100.97	304.7
2A.10	07/11/91	97.93	300.4
2A.11	07/10/91	101.14	309.8
2A.12	07/12/91	101.25	297.6

performed with the bare charges and with charges that were totally enclosed by two different thicknesses (6.35 and 9.53 mm) of steel casing.

The most convenient measuring device for obtaining total impulse is a ballistic pendulum. Such a device was designed and constructed for this project. It was desired to have the pendulum face correspond in size to the large pendulum at BRL's test range.

2.4.1 Design of Pendulum. The existing BRL pendulum has a loaded area of approximately 0.45 square meters; a circular face of this area would have a diameter of 0.75 m. The pendulum for our tests was designed on this basis. The pendulum head was constructed of two 0.77-m-diameter, 7.6-cm-thick steel plates (parts A and B) with a 15.0-cm clear spacing (Figures 14 and 15). The plates were held apart by a 15.0-cm length of 15.0-cm-diameter steel rod (part G) and four lengths of 3.2-cm Schedule 80 steel pipe (part C). This head was suspended on a 1.52-m length of 5.1-cm-diameter steel rod (part J).



Note: all dimensions in meters.

Figure 14. Ballistic Pendulum.

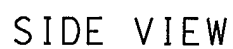


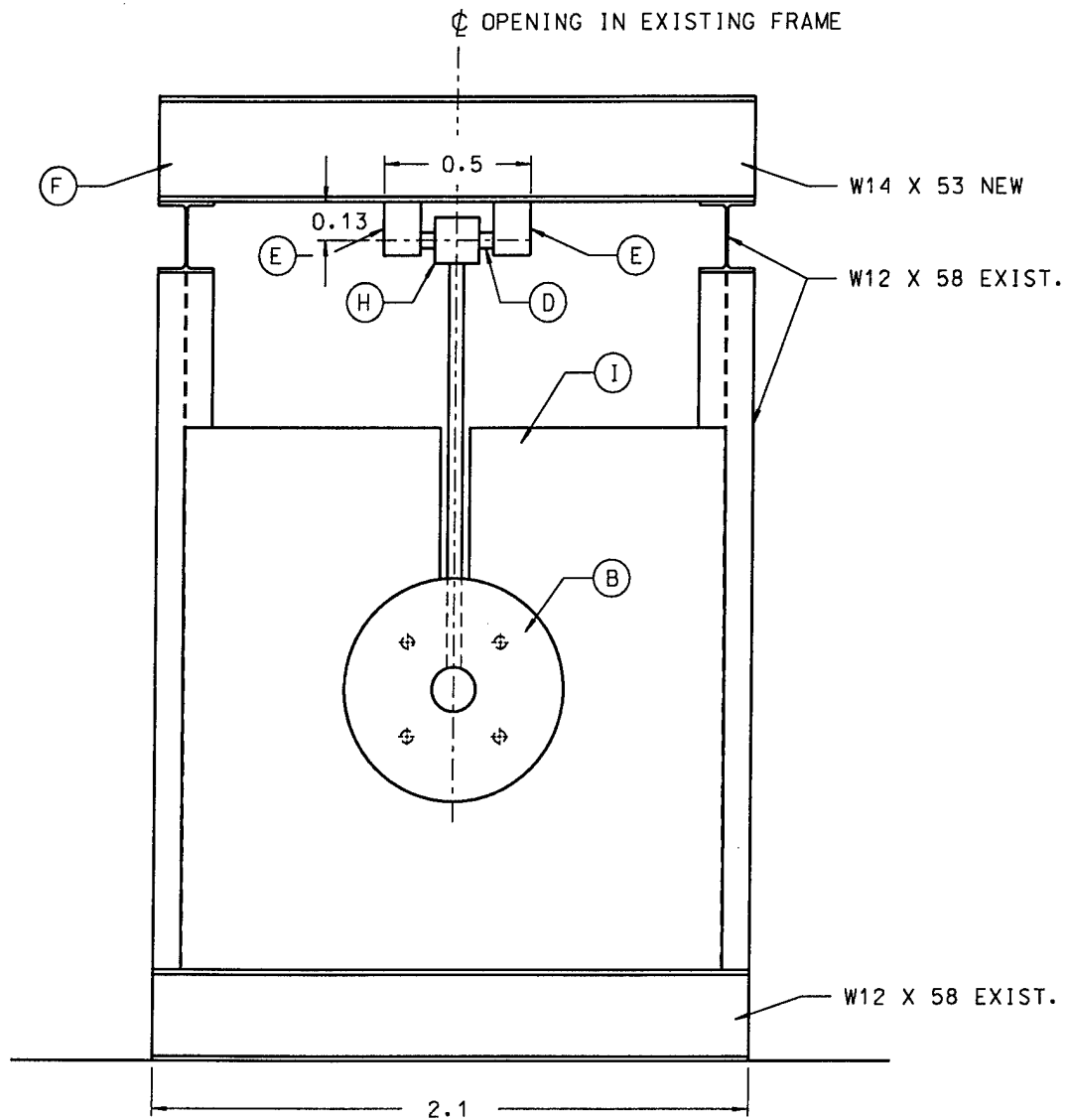
Figure 15. Side View of the Ballistic Pendulum Fixture.

After the initial test with cased charges, the front pendulum plate was machined to accept a 3.2-cm-diameter, 2.5-cm-thick sacrificial plate, which was replaced after each test. This plate was made of rolled homogeneous armor (RHA).

The pendulum was mounted into a large steel fixture (Figure 15) which suspended the centerpoint of the pendulum approximately 1.23 m off the ground. The pendulum was hung from a pivot assembly (Figure 16). A steel block (part H) was mounted into an axle (part D) and connected to the pendulum rod. The ends of the axle contained bearings to allow easy rotation of the pendulum assembly. The axle was hung from a top I-beam member by two axle supports (part E). Shown in Figures 16 and 17 is a large coverplate (part I) which was used on some of the tests to prevent the blast wave from encircling the pendulum face during a test. The coverplate measured 1.9 square meters, and was cut in a keyway manner to allow the pendulum face and rod to pass through as it swung. A fragment mat (Figure 17) was made of woven steel cable, 1.6 cm in diameter. The mats were suspended in a framework made of angle iron. The mats were designed to capture the fragments generated during a test with a cased charge, while allowing the blast wave to pass through relatively unimpeded. In this manner, reflected pressures on the pendulum face could be minimized. Figures 18 through 21 show the pendulum fixture and a closeup of the pivot axle.

2.4.2. Explosives. All of the explosive charges used with the ballistic pendulum were made of Comp B and were supplied by BRL from the same batch as those used in the baseplate experiments. The charges were 8.8 cm in diameter and 8.8 cm in length. The nominal explosive mass for each of the charges was 900 grams.

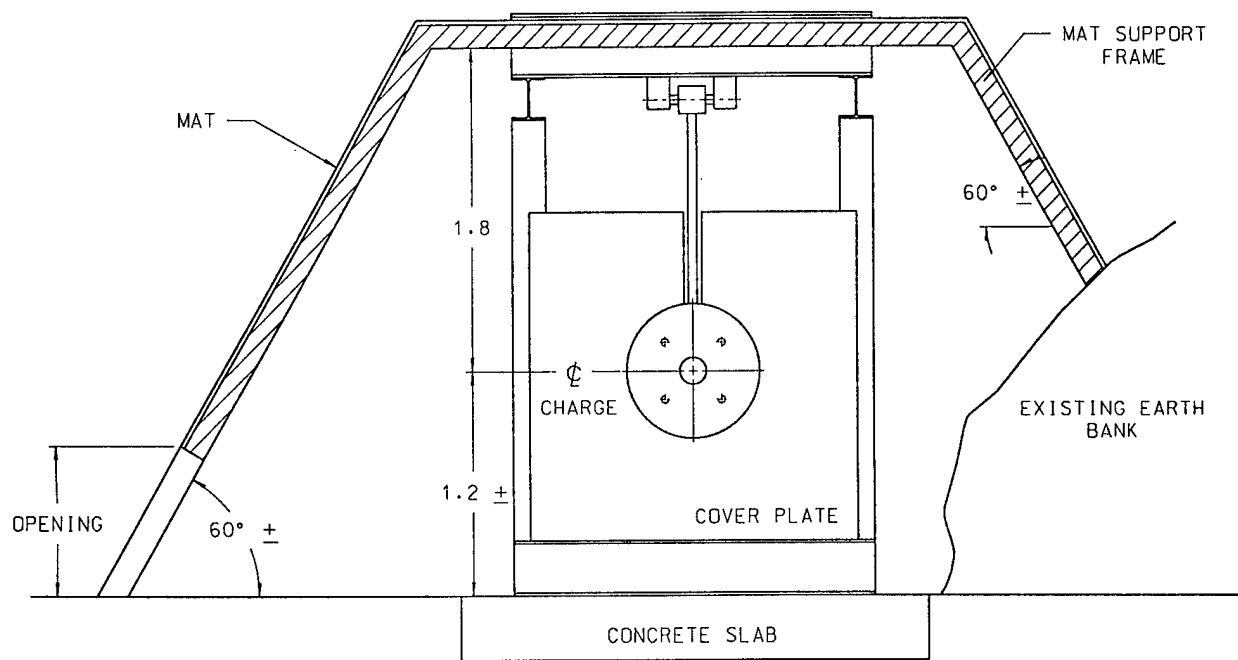
Charges were also supplied completely encased in steel. The casings were made of two pieces: a single cup-shaped piece and a circular top plate. They were formed by machining the cup piece from steel barstock to the proper dimensions. The explosive was poured into the cup and allowed to solidify. The top plates were bonded to the top of the assembly. The steel thickness was nominally 0.635 cm or 0.953 cm. These charges were exploded to determine the contribution that the casing material would add to the total impulse applied to the pendulum face. Figure 22 depicts the nominal dimensions of the charges. Table 7 shows the actual masses of all charges used in this test program.



FRONT VIEW

Note: all dimensions in meters.

Figure 16. Front View of Ballistic Pendulum.



FRONT OF PENDULUM

Note: all dimensions in meters.

Figure 17. View of Pendulum and Fragment Capture Matting.



Figure 18. Photograph of the Ballistic Pendulum Fixture, Showing the Coverplate.



Figure 19. Photograph of the Ballistic Pendulum Fixture, Showing the Rails Used to Interpret Pendulum Swing.

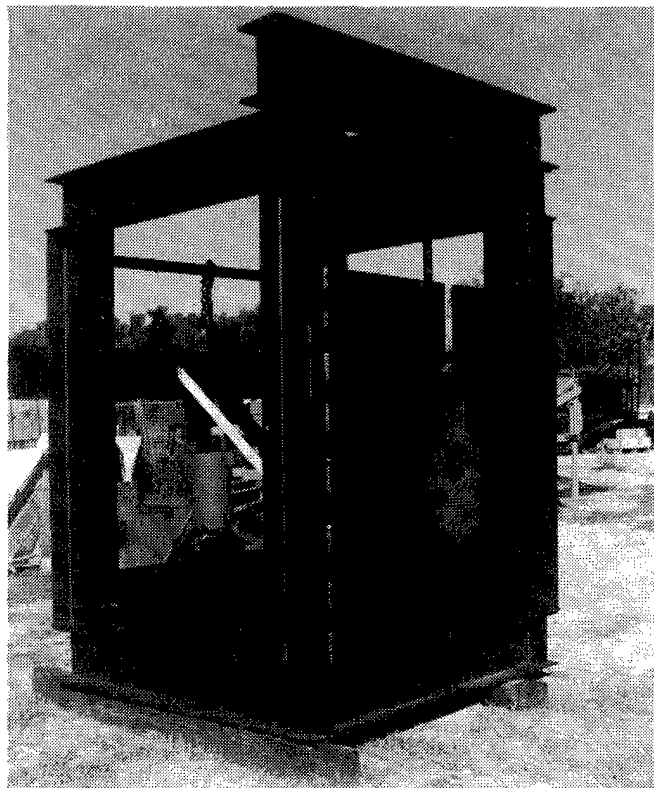


Figure 20. Photograph of the Ballistic Pendulum Fixture.

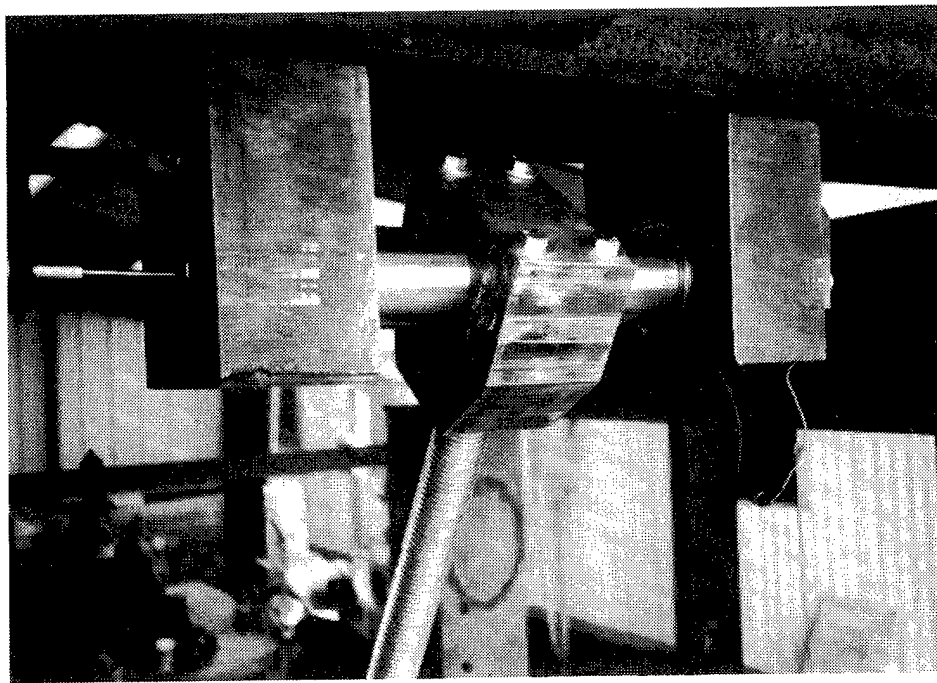


Figure 21. Closeup Photo of the Pendulum Pivot Axle.

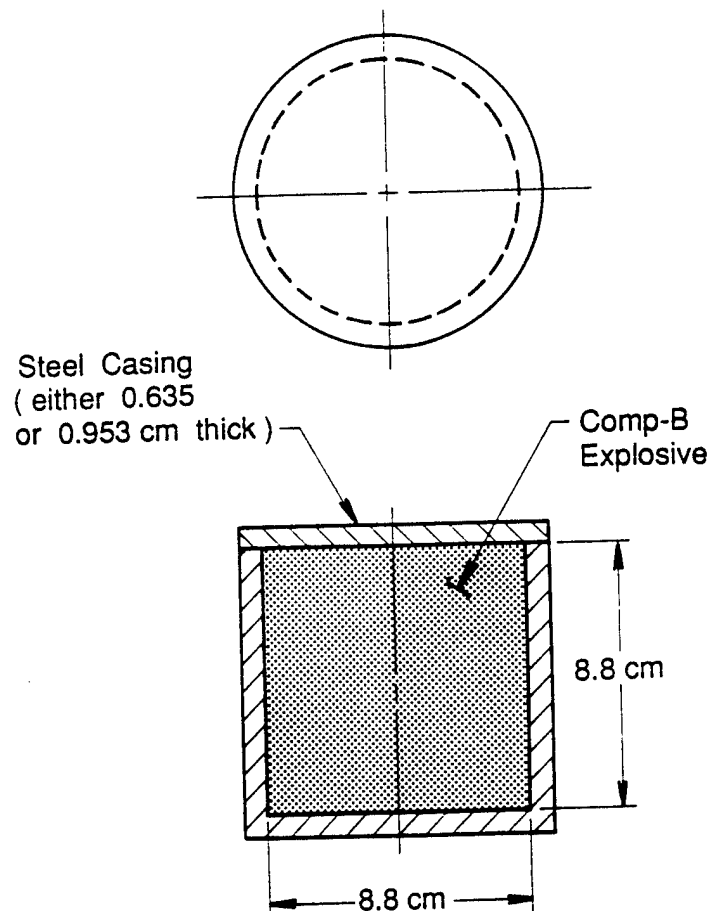


Figure 22. Explosive Configuration for Pendulum Tests.

The detonator used to initiate all the charges was a Reynolds Industries RP-80, placed within a small (4.0-g) booster charge hand-formed from C-4 explosive. The booster, cylindrical in shape, was bonded to the top center of the bare charges. For the cased charges, a hole 1.27 cm in diameter was drilled into the center of the top casing plate to accept the booster.

A holder device was designed to properly place the charge on the pendulum face. The charges were centered on the pendulum face with the bottom surface parallel to the plane of the face, and the axis of symmetry perpendicular and located such that the HOB was maintained within required tolerances. The precision holder allowed for placement within ± 1 -mm on centering and HOB. Additionally, the holder was unobtrusive so as to minimize its effect on the test. The holder was made of 5-cm-thick styrofoam, which provided adequate stiffness, but not significant mass or impedance to the charge. The holder was a 0.3-m-square styrofoam plate with a hole cut through the center equal to the charge diameter. Four legs were cut to the proper length to place the plate at the HOB for each charge. The legs were glued to the corners of the plate, making a table-like assembly. All dimensions were cut by a machine shop to ± 0.1 mm to stay within required placement tolerances. The holder was aligned with scribe lines on the pendulum face to center the charge. The holder was then taped securely to the face prior to blasting. Figure 23 shows the holder device in place on an early preliminary test. Figure 24 shows the holder device in place during real testing. Note the placement of the booster charge on Figure 16, and the damage done to the pendulum face by the cased charges.

2.4.3 Instrumentation and Data Acquisition. Several instrumentation types were considered to measure the swing of the pendulum, including radial variable displacement transducers (RVDT), contact pins, video, and high speed filming. It was decided that the most rugged and reliable readings could be obtained with RVDT gages, using the video or film as a backup.

Table 7. Ballistic Pendulum Explosive Charges

Test Number	Charge Number	Main Charge Mass (g)	Booster Explosive Mass (g)	Total Charge Mass (g)
2	(1) 11	905.5	4.0	905.5
3	(1) 12	905.4	"	905.4
4	(1) 13	898.0	"	898.0
5	(1) 15	897.0	"	897.0
6	(2) 5	910.0	"	2974.0
7	(2) 1	900.0	"	2883.0
8	(2) 6	908.0	"	2974.0
9	(2) 2	901.0	"	3064.0
10	(3) 2	901.0	"	4744.0
11	(3) 4	877.0	"	4858.0
12	(3) 6	907.0	"	4631.0
13	(3) 1	881.0	"	4835.0
14	(1) 16	897.5	"	897.5
15	(1) 14	898.3	"	898.3
16	(3) 5	879.0	"	4722.0
17	(3) 3	906.0	"	4404.0
18	(2) 4	901.0	"	2974.0
19	(2) 3	905.0	"	2974.0
Notes: 1. Lot number ABY90M0E1S017B 2. Lot number ABY90B0E1S017B 3. Lot number ABY90C0E1S017B				

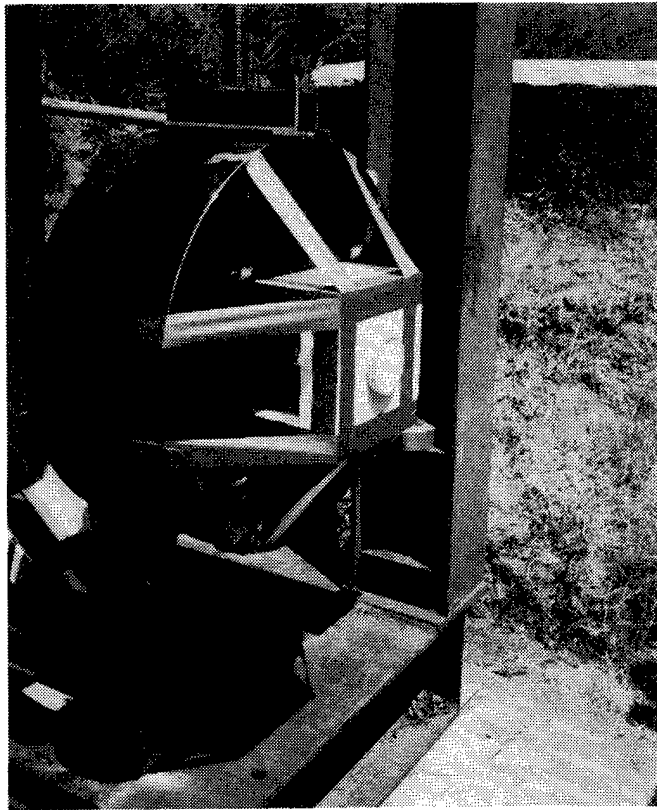


Figure 23. Explosive Charge Holder Device Without Coverplate.

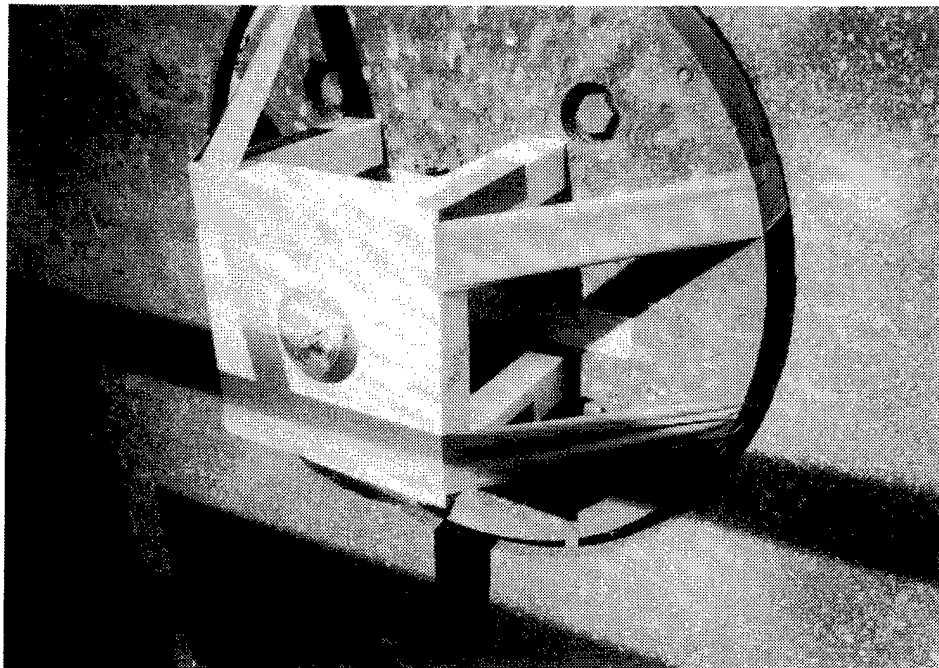


Figure 24. Charge Holder Device for a Test With the Coverplate.

A pair of RVDT gages was used to measure pendulum rotation and provide redundant readings. These gages were calibrated and installed on the fixture. They were directly connected on each end of the pendulum pivot axle (edge of Figure 21). At this point, the pendulum was swung by hand to check its operation and the recording of the gages. A set of rails was then installed below the swing arc of the pendulum for use in interpreting the amount of swing when the pendulum was filmed (Figures 19, 20, and 23). A steel bar was welded to the bottom of the back pendulum face and painted black. This bar (Figure 23) would slide between the white rails, providing a contrast for easier viewing on the film and video. The pendulum swing tests went well, and the gages performed well, so the fixture was moved to the site for the explosive testing.

The fixture was placed on a smooth, level concrete pad at the blast site. The fixture itself was leveled, then bolted to the concrete.

A videocamera was installed at the site to monitor pendulum motion. This system was used prior to the installation of the high-speed camera to evaluate the picture clarity (or lack thereof). With the videocamera in a permanent location, the rails below the pendulum were marked to indicate pendulum swing, in one-degree increments from 5 through 40 degrees. This was done by moving the pendulum by hand with a "come-along" and measuring angle with an inclinometer. The view from the camera was used to indicate placement of markings on the rail, thereby eliminating any parallax in the video image. The image provided by the video would provide a doublecheck for the output from the RVDT gages. Additionally, the calibration of each gage was checked during the marking of the rail.

The initial test on the system was performed with a 900-gm disk of C-4, approximately 8.7 cm in diameter and 8.7 cm long. This test was intended to evaluate the pendulum and gage performance. No damage was incurred by the pendulum, and both RVDTs performed well. The video image shows a flash and dust on the initial pendulum swing. In subsequent swings the pendulum can be observed because the dust settled sufficiently. Since the videocamera provided a high quality image of the pendulum swing, the use of the high-speed camera was not warranted.

2.4.4 Data Analysis. The following relationship describes the motion of the compound pendulum used in this research effort. Whereas a simple pendulum is one whose mass is considered to be concentrated in a particle and attached to a pivot point by a light "massless" string, all real pendulums, including the one used herein, are actually compound pendulums, whose mass is distributed throughout the pendulum body. The pendulum used for these experiments was close to a simple pendulum (the main mass was 1263 lbm, while the support rod was 78 lbm), but compound pendulum equations are used to be more exact.

Consider a pendulum swinging in a plane about a pivot point. An equation of motion results from the conservation of energy. Relative to the pivot point, the potential energy is:

$$U = M g L \cos\theta \quad (1)$$

where M = pendulum mass (kg)
 g = acceleration of gravity (m/s^2)
 L = distance from pivot to center of gravity (m)
 θ = swing angle (degrees)

and the rotational kinetic energy is:

$$T = 1/2 I (\dot{\theta})^2 \quad (2)$$

where I = mass moment of inertia about pivot (kg-m^2) and
 $\dot{\theta}$ = rotational velocity (rad/s).

The conservation of energy states that:

$$U + T = 1/2 I (\dot{\theta})^2 - M g L \cos\theta = E \quad (3)$$

where E = a constant. If we assume that the pendulum starts with C directly below O and with an angular velocity ω , then

$$E = 1/2 I \omega^2 - M g L \quad (4)$$

and plugging into equation 3 gives:

$$(\dot{\theta})^2 = \omega^2 - \frac{4 g L M}{I} \sin^2(\theta/2) \quad (5)$$

The maximum swing of the pendulum will occur when $\dot{\theta}$ goes to zero, which relates the maximum swing θ_{\max} to the initial angular velocity:

$$\sin^2\left(\frac{\theta_{\max}}{2}\right) = \frac{I \omega^2}{4 g L M} \quad (6)$$

The impulse can be calculated from knowledge of the initial angular velocity, the pendulum's mass moment of inertia, and the impulse-momentum relationship:

$$H = I \omega$$

where H = angular momentum ($\text{kg-m}^2/\text{s}$)

$$\mathfrak{L} = \Delta H = H_{\text{initial}} - H_{\text{final}} = H_{\text{initial}} \quad (7)$$

where \mathfrak{L} = angular impulse ($\text{kg m}^2/\text{s}$).

Using Equation 6 gives:

$$\mathfrak{L} = 2(g L M)^{1/2} \sin\left(\frac{\theta_{\max}}{2}\right) \quad (8)$$

The impulse of interest here is actually the linear impulse, which is equal to the angular impulse through the moment arm L :

$$\begin{aligned} J &= \mathfrak{L} / L \\ &= 2\left(\frac{g M}{L}\right)^{1/2} \sin\left(\frac{\theta_{\max}}{2}\right) \end{aligned} \quad (9)$$

where J = linear impulse (kg-m/s).

The pendulum's swing is measured, but its mass moment of inertia is usually calculated. The mass moment of inertia can be checked with knowledge of the pendulum's natural period. The period of the pendulum can be derived by solving the equation, which results from differentiation of Eq. 3:

$$I \ddot{\theta} + M g L \sin \theta = 0 \quad (10)$$

This equation is most typically solved by making the substitution $\sin \theta \approx \theta$ which leads to the solution

$$\theta = C_1 \cos\left(\frac{2\pi t}{T} + C_2\right) \quad (11)$$

where C_1 and C_2 are integration constants.

The pendulum has the natural period

$$T = 2\pi \sqrt{\frac{I}{M g L}} \quad (12)$$

The substitution of θ for $\sin \theta$ is strictly valid only for small swings of the pendulum. For example, at 30 degrees of rotation, θ equals 0.52 rad, while $\sin 30$ degrees equals 0.50 rad. Although this is not a large difference, a more exact solution was used for this data analysis.

However, solving Eq. (10) is much more difficult, and leads to the following relationship of natural period to swing angle:

$$T = 2\pi \sqrt{\frac{I}{M g L}} \left[1 + \frac{\theta^2}{16} + \frac{11 \theta^4}{3072} \right] \quad (13)$$

Eq. (13) accurately describes the period of swing of the pendulum for all of the maximum swing angles encountered in this project.

The validity of Eq. (13) was doublechecked through careful measurements of the swing period from several of the tests. Table 8 shows the period measured from the RVDT gage output, along with the corresponding swing angle. It can be seen that there is a slight increase in natural period as the swing angle increases, as Eq. (13) predicts. The values in Table 8 were used to determine the portion of Eq. (13) uncorrected for the swing angle—that is, that portion represented by Eq. (12).

Table 8. Ballistic Pendulum Period Calculations

Test Number	Peak Swing (degrees)	Experimentally Measured Period (sec)	Computed Period by Eq. (13) (sec)
4	16.8	2.536	2.540
2	17.9	2.546	2.541
3	18.0	2.544	2.542
15	20.1	2.544	2.545
14	20.6	2.544	2.547
6	25.2	2.554	2.557
8	25.2	2.556	2.557
12	29.8	2.578	2.569

This value, determined by averaging results, was found to be 2.526 sec, which corresponds to the natural period of the pendulum for small angle swings. The last column in Table 8 compares the natural period to the measured period computed using Eq. (13). It can be seen that Eq. (13) accurately represents the motion of the pendulum, especially considering that the period measurements were accurate only to ± 0.004 sec.

The moment of inertia originally calculated for the pendulum resulted in a natural period of 2.519 sec. This value is very close to the value determined from the experimental swing (2.526 sec). The calculated moment of inertia was increased by 0.5% to provide a calculated period equal to the experimentally determined value. Considering that several simplifying assumptions were used to calculate the moment of inertia, this increase is not unreasonable. Table 9 summarizes the pendulum properties used to calculate the total impulse provided by the explosive blast.

Table 9. Ballistic Pendulum Properties

I (mass moment of inertia about pivot)	=	1470.73 kg-m ²
M (pendulum mass)	=	608.4 kg
L (distance from pivot to center of gravity)	=	1.524 m

3. RESULTS

The results of computational and empirical measurements are presented in four sections: computational analysis of bare charge explosives; baseplate measurements of bare charge explosives; ballistic pendulum measurements of cased and bare charge explosives; and comparison of analytical and empirical measurements.

3.1 Computational Analysis of Bare Explosives. The following tables and figures display the results of the simulations described in paragraph 2.2. Tables 10 and 11 are for Comp B; Tables 12 and 13 are for Pentolite. Figures 25 through 28 display the peak pressure and specific impulse graphically. Specific impulse for each location resulted from integrating the pressure pulse for the duration of the positive phase. Results are given for selected points on the baseplate, as well as in the freefield at the HOB. It can be seen that pressure and impulse are slightly higher for Comp B than Pentolite. The figures also depict the rapid dropoff of both pressure and impulse as you move out from the centerline.

Table 10. Computational Data at Baseplate, Comp B at 20-cm HOB

Distance from Centerline (cm)	Peak Pressure (GPa)	Peak TOA (μ sec)	Specific Impulse (MPa-sec)
0	1.91	42	0.039
1	1.70	41	0.037
2	1.48	34	0.031
2.5	1.48	34	0.029
3	1.37	35	0.025
4	1.13	35	0.019
5	0.87	36	0.014
6	0.62	37	0.011
7	0.45	38	0.0083
10	0.18	46	0.0042
13	0.083	55	0.0024
16	0.045	66	0.0017
Total Impulse (to $r = 50$ cm and 400μ sec) = 1120 N-sec			
Freefield at HOB			
25	0.015	46	N/A
35	0.011	74	N/A
45	0.0081	101	N/A

Table 11. Computational Data at Baseplate, Comp B at 15-cm HOB

Distance from Centerline (cm)	Peak Pressure (GPa)	Peak TOA (μ sec)	Specific Impulse (MPa-sec)
0	3.04	31	0.056
1	3.00	32	0.052
2	2.65	32	0.045
2.5	2.41	31	0.041
3	1.95	31	0.035
4	1.26	28	0.025
5	0.71	28	0.017
6	0.49	29	0.012
7	0.29	31	0.0083
10	0.18	39	0.0041
13	0.068	47	0.0025
16	0.047	53	0.0017
Total Impulse (to $r = 50$ cm and 400 μ sec) = 1090 N-sec			
Freefield at HOB			
25	0.015	46	N/A
35	0.011	74	N/A
45	0.0081	101	N/A

Table 12. Computational Data at Baseplate, Pentolite at 20-cm HOB

Distance from Centerline (cm)	Peak Pressure (GPa)	Peak TOA (μ sec)	Specific Impulse (MPa-sec)
0	1.75	44	0.037
1	1.63	43	0.035
2	1.39	36	0.030
2.5	1.36	36	0.028
3	1.25	37	0.024
4	1.00	37	0.018
5	0.81	38	0.014
6	0.59	39	0.010
7	0.41	40	0.0079
10	0.17	49	0.0040
13	0.075	58	0.0023
16	0.048	69	0.0017
Total Impulse (to $r = 50$ cm and 400μ sec) = 1050 N-sec			
Freefield at HOB			
25	0.014	47	N/A
35	0.0098	76	N/A
45	0.0074	104	N/A

Table 13. Computational Data at Baseplate, Pentolite at 15-cm HOB

Distance from Centerline (cm)	Peak Pressure (GPa)	Peak TOA (μ sec)	Specific Impulse (MPa-sec)
0	2.78	34	0.053
1	2.77	34	0.050
2	2.56	33	0.043
2.5	2.32	33	0.040
3	1.87	33	0.034
4	1.19	30	0.023
5	0.65	30	0.016
6	0.44	31	0.011
7	0.27	32	0.0080
10	0.15	42	0.0039
13	0.077	44	0.0026
16	0.069	45	0.0018
Total Impulse (to $r = 50$ cm and 400 μ sec) = 1110 N-sec)			
Freefield at HOB			
25	0.014	47	N/A
35	0.0097	76	N/A
45	0.0075	104	N/A

Simulations of Comp-B at 15 and 20 cm Peak Pressure at Base Plate

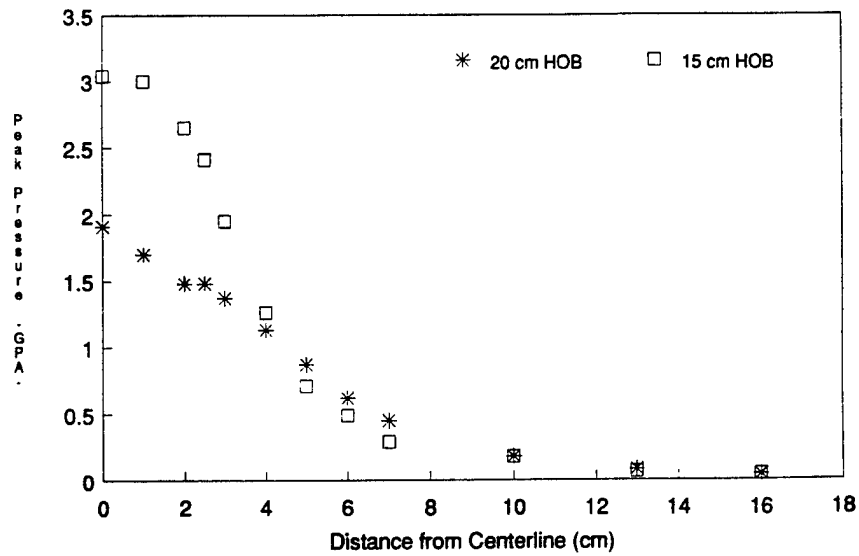


Figure 25. Peak Pressure vs. Location From Comp B Simulations at 15- and 20-cm HOB.

Simulations of Pentolite at 15 and 20 cm Peak Pressure at Base Plate

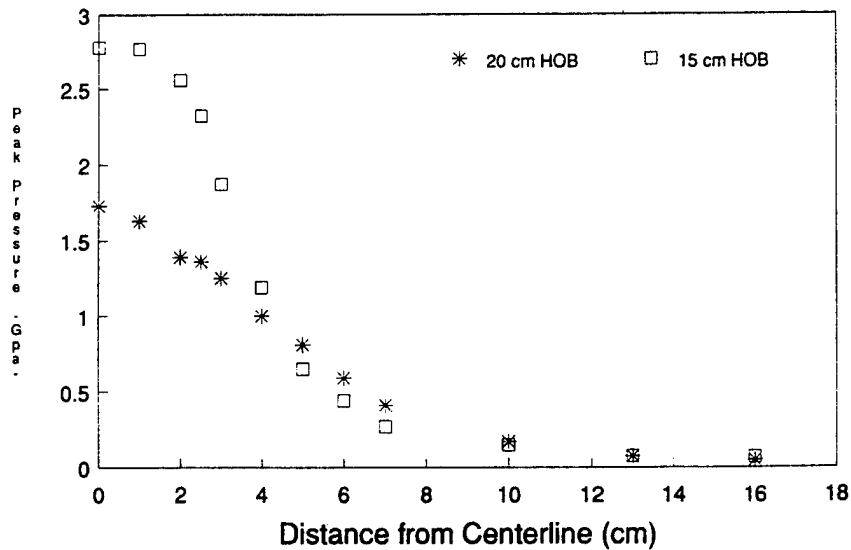


Figure 26. Peak Pressure vs. Location From Pentolite Simulations at 15- and 20-cm HOB.

Simulations of Comp-B at 15 and 20 cm Specific Impulse at Base Plate

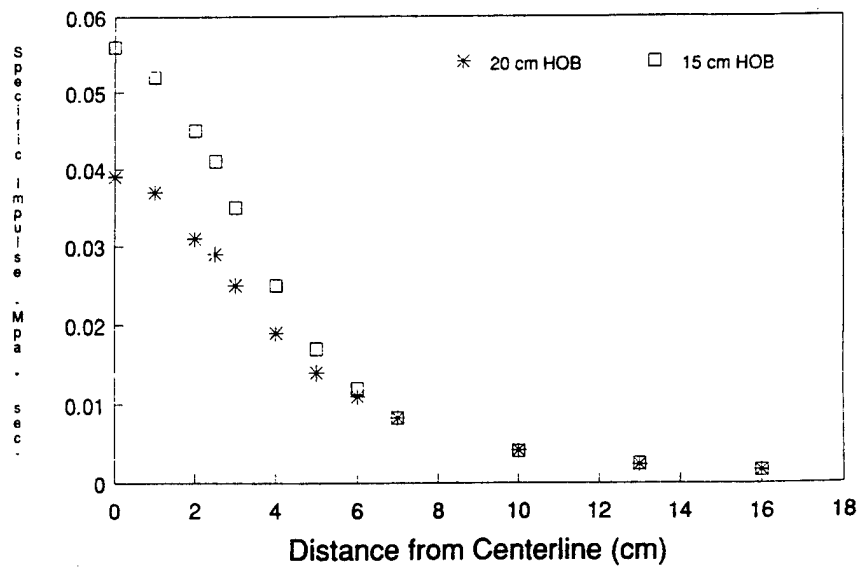


Figure 27. Specific Impulse vs. Location From Comp B Simulations at 15- and 20-cm HOB.

Simulations of Pentolite at 15 and 20 cm Specific Impulse at Base Plate

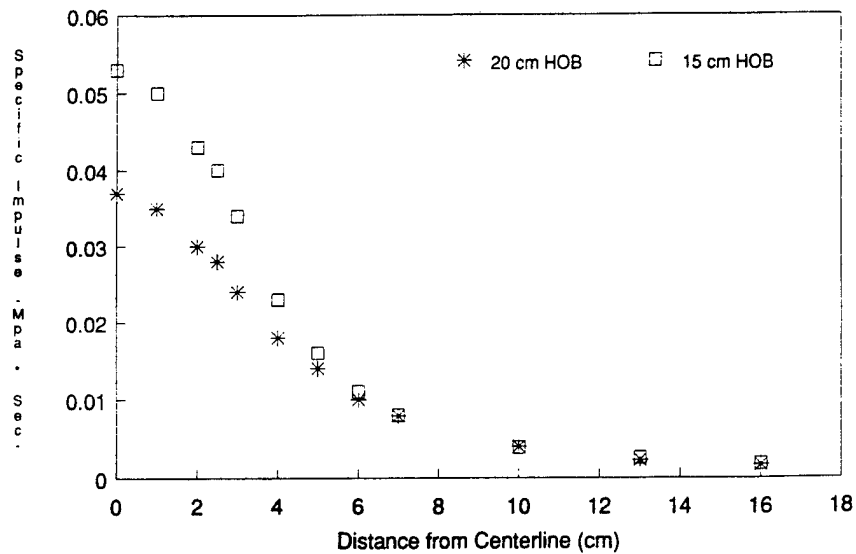


Figure 28. Specific Impulse vs. Location From Pentolite Simulations at 15- and 20-cm HOB.

The time of arrival (TOA) of the pressure peak indicates the planarity of the pressure wave on the baseplate. The zero time reference is the start of the detonation upon the top surface of the charge. The point on the centerline curiously shows a peak pressure at a time slightly later than adjacent points. Pressure and specific impulse increase on the baseplate as the HOB is reduced, but total impulse is nearly constant.

Figures 29 through 32 depict selected pressure-time traces from the computer simulations. A complete set of these traces appears in Appendix D.

3.2 Baseplate Measurements. The results of the baseplate measurements are presented in two parts: results of individual gage type and results by test configuration. Included in the discussion of individual gage types are: signal-to-noise (S/N) ratios; overall data return; and assumptions and problems encountered in the areas of design, fabrication, fielding and interpretation of results. The results of individual tests are grouped into four sections based on the four unique configurations tested. Data reduction procedures for all gage types are included in Appendix C.

3.2.1 Results of Individual Gage Types. The following sections describe the experimental results of all individual gage types. A complete set of stress and impulse records from ytterbium and pressure bar stress gages are contained in Appendixes A and B. The peak stress, TOA, specific impulse and duration of the piezoresistant gages are contained in Table 14. Table 15 contains the velocities and total specific impulse measured from the impulse plug gages.

Records obtained by the pressure transducers are judged by reproducibility (both within and between tests), S/N ratios, TOAs and usable duration.

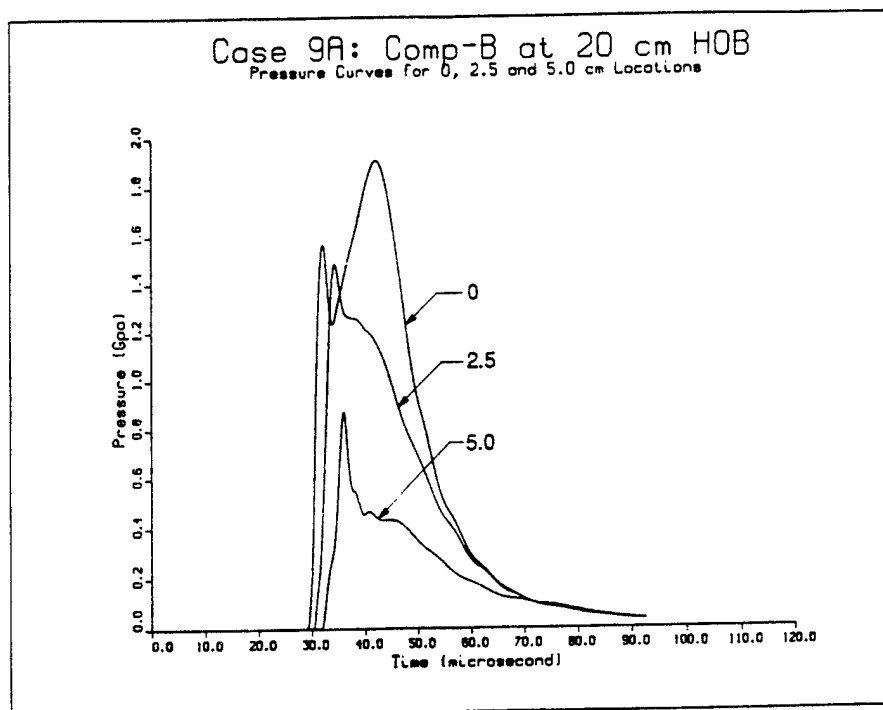


Figure 29. Pressure-Time Traces From Simulation of Comp B at 20-cm HOB.

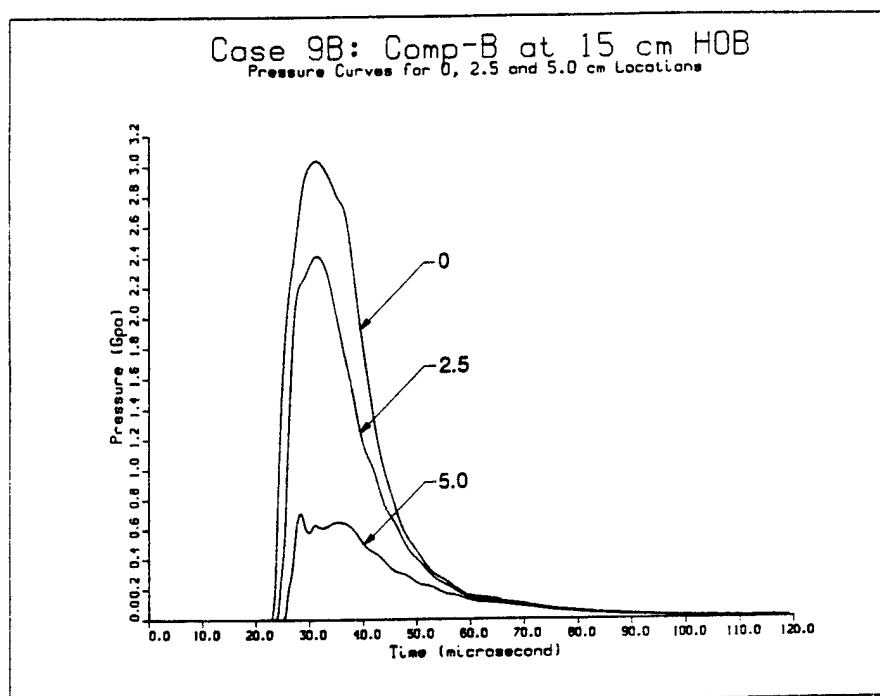


Figure 30. Pressure-Time Traces From Simulation of Comp B at 15-cm HOB.

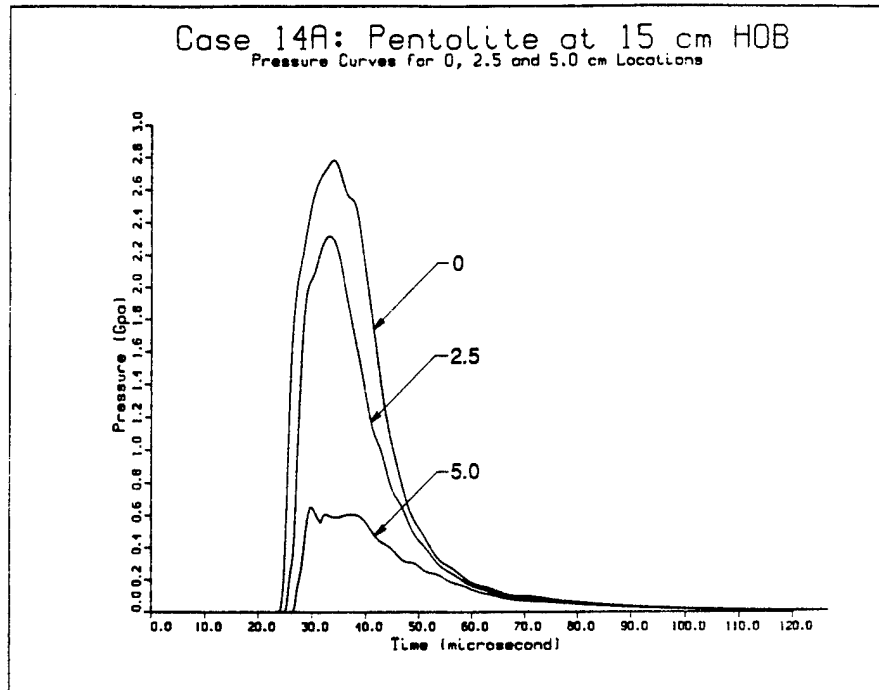


Figure 31. Pressure-Time Traces From Simulation of Pentolite at 15-cm HOB.

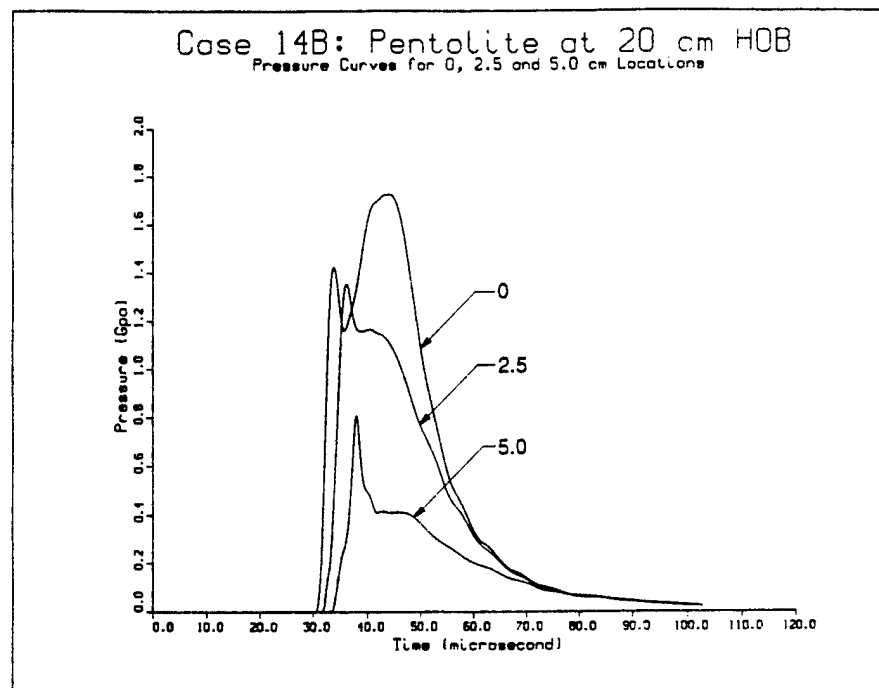


Figure 32. Pressure-Time Traces From Simulation of Pentolite at 20-cm HOB.

**Table 14. TOA, Peak Stress and Specific Impulse From Piezoresistant Gages,
Baseplate Tests 2A.1–2A.12**

Gage	TOA (μ sec)	Peak Stress (MPa)	Specific Impulse (MPa-sec)	Usable Duration (μ sec)	Comments
Test 2A.1					
Yb-1	33.76	1115	0.014	89	Complete record
Mn-2	–	–	–	0	Noisy
Yb-3	31.84	1520	0.028	89	Complete record
Mn-4	–	–	–	–	Low signal, noisy
Test 2A.2					
Yb-1	41.84	818	0.012	120	Complete record
Mn-2	40.10	–	–	–	Low signal, noisy
Yb-3	40.08	1082	0.024	72	Complete record
Mn-4	41.80	–	–	–	Low signal, noisy
Test 2A.3					
Yb-1	32.30	921	0.014	120	Complete record
Mn-2	30.70	–	–	–	Low signal, noisy
Yb-3	33.40	1542	0.031	120	Complete record
Mn-4	34.30	–	–	–	Low signal, noisy
Test 2A.4					
Yb-1	42.40	1215	0.014	83	Complete record
Mn-2	41.40	–	–	–	Low signal, noisy
Yb-3	41.97	940	0.020	108	Complete record
Mn-4	42.25	–	–	–	Low signal, noisy
Test 2A.5					
Yb-1	32.72	1060	0.013	52	No hysteresis
Yb-2	32.16	1732	0.030	158	Complete record
Yb-3	31.84	1704	0.030	–	Near complete
Yb-4	32.64	1136	0.013	62	Near complete
Yb-5	31.92	1500	0.035	58	Near complete

Table 14. TOA, Peak Stress and Specific Impulse From Piezoresistant Gages, Baseplate Tests 2A.1–2A.12 (continued)

Gage	TOA (μ sec)	Peak Stress (MPa)	Specific Impulse (MPa-sec)	Usable Duration (μ sec)	Comments
Test 2A.6					
Yb-1	42.32	1502	0.015	120	Complete, some noise
Yb-2	42.16	1235	0.024	120	Complete, some noise
Yb-3	42.16	1324	0.024	100	Complete, some noise
Yb-4	42.40	1671	0.015	100	Complete, some noise
Yb-5	39.97	none	–	0	Broke at arrival
Test 2A.7					
Yb-1	34.16	1057	0.015	40	No hysteresis
Yb-2	33.84	1455	0.027	90	Complete record
Yb-3	33.76	1562	0.030	120	Complete record
Yb-4	34.08	–	0.015	40	No hysteresis
Yb-5	32.30	–	0.036	40	
Test 2A.8					
Yb-1	42.88	1202	0.013	120	Complete record
Yb-2	40.88	1606	0.022	120	Complete, some noise
Yb-3	–	–	–	–	No record
Yb-4	40.88	1967	0.017	120	Complete, some noise
Yb-5	40.88	3641	–	100	Questionable
Test 2A.9					
Yb-1	33.08	–	–	54	Very noisy
Yb-2	33.26	–	0.31	54	Very noisy
Yb-3	34.48	–	–	0	Breaks on arrival
Yb-4	38.12	–	–	0	Breaks on arrival
Yb-5	34.12	–	0.014	90	Noisy after peak

Table 14. TOA, Peak Stress and Specific Impulse From Piezoresistant Gages, Baseplate Tests 2A.1–2A.12 (continued)

Gage	TOA (μ sec)	Peak Stress (MPa)	Specific Impulse (MPa-sec)	Usable Duration (μ sec)	Comments
Test 2A.10					
Yb-1	41.11	–	–	0	Breaks on peak
Yb-2	40.92	1159	0.023	120	Complete record
Yb-3	41.72	1271	0.023	120	Complete record
Yb-4	41.80	1032	0.014	120	Complete record
Yb-5	42.52	742	0.014	120	Complete record
Test 2A.11					
Yb-1	33.98	–	–	0	Breaks at peak
Yb-2	34.38	1638	0.024	120	Complete, some noise
Yb-3	34.14	1265	0.016	120	Complete
Yb-4	34.14	–	–	0	Breaks after arrival
Yb-5	33.05	803	0.016	80	Complete
Test 2A.12					
Yb-1	43.12	1108	0.010	40	Nearly complete
Yb-2	42.48	1312	0.019	60	Nearly complete
Yb-3	42.35	1156	0.021	120	Complete
Yb-4	43.12	1072	0.012	120	Complete
Yb-5	42.05	1080	0.027	120	Complete

Table 15. Impulse Plug Data, Tests 2A.1–2A.8

Gage No.	Test No.	Vel 1	Vel 2	Vel 3	Vel 4	Ave Vel	Impulse (MPa-sec)
		(ft/sec)					
Imp-8	2A.1	None	None	None	None	N/A	N/A
Imp-9	2A.1	None	None	None	None	N/A	N/A
Imp-8	2A.2	None	None	None	None	N/A	N/A
Imp-9	2A.2	None	None	None	None	N/A	N/A
Imp-8	2A.3	270	200	218	200	222	0.042
Imp-9	2A.3	97	50	66	59	68	0.013
Imp-8	2A.4	133	78	92	78	95	0.018
Imp-9	2A.4	50	35	37	33	39	0.007
Imp-8	2A.5	None	None	237	228	232	0.044
Imp-9	2A.5	91	57	70	62	70	0.013
Imp-8	2A.6	204	251	None	None	227	0.043
Imp-9	2A.6	70	47	55	47	55	0.011
Imp-8	2A.7	234	228	228	179	217	0.041
Imp-9	2A.7	None	None	71	58	65	0.012
Imp-8	2A.8	None	None	None	None	N/A	N/A
Imp-9	2A.8	60	43	48	40	48	0.009

3.2.1.1 Ytterbium Gages. Ytterbium elements had the highest rate of return and the highest quality of all gages. Fifty-four standard ytterbium elements were fielded and 46 returned very high quality data—that is, reproducible peak stresses, high S/N ratios, consistent TOAs and long durations. Four gages had good S/N ratios but failed prior to complete unloading; two elements failed at shock arrival.

Due to the complexity of the stress histories, comparison plots were not generated. Instead, it is left to the reader to compare stress-time records by using the plots found in Appendix A.

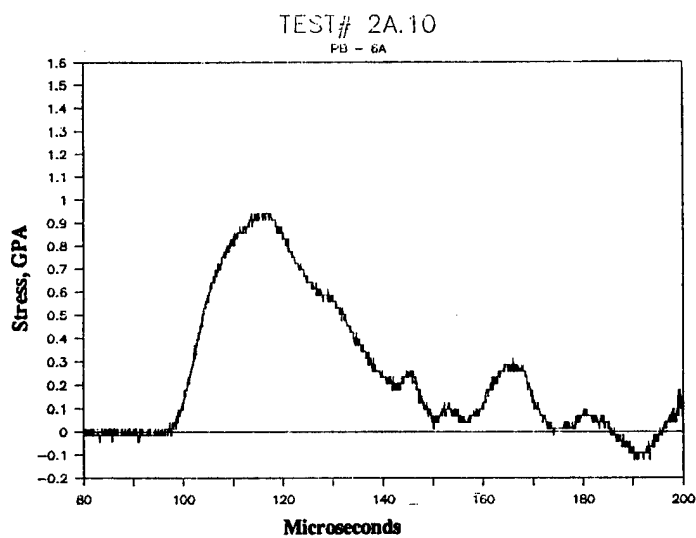
Impulse histories are generated by integrating the stress-time histories. A complete set of impulse histories obtained from ytterbium gages is included in Appendix A; comparison plots of selected impulse histories are contained in paragraph 3.3.

An assessment of the quality of the gage records can be completed by comparing records within and between tests. For each unique test configuration, five ytterbium elements were fielded at both the 2.5- and 5.0-cm locations. By comparing the records obtained from gages at the same range from ground zero (GZ), it is apparent that the records faithfully reproduce each other. In addition, records from different ranges and/or different test configurations produce distinct waveforms, demonstrating that the signals received are being produced by explosive products, not by spurious electrical signals.

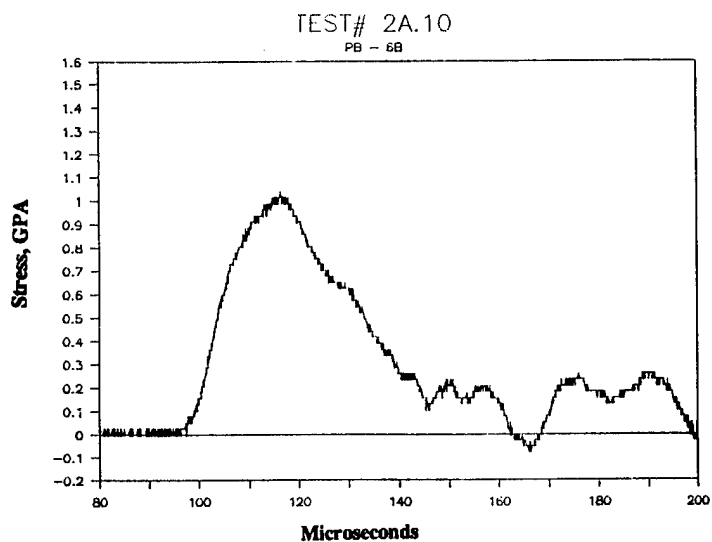
3.2.1.2 Manganin Gages. The initial four tests employed the use of both manganin and ytterbium elements because the range of expected peak pressures did not clearly define the use of one or the other. In these first four tests, manganin elements returned very low quality data: low S/N ratios, large variations in peak pressures and inconsistent waveshape. Based on these results, ytterbium was selected for all piezoresistant gage locations for the remaining eight tests. TOA, peak stress and durations from the manganin elements are summarized in Table 14. Selected manganin traces are included in Appendix A.

3.2.1.3 Pressure Bar Gages. Records obtained from bar gages generally had fair to good S/N ratios and long durations but had long risetimes and therefore did not produce the complex waveforms made by the ytterbium gages. The records were inconsistent in their reproducibility, partially due to the fact that, due to space constraints, only one bar gage could be fielded at each range from GZ.

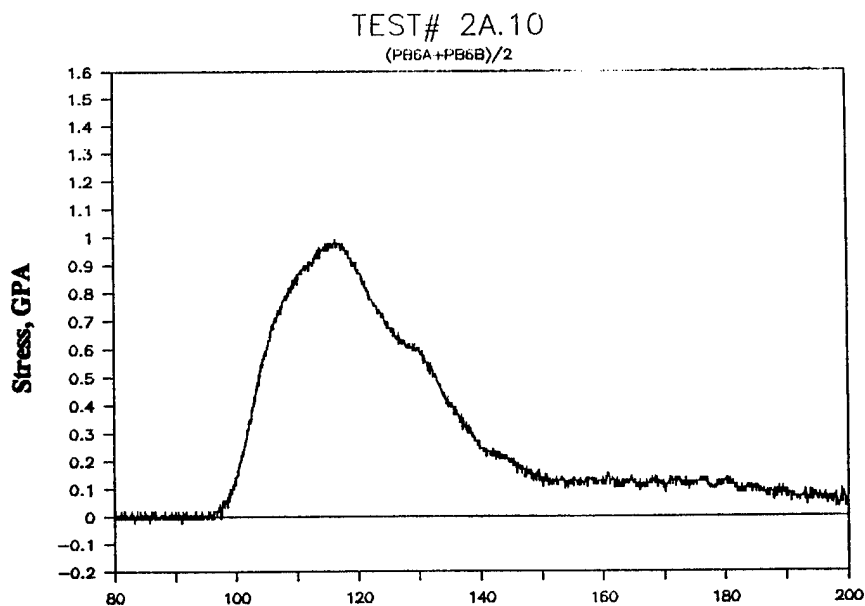
Strain signals generated by a bending mode in the bar were compensated by using two symmetrically located strain elements. Where both strain elements from a single bar were cleanly recorded, the records were combined. The voltages produced by each strain element for each time step were added together and the sum divided by two. As shown in Figure 33, the combination effectively cancels the effects of a bending mode strain signal.



a. Single Strain Record



b. Single Strain Record



c. Combined Strain Record

Figure 33. Individual and Combined Stress-Time Records From Two Pressure Bar Strain Elements.

3.2.1.4 Impulse Plug Gages. The data from the impulse plug gages for tests 2A.1 through 2A.8 are summarized in Table 15. The apparatus was damaged on test 2A.9 and not repaired for tests 2A.9 - 2A.12. Arrival and departure times were read directly from a Nicolet oscilloscope and the velocity computed and recorded in Table 15. It is possible to get four velocities from each setup and these velocities are averaged and a specific impulse computed from that average velocity. This single number may be compared with that derived from the pressure bars and stress gages.

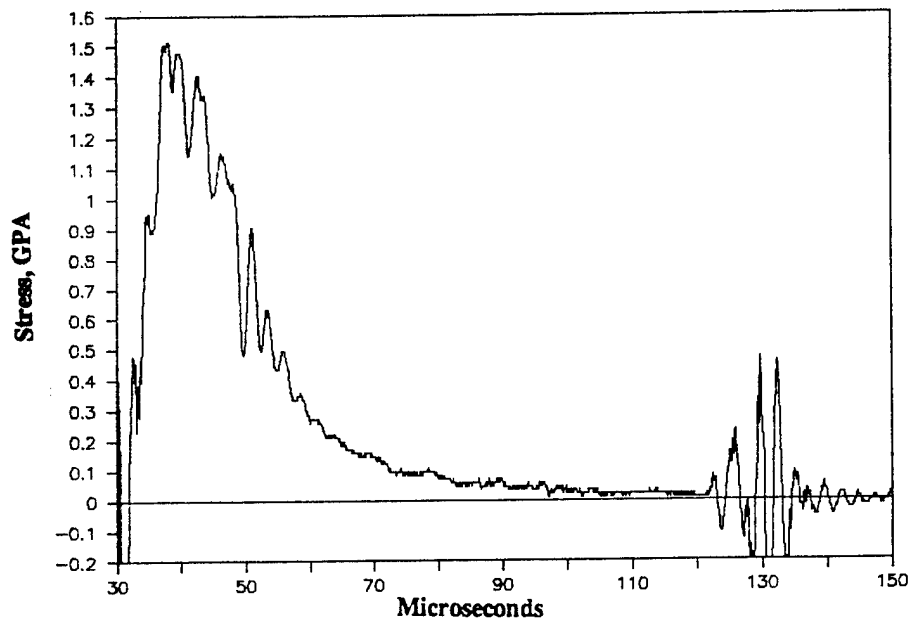
3.2.1.5 Airblast Gages. No data was obtained from the airblast gages. Both gages were destroyed on test 2A.1 due to the close proximity of the baffleplates and support hardware to the explosive. These gages demonstrated the difficulty involved in designing a gage system delicate enough to measure pressures, yet robust enough to survive the event.

3.2.2 Baseplate Tests, Comp B at 15-cm HOB. Three tests (2A.1, 2A.5 and 2A.9) were performed using Comp B explosive at 15-cm HOB. High quality, reproducible data were obtained at the 2.5- and 5.0-cm gage locations. Limited data were obtained at the 0.0-cm location.

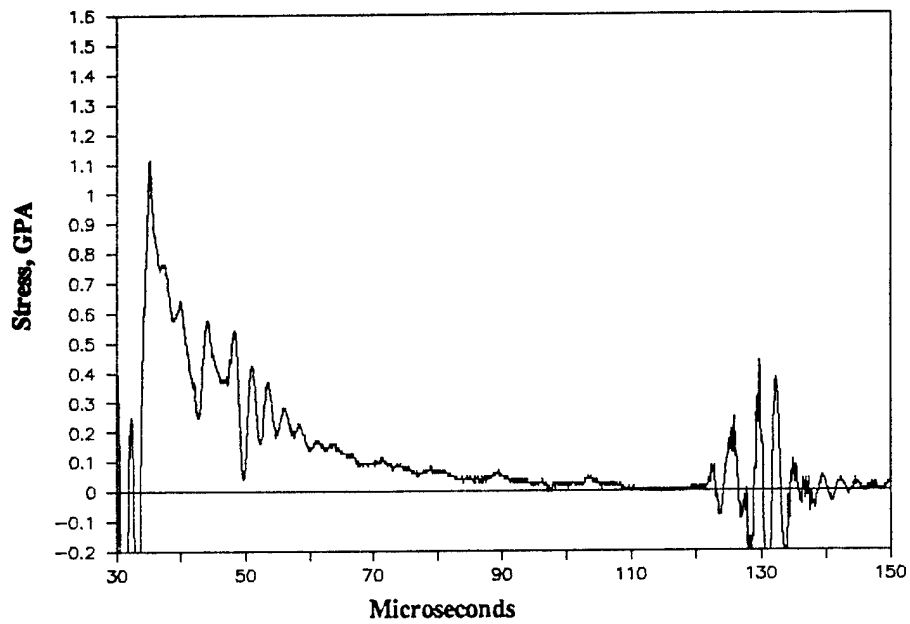
Ytterblum. While gages located at the same range produced nearly identical waveforms, records from ytterbium elements located at different ranges showed distinct differences in both peak pressure and waveshape. Stress histories from gage Yb-3, Test 2A.1, and gage Yb-1, Test 2A.1 were selected as representative results from the 2.5-cm and 5.0-cm ranges, respectively (Figure 34).

2.5-cm Range. At 2.5 cm from GZ, three stress-time records (Yb-2 and 3, test 2A.5 and Yb-3, test 2A.1) were deemed reliable. All three had reproducible peak stresses and waveshapes. Record Yb-3 from test 2A.5 showed an anomalous spike about 60 μ sec after TOA. This feature was not seen on any other records and is not believed to be a pressure pulse.

5.0-cm Range. At 5.0 cm from GZ, three stress-time records (Yb-1 and 4, test 2A.5 and Yb-1, test 2A.1) were deemed reliable. All had high S/N ratios and reproducible peak stresses and waveshapes.



a. 2.5-cm Range From GZ



b. 5.0-cm Range From GZ

Figure 34. Representative Stress-Time Records From Comp B Tests at 15-cm HOB.

0.0-cm Range. One record (Yb-5, test 2A.5) had a moderate S/N ratio and reasonable waveshape. The peak stress (1.5 GPa) recorded by this gage was equivalent to stresses measured at the 2.5-cm location, but had a more symmetric shape and therefore a greater specific impulse. A second record at this location had a low S/N ratio and was deemed unreliable. Because of the lack of symmetry and the intense environment, records from gages at the 0.0-cm location were difficult to assess.

Glycerol Ytterbium Gages. On test 2A.9, two ytterbium elements (Yb-3 and 4) were suspended in glycerol and fielded 2.5 and 5.0 cm from GZ. These elements failed at shock arrival due to load failure and returned TOA data only.

Analysis. In the initial 20-30 μ sec, records from the 2.5-cm range showed numerous, narrow pulses ranging from 0.9 to 1.9 GPa. At 5.0 cm from GZ, however, the first pressure spike observed was the peak stress, which ranged from 1.0 to 1.3 GPa. In addition, the pressures observed in the overall waveshape were considerably lower than at the 2.5-cm location. The records further indicated that the pressures at both locations had equilibrated approximately 50 μ sec after TOA.

The reproducibility of the gage records can also be seen when specific impulse histories are compared (Figures 35 and 36). Gages located at the same range yielded very similar records while records from different ranges yielded differences both in waveform and total specific impulse. Total specific impulses measured from the 2.5-cm locations roughly doubled those measured at the 5.0-cm location.

Pressure Bars. Four stress-time records were obtained from pressure bar gages: three from the 5.0- and one from the 2.5-cm locations. The records were deemed unreliable due to low S/N ratios and inconsistent peak stresses or TOAs.

Impulse Plugs. Total specific impulse measurements were obtained from tests 2A.1 and 2A.5 (Table 15). The specific impulse measured was higher than that measured by the ytterbium elements.

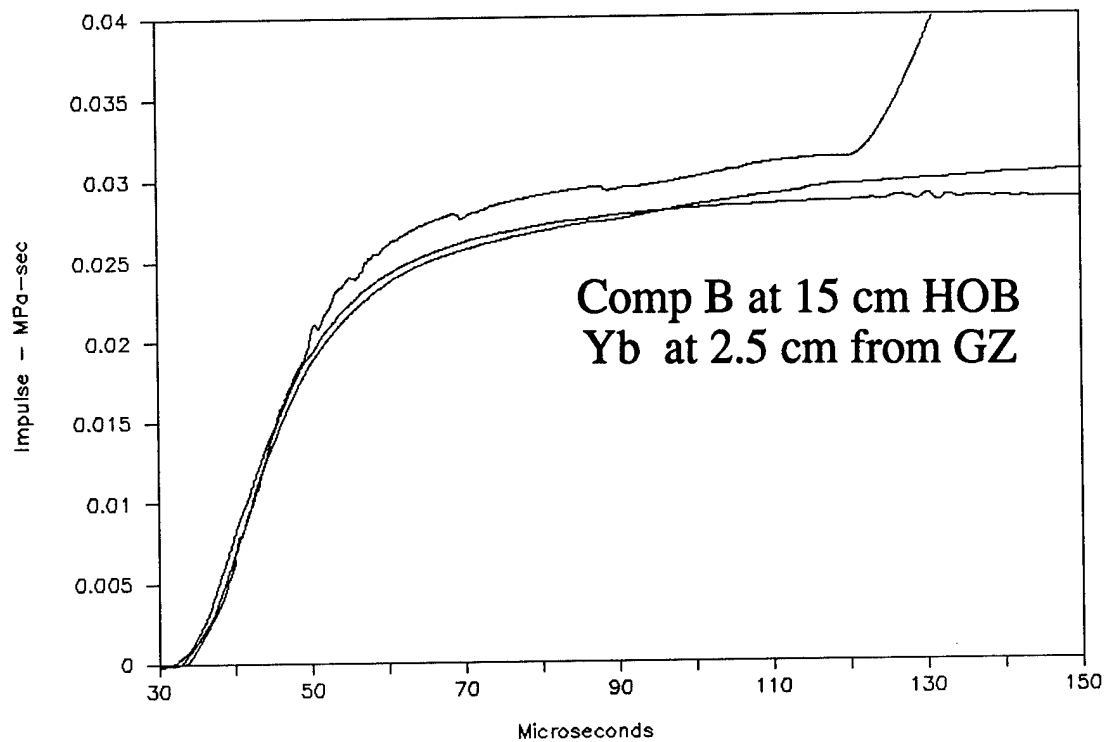


Figure 35. Impulse-Time Records, Comp B at 15-cm HOB, Ytterbium, 2.5-cm Range.

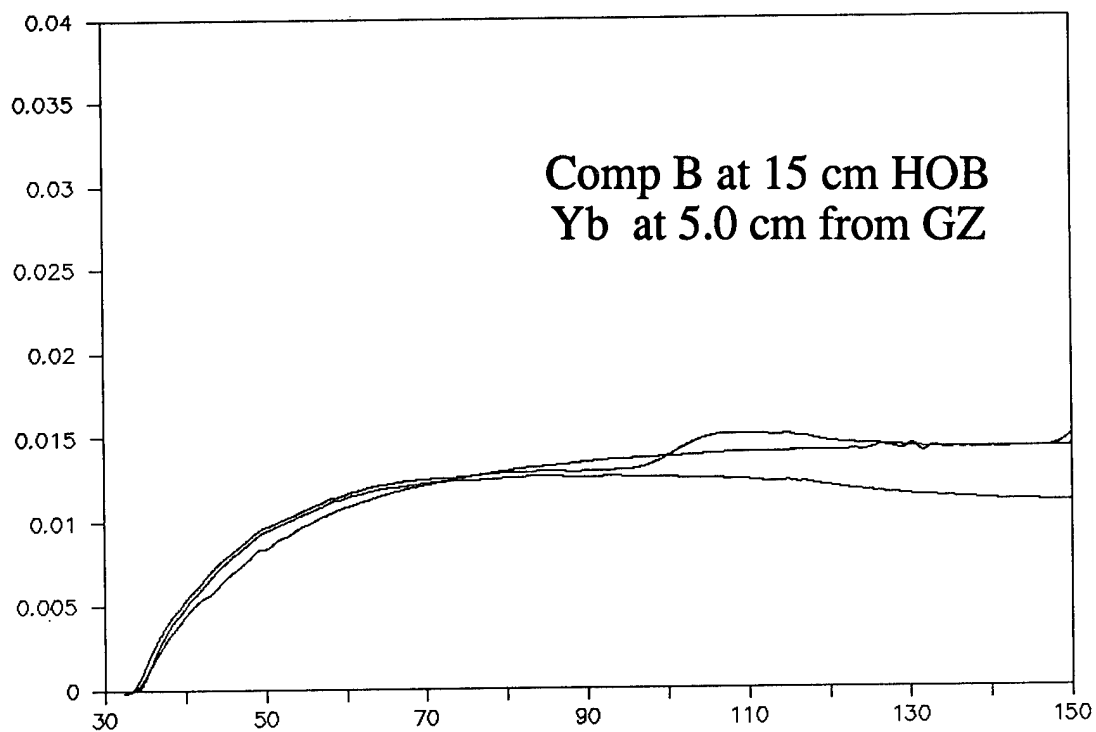


Figure 36. Impulse-Time Records, Comp B at 15-cm HOB, Ytterbium, 5.0-cm Range.

3.2.3 Baseplate Tests, Comp B at 20-cm HOB. Three tests (2A.2, 2A.6 and 2A.10) were performed using Comp B explosive at 20-cm HOB. High quality, reproducible data were obtained at the 2.5- and 5.0-cm ranges and limited data were obtained at GZ.

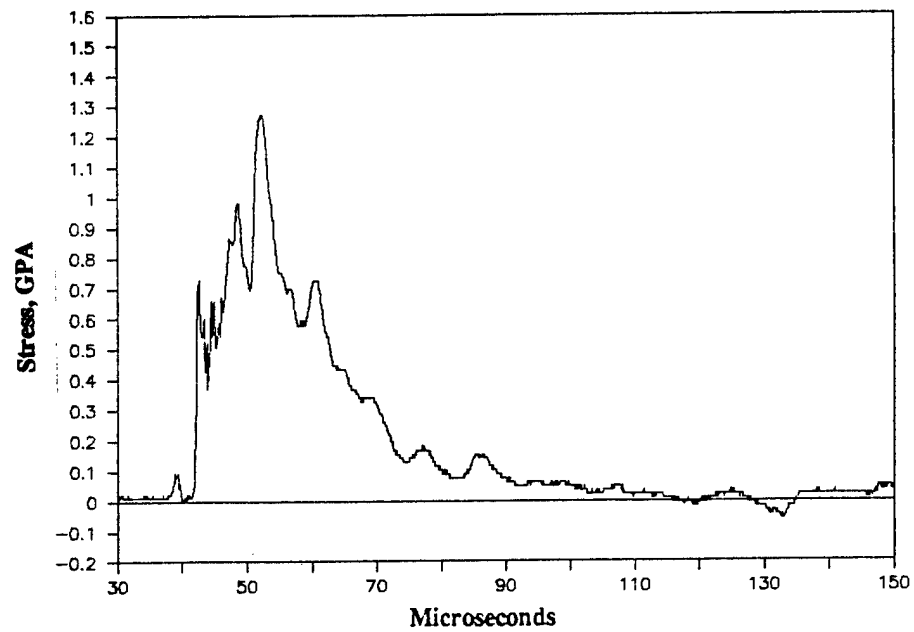
Ytterbium. Again, gages at the same range from GZ produced near identical waveforms; gages from different ranges produced records with distinct shapes. Comparison of records from ytterbium elements from the Comp B tests showed the same general trends in peak pressure and waveshape. As expected, measured peak pressures and total specific impulse were lower at 20-cm HOB than at 15-cm HOB. Stress histories from gage Yb-3, Test 2A.10 and Yb-4, Test 2A.10 were selected as representative results from the 2.5 cm and 5.0 cm ranges, respectively (Figure 37). The specific impulse for the 2.5-cm range is shown in Figure 38, and that for the 5.0-cm range is shown in Figure 39.

2.5-cm Range. All five ytterbium elements fielded at the 2.5-cm range returned usable data. Two records (Yb-2 and 3, test 2A.10) had very high S/N ratios and were very reproducible. The other three records had somewhat lower S/N ratios but very similar peak pressures and overall waveshape.

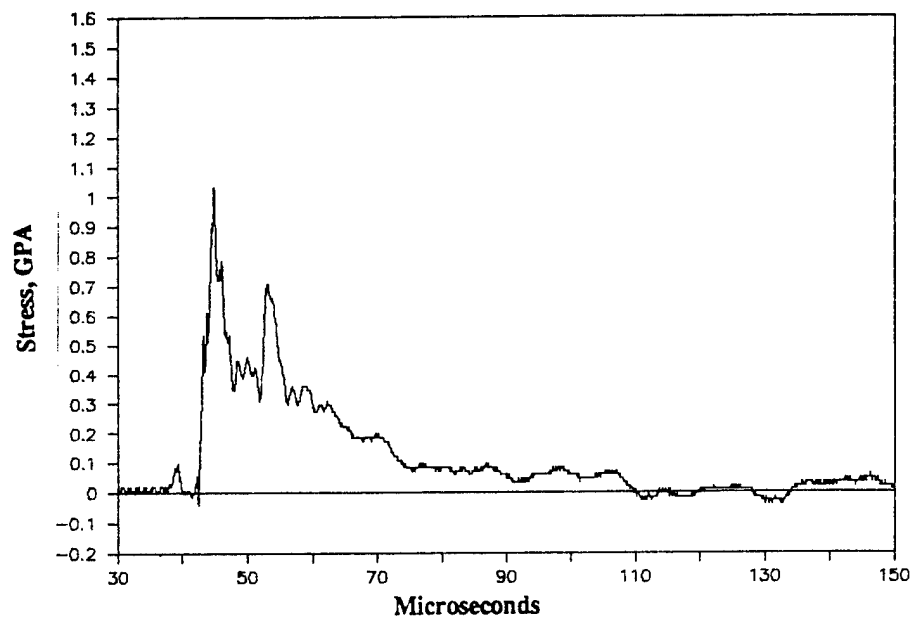
5.0-cm Range. Four records were obtained at the 5.0-cm range: one with a very high S/N ratio (Yb-4, test 2A.10) one with a moderate S/N ratio (Yb-1, test 2A.2), and two with somewhat low S/N ratios (Yb-1 and 4, test 2A.6).

0.0-cm Range. One record (Yb-5, test 2A.5) with an excellent S/N ratio was obtained from the gages fielded at 0.0-cm range. This record is somewhat perplexing in that the stresses observed are considerably lower than records from the 2.5- and 5.0-cm locations. Again, the lack of symmetry precluded a direct comparison with one from the same test and made evaluation difficult.

Analysis. The stress-time records from gages located at the 2.5-cm range displayed numerous stress pulses ranging from 0.7 to 1.3 GPa during the initial 20-30 μ sec. At the 5.0-cm location, however, the first pressure spike observed is the peak stress, ranging from 0.9 to 1.05 GPa on the "clean" records. The pressures observed in the overall waveshape are considerably lower than at the 2.5-cm location until about 40 μ sec after TOA, at which time the records converge.



a. 2.5-cm Range from GZ



b. 5.0-cm Range from GZ

Figure 37. Representative Stress-Time Records, Comp B at 20-cm HOB.

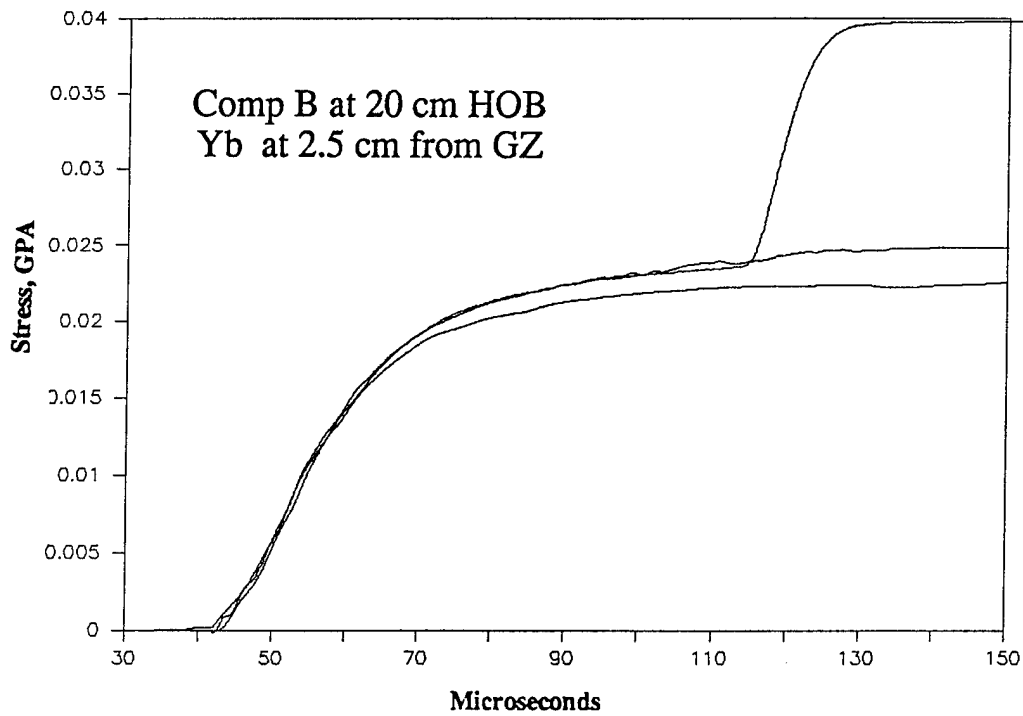


Figure 38. Impulse-Time Records, Comp B at 20-cm HOB, Ytterbium, 2.5-cm Range.

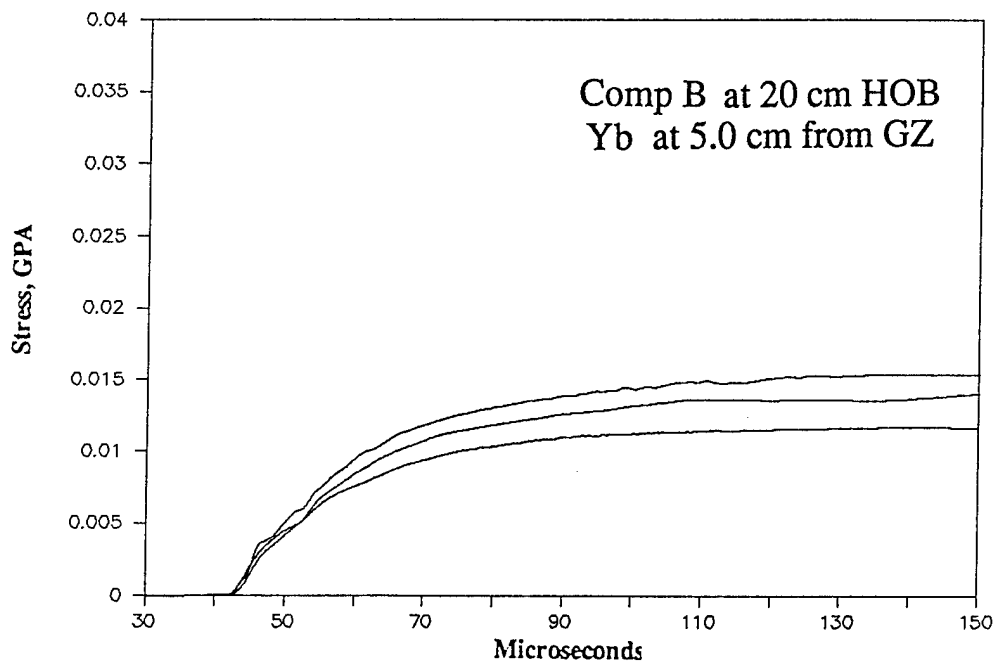


Figure 39. Impulse-Time Records, Comp B at 20-cm HOB, Ytterbium, 5.0-cm Range.

Specific impulse histories from the ytterbium gages were plotted together in Figures 38 and 39. The records from the 2.5-cm range were slightly lower than the specific impulses measured at the same range using Comp B at 15-cm HOB. At the 5.0-cm range, however, the specific impulses measured from the two HOBs did not show distinct differences.

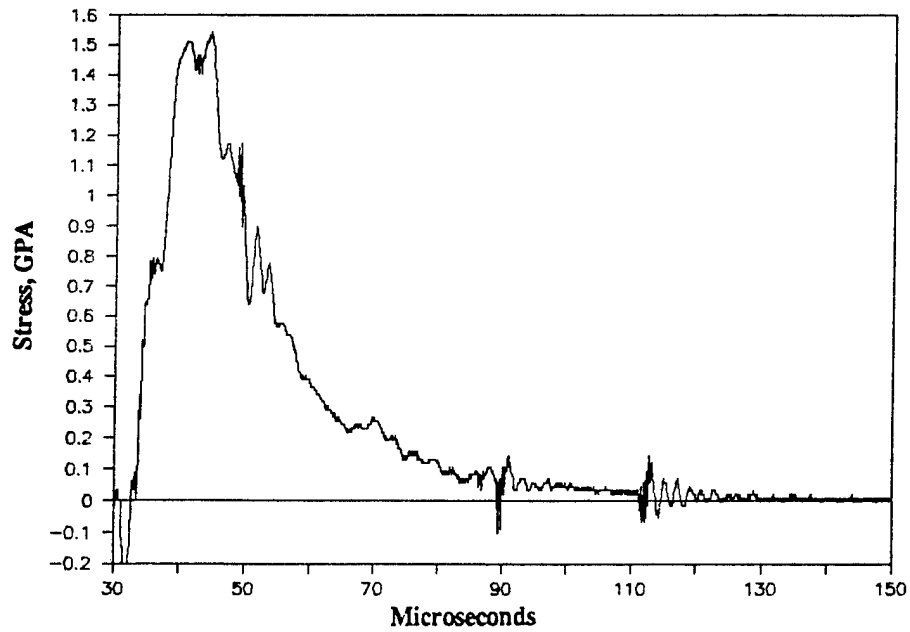
Pressure Bars. Five stress-time records were obtained from pressure bar gages: three from the 5.0- and two from the 2.5-cm locations. One record (Pb-6, test 2A.10) had an excellent S/N ratio and long duration; the remaining records had low S/N ratios and inconsistent peak stresses or TOAs and were deemed unreliable. In addition, the one clean record did not return to zero stress and, because of the long risetime, did not produce a detailed stress history. Little useful data appeared to have been gained from these gages.

Impulse Plugs. Total specific impulse was measured for tests 2A.2 and 2A.6 and is listed in Table 15.

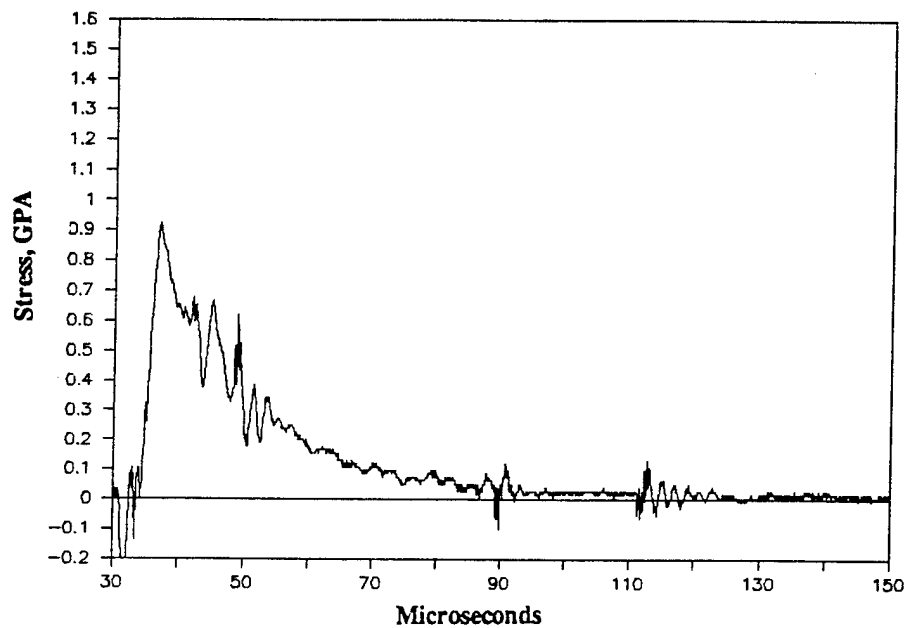
3.2.4 Baseplate Tests, Pentolite at 15-cm HOB. Three tests (2A.3, 2A.7 and 2A.11) were performed using Pentolite at 15-cm HOB. High quality, reproducible data was obtained at the 2.5- and 5.0-cm ranges and limited data were obtained at GZ.

Ytterbium. Comparison of stress-time records with those obtained from the Comp B experiments at the same HOB show similar waveshapes, peak pressures and TOAs. As with the records from the Comp B tests, ytterbium elements at the same range from GZ produced near identical waveforms; stress-time records from gages at different ranges from GZ showed distinct differences in both peak pressure and waveshape. Stress histories from gage Yb-3, Test 2A .3 and gage Yb-4, Test 2A.3 were selected as representative results from the 2.5-cm and 5.0-cm ranges, respectively (Figure 40).

2.5-cm Range. Three reliable records were obtained from ytterbium at the 2.5-cm range (Yb-2 and 3, test 2A.7 and Yb-3, test 2A.3). One record (Yb-2, test 2A.11) displayed large spurious signals attributed to electrical noise and was deemed unreliable. The two records from the same test were nearly identical and showed the familiar multiple peak waveshape seen with Comp B. The record obtained from test 2A.3 had multiple peaks as well, but the peaks were slightly higher and more sustained.



a. 2.5-cm Range From GZ



b. 5.0-cm Range From GZ

Figure 40. Representative Stress-Time Records, Pentolite at 15-cm HOB.

5.0-cm Range. At the 5.0-cm location, three gages produced reportable data. One record (Yb-1, test 2A.3) had a high S/N ratio and long duration while two records (Yb-1 and 4, test 2A.7) stopped reporting about 40 μ sec after TOA. Because of the overall high quality of the data, records that terminated early still provided some information on the peak pressures and early waveshape. These records closely reproduced the long duration record.

0.0-cm Range. Two records were obtained from the 0.0-cm range. One record (Yb-5, test 2A.7) broke after about 40 μ sec, but showed a wave structure similar to the Comp B test at 15-cm HOB. The second record (Yb-5, 2A.11) appeared to have an adequate S/N ratio and long duration but displayed an unusually low waveshape both in peak pressure and profile.

Analysis. The records obtained from these tests closely resembled the results from tests of Comp B at 15-cm HOB. Nearly identical stress-time waveforms were seen when comparisons were made within the 2.5- and 5.0-cm ranges. The differences seen when compared between ranges were consistent with earlier results.

Specific impulse histories from all ytterbium records are plotted together in Figures 41 and 42. Comparing these data with Figures 35 and 36, it appeared that the specific impulse from the Pentolite was delivered slightly sooner than from the Comp B but that Comp B delivered a few percent more total specific impulse.

Pressure Bars. Four stress-time records were obtained from pressure bar gages: two each from the 2.5- and 5.0-cm locations. Again, the records had low S/N ratios, inconsistent peak stresses or TOAs, did not return to zero stress and were deemed unreliable.

Impulse Plugs. Total specific impulse was measured for tests 2A.3 and 2A.7 and is listed in Table 15.

3.2.5 Baseplate Tests, Pentolite at 20-cm HOB. Three tests (2A.4, 2A.8 and 2A.12) were performed using Pentolite explosive at 20-cm HOB. High quality, reproducible data were obtained from ytterbium gages at all three distinct gage locations.

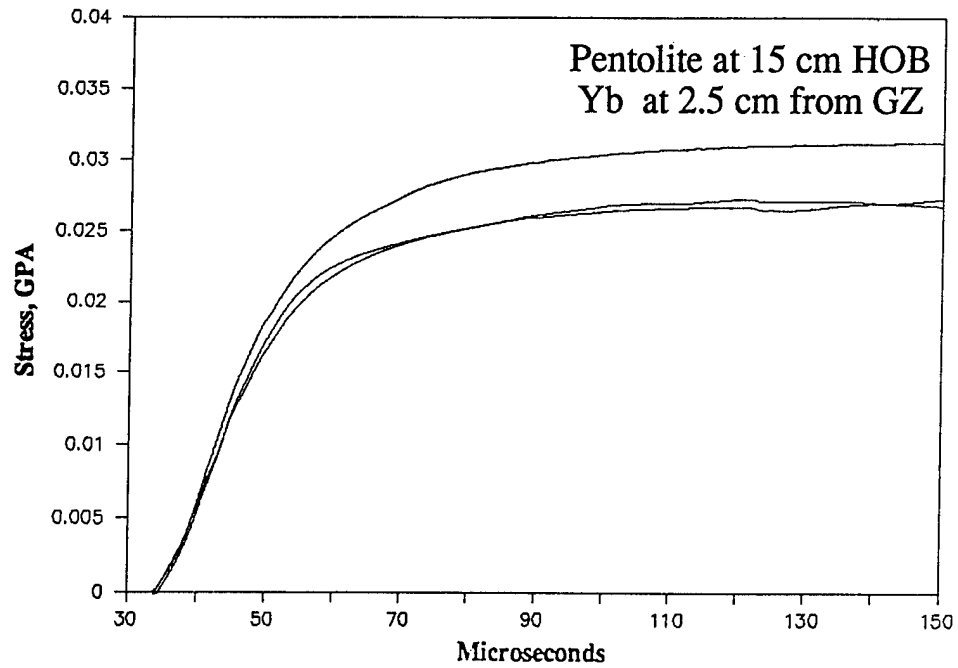


Figure 41. Impulse-Time Records, Pentolite at 15-cm HOB, Ytterbium, 2.5-cm Range.

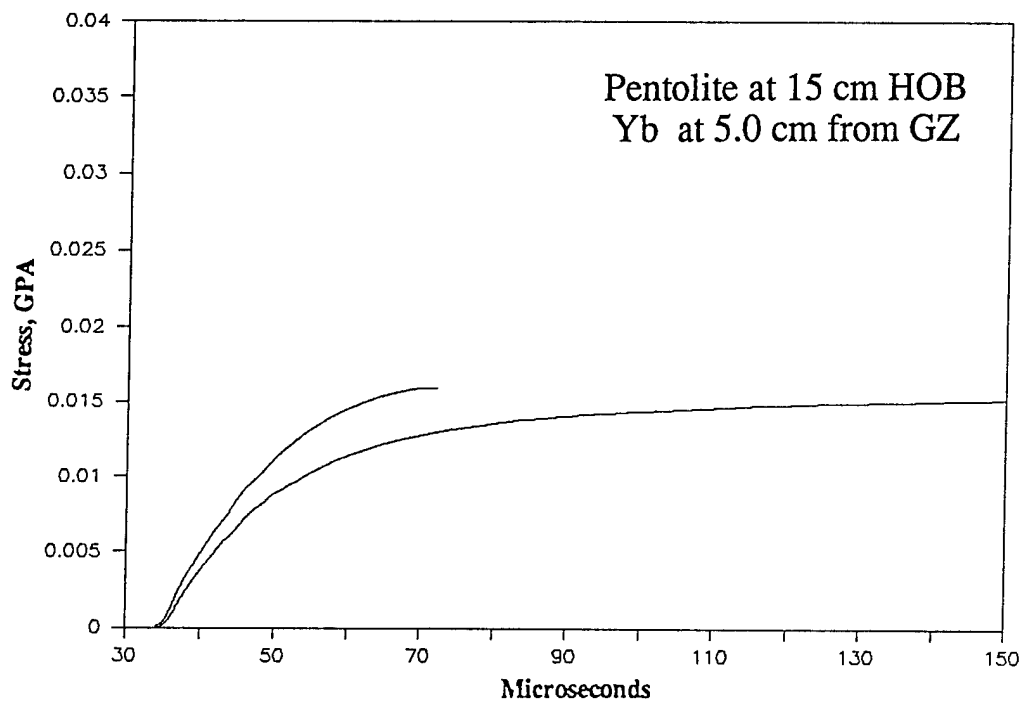


Figure 42. Impulse-Time Records, Pentolite at 15-cm HOB, Ytterbium, 5.0-cm Range.

Ytterbium. As with the previous tests, gages at the same range from GZ produced near identical waveforms. Comparison of records from ytterbium elements with the Comp B and Pentolite tests at 15-cm HOB showed the same general trends in peak pressure and waveshape: multiple peaks at 2.5 cm and single peaks at 5.0 cm. As expected, measured peak pressures and total specific impulses were lower at 20-cm HOB than at 15-cm HOB. Stress histories from gage Yb-3, Test 2A.4, and gage Yb-1, Test 2A.4, were selected as representative results from the 2.5-cm and 5.0-cm ranges, respectively (Figure 43).

2.5-cm Range. At 2.5 cm from GZ, four records returned reportable data: three (Yb-2 and 3, test 2A.12 and Yb-3, test 2A.4) had excellent early S/N ratios, while one (Yb-2, test 2A.8) produced some early noise spikes.

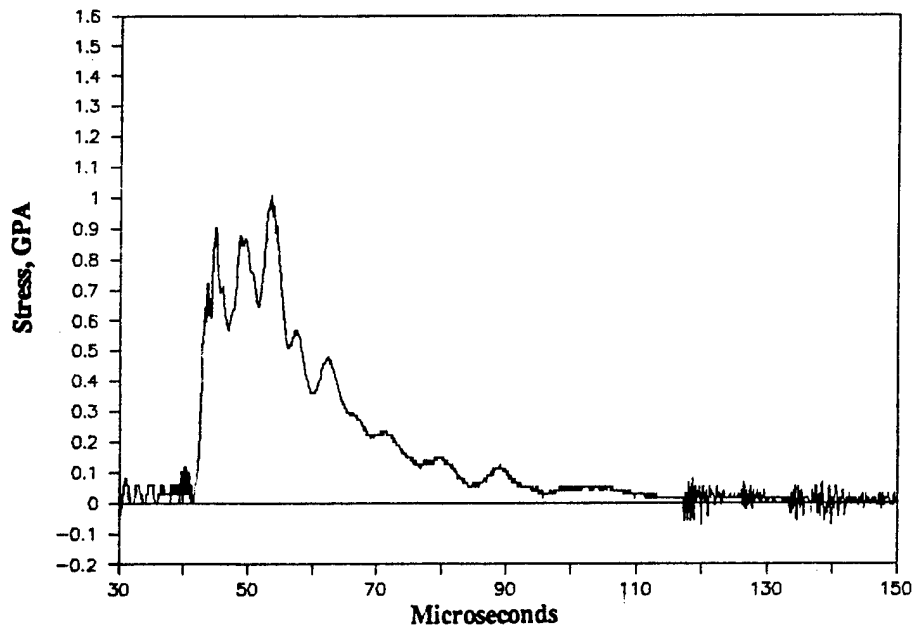
5.0-cm range. All five ytterbium elements fielded at 5.0 cm from GZ returned reportable data. Three (Yb-1, tests 2A.4, 2A.8 and 2A.12) had excellent S/N ratios and long durations; one (Yb-4, test 2A.12) had an excellent S/N ratio but stopped reporting about 40 μ sec after TOA; and one (Yb-4, test 2A.8) had a fair S/N (showing apparent noise spikes in the first 40 μ sec) and a long duration.

0.0-cm Range. A single stress-time record (Yb-5, test 2A.12) was obtained at this range. This record had a good S/N ratio and a long duration. The peak stresses measured were slightly lower than those measured at the 2.5-cm range from similar tests.

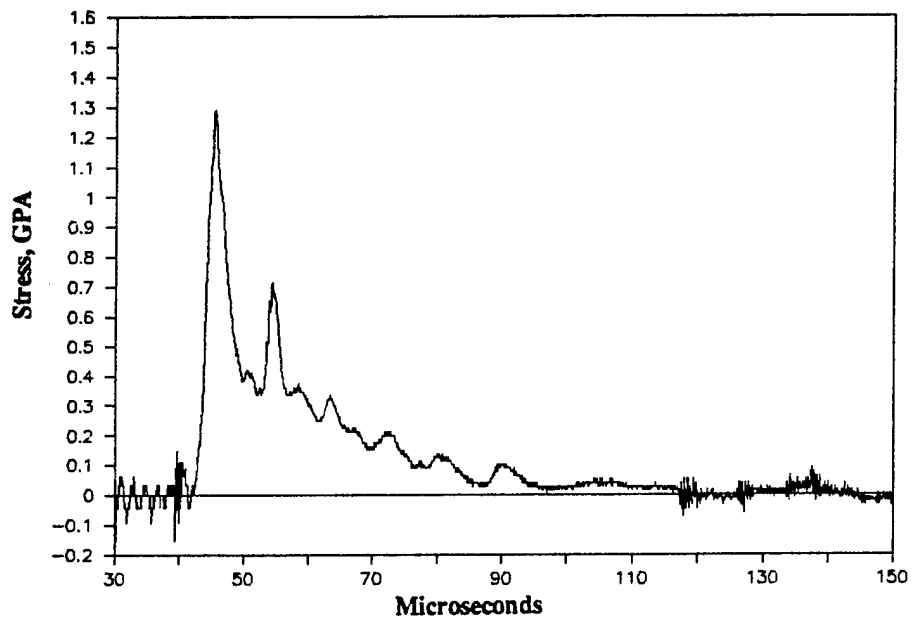
Analysis. As with Comp B, overall peak pressures and waveshapes were lower than tests at 15-cm HOB. The stress profiles were smoother and fewer differences between Pentolite and Comp B explosives were observed. Again, multiple peaks were present in the first 20 μ sec at the 2.5-cm range, whereas only single peaks were present at 5.0 cm during this time.

Specific impulse histories from all ytterbium records from the Pentolite tests at 20-cm HOB are plotted together in Figures 44 and 45. Comparison of these plots with Figures 38 and 39 confirmed the observation that the Comp B explosive delivered about 10% more specific impulse than Pentolite.

Pressure Bars. Five stress-time records were obtained from pressure bar gages: two from the 2.5-cm and three from the 5.0-cm locations. Again, since the records had low S/N ratios,



a. 2.5-cm Range from GZ



b. 5.0-cm Range from GZ

Figure 43. Representative Stress-Time Records, Pentolite at 20-cm HOB.

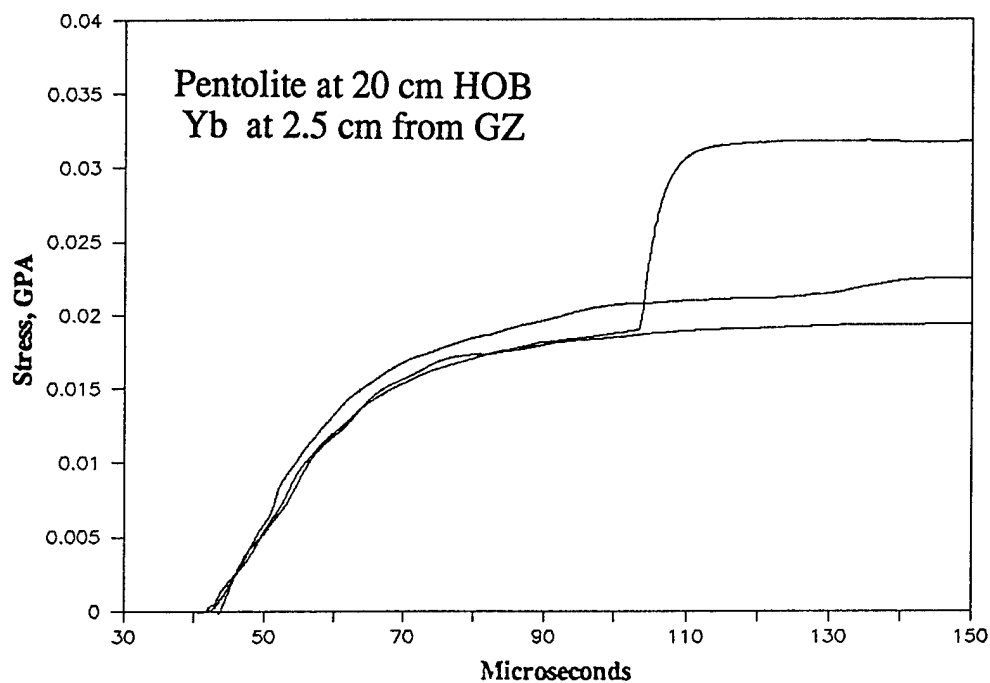


Figure 44. Impulse-Time Records, Pentolite at 20-cm HOB, Ytterbium, 2.5-cm Range.

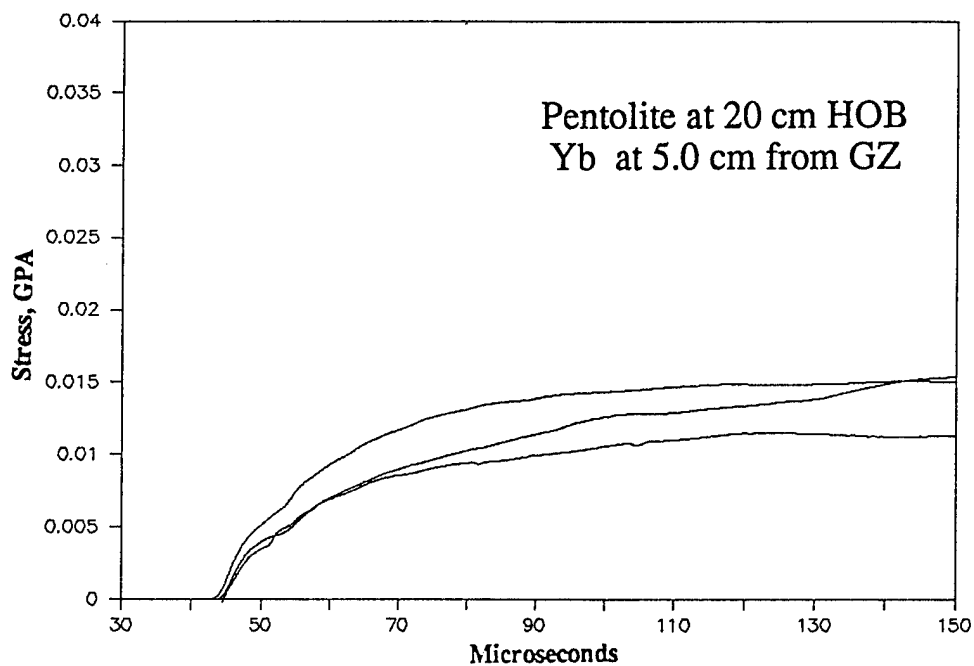


Figure 45. Impulse-Time Records, Pentolite at 20-cm HOB, Ytterbium, 5.0-cm Range.

inconsistent peak stresses or TOAs and did not return to zero stress, the readings were deemed unreliable.

Impulse Plugs. Total specific impulses were measured for tests 2A.4 and 2A.8 and are listed in Table 15.

3.3 Ballistic Pendulum Measurements. The experimental tests required by the statement of work included detonations of bare Comp B, 6.35-mm cased, and 9.53-mm cased explosive charges at 15- and 20-cm HOB. Each test was repeated to assess test-to-test variation. The information on these tests is shown in the required format in Tables 16 through 18.

The masses in Table 16 included the lid of each cased charge after a 1.2-cm-diameter hole was drilled through it to accept the booster charge. For tests 2 through 13, the region adjacent to the pendulum face was not surrounded by a coverplate, but was left as an open space, as with the large BRL pendulum.

Table 16. Ballistic Pendulum Explosive Charges

Test Number	Charge Number	Main Charge Explosive Type	Main Charge Mass (g)	Det. or Primary Explosive Type	Primary Explosive Mass (g)	Booster Explosive Type	Booster Explosive Mass (g)	Total Charge Mass (g)
2	(1) 11	Comp B	905.5	RP-80	N/A	C-4	4.0	905.5
3	(1) 12	"	905.4	"	"	"	"	905.4
4	(1) 13	"	898.0	"	"	"	"	898.0
5	(1) 15	"	897.0	"	"	"	"	897.0
6	(2) 5	"	910.0	"	"	"	"	2974.
7	(2) 1	"	900.0	"	"	"	"	2883.
8	(2) 6	"	908.0	"	"	"	"	2074.
9	(2) 2	"	901.0	"	"	"	"	3064.
10	(3) 2	"	901.0	"	"	"	"	4744.
11	(3) 4	"	877.0	"	"	"	"	4858.
12	(3) 6	"	907.0	"	"	"	"	4631.
13	(3) 1	"	881.0	"	"	"	"	4835.
14	(1) 16	"	897.5	"	"	"	"	897.5
15	(1) 14	"	898.3	"	"	"	"	898.3
16	(3) 5	"	879.0	"	"	"	"	4722.
17	(3) 3	"	906.0	"	"	"	"	4404.
18	(2) 4	"	901.0	"	"	"	"	2974.
19	(2) 3	"	905.0	"	"	"	"	2974.
Notes: 1. Lot number ABY90M0E1S017B 2. Lot number ABY90B0E1S017B 3. Lot number ABY90C0E1S017B								

Table 17. Ballistic Pendulum Shot Geometry

Test Number	Charge Number	HOB (cm)	Charge Shape	Charge Type	Charge Diameter (cm)	Charge Length (cm)	Detonation Initiation Point
2	(1) 11	15	Right Circular Cylinder	Bare	8.79	8.81	Top Center
3	(1) 12	15	"	Bare	8.79	8.81	"
4	(1) 13	20	"	Bare	8.79	8.81	"
5	(1) 15	20	"	Bare	8.79	8.80	"
6	(2) 5	15	"	6.35-mm case	10.10	10.10	"
7	(2) 1	15	"	"	10.08	9.98	"
8	(2) 6	20	"	"	10.08	10.10	"
9	(2) 2	20	"	"	10.08	10.13	"
10	(3) 2	15	"	9.53-mm case	10.71	11.32	"
11	(3) 4	15	"	"	10.71	11.35	"
12	(3) 6	20	"	"	10.60	11.34	"
13	(3) 1	20	"	"	10.72	11.34	"
14	(1) 16	15	"	Bare	8.79	8.79	"
15	(1) 14	20	"	Bare	8.79	8.80	"
16	(3) 5	15	"	9.53-mm case	10.67	11.34	"
17	(3) 3	20	"	"	11.55	11.34	"
18	(2) 4	15	"	6.35-mm case	10.09	10.09	"
19	(2) 3	20	"	"	10.09	10.09	"

Table 18. Ballistic Pendulum Shot Conditions

Test Number	Charge Number	Date	Barometric Pressure (kPa)	Ambient Temperature (K)	Supplemental Notes
2	(1) 11	8/28/90	100.0	308	First real test
3	(1) 12	8/28/90	98.9	309	
4	(1) 13	8/29/90	103.6	300	
5	(1) 15	8/29/90	104.3	302	
6	(2) 5	8/29/90	101.9	306	
7	(2) 1	9/7/90	101.9	302	
8	(2) 6	9/7/90	101.9	305	
9	(2) 2	9/10/90	101.9	303	
10	(3) 2	9/11/90	101.9	300	
11	(3) 4	9/12/90	101.9	295	
12	(3) 6	9/12/90	101.9	297	
13	(3) 1	9/12/90	101.9	299	
14	(1) 16	9/14/90	101.9	301	Coverplate added for this and all subsequent tests
15	(1) 14	9/14/90	101.9	303	
16	(3) 5	9/14/90	101.9	303	
17	(3) 3	9/17/90	101.9	300	
18	(2) 4	9/17/90	101.9	300	
19	(2) 3	9/17/90	101.9	302	

A second set of tests involved the addition of a large (2-m-square) coverplate surrounding the pendulum face. The coverplate had a keyway cut to allow the pendulum to swing freely through it. The goal of this modification was to assess the possibility that edge effects or blastwave wraparound was impeding the pendulum swing. The coverplate was procured and welded to the fixture. A gap of approximately 2.5 cm was cut between the outer edge of the pendulum face and the keyway to prevent interference.

When the coverplate was in place, six tests were performed (tests 14 through 19), one for each explosive type at each HOB. The information for these tests is shown on Tables 16 through 18.

Table 19 shows the peak swing measurements for each test. These values were derived from careful analysis of the videotape recording and the signals from the RVDT gages. The RVDT signals were lost from several tests due to excessive vibration, or in some cases, fragments hitting cables. On tests where the RVDTs provided a signal, some inconsistencies were noted in magnitude of swing angle when compared to the video images. Although the gages were removed and recalibrated several times, the inconsistencies were not overcome. Hence, it is surmised that these gages were affected by shock transmission from the fragment impacts on the fixture (the gages appeared to work well during the bare charge tests). For this reason, the measurement derived from the videocamera was used in all cases where the camera and gage outputs differed. The RVDT gages did, however, provide excellent records of pendulum swing over many cycles, from which the pendulum period could be measured.

Table 19. Pendulum Swing Results (Degrees at Peak)

HOB	Bare	Test No.	6.35-mm Steel Cased	Test No.	9.53-mm Steel Cased	Test No.
15-cm	17.9	2	25.2	6	31.8	10
15-cm	18.0	3	24.7	7	32.0	11
20-cm	16.8	4	25.2	8	29.8	12
20-cm	17.0	5	25.5	9	30.1	13
15-cm w/plate	20.6	14	28.5	18	31.2	16
20-cm w/plate	20.1	15	27.3	19	31.4	17

The videocamera provided good data for all tests. The camera view was frequently obscured by smoke and dust on the first one or two swings of the pendulum. Hence, the readings taken from the video were corrected to account for the slight reduction in swing angle for later swing observations. The correction involved adding a small amount ($0.067^\circ/\text{swing}$) to the observed swing to predict the initial swing value. (The factor which accounts for swing decrement is explained in the next paragraph.) Taking into account errors in setting up and interpreting the video image, and the resolution capability of the RVDT signal processing, it is conservatively estimated that the readings on Table 19 are accurate within $\pm 0.3^\circ$.

Figures 46 through 56 depict the output from the RVDT gages on all tests where it was deemed fairly reliable. Time zero in these figures corresponds to the detonation pulse. Figures 46 through 49 are from test 2 (bare charge at 15-cm HOB), which was the first real test. Figure 46 shows the initial pendulum swing, and a peak value of about 17.8° . This value was doublechecked and found to be actually 17.9° , the value which appears in Table 19. Figure 46 shows the shock-induced vibration evident on the gage trace. The initial shock causes the negative dip at time zero seen on some of the plots. The dip does not represent a baseline shift. Figure 47 from the same test and shows how the gage trace smooths out appreciably after the first swing. This figure also indicates a period of 2.55 sec, later corrected to 2.541 sec. Figures 46 and 49 show the long term swing of the pendulum. From these figures, and similar ones from other tests, it was determined that the pendulum swing amplitude decayed about 0.067° per swing (period). This value was doublechecked on the video output by observing swing magnitude after 20 or more swings.

Figures 50 and 51 provide data for test 3 (also a bare charge at 15-cm HOB). The peak value shown on Figure 50 was later corrected to 18.0° . Figures 52 and 53 are from different RVDT gages on test 4 (bare charge at 20-cm HOB). The peak swing for test 4 was determined to be 16.8° , which was seen on the video and represented an average of the values seen on Figures 52 and 53. Figure 54 depicts the swing record for test 5 (bare charge at 20-cm HOB). This record showed a peak of 16.37° , but the video image of 17.0° was deemed to be more reliable. Similarly, Figure 55 shows a peak of 24.94° for test 6 (6.35-mm cased charge at 15-cm HOB), but the video result of 25.2° was chosen as being better. Figure 56 shows the swing record from test 13 (9.53-mm cased charge at 20-cm HOB). The peak for this test was 30.1° .

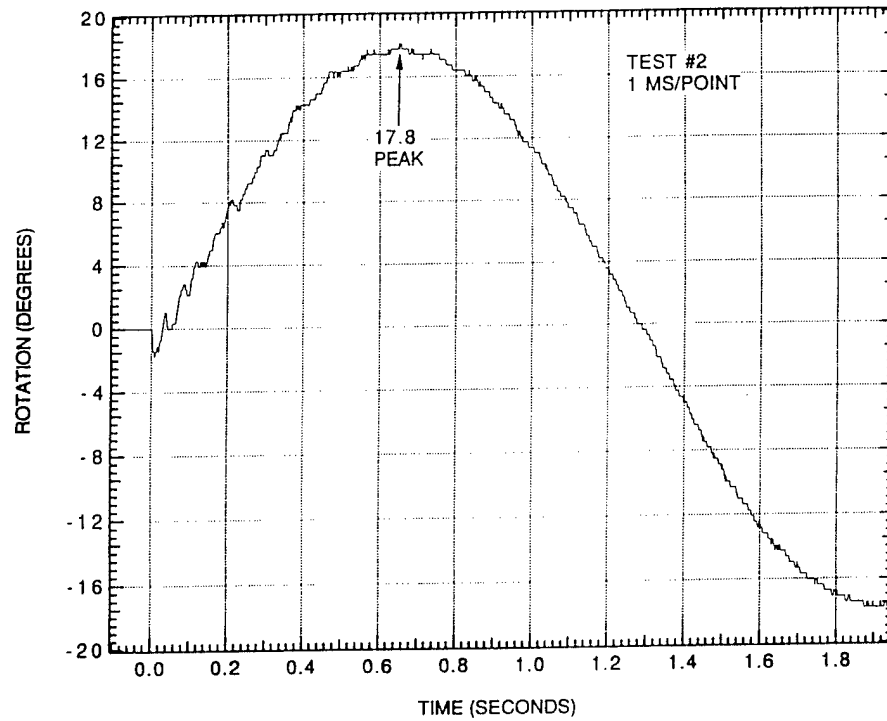


Figure 46. RVDT Record, One Swing, Test 2 (Bare Charge - 15-cm HOB).

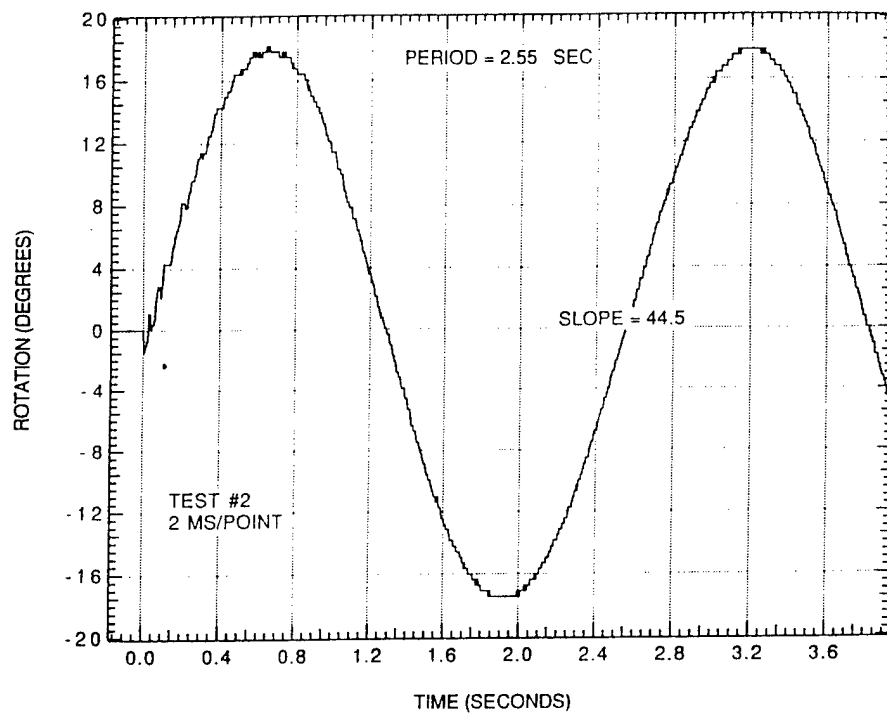


Figure 47. RVDT Record, Two Swings, Test 2 (Bare Charge - 15-cm HOB).

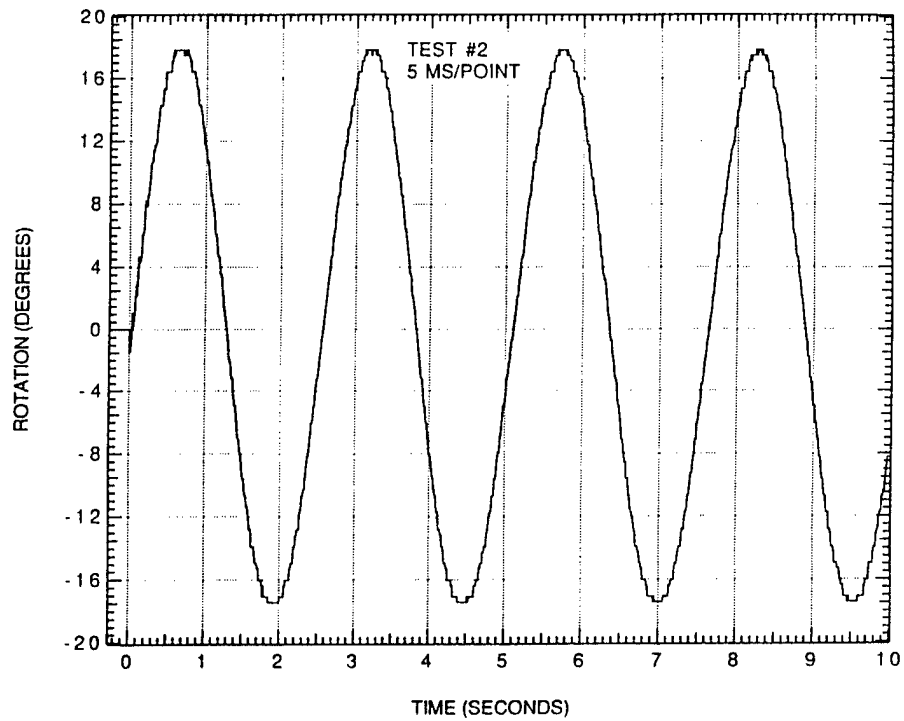


Figure 48. RVDT Record, Four Swings, Test 2 (Bare Charge - 15-cm HOB).

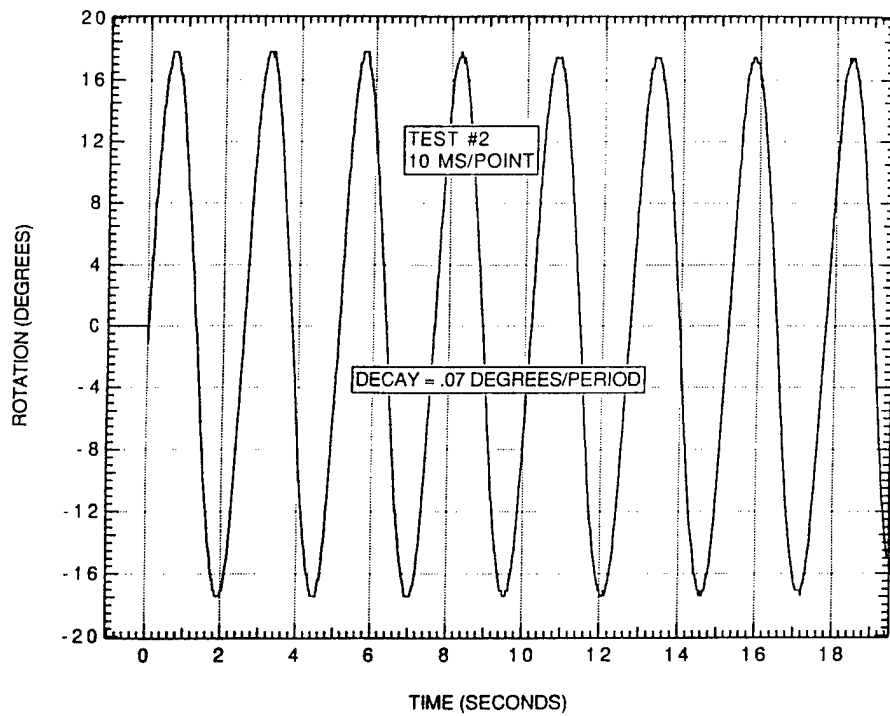


Figure 49. RVDT Record, Eight Swings, Test 2 (Bare Charge - 15-cm HOB).

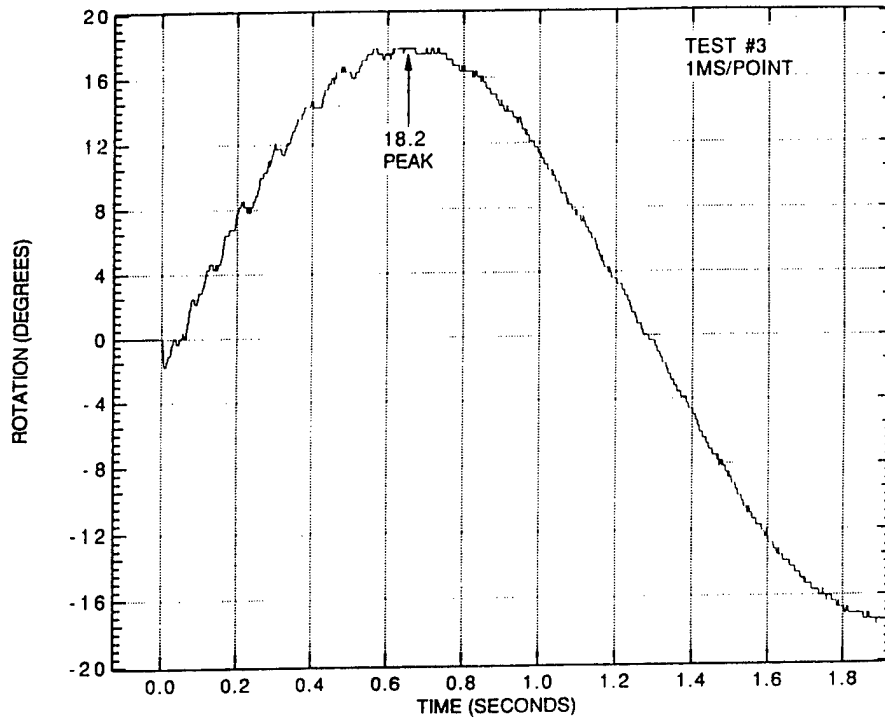


Figure 50. RVDT Record, One Swing, Test 3 (Bare Charge - 15-cm HOB).

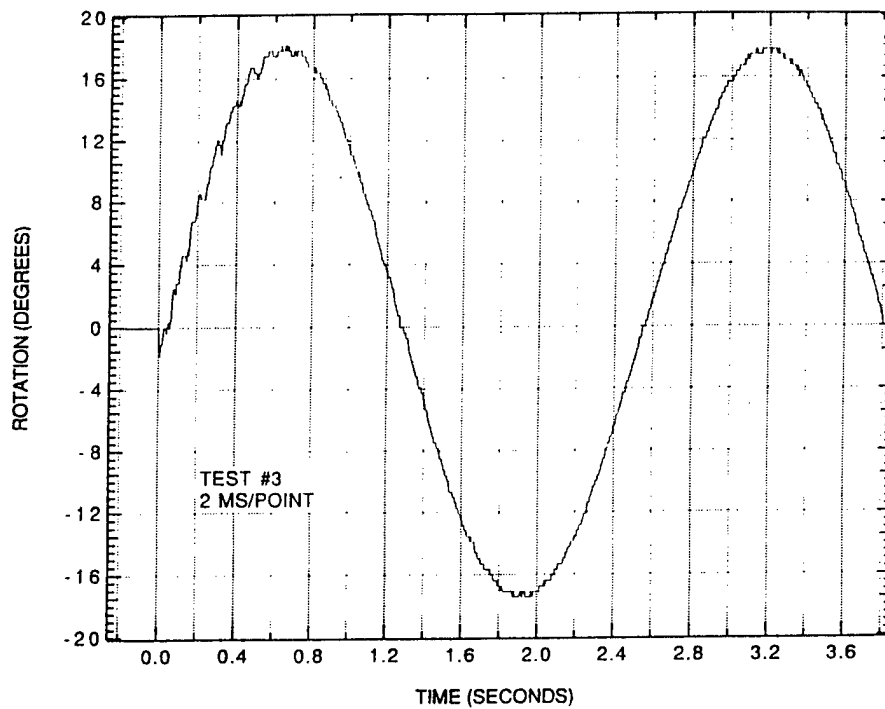


Figure 51. RVDT Record, Two Swings, Test 3 (Bare Charge - 15-cm HOB).

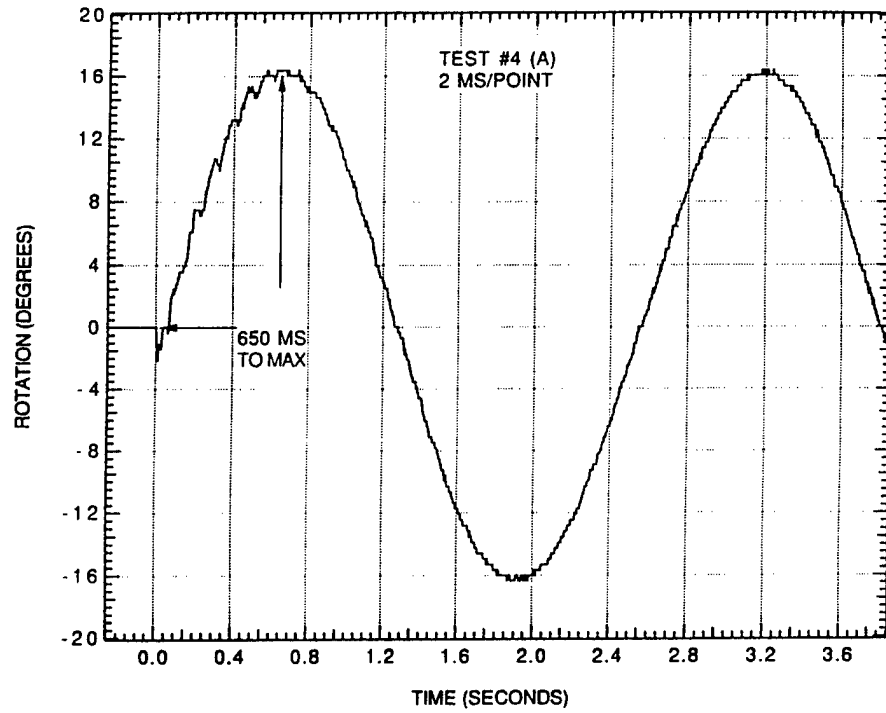


Figure 52. RVDT Record A, Two Swings, Test 4 (Bare Charge - 20-cm HOB).

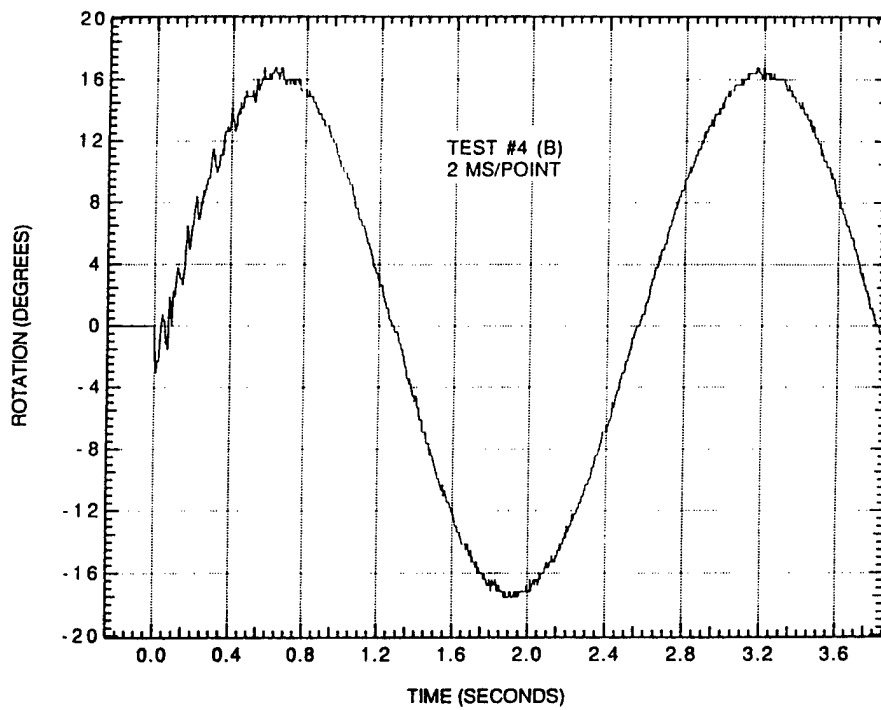


Figure 53. RVDT Record B, Two Swings, Test 4 (Bare Charge - 20-cm HOB).

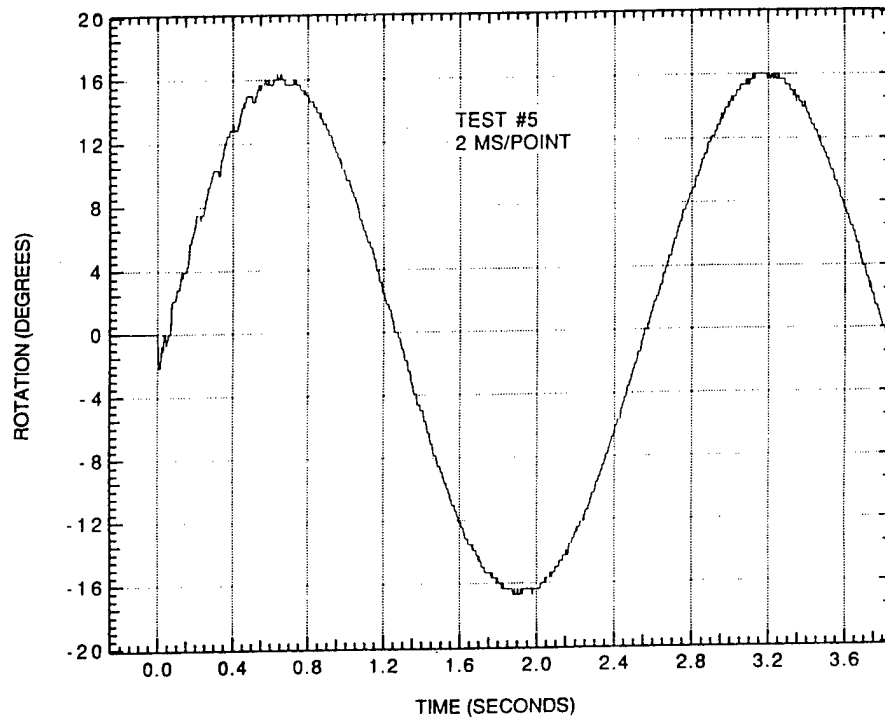


Figure 54. RVDT Record, Two Swings, Test 5 (Bare Charge - 20-cm HOB).

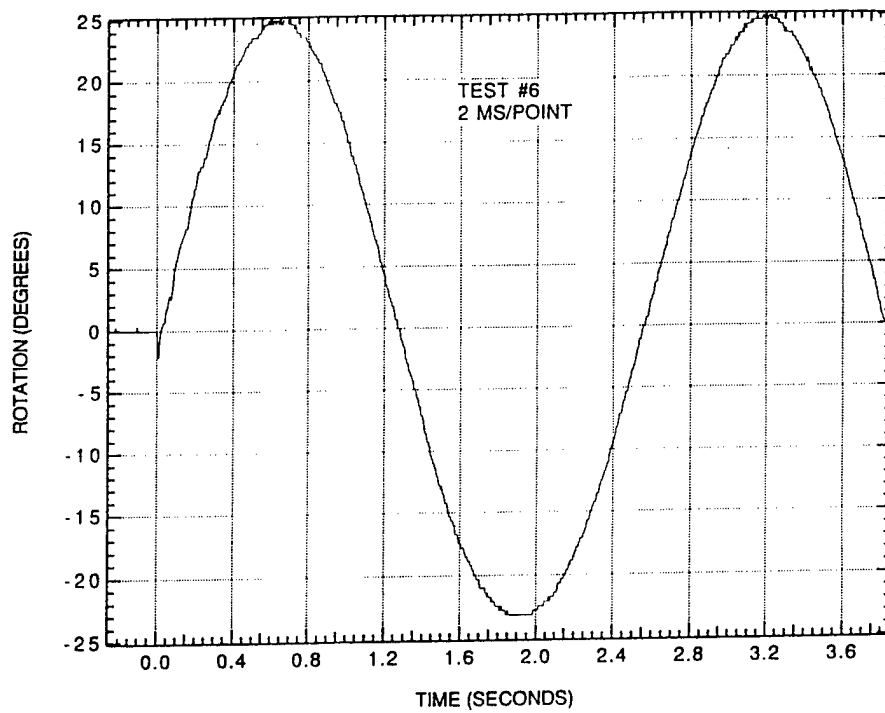


Figure 55. RVDT Record, Two Swings, Test 6 (6.35-mm Cased Charge - 15-cm HOB).

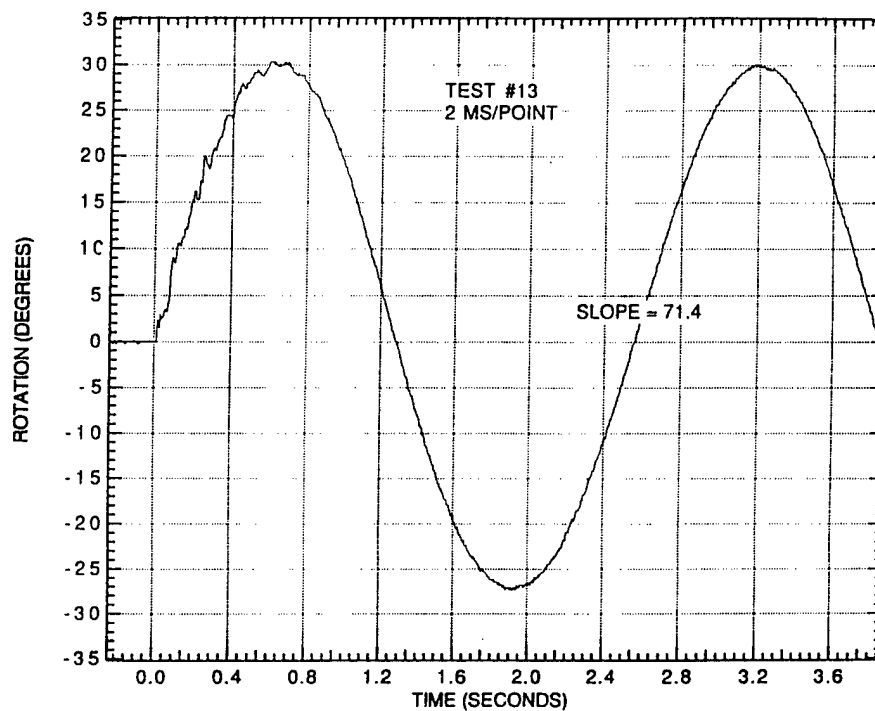


Figure 56. RVDT Record, Two Swings, Test 13 (9.53-mm Cased Charge - 20-cm HOB).

The results shown in Table 19 are averaged and plotted in Figure 57. Several important features are evident. First, the test arrangement demonstrated excellent repeatability. The maximum test-to-test variation seen when repeated tests were compared is 2% for tests 6 and 7. It should be noted that total charge mass varied almost 4% in those tests. Second, a trend was seen in that swing angle (and therefore impulse) increased as steel case thickness increased. More relative change was seen between the 6.35-mm cases and the bare charges than between the 9.53-mm and 6.35-mm cases. Third, the 15-cm HOB provided slightly higher load than the 20-cm HOB in all but one case, although the difference was relatively small (2-6%). Fourth, the addition of the coverplate increased the swing angle for the bare and 6.35-mm cased charge, but did not appear to change the results for the 9.53-mm charges. Table 20 shows the impulse and natural periods calculated for each test in this program. The natural period was calculated using the values in Tables 19 and 9 and Eq. (13). The impulse was then computed using Eq. (9), with the maximum swing results coming from Table 19. Figure 58 plots the results of Table 20.

Pendulum Swing Angles For Comp-B Charges Bare, 6.35 & 9.53 mm Steel Cased Charges

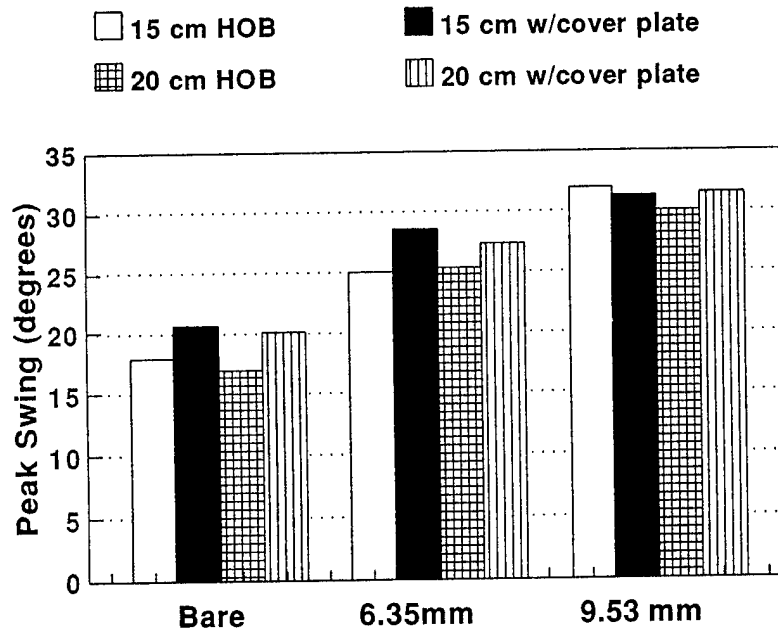


Figure 57. Averaged Pendulum Swing Angles for All Tests.

Table 20. Impulse and Natural Period

Test Number	Charge Type	HOB (cm)	Natural Period (sec)	Total Impulse (N-sec)
2	Bare	15	2.541	746.6
3	Bare	15	2.542	750.7
4	Bare	20	2.540	701.0
5	Bare	20	2.540	709.3
6	6.35-mm case	15	2.557	1046.9
7	6.35-mm case	15	2.556	1026.4
8	6.35-mm case	20	2.557	1046.9
9	6.35-mm case	20	2.558	1059.1
10	9.53-mm case	15	2.575	1314.7
11	9.53-mm case	15	2.576	1322.8
12	9.53-mm case	20	2.569	1234.0
13	9.53-mm case	20	2.570	1246.1
14	Bare w/plt	15	2.547	858.1
15	Bare w/plt	20	2.546	837.4
16	9.53-mm case w/plt	15	2.574	1290.5
17	9.53-mm case w/plt	20	2.574	1298.6
18	6.35-mm case w/plt	15	2.566	1181.3
19	6.35-mm case w/plt	20	2.562	1132.5

Impulse Calculated From Pendulum Swing Bare, 6.35 & 9.53 mm Steel Cased Charges

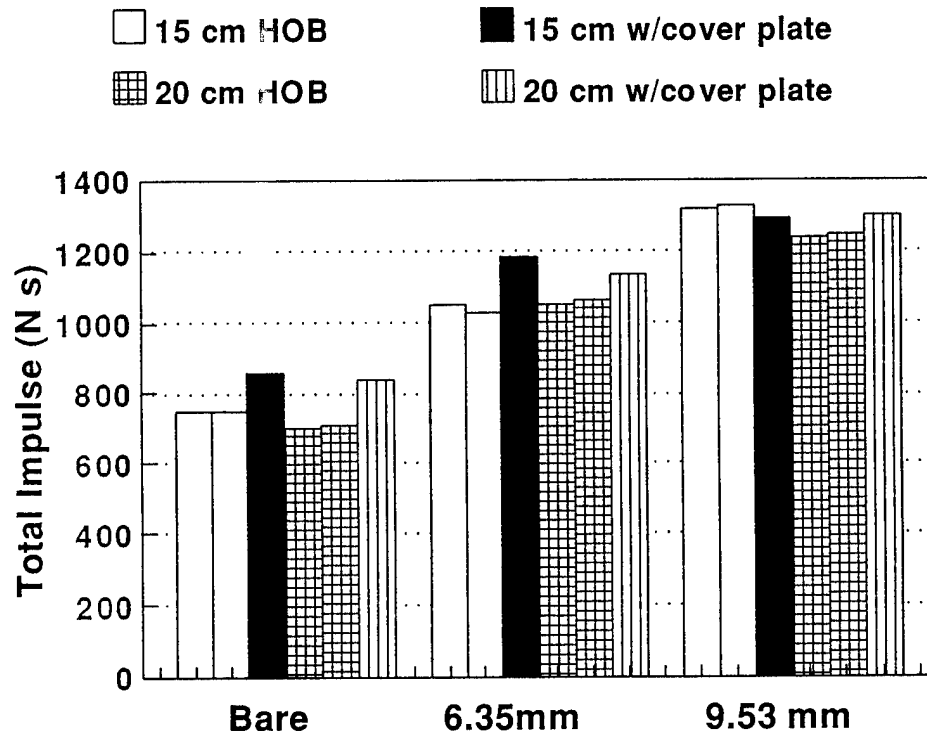


Figure 58. Calculated Impulse for All Tests.

3.4 Comparison of Computational and Experimental Results. It was possible to directly compare the results of the computational simulations with the experimental results because the same explosive and geometry were used in both cases. One difference did occur, however, in the method of detonation. The computer simulations used an initiation at the center and at a point (actually a ring, due to axisymmetry) 2.2 cm from center. This approach followed the original plan, which was to generate a detonation wave which was near planar. The multipoint initiation was not used in the experiments because it was later decided that the timing precision was not sufficiently good to ensure a more planar wave than that which could be generated by the singlepoint initiation.

The following comparisons concentrate on records from the ytterbium gages because they generally provided the best results. The time zero of the computational records was increased

by about 8 μ sec to correspond to the time zero of the experimental records. The computational time zero started at the initiation of the main charge; time zero for the experiments started at the firing panel, and thus included time for signal transmission, detonator operation, and booster pellet detonation.

Several general trends can be noticed for both Comp B and Pentolite. The computer simulations indicated higher peak pressure at the 2.5-cm location than the experimental records (see for example Figures 59 through 62). The traces for the 20-cm HOB were less different than those at 15-cm HOB. (Notice that the pulsewidths and the pressure decay agreed very closely for all the records). Due to the higher pressures seen on the computer simulations, the specific impulse integrated at the 2.5-cm location was greater than that recorded with the gages (see for example Figures 63 through 66).

At the location 5.0-cm from center, the experimental records showed a peak pressure slightly higher than the computational simulations (see for example Figures 67 through 70). All traces showed very similar risetimes, pulsewidths, and decay profiles. The specific impulse computed at 5.0 cm from center was in good agreement in both waveshape and total impulse, primarily due to the similarity of the pressure traces (see for example Figures 71 through 74 and note the excellent correlation evident on Figure 72).

The close similarity of the pressure traces seen from the experiments and the computer simulations was encouraging. The higher peak seen in the computer simulations at the 2.5-cm location may have been due to the differences in the initiation scheme. It is possible that the multipoint initiation used in the computer simulations tended to focus the energy more, causing the higher peak pressure directly under the charge. This may also explain why the pressures seen at the 5.0-cm location were slightly lower in the computations: the simulations would tend to have more focused energy directly under the charge and less contribution at locations outside the charge diameter (such as the 5.0-cm location).

Pressure Curves For Blast

Case 9B and 2alyb3 Test Data

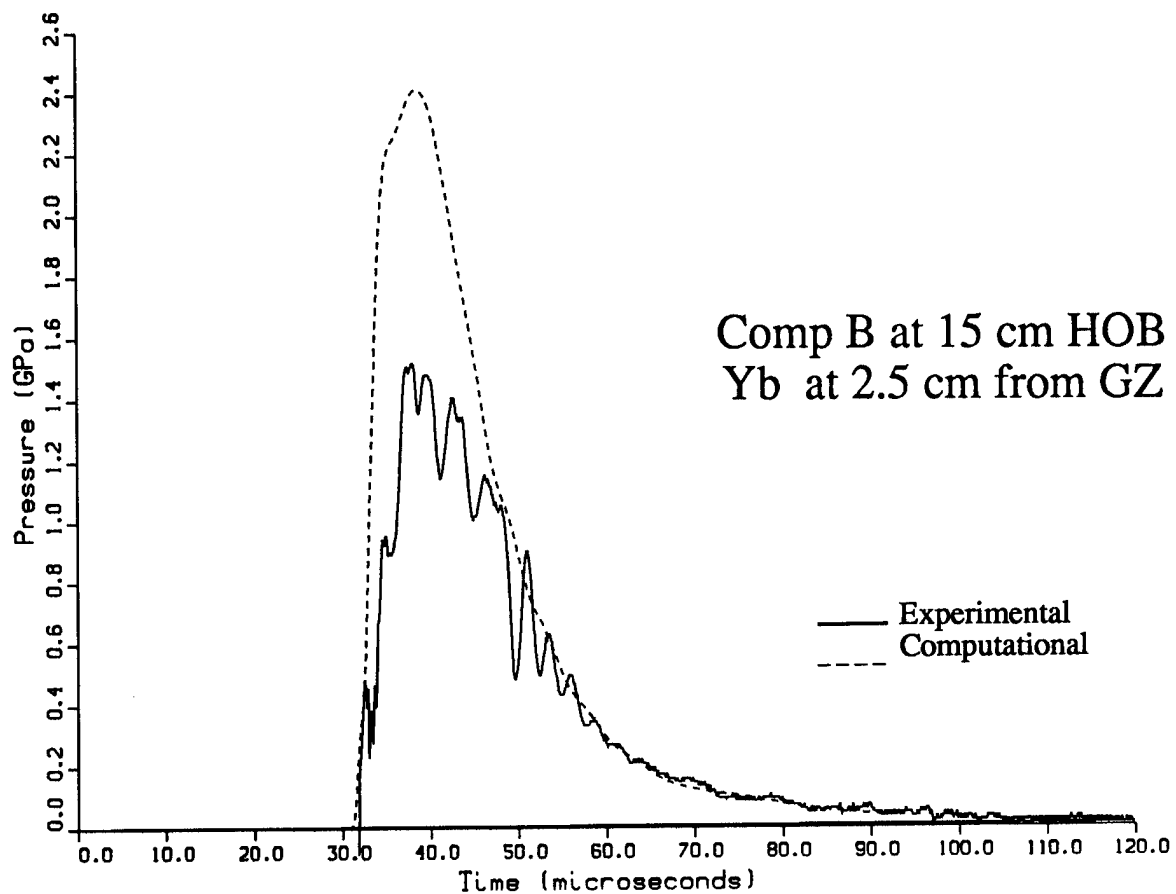


Figure 59. Computation (Dashed Line) vs. Experimental Record (Solid Line), Comp B at 15-cm HOB, 2.5-cm Range.

Pressure Curves For Blast

Case 9A and 2a10yb2 Test Data

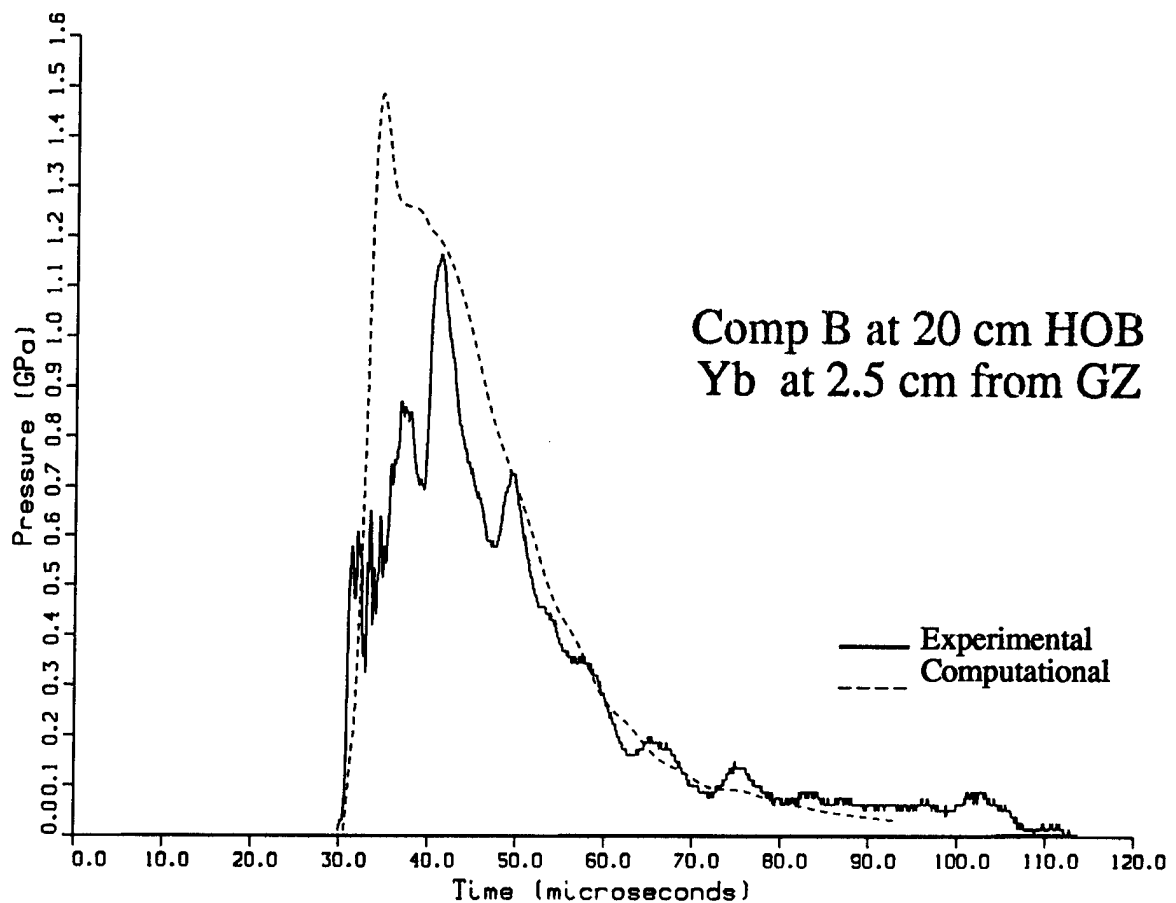


Figure 60. Computation (Dashed Line) vs. Experimental Record (Solid Line), Comp B at 20-cm HOB, 2.5-cm Range.

Pressure Curves For Blast

Case 14A and 2a7yb3 Test Data

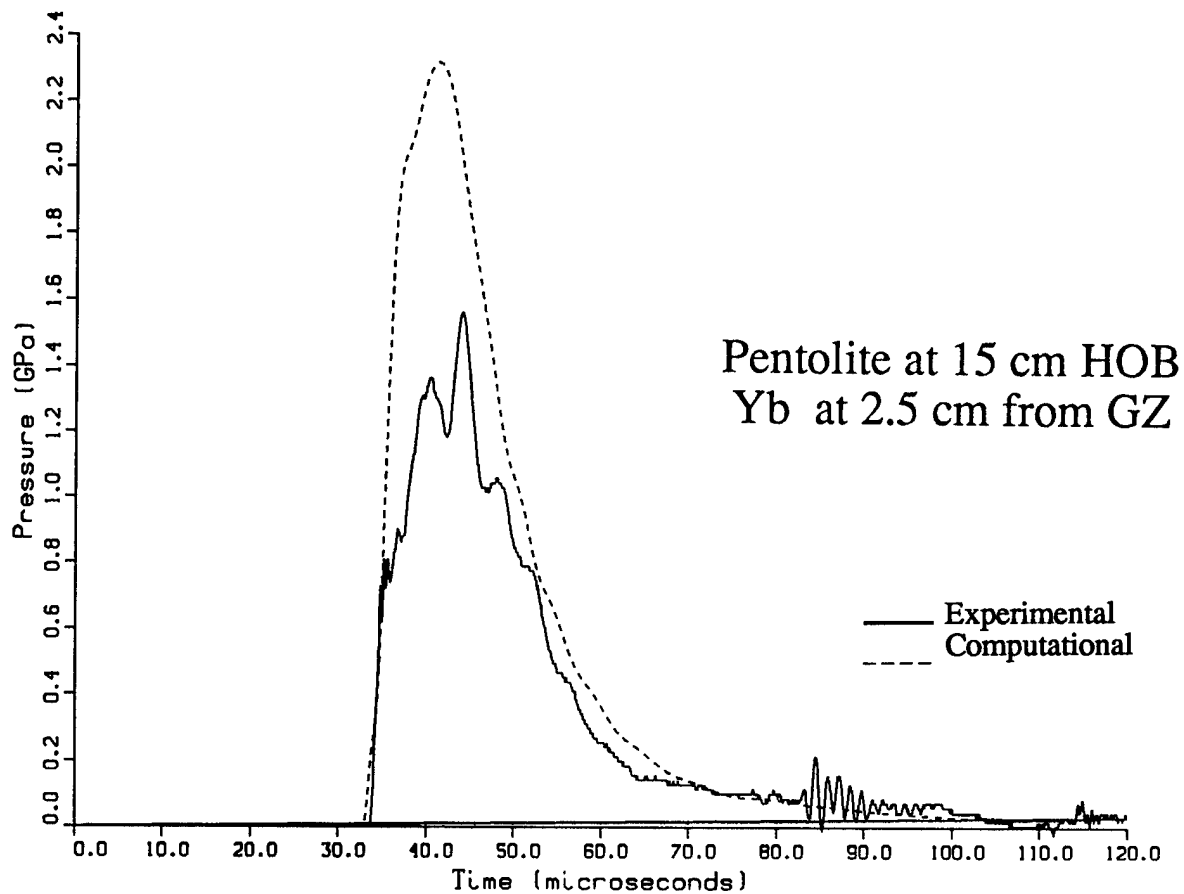


Figure 61. Computation (Dashed Line) vs. Experimental Record (Solid Line), Pentolite at 15-cm HOB, 2.5-cm Range.

Pressure Curves For Blast

Case 14B and 2a12yb2 Test Data

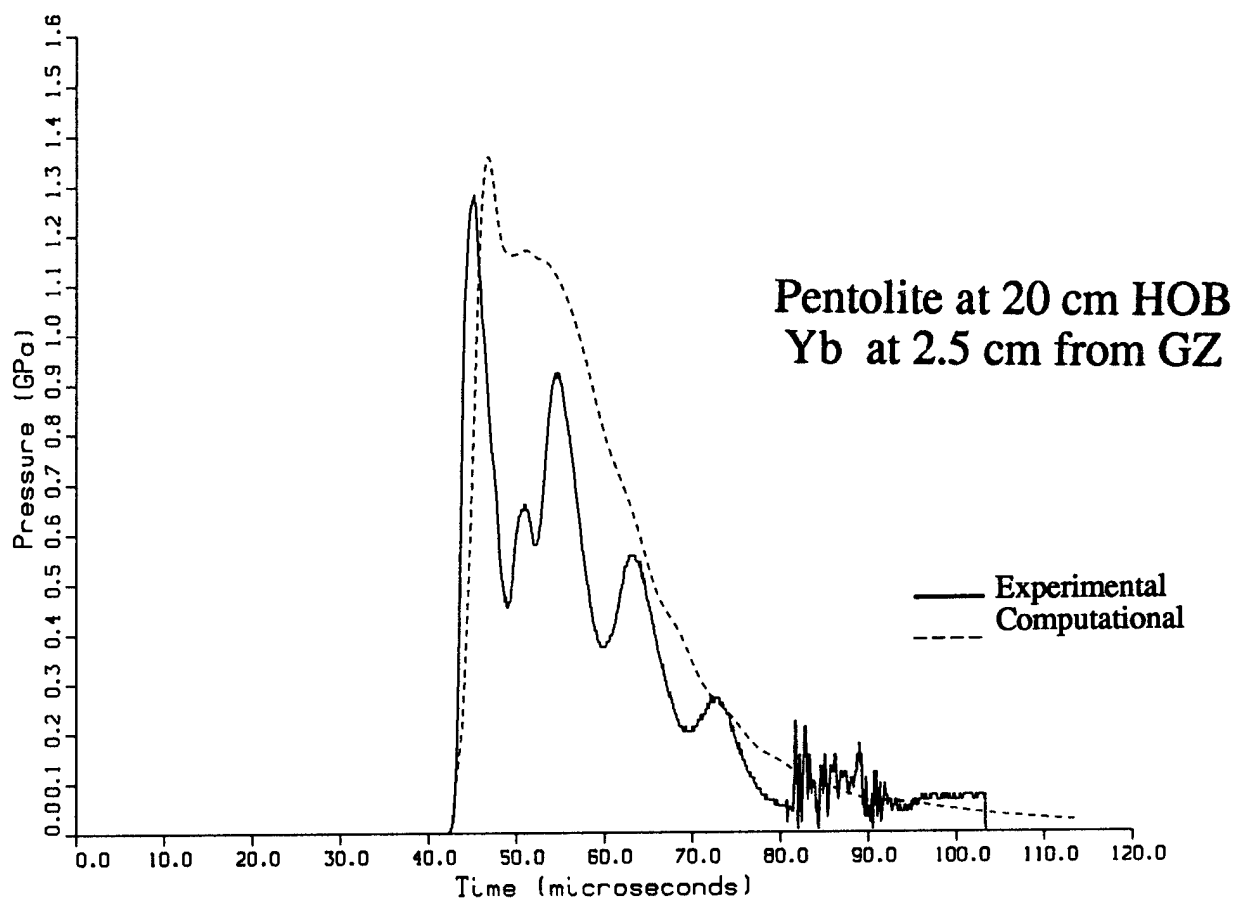


Figure 62. Computation (Dashed Line) vs. Experimental Record (Solid Line), Pentolite at 20-cm HOB, 2.5-cm Range.

Specific Impulse Curves For Blast

Case 9B and 2alyb3 Test Data

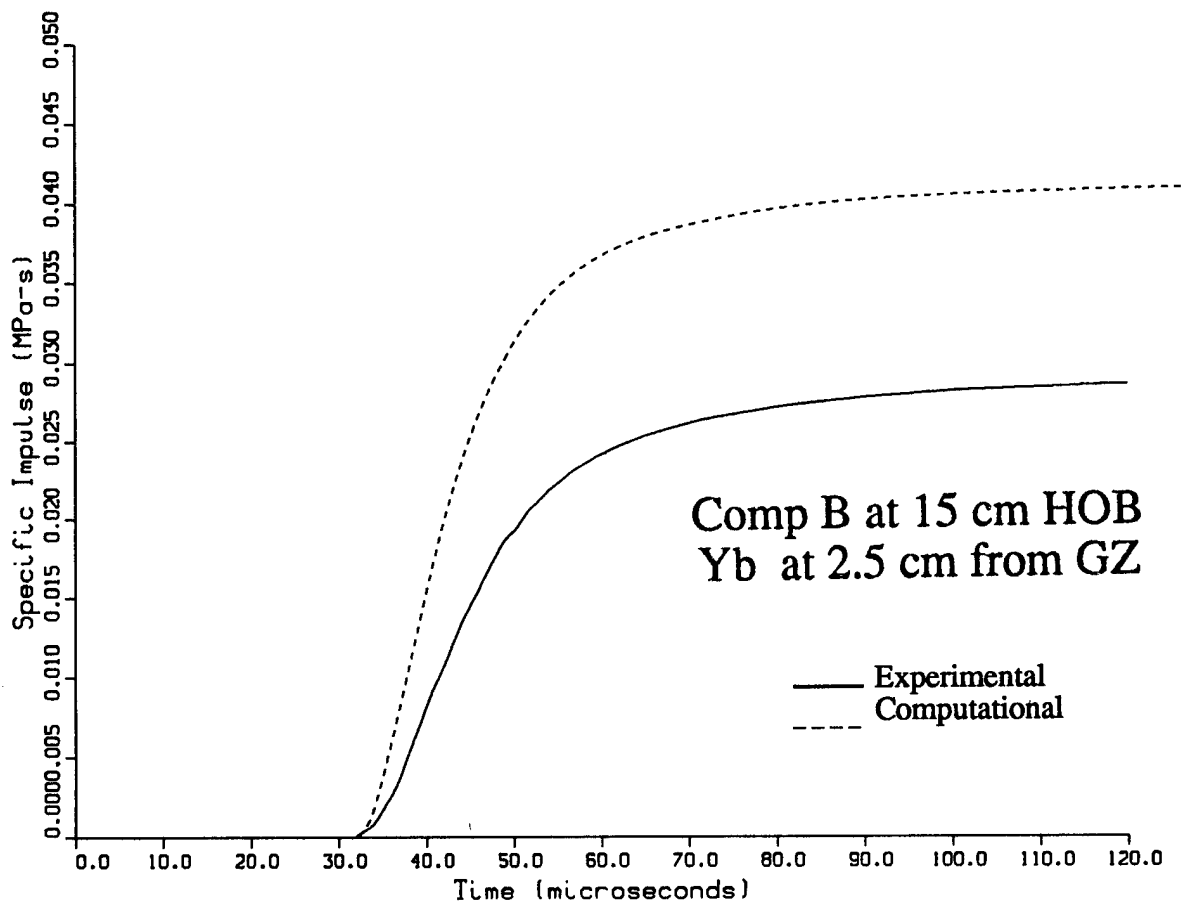


Figure 63. Computation (Dashed Line) vs. Experimental Record (Solid Line), Comp B at 15-cm HOB, 2.5-cm Range.

Specific Impulse Curves For Blast

Case 9A and 2a10yb2 Test Data

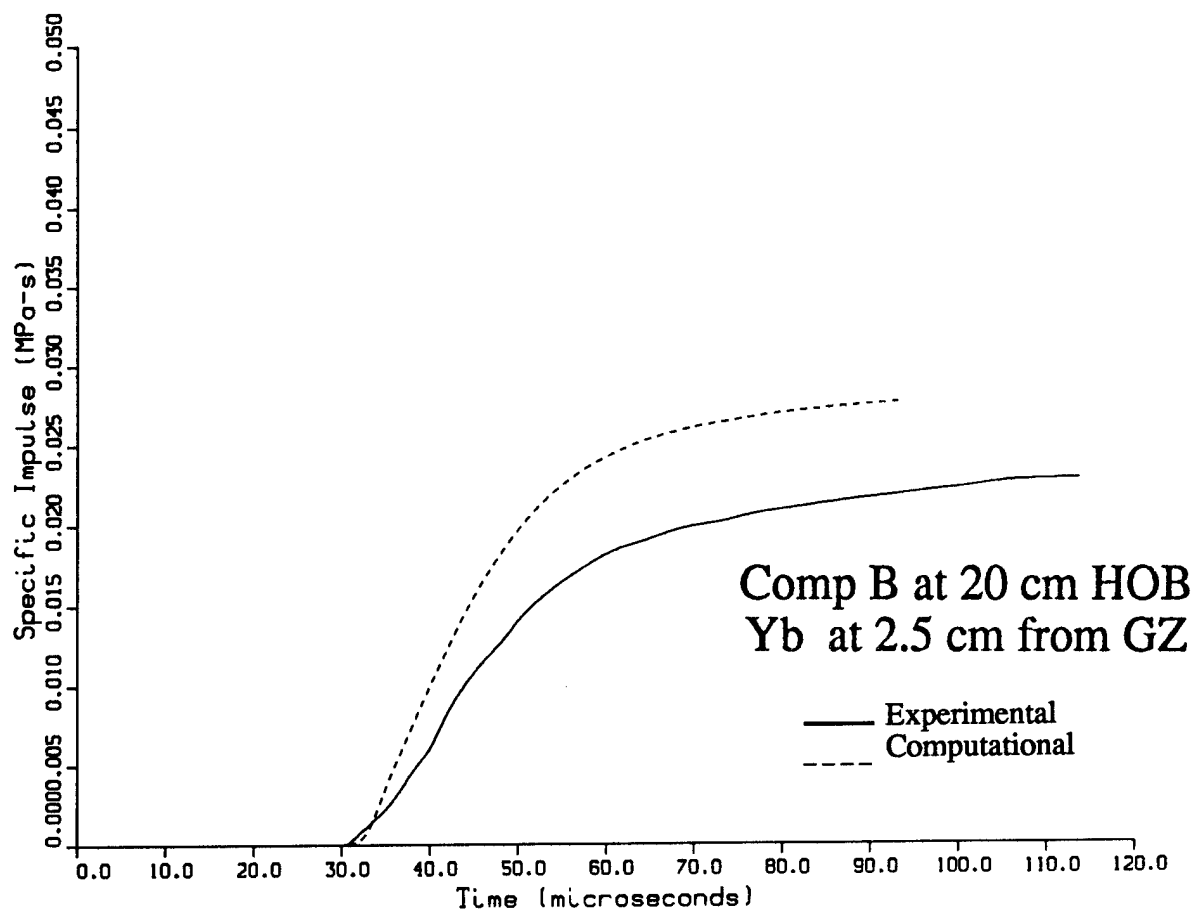


Figure 64. Computation (Dashed Line) vs. Experimental Record (Solid Line), Comp B at 20-cm HOB, 2.5-cm Range.

Specific Impulse Curves For Blast

Case 14A and 2a7yb3 Test Data

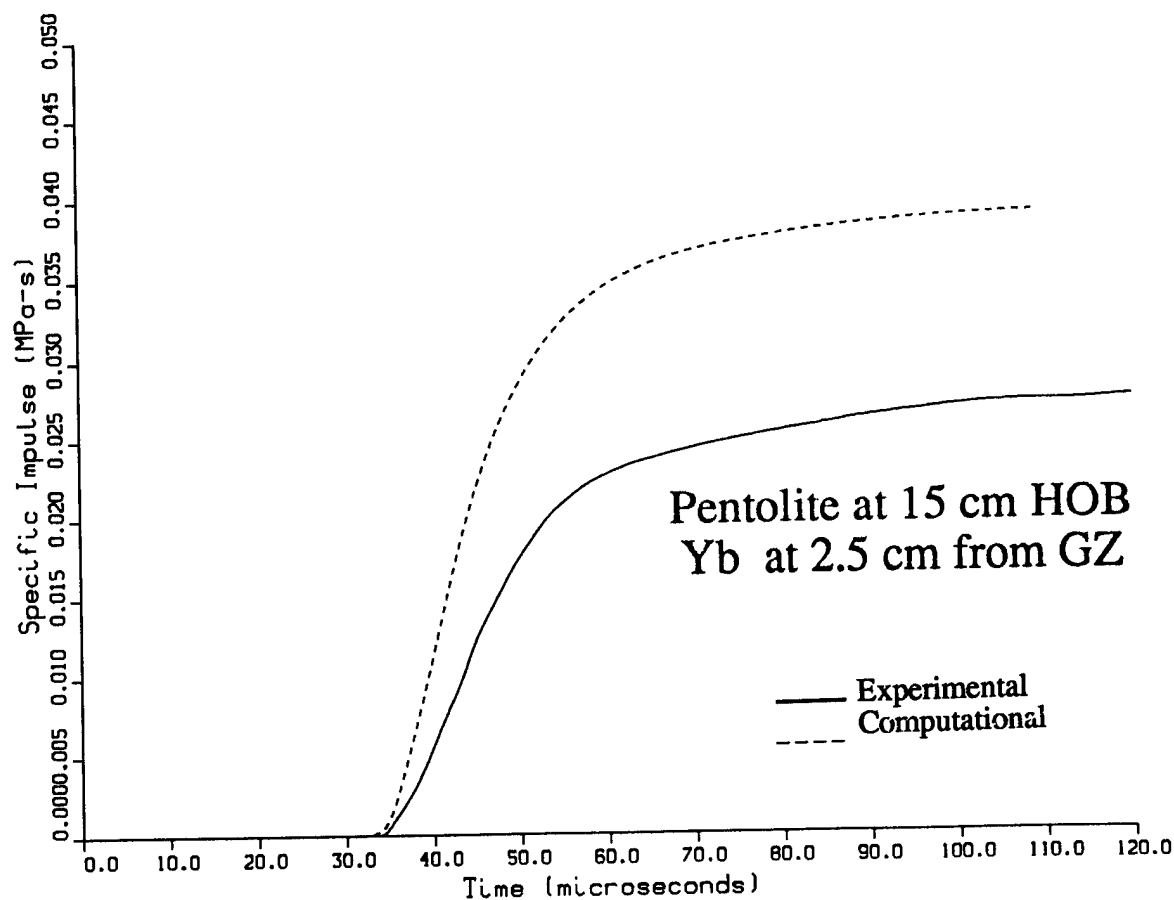


Figure 65. Computation (Dashed Line) vs. Experimental Record (Solid Line), Pentolite at 15-cm HOB, 2.5-cm Range.

Specific Impulse Curves For Blast

Case 14B and 2a12yb2 Test Data

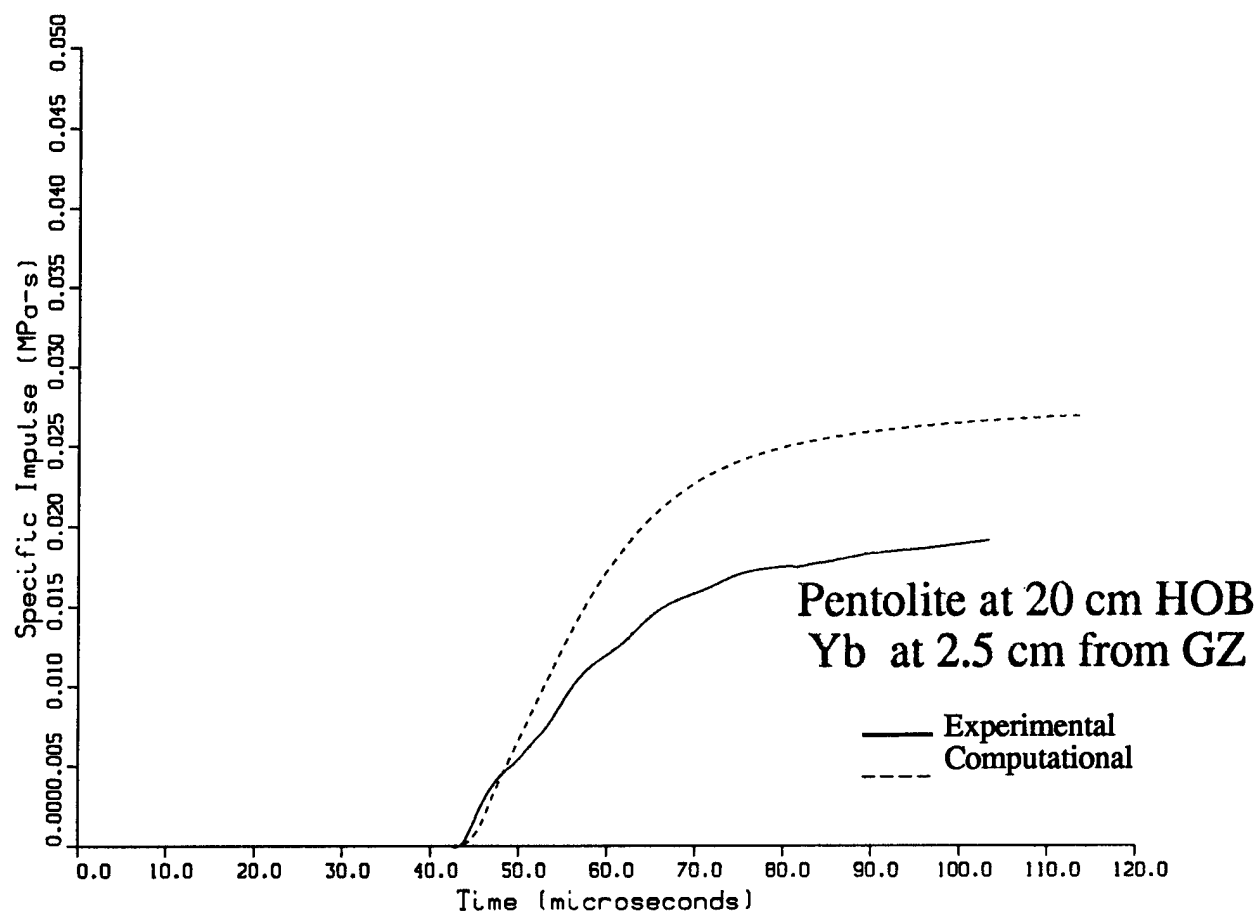


Figure 66. Computation (Dashed Line) vs. Experimental Record (Solid Line), Pentolite at 20-cm HOB, 2.5-cm Range.

Pressure Curves For Blast

Case 9B and 2a5yb4 Test Data

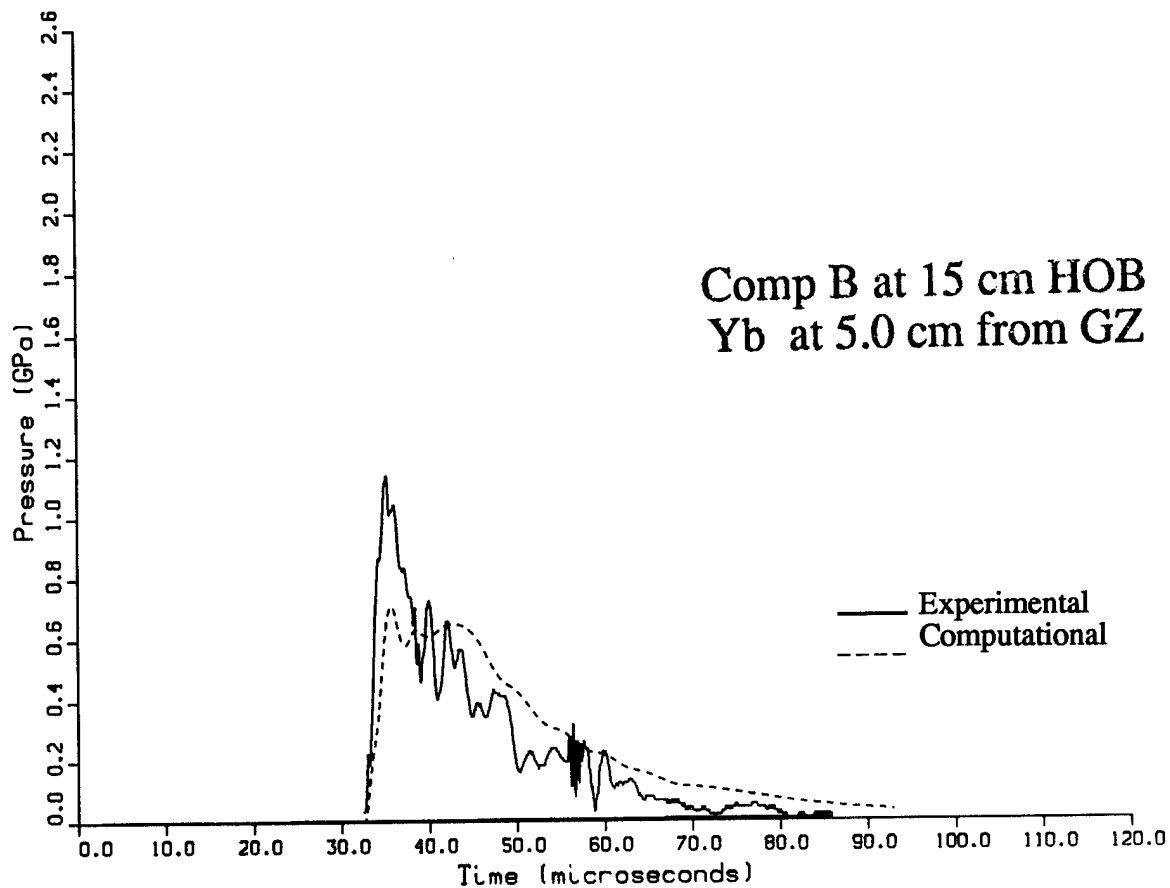


Figure 67. Computation (Dashed Line) vs. Experimental Record (Solid Line), Comp B at 15-cm HOB, 5.0-cm Range.

Pressure Curves For Blast

Case 9A and 2a10yb4 Test Data

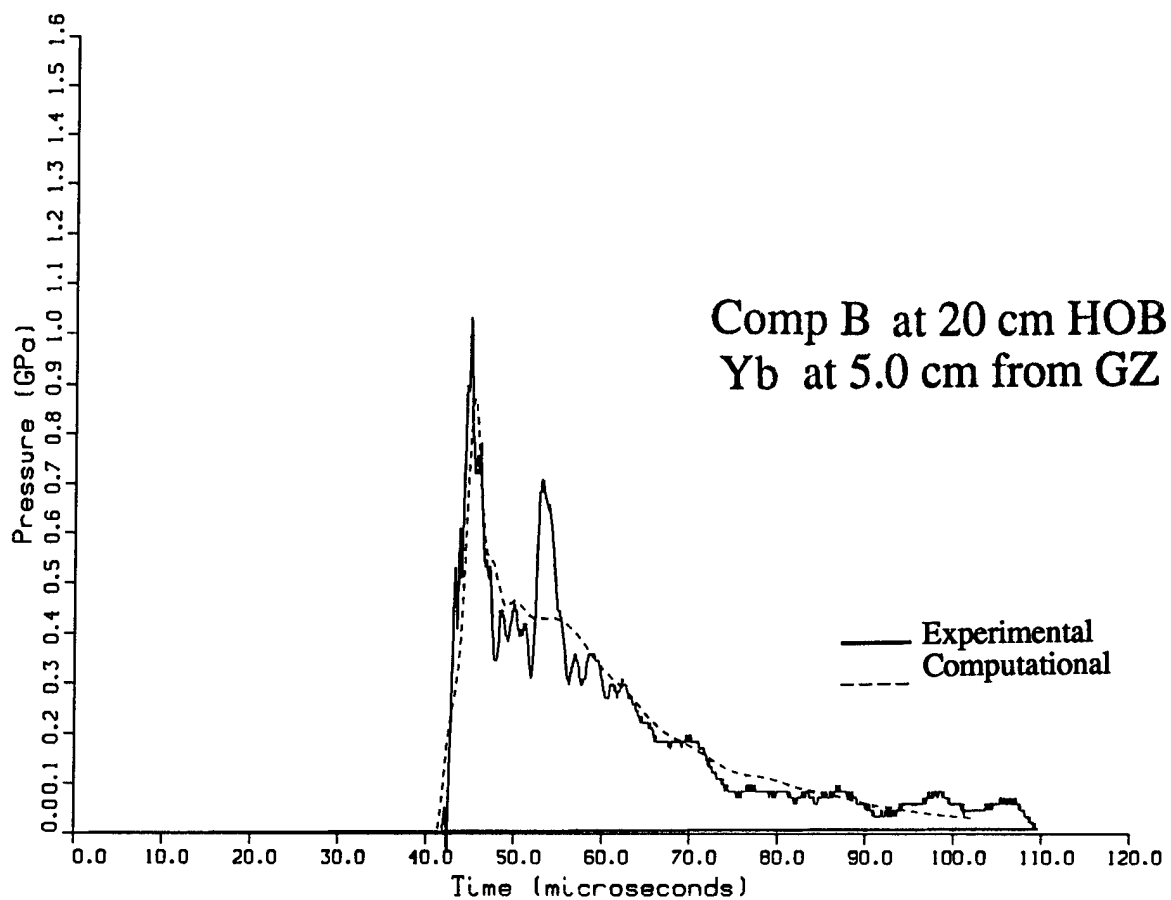


Figure 68. Computation (Dashed Line) vs. Experimental Record (Solid Line), Comp B at 20-cm HOB, 5.0-cm Range.

Pressure Curves For Blast

Case 14A and 2a3yb1 Test Data

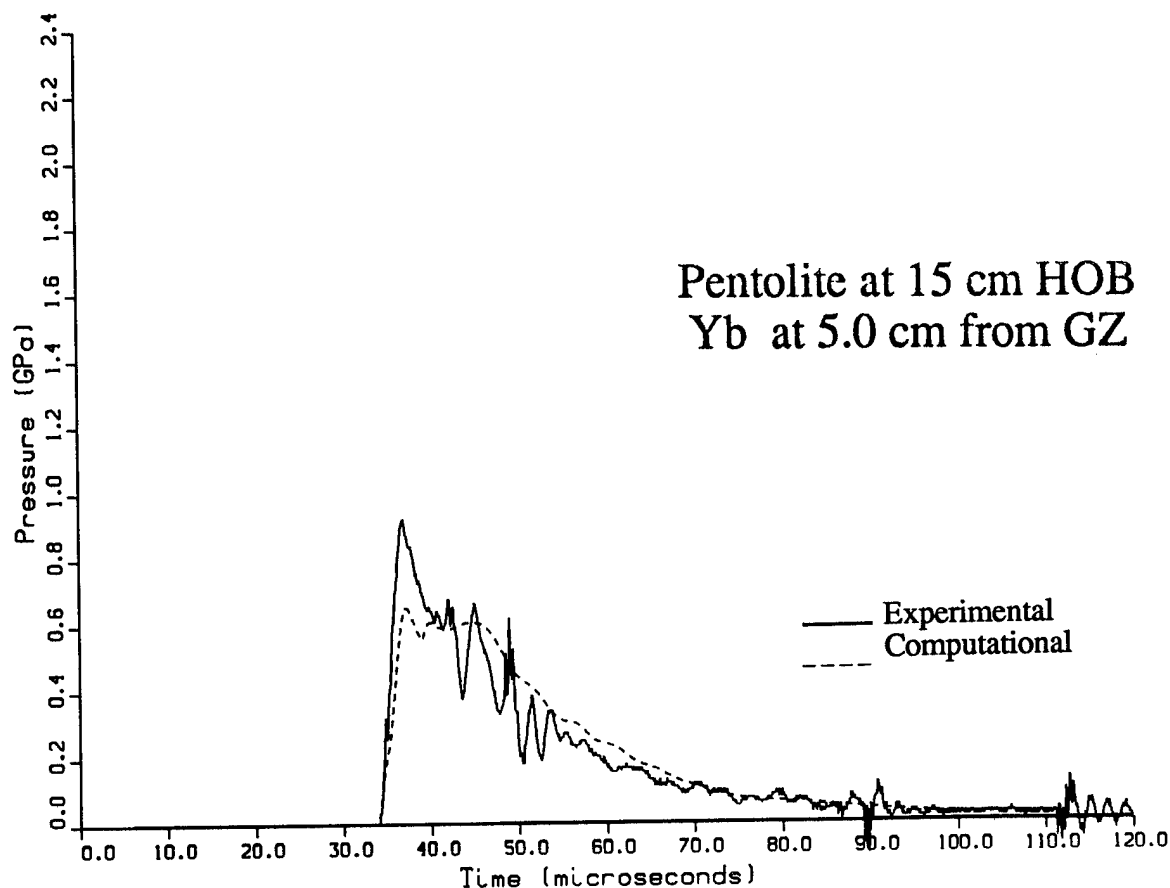


Figure 69. Computation (Dashed Line) vs. Experimental Record (Solid Line), Pentolite at 15-cm HOB, 5.0-cm Range.

Pressure Curves For Blast

Case 14B and 2a4yb1 Test Data

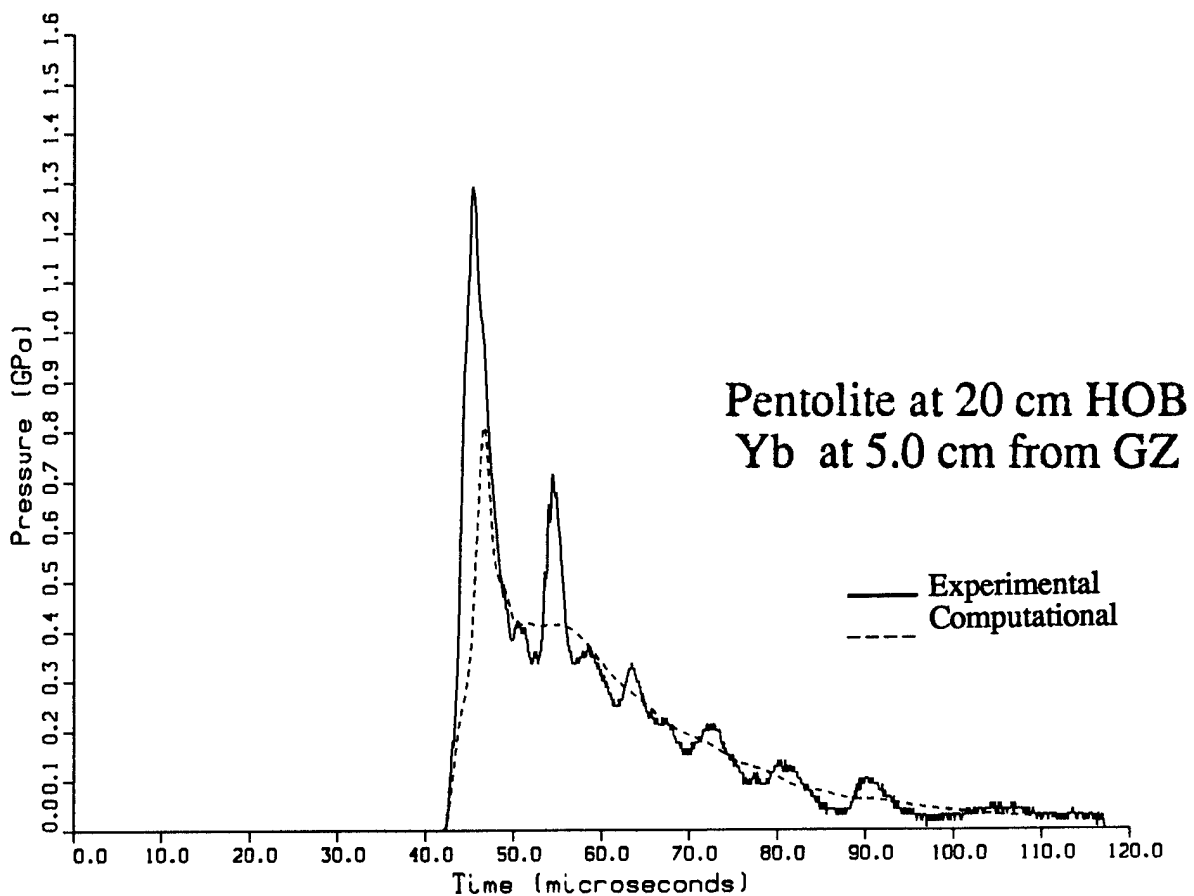


Figure 70. Computation (Dashed Line) vs. Experimental Record (Solid Line), Pentolite at 20-cm HOB, 5.0-cm Range.

Specific Impulse Curves For Blast

Case 9B and 2a5yb4 Test Data

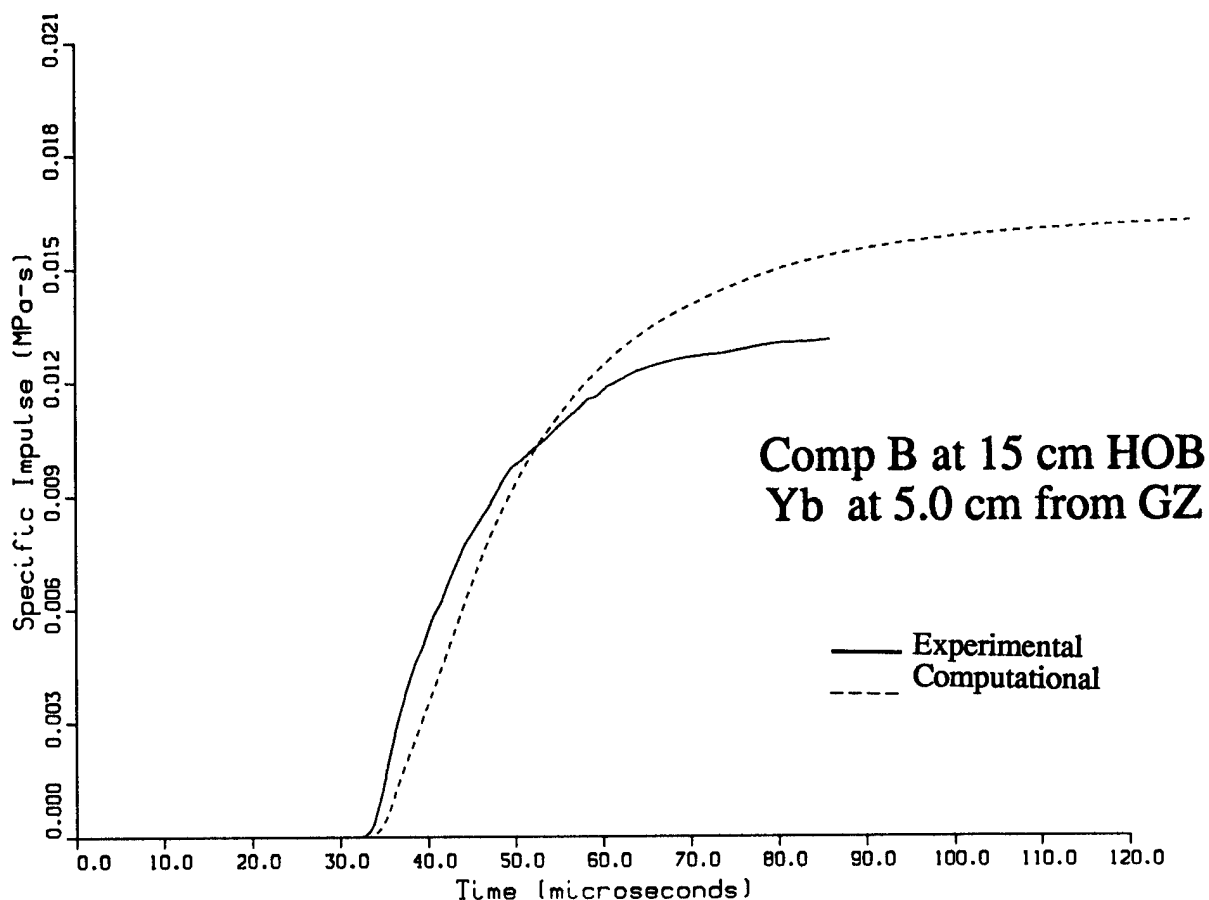


Figure 71. Computation (Dashed Line) vs. Experimental Record (Solid Line), Comp B at 15-cm HOB, 5.0-cm Range.

Specific Impulse Curves For Blast

Case 9A and 2a10yb4 Test Data

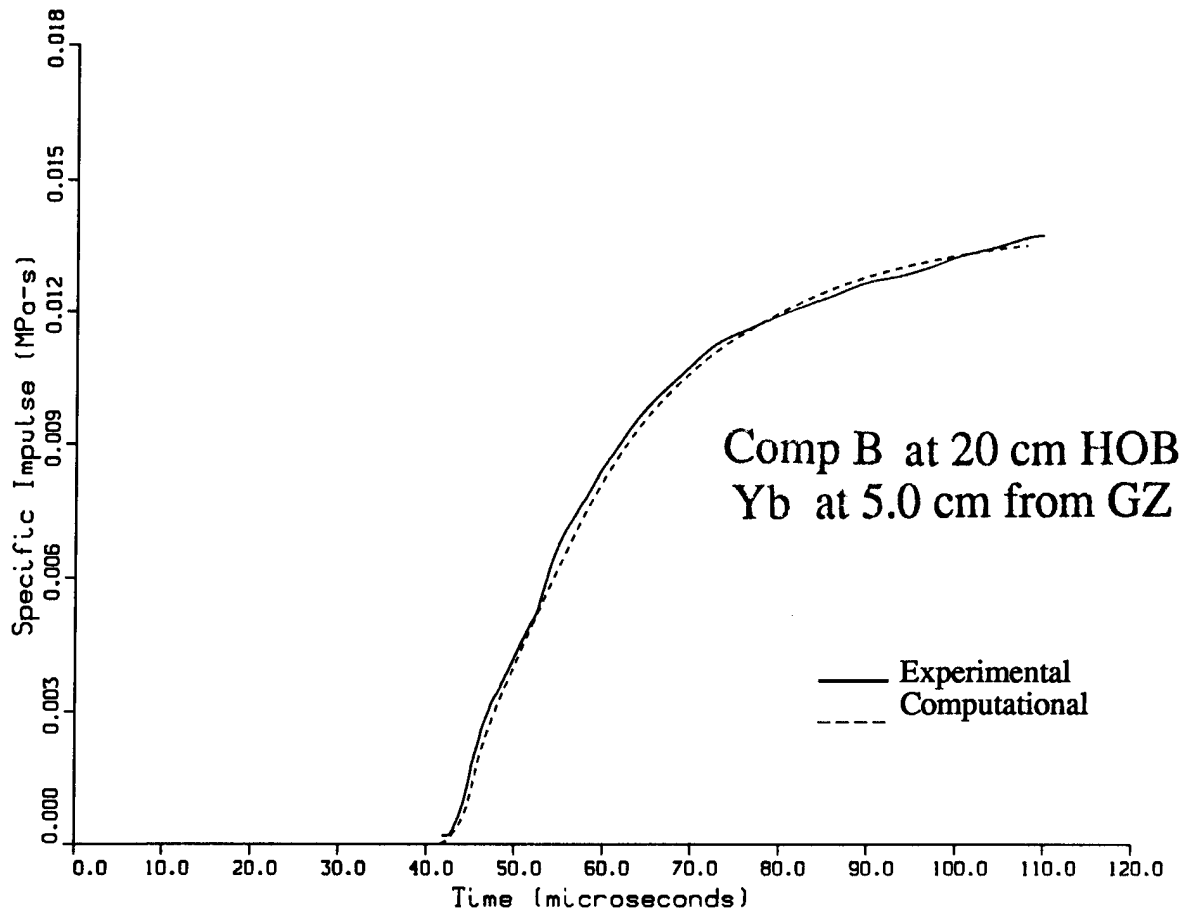


Figure 72. Computation (Dashed Line) vs. Experimental Record (Solid Line), Comp B at 20-cm HOB, 5.0-cm Range.

Specific Impulse Curves For Blast

Case 14A and 2a3yb1 Test Data

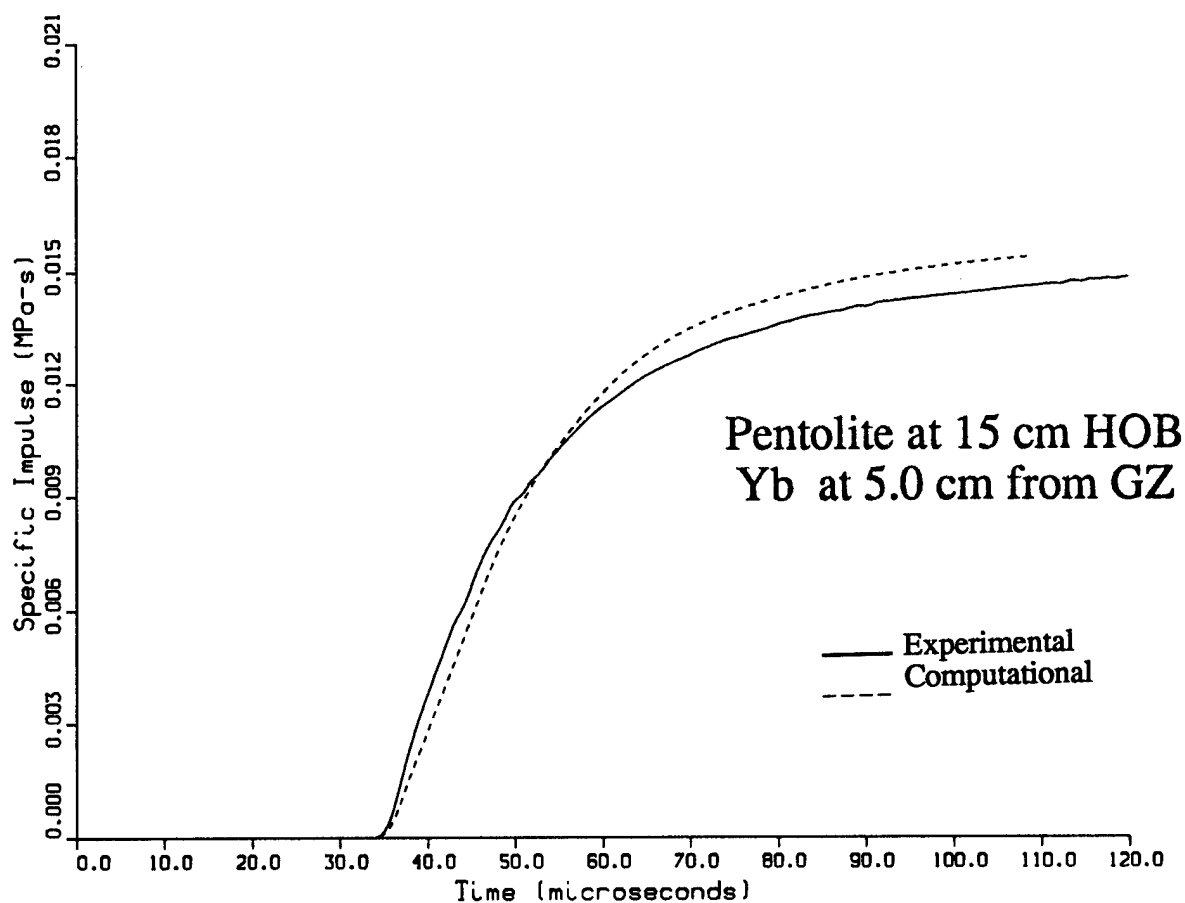


Figure 73. Computation (Dashed Line) vs. Experimental Record (Solid Line), Pentolite at 15-cm HOB, 5.0-cm Range.

Specific Impulse Curves For Blast

Case 14B and 2a4yb1 Test Data

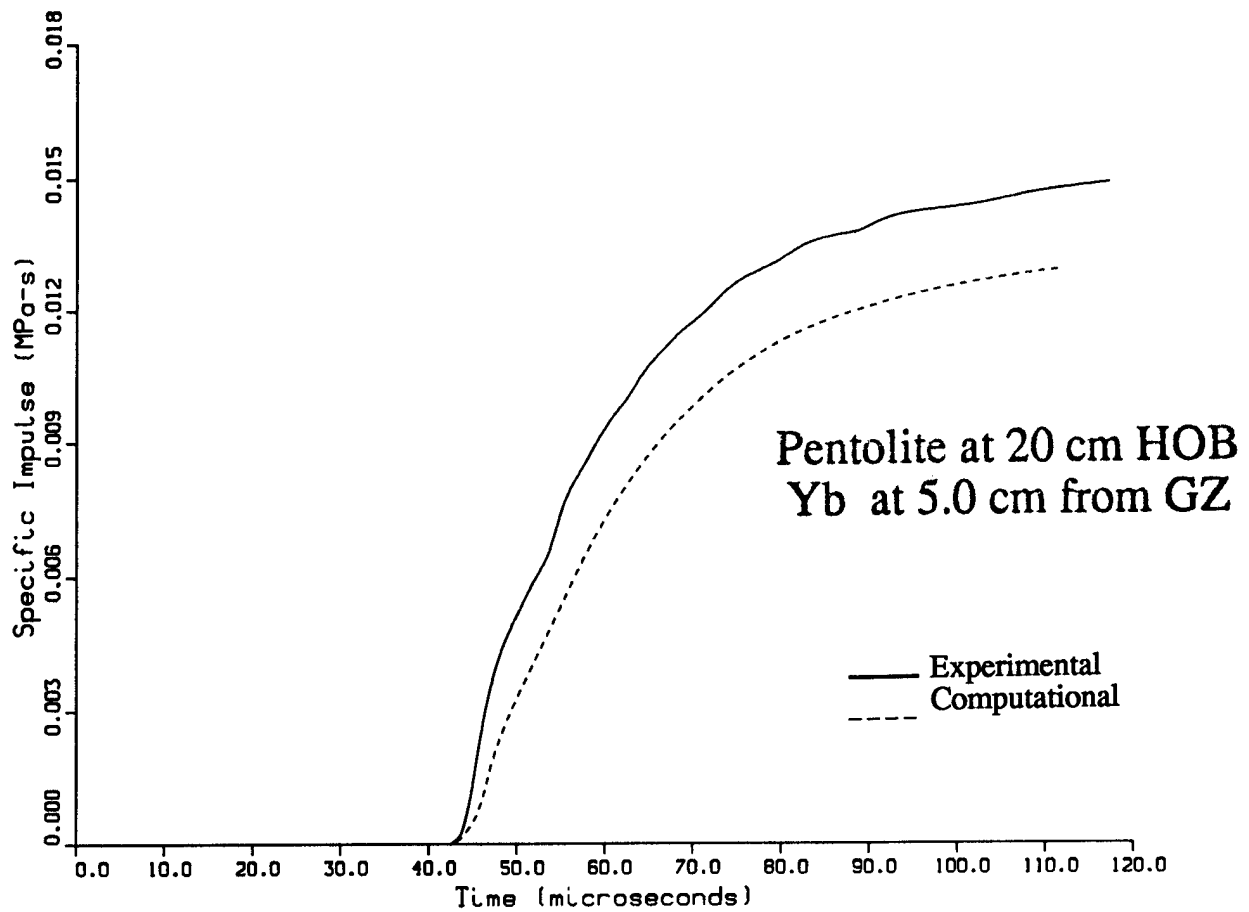


Figure 74. Computation (Dashed Line) vs. Experimental Record (Solid Line), Pentolite at 20-cm HOB, 5.0-cm Range.

4. CONCLUSIONS

Under this contract, FMC has developed an analytical model capable of generating stress and impulse histories produced from bare charge explosives at close-in ranges that compare well but with some significant variability to experimentally measured loading curves produced from actual military bare charges at close-in ranges (15 and 20 cm). Reproducible peak stresses ranging from 0.8 to 2.0 GPa were measured using ytterbium gage instrumentation. These records are the first known repeatable measurements of stress and impulse histories at close-in ranges. In addition, the use of a ballistic pendulum showed that there is an increase in total impulse delivered when a steel casing is placed around a bare military charge.

Specifically, the following results and conclusions were drawn:

- Ytterbium elements returned the highest quality and quantity of data.
- Calculated stress and impulse histories were generally higher than measured at 0- and 2.5-cm ranges from GZ and lower at 5.0-cm ranges from GZ.
- The differences observed between analytical and empirical measurements could be attributed to the different initiation schemes used.
- Records obtained from bar gages generally had fair S/N ratios and long durations but did not yield detailed stress waveforms, reproducible peak stresses or accurate TOAs and were deemed unreliable.
- Manganin elements did not return any usable stress or impulse data because the pressures present in these experiments were not within the effective range for manganin.
- Repeatable ytterbium measurements were not obtained at the 0.0-cm range from ground zero.

- Reproducible impulse plug measurements were obtained from the initial eight tests. However, data obtained from this gage type is in the form of a single total specific impulse, which made it difficult to ascertain measurement accuracy.
- The baffle constructed to house the airblast gages was not properly designed to withstand the severe environment produced in a close-in blast environment.
- The ballistic pendulum proved reliable, repeatable and relatively easy to use for measuring total impulse imparted by a charge at close-in ranges.
- A coverplate is needed surrounding the face of the pendulum to prevent blast wave wraparound.
- The total impulse delivered increased sharply as the steel casing thickness was increased from 0.0 to 6.35 mm. However, an increase in casing thickness to 9.53 mm produced only a marginal increase in total impulse.

5. RECOMMENDATIONS

Based on the results of this program, the following recommendations are provided for continuing research in the area of close-in blast:

- A computer simulation should be run with a singlepoint initiation at the center top of a bare charge. This analysis could determine if the multipoint initiation used in this program focused the charge and led to the higher peak stresses and specific impulses seen in the computations. The setup for such a run would essentially be the same as that described in this report and would require about 6 Cray hours to complete.
- Additional baseplate tests, using different explosive geometries, should be performed using the successful experimental techniques developed in this program. Such measurements would provide a more complete database and should include actual military ordnance, such as TOW missiles. Further baseplate tests should include a focused effort to determine stress-time profiles directly under the charge as well as outside of the charge diameter.

- In conjunction with additional baseplate tests, the analytical model developed in this program should be used to simulate the loadings produced by actual military ordnance.
- Ytterbium elements should be used exclusively for any future experiments conducted in this regime.
- A smaller, more robust airblast baffle should be designed for any future tests.
- Impulse plug gages should either not be used or the impulse plug photodiode housing should be redesigned for any future tests.

INTENTIONALLY LEFT BLANK.

6. REFERENCES

1. R.E. Lottero and J.D. Wortman, "Computational Predictions of Close-In Blast Loading from Bare Spherical Charges," Proceedings of the 1988 Army Science Conference, Ft. Monroe, Virginia, October 26-27, 1988.
2. J.W. Kury, H.C. Hornig, E.L. Lee, J.L. McDonnell, D.L. Ornellas, M. Finger, F.M. Strange, and M.L. Wilkins, "Metal Acceleration by Chemical Explosives," Proceedings of the Fourth Symposium (International) on Detonation, ACR-126, U.S. Naval Ordnance Laboratory, White Oak, Maryland, October 12-15, 1965.
3. D.A. Matuska, and J.J. Osborn, "HULL Technical Manual," vol. 1, Orlando Technology, Inc., P. O. Box 815, Shalimar, Florida, 1986.
4. J.E. Crepeau, H.J. Happ, C.E. Needham, and S. Hikida, "HULL Computer Calculations of Bare Spherical HE Charges Detonated over a Reflecting Surface," SSS-88-9181 under BRL contract DAAL03-86-D-0001, S-Cubed, La Jolla, California, December 1987.
5. B.M. Dobratz and P.C. Crawford (Editors), "LLNL Explosives Handbook, Properties of Chemical Explosives and Explosive Simulants," UCRL-52997, Change 2, Lawrence Livermore National Laboratory, University of California, Livermore, California January 31, 1985.
6. N.J. Huffington and W.O. Ewing, "Reflected Impulse Near Spherical Charges," BRL-TR-2678, U. S. Army Ballistic Research Laboratory, Aberdeen Proving Ground, Maryland, September 1985.
7. S.A. Mullin, E.D. Esparza, L.R. Garza, "Explosive Shock Test: Fixture Design, Operational Procedures, Test Results," prepared for FMC Corporation by Southwest Research Institute under project 06-1882, December 1987.
8. C.E. Anderson, Jr., P.E. O'Donoghue, P. A. Cox, S.A. Mullin, "Explosive Loading of Metal and Composite Panels: Comparisons of Experiments and Numerical Simulations," prepared for FMC Corporation by Southwest Research Institute under project 06-1882, January 1988.
9. S.A. Mullin and E.D. Esparza, "Explosive Shock Testing: Materials Evaluation," prepared by Southwest Research Institute for FMC Corporation under project 06-2403, January 1989.
10. S.A. Mullin, G.J. Friesenhahn, E.D. Esparza, "Explosive Shock Testing: Close Proximity Blast Measurements," prepared by Southwest Research Institute for FMC Corporation under project 06-2403, April 1989.
11. D. D. Keough, 1991, personal communication.

12. J. Ginsberg, "Effects of Stress on the Electrical Resistance of Ytterbium and Calibration of Ytterbium Stress Transducers," Stanford Research Institute, Menlo Park, California, Final Report DNA001-72-C-0146 (1973).
13. P. W. Bridgman, Proc. Amer. Acad. Arts Sci., vol. 47, p. 321, 1911.
14. D. Bernstein and D. D. Keough, J. Appl. Phy., vol. 35, p. 1471-1474, 1964.

APPENDIX A:

STRESS AND IMPULSE HISTORIES
FROM YTTERBIUM AND MANGANIN ELEMENTS,
BASEPLATE TESTS 2A.1-2A.12

INTENTIONALLY LEFT BLANK.

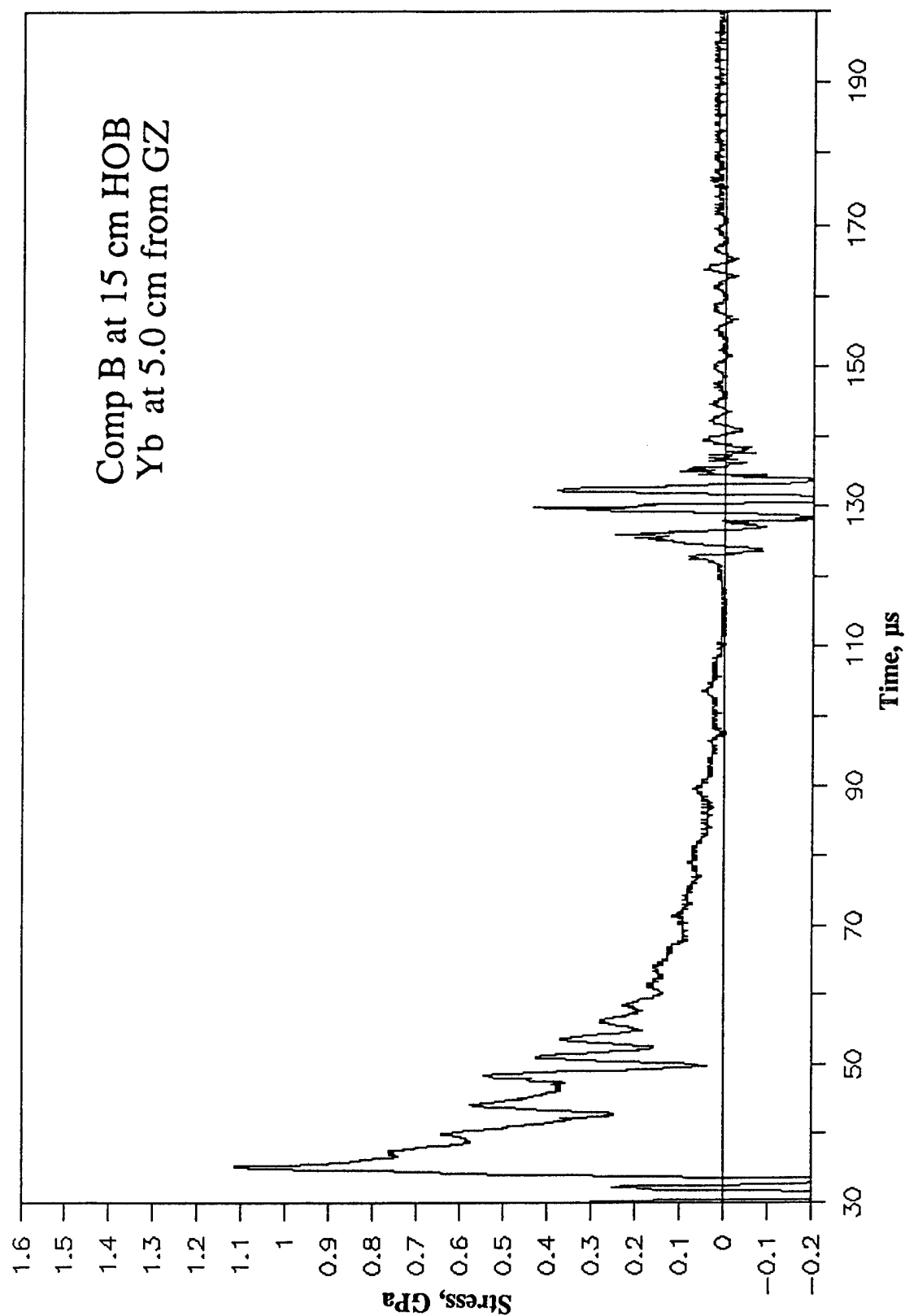


Figure A-1. Stress-Time Record From Ytterbium Element Yb-1, 5.0 cm From Centerline, Baseplate Test 2A.1, Comp B at 15-cm HOB.

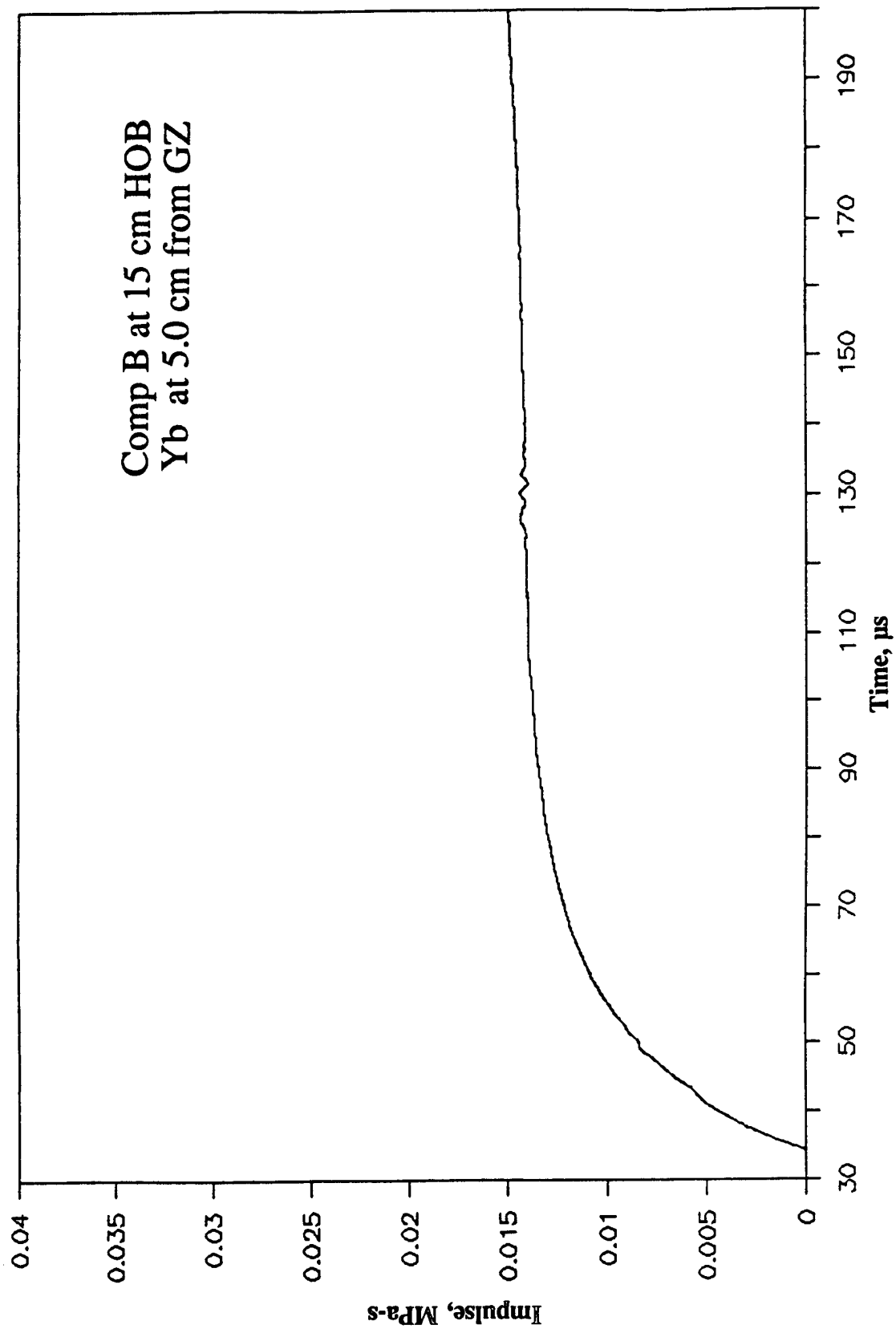


Figure A-2. Impulse-Time Record From Ytterbium Element Yb-1, 5.0 cm From Centerline, Baseplate Test 2A.1, Comp B at 15-cm HOB.

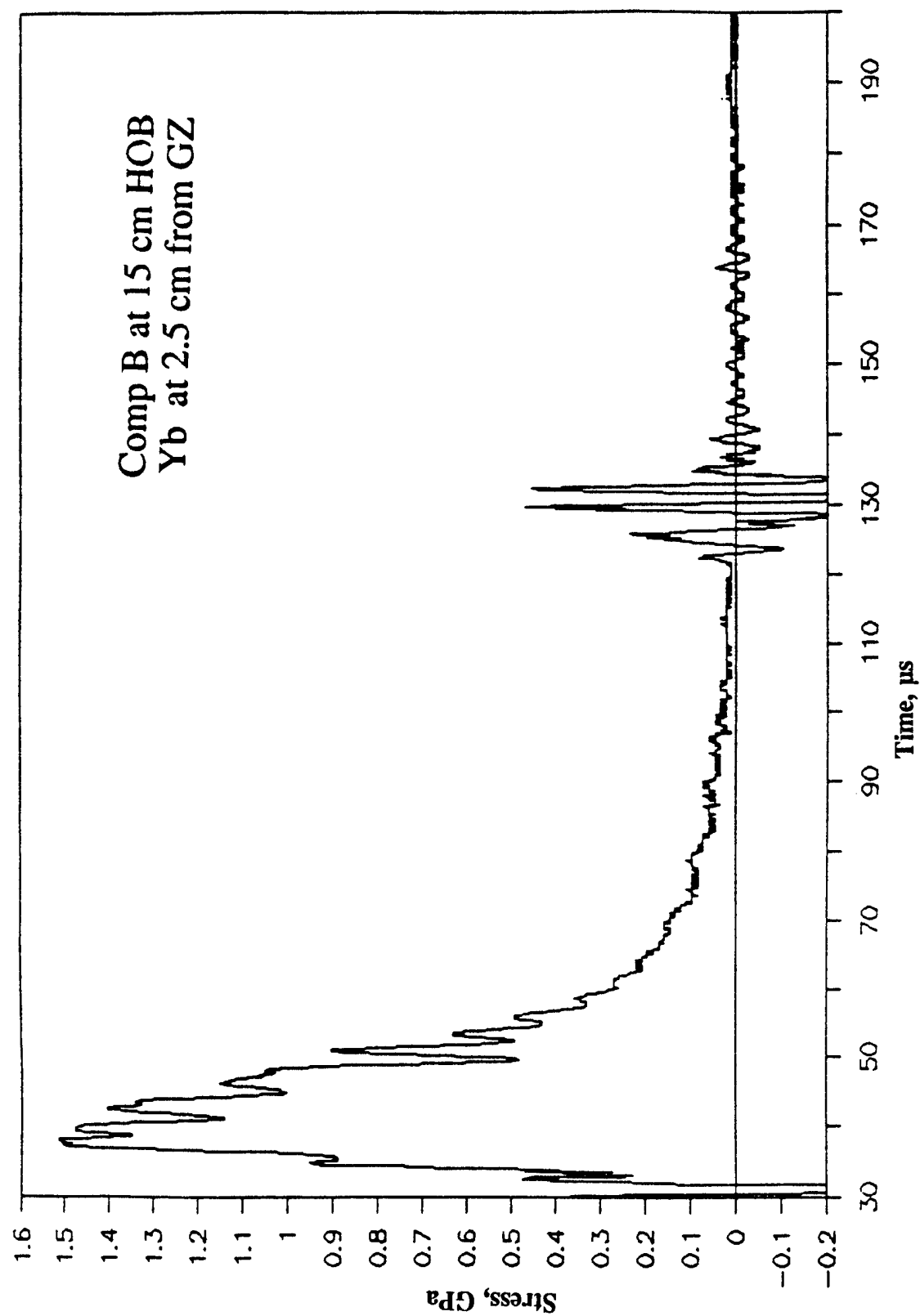


Figure A-3. Stress-Time Record From Ytterbium Element Yb-3, 2.5 cm From Centerline, Baseplate Test 2A.1, Comp B at 15-cm HOB.

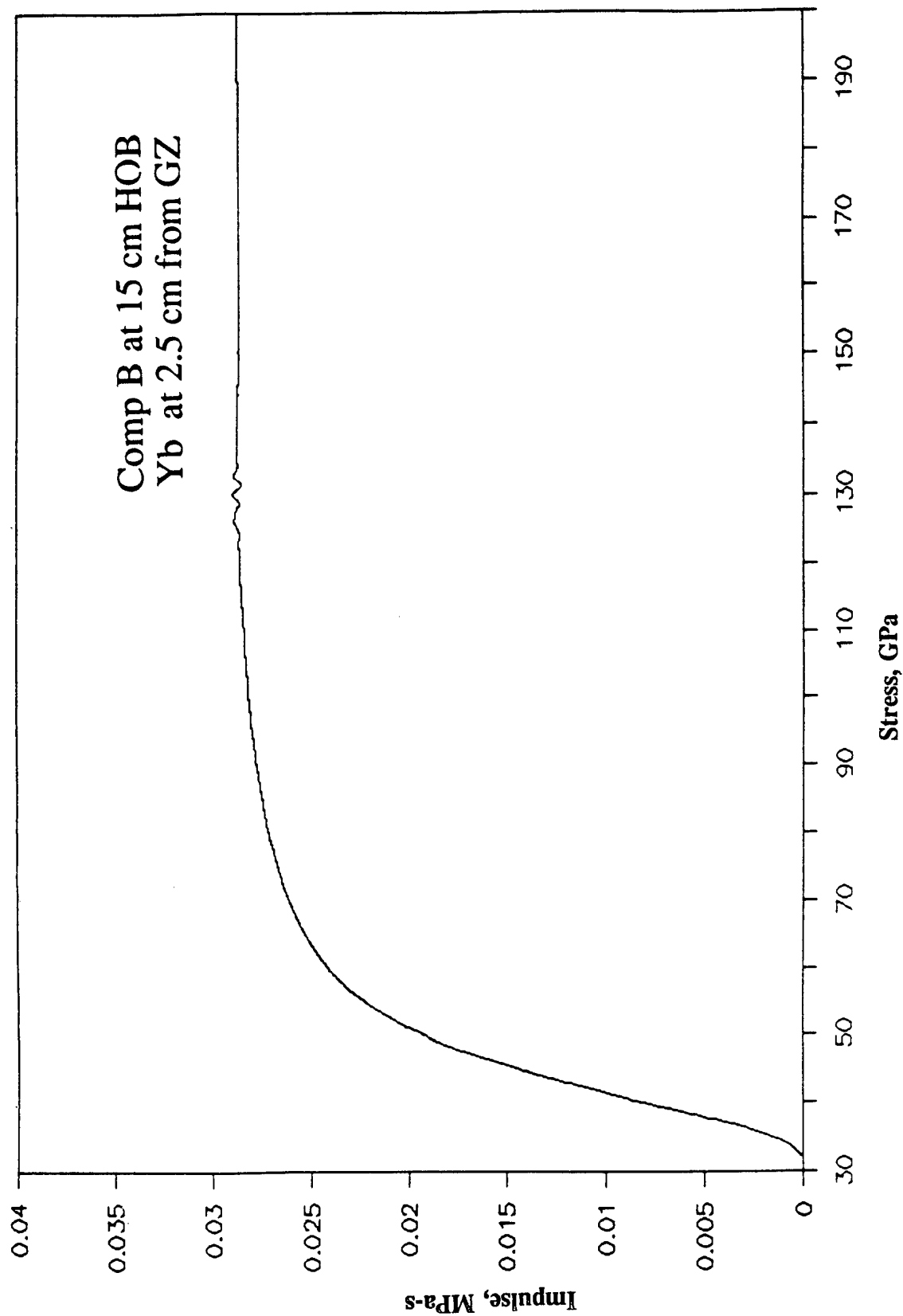


Figure A-4. Impulse-Time Record From Ytterbium Element Yb-3, 2.5 cm From Centerline, Baseplate Test 2A.1, Comp B at 15-cm HOB.

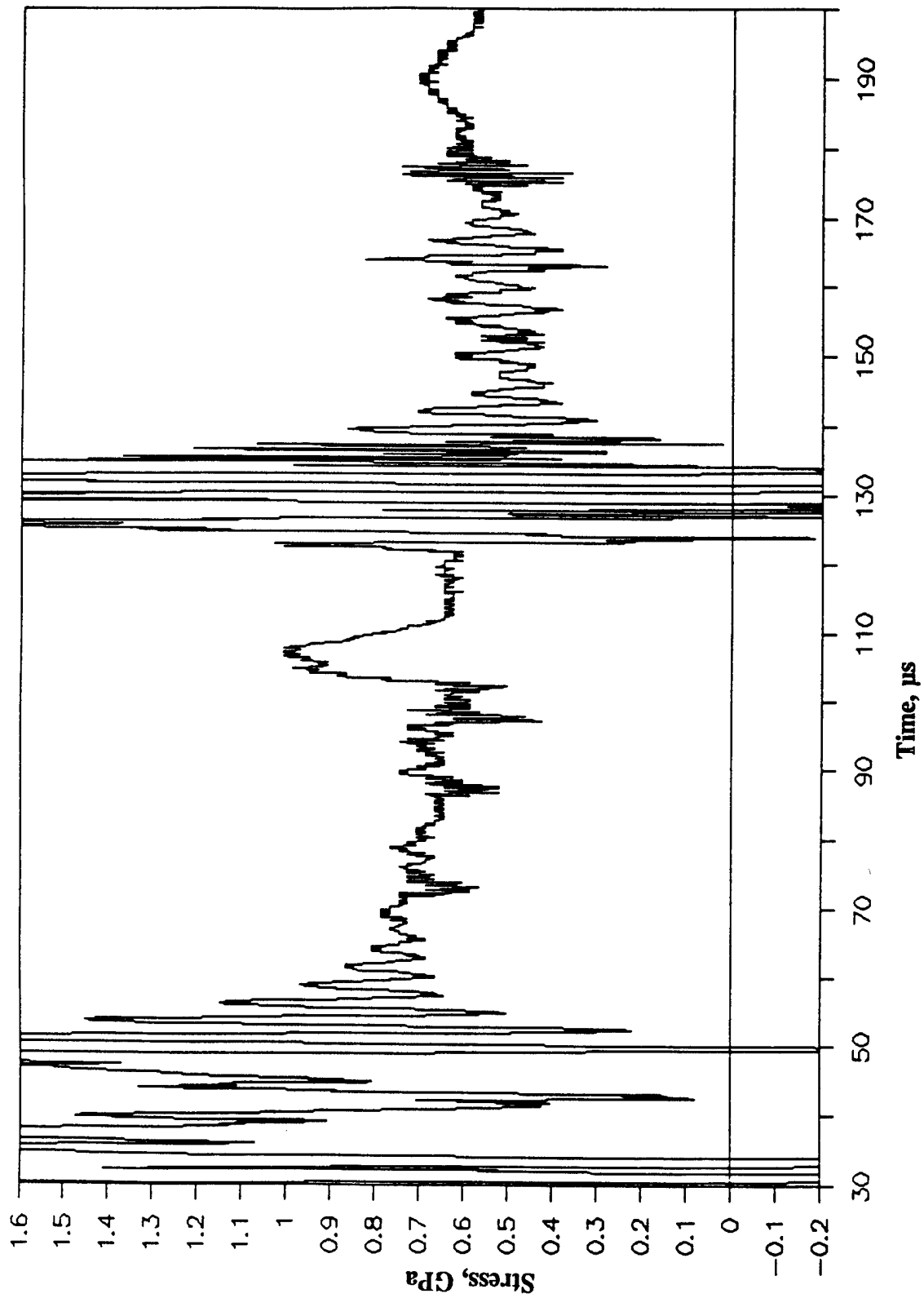


Figure A-5. Stress-Time Record From Manganin Element Mn-2, 2.5 cm From Centerline, Baseplate Test 2A.1, Comp B at 15-cm HOB.

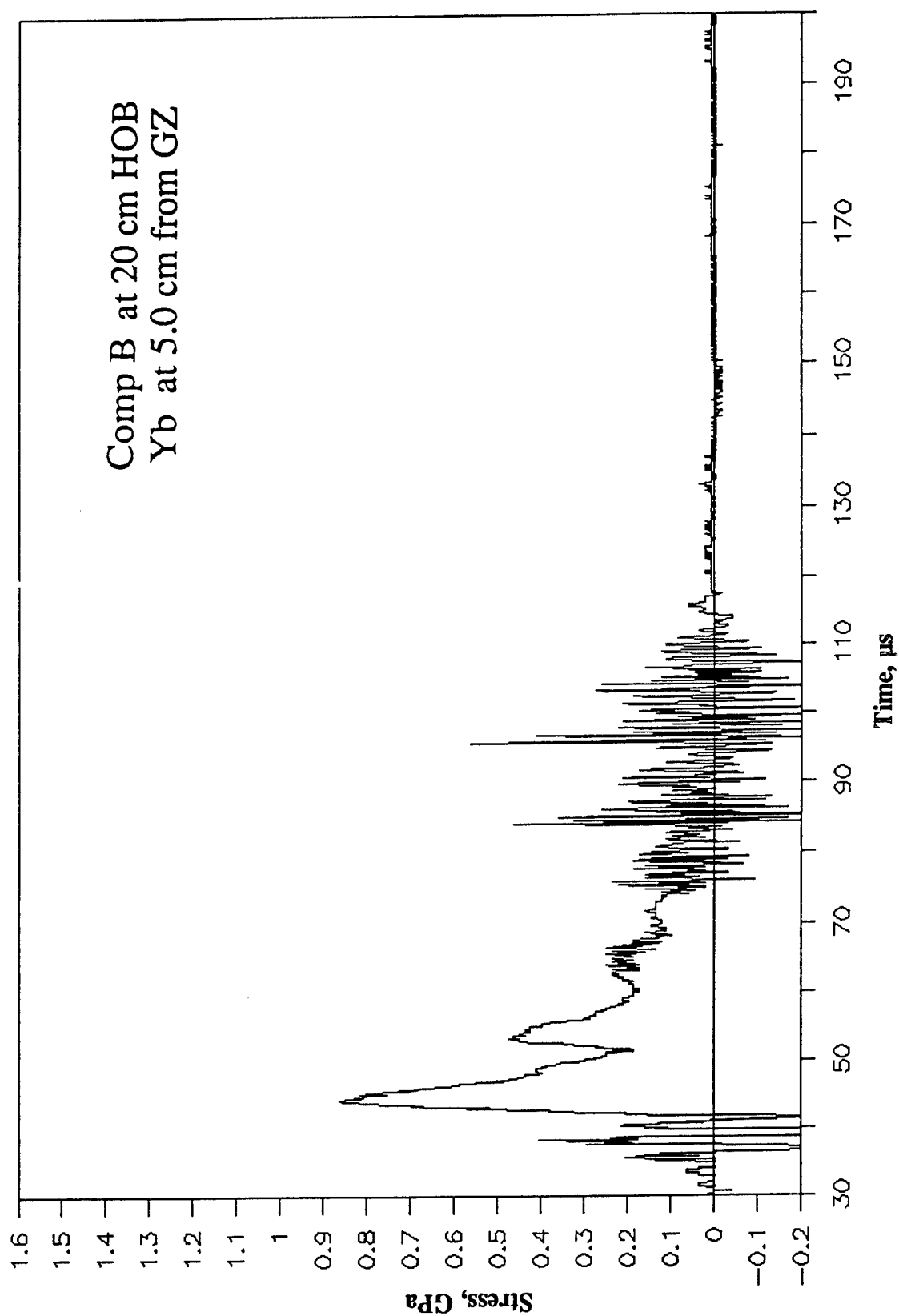


Figure A-6. Stress-Time Record From Ytterbium Element Yb-1, 5.0 cm From Centerline, Baseplate Test 2A.2, Comp B at 20-cm HOB.

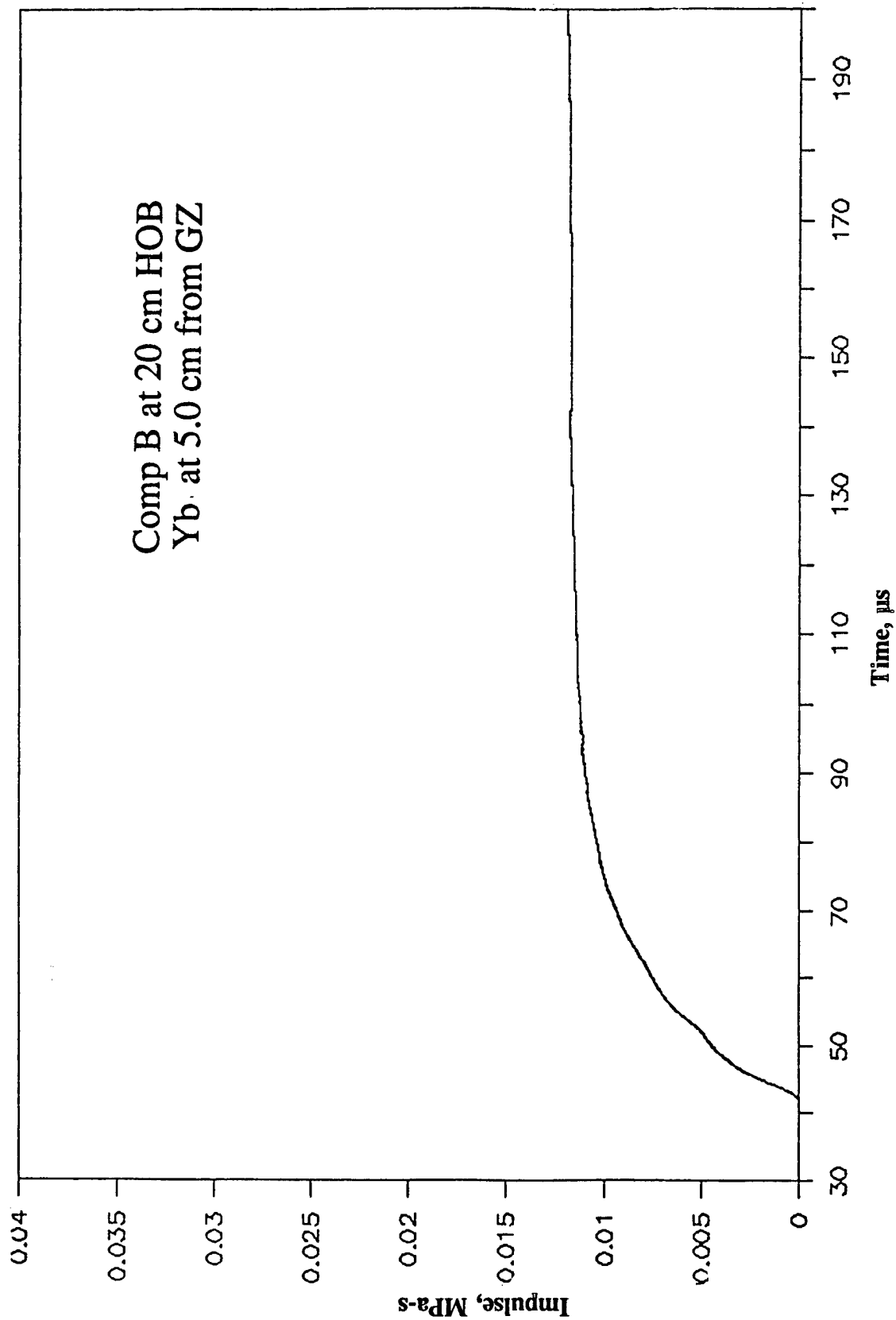


Figure A-7. Impulse-Time Record From Ytterbium Element Yb-1, 5.0 cm From Centerline, Baseplate Test 2A.2, Comp B at 20-cm HOB.

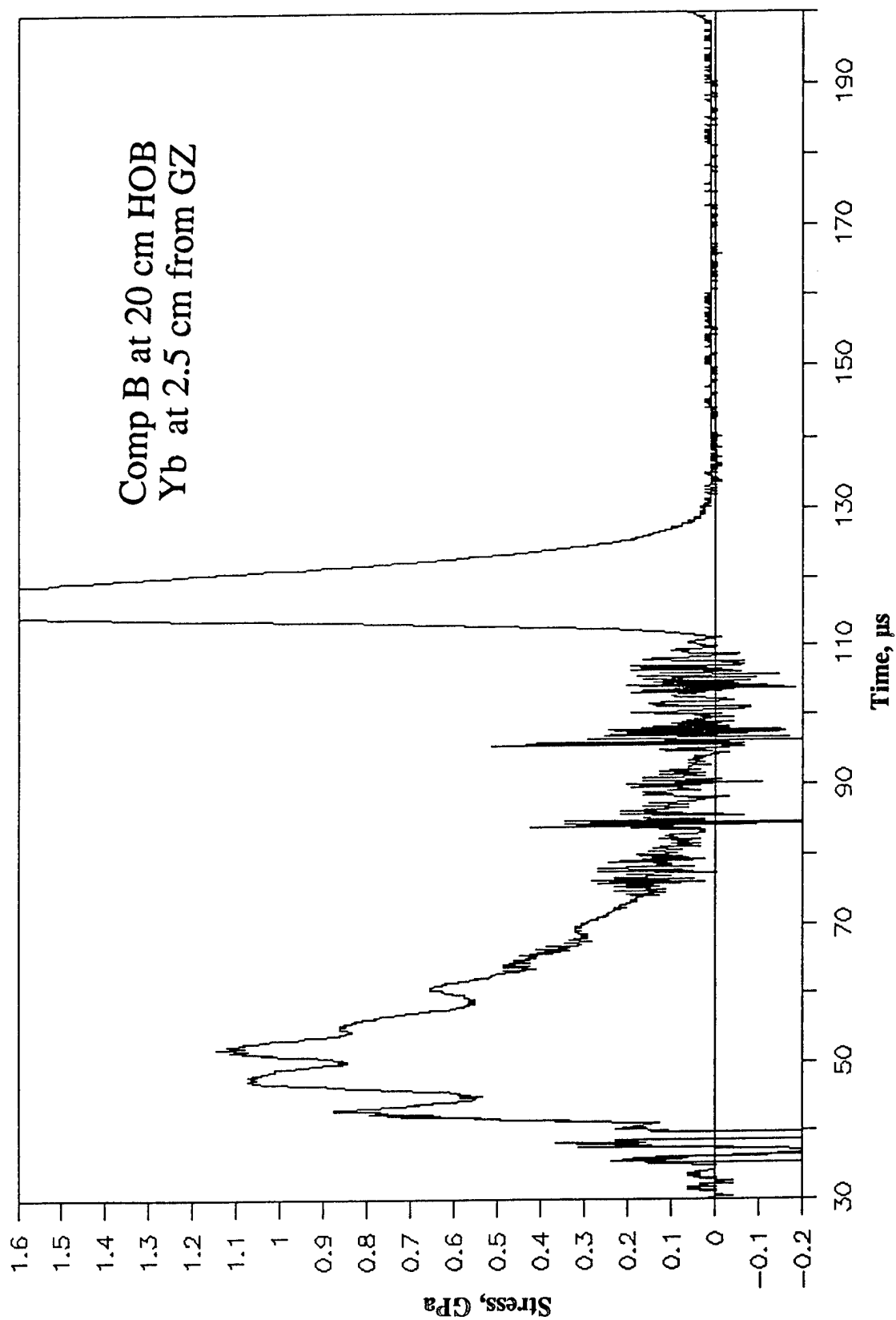


Figure A-8. Stress-Time Record From Ytterbium Element Yb-3, 2.5 cm From Centerline, Baseplate Test 2A.2, Comp B at 20-cm HOB.

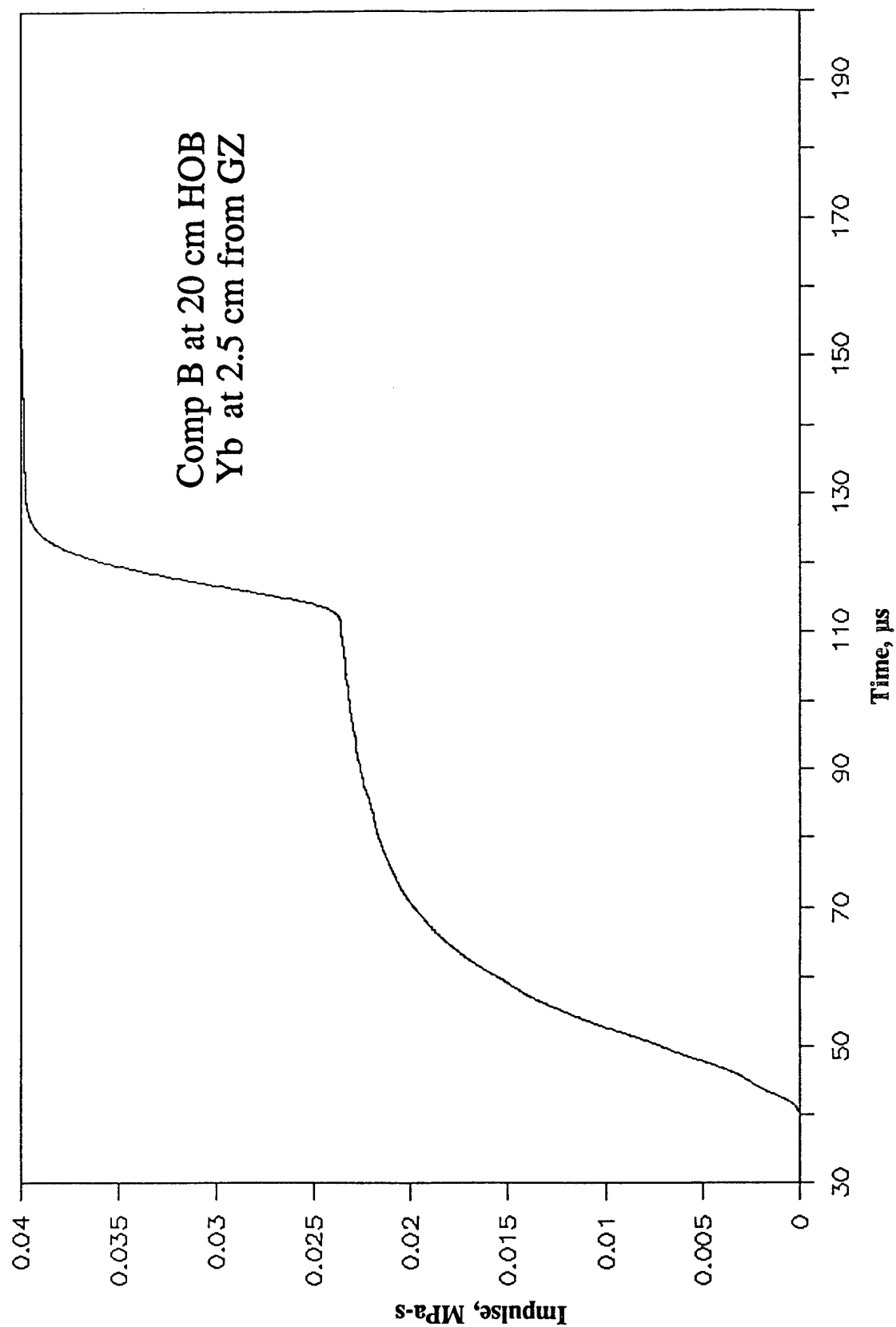


Figure A-9. Impulse-Time Record From Ytterbium Element Yb-3, 2.5 cm From Centerline, Baseplate Test 2A.2, Comp B at 20-cm HOB.

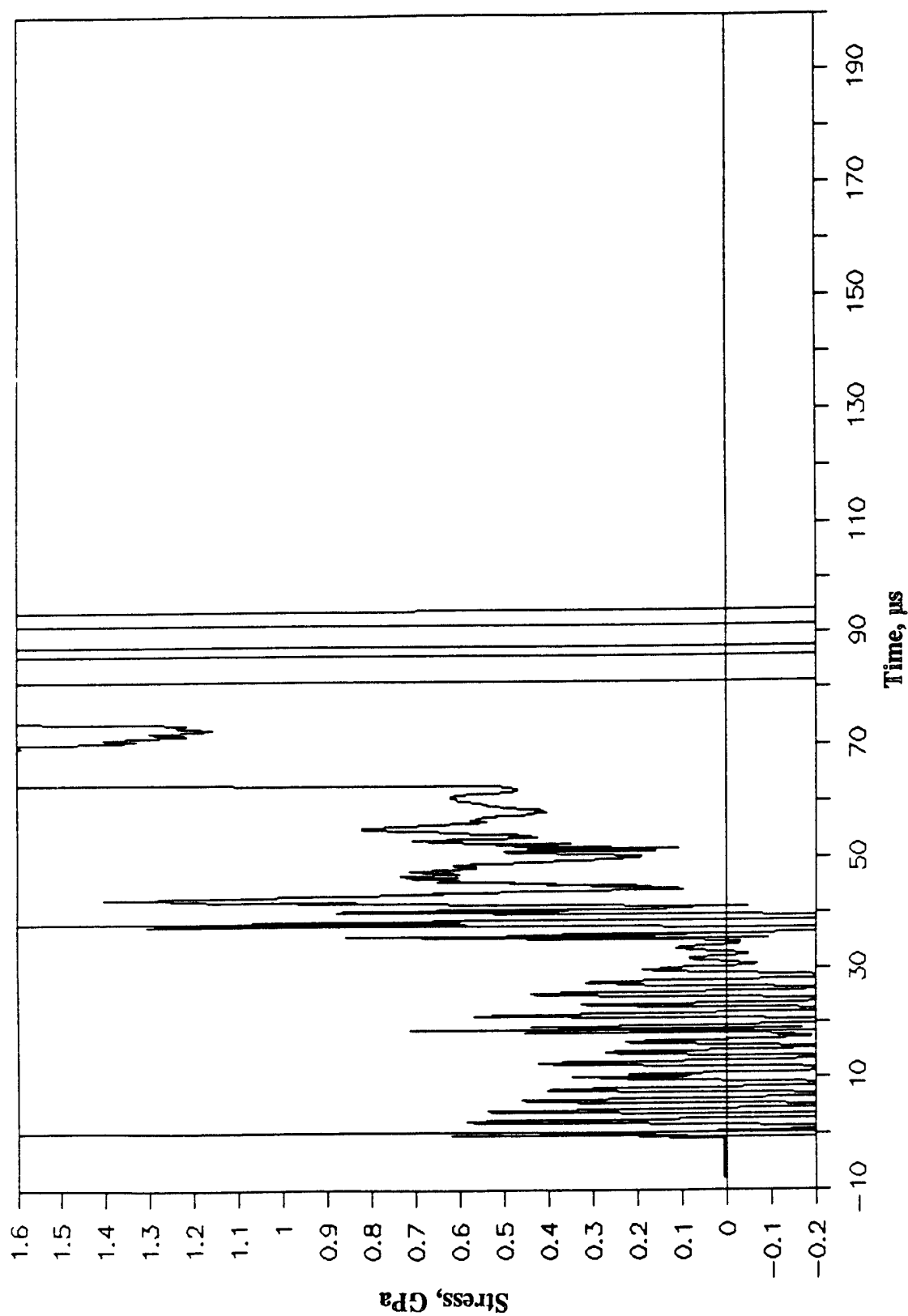


Figure A-10. Stress-Time Record From Manganin Element Mn-4, 5.0 cm From Centerline, Baeplate Test 2A.2, Comp B at 20-cm HOB.

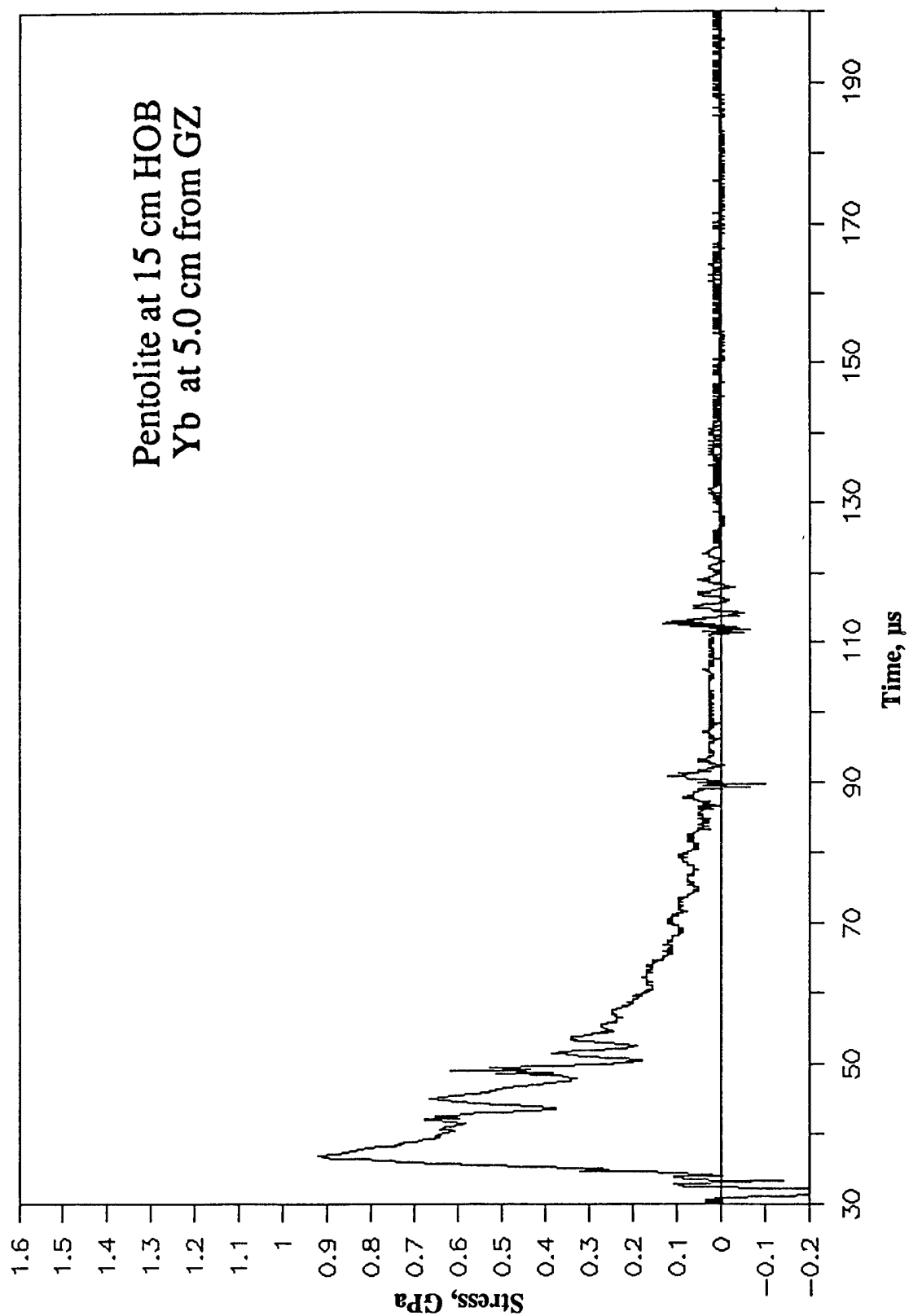


Figure A-11. Stress-Time Record From Ytterbium Element Yb-1, 5.0 cm From Centerline, Baseplate Test 2A.3, Pentolite at 15-cm HOB.

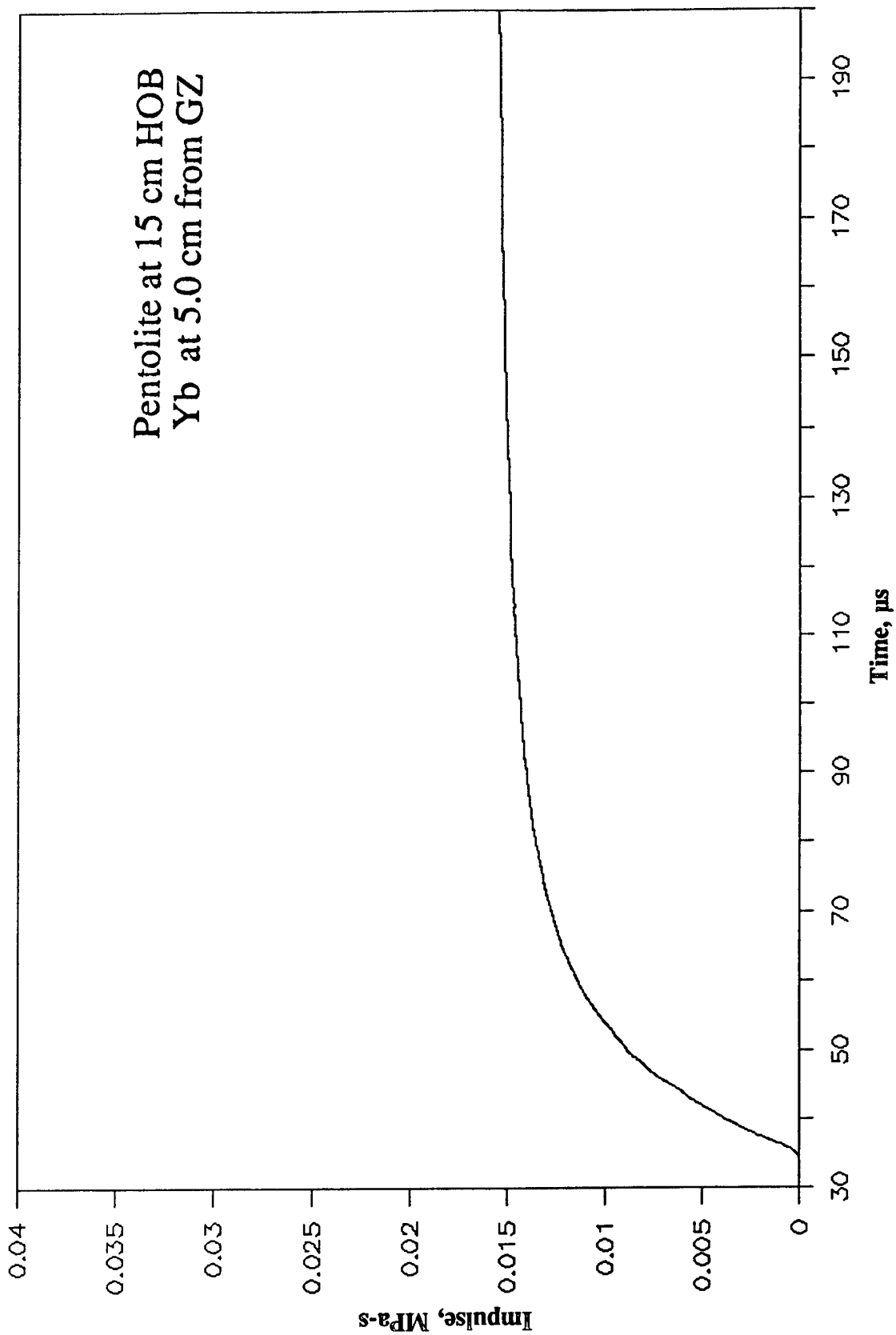


Figure A-12. Impulse-Time Record From Ytterbium Element Yb-1, 5.0 cm From Centerline, Baseplate Test 2A.3, Pentolite at 15-cm HOB.

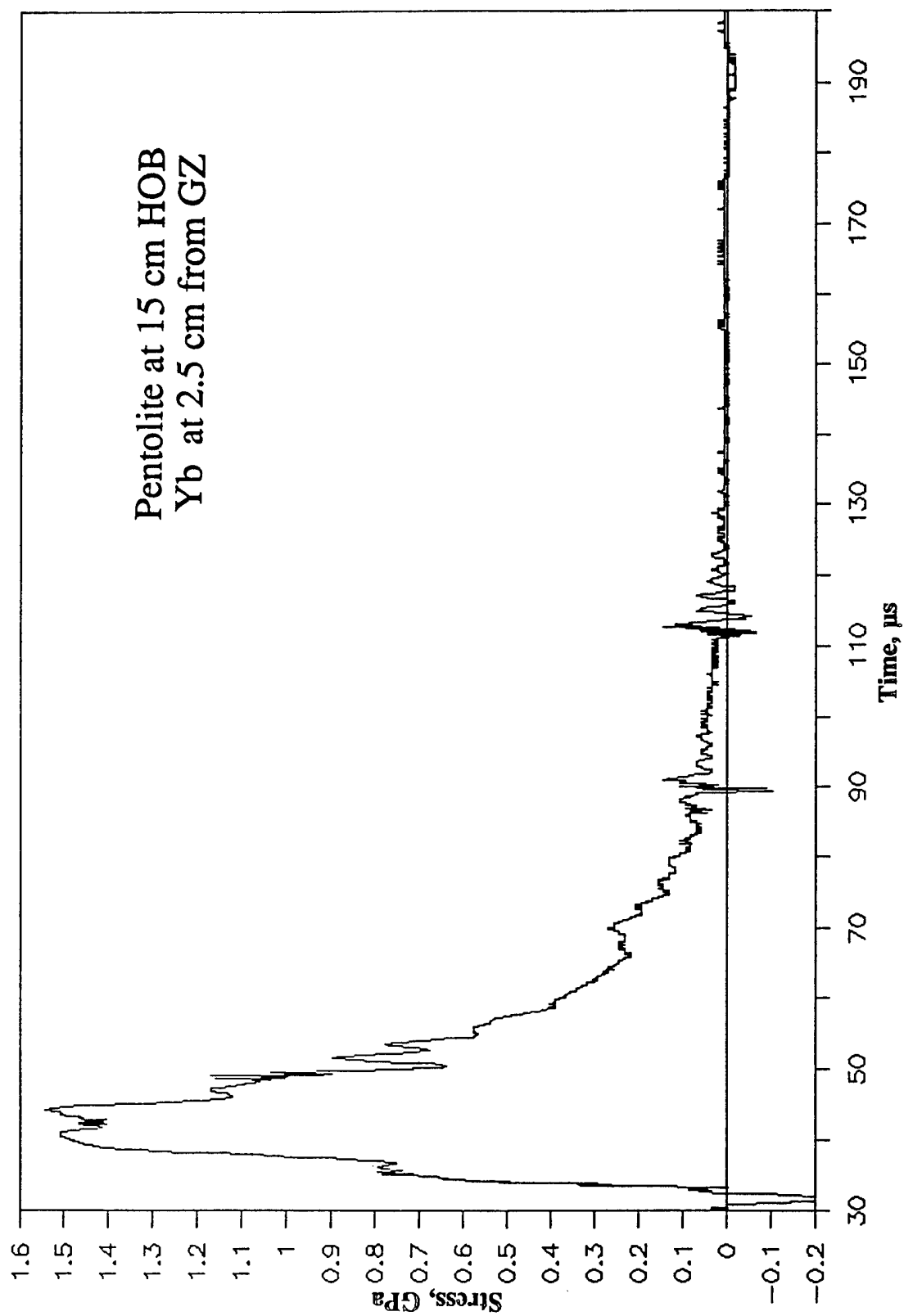


Figure A-13. Stress-Time Record From Ytterbium Element Yb-3, 2.5 cm From Centerline, Baseplate Test 2A.3, Pentolite at 15-cm HOB.

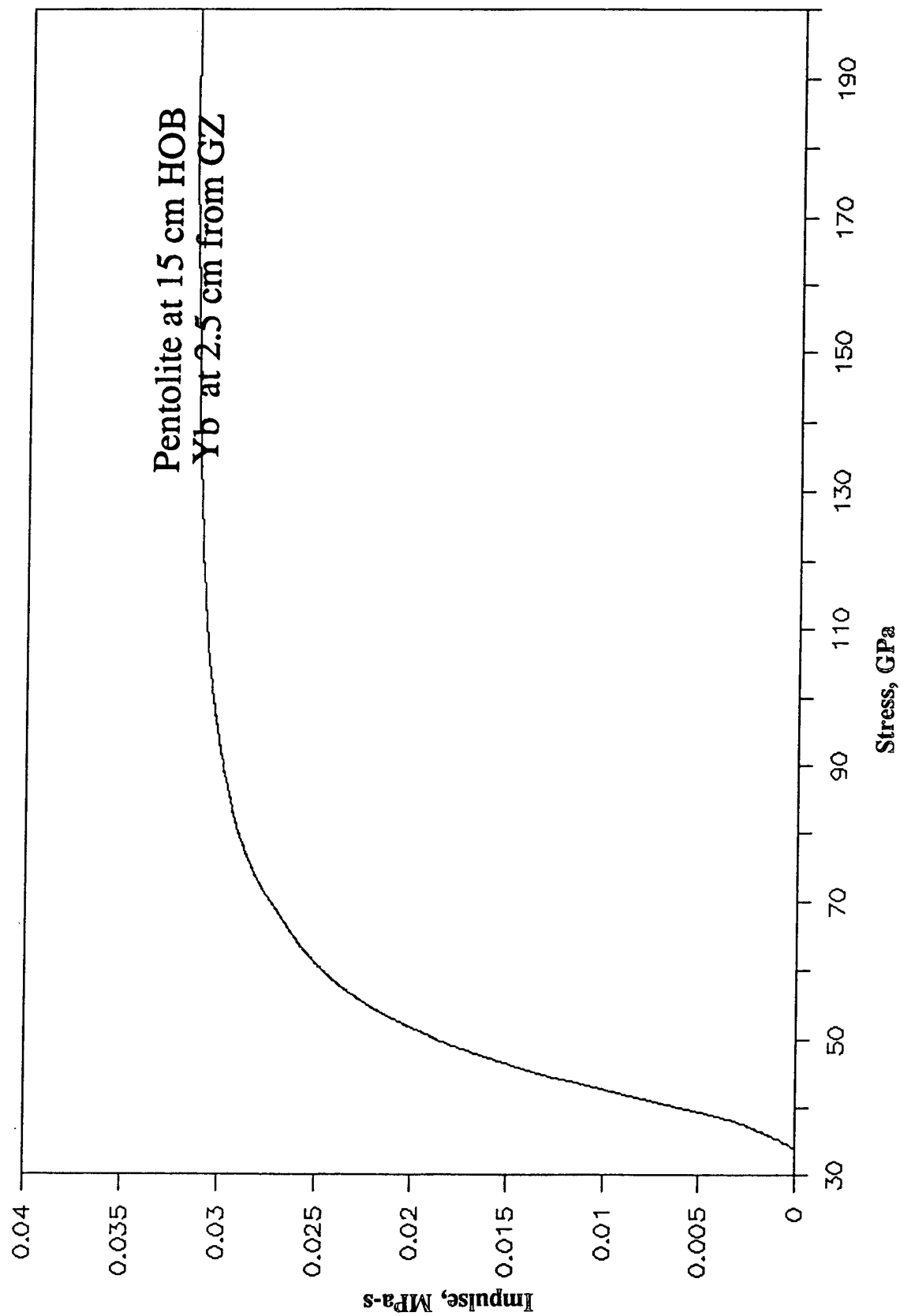


Figure A-14. Impulse-Time Record From Ytterbium Element Yb-3, 2.5 cm From Centerline, Baseplate Test 2A.3, Pentolite at 15-cm HOB.

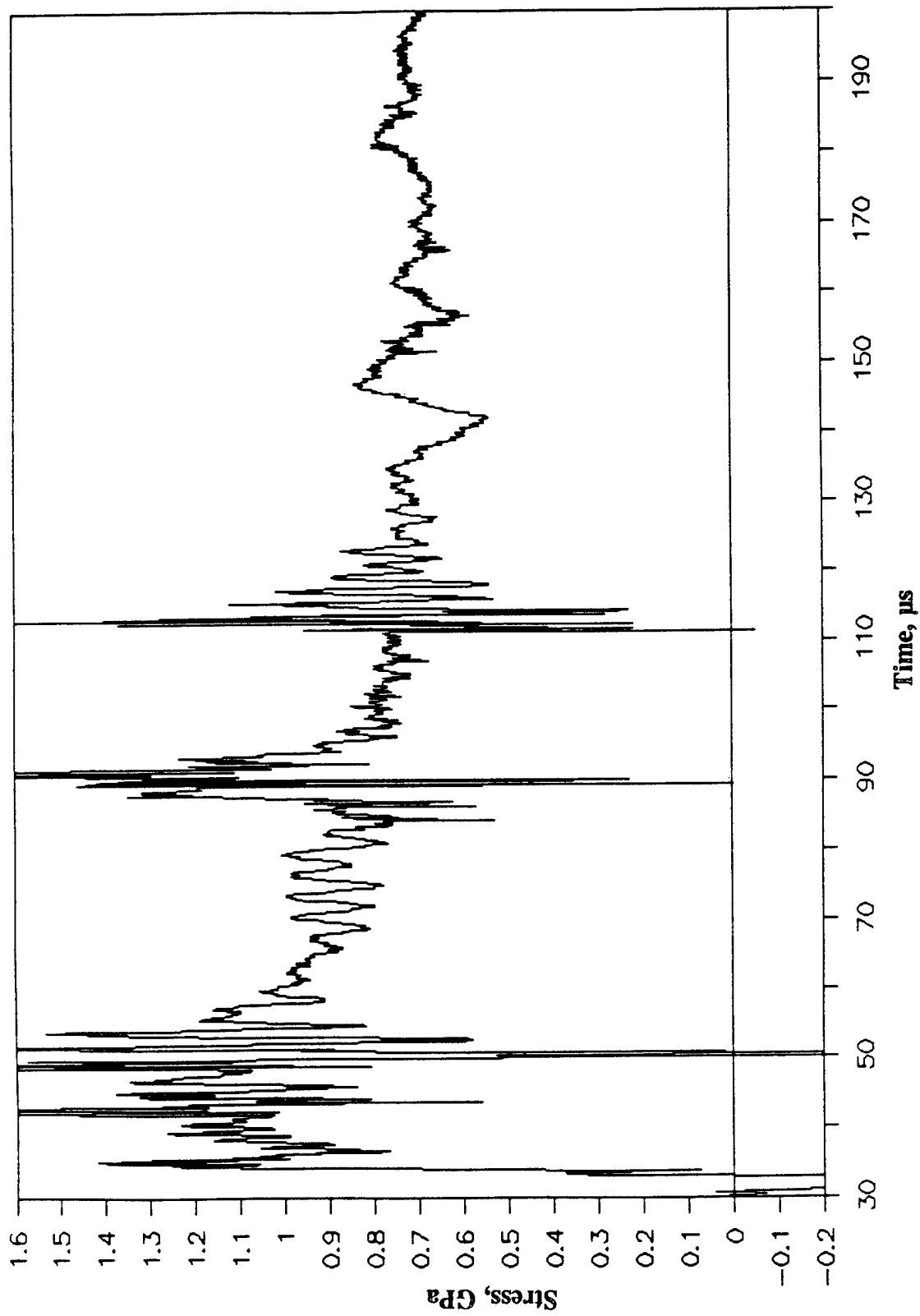


Figure A-15. Stress-Time Record From Manganin Element Mn-2, 2.5 cm From Centerline, Baseplate Test 2A.3, Pentolite at 15-cm HOB.

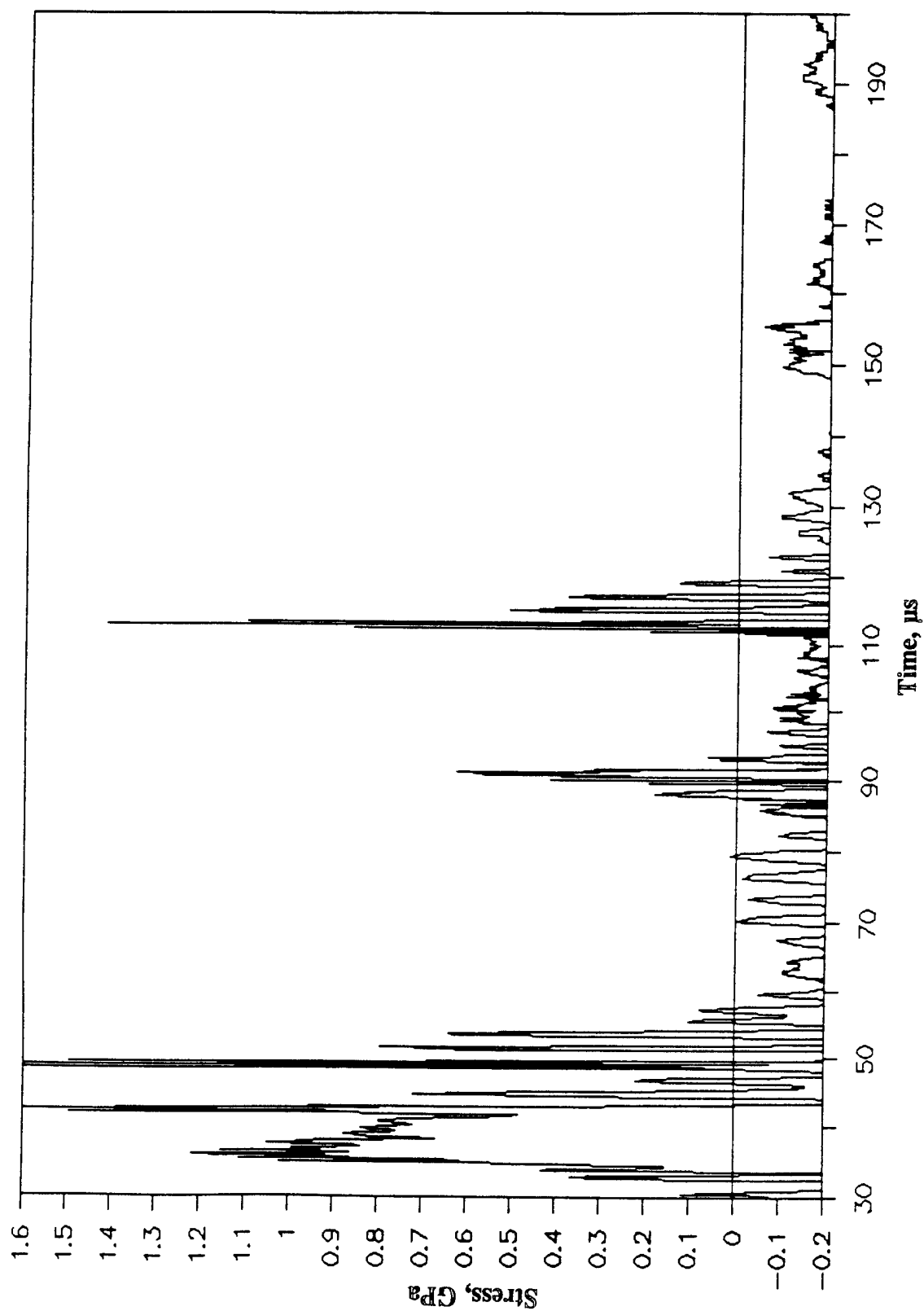


Figure A-16. Stress-Time Record From Manganin Element Mn-4, 5.0 cm From Centerline, Baseplate Test 2A.3, Pentolite at 15-cm HOB.

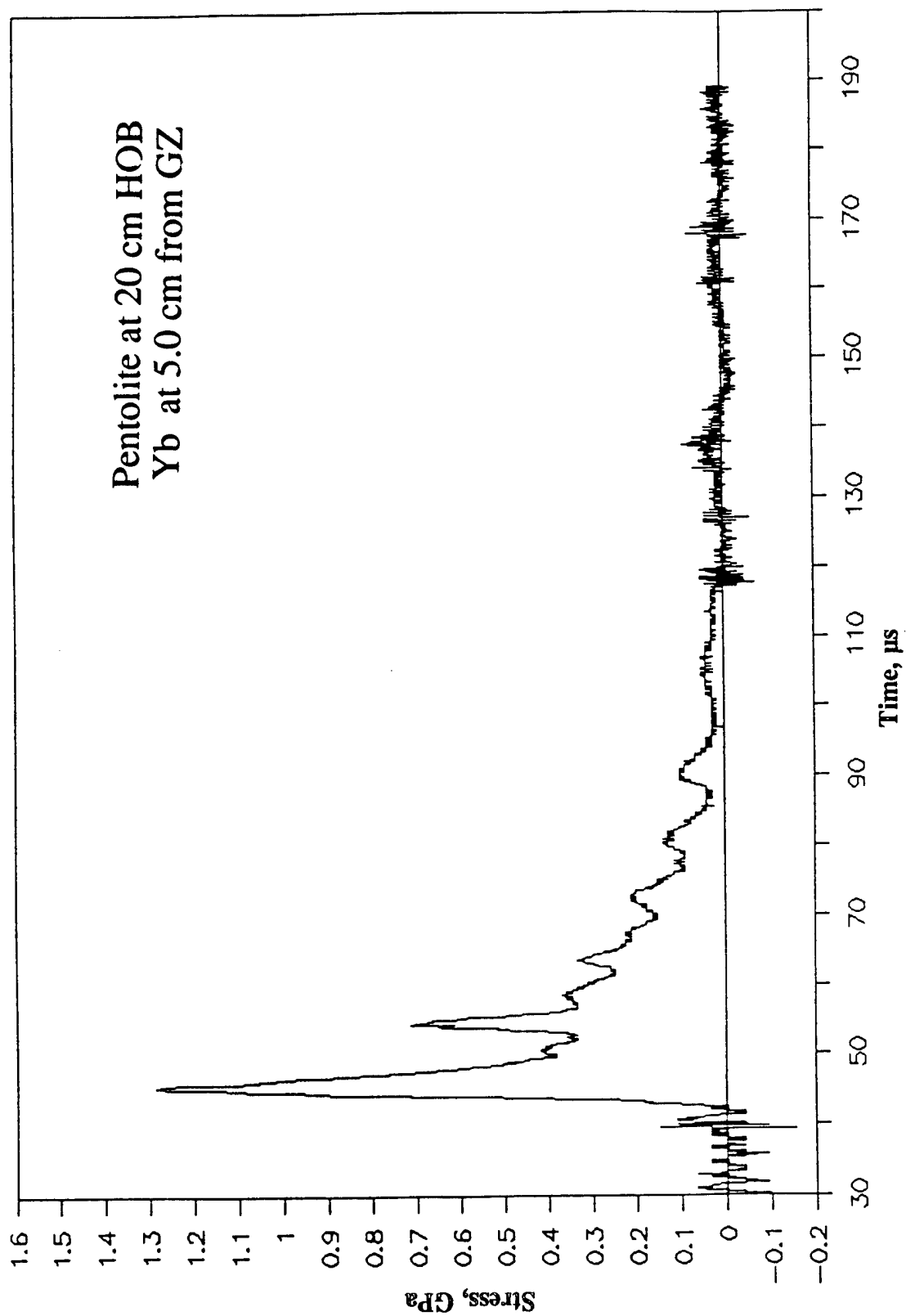


Figure A-17. Stress-Time Record From Ytterbium Element Yb-1, 5.0 cm From Centerline, Baseplate Test 2A.4, Pentolite at 20-cm HOB.

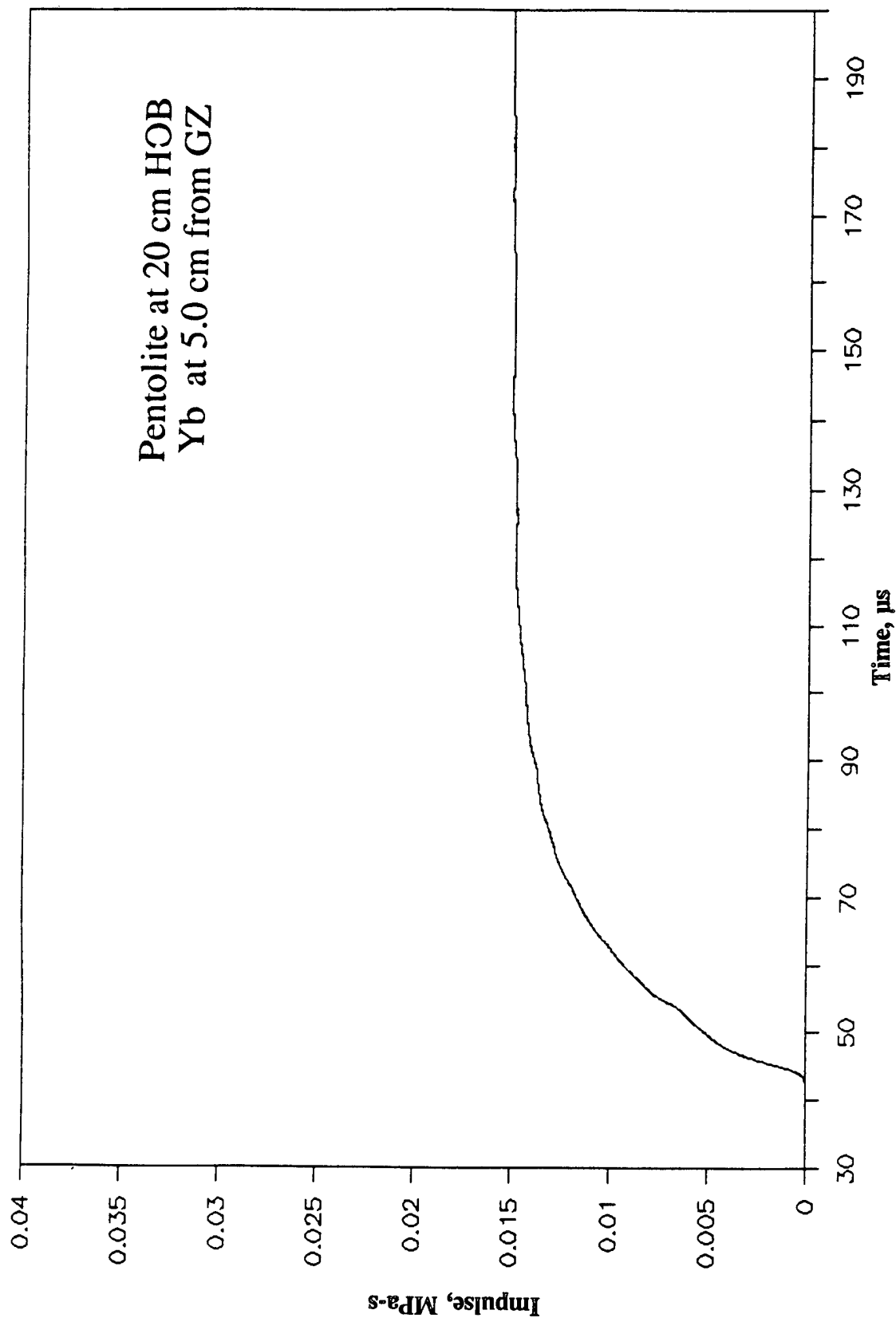


Figure A-18. Impulse-Time Record From Ytterbium Element Yb-1, 5.0 cm From Centerline, Baseplate Test 2A.4, Pentolite at 20-cm HOB.

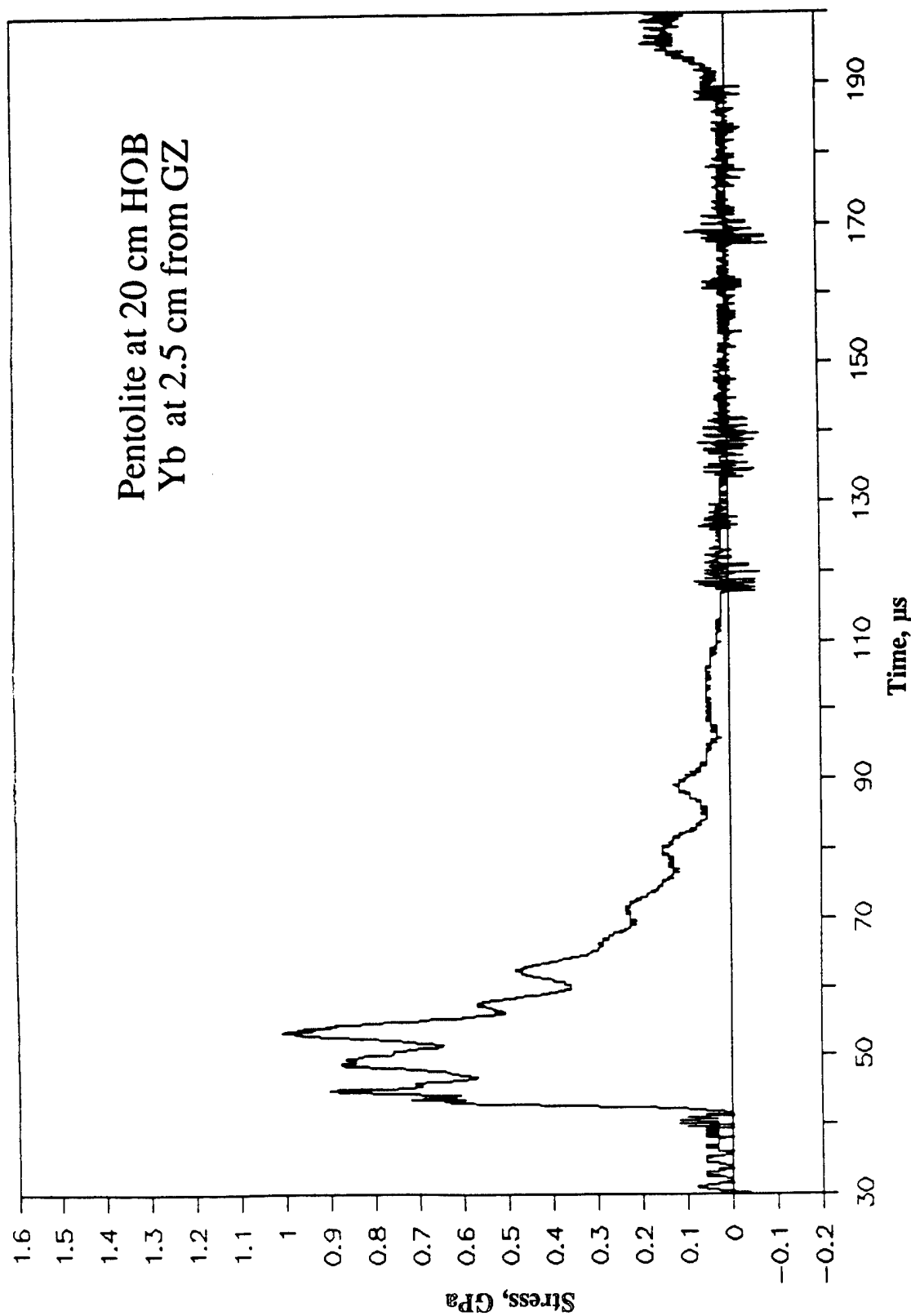


Figure A-19. Stress-Time Record From Ytterbium Element Yb-3, 2.5 cm From Centerline, Baseplate Test 2A.4, Pentolite at 20-cm HOB.

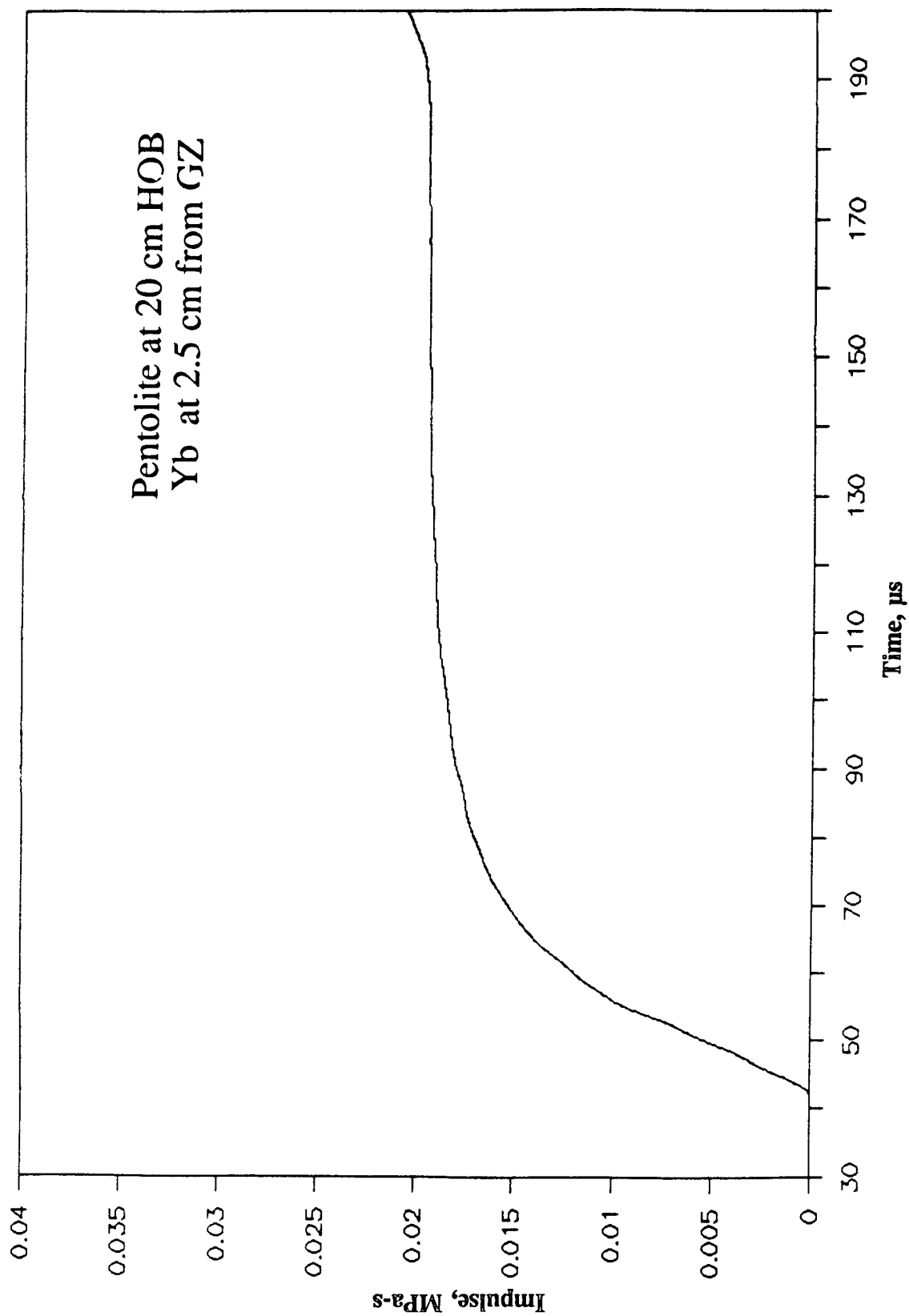


Figure A-20. Impulse-Time Record From Ytterbium Element Yb-3, 2.5 cm From Centerline, Baseplate Test 2A.4, Pentolite at 20-cm HOB.

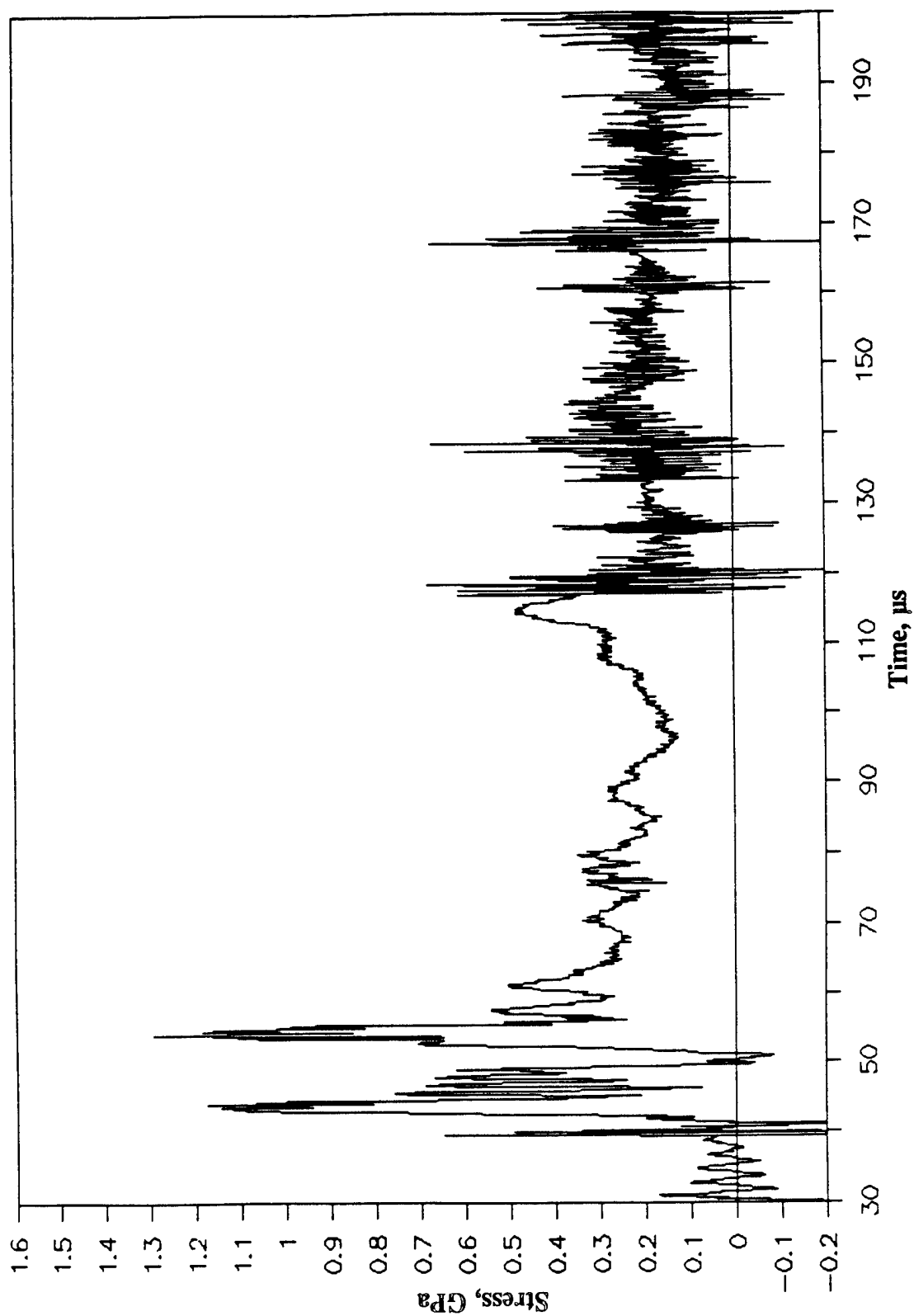


Figure A-21. Stress-Time Record From Manganin Element Mn-2, 2.5 cm From Centerline, Baseplate Test 2A.4, Pentolite at 20-cm HOB.

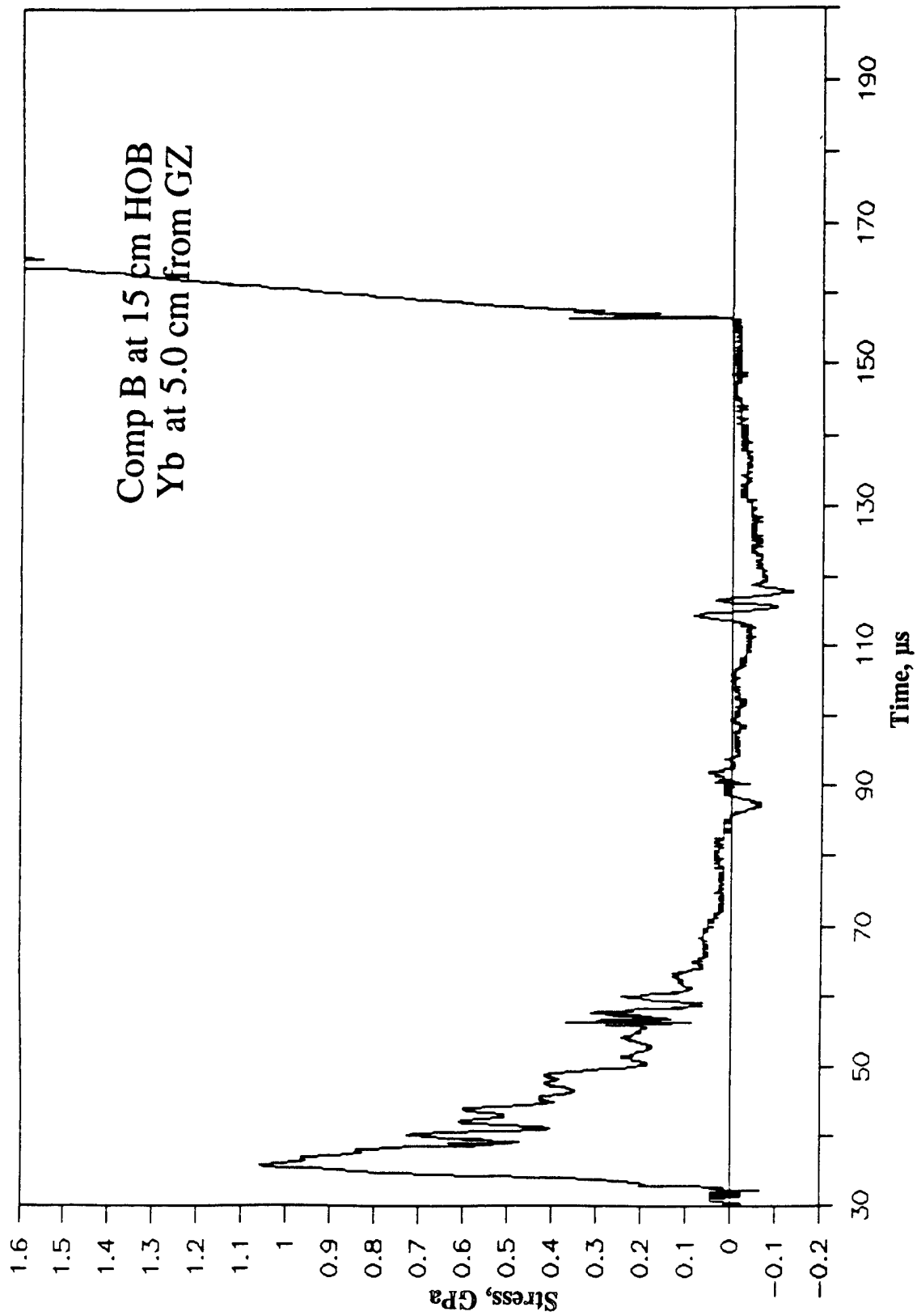


Figure A-22. Stress-Time Record From Ytterbium Element Yb-1, 5.0 cm From Centerline, Baseplate Test 2A.5, Comp B at 15-cm HOB.

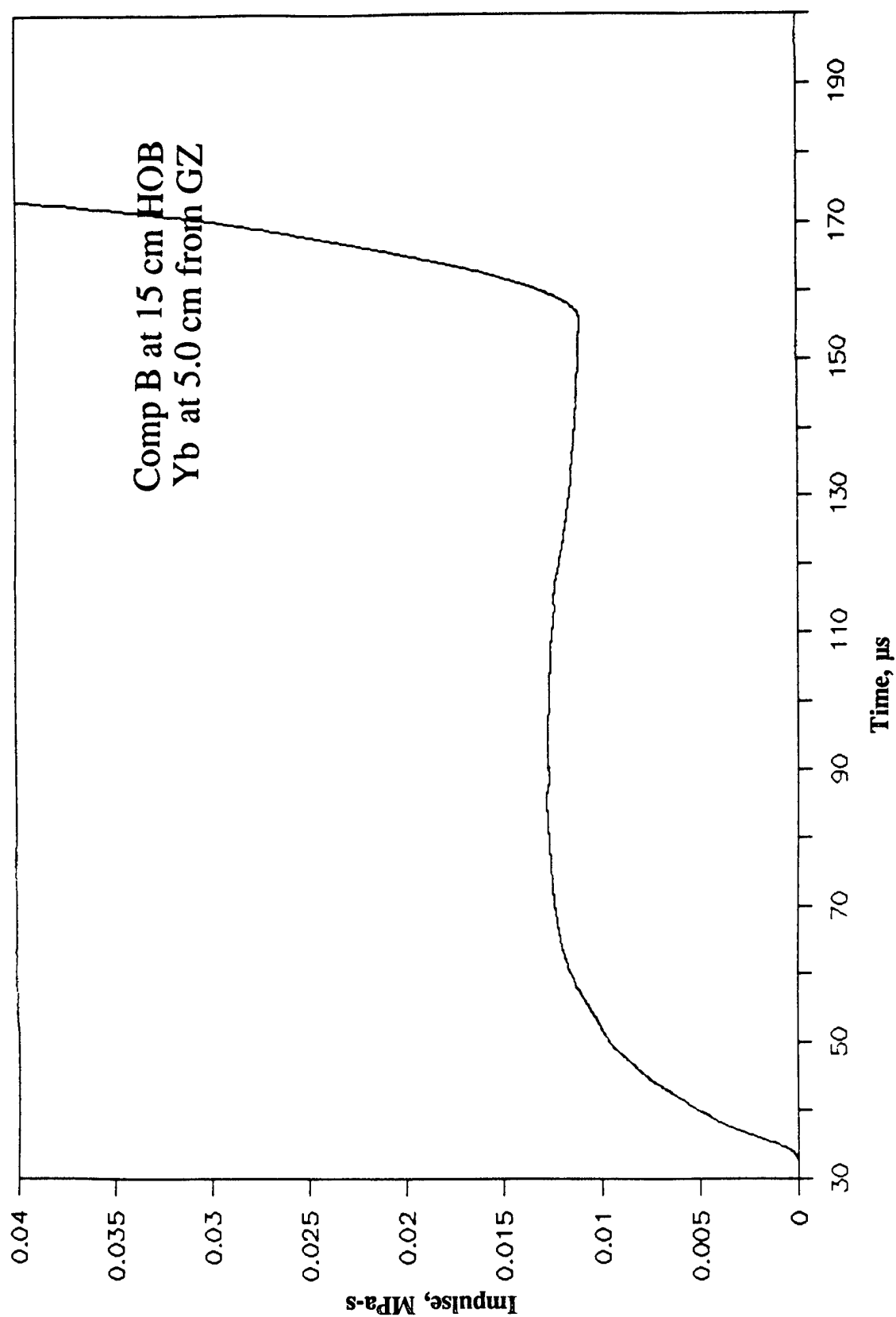


Figure A-23. Impulse-Time Record From Ytterbium Element Yb-1, 5.0 cm From Centerline, Baseplate Test 2A.5, Comp B at 15-cm HOB.

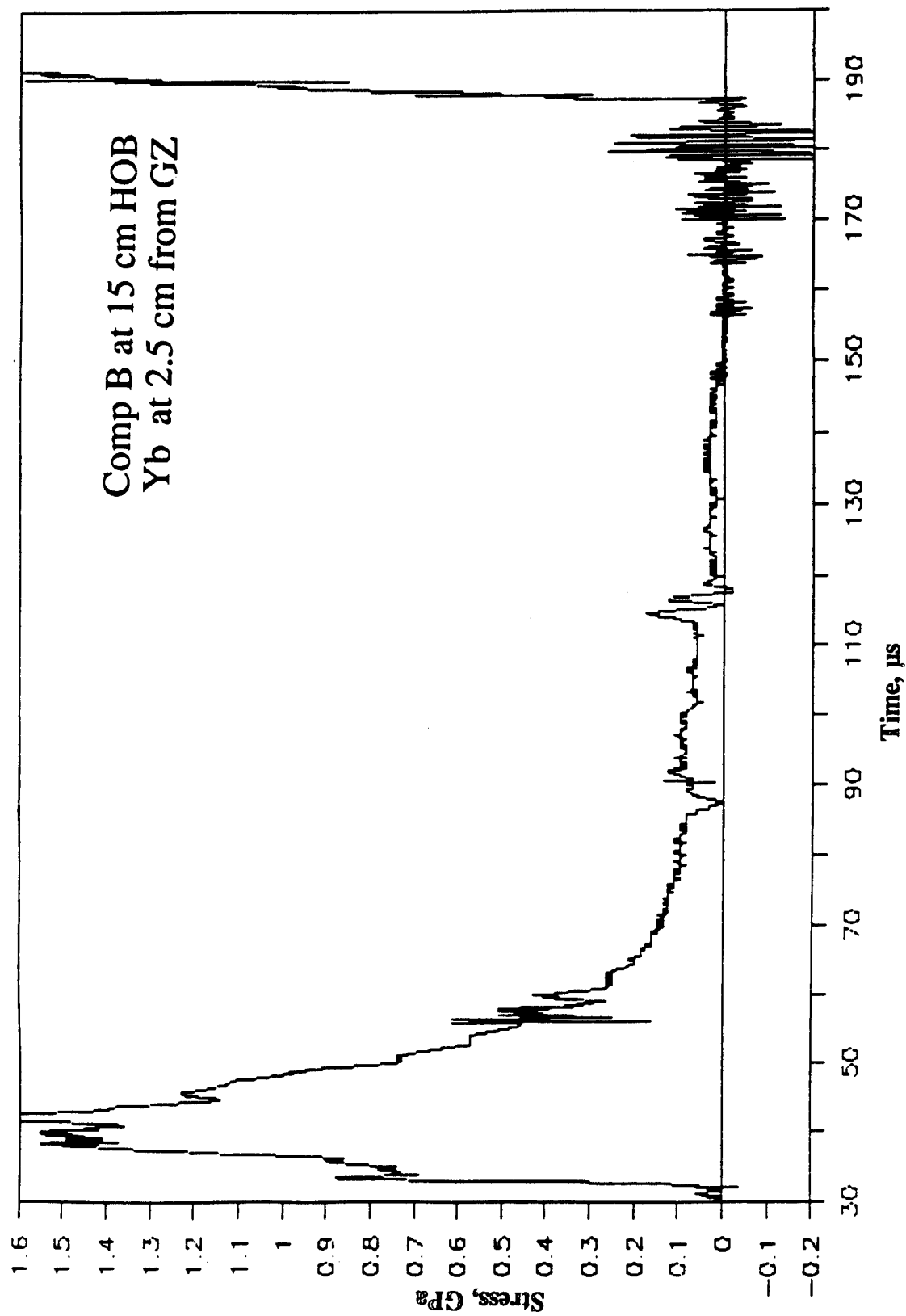


Figure A-24. Stress-Time Record From Ytterbium Element Yb-2, 2.5 cm From Centerline, Baseplate Test 2A.5, Comp B at 15-cm HOB.

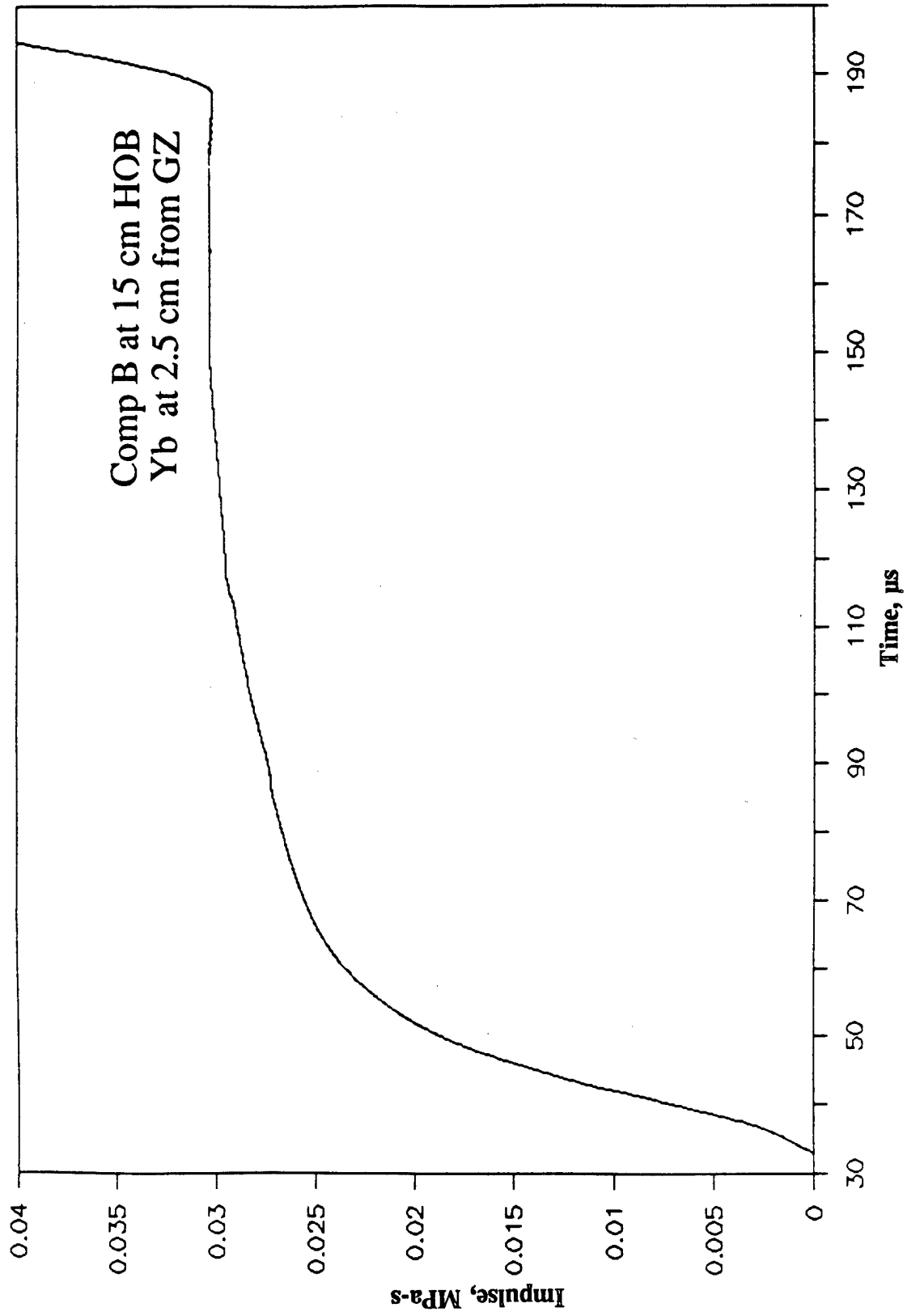


Figure A-25. Impulse-Time Record From Ytterbium Element Yb-2, 2.5 cm From Centerline, Baseplate Test 2A.5, Comp B at 15-cm HOB.

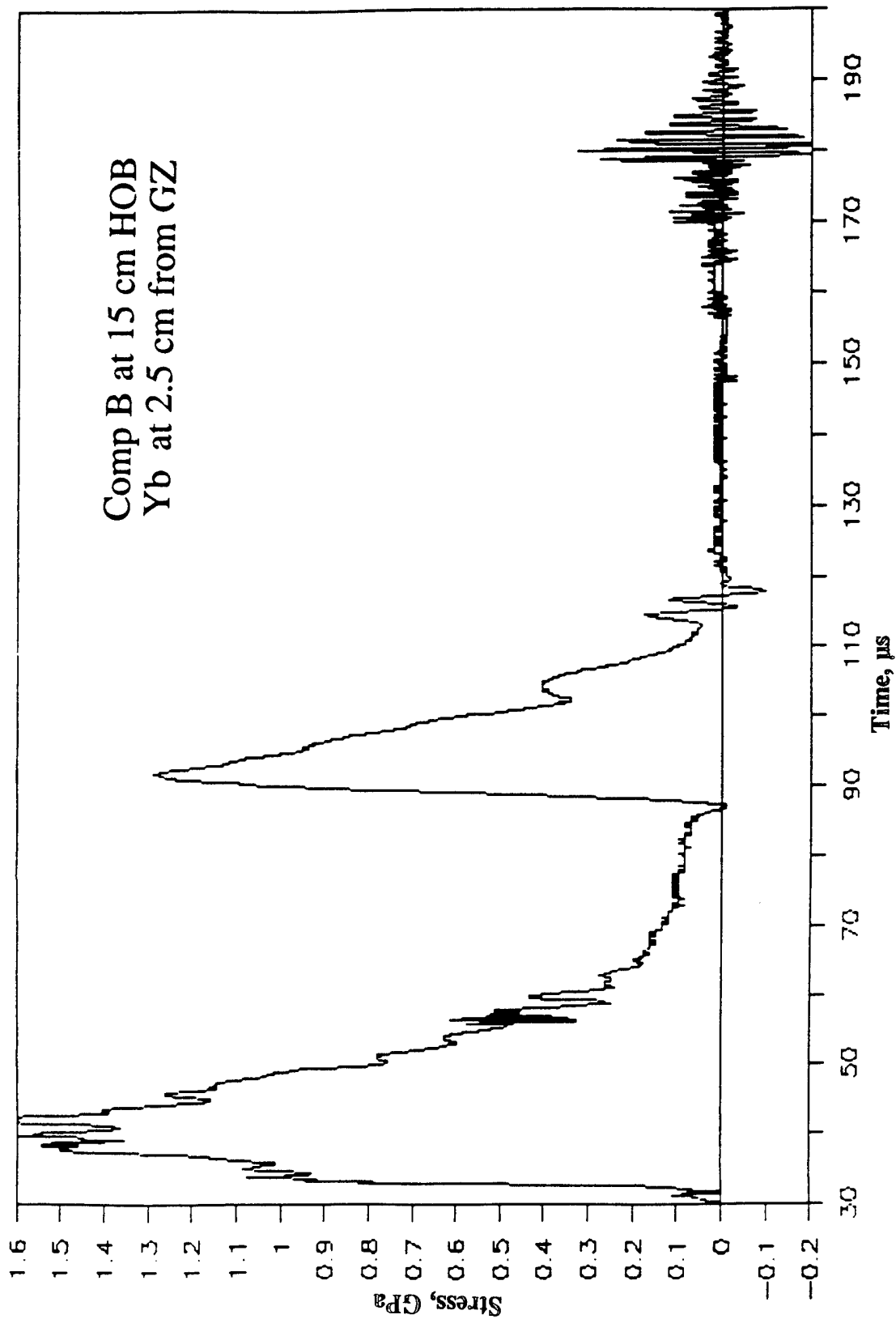


Figure A-26. Stress-Time Record From Ytterbium Element Yb-3, 2.5 cm From Centerline, Baseplate Test 2A.5, Comp B at 15-cm HOB.

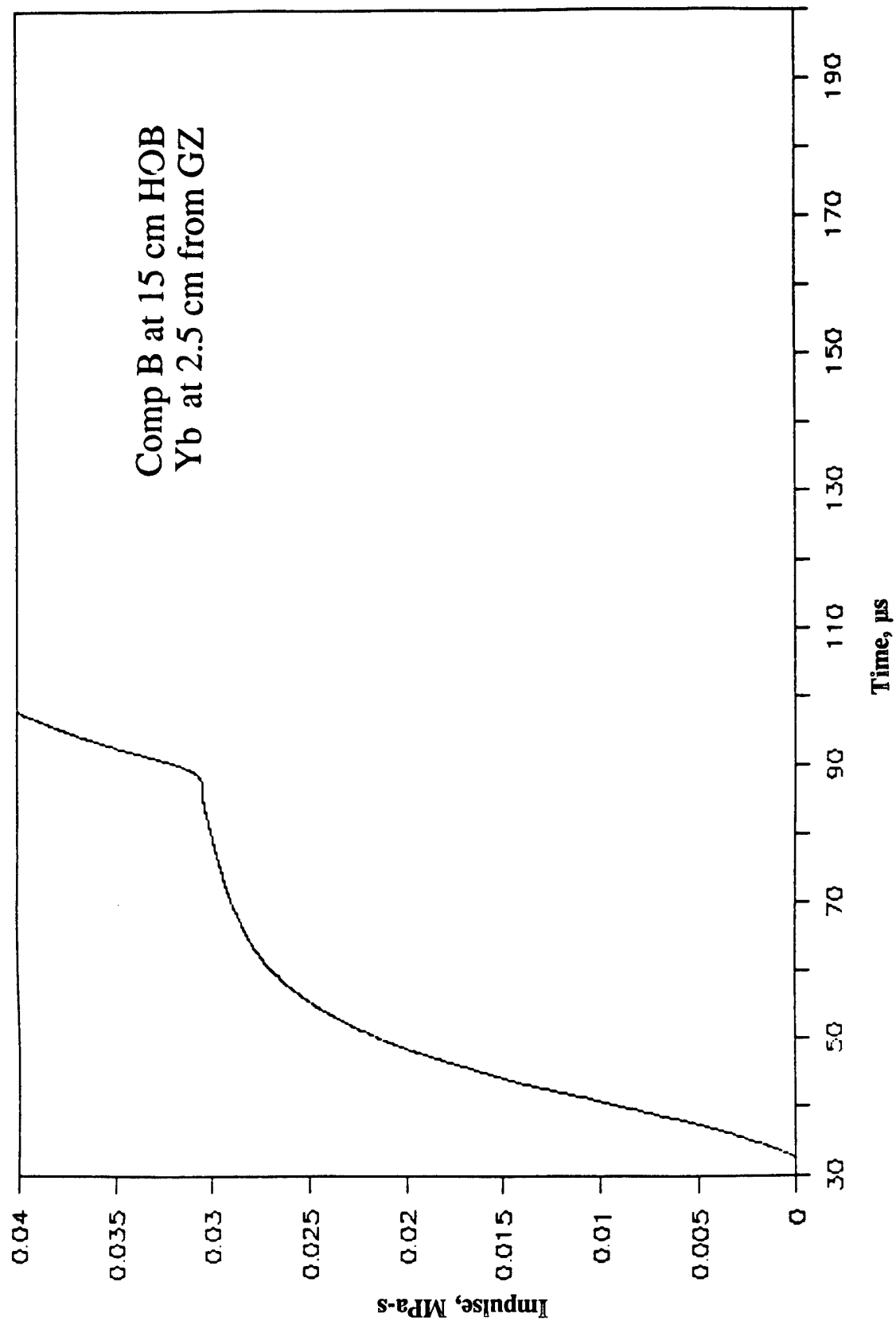


Figure A-27. Impulse-Time Record From Ytterbium Element Yb-3, 2.5 cm From Centerline, Baseplate Test 2A.5, Comp B at 15-cm HOB.

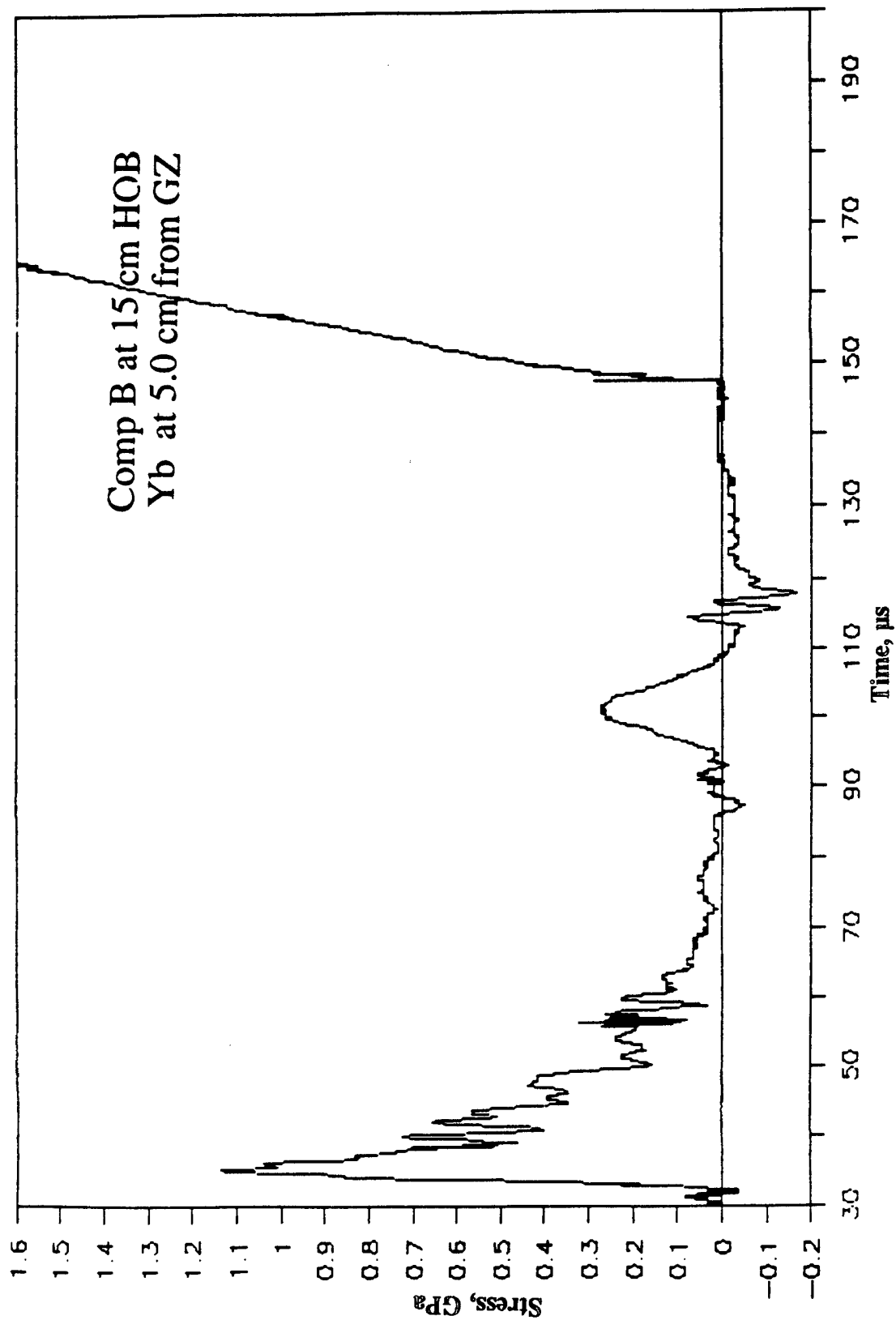


Figure A-28. Stress-Time Record From Ytterbium Element Yb-4, 5.0 cm From Centerline, Baseplate Test 2A.5, Comp B at 15-cm HOB.

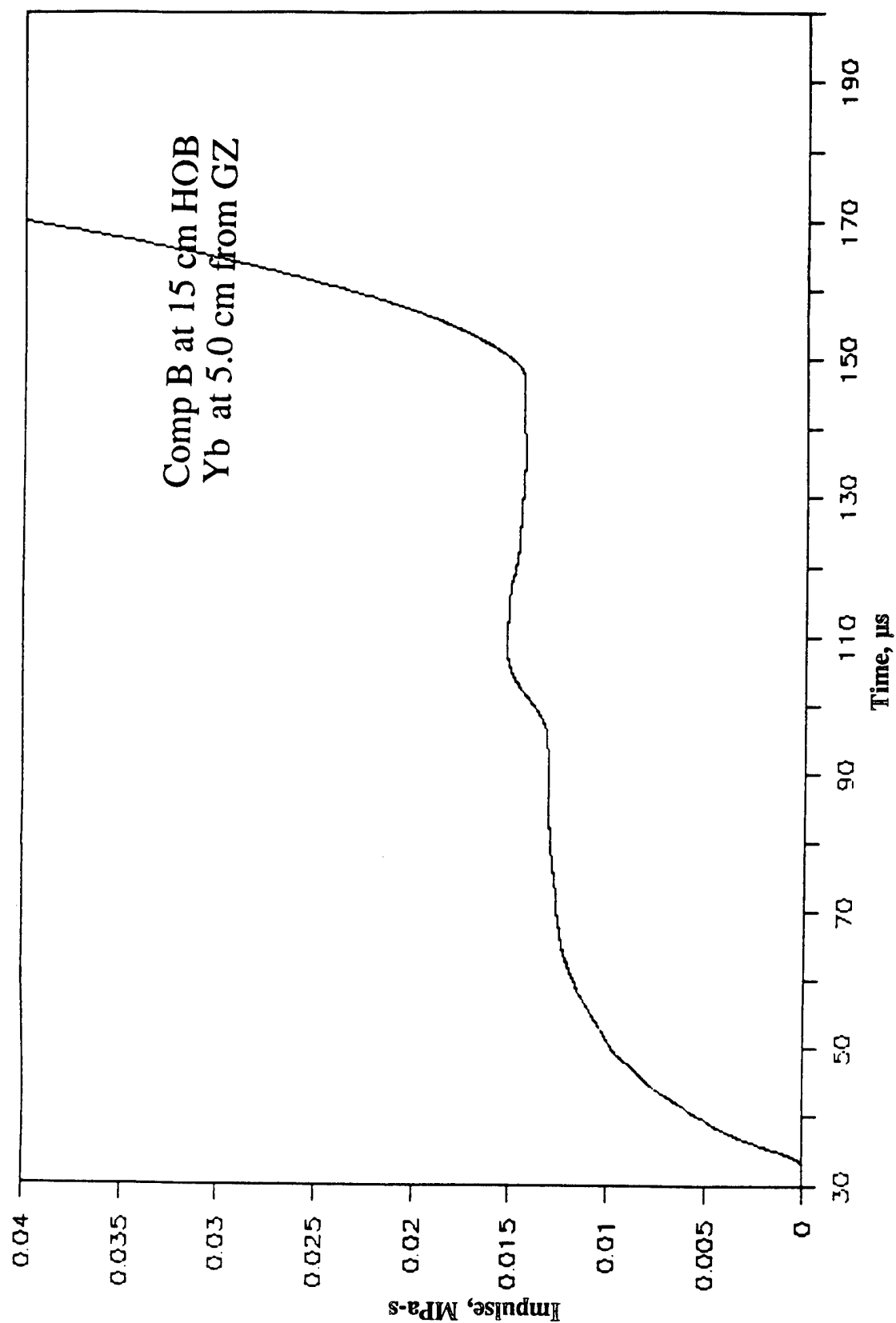


Figure A-29. Impulse-Time Record From Ytterbium Element Yb-4, 5.0 cm From Centerline, Baseplate Test 2A.5, Comp B at 15-cm HOB.

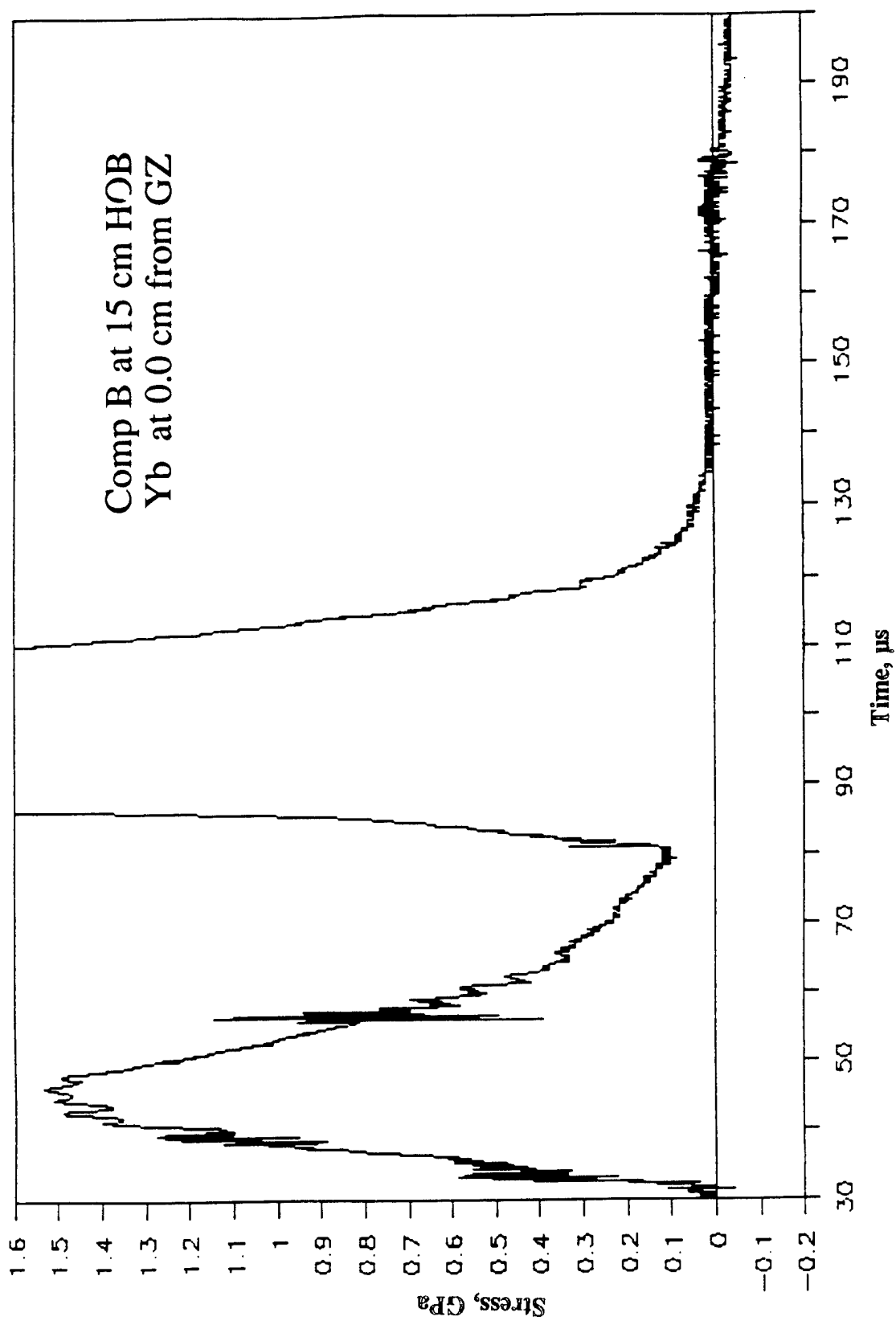


Figure A-30. Stress-Time Record From Ytterbium Element Yb-5, 0.0 cm From Centerline, Baseplate Test 2A.5, Comp B at 15 cm HOB.

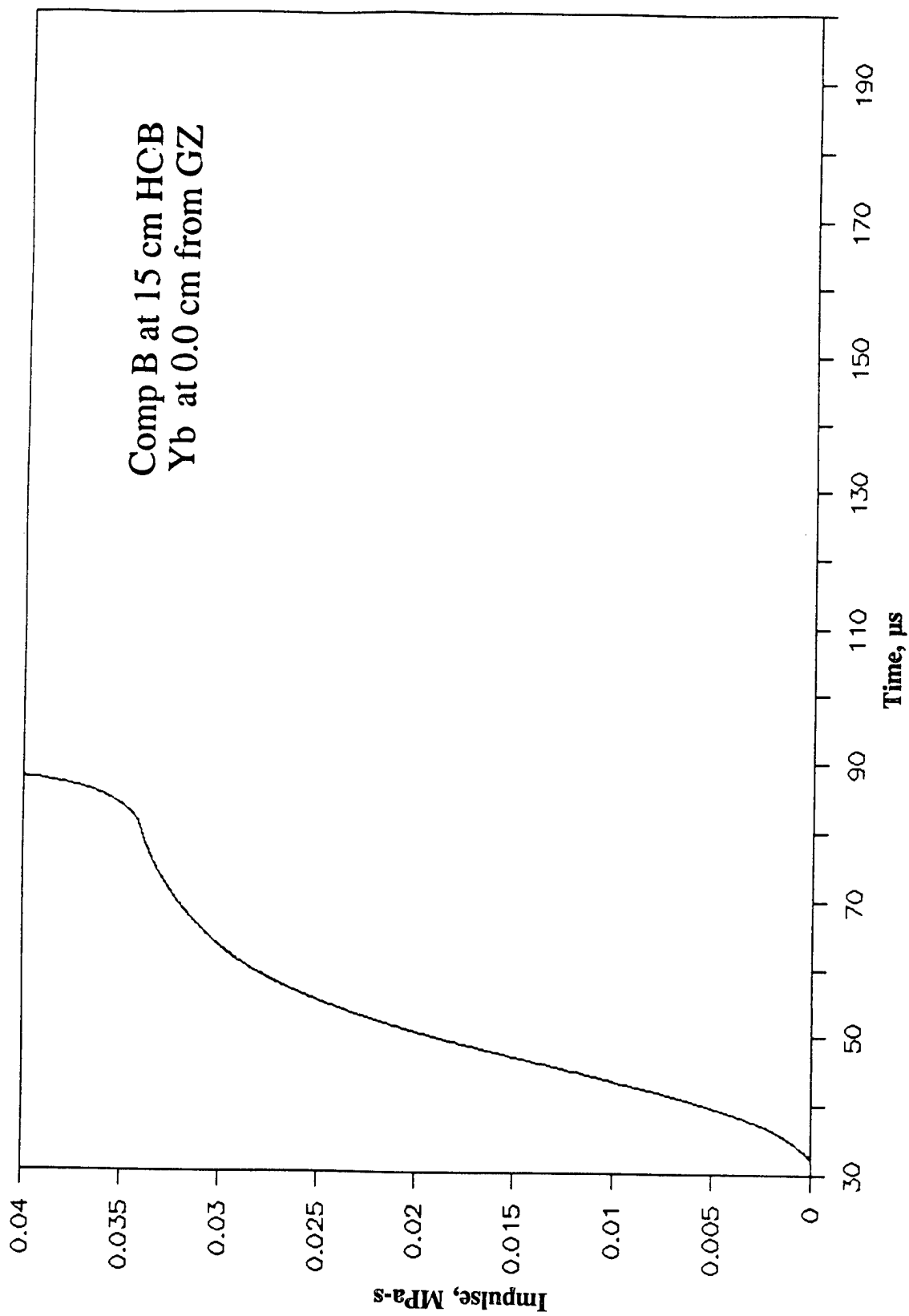


Figure A-31. Impulse-Time Record From Ytterbium Element Yb-5, 0.0 cm From Centerline, Baseplate Test 2A.5, Comp B at 15-cm HOB.

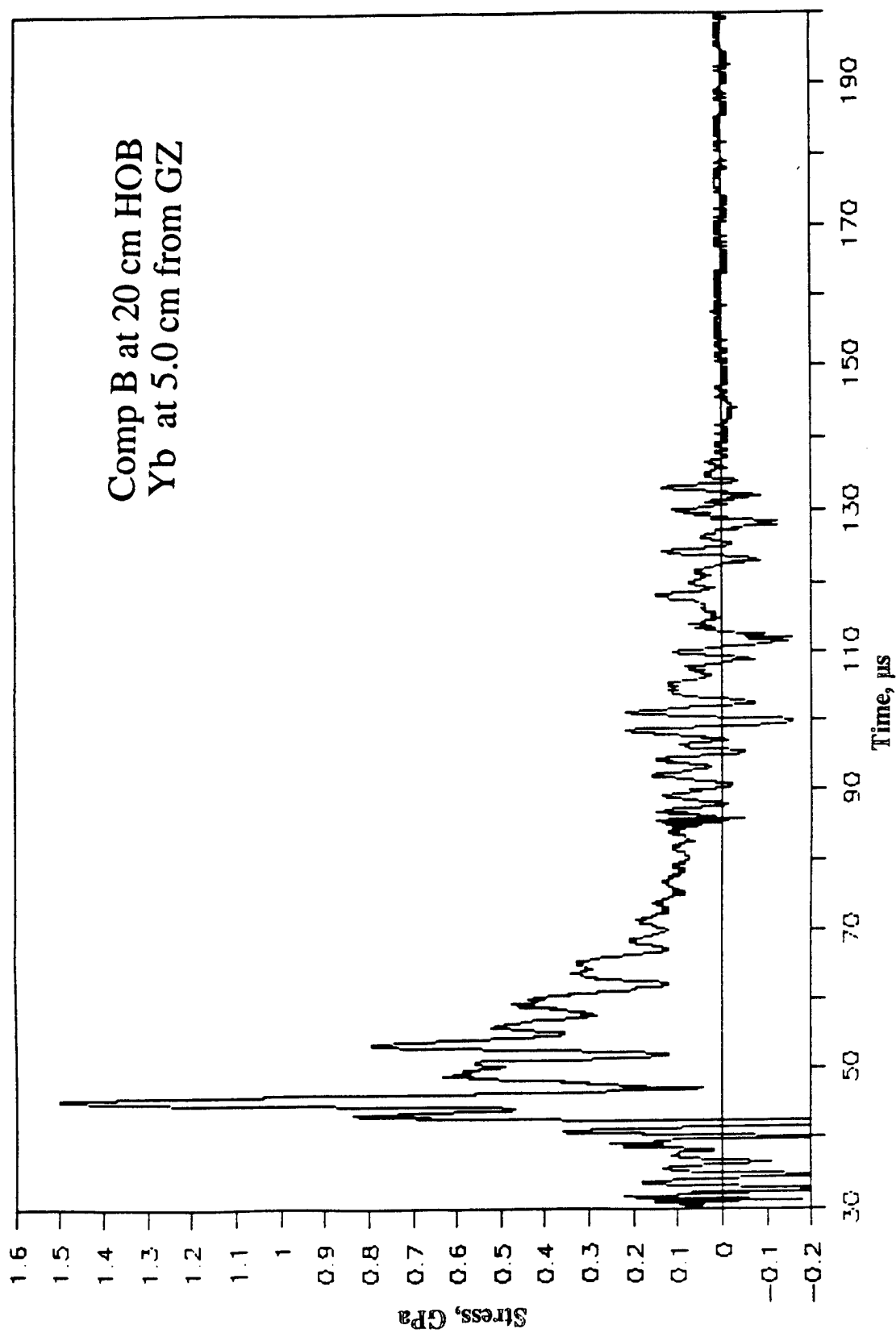


Figure A-32. Stress-Time Record From Ytterbium Element Yb-1, 5.0 cm From Centerline, Baseplate Test 2A.6, Comp B at 20-cm HOB.

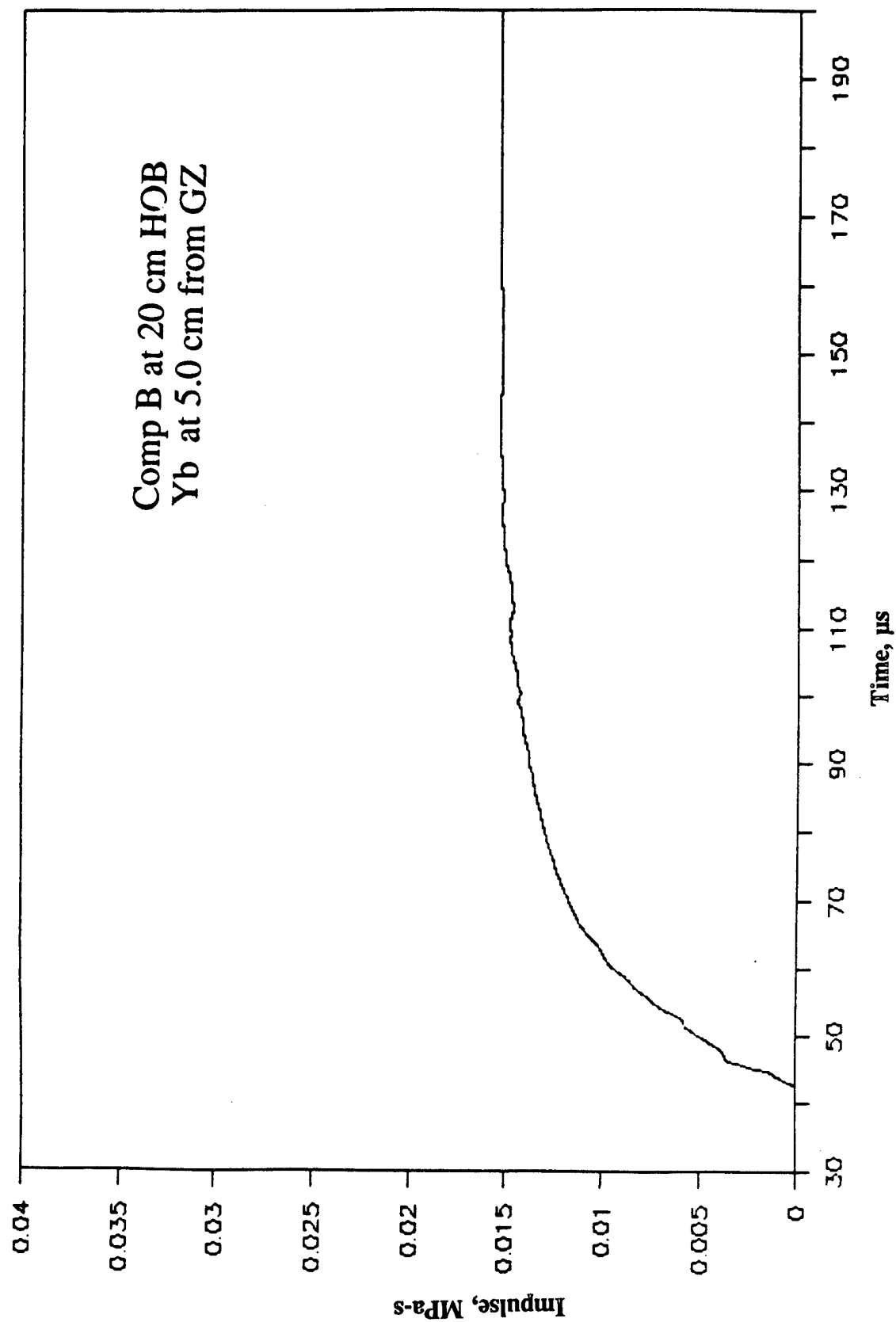


Figure A-33. Impulse-Time Record From Ytterbium Element Yb-1, 5.0 cm From Centerline, Baseplate Test 2A.6, Comp B at 20-cm HOB.

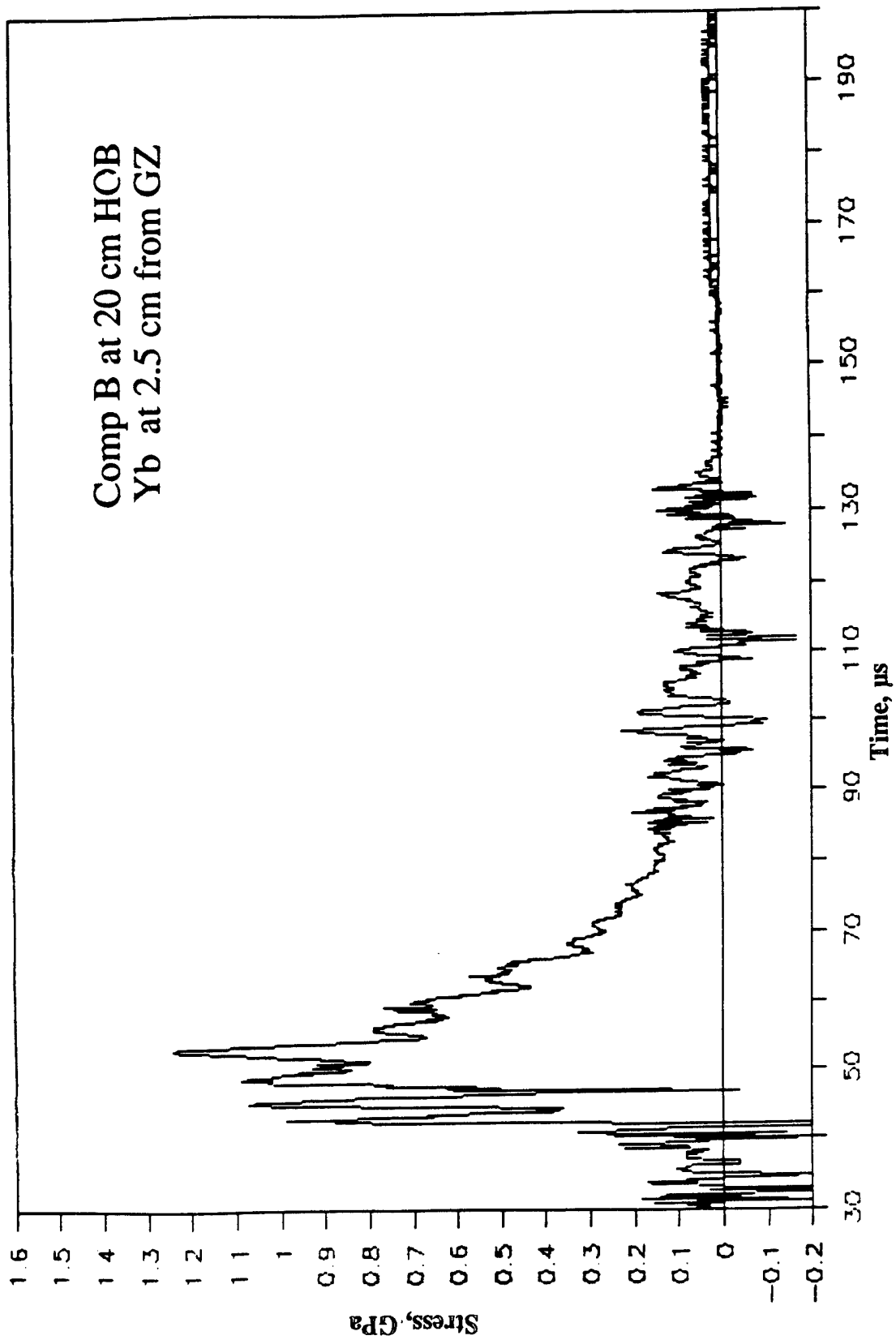


Figure A-34. Stress-Time Record From Ytterbium Element Yb-2, 2.5 cm From Centerline, Baseplate Test 2A.6, Comp B at 20-cm HOB.

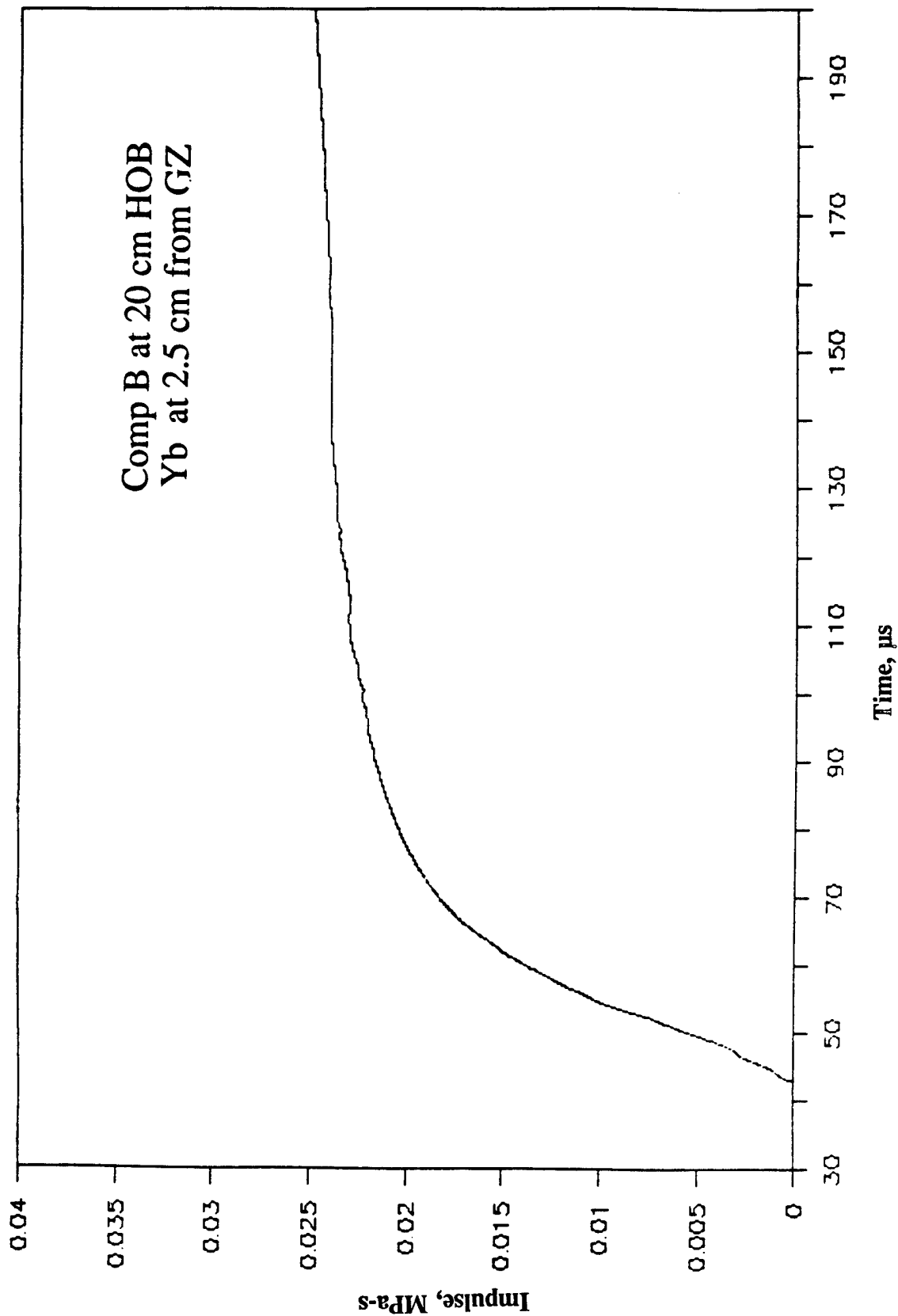


Figure A-35. Impulse-Time Record From Ytterbium Element Yb-2, 2.5 cm From Centerline, Baseplate Test 2A.6, Comp B at 20-cm HOB.

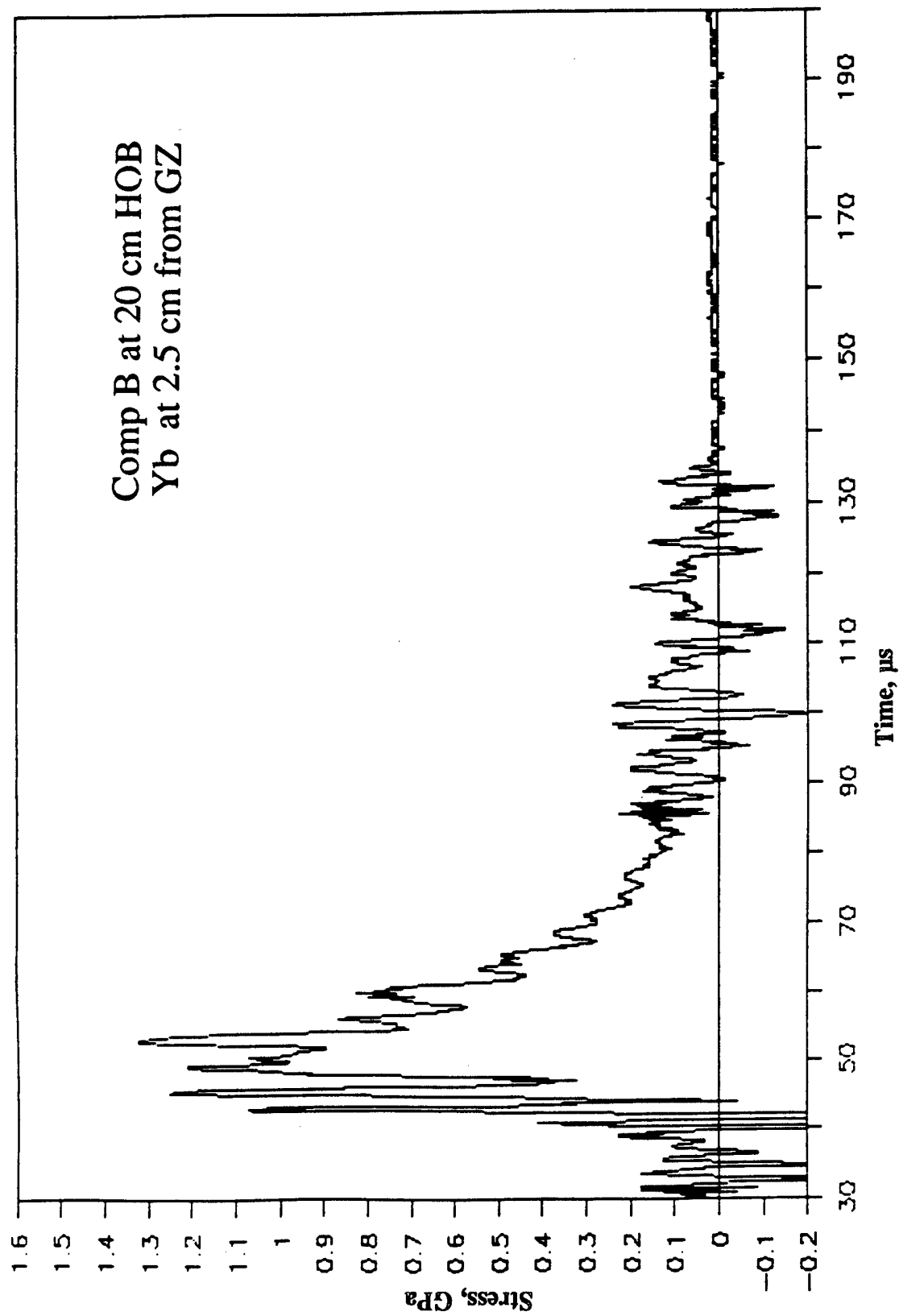


Figure A-36. Stress-Time Record From Ytterbium Element Yb-3, 2.5 cm From Centerline, Baseplate Test 2A.6, Comp B at 20-cm HOB.

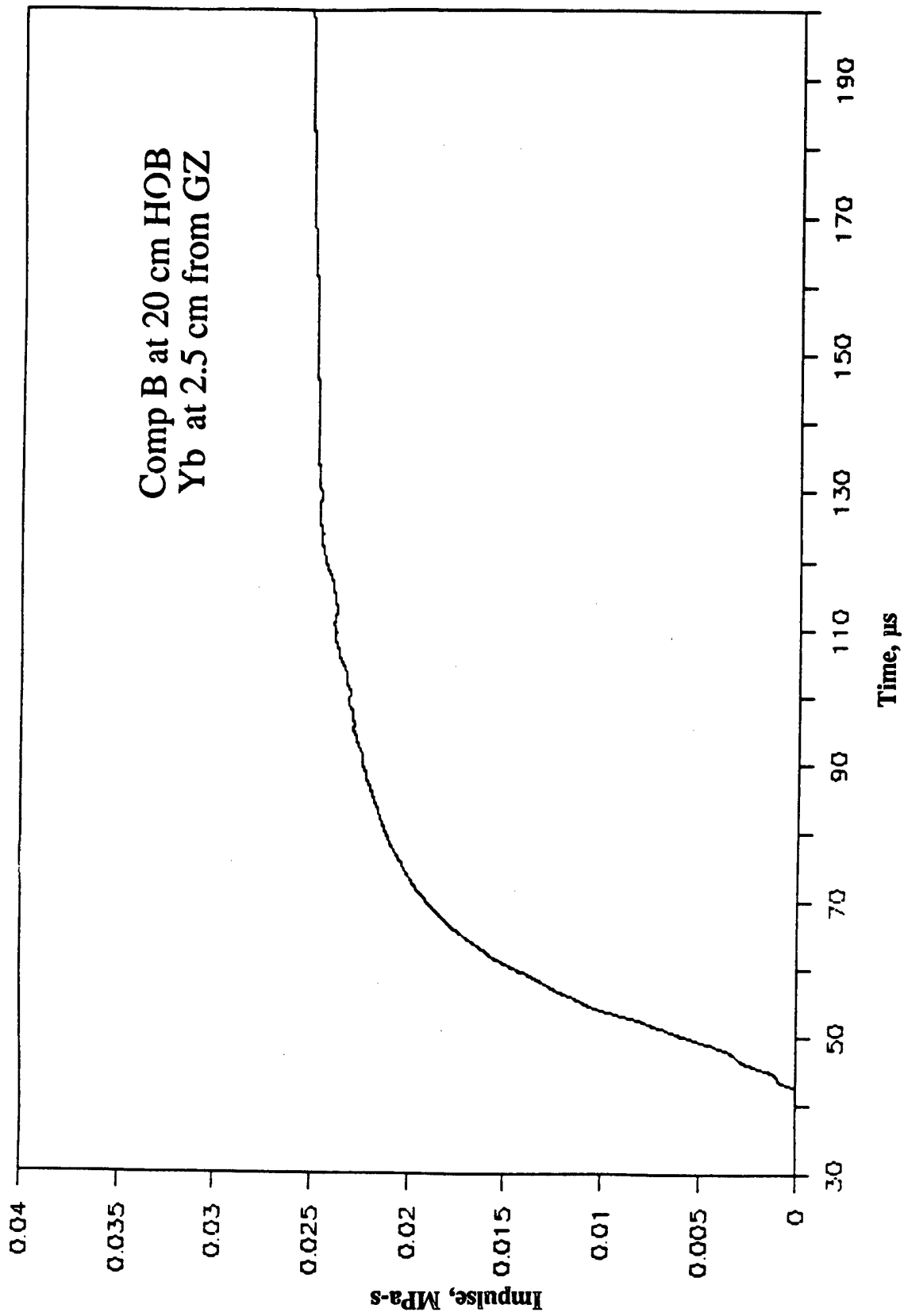


Figure A-37. Impulse-Time Record From Ytterbium Element Yb-3, 2.5 cm From Centerline, Baseplate Test 2A.6, Comp B at 20-cm HOB.

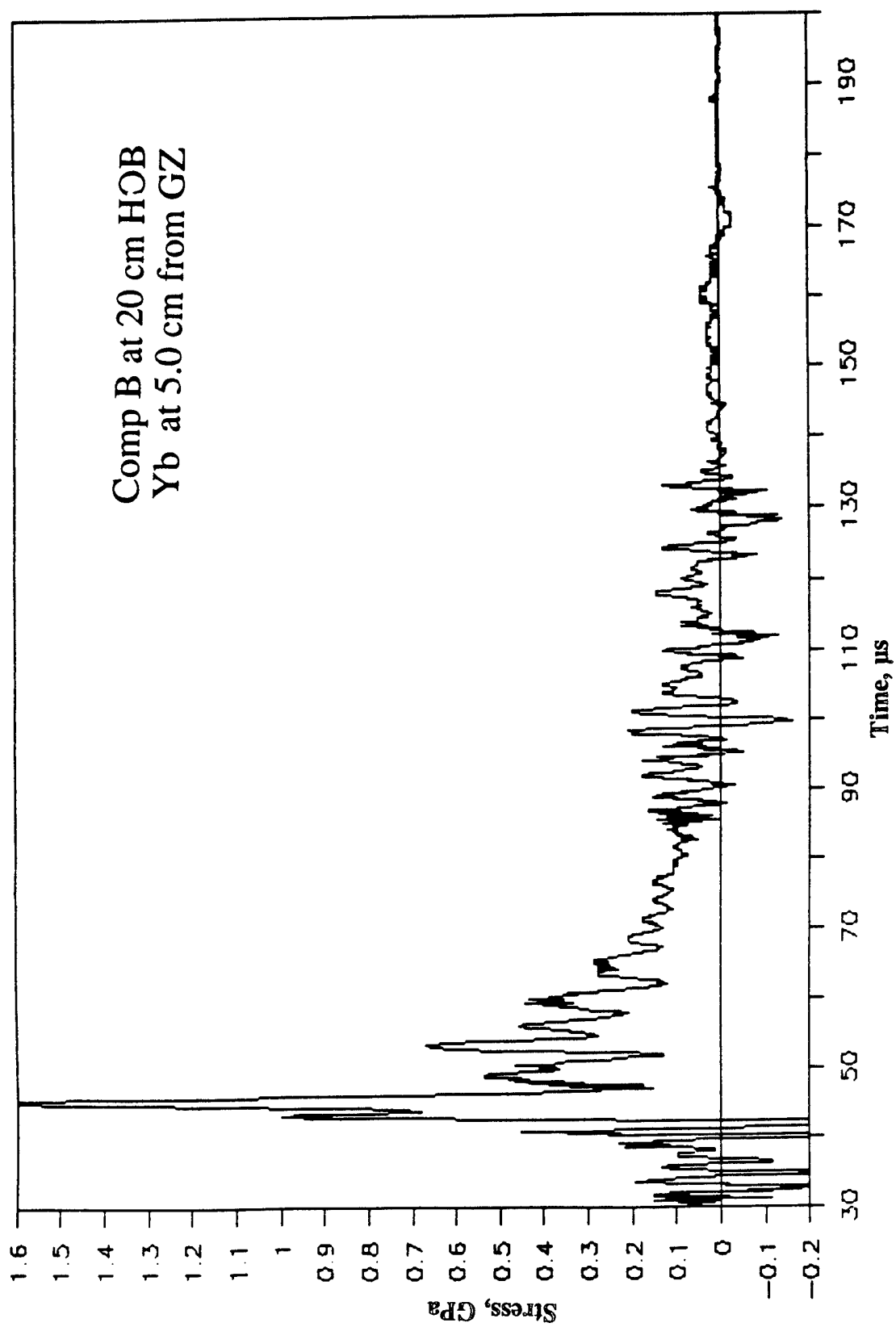


Figure A-38. Stress-Time Record From Ytterbium Element Yb-4, 5.0 cm From Centerline, Baseplate Test 2A.6, Comp B at 20-cm HOB.

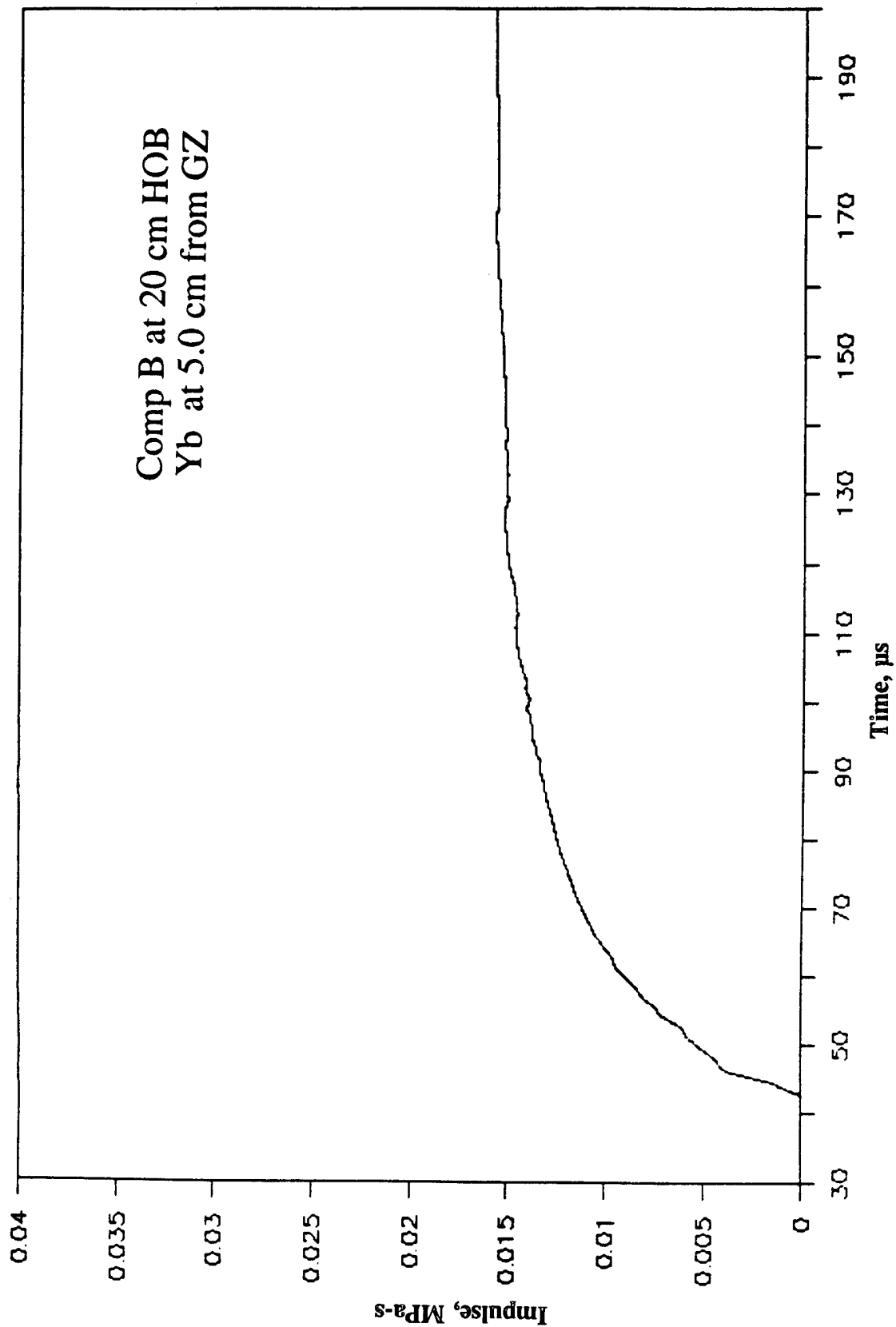


Figure A-39. Impulse-Time Record From Ytterbium Element Yb-4, 5.0 cm From Centerline, Baseplate Test 2A.6, Comp B at 20-cm HOB.

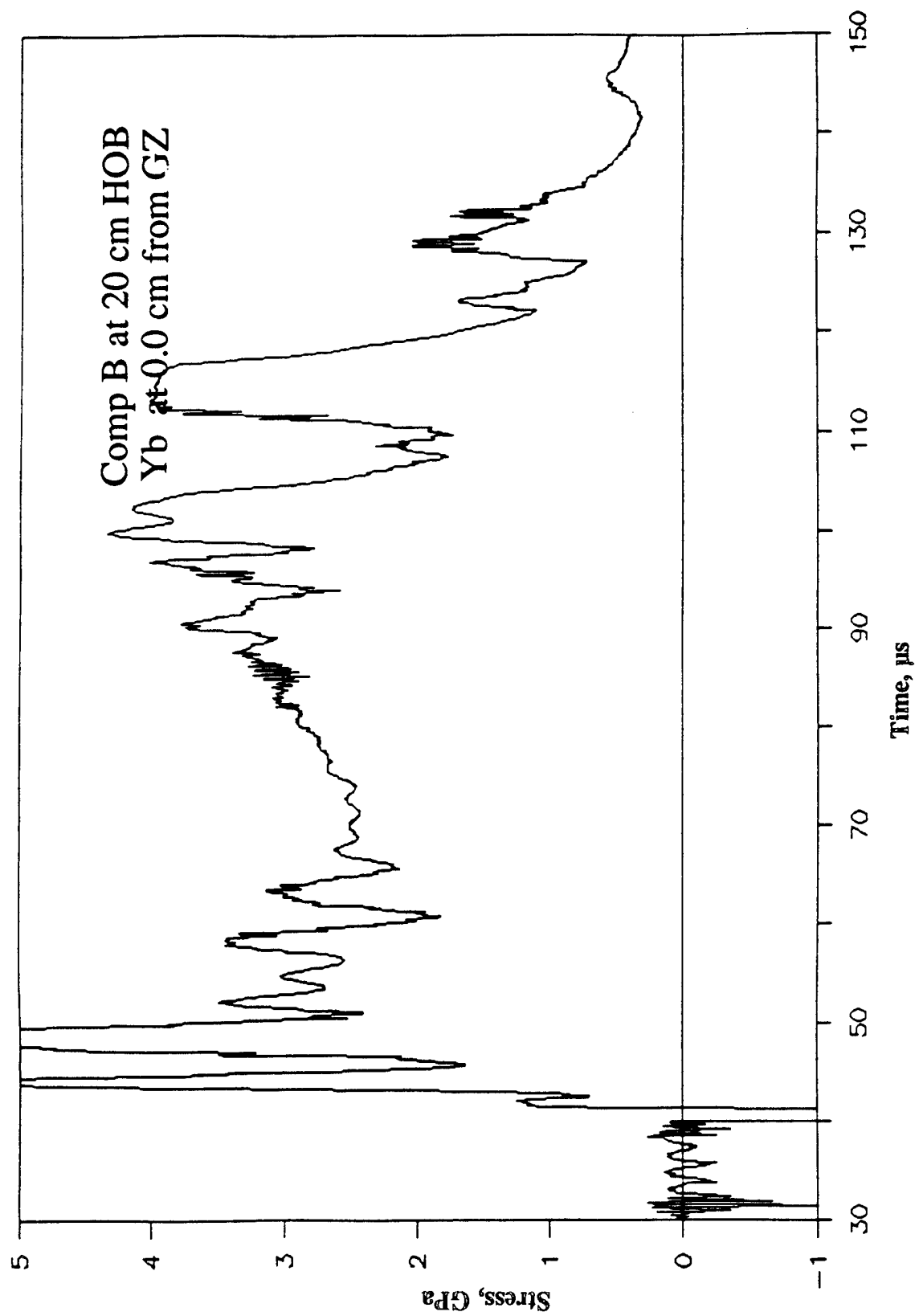


Figure A-40. Stress-Time Record From Ytterbium Element Yb-5, 0.0 cm From Centerline, Baseplate Test 2A.6, Comp B at 20-cm HOB.

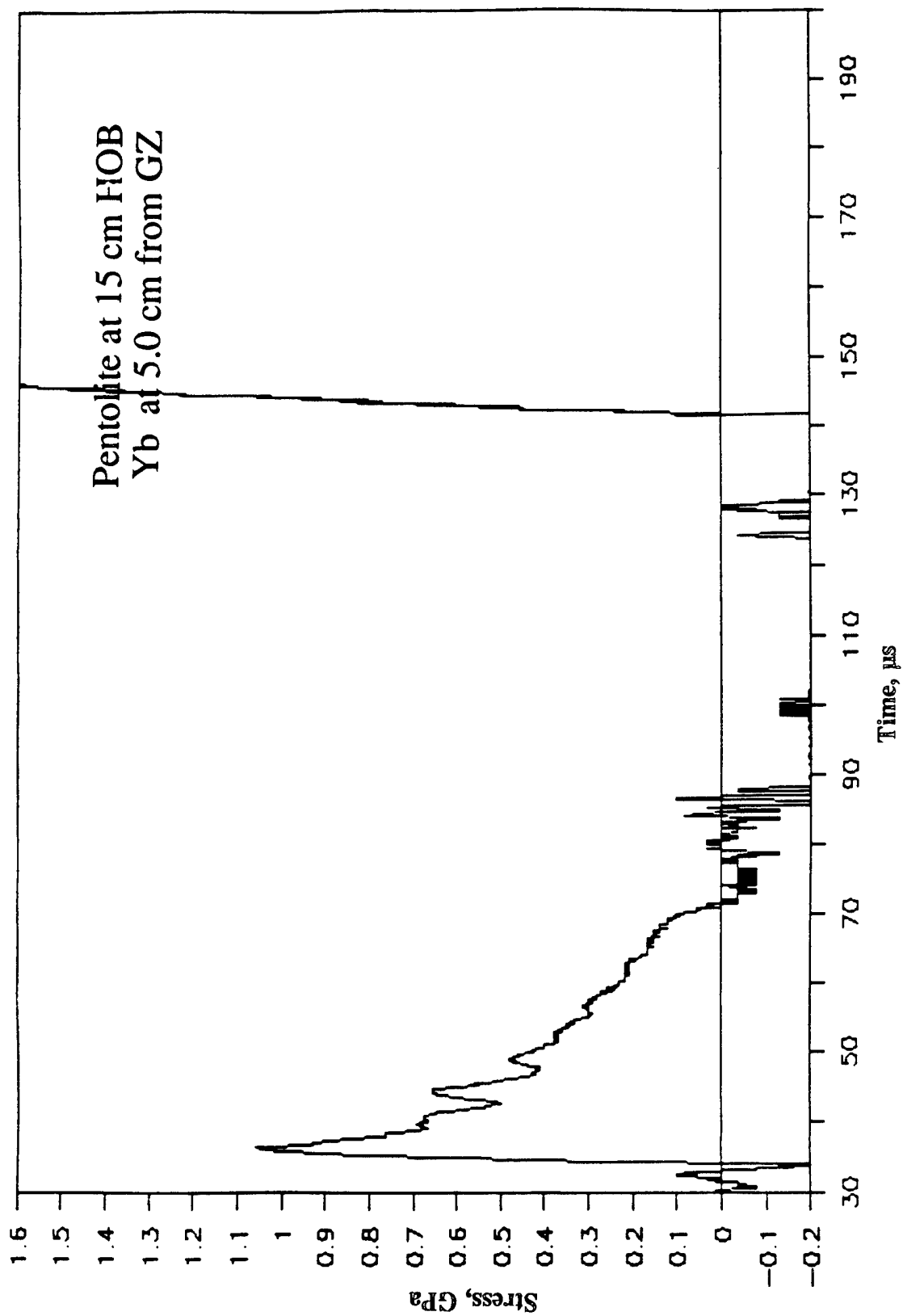


Figure A-41. Stress-Time Record From Ytterbium Element Yb-1, 5.0 cm From Centerline, Baseplate Test 2A.7, Pentolite at 15-cm HOB.

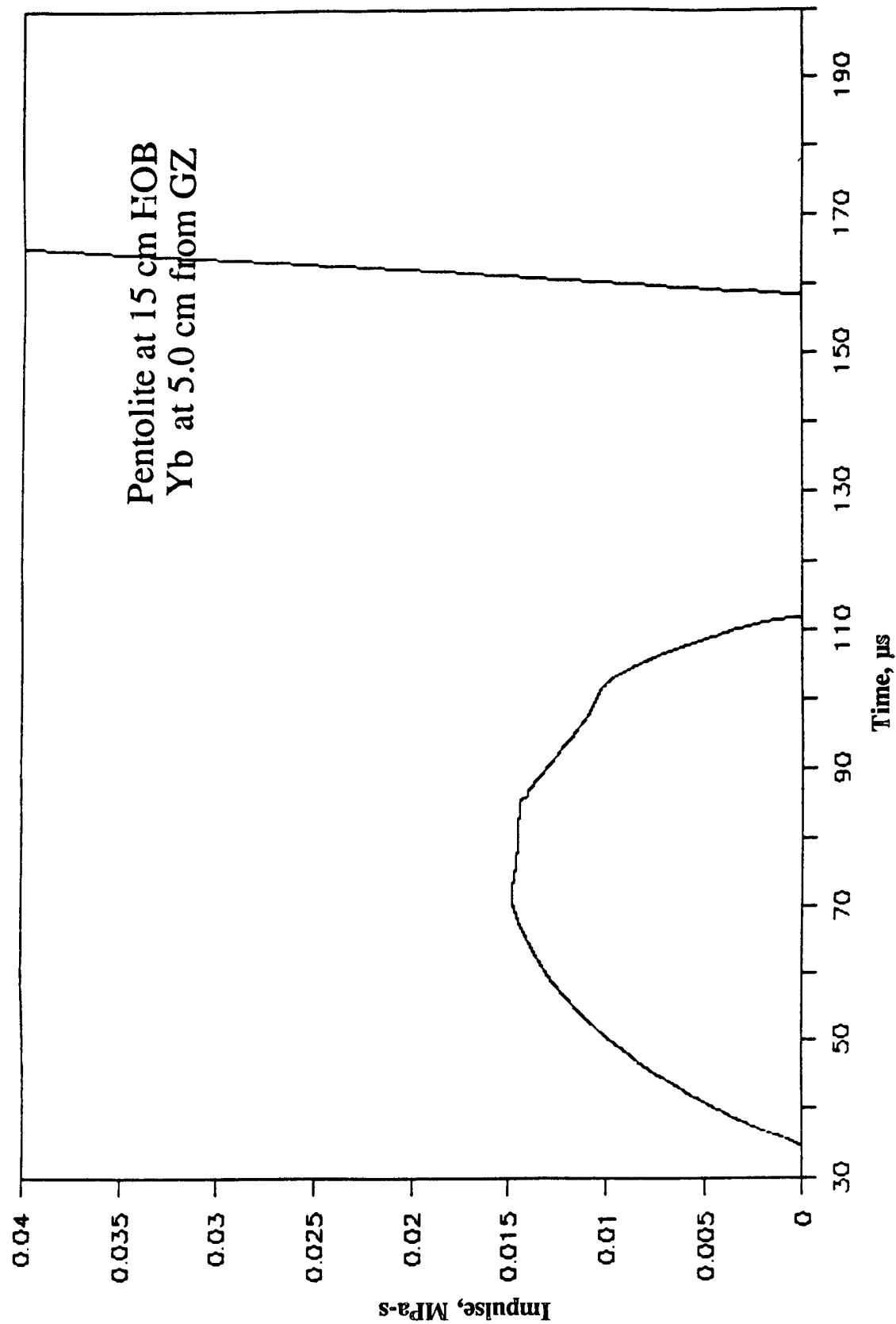


Figure A-42. Impulse-Time Record From Ytterbium Element Yb-1, 5.0 cm From Centerline, Baseplate Test 2A.7, Pentolite at 15-cm HOB.

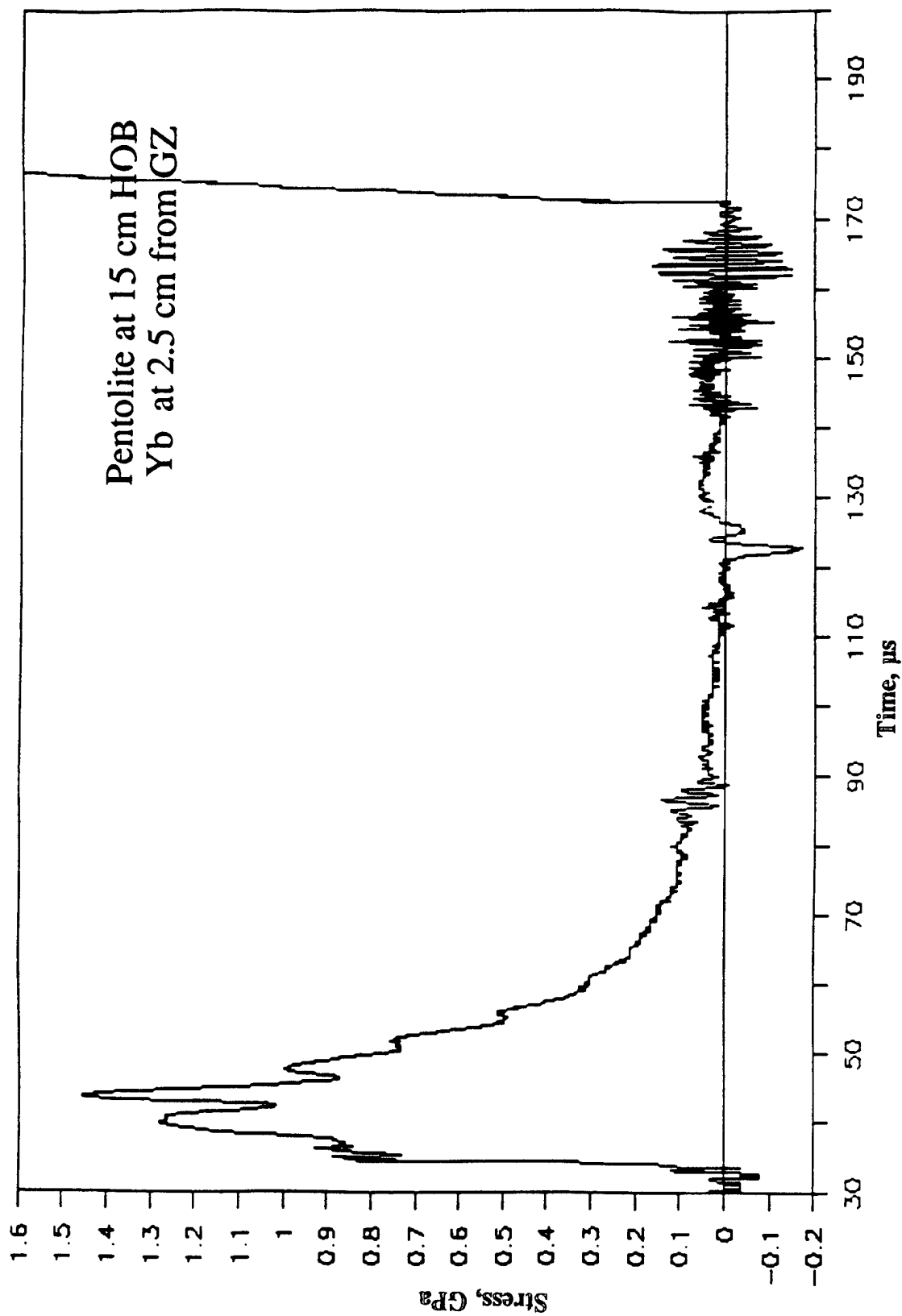


Figure A-43. Stress-Time Record From Ytterbium Element Yb-2, 2.5 cm From Centerline, Baseplate Test 2A.7, Pentolite at 15-cm HOB.

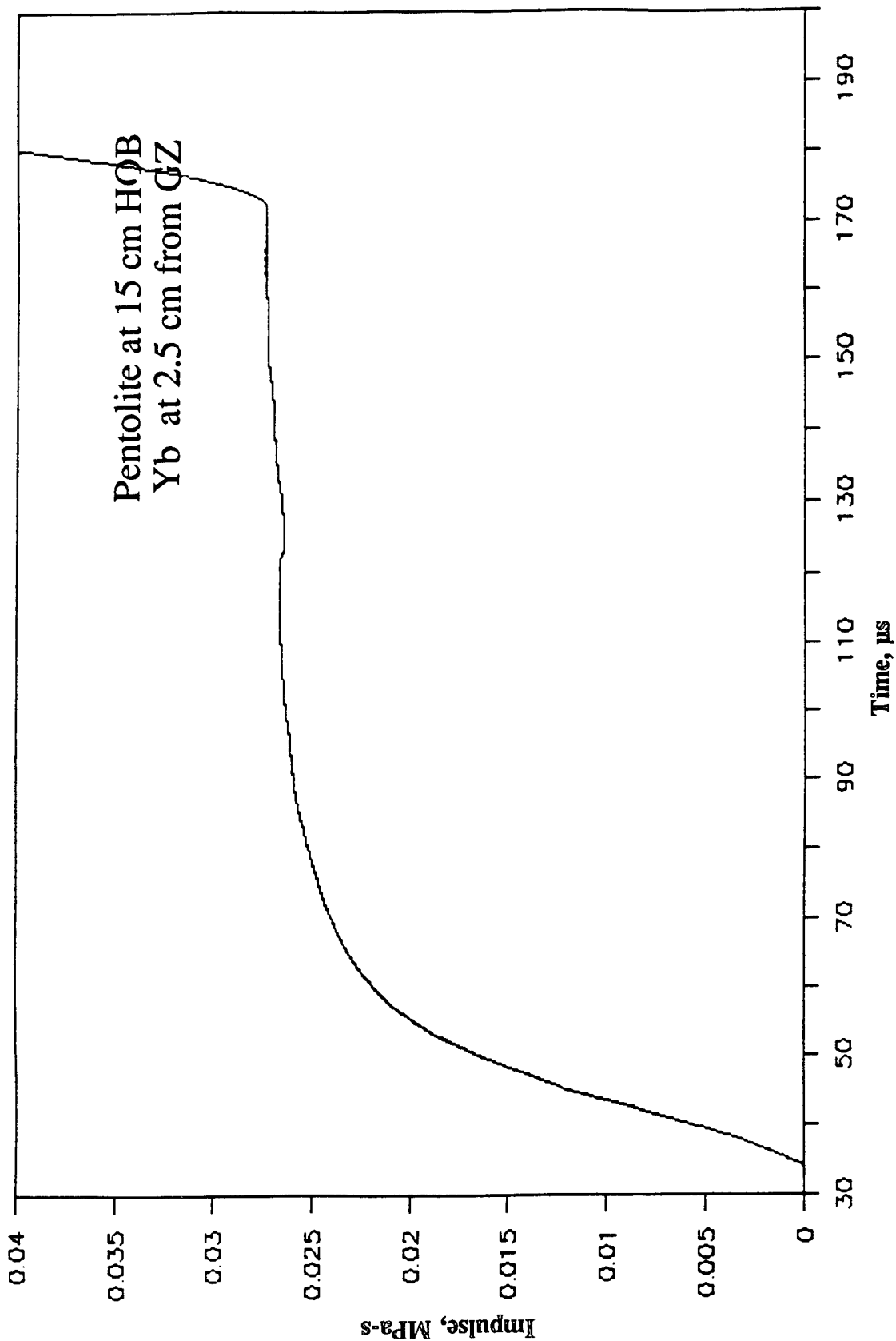


Figure A-44. Impulse-Time Record From Ytterbium Element Yb-2, 2.5 cm From Centerline, Baseplate Test 2A.7, Pentolite at 15-cm HOB.

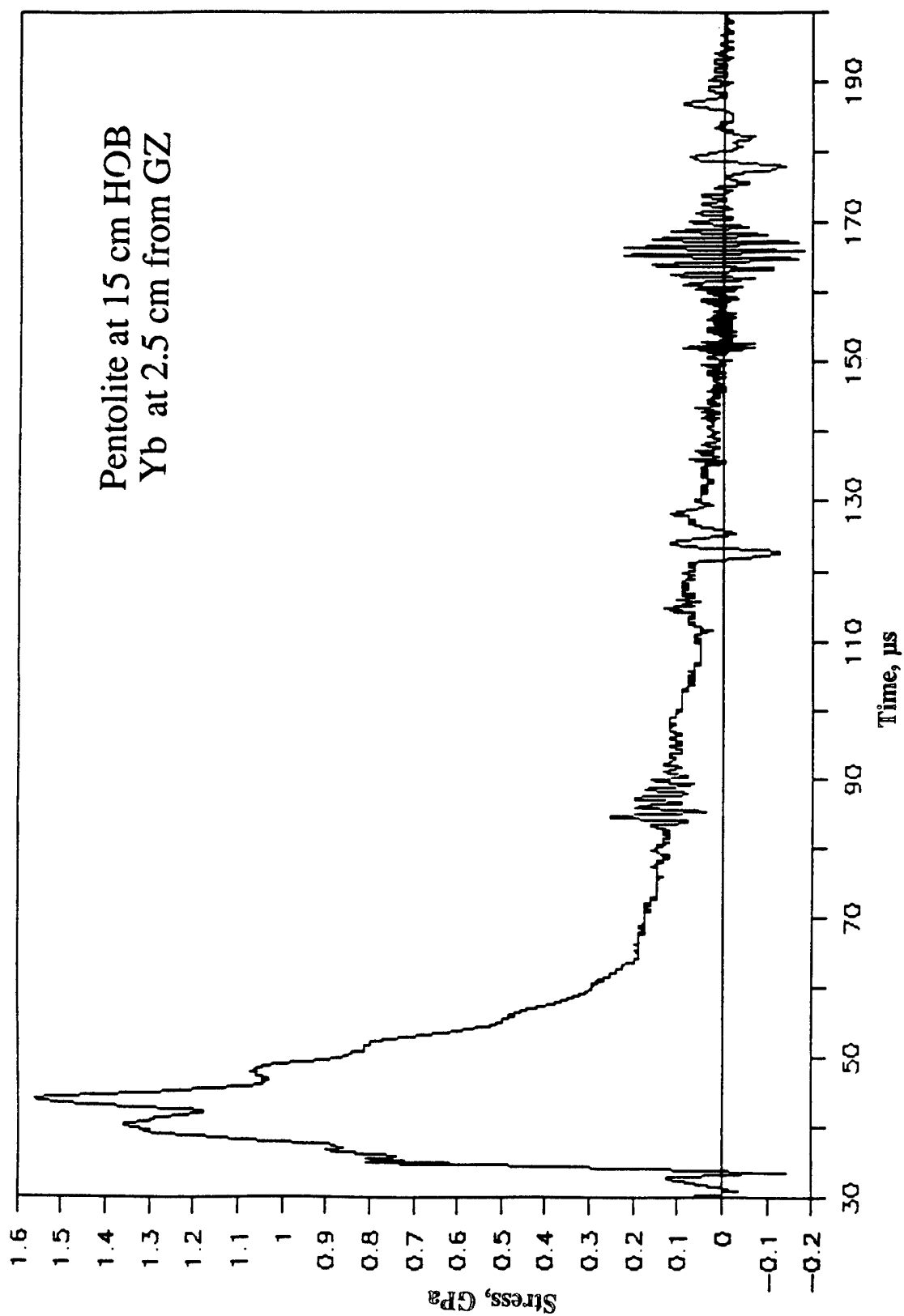


Figure A-45. Stress-Time Record From Ytterbium Element Yb-3, 2.5 cm From Centerline, Baseplate Test 2A.7, Pentolite at 15-cm HOB.

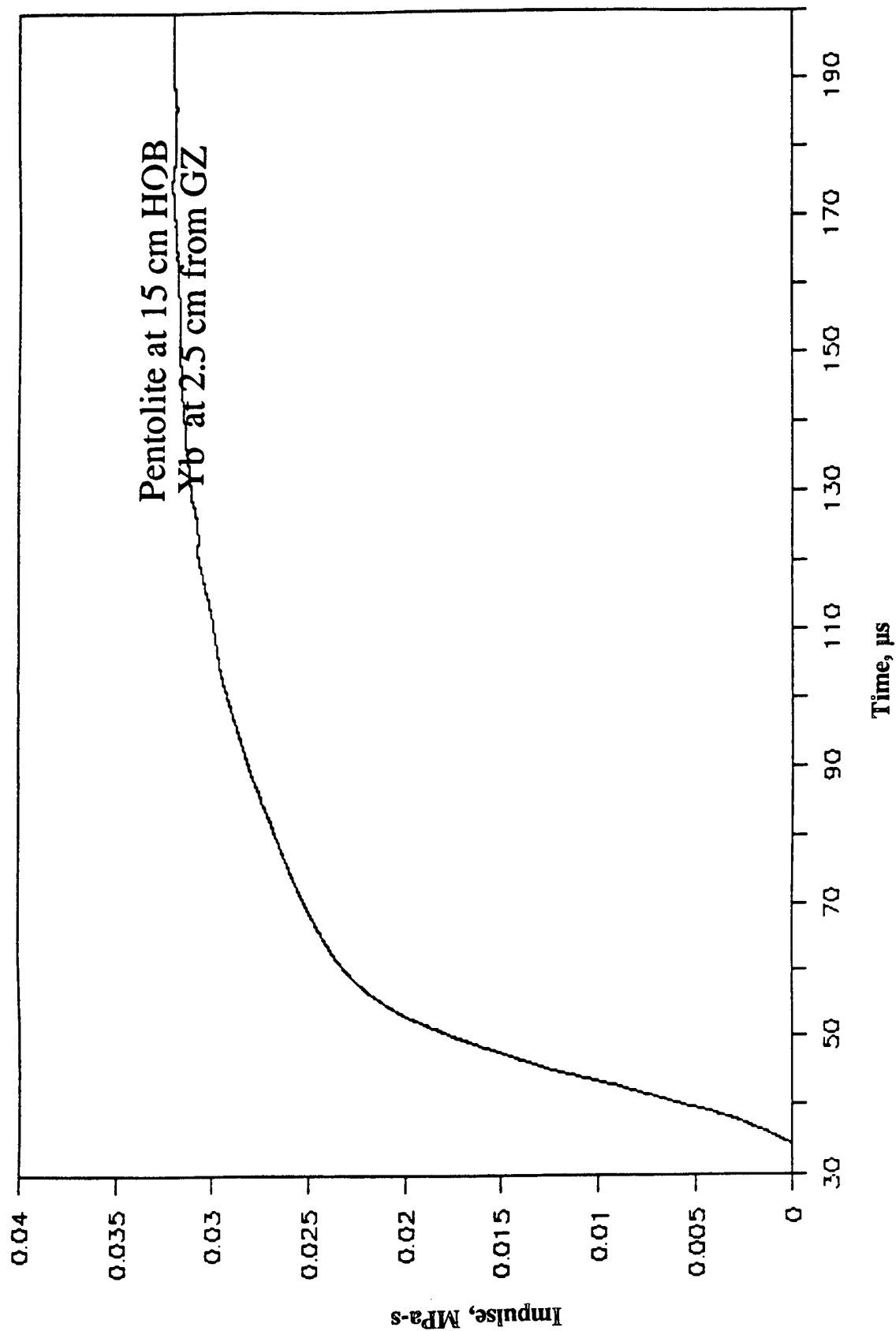


Figure A-46. Impulse-Time Record From Ytterbium Element Yb-3, 2.5 cm From Centerline, Baseplate Test 2A.7, Pentolite at 15-cm HOB.

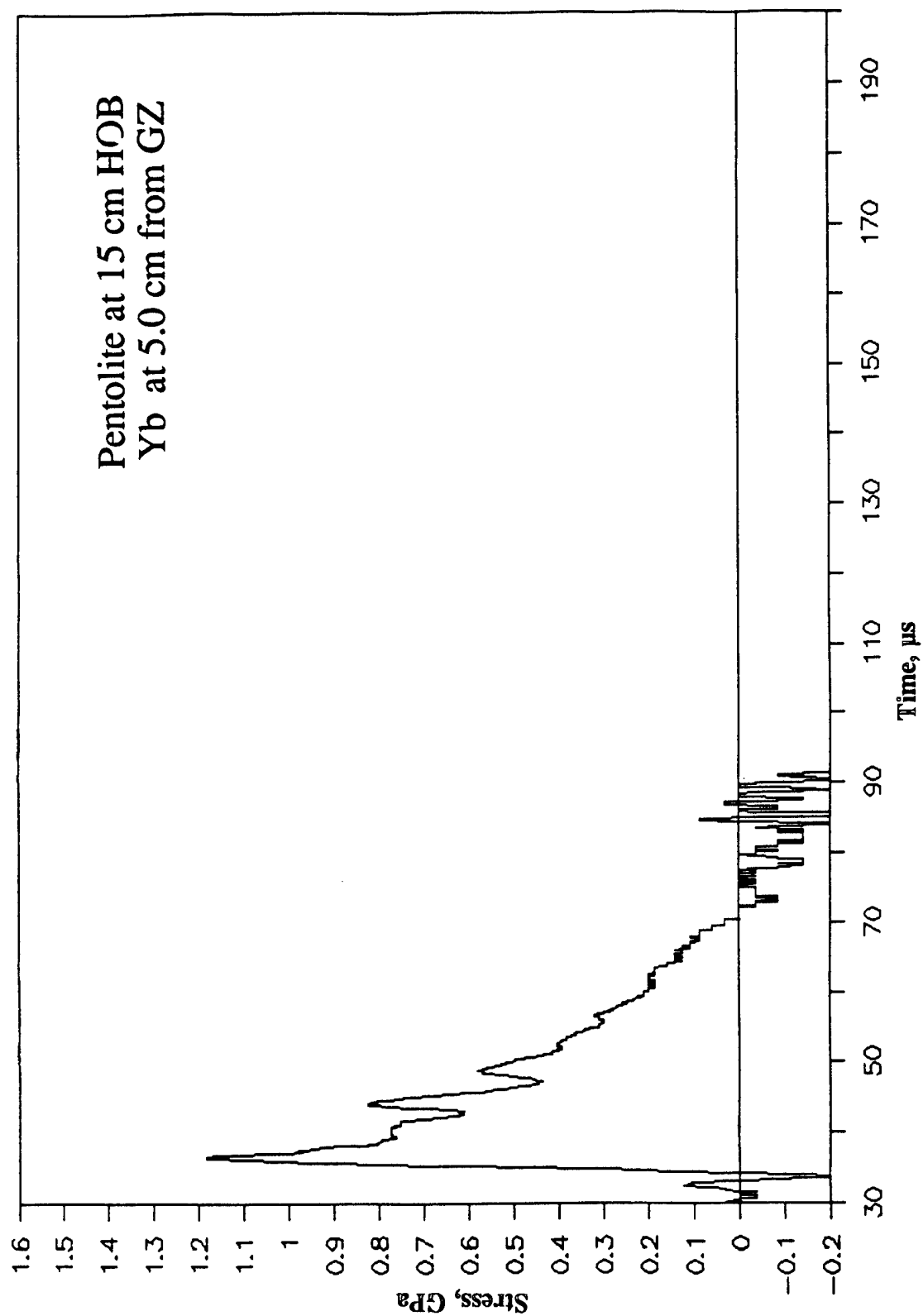


Figure A-47. Stress-Time Record From Ytterbium Element Yb-4, 5.0 cm From Centerline, Baseplate Test 2A.7, Pentolite at 15-cm HOB.

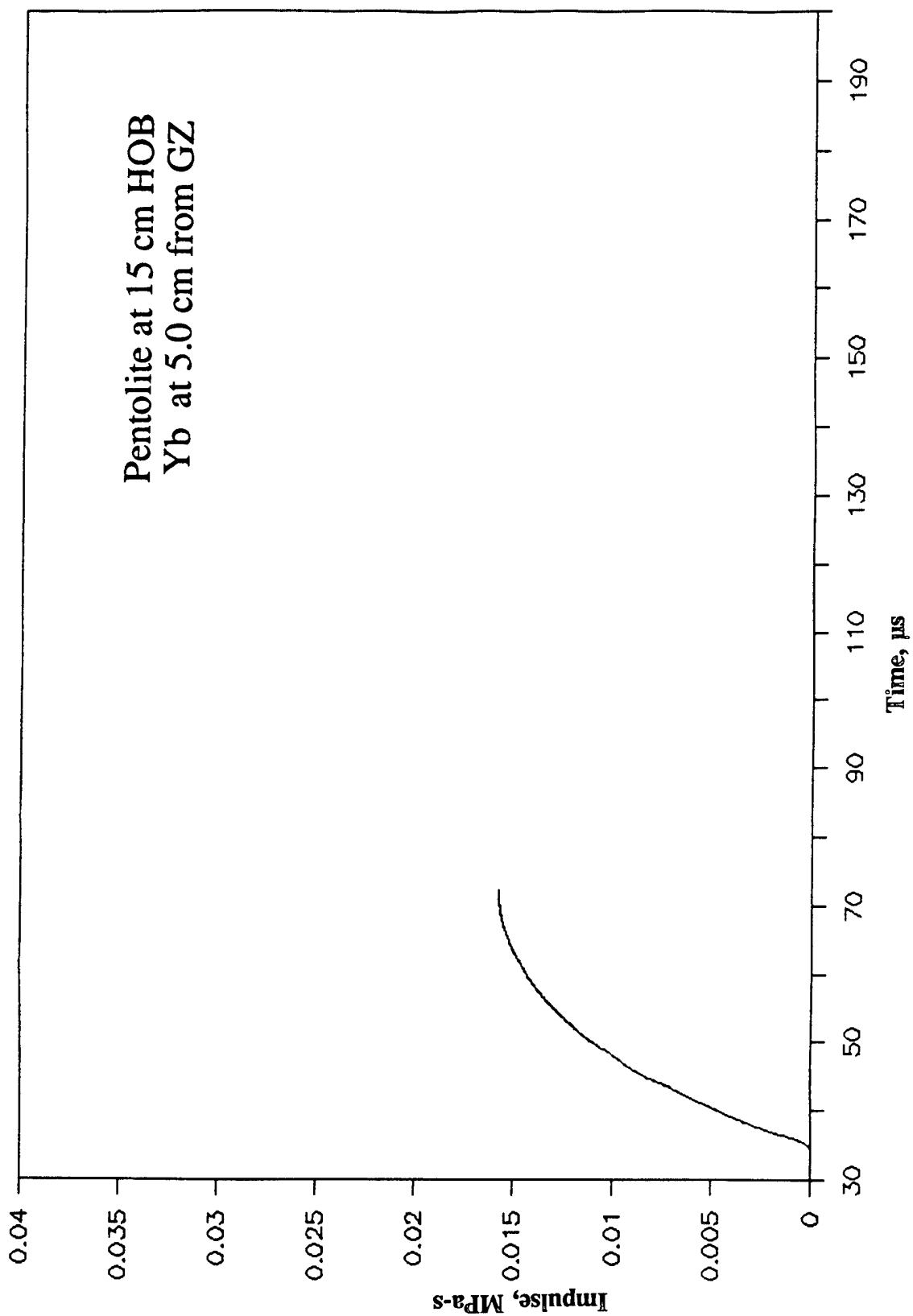


Figure A-48. Impulse-Time Record From Ytterbium Element Yb-4, 5.0 cm From Centerline, Baseplate Test 2A.7, Pentolite at 15-cm HOB.

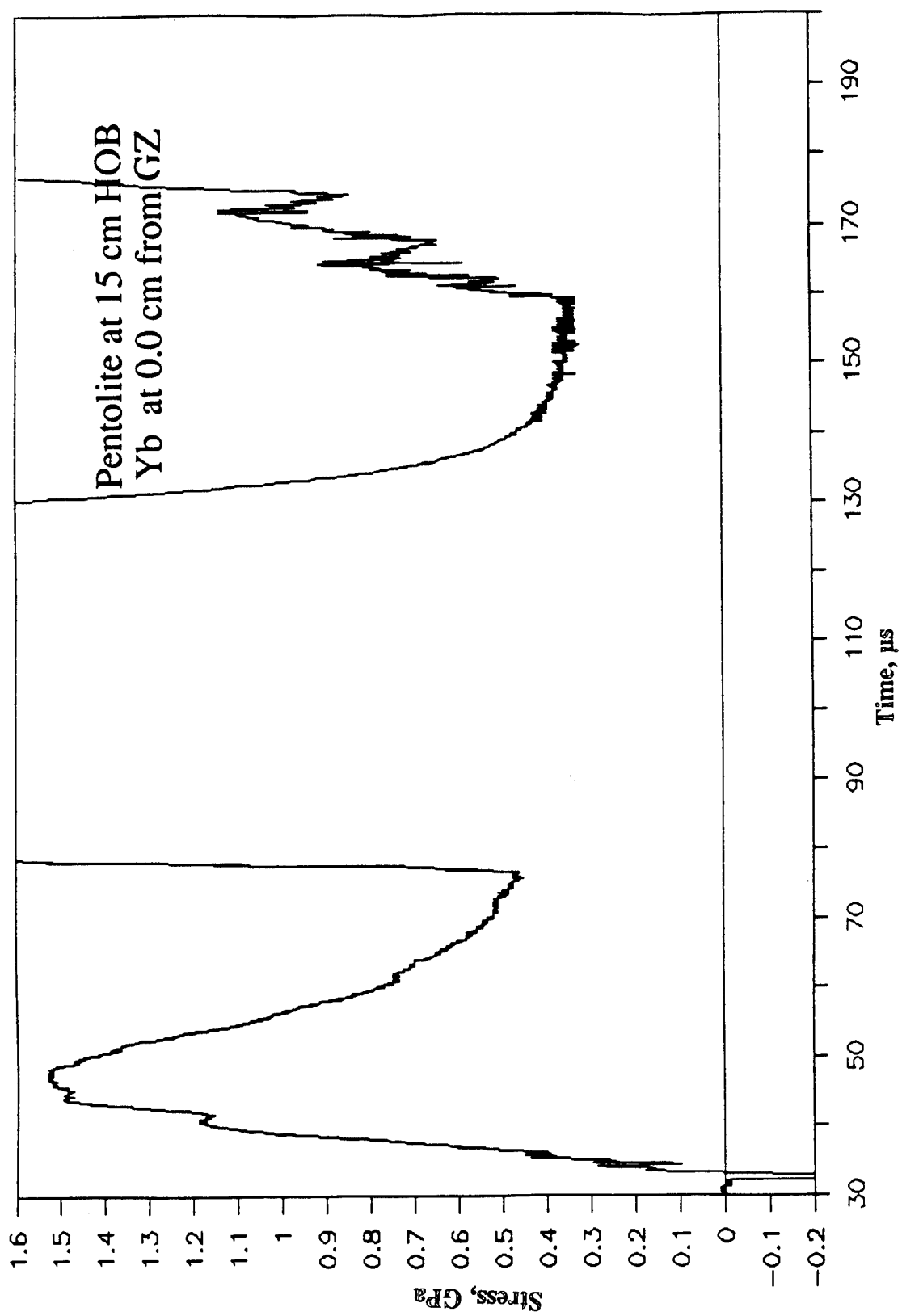


Figure A-49. Stress-Time Record From Ytterbium Element Yb-5, 0.0 cm From Centerline, Baseplate Test 2A.7, Pentolite at 15-cm HOB.

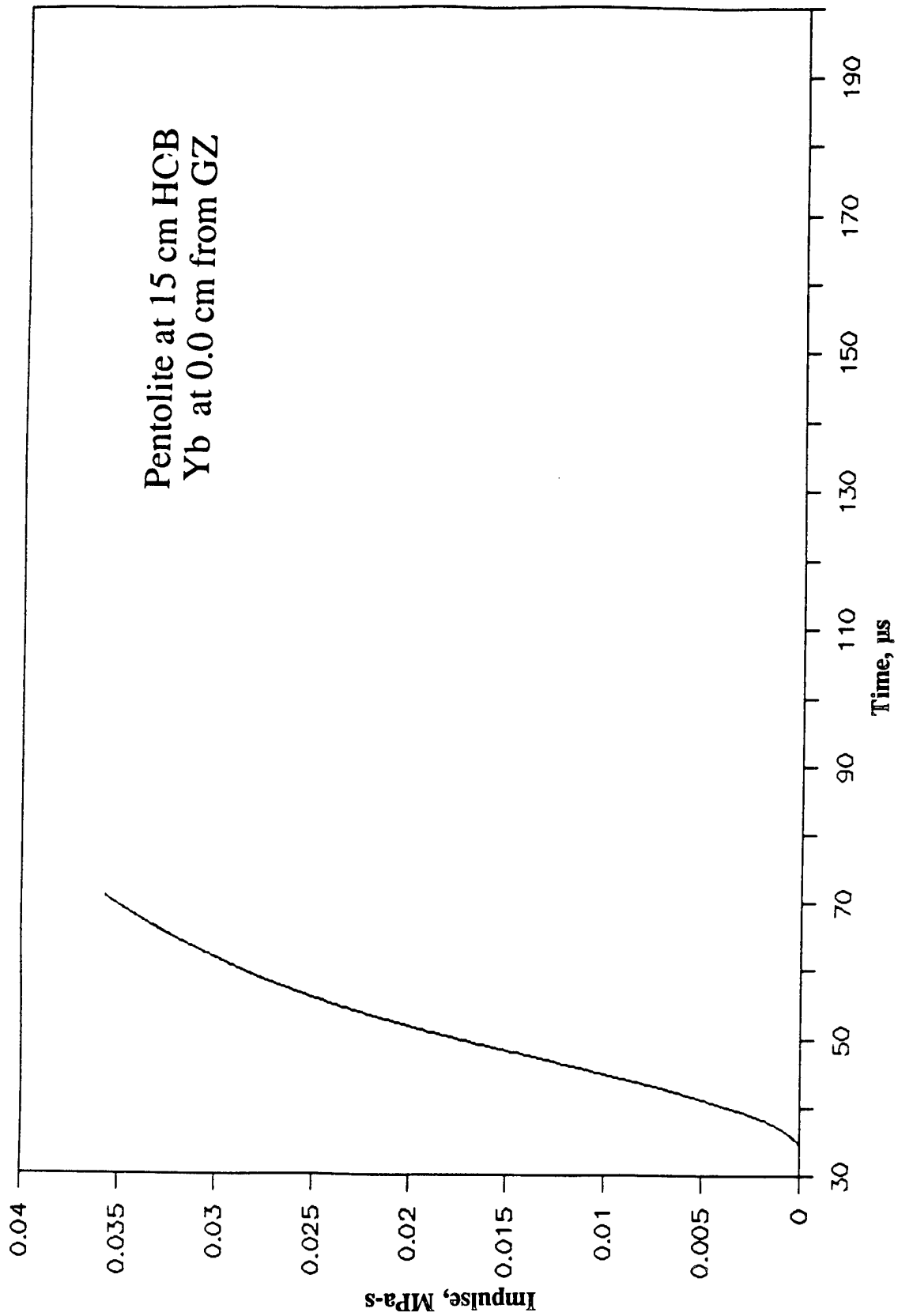


Figure A-50. Impulse-Time Record From Ytterbium Element Yb-5, 0.0 cm From Centerline, Baseplate Test 2A.7, Pentolite at 15-cm HOB.

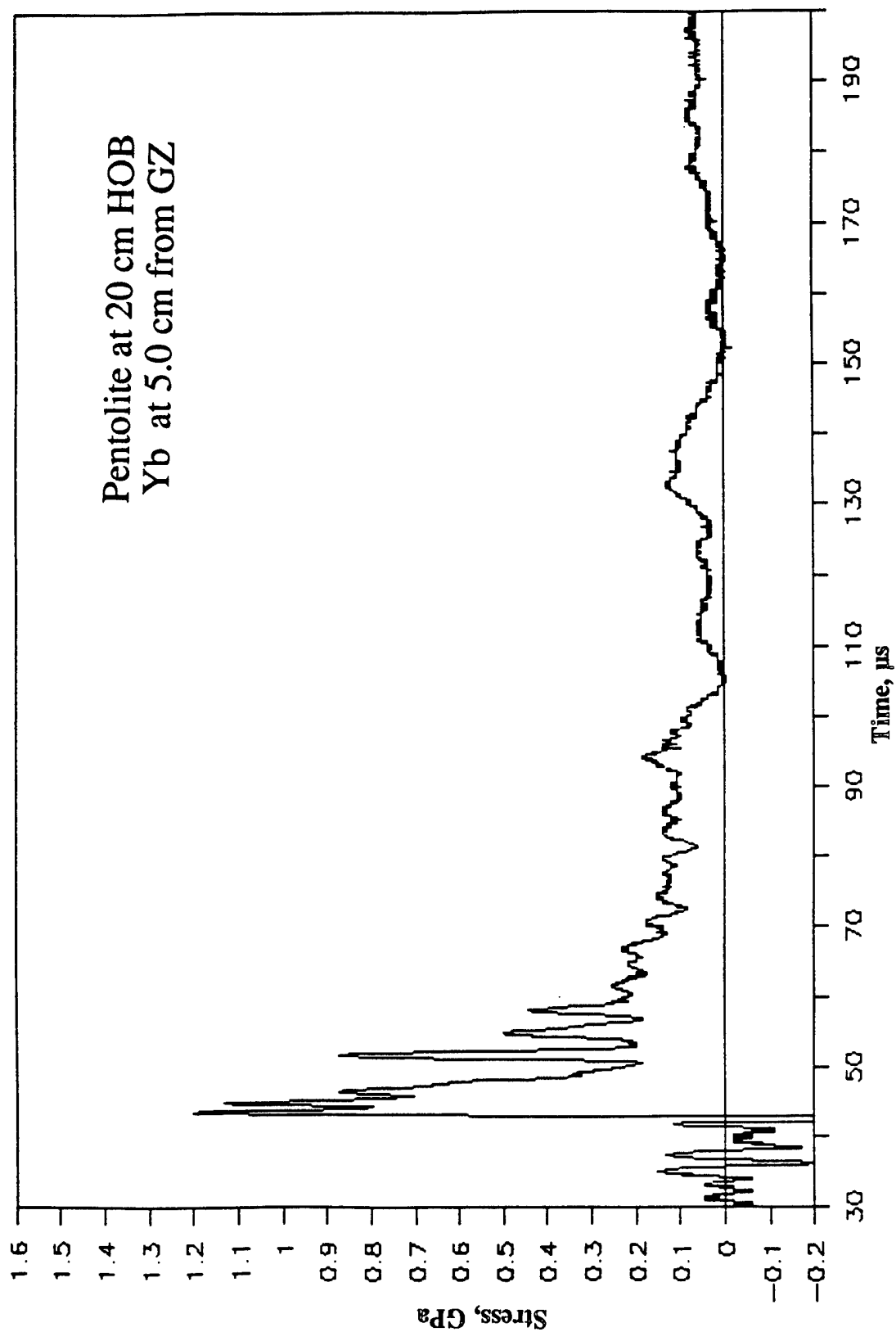


Figure A-51. Stress-Time Record From Ytterbium Element Yb-1, 5.0 cm From Centerline, Baseplate Test 2A.8, Pentolite at 20-cm HOB.

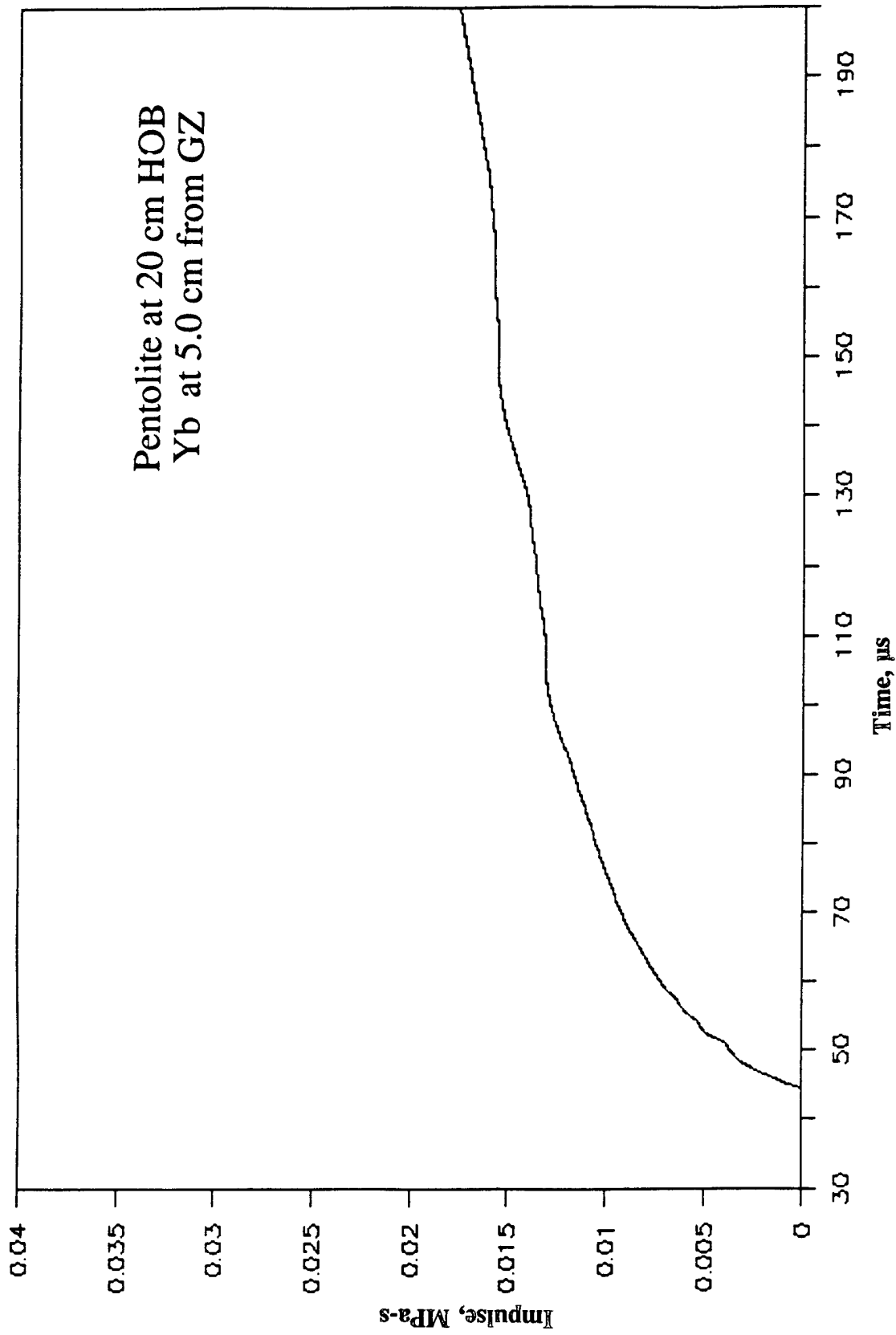


Figure A-52. Impulse-Time Record From Ytterbium Element Yb-1, 5.0 cm From Centerline, Baseplate Test 2A.8, Pentolite at 20-cm HOB.

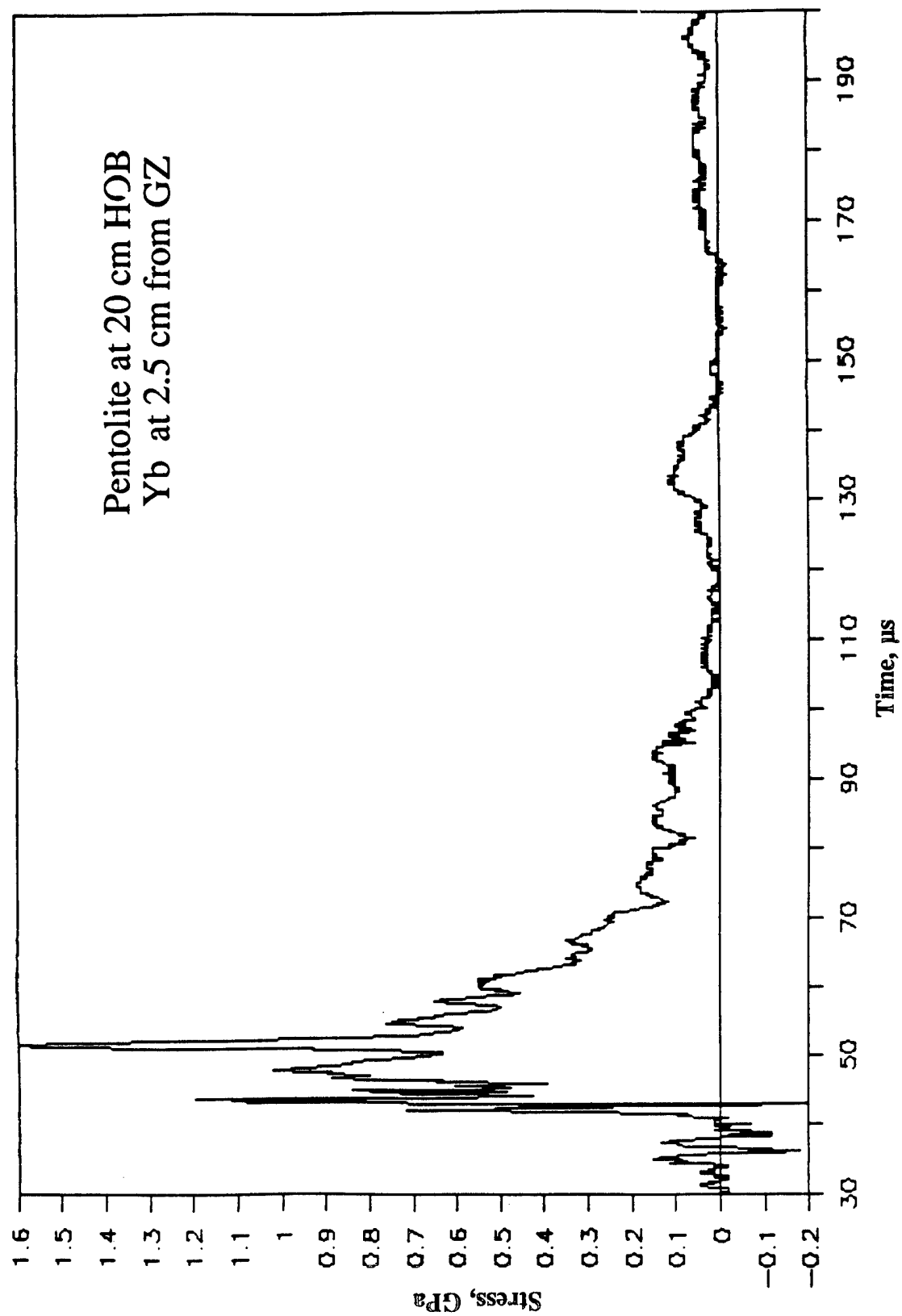


Figure A-53. Stress-Time Record From Ytterbium Element Yb-2, 2.5 cm From Centerline, Baseplate Test 2A.8, Pentolite at 20-cm HOB.

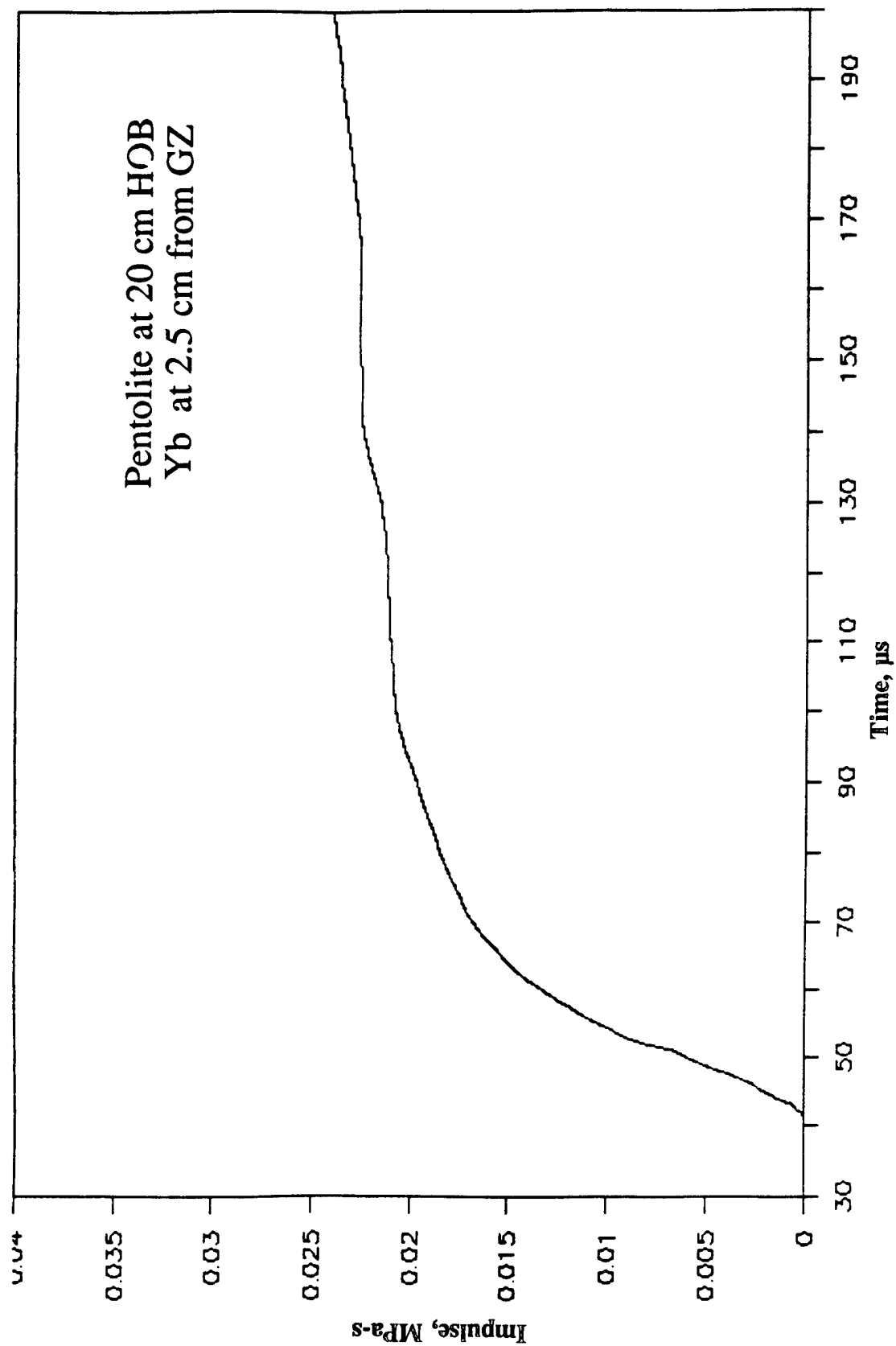


Figure A-54. Impulse-Time Record From Ytterbium Element Yb-2, 2.5 cm From Centerline, Baseplate Test 2A.8, Pentolite at 20-cm HOB.

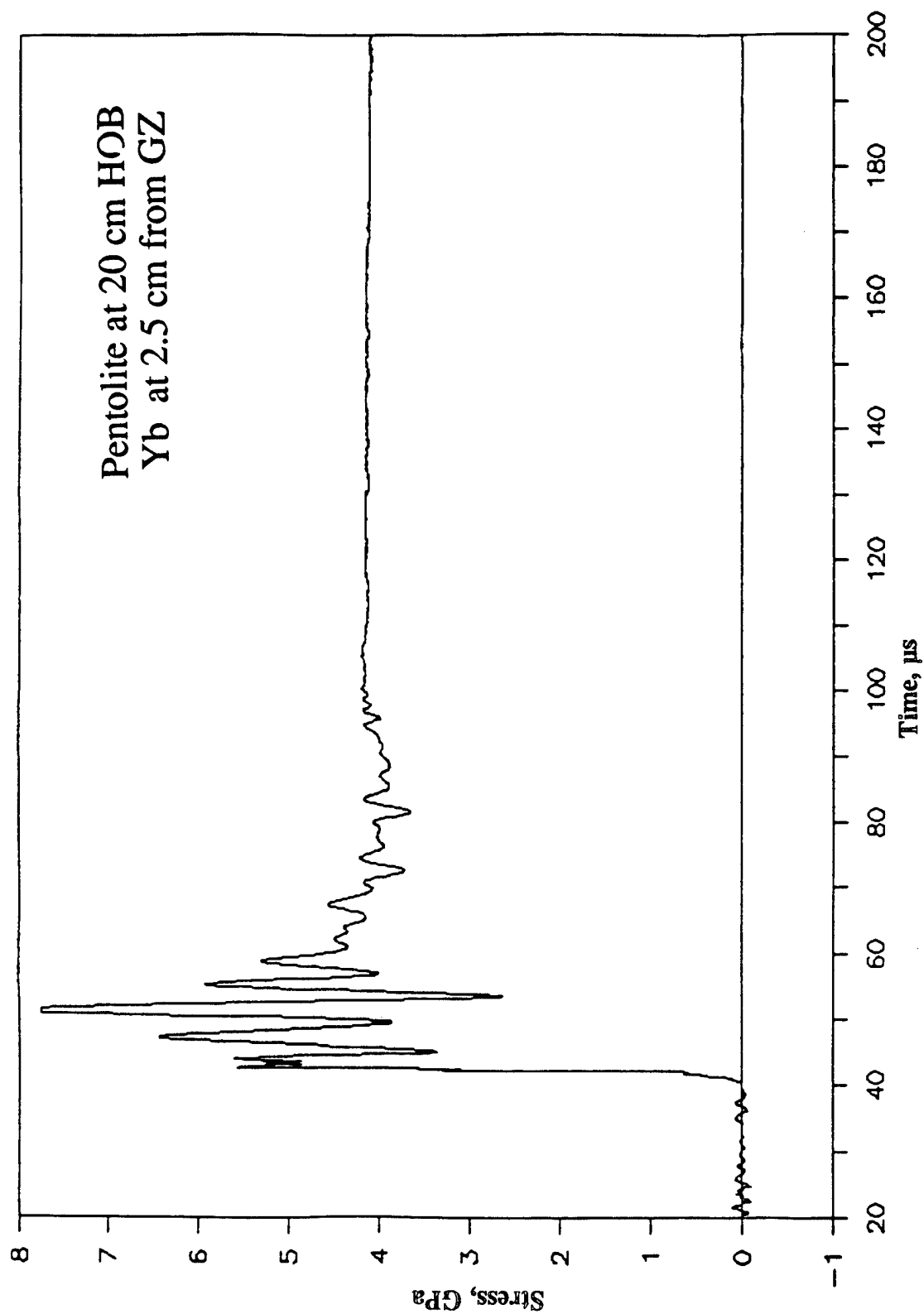


Figure A-55. Stress-Time Record From Ytterbium Element Yb-3, 2.5 cm From Centerline, Baseplate Test 2A.8, Pentolite at 20-cm HOB.

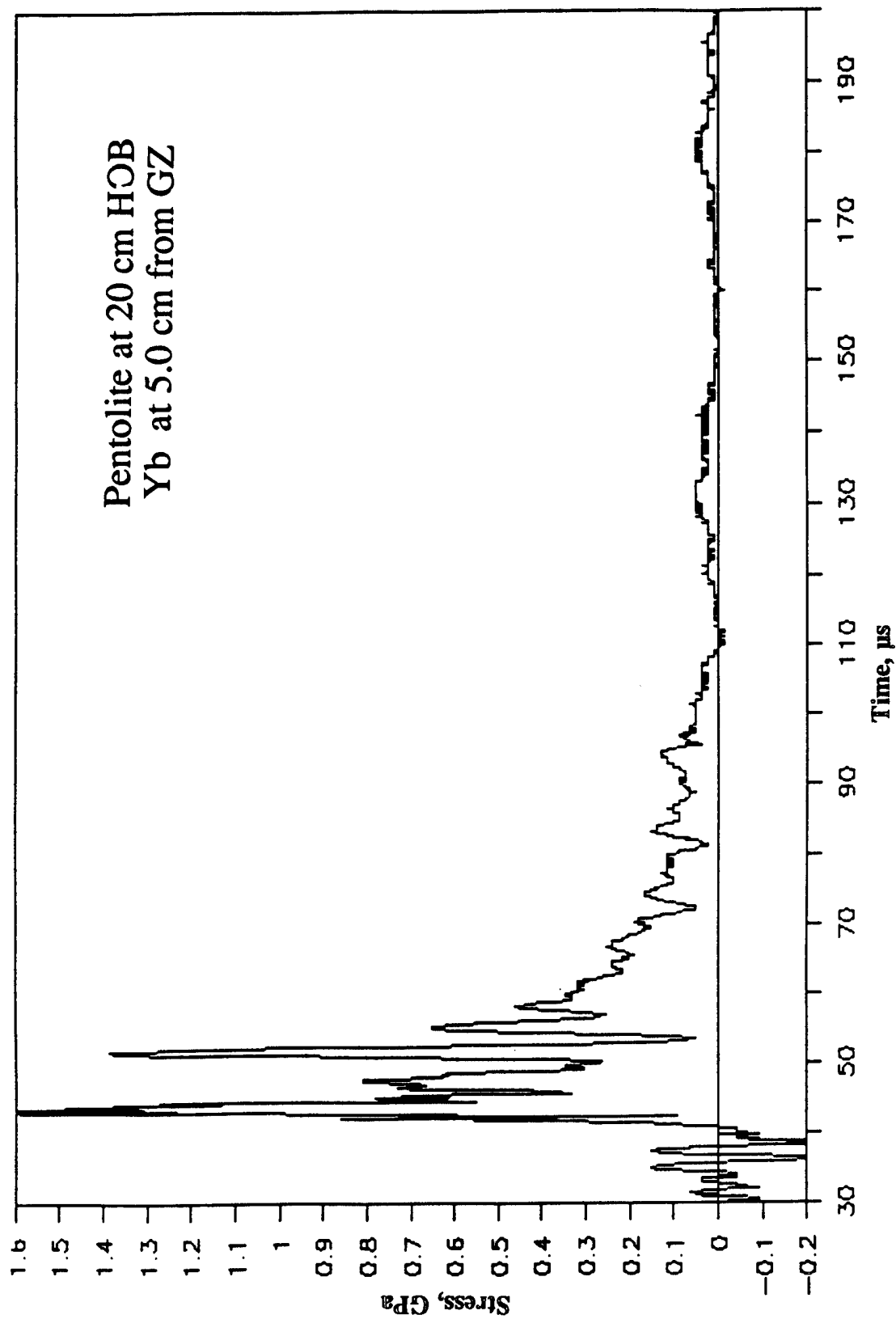


Figure A-56. Stress-Time Record From Ytterbium Element Yb-4, 5.0 cm From Centerline, Baseplate Test 2A.8, Pentolite at 20-cm HOB.

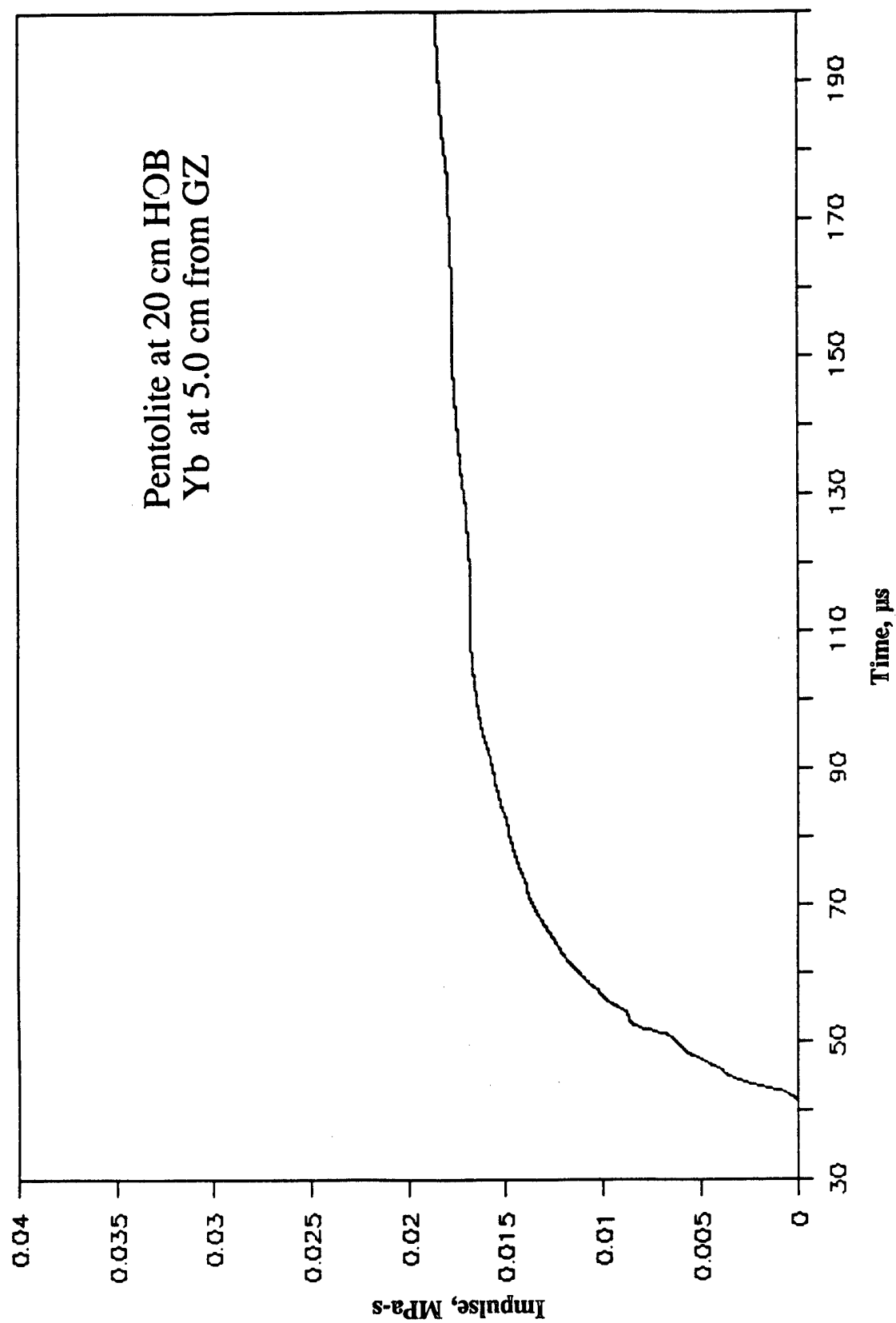


Figure A-57. Impulse-Time Record From Ytterbium Element Yb-4, 5.0 cm From Centerline, Baseplate Test 2A.8, Pentolite at 20-cm HOB.

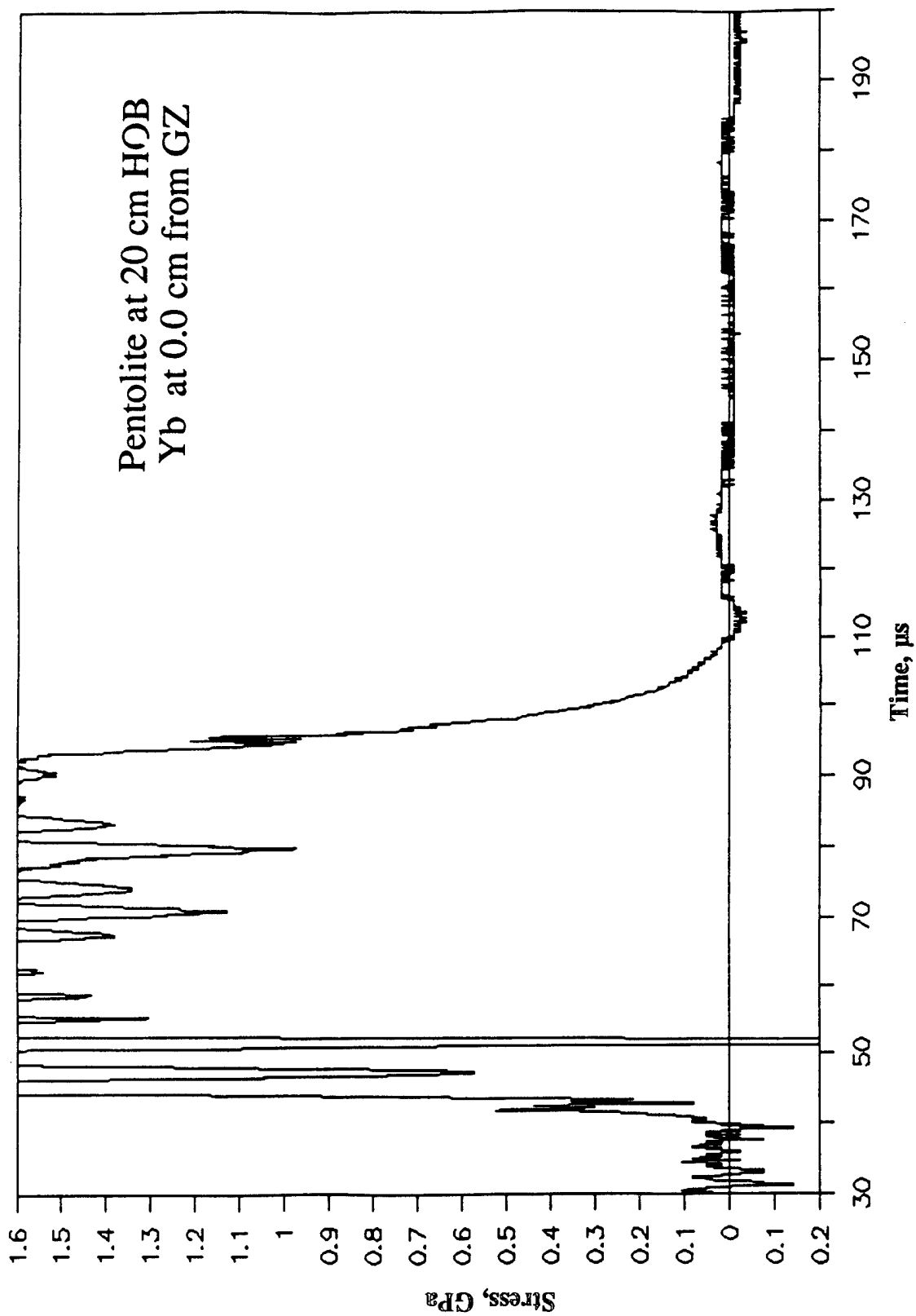


Figure A-58. Stress-Time Record From Ytterbium Element Yb-5, 0.0 cm From Centerline, Baseplate Test 2A.8, Pentolite at 20-cm HOB.

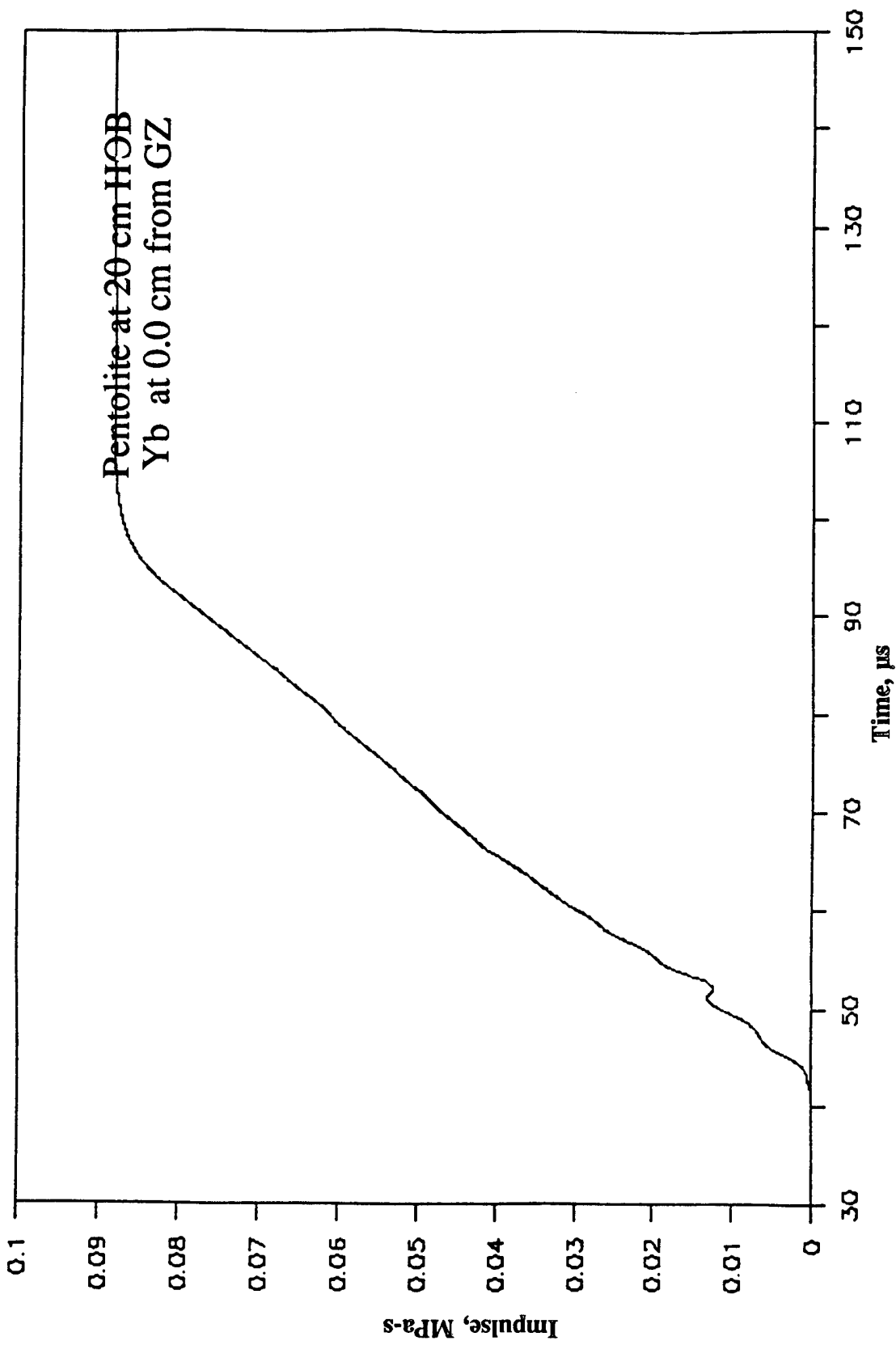


Figure A-59. Impulse-Time Record From Ytterbium Element Yb-5, 0.0 cm From Centerline, Baseplate Test 2A.8, Pentolite at 20-cm HOB.

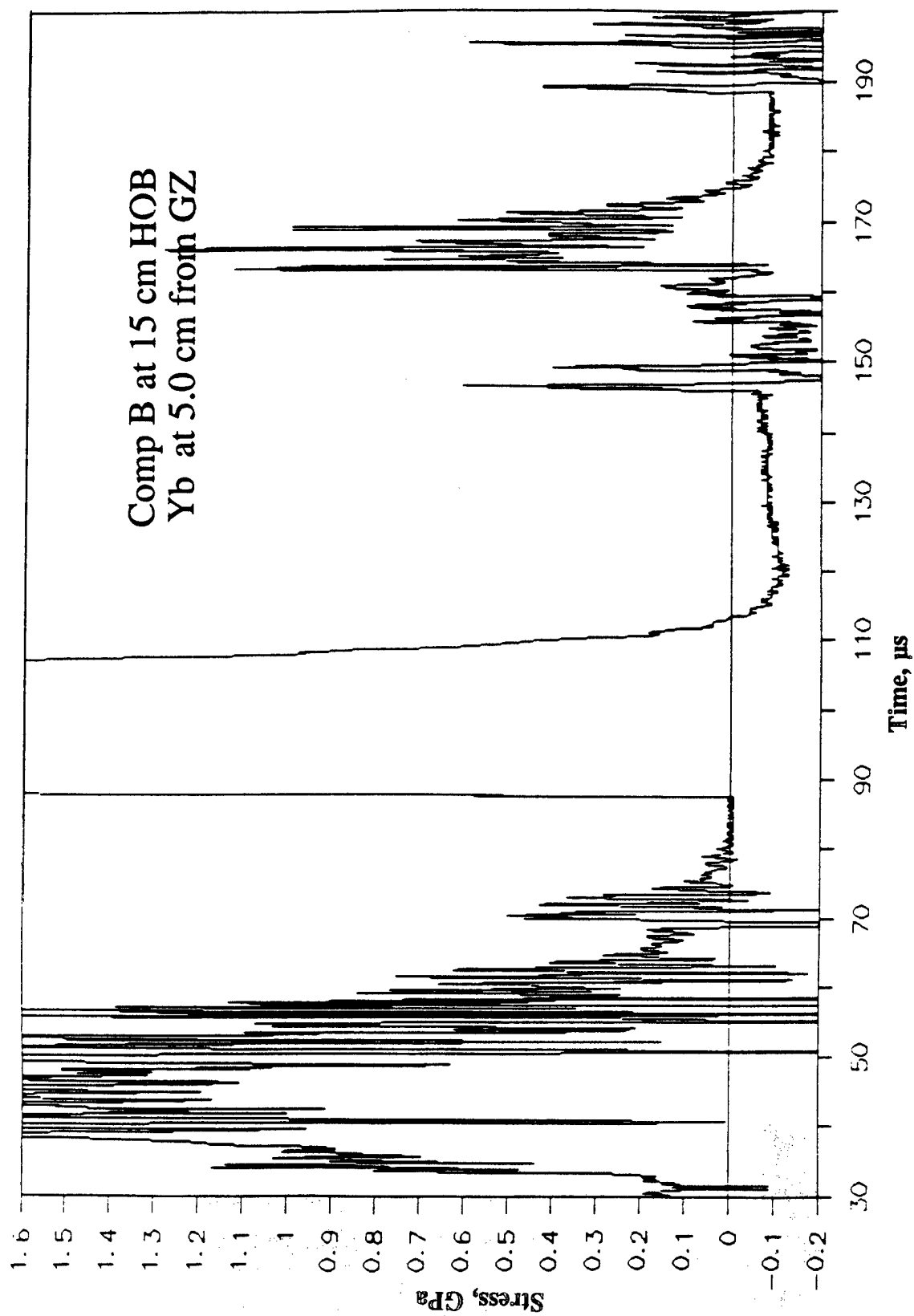


Figure A-60. Stress-Time Record From Ytterbium Element Yb-1, 5.0 cm From Centerline, Baseplate Test 2A.9, Comp B at 15-cm HOB.

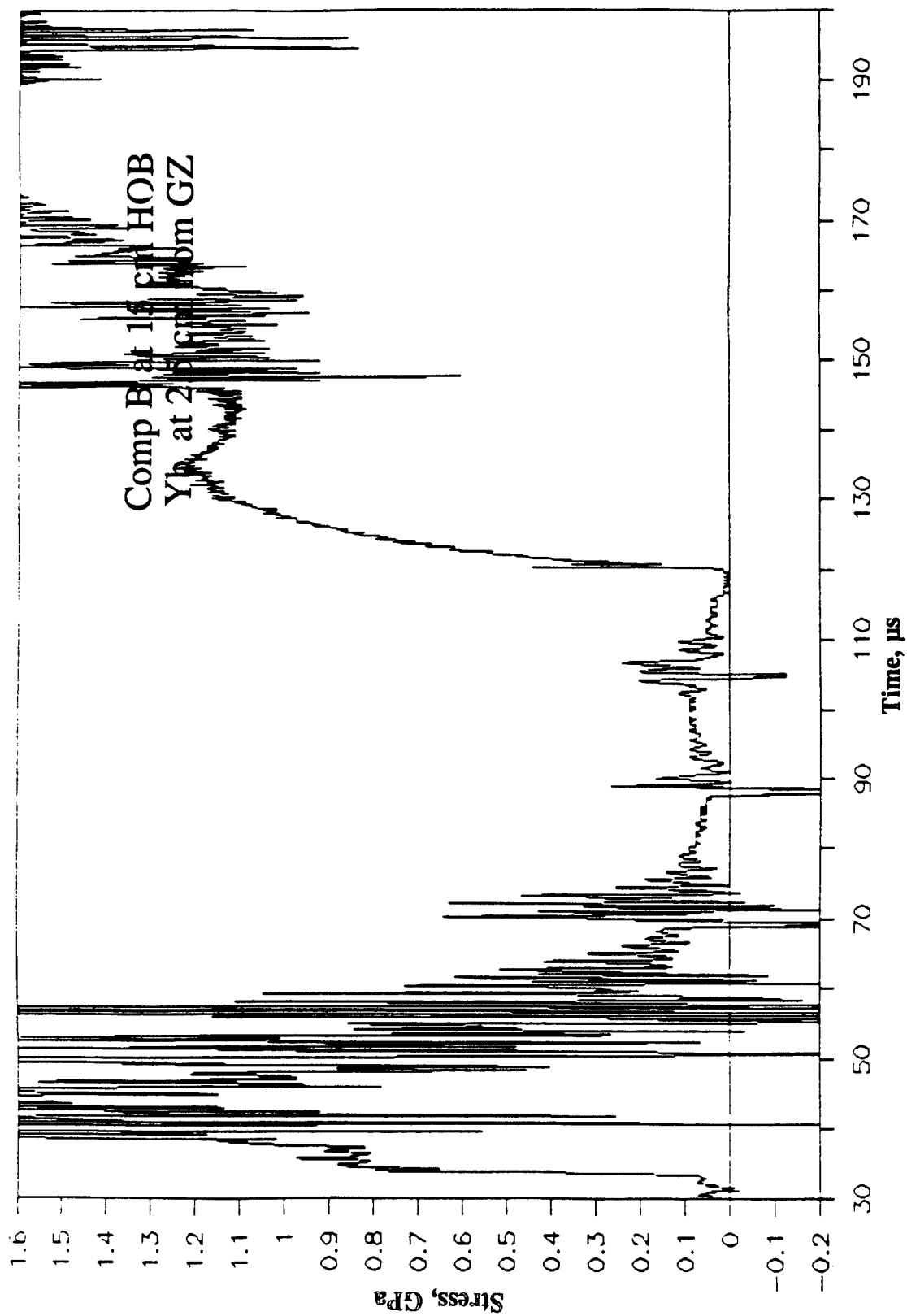


Figure A-61. Stress-Time Record From Ytterbium Element Yb-2, 2.5 cm From Centerline, Baseplate Test 2A.9, Comp B at 15-cm HOB.

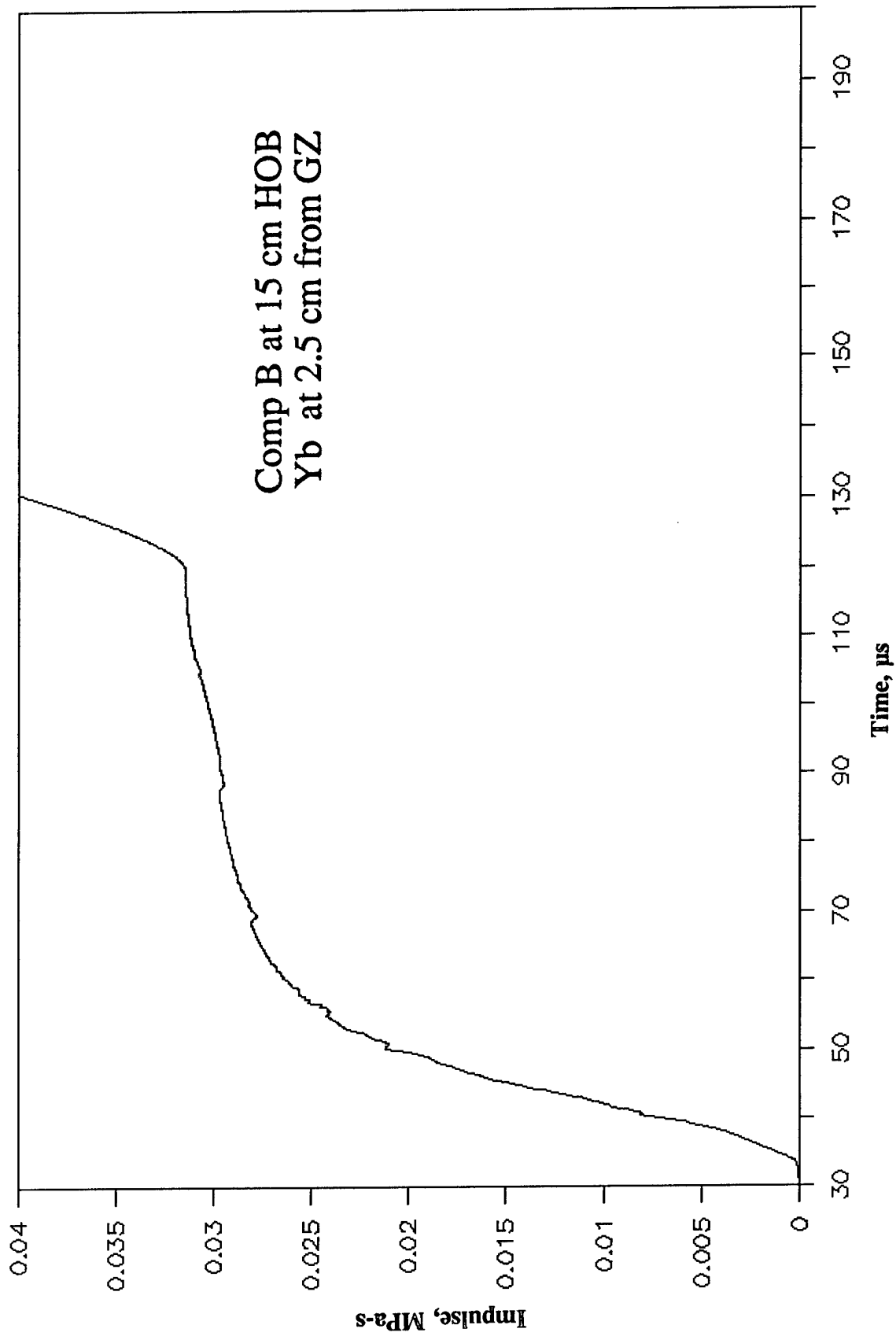


Figure A-62. Impulse-Time Record From Ytterbium Element Yb-2, 2.5 cm From Centerline, Baseplate Test 2A.9, Comp B at 15-cm HOB.

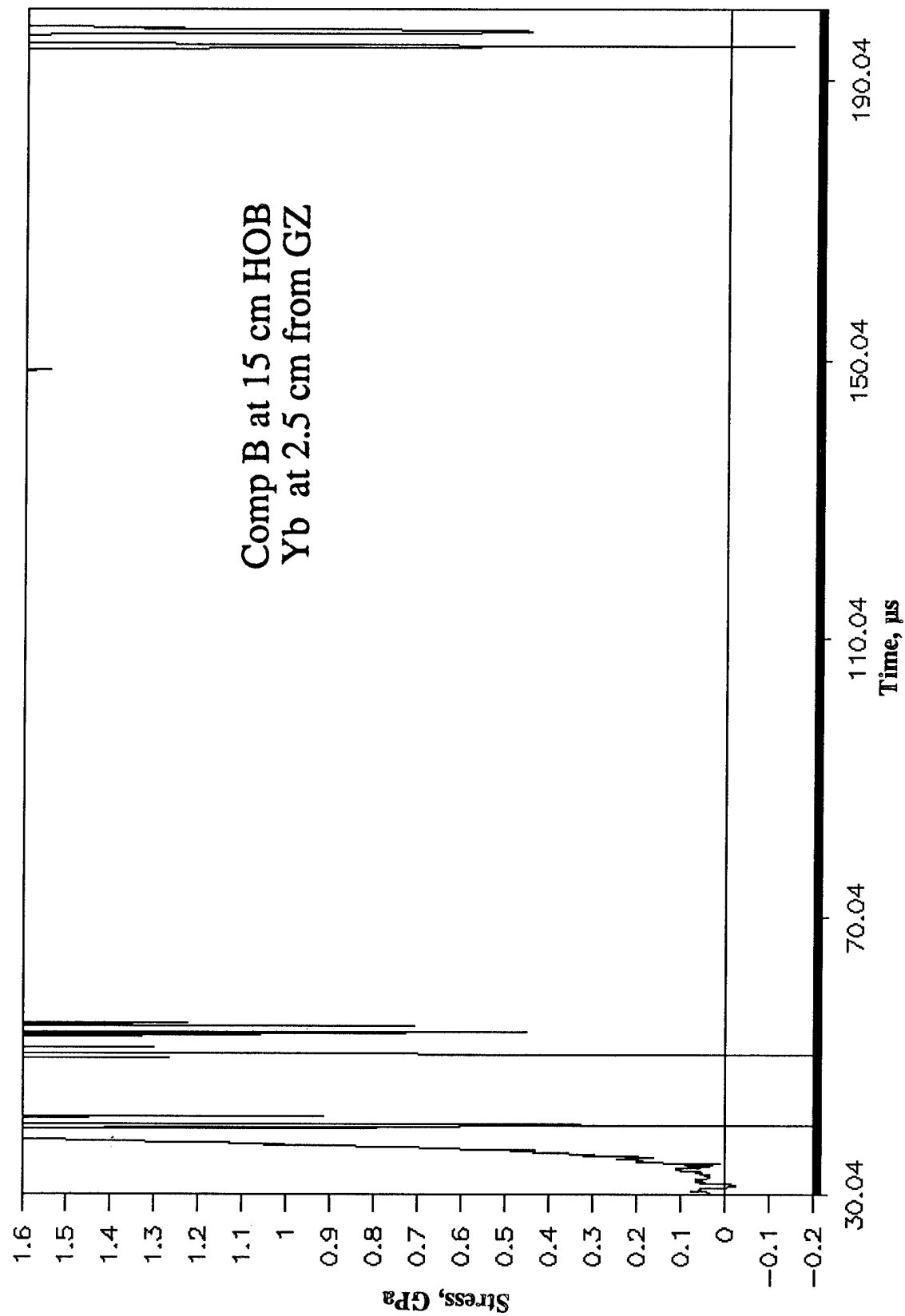


Figure A-63. Stress-Time Record From Ytterbium (in Glycerol) Element Yb-3, 2.5 cm From Centerline, Baseplate Test 2A.9, Comp B at 15-cm HOB.

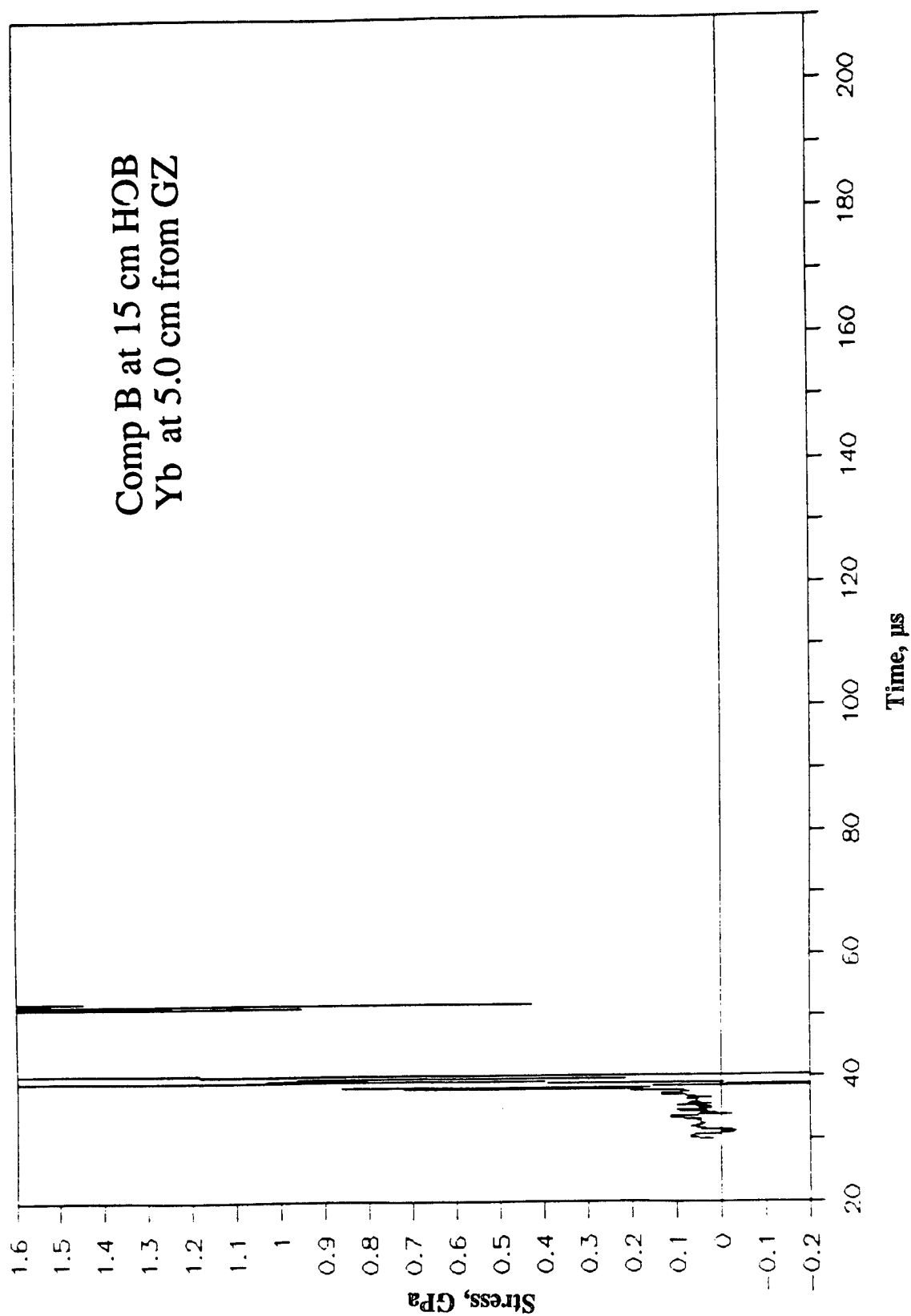


Figure A-64. Stress-Time Record From Ytterbium (in Glycerol) Element Yb-4, 5.0 cm From Centerline, Baseplate Test 2A.9, Comp B at 15-cm HOB.

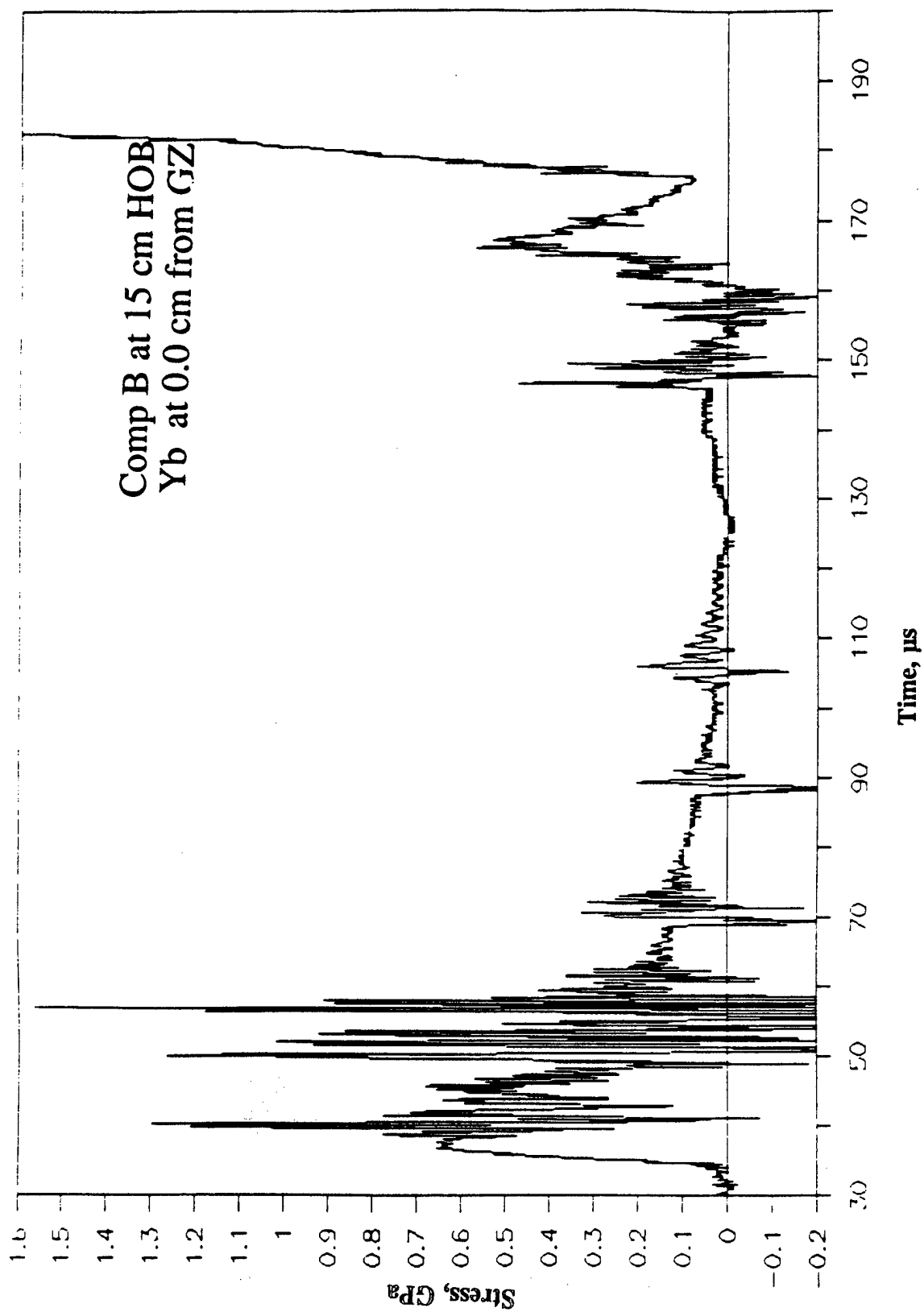


Figure A-65. Stress-Time Record From Ytterbium Element Yb-5, 0.0 cm From Centerline, Baseplate Test 2A.9, Comp B at 15-cm HOB.

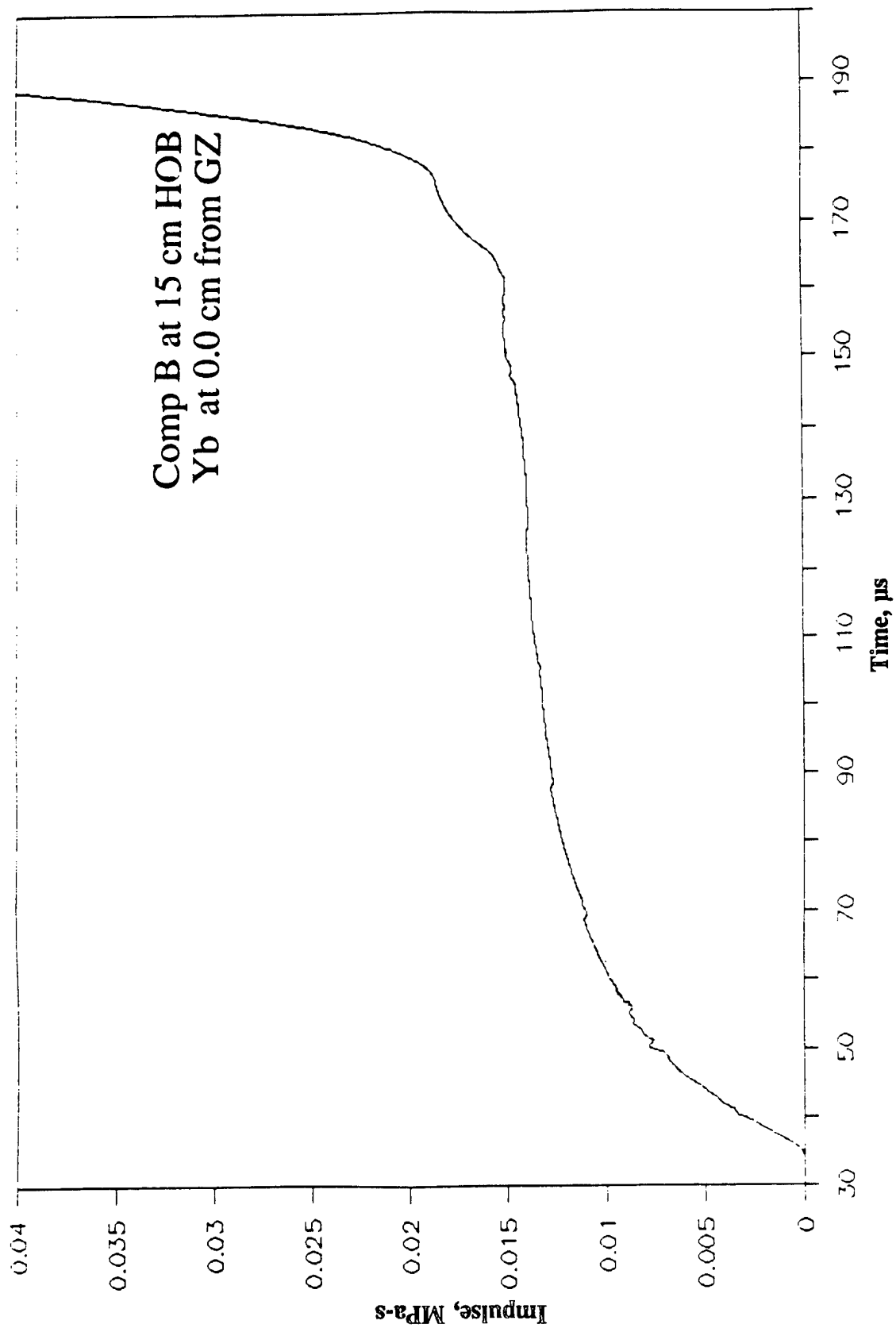


Figure A-66. Impulse-Time Record From Ytterbium Element Yb-5, 0.0 cm From Centerline, Baseplate Test 2A.9, Comp B at 15-cm HOB.

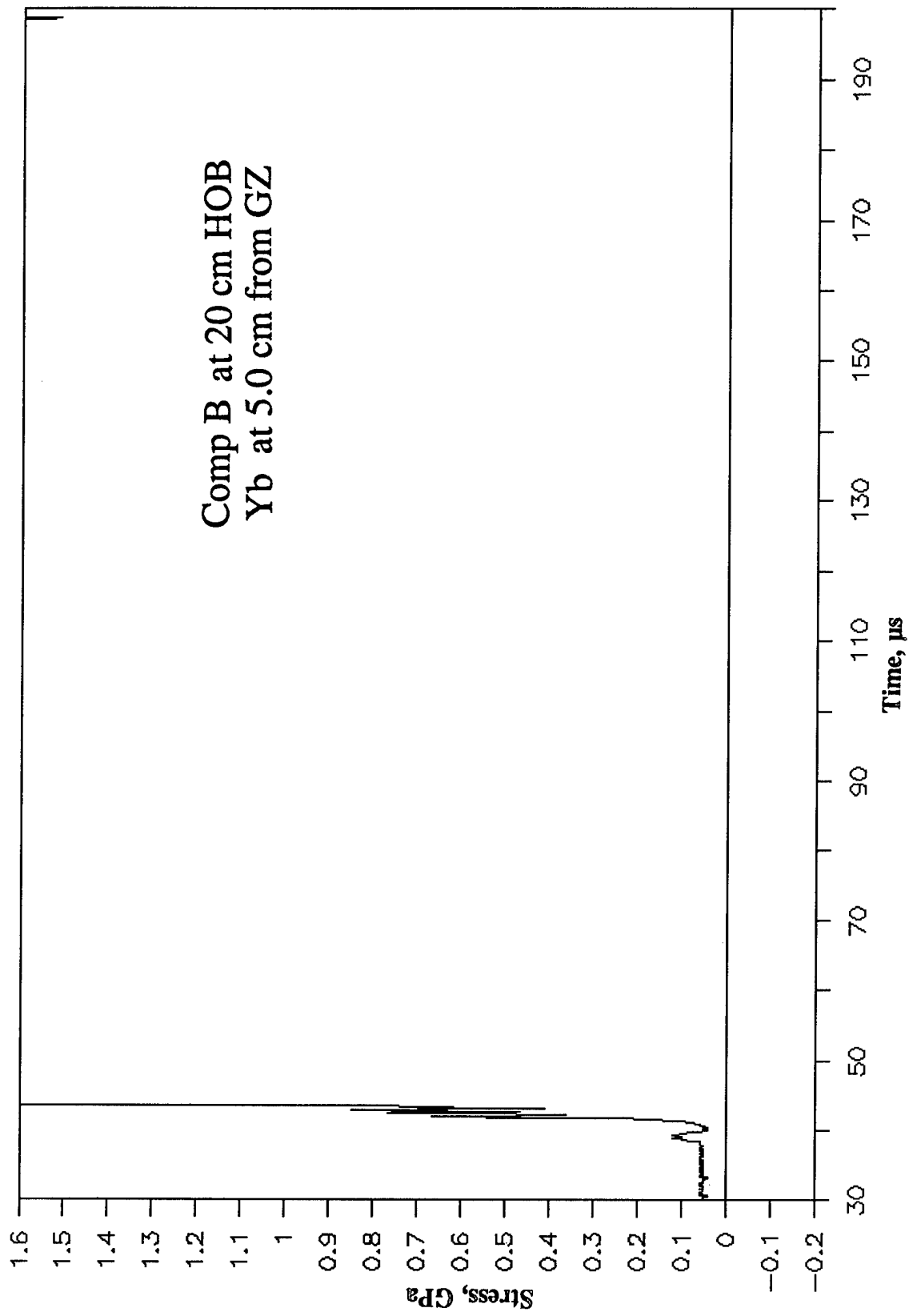


Figure A-67. Stress-Time Record From Ytterbium Element Yb-1, 5.0 cm From Centerline, Baseplate Test 2A.10, Comp B at 20-cm HOB.

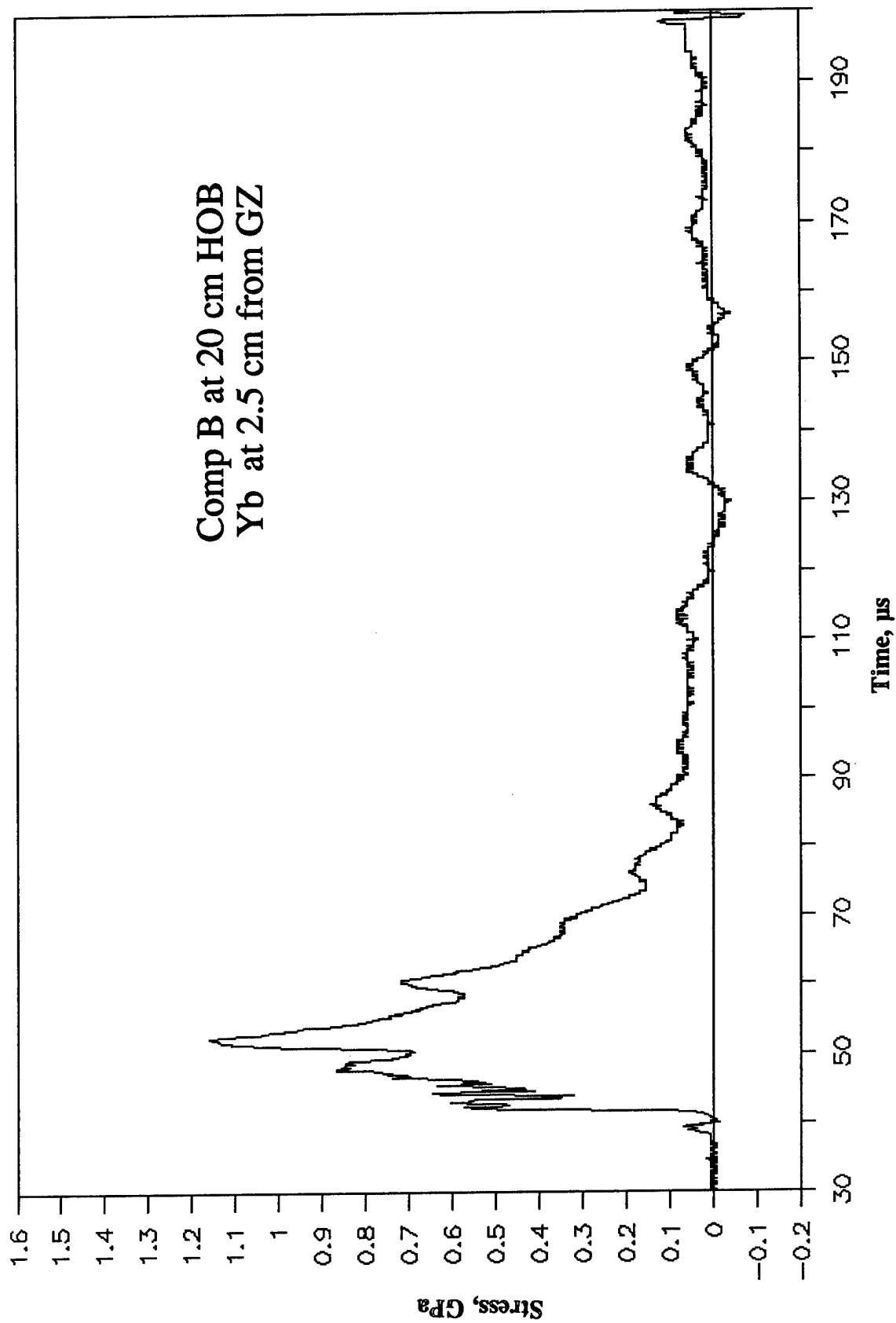


Figure A-68. Stress-Time Record From Ytterbium Element Yb-2, 2.5 cm From Centerline, Baseplate Test 2A.10, Comp B at 20-cm HOB.

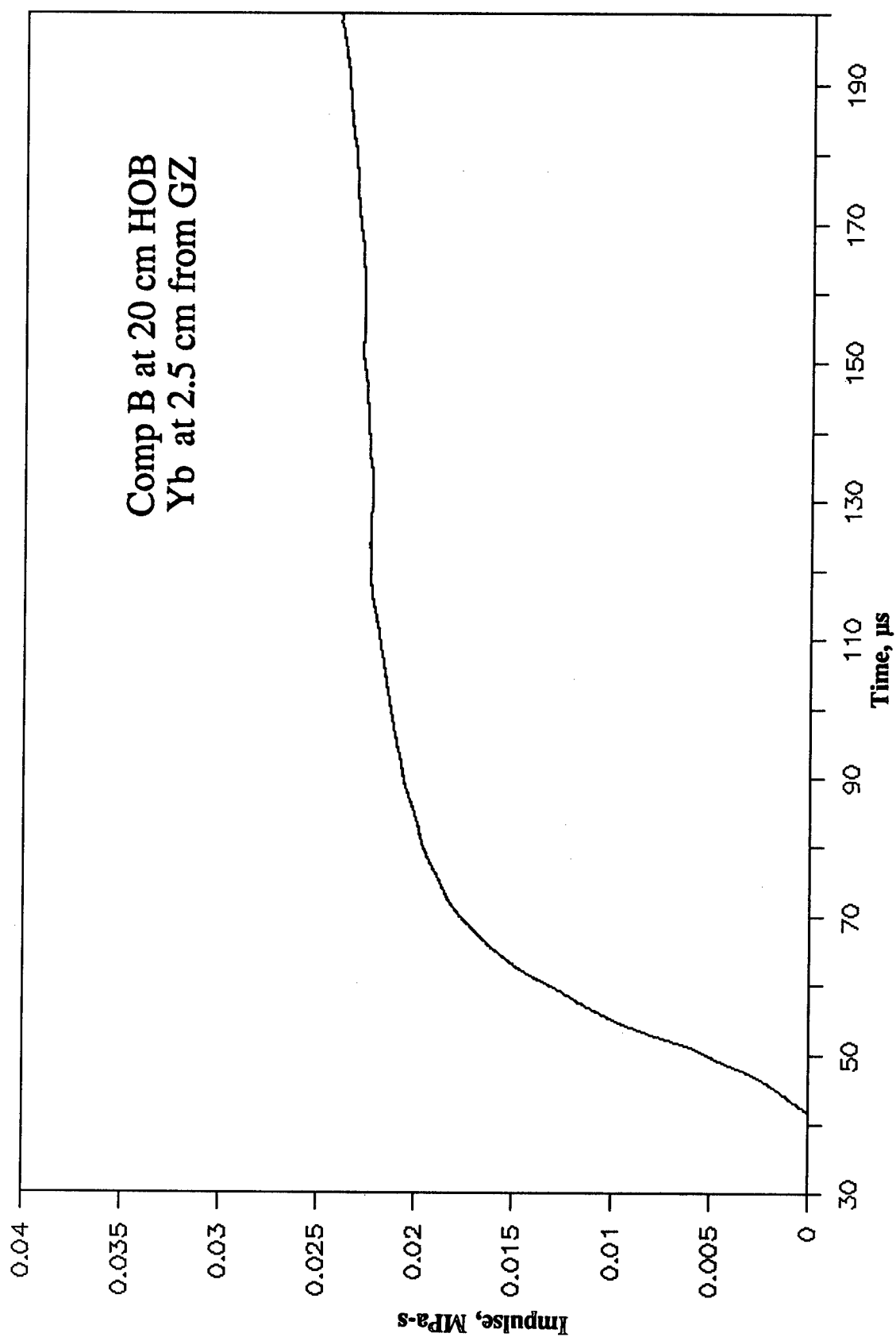


Figure A-69. Impulse-Time Record From Ytterbium Element Yb-2, 2.5 cm From Centerline, Baseplate Test 2A.10, Comp B at 20-cm HOB.

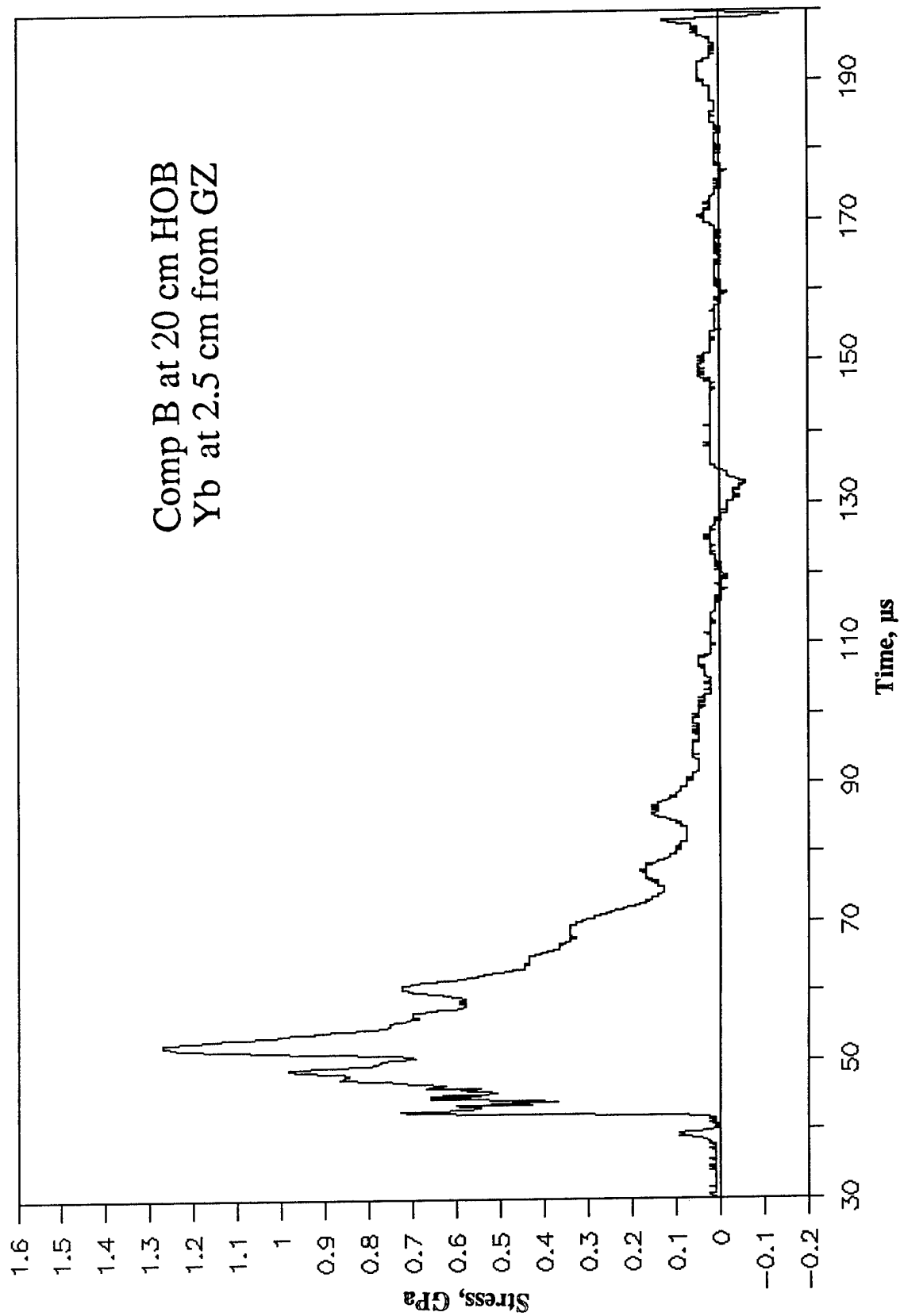


Figure A-70. Stress-Time Record From Ytterbium Element Yb-3, 2.5 cm From Centerline, Baseplate Test 2A.10, Comp B at 20-cm HOB.

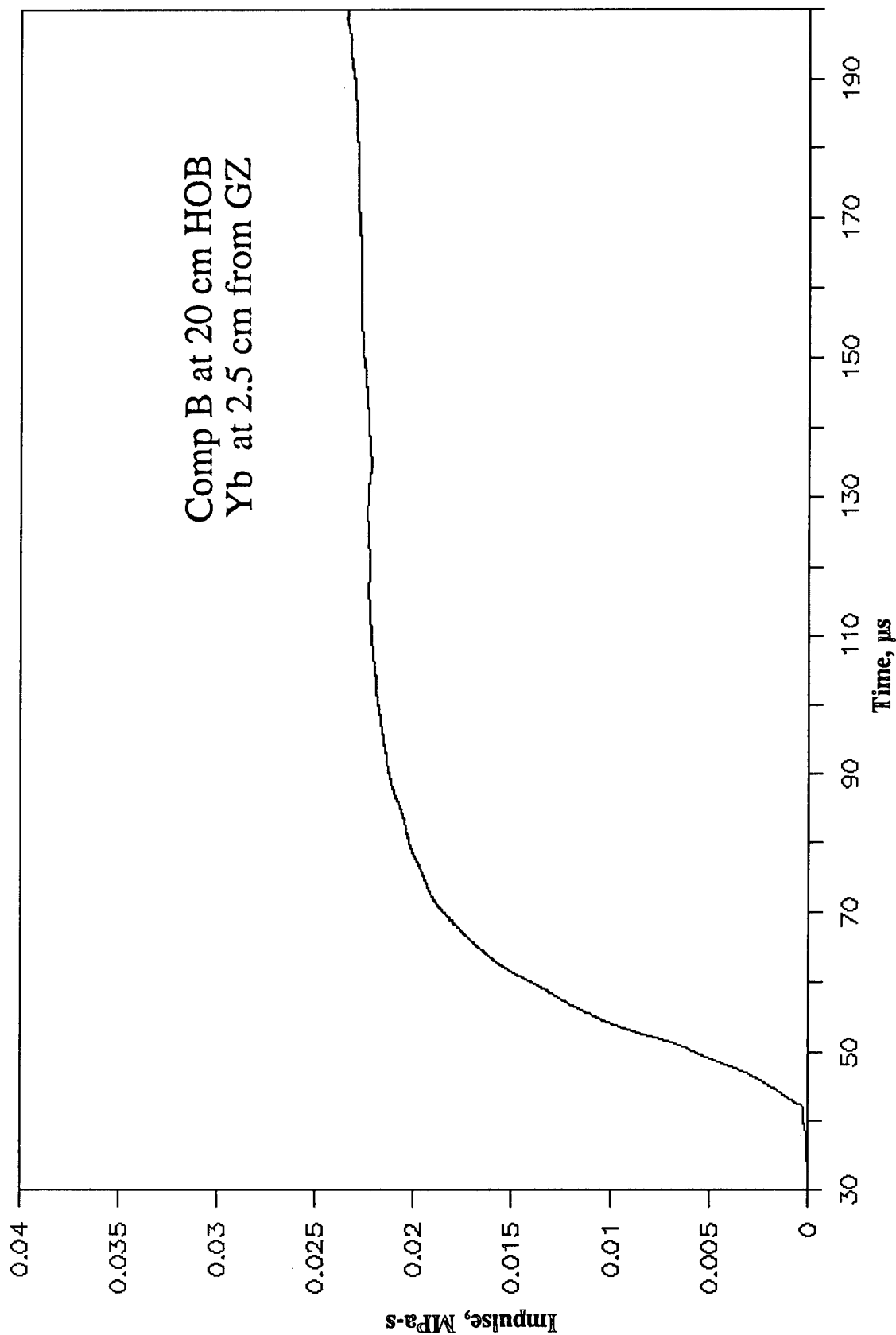


Figure A-71. Impulse-Time Record From Ytterbium Element Yb-3, 2.5 cm From Centerline, Baseplate Test 2A.10, Comp B at 20-cm HOB.

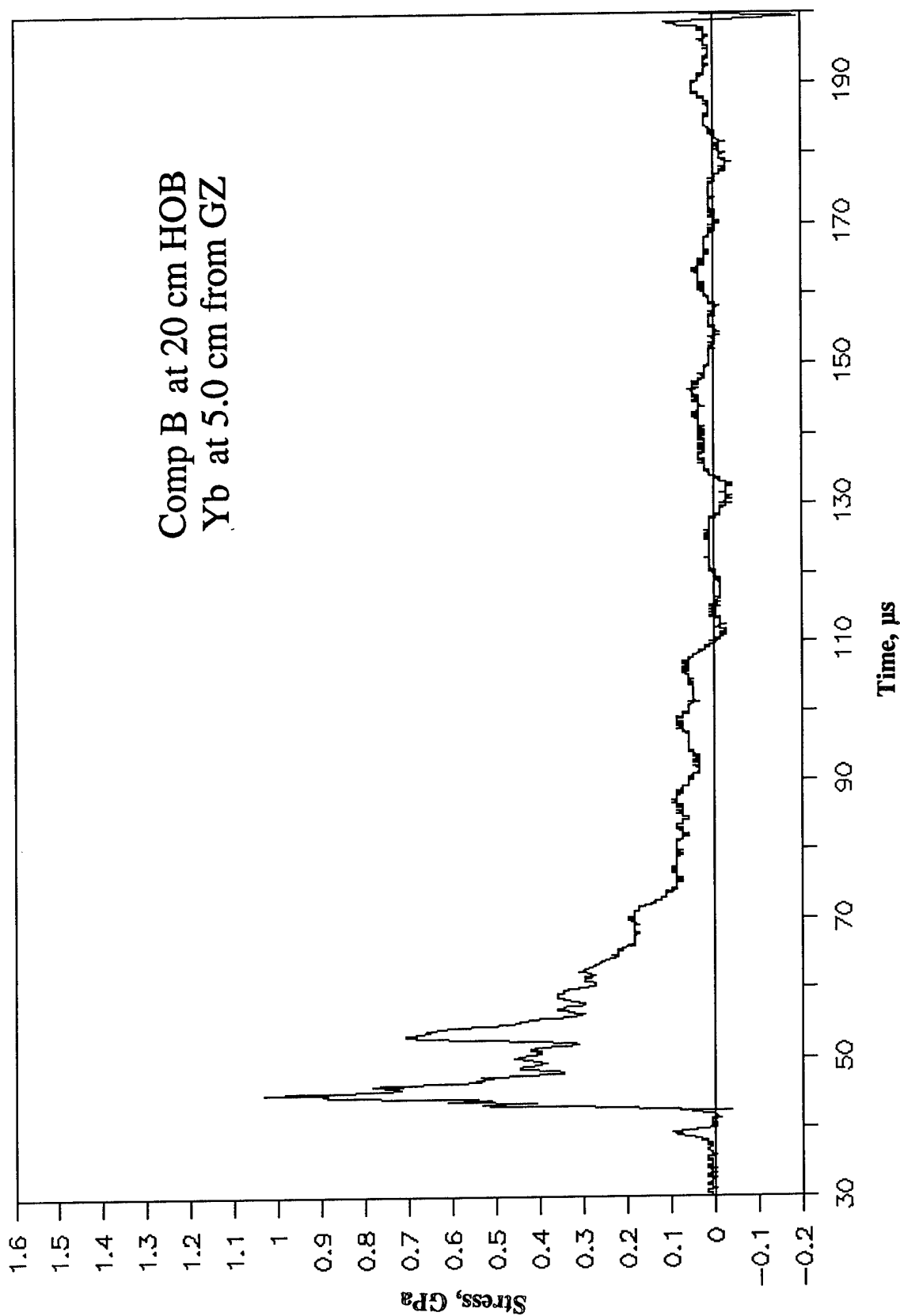


Figure A-72. Stress-Time Record From Ytterbium Element Yb-4, 5.0 cm From Centerline, Baseplate Test 2A.10, Comp B at 20-cm HOB.

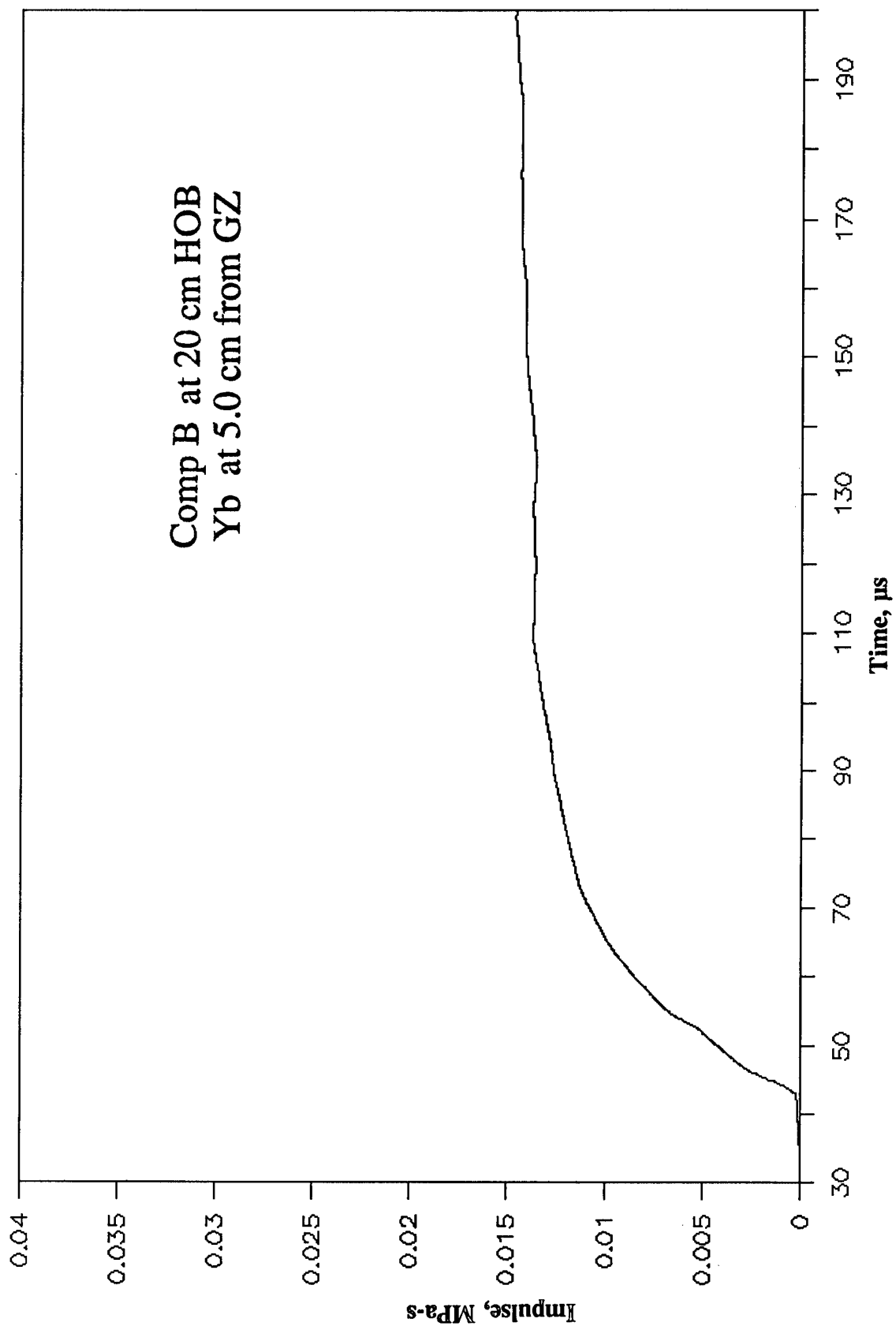


Figure A-73. Impulse-Time Record From Ytterbium Element Yb-4, 5.0 cm From Centerline, Baseplate Test 2A.10, Comp B at 20-cm HOB.

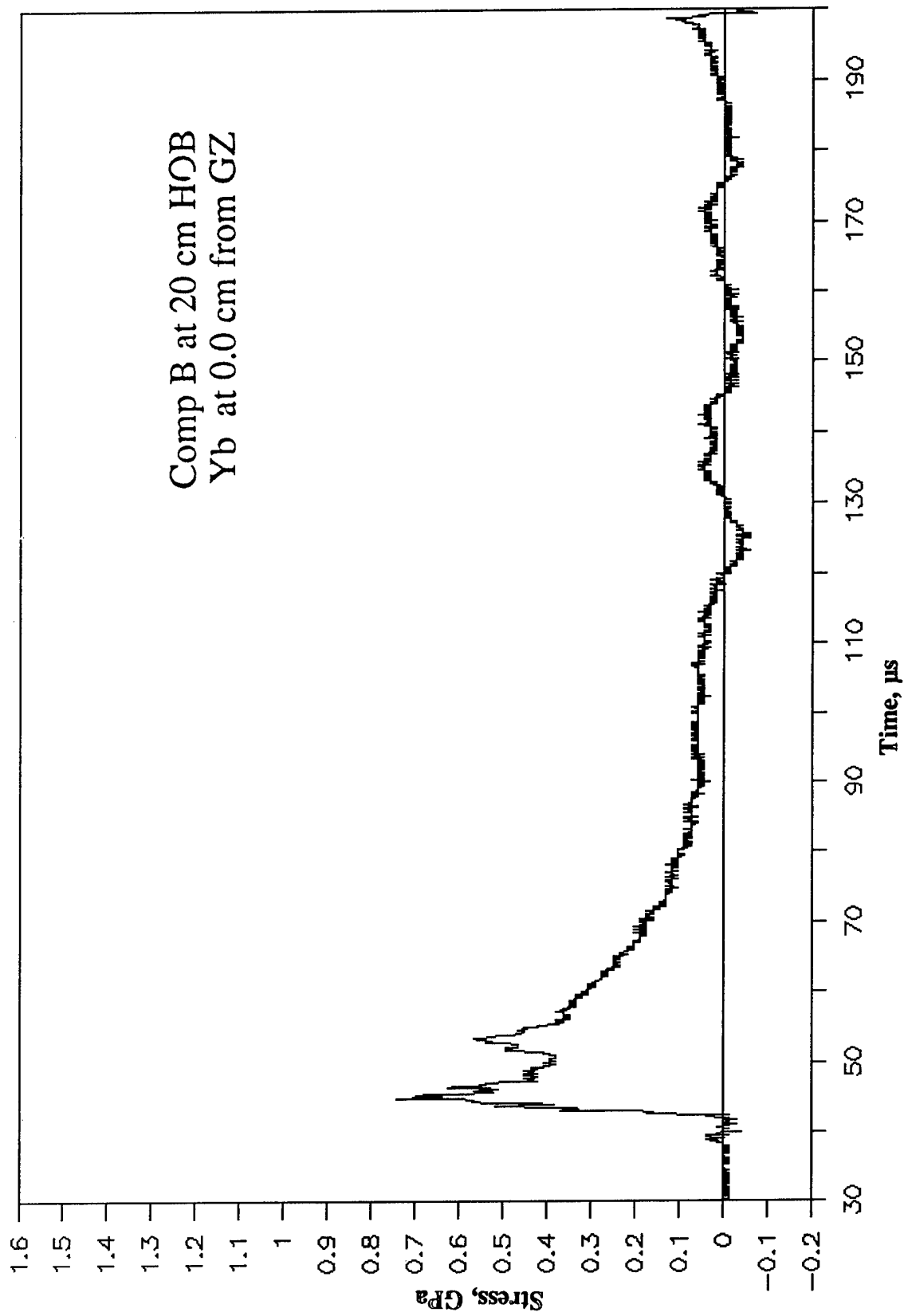


Figure A-74. Stress-Time Record From Ytterbium Element Yb-5, 0.0 cm From Centerline, Baseplate Test 2A.10, Comp B at 20-cm HOB.

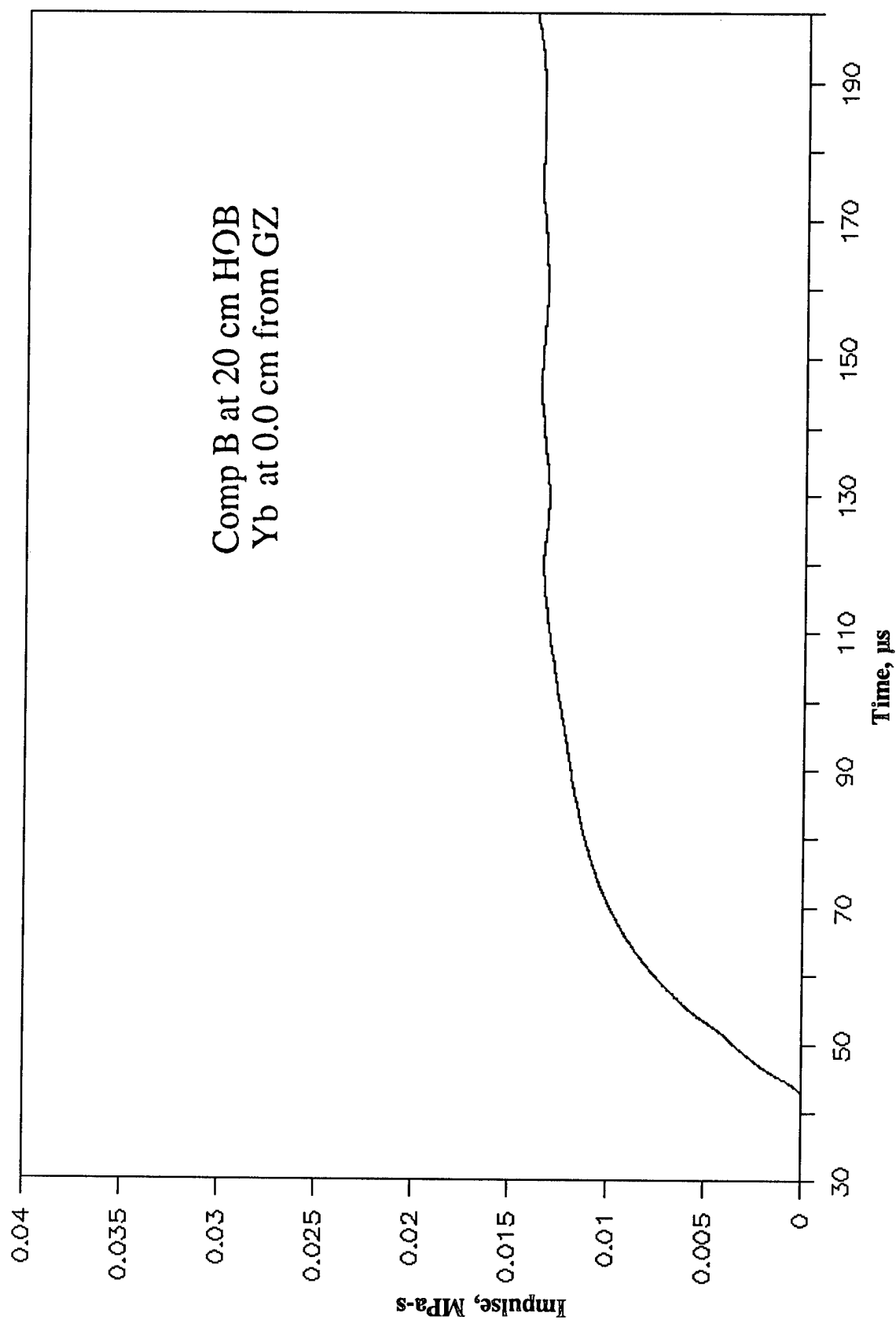
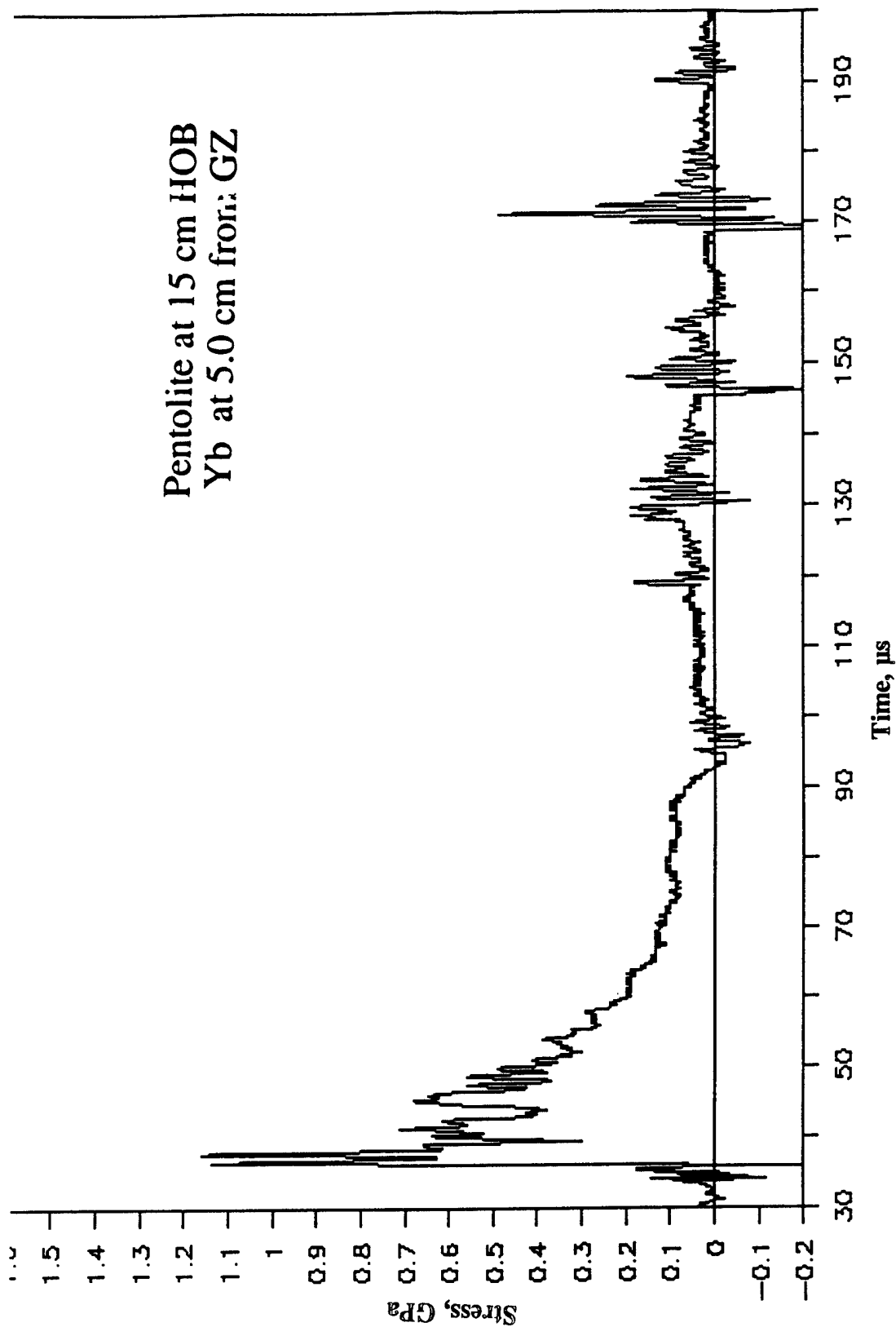


Figure A-75. Impulse-Time Record From Ytterbium Element Yb-5, 0.0 cm From Centerline, Baseplate Test 2A.10, Comp B at 20-cm HOB.



Pentolite at 15 cm HOB
Yb at 5.0 cm from GZ

Figure A-76. Stress-Time Record From Ytterbium Element Yb-1, 5.0 cm From Centerline, Baseplate Test 2A.11, Pentolite at 15-cm HOB.

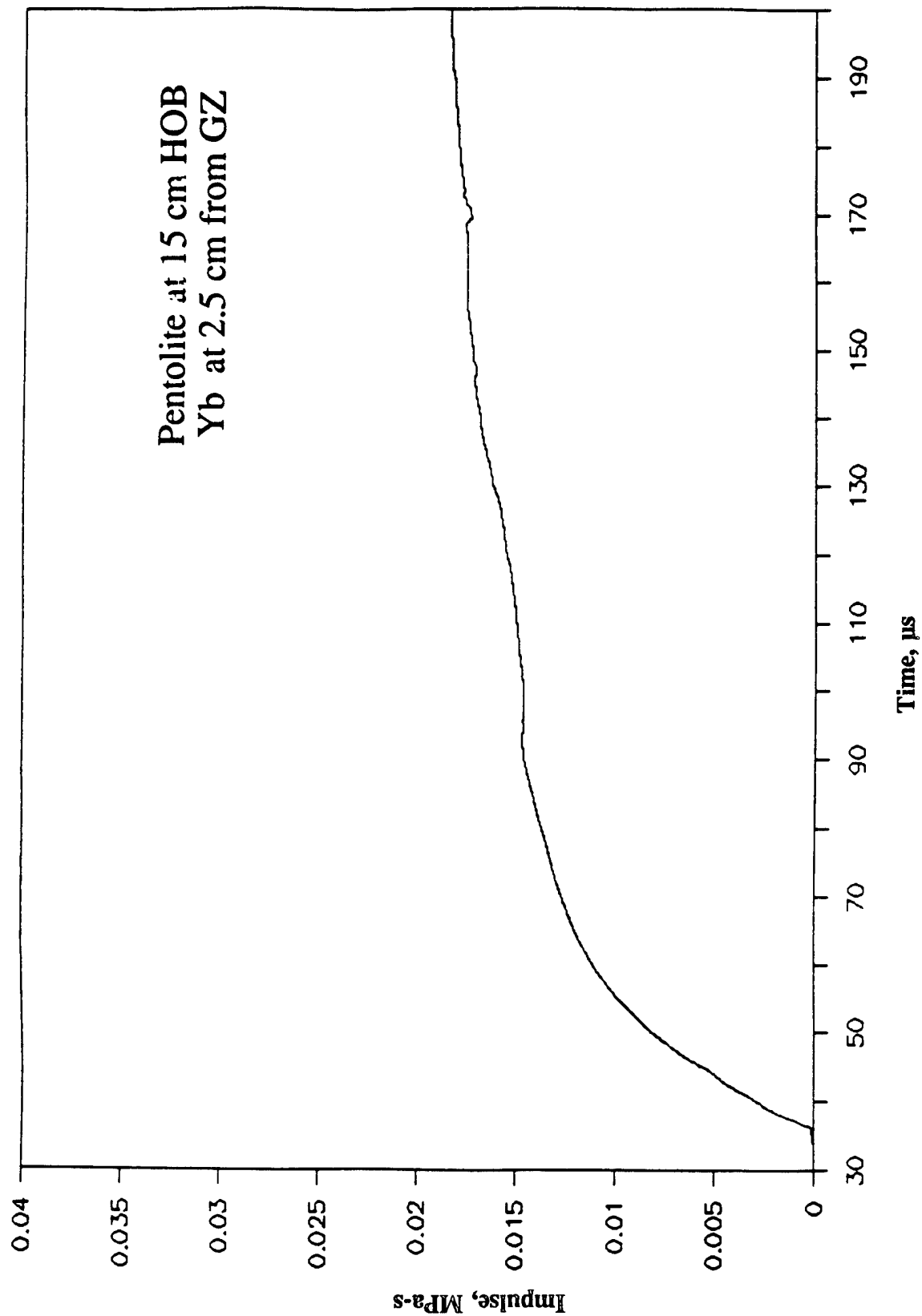


Figure A-77. Impulse-Time Record From Ytterbium Element Yb-1, 5.0 cm From Centerline, Baseplate Test 2A.11, Pentolite at 15-cm HOB.

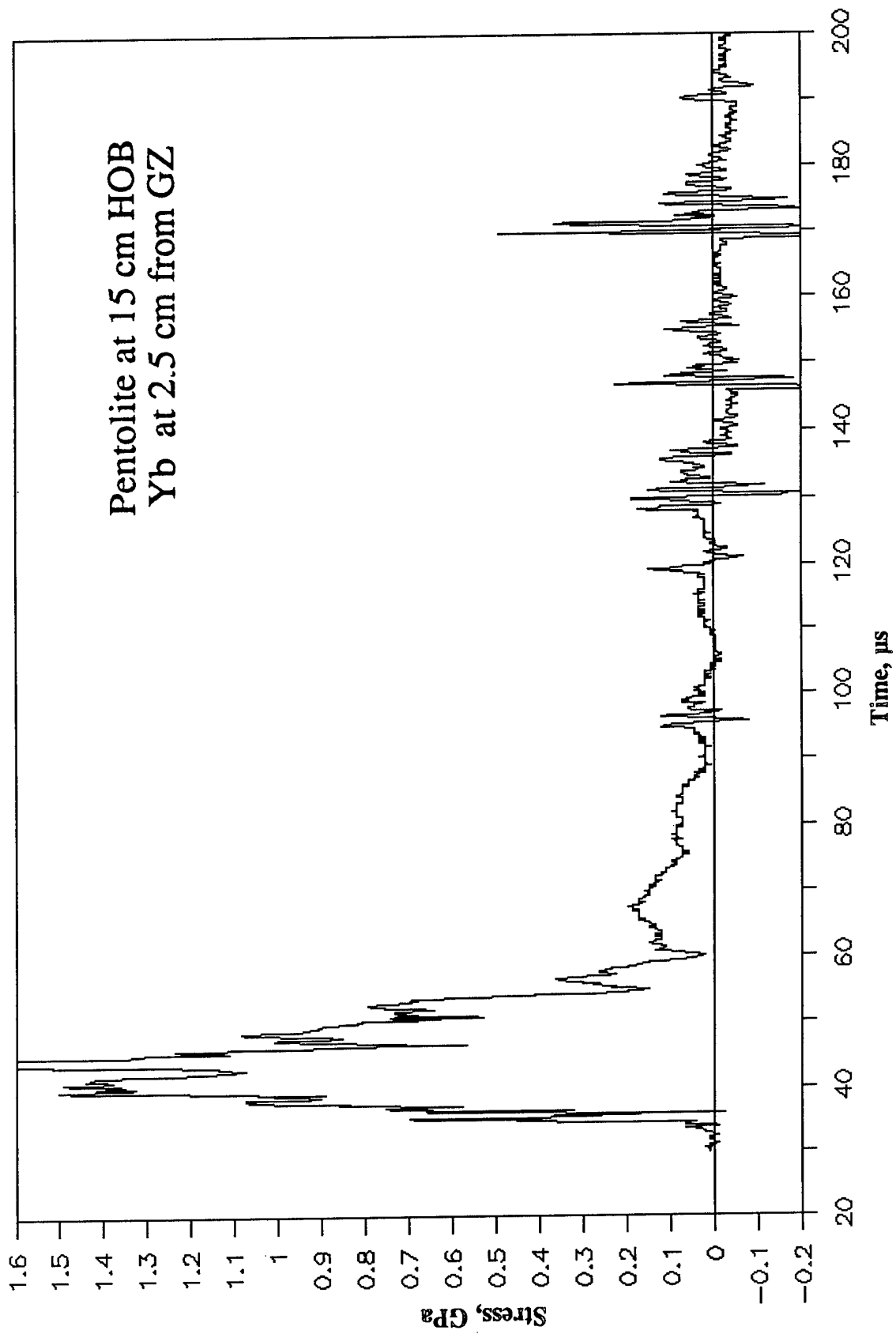


Figure A-78. Stress-Time Record From Ytterbium Element Yb-2, 2.5 cm From Centerline, Baseplate Test 2A.11, Pentolite at 15-cm HOB.

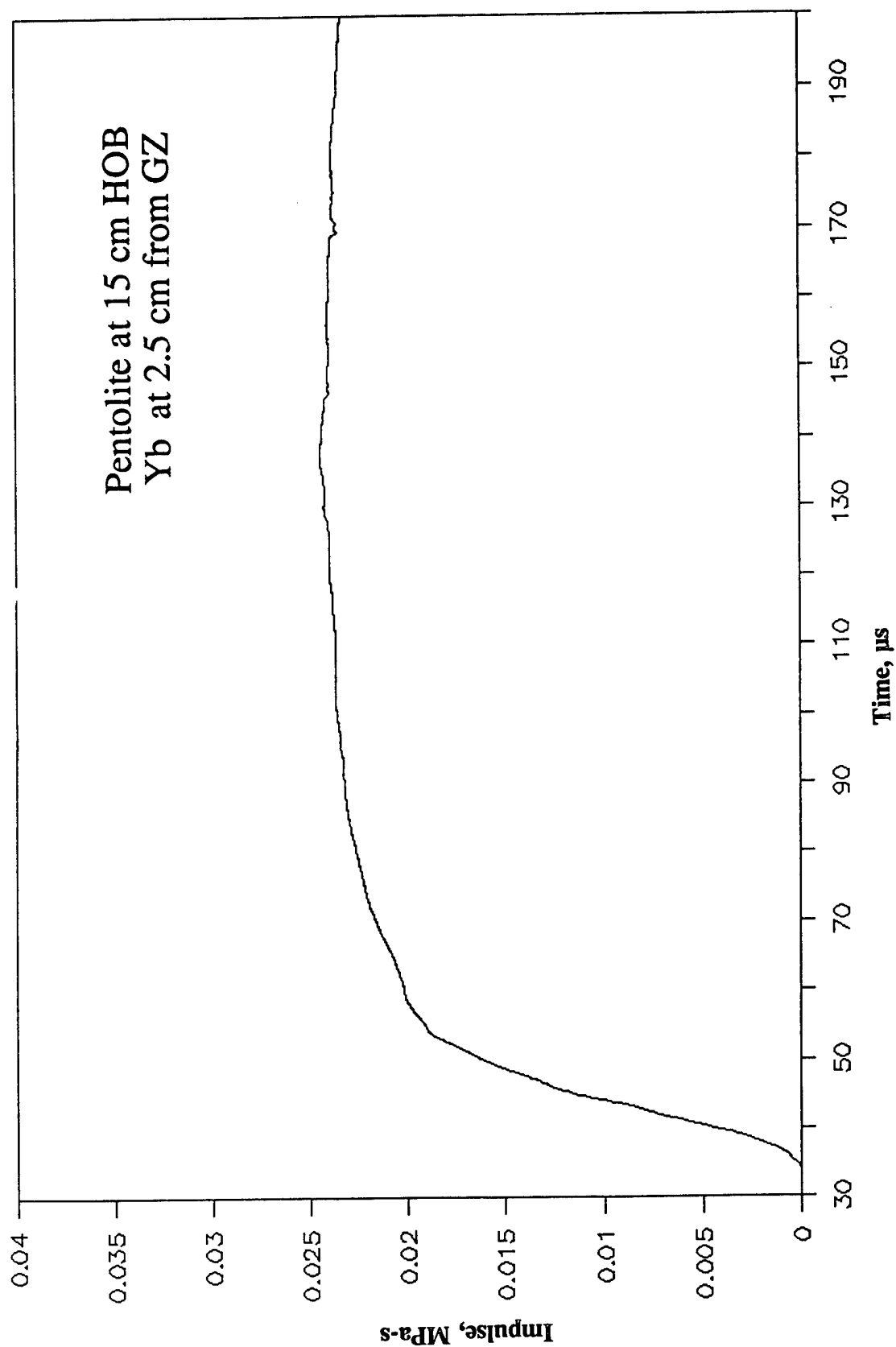


Figure A-79. Impulse-Time Record From Ytterbium Element Yb-2, 2.5 cm From Centerline, Baseplate Test 2A.11, Pentolite at 15-cm HOB.

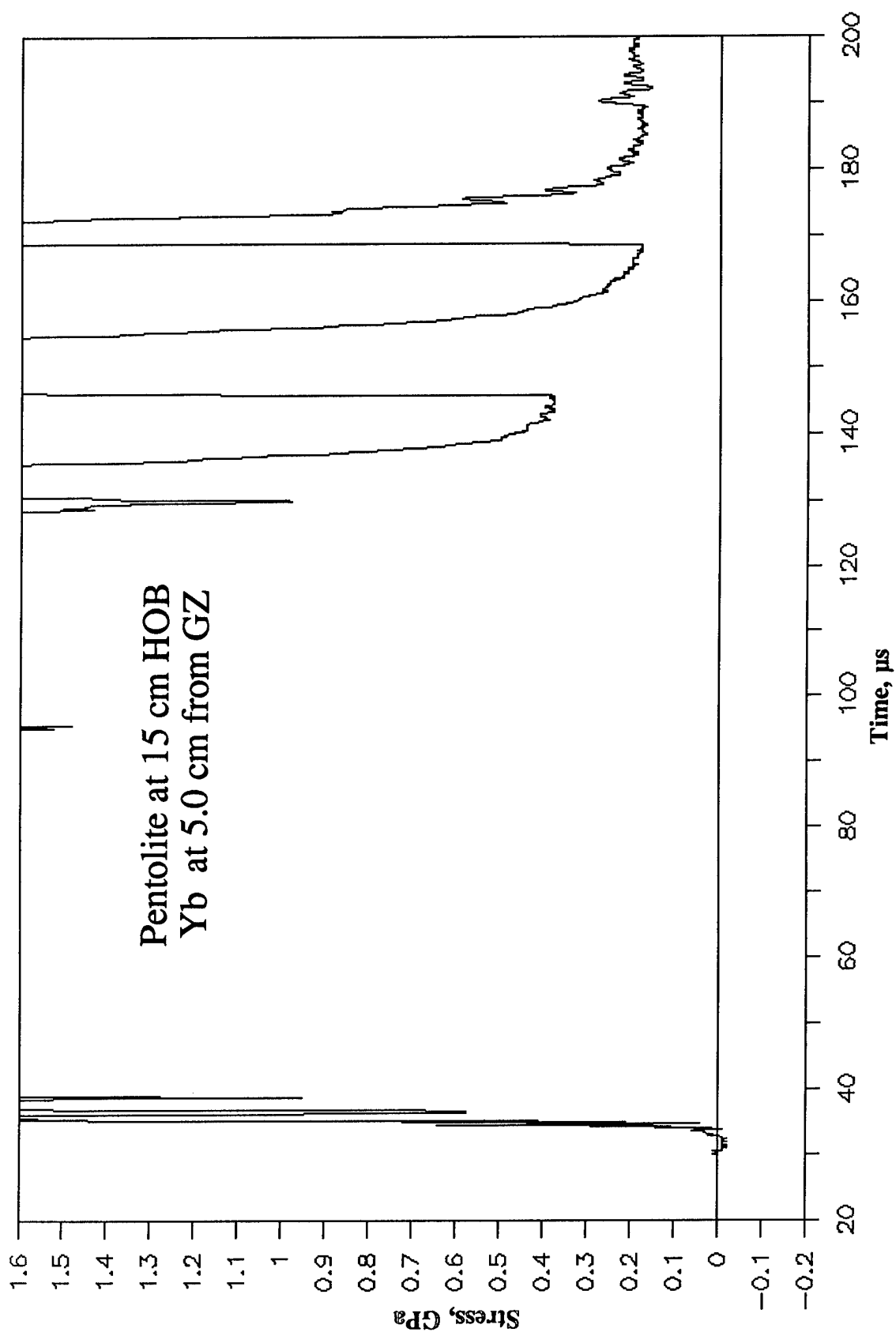


Figure A-80. Stress-Time Record From Ytterbium Element Yb-3, 2.5 cm From Centerline, Baseplate Test 2A.11, Pentolite at 15-cm HOB.

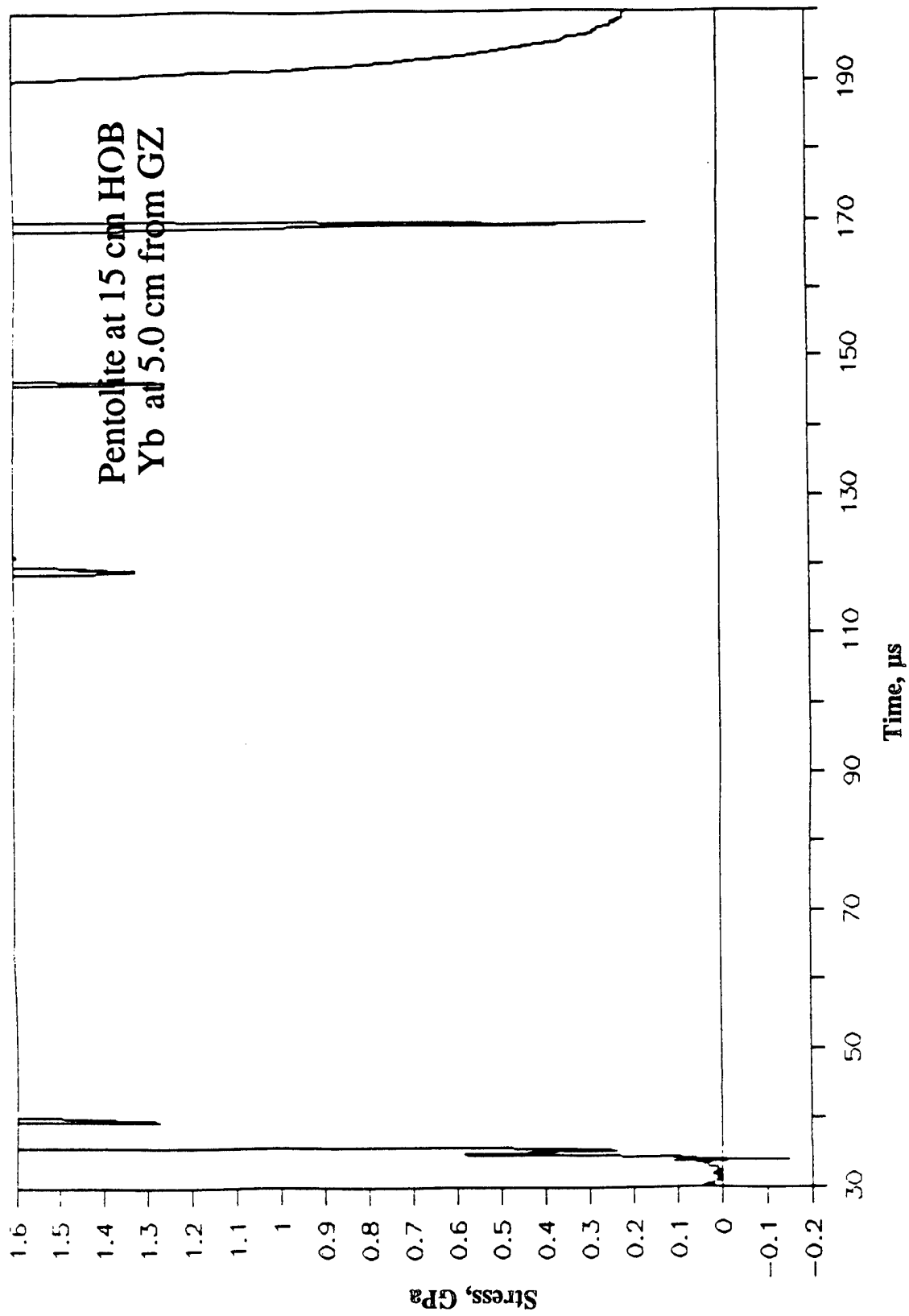


Figure A-81. Stress-Time Record From Ytterbium Element Yb-4, 5.0 cm From Centerline, Baseplate Test 2A.11, Pentolite at 15-cm HOB.

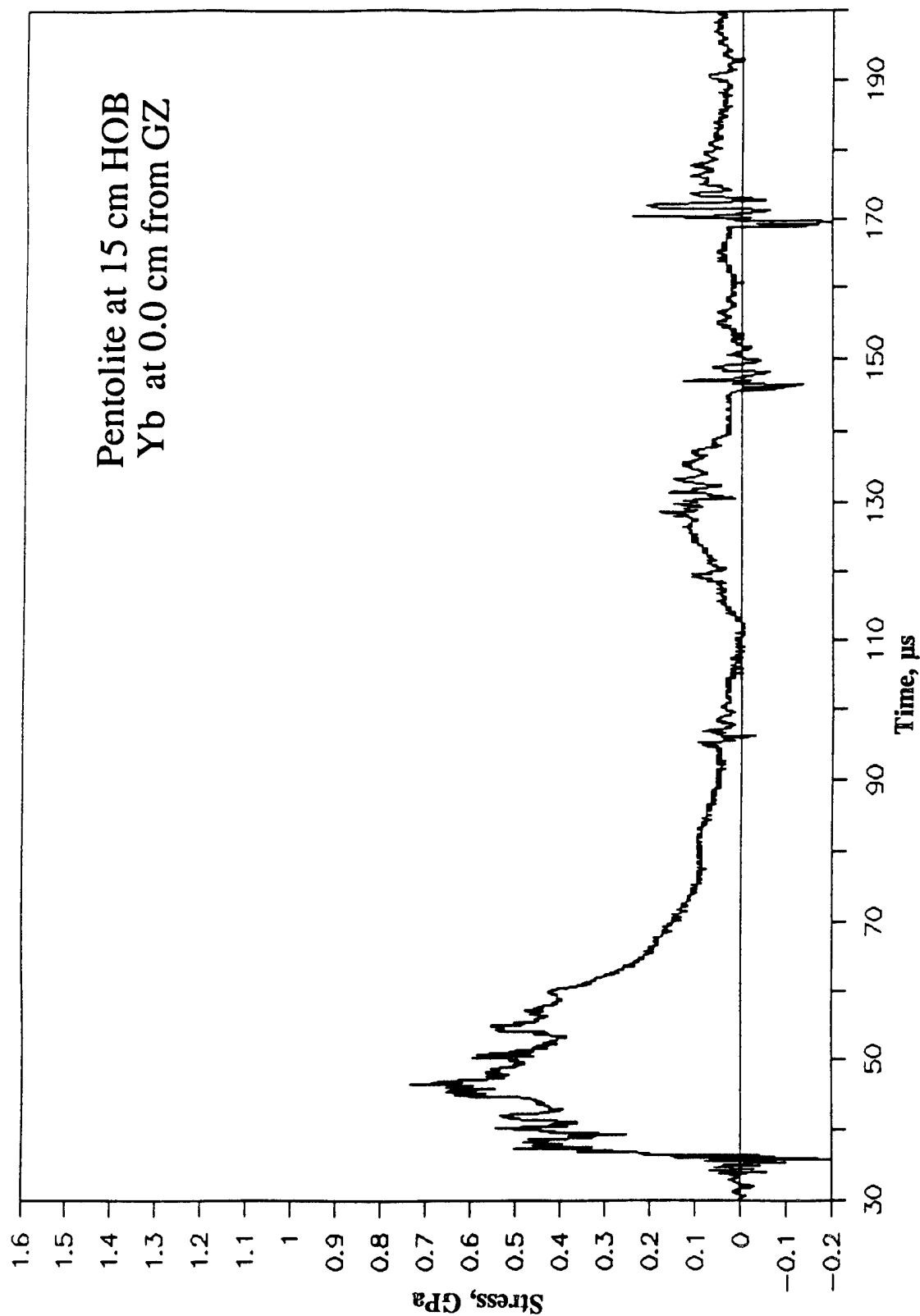


Figure A-82. Stress-Time Record From Ytterbium Element Yb-5, 0.0 cm From Centerline, Baseplate Test 2A.11, Pentolite at 15-cm HOB.

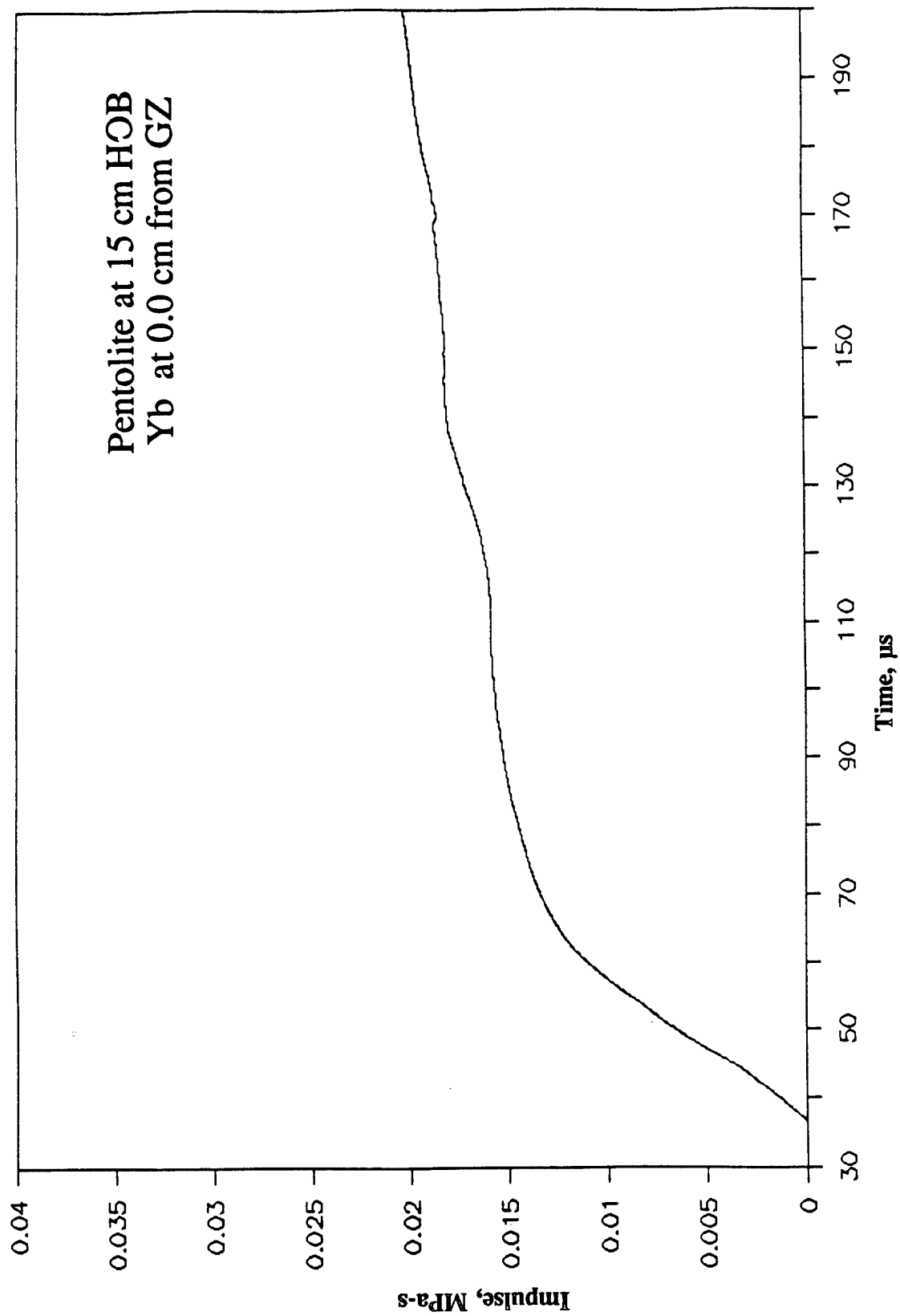


Figure A-83. Impulse-Time Record From Ytterbium Element Yb-5, 0.0 cm From Centerline, Baseplate Test 2A.11, Pentolite at 15-cm HOB.

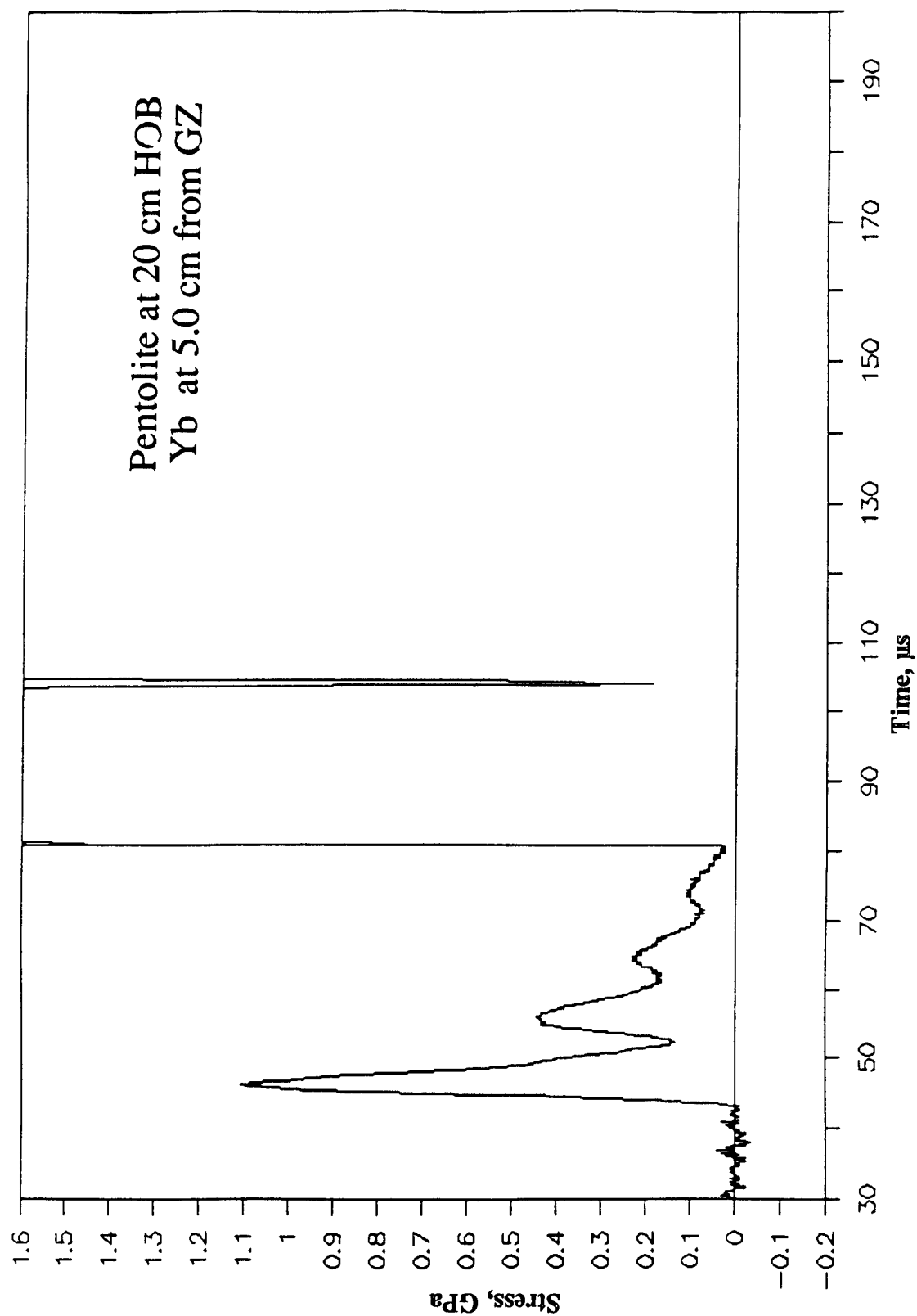


Figure A-84. Stress-Time Record From Ytterbium Element Yb-1, 5.0 cm From Centerline, Baseplate Test 2A.12, Pentolite at 20-cm HOB.

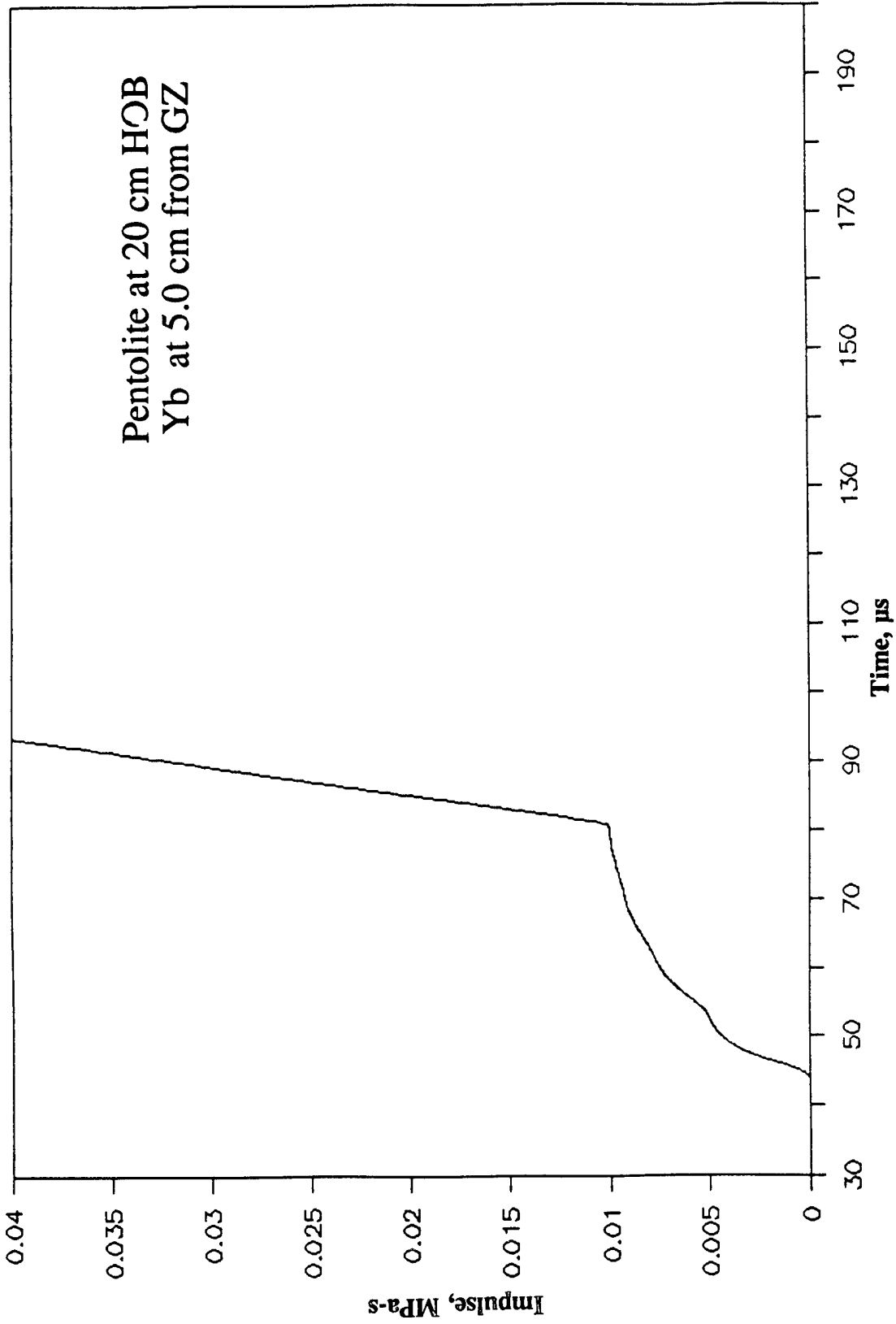


Figure A-85. Impulse-Time Record From Ytterbium Element Yb-1, 5.0 cm From Centerline, Baseplate Test 2A.12, Pentolite at 20-cm HOB.

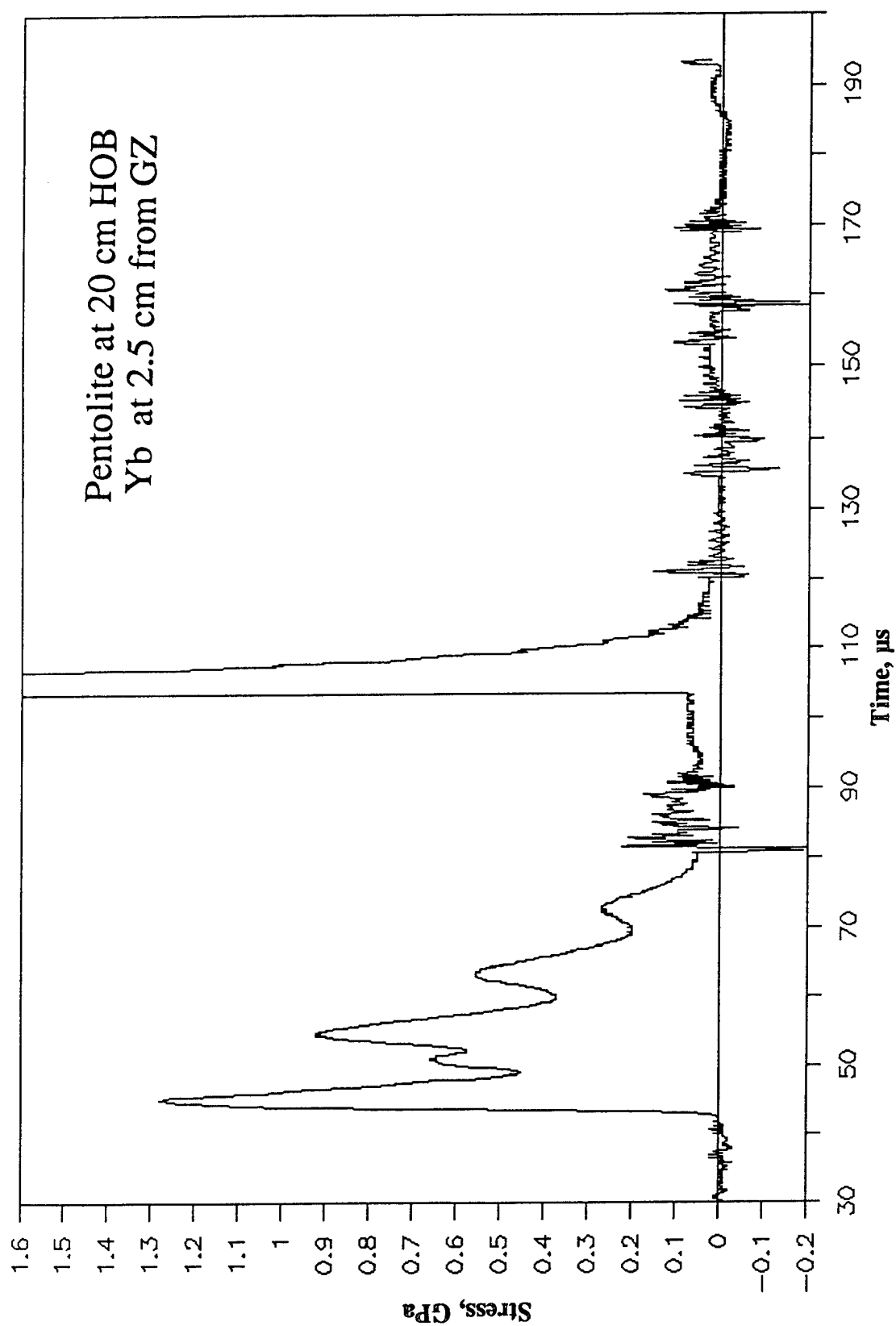


Figure A-86. Stress-Time Record From Ytterbium Element Yb-2, 2.5 cm From Centerline, Baseplate Test 2A.12, Pentolite at 20-cm HOB.

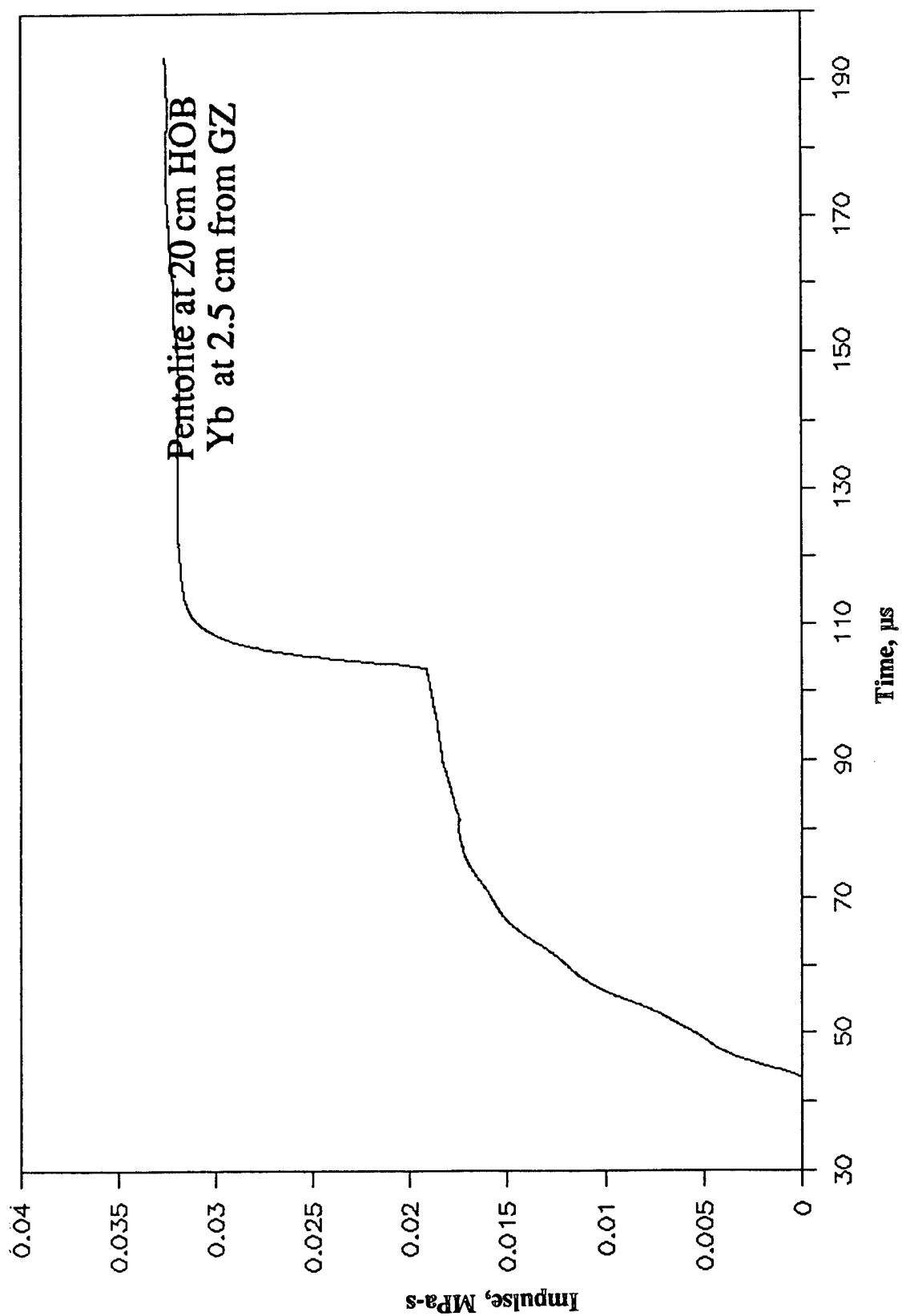


Figure A-87. Impulse-Time Record From Ytterbium Element Yb-2, 2.5 cm From Centerline, Baseplate Test 2A.12, Pentolite at 20-cm HOB.

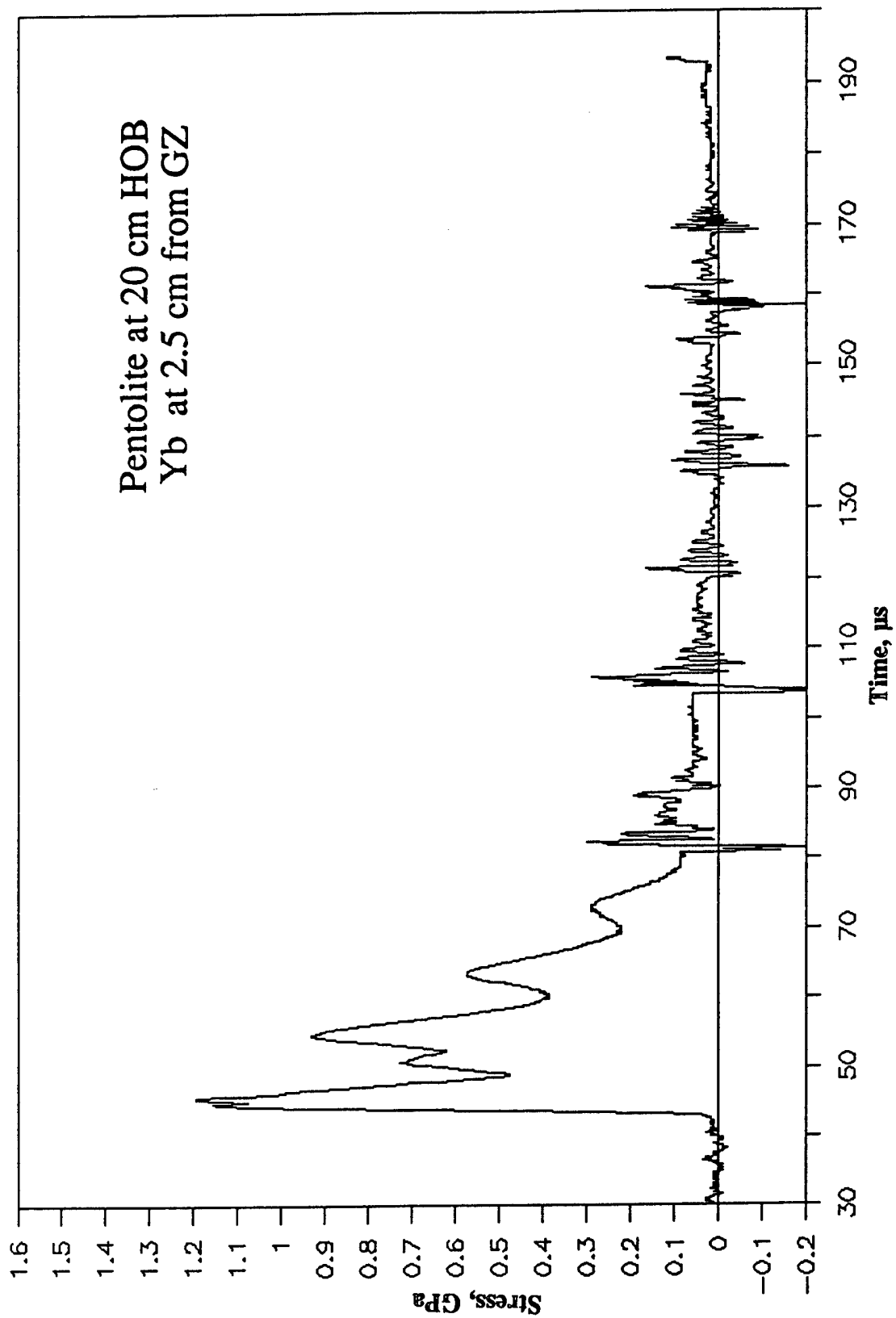


Figure A-88. Stress-Time Record From Ytterbium Element Yb-3, 2.5 cm From Centerline, Baseplate Test 2A.12, Pentolite at 20-cm HOB.

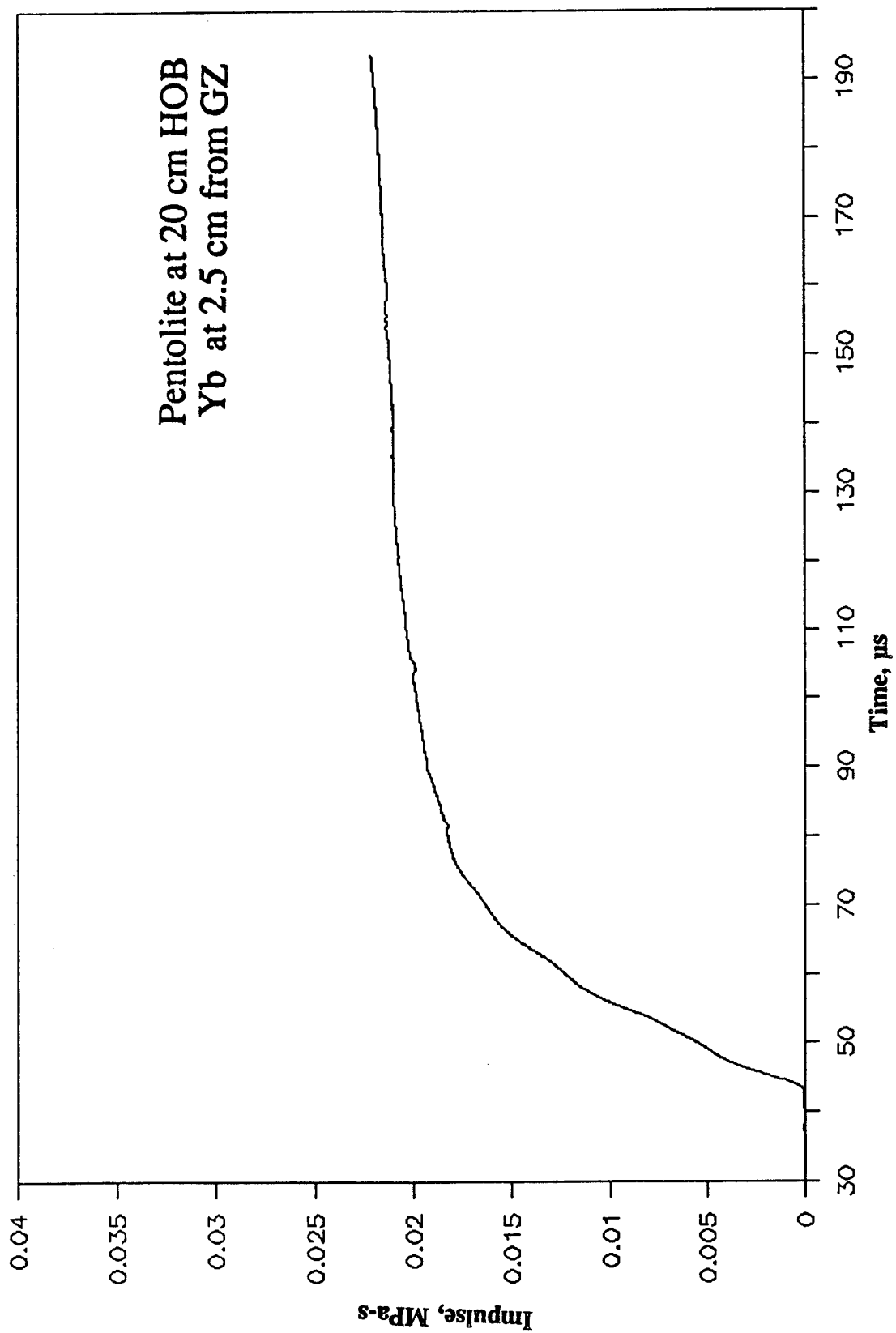


Figure A-89. Impulse-Time Record From Ytterbium Element Yb-3, 2.5 cm From Centerline, Baseplate Test 2A.12, Pentolite at 20-cm HOB.

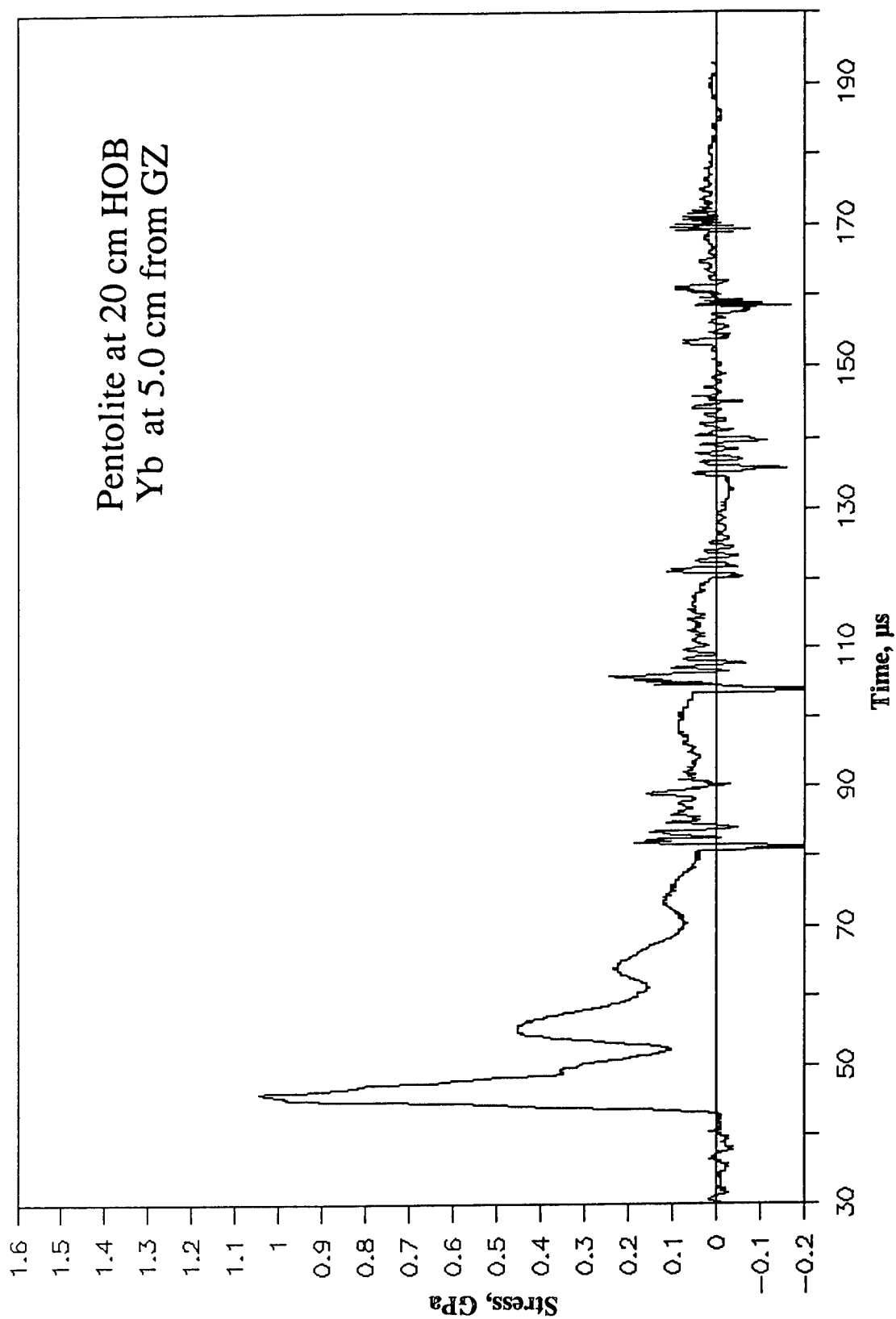


Figure A-90. Stress-Time Record From Ytterbium Element Yb-4, 5.0 cm From Centerline, Baseplate Test 2A.12, Pentolite at 20-cm HOB.

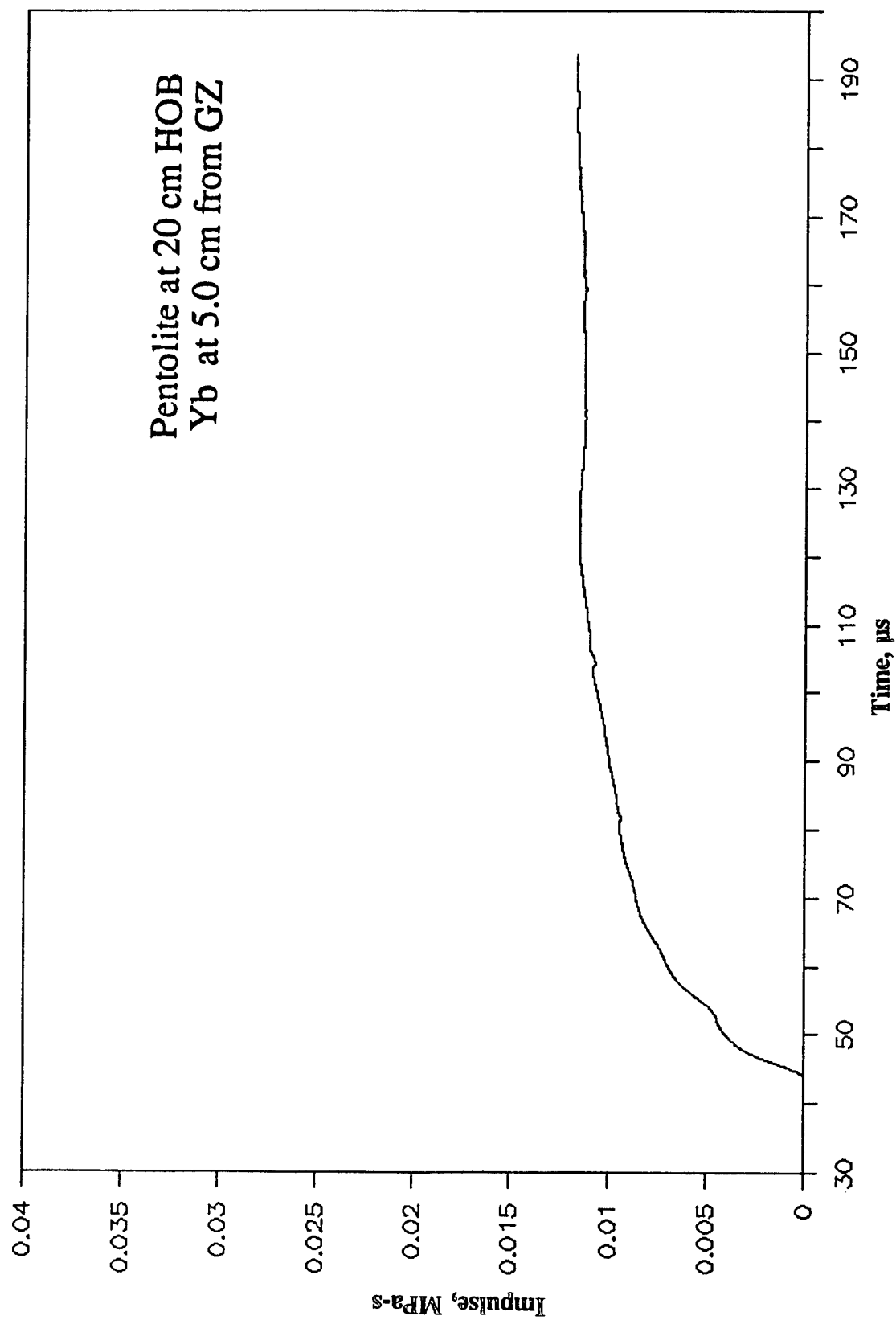


Figure A-91. Impulse-Time Record From Ytterbium Element Yb-4, 5.0 cm From Centerline, Baseplate Test 2A.12, Pentolite at 20-cm HOB.

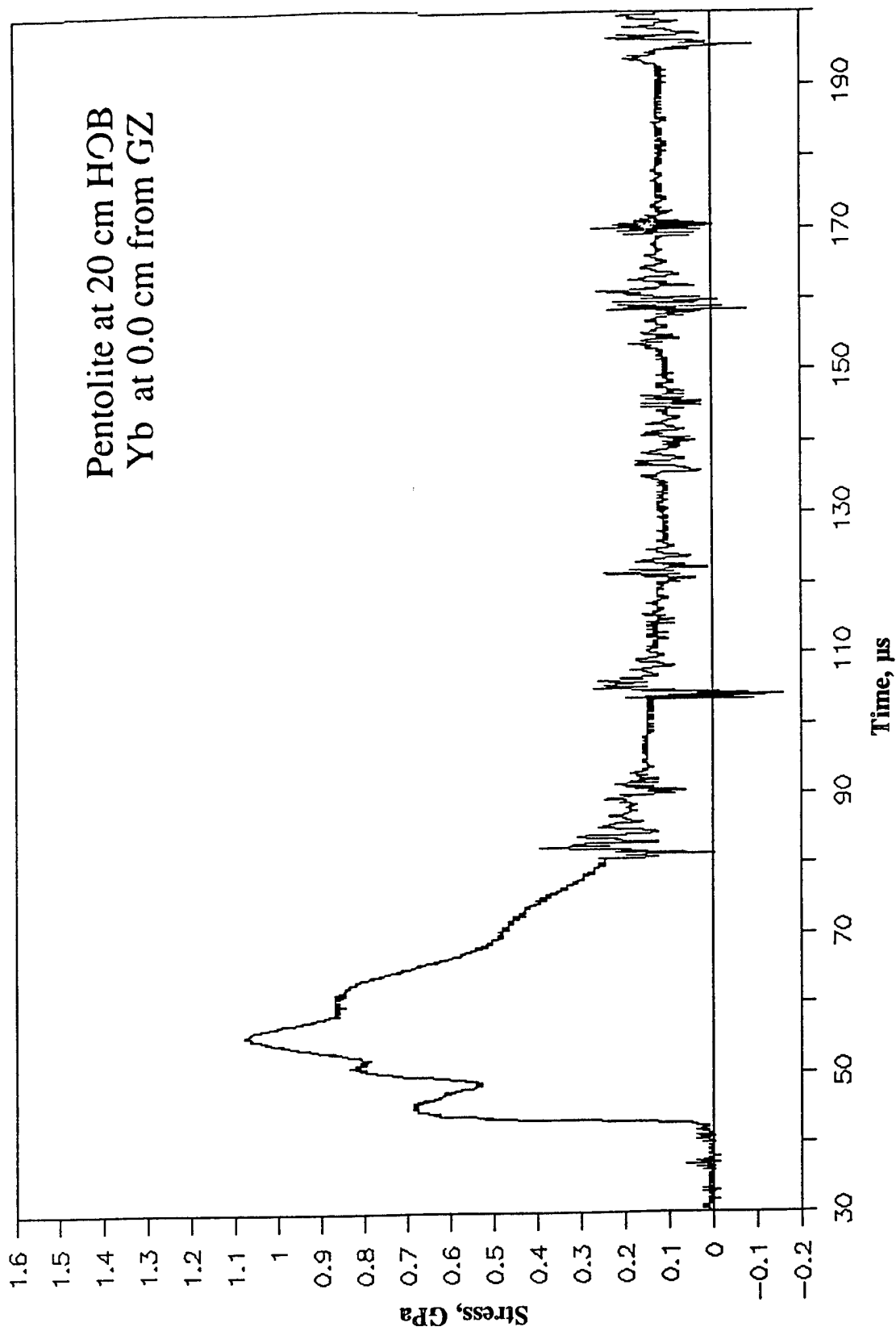


Figure A-92. Stress-Time Record From Ytterbium Element Yb-5, 0.0 cm From Centerline, Baseplate Test 2A.12, Pentolite at 20-cm HOB.

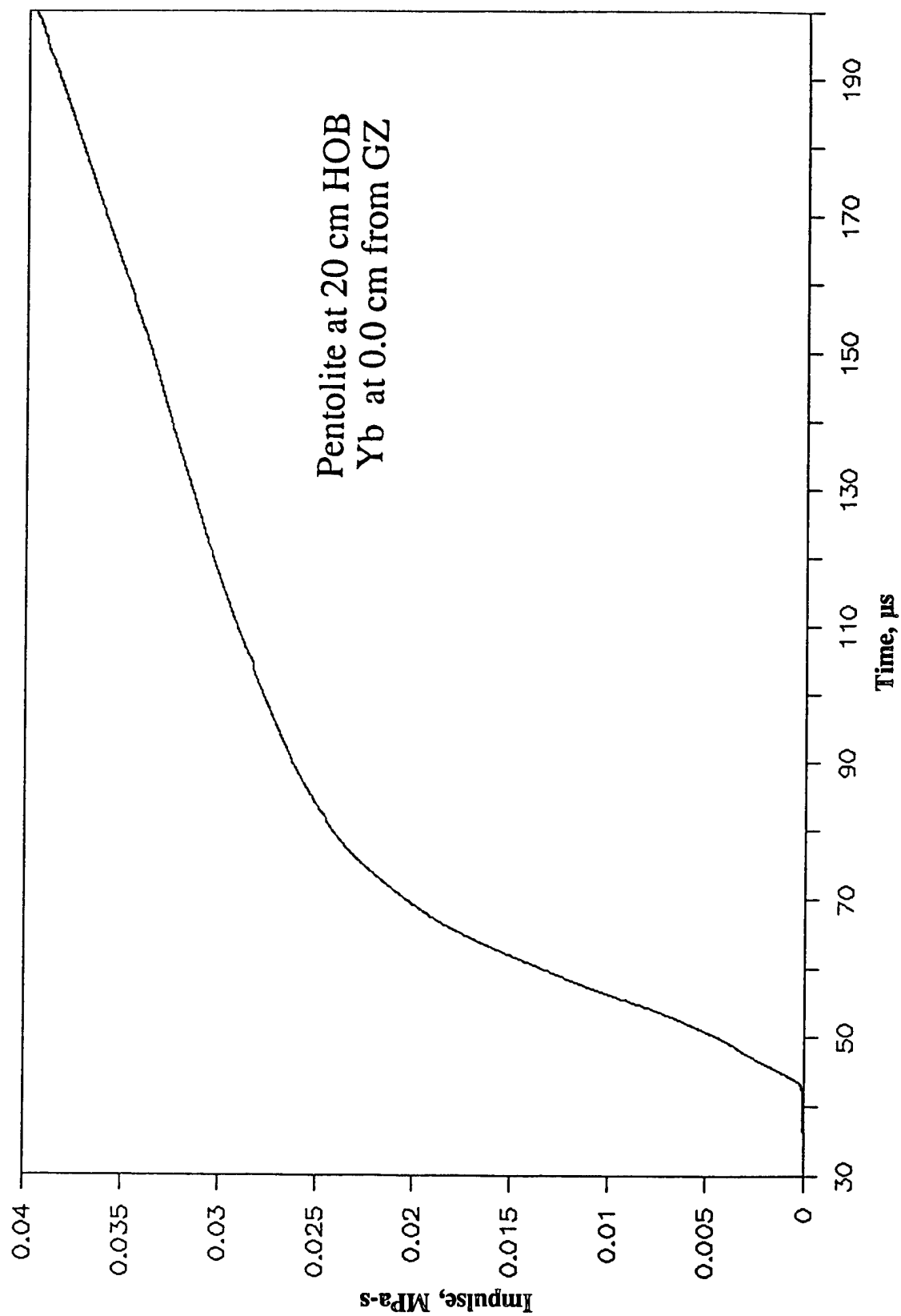


Figure A-93. Impulse-Time Record From Ytterbium Element Yb-5, 0.0 cm From Centerline, Baseplate Test 2A.12, Pentolite at 20-cm HOB.

INTENTIONALLY LEFT BLANK.

APPENDIX B:
STRESS AND IMPULSE HISTORIES
FROM BAR GAGES
BASEPLATE TESTS 2A.1-2A.12

INTENTIONALLY LEFT BLANK.

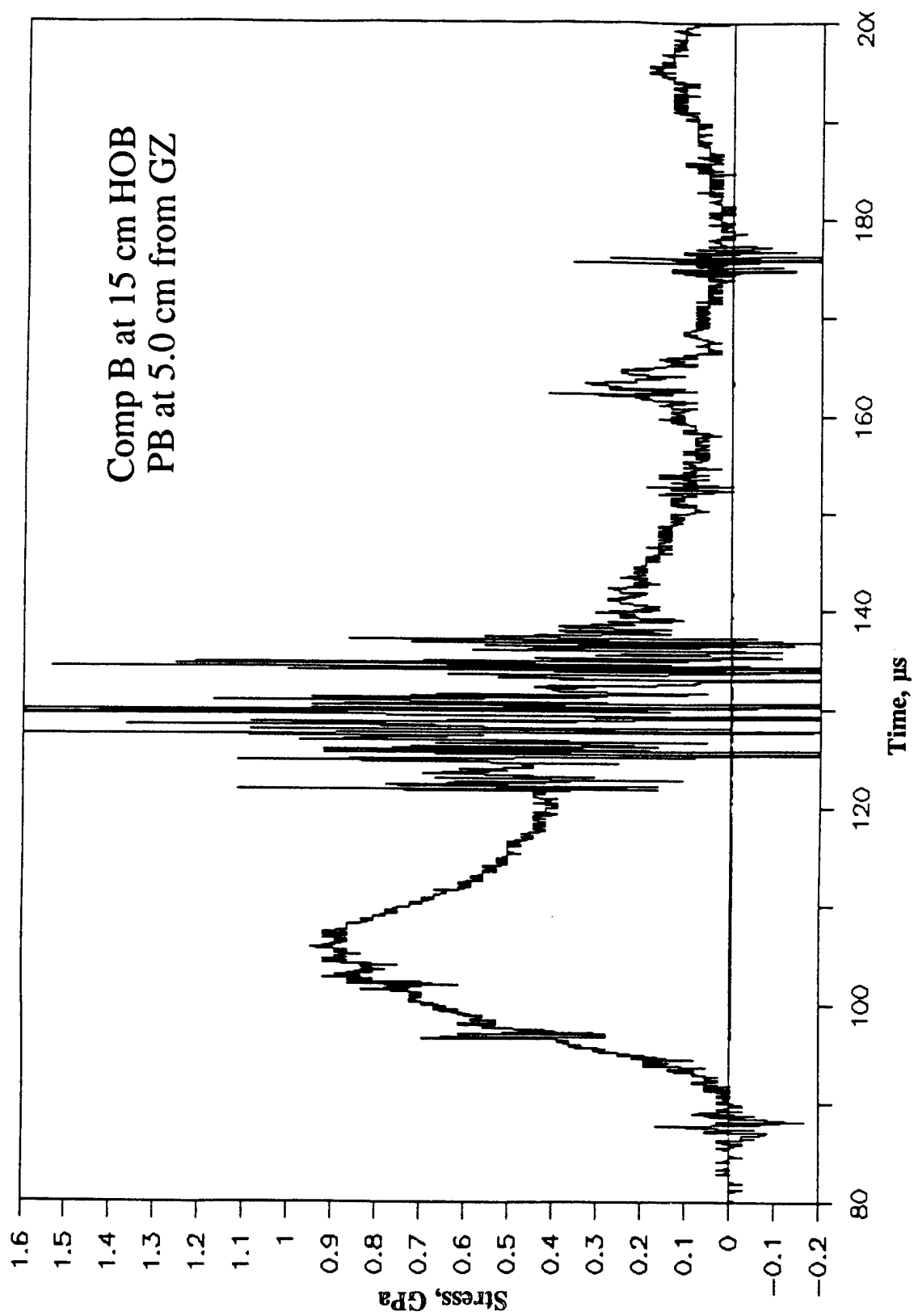


Figure B-1. Stress-Time Record From Bar Gage PB-7, 5.0 cm From Centerline, Baseplate Test 2A.1, Comp B at 15 cm.

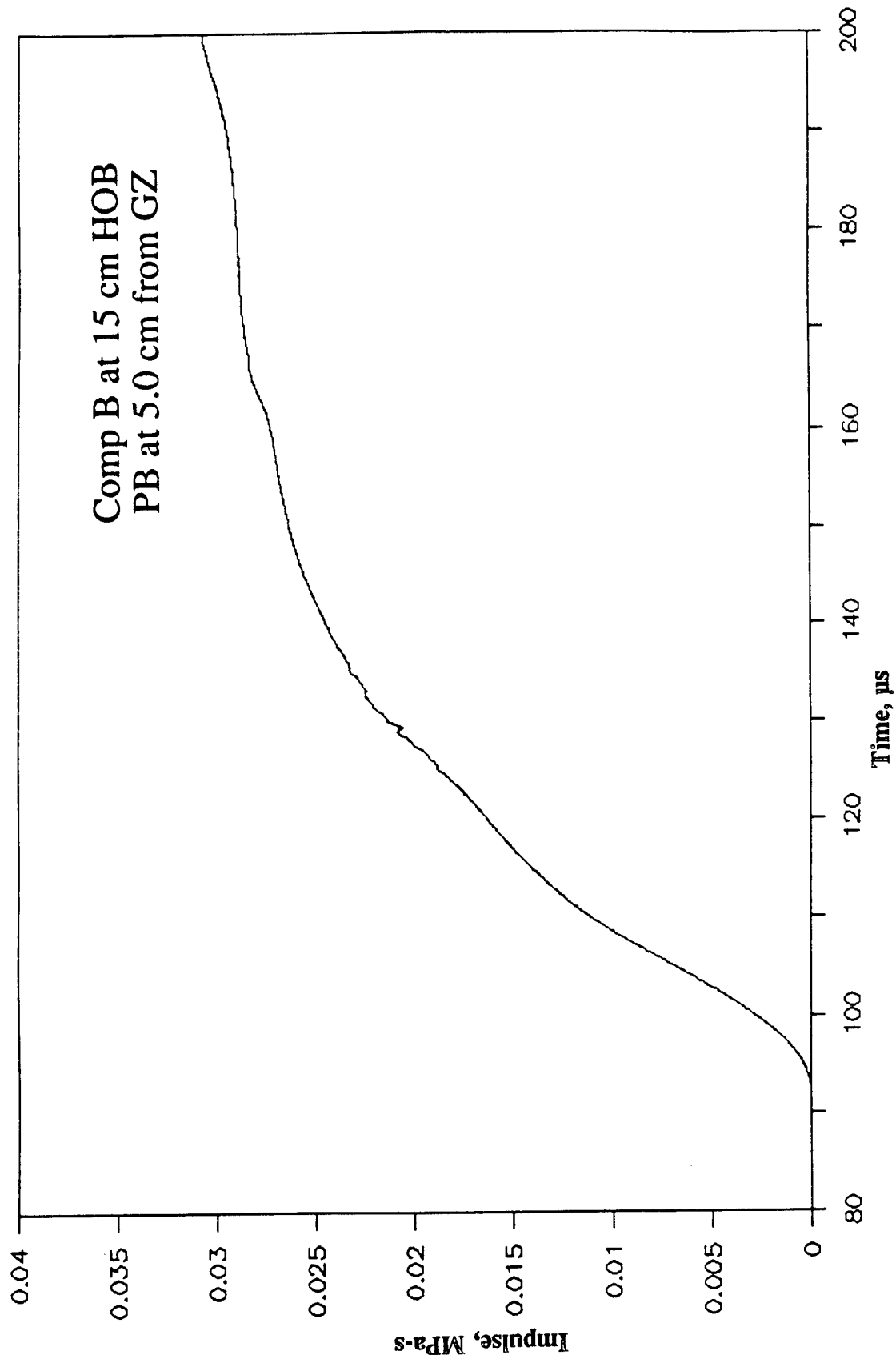


Figure B-2. Impulse-Time Record From Bar Gage PB-7, 5.0 cm From Centerline, Baseplate Test 2A.1, Comp B at 15 cm.

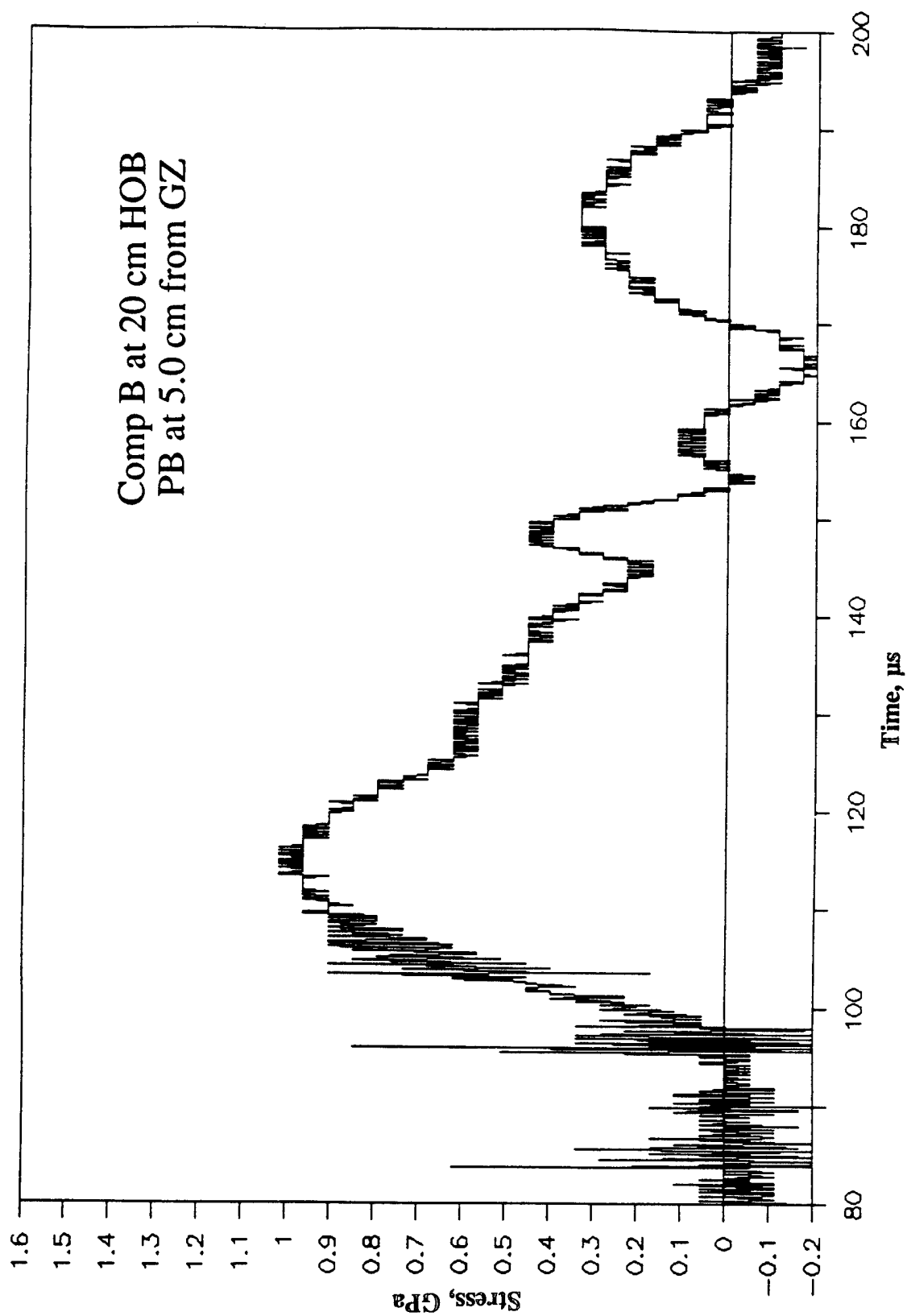


Figure B-3. Stress-Time Record From Bar Gage PB-7, 5.0 cm From Centerline, Baseplate Test 2A.2, Comp B at 20 cm.

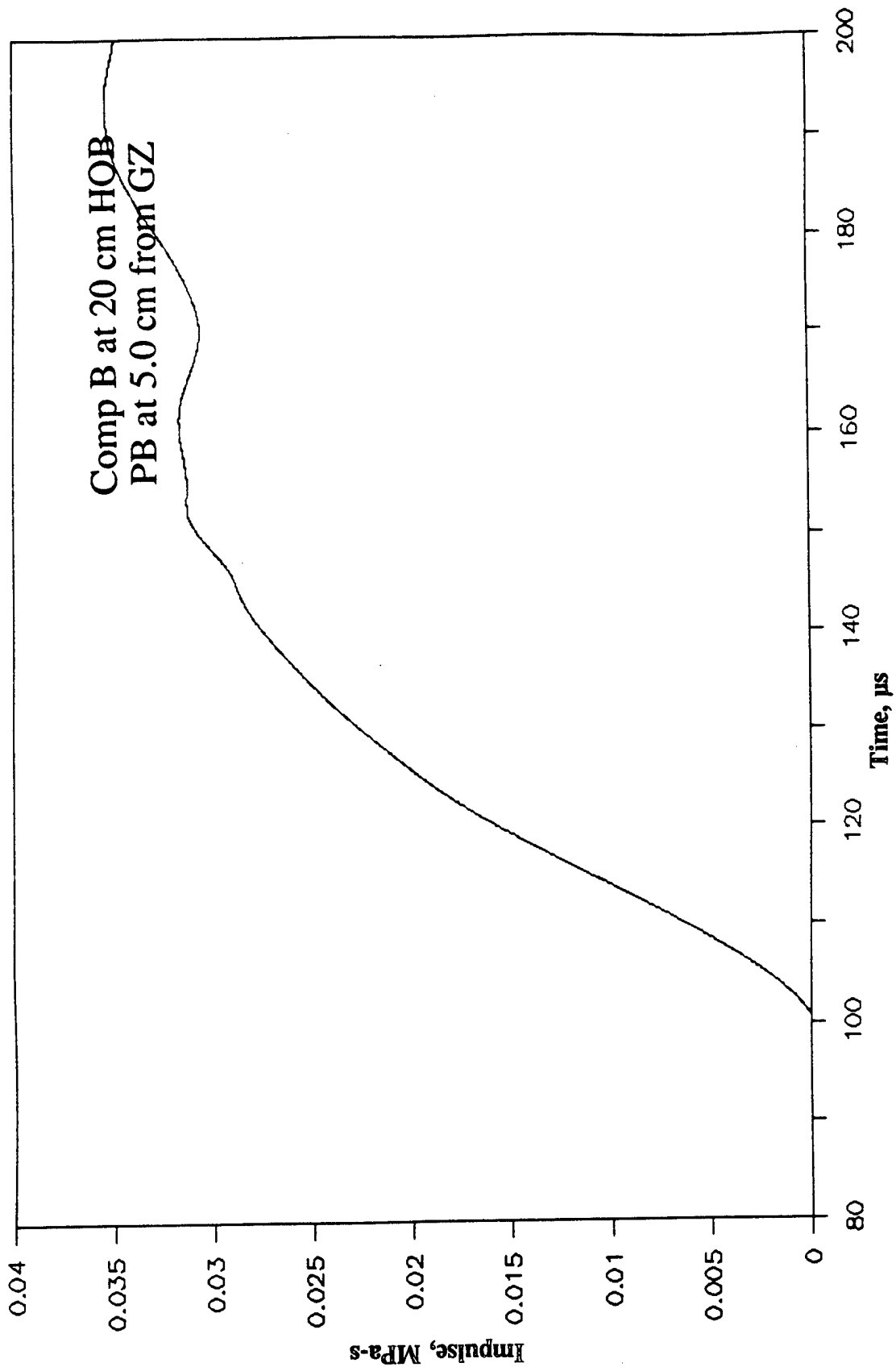


Figure B-4. Impulse-Time Record From Bar Gage PB-7, 5.0 cm From Centerline, Baseplate Test 2A.2, Comp B at 20 cm.

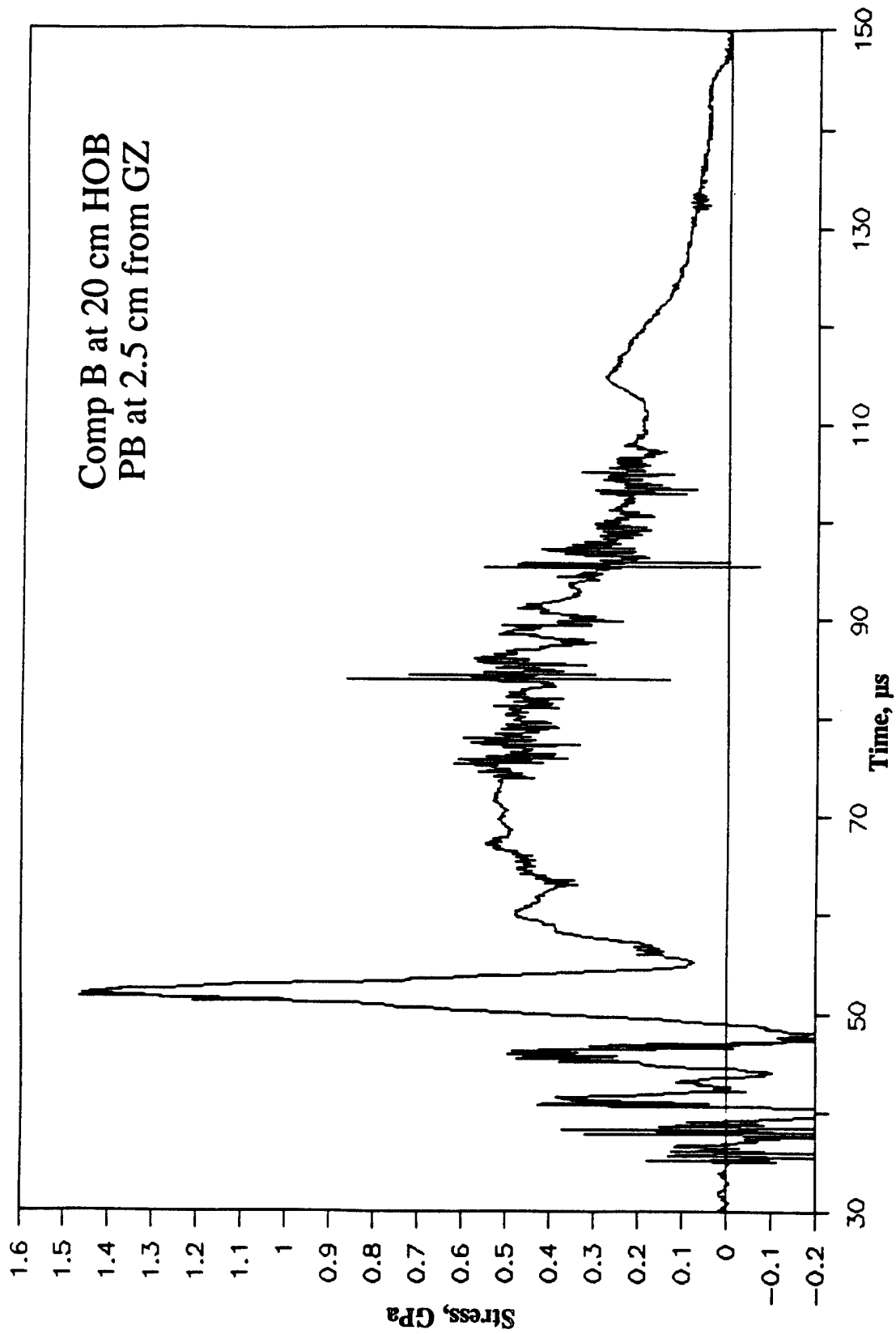


Figure B-5. Stress-Time Record From Bar Gage PB-6, 2.5 cm From Centerline, Baseplate Test 2A.2, Comp B at 20 cm.

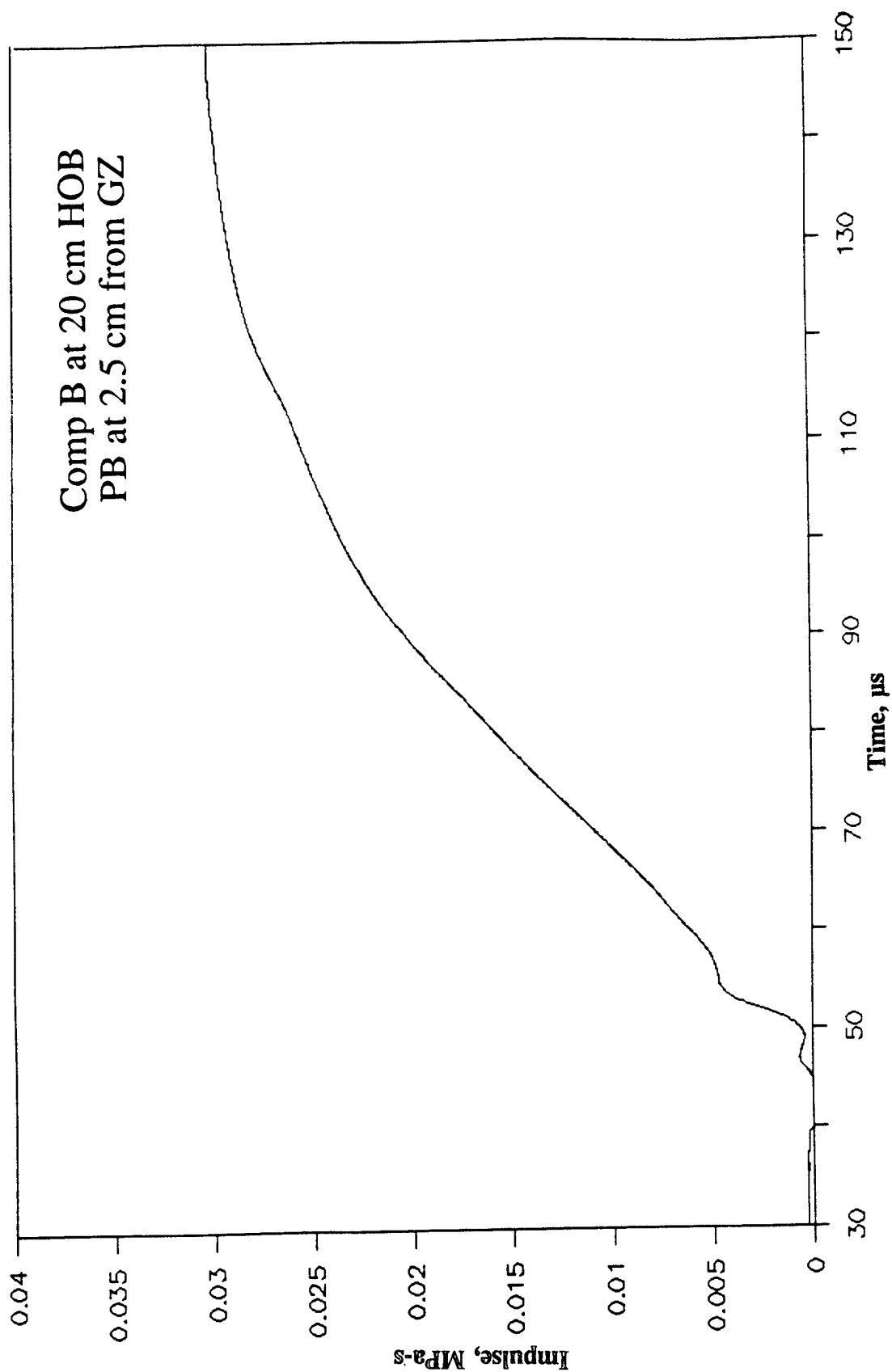


Figure B-6. Impulse-Time Record From Bar Gage PB-6, 2.5 cm From Centerline, Baseplate Test 2A.2, Comp B at 20 cm.

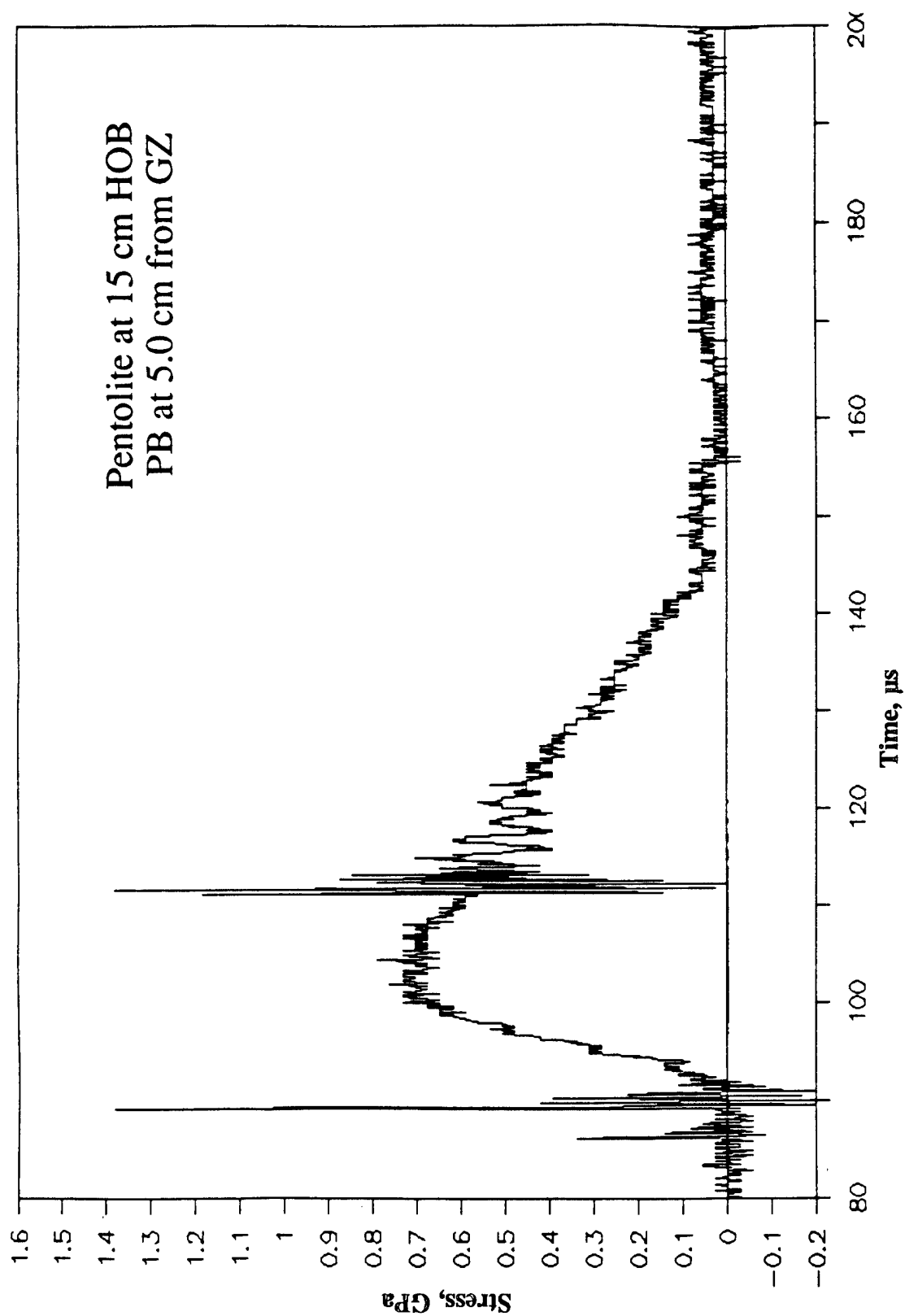


Figure B-7. Stress-Time Record From Bar Gage PB-7, 5.0 cm From Centerline, Baseplate Test 2A.3, Pentolite at 15 cm.

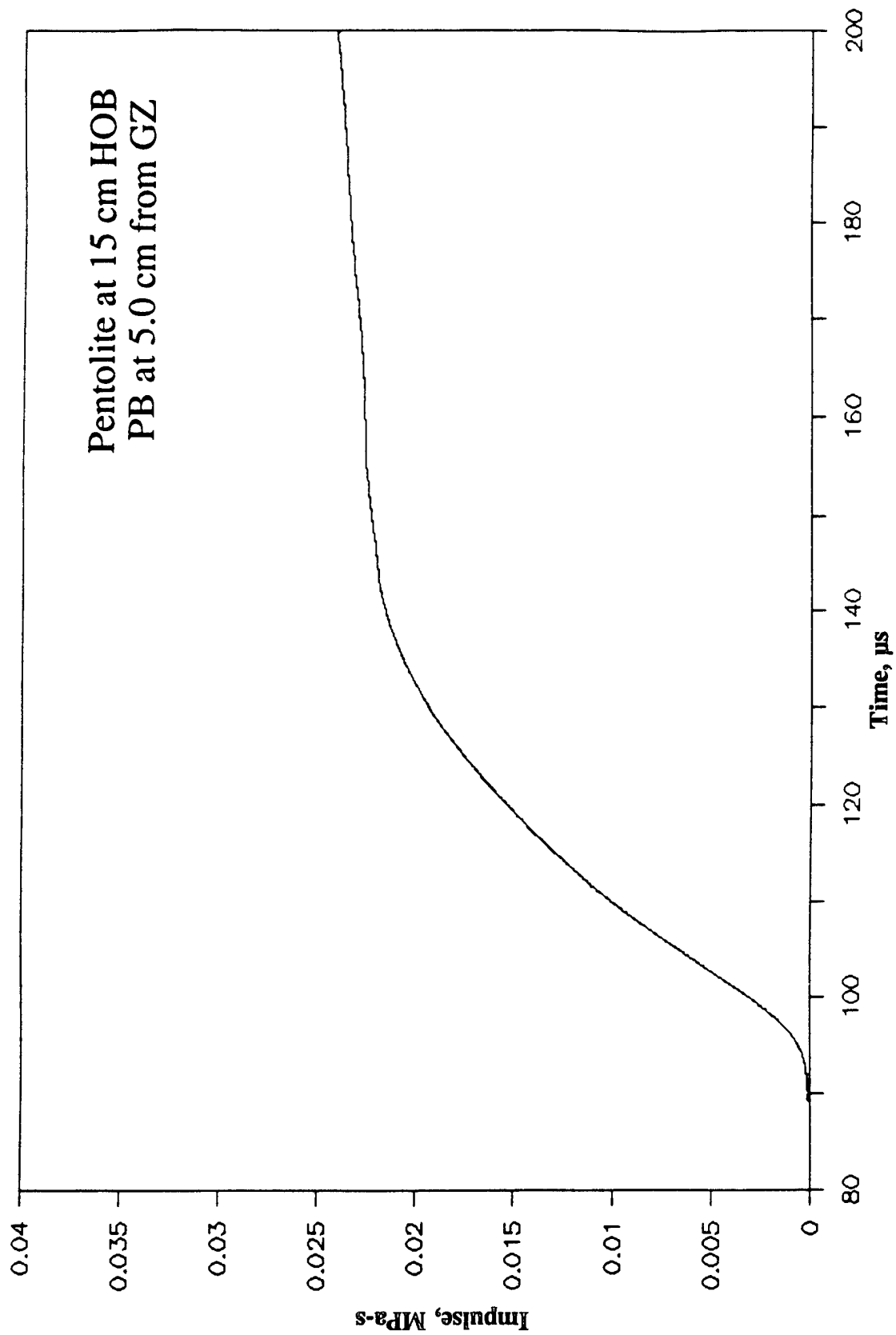


Figure B-8. Impulse-Time Record From Bar Gage PB-7, 5.0 cm From Centerline, Baseplate Test 2A.3, Pentolite at 15 cm.

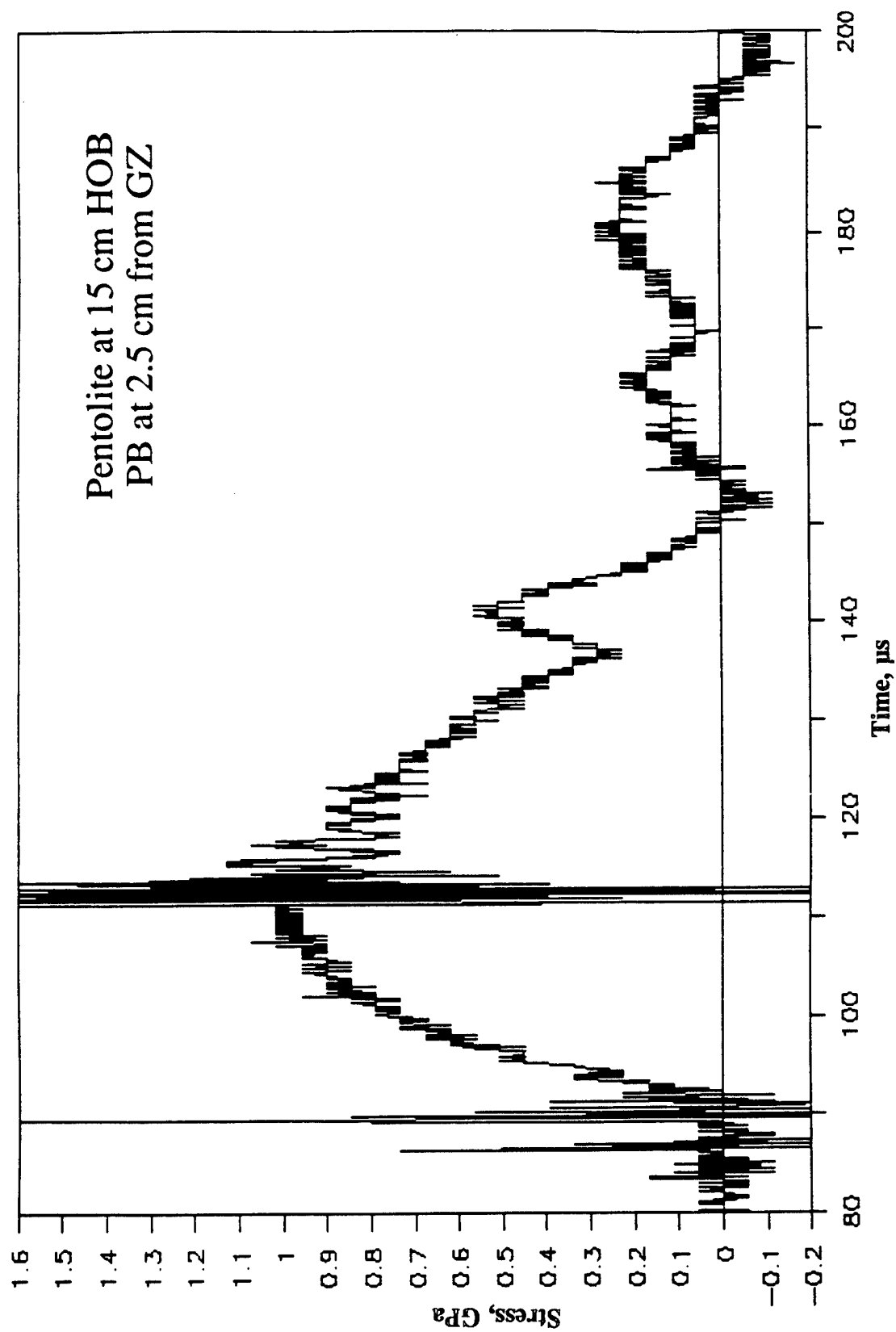


Figure B-9. Stress-Time Record From Bar Gage PB-6, 2.5 cm From Centerline, Baseplate Test 2A.3, Pentolite at 15 cm.

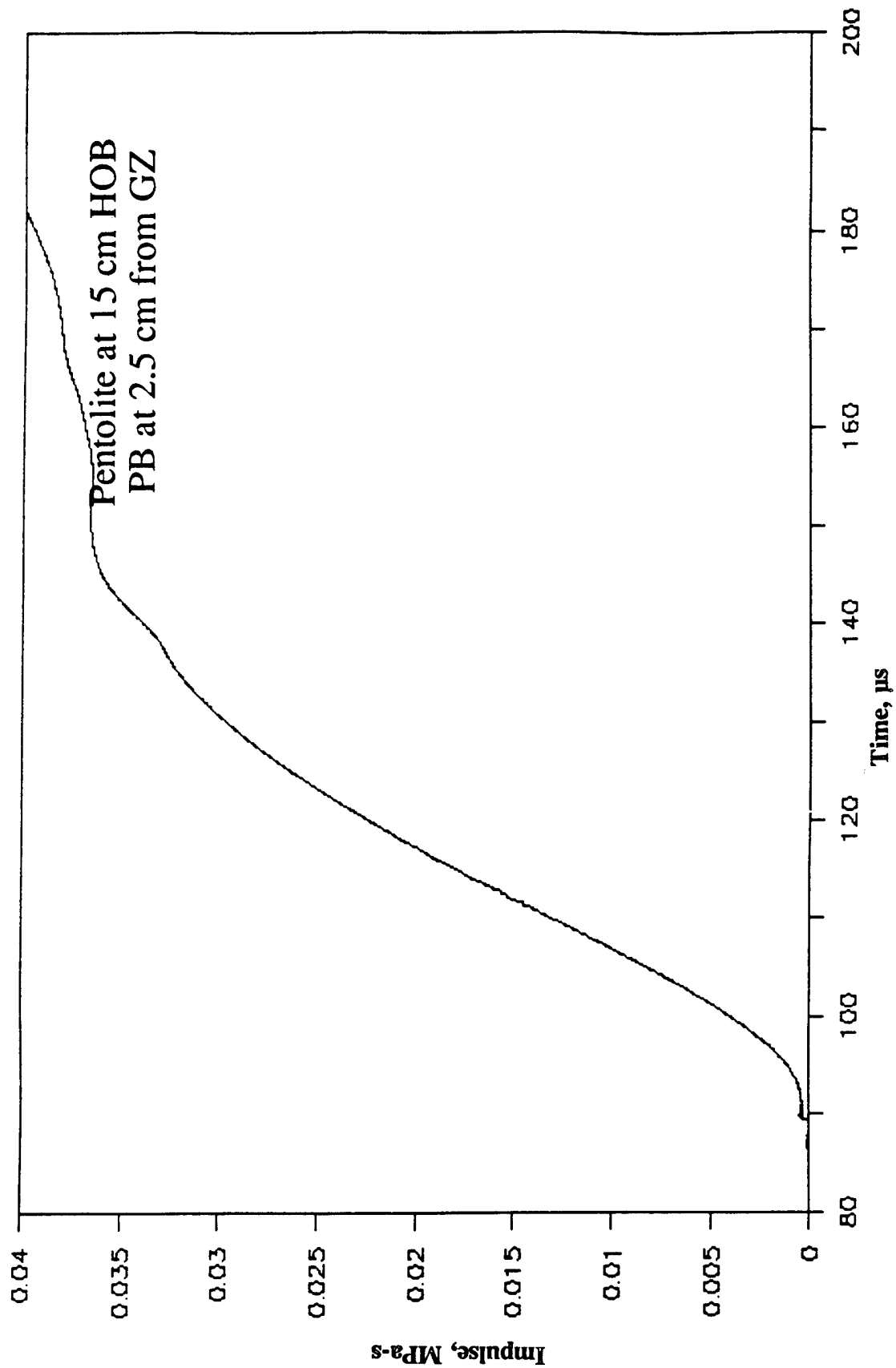


Figure B-10. Impulse-Time Record From Bar Gage PB-6, 2.5 cm From Centerline, Baseplate Test 2A.3, Pentolite at 15 cm.

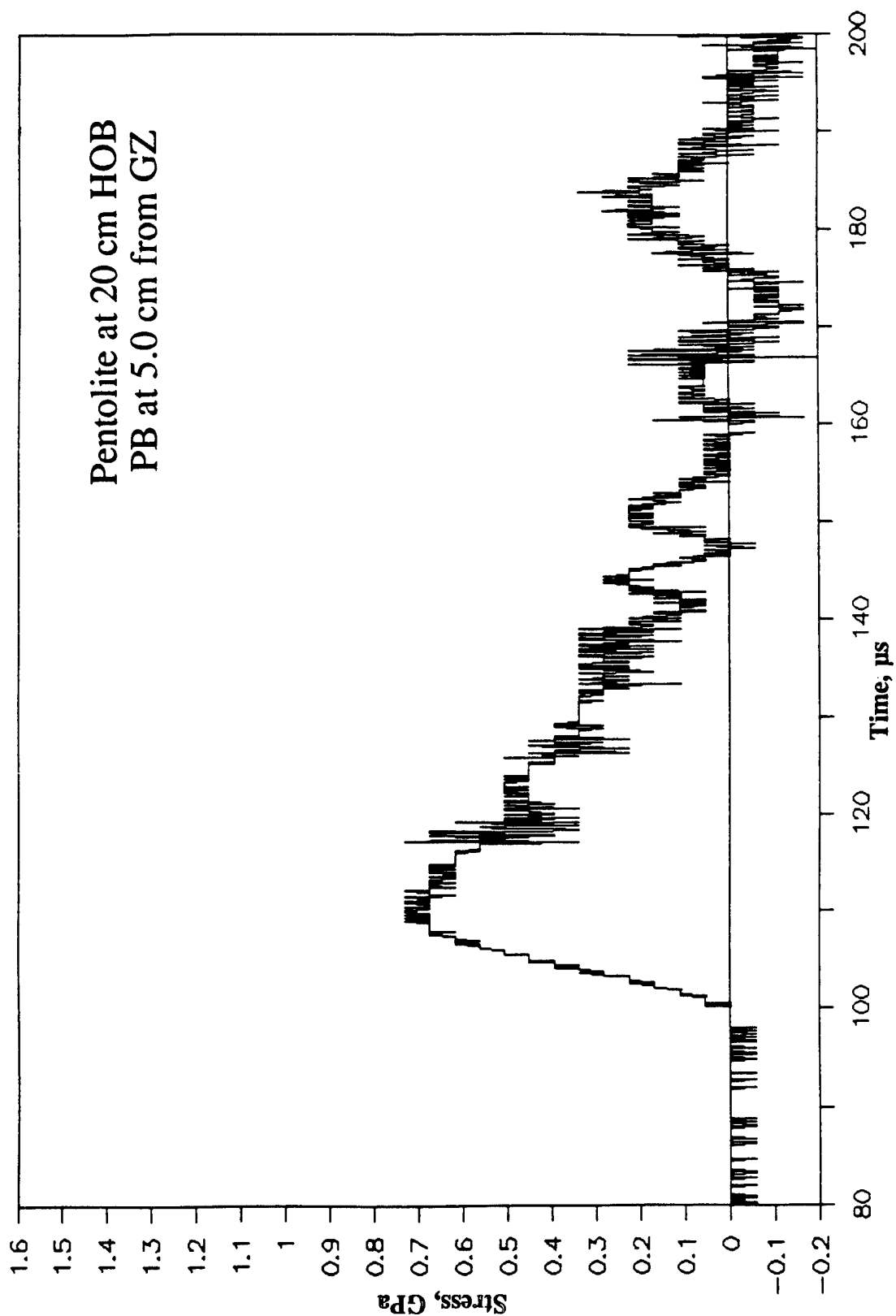


Figure B-11. Stress-Time Record From Bar Gage PB-7, 5.0 cm From Centerline, Baseplate Test 2A.4, Pentolite at 20 cm.

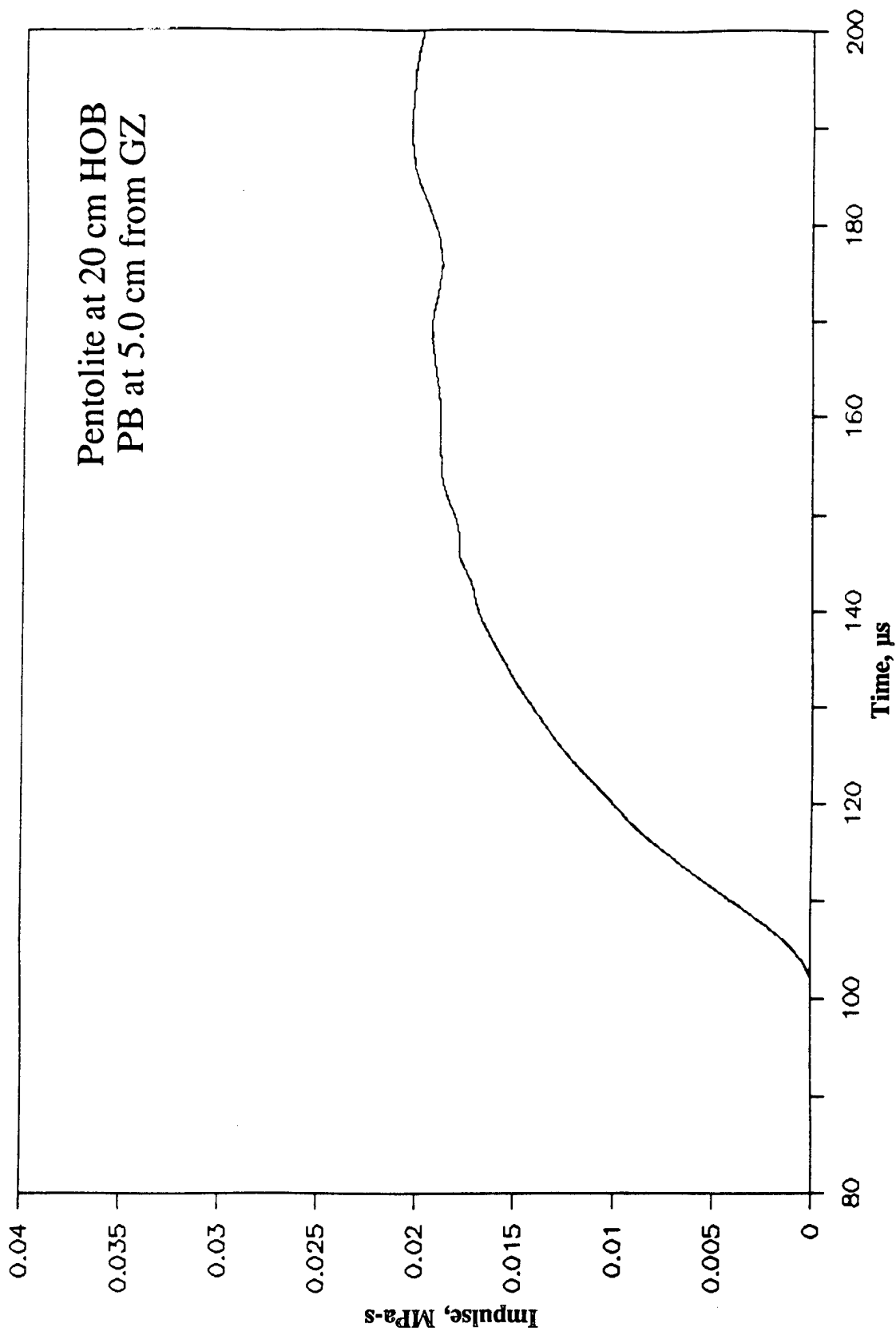


Figure B-12. Impulse-Time Record From Bar Gage PB-7, 5.0 cm From Centerline, Baseplate Test 2A.4, Pentolite at 20 cm.

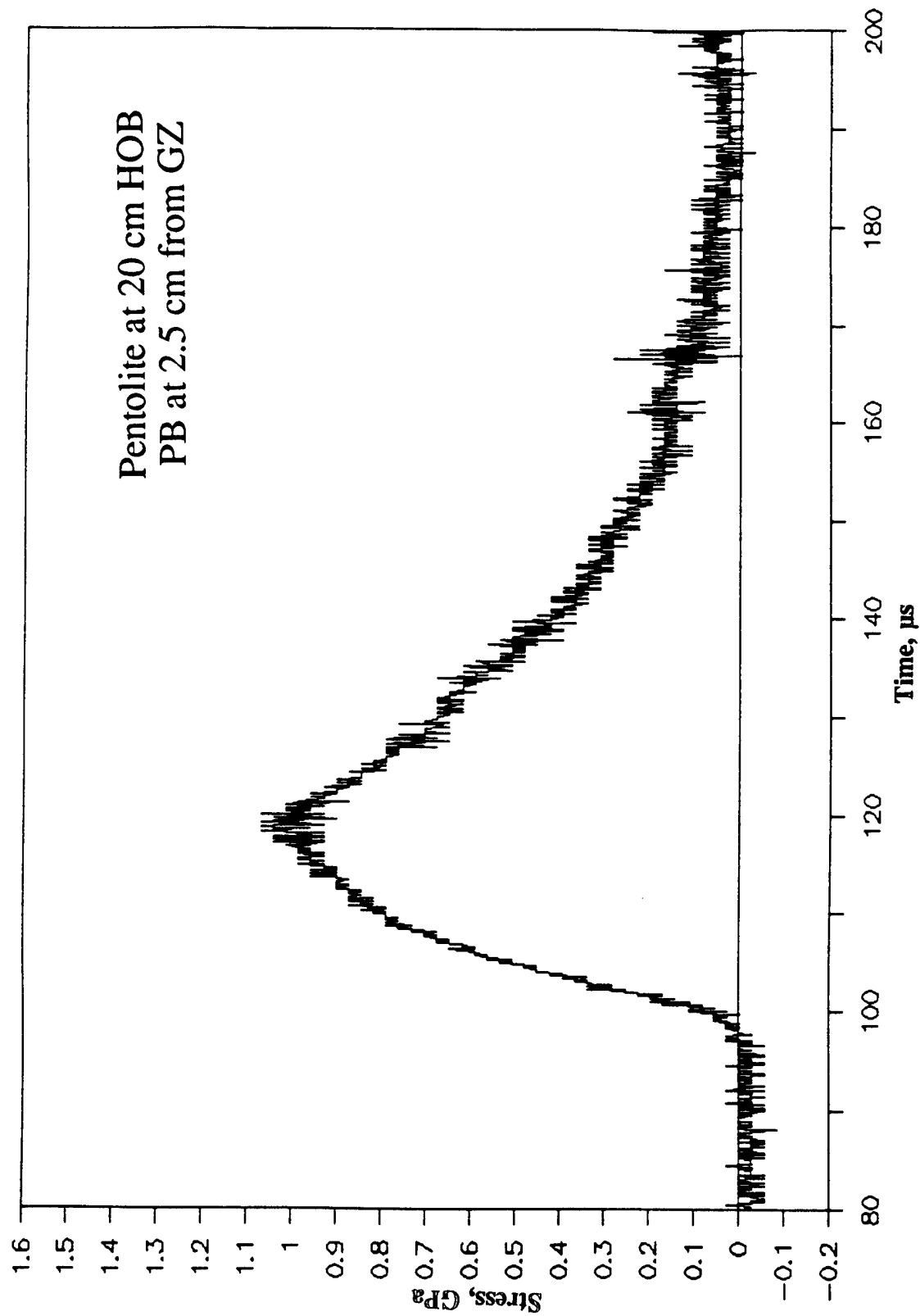


Figure B-13. Stress-Time Record From Bar Gage PB-6, 2.5 cm From Centerline, Baseplate Test 2A.4, Pentolite at 20 cm.

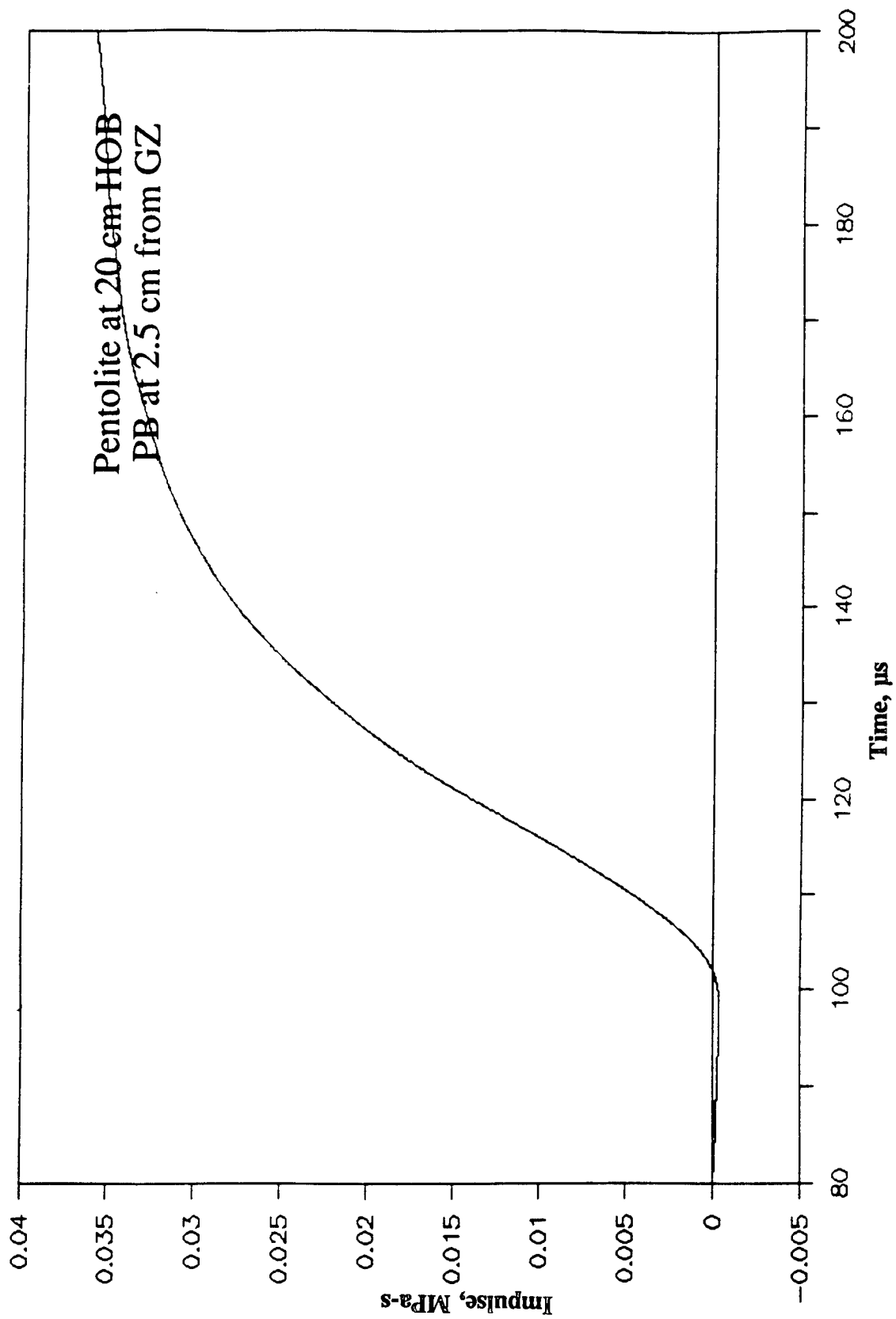


Figure B-14. Impulse-Time Record From Bar Gage PB-6, 2.5 cm From Centerline, Baseplate Test 2A.4, Pentolite at 20 cm.

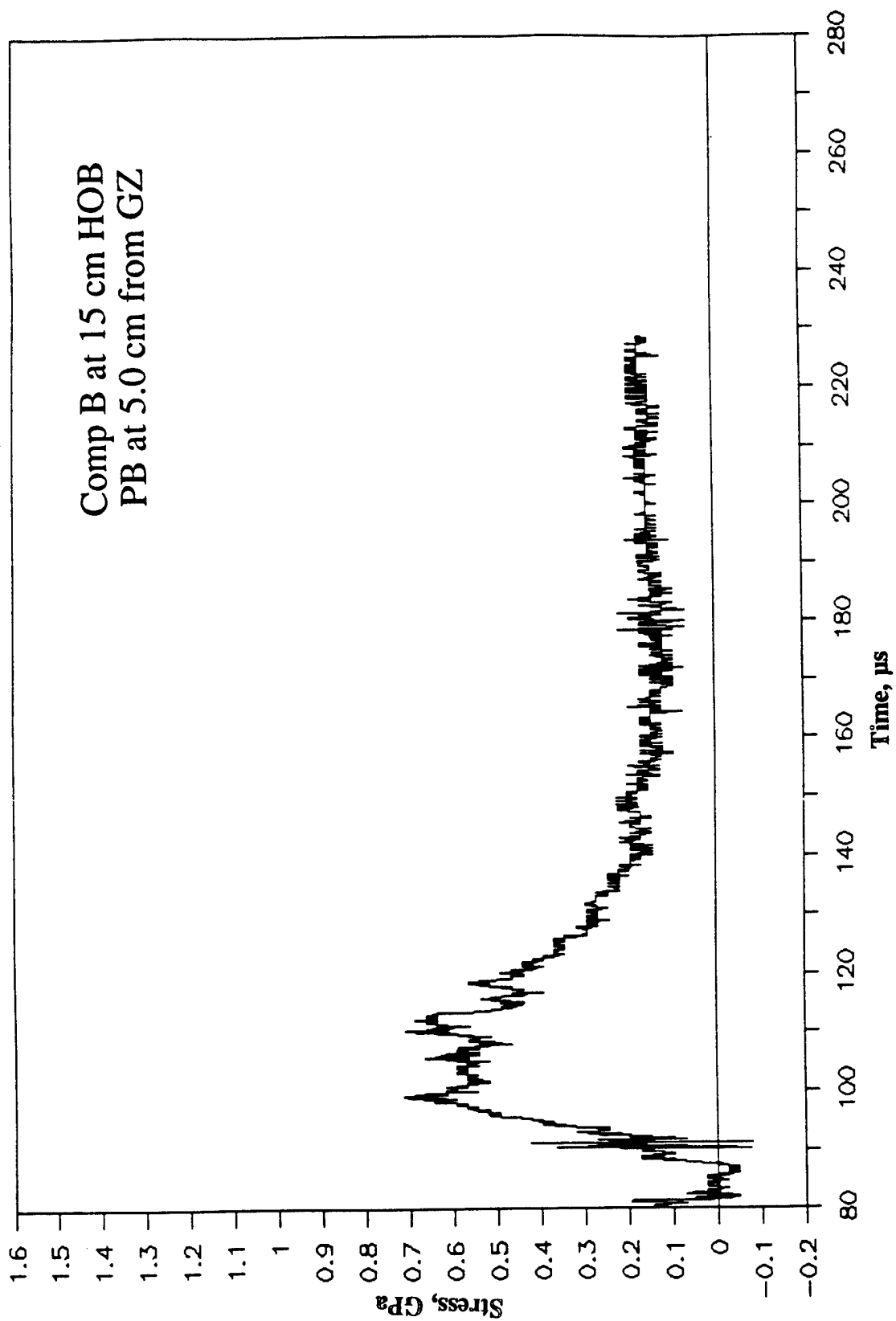


Figure B-15. Stress-Time Record From Bar Gage PB-7, 5.0 cm From Centerline, Baseplate Test 2A.5, Comp B at 15-cm HOB.

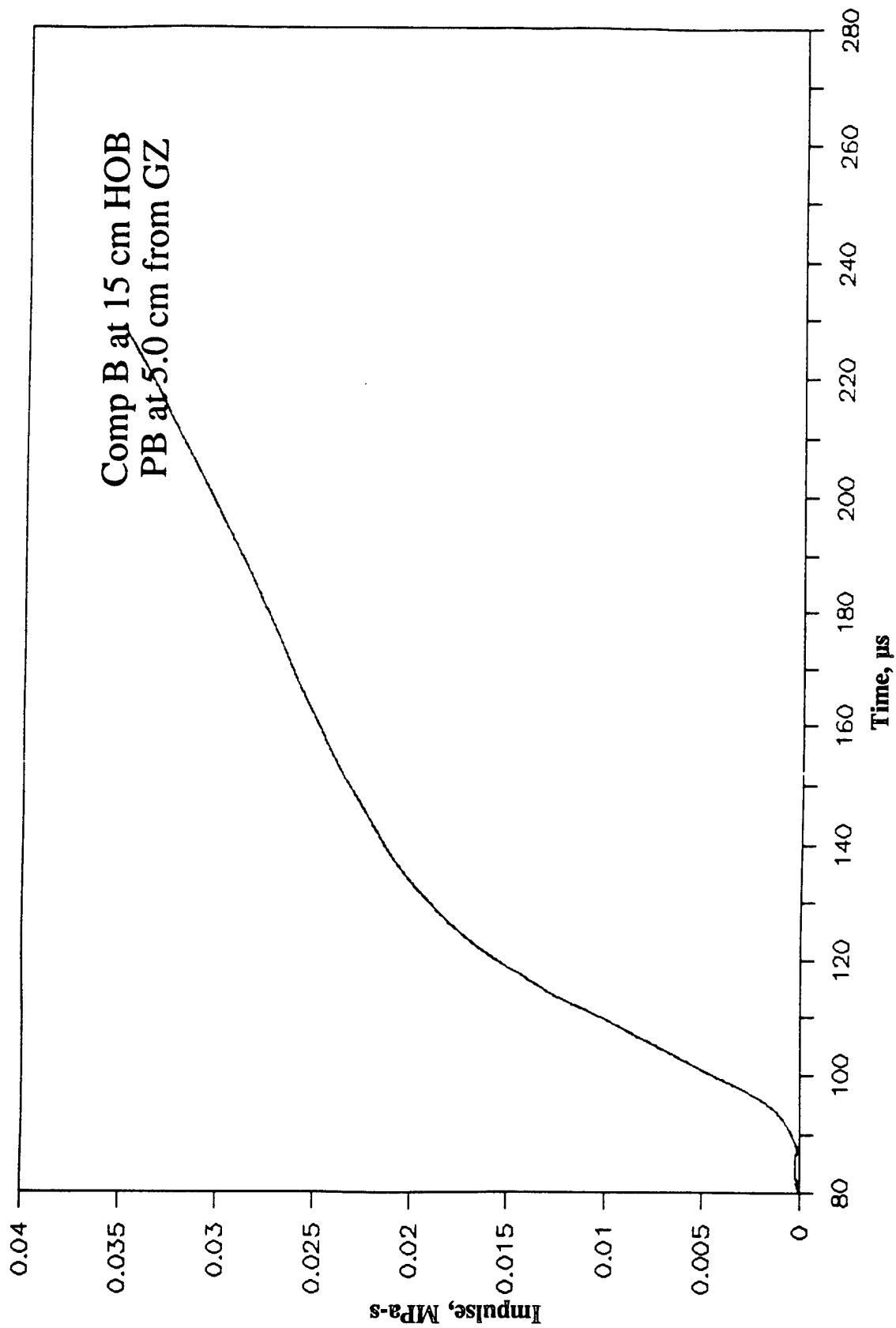


Figure B-16. Impulse-Time Record From Bar Gage PB-7, 5.0 cm From Centerline, Baseplate Test 2A.5, Comp B at 15-cm HOB.

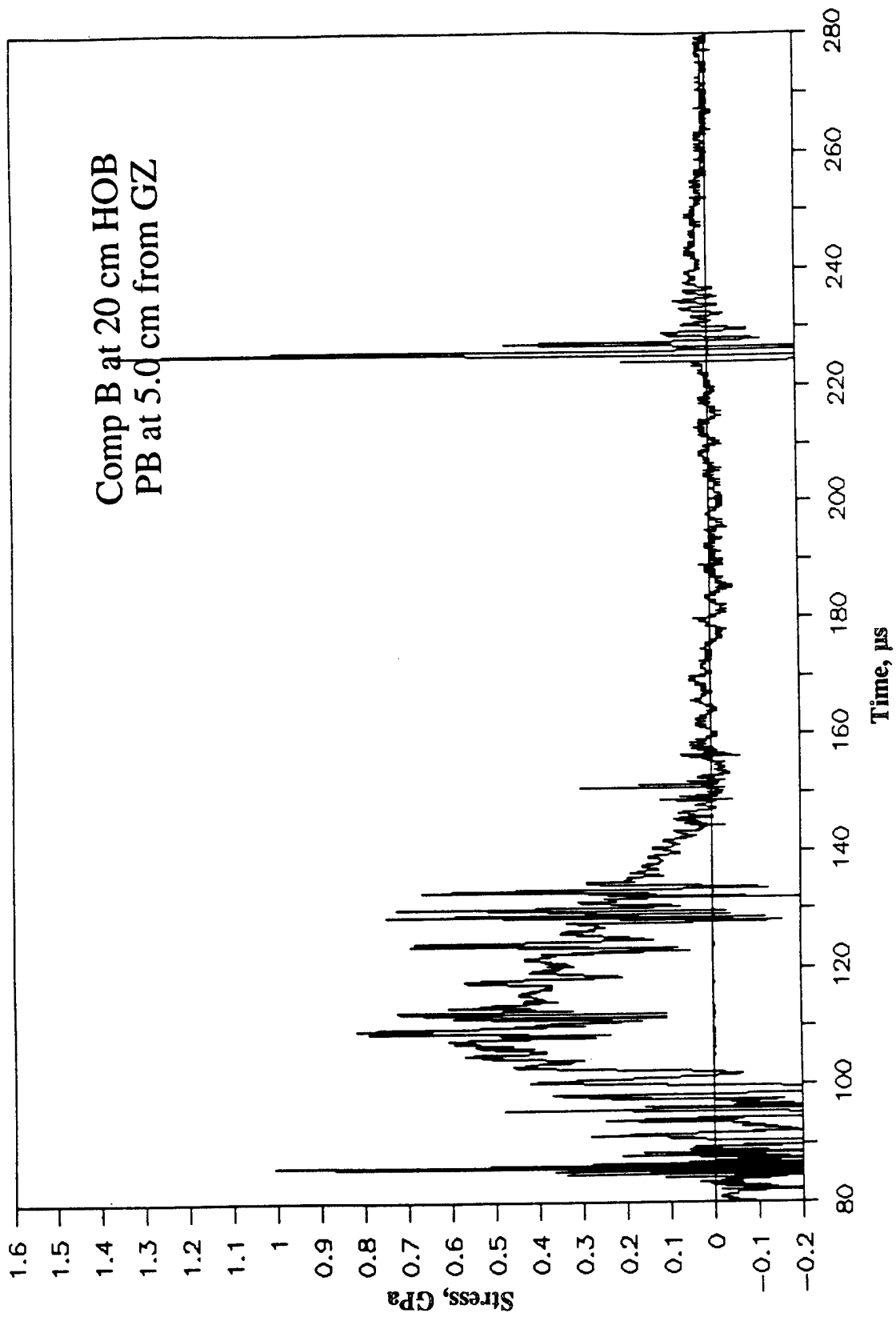


Figure B-17. Stress-Time Record From Bar Gage PB-7, 5.0 cm From Centerline, Baseplate Test 2A.6, Comp B at 20-cm HOB.

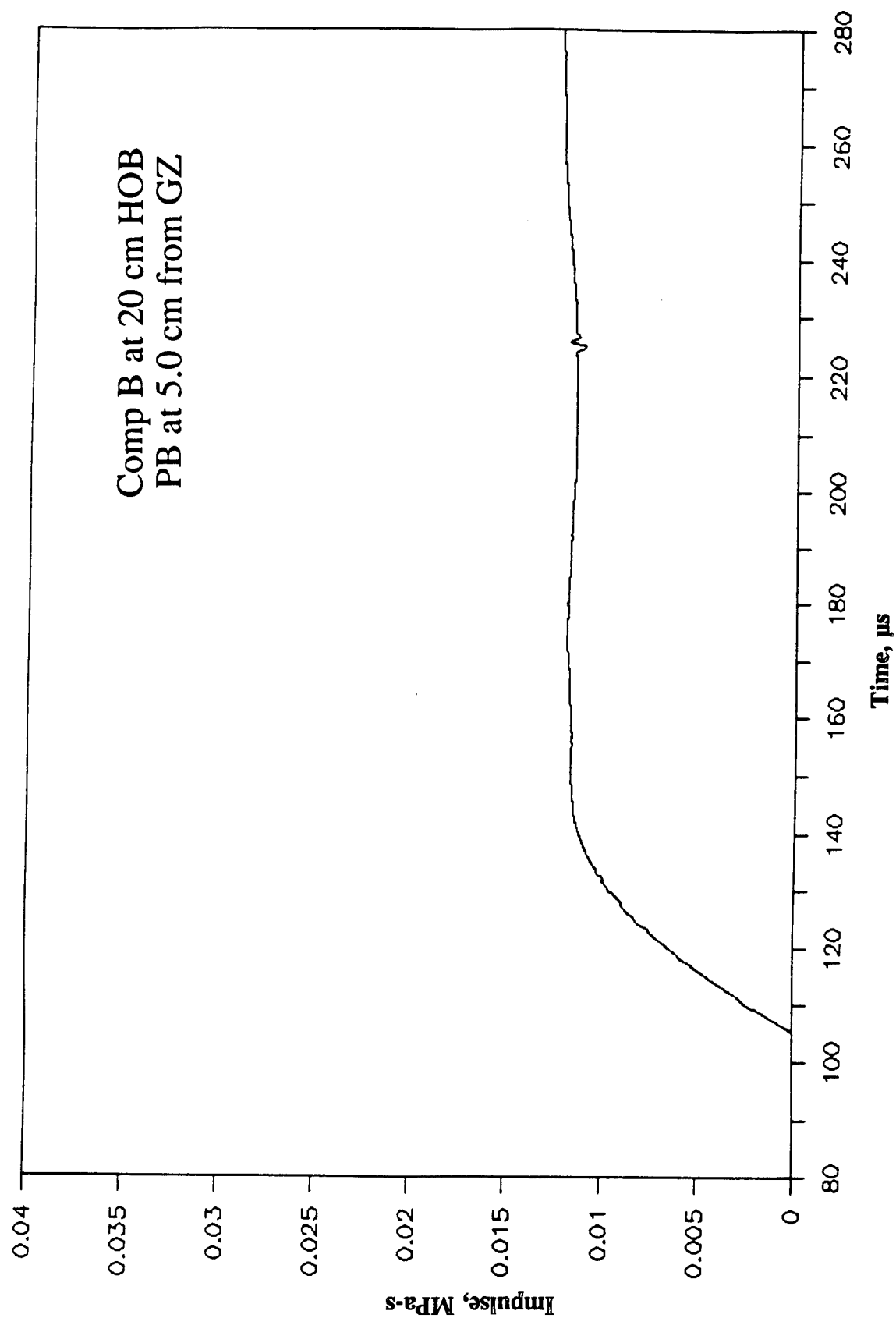


Figure B-18. Impulse-Time Record From Bar Gage PB-7, 5.0 cm From Centerline, Baseplate Test 2A.6, Comp B at 20-cm HOB.

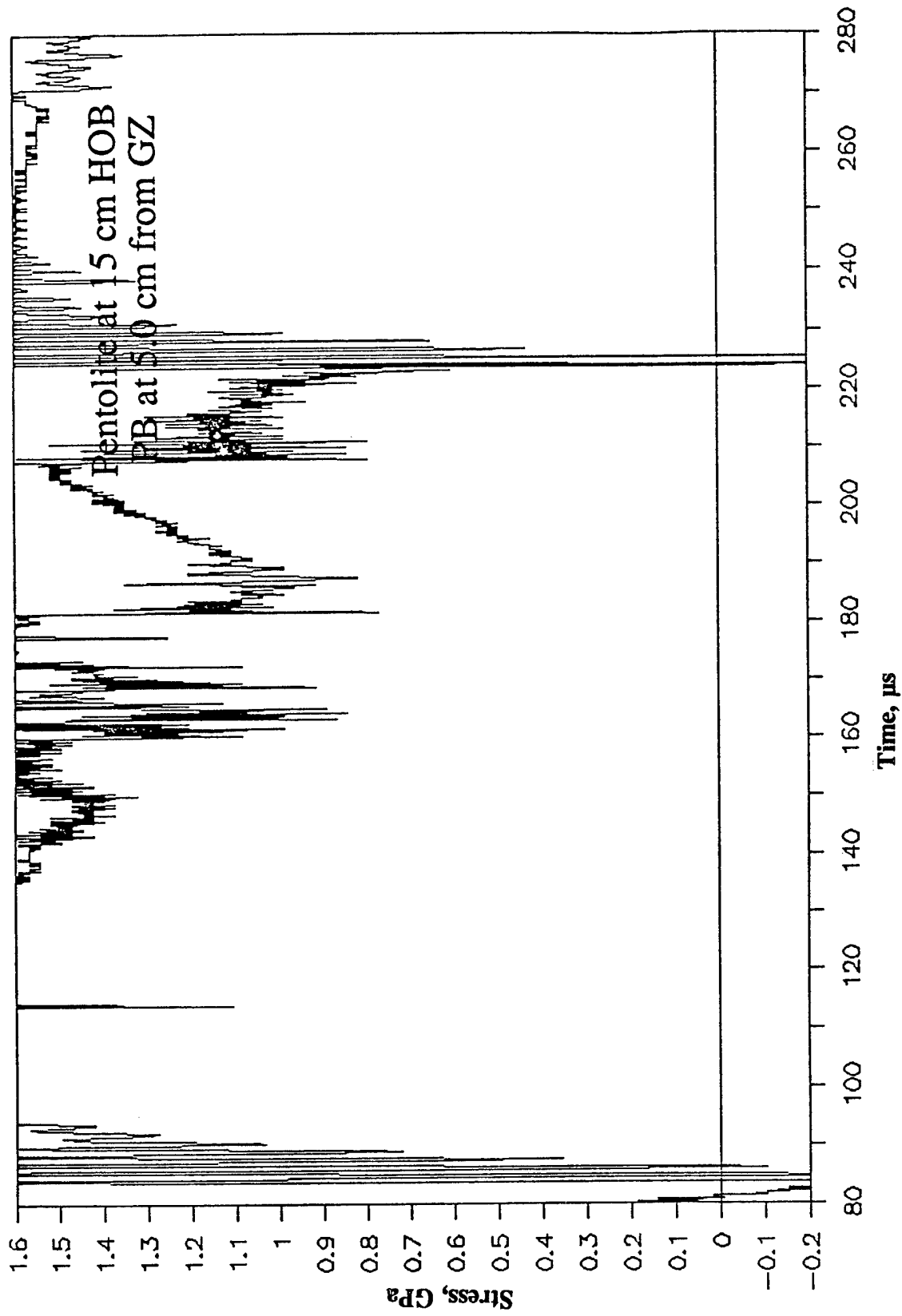


Figure B-19. Stress-Time Record From Bar Gage PB-7, 5.0 cm From Centerline, Baseplate Test 2A.7, Pentolite at 15-cm HOB.

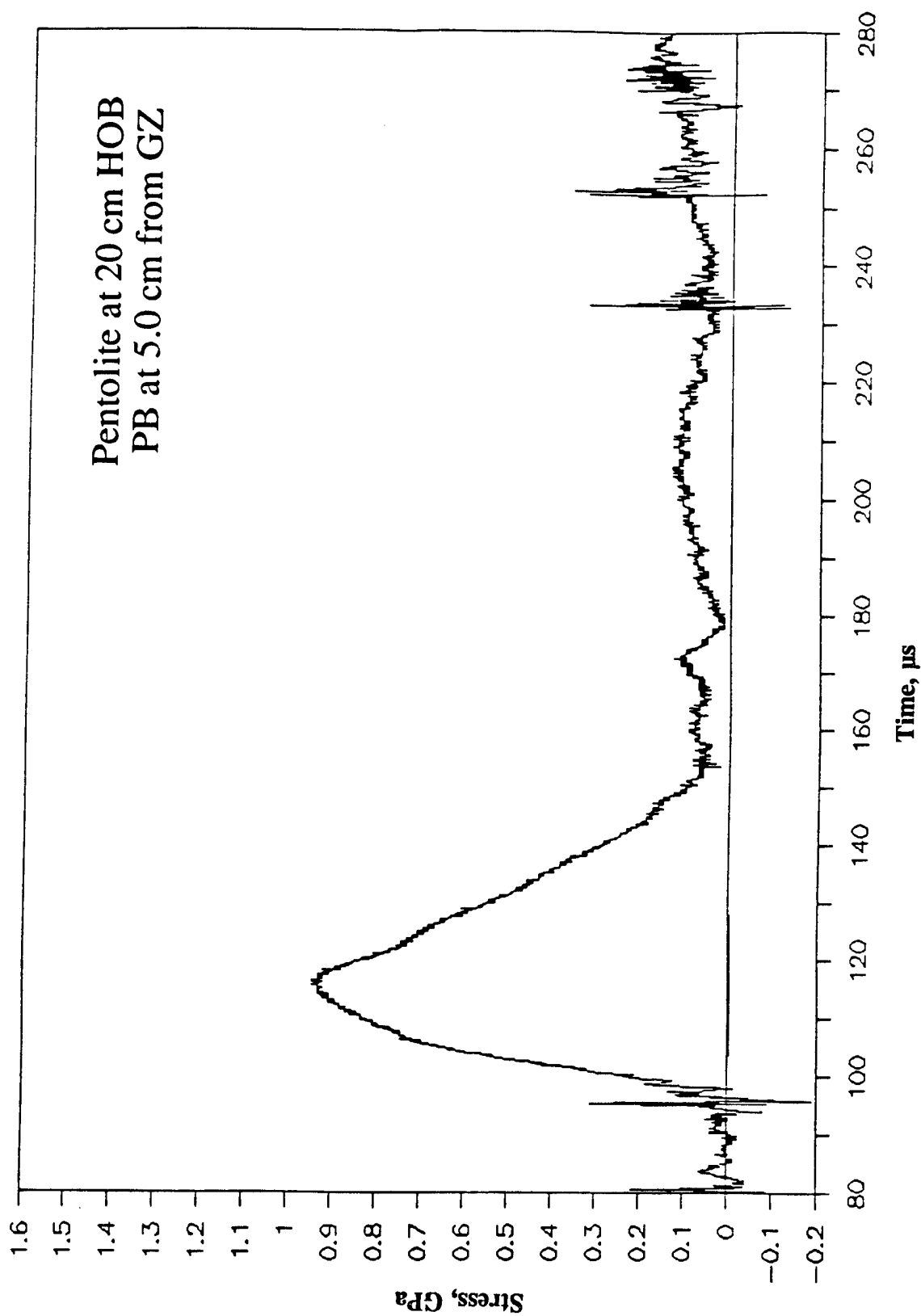


Figure B-20. Stress-Time Record From Bar Gage PB-7, 5.0 cm From Centerline, Baseplate Test 2A.8, Pentolite at 20-cm HOB.

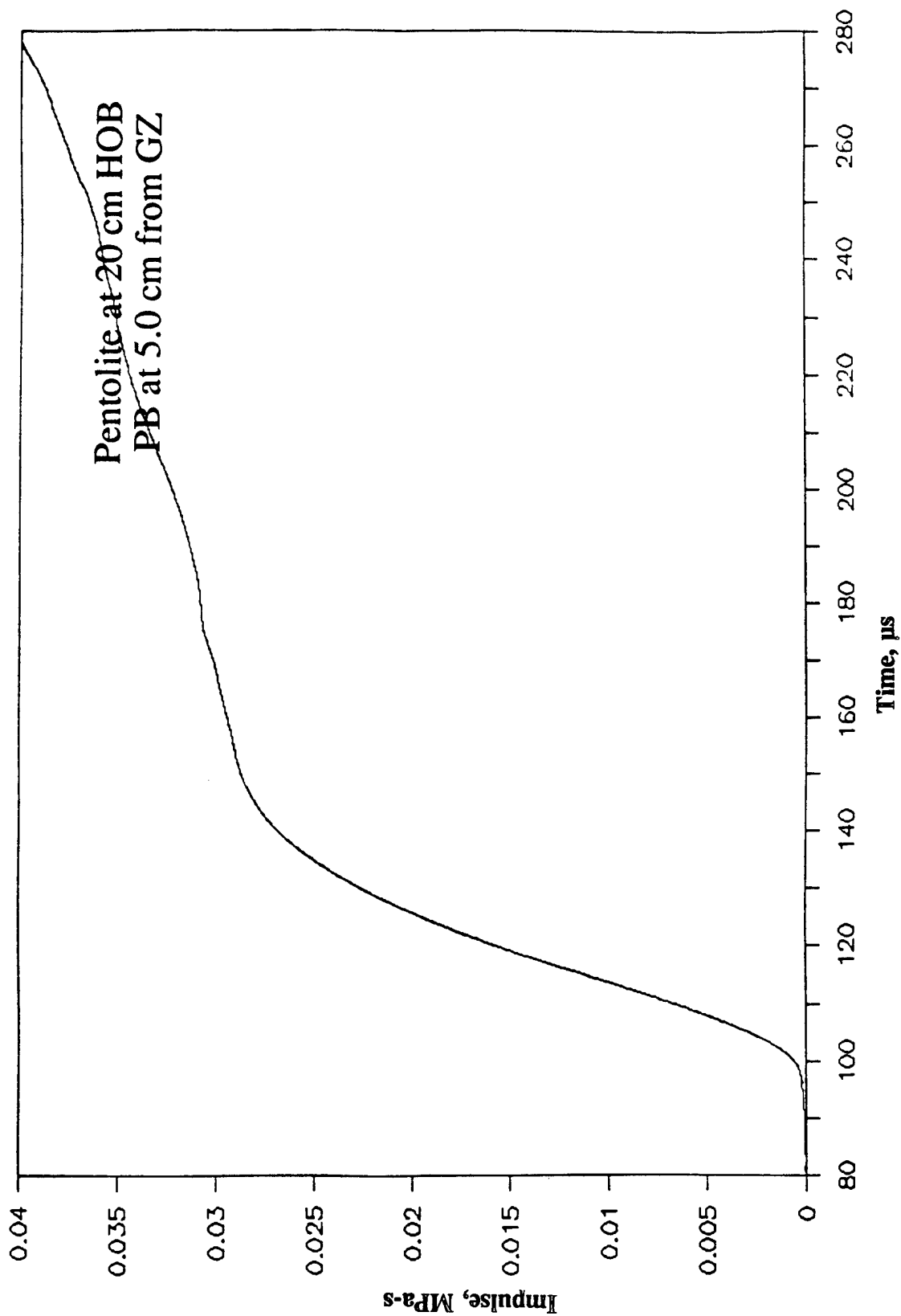


Figure B-21. Impulse-Time Record From Bar Gage PB-7, 5.0 cm From Centerline, Baseplate Test 2A.8, Pentolite at 20-cm HOB.

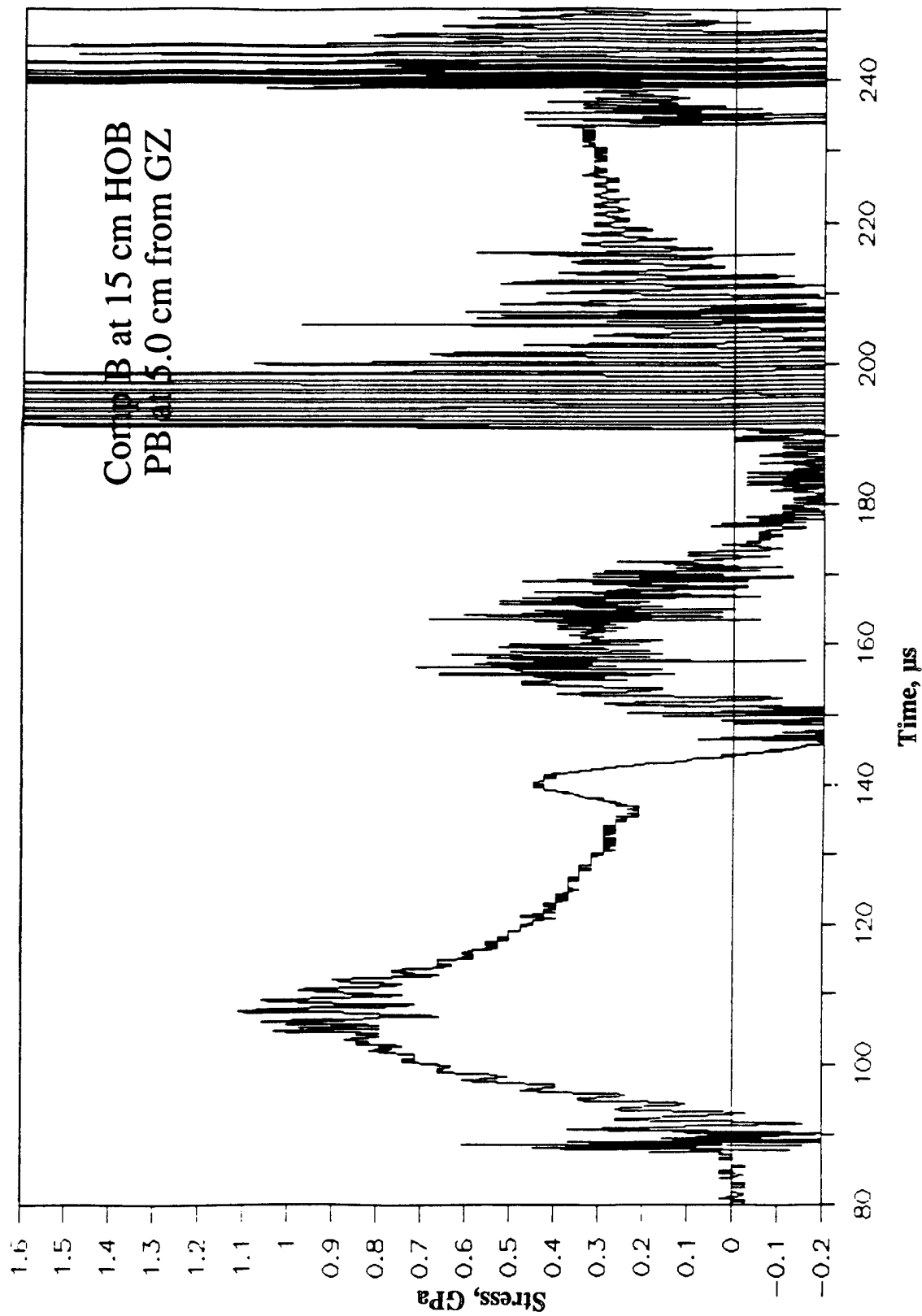


Figure B-22. Stress-Time Record From Bar Gage PB-7, 5.0 cm From Centerline, Baseplate Test 2A.9, Comp B at 15-cm HOB.

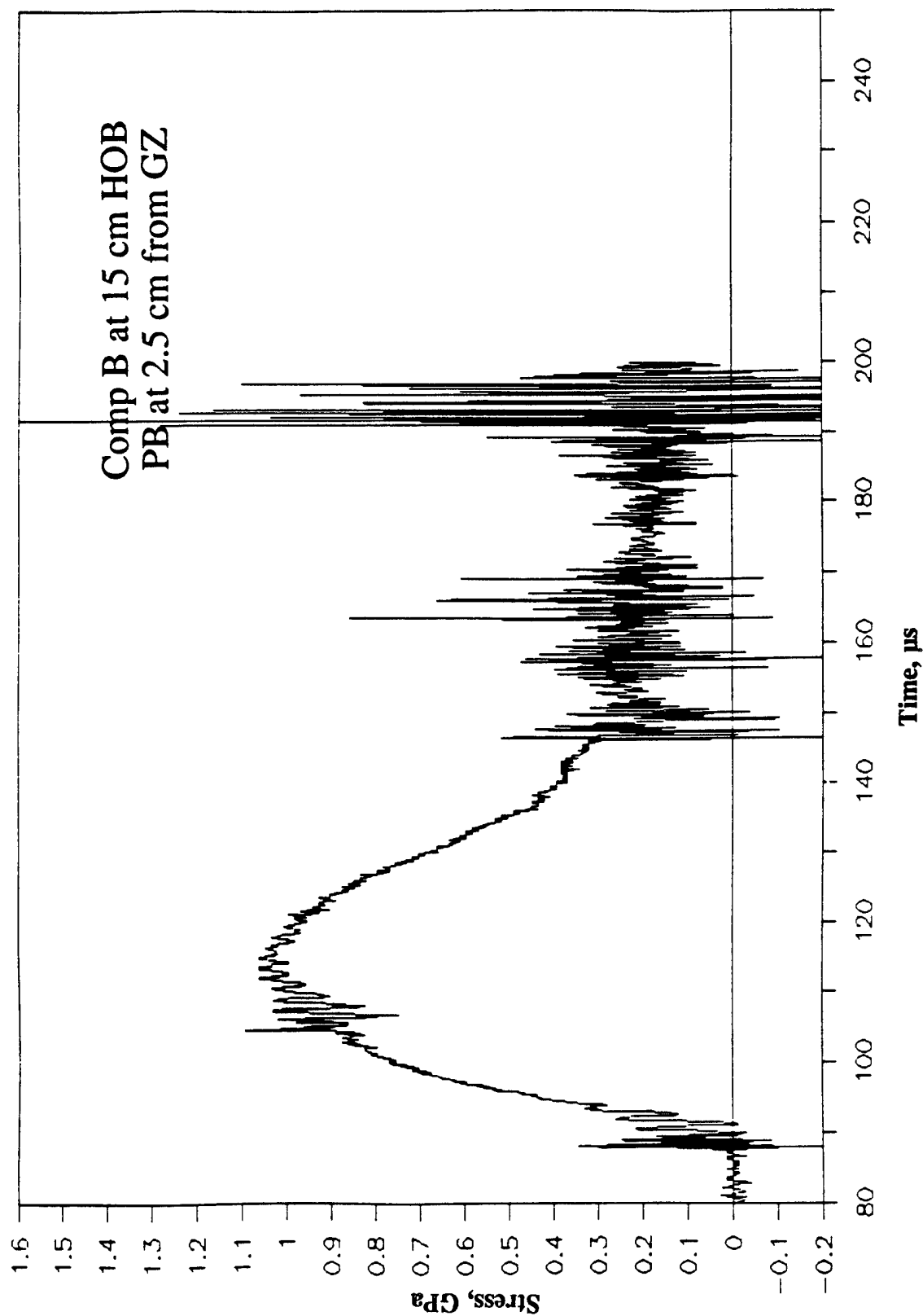


Figure B-23. Stress-Time Record From Bar Gage PB-6, 2.5 cm From Centerline, Baseplate Test 2A.9, Comp B at 15-cm HOB.

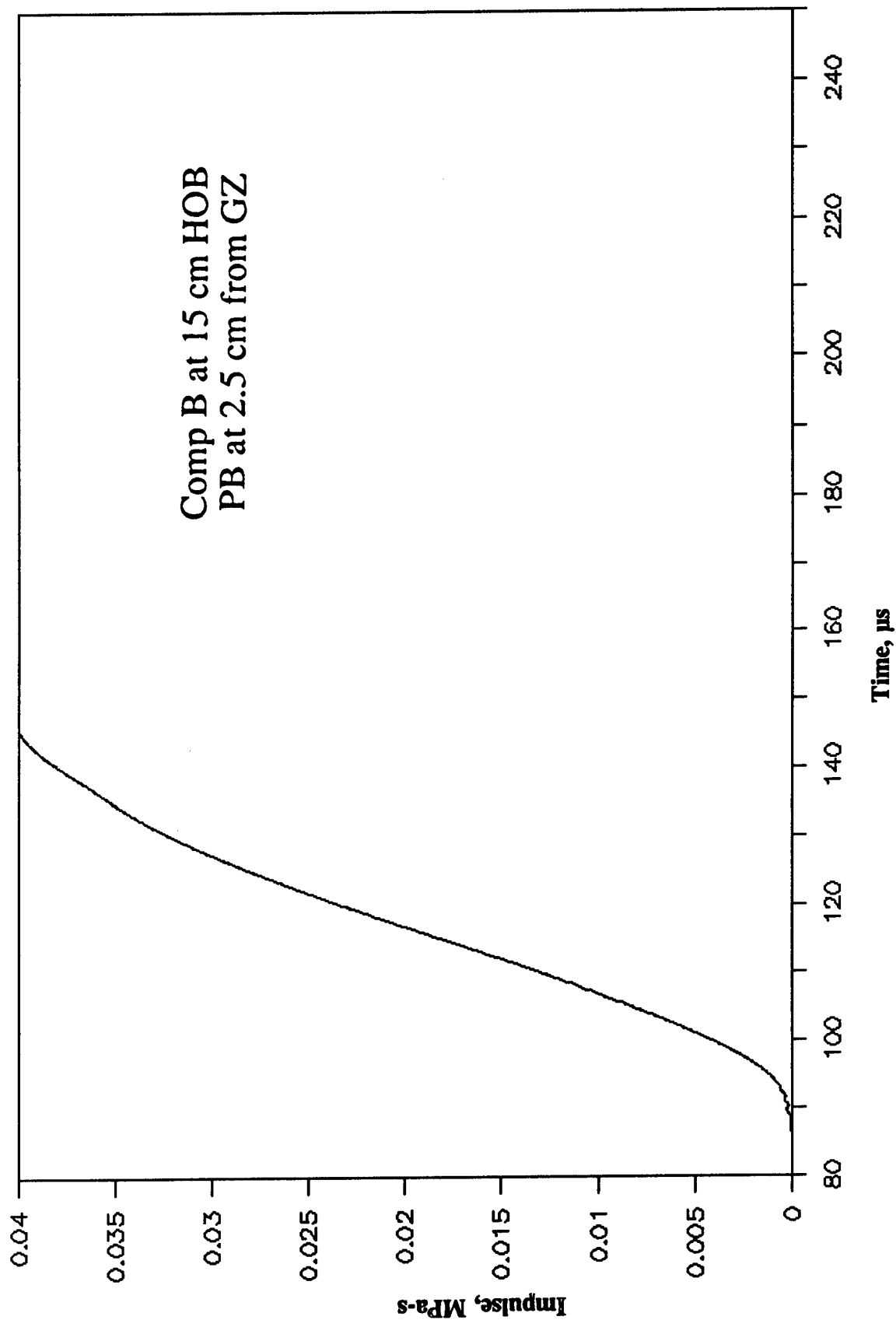


Figure B-24. Impulse-Time Record From Bar Gage PB-6, 2.5 cm From Centerline, Baseplate Test 2A.9, Comp B at 15-cm HOB.

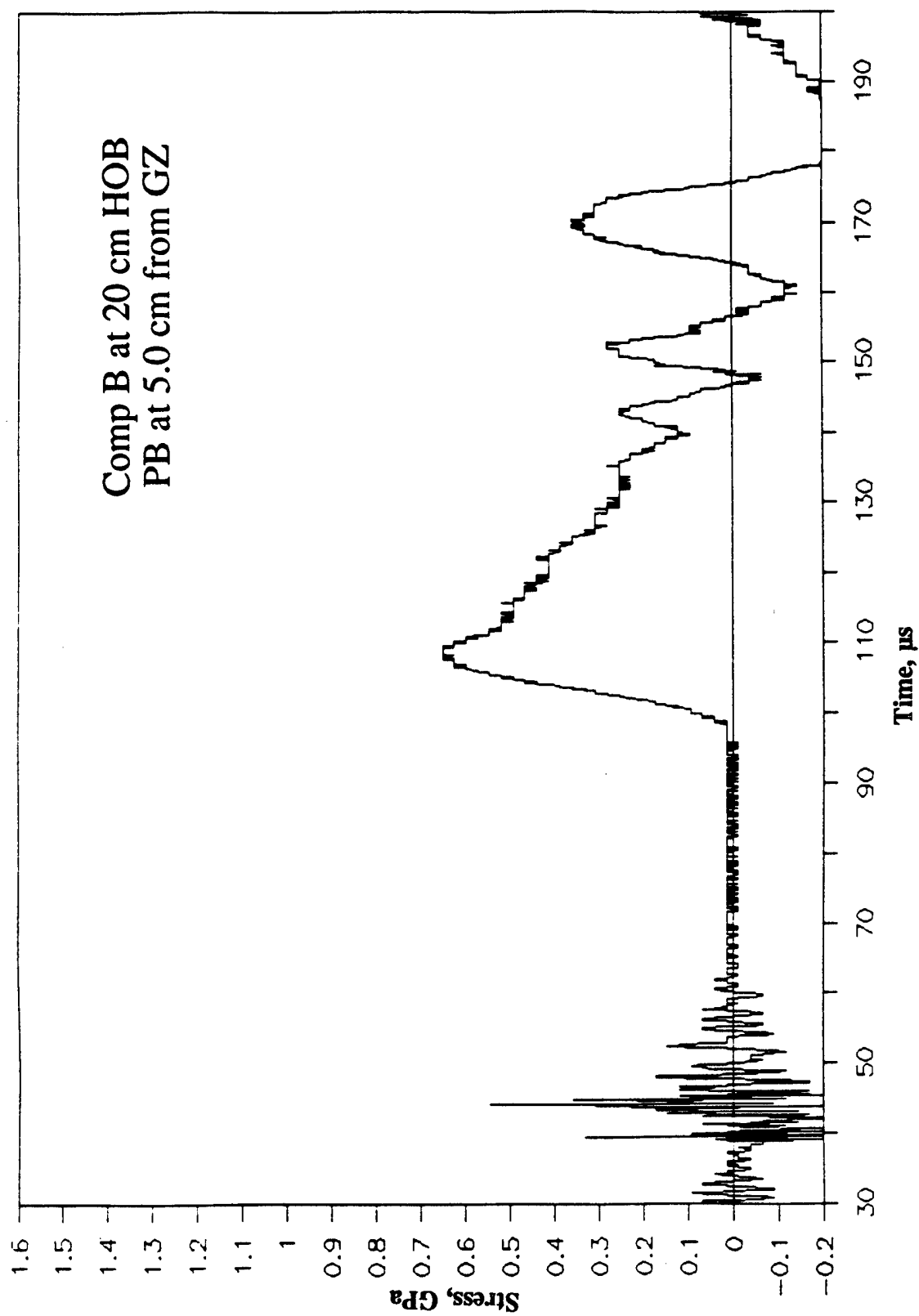


Figure B-25. Stress-Time Record From Bar Gage PB-7, 5.0 cm From Centerline, Baseplate Test 2A.10, Comp B at 20-cm HOB.

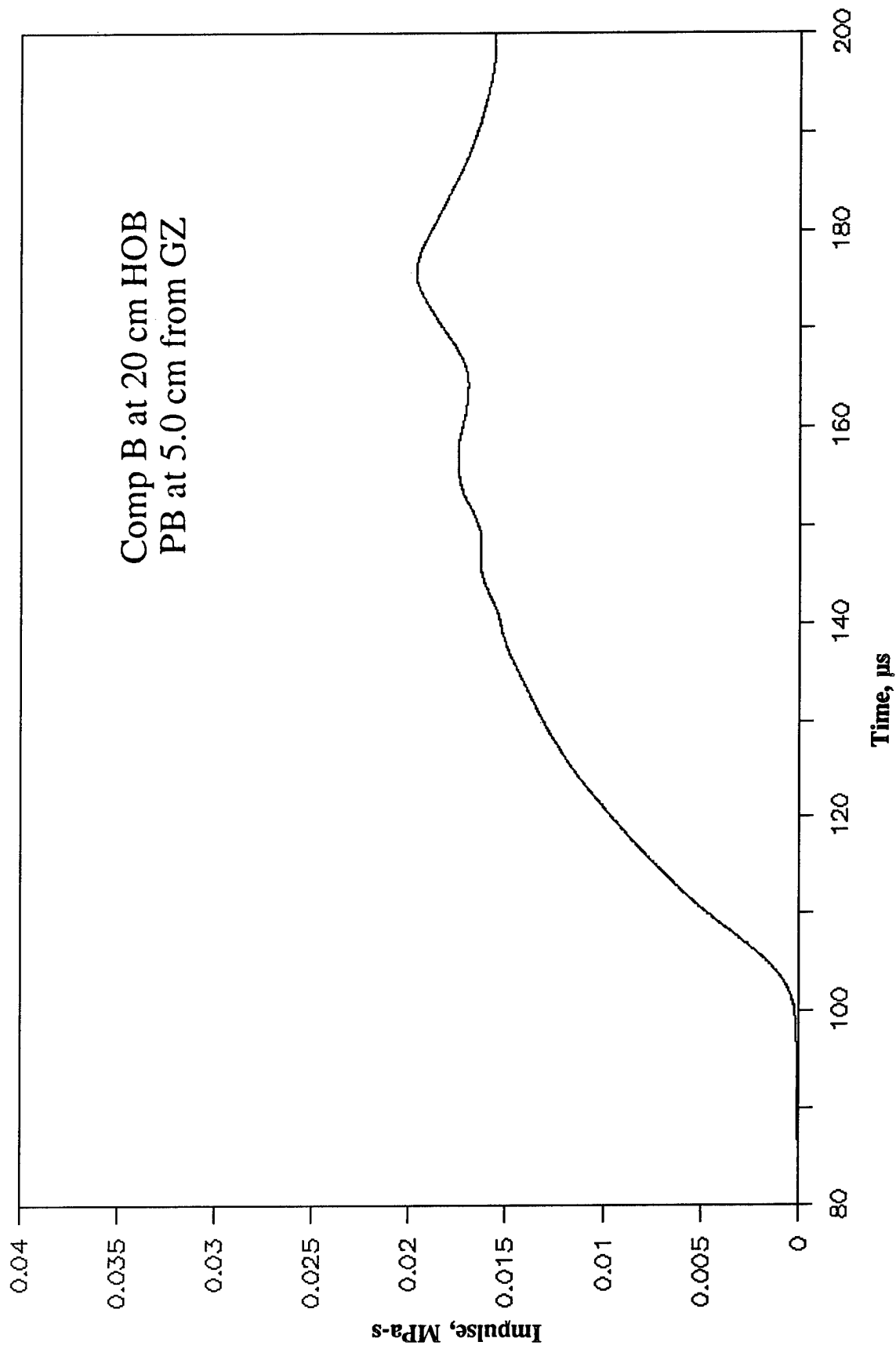


Figure B-26. Impulse-Time Record From Bar Gage PB-7, 2.5 cm From Centerline, Baseplate Test 2A.10, Comp B at 20-cm HOB.

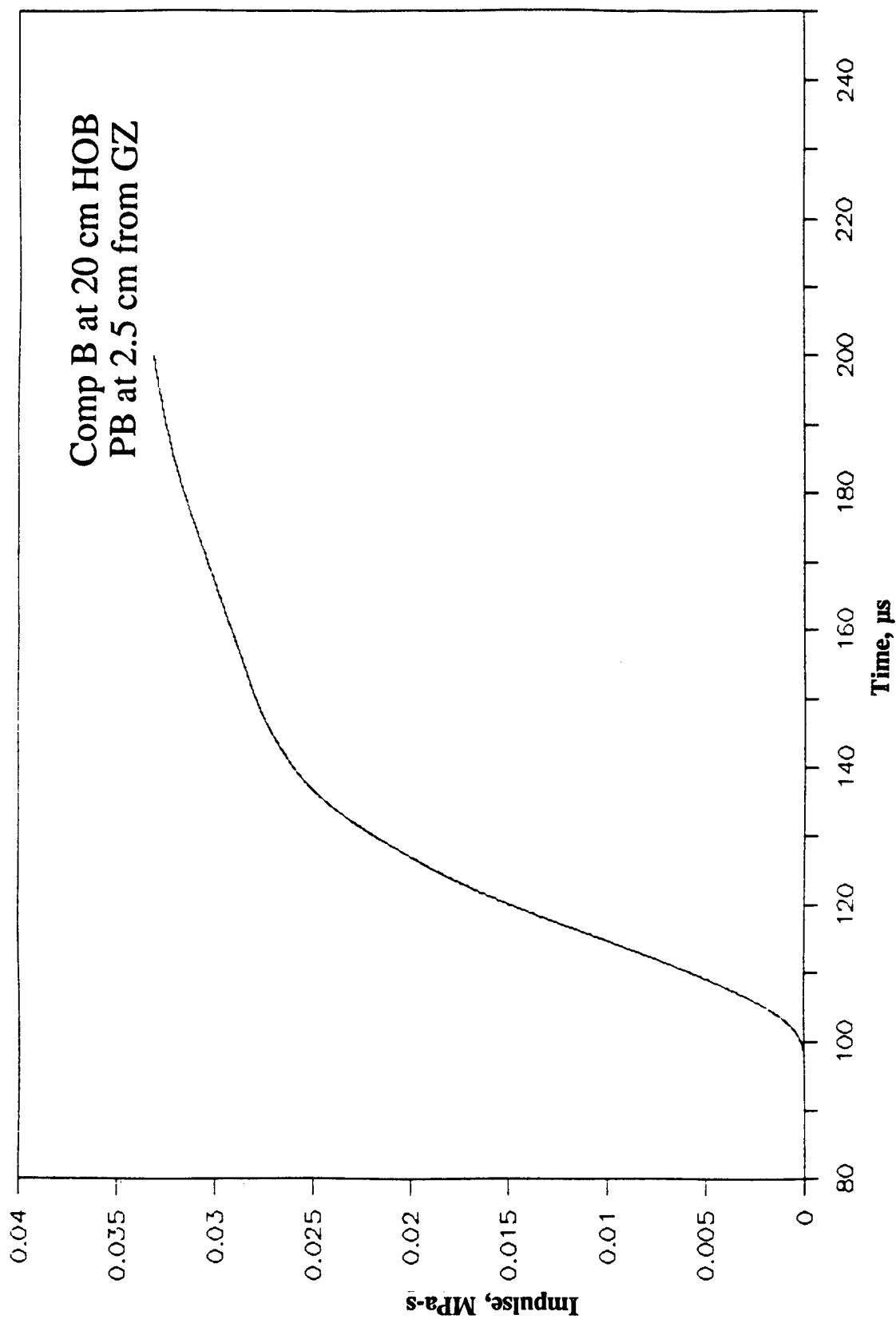


Figure B-27. Impulse-Time Record From Bar Gage PB-6, 2.5 cm From Centerline, Baseplate Test 2A.10, Comp B at 20-cm HOB.

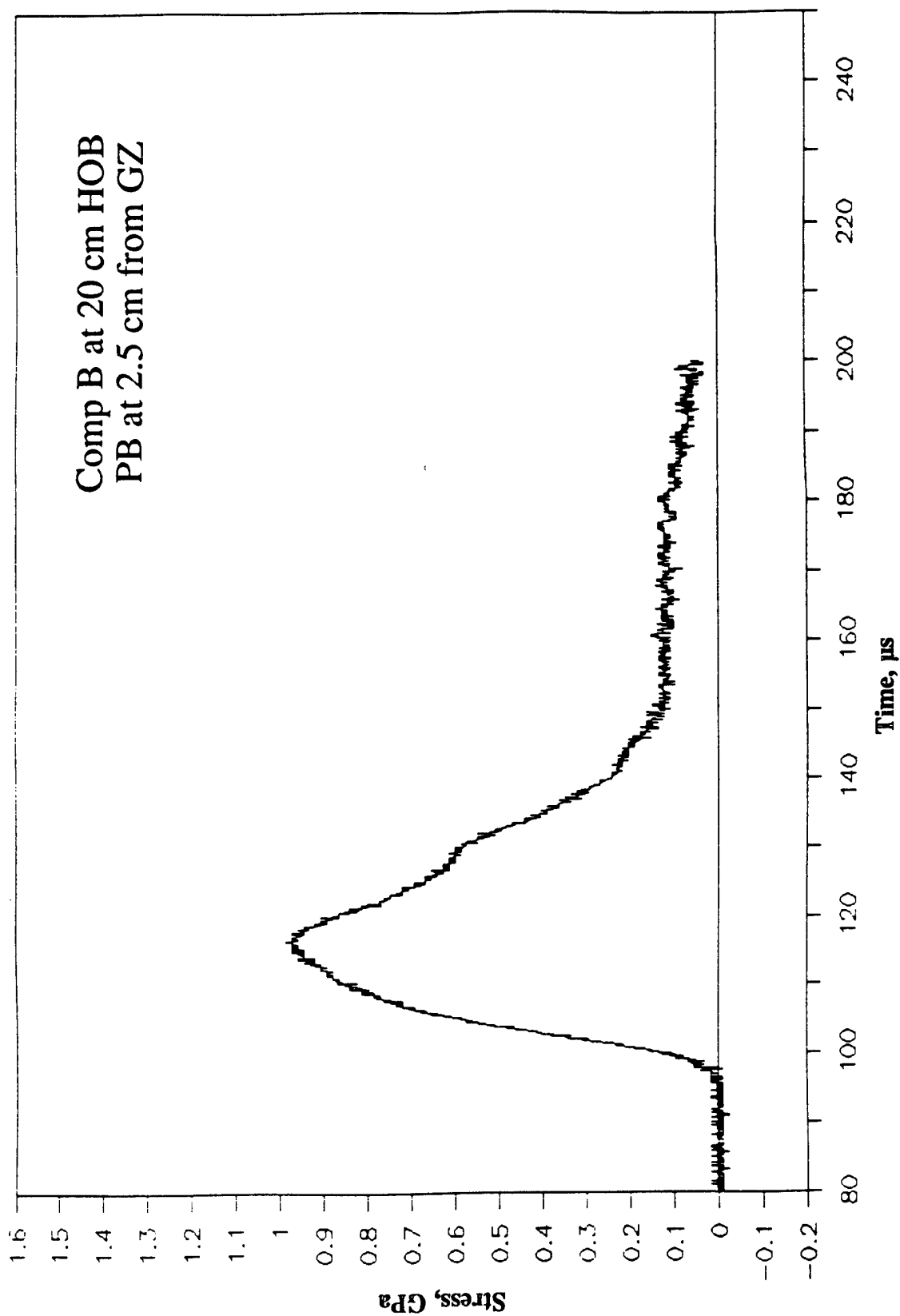


Figure B-28. Stress-Time Record From Bar Gage PB-6, 2.5 cm From Centerline, Baseplate Test 2A.10, Comp B at 20-cm HOB.

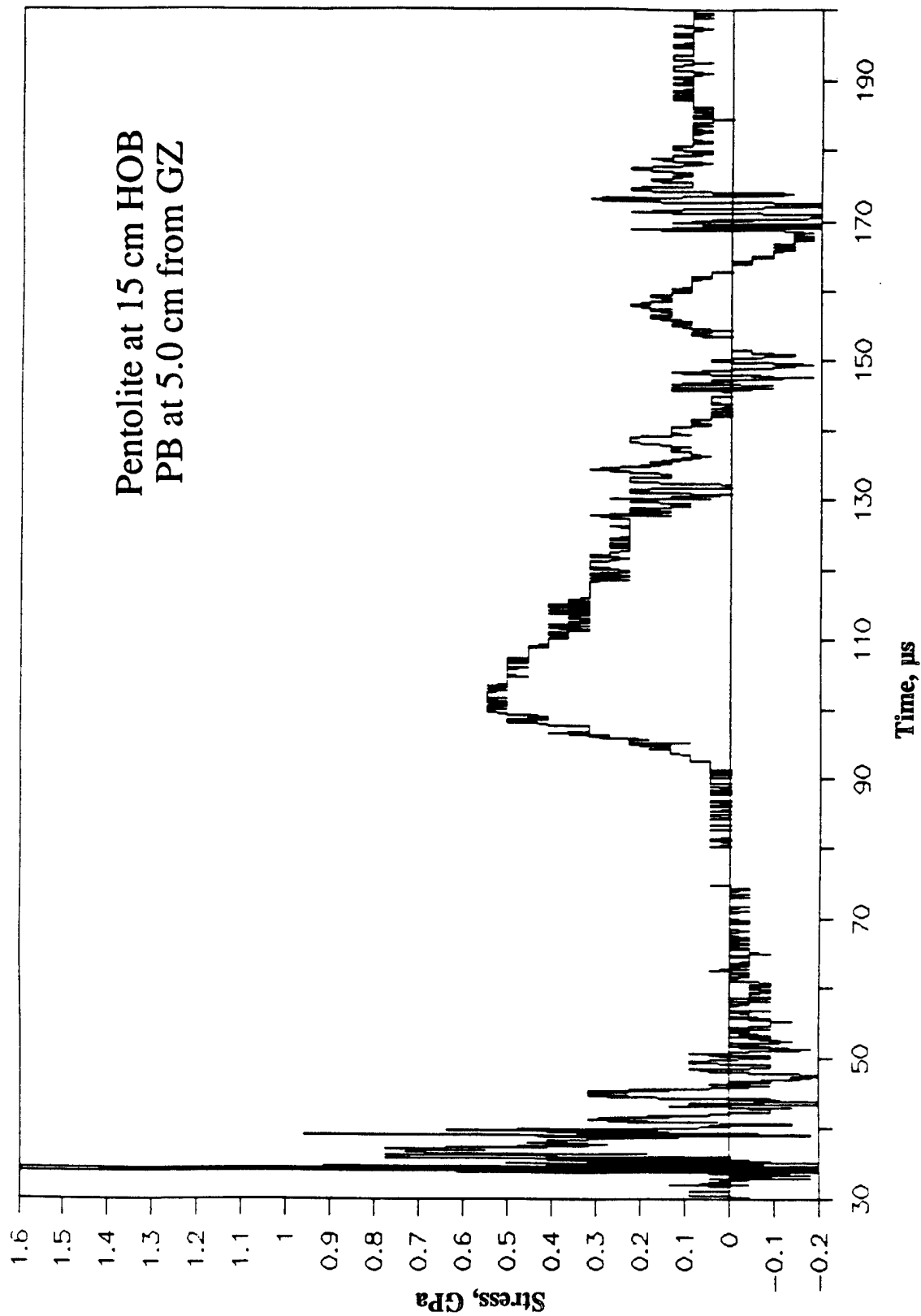


Figure B-29. Stress-Time Record From Bar Gage PB-7, 5.0 cm From Centerline, Baseplate Test 2A.11, Pentolite at 15-cm HOB.

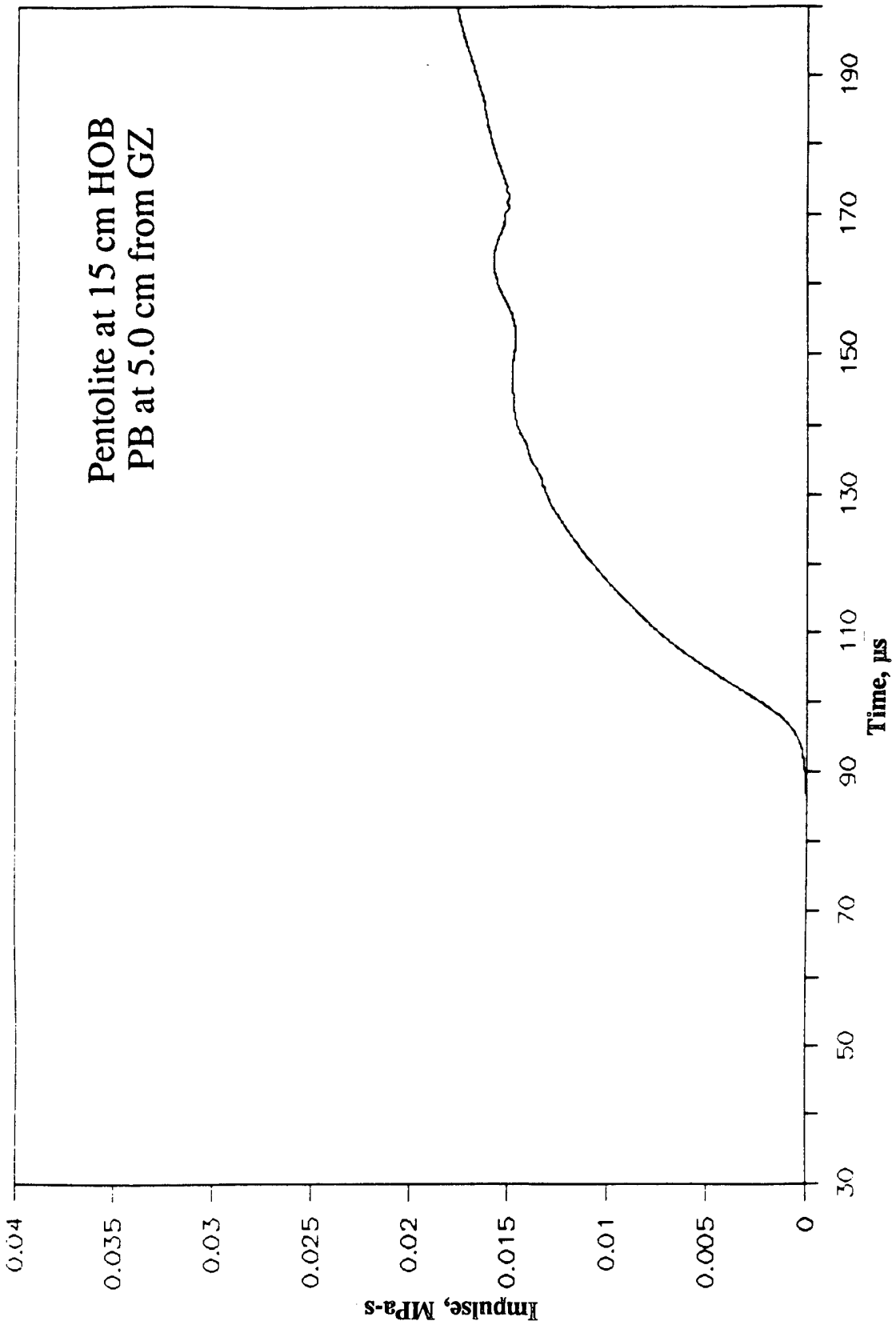


Figure B-30. Impulse-Time Record From Bar Gage PB-7, 5.0 cm From Centerline, Baseplate Test 2A.11, Pentolite at 15-cm HOB.

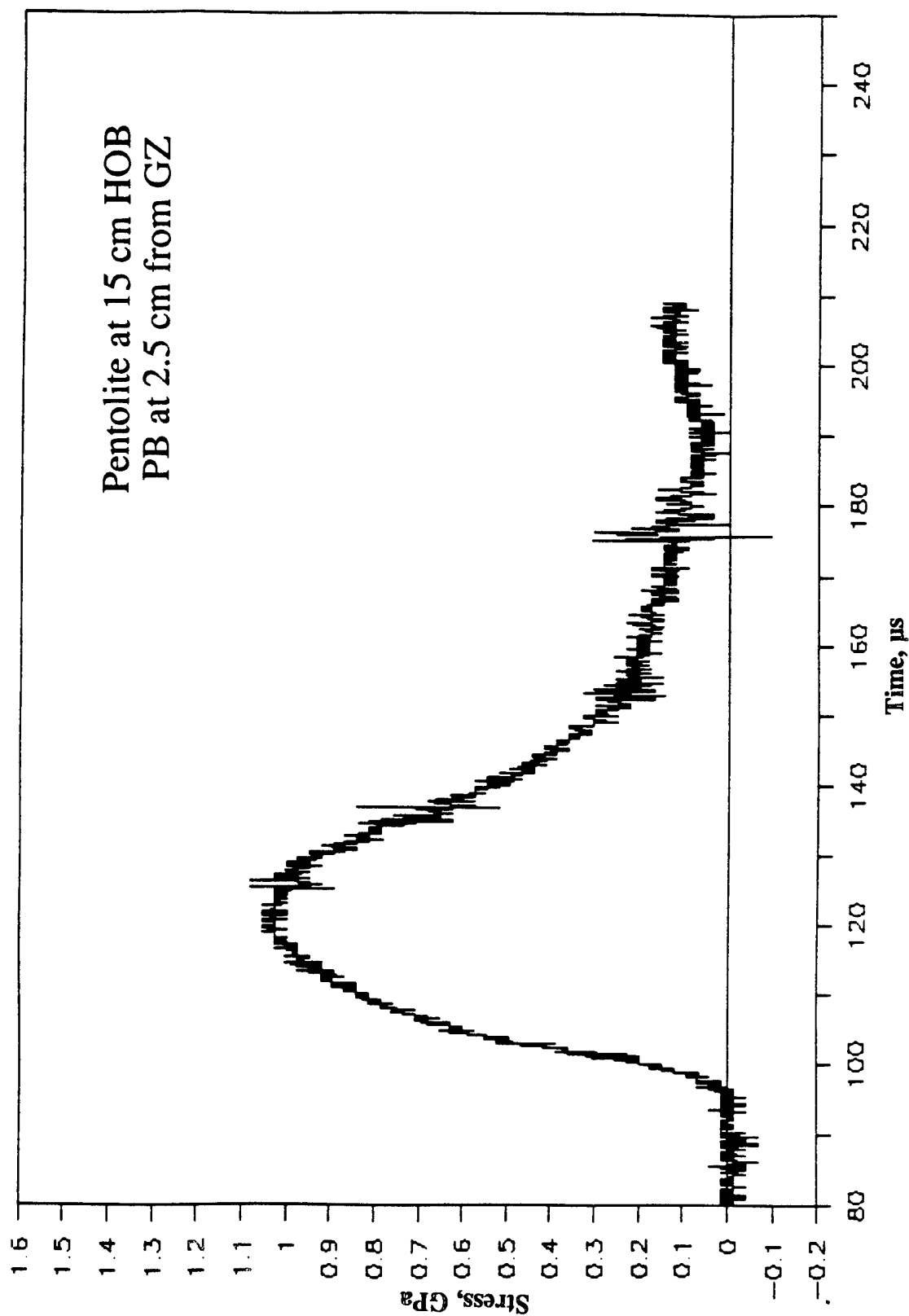


Figure B-31. Stress-Time Record From Bar Gage PB-6, 2.5 cm From Centerline, Baseplate Test 2A.11, Pentolite at 15-cm HOB.

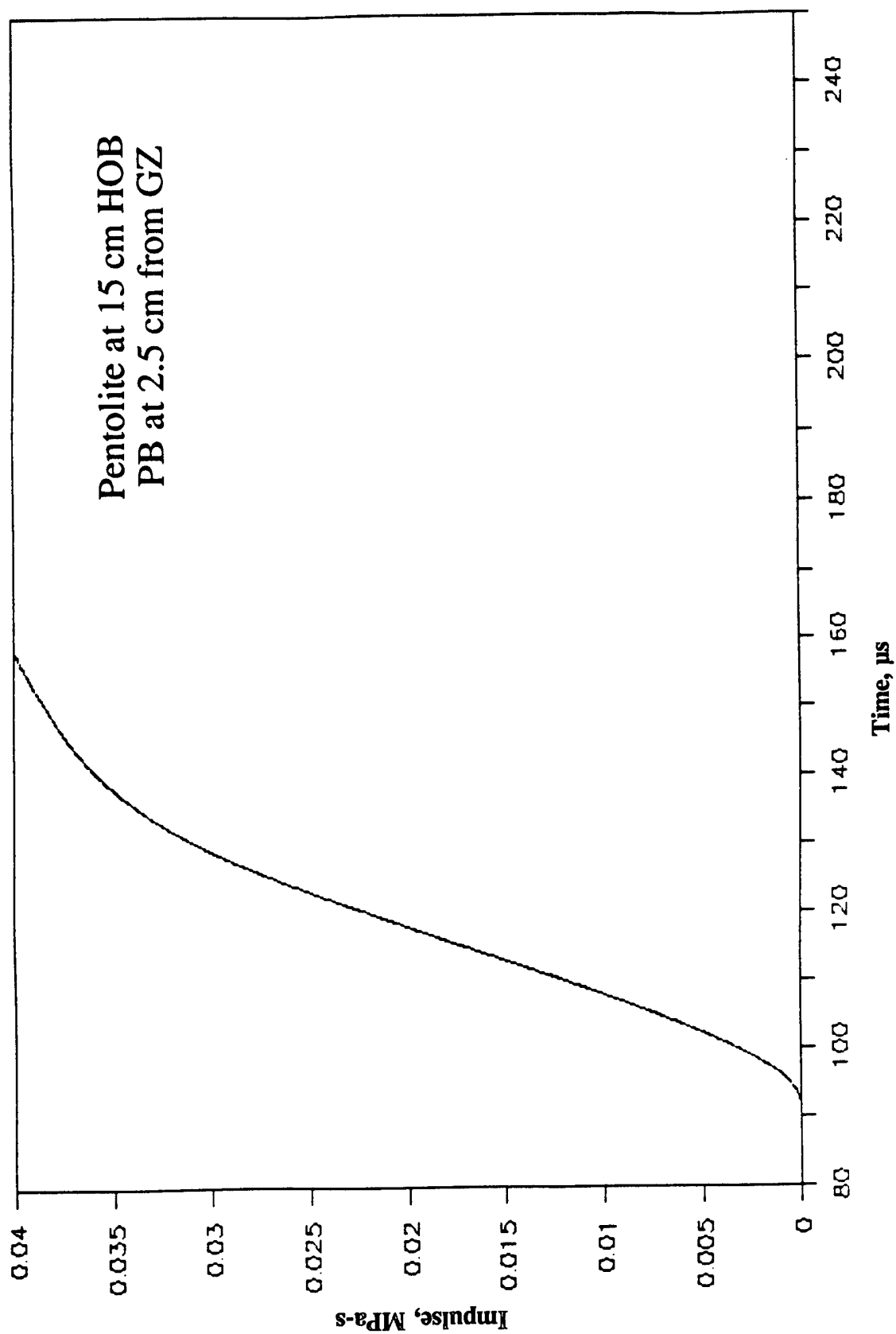


Figure B-32. Impulse-Time Record From Bar Gage PB-6, 2.5 cm From Centerline, Baseplate Test 2A.11, Pentolite at 15-cm HOB.

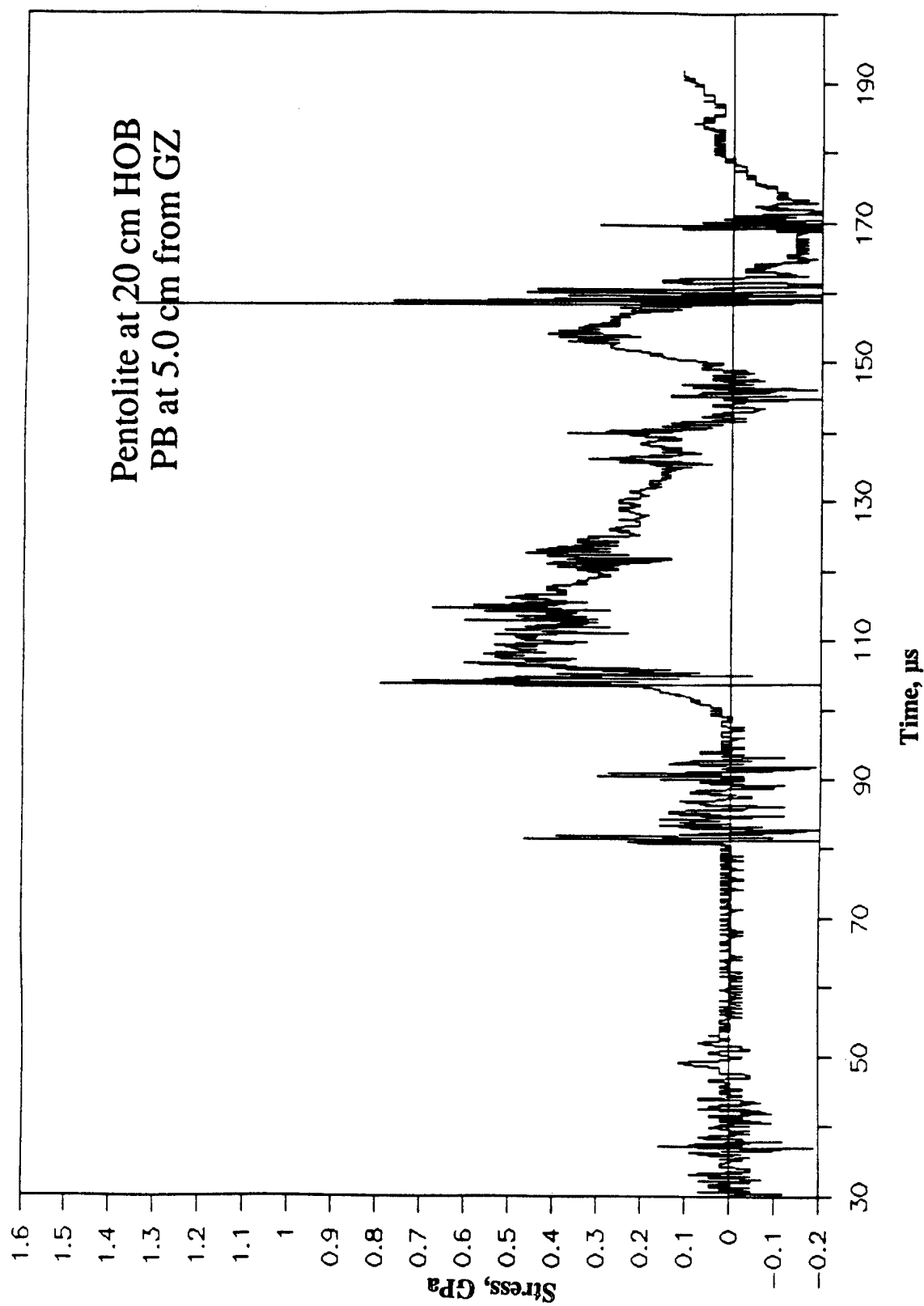


Figure B-33. Stress-Time Record From Bar Gage PB-7, 5.0 cm From Centerline, Baseplate Test 2A.12, Pentolite at 20-cm HOB.

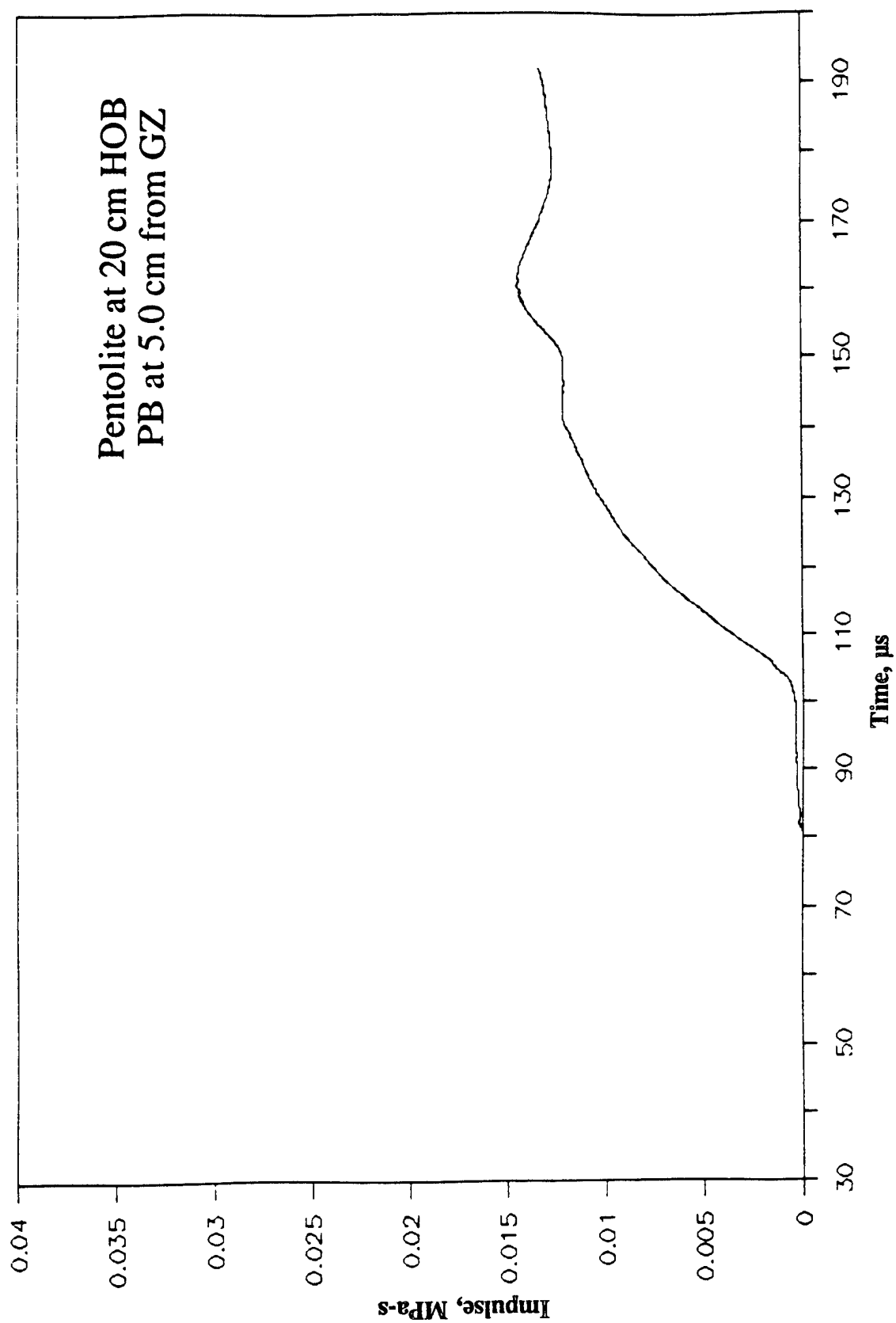


Figure B-34. Impulse-Time Record From Bar Gage PB-7, 5.0 cm From Centerline, Baseplate Test 2A.12, Pentolite at 20-cm HOB.

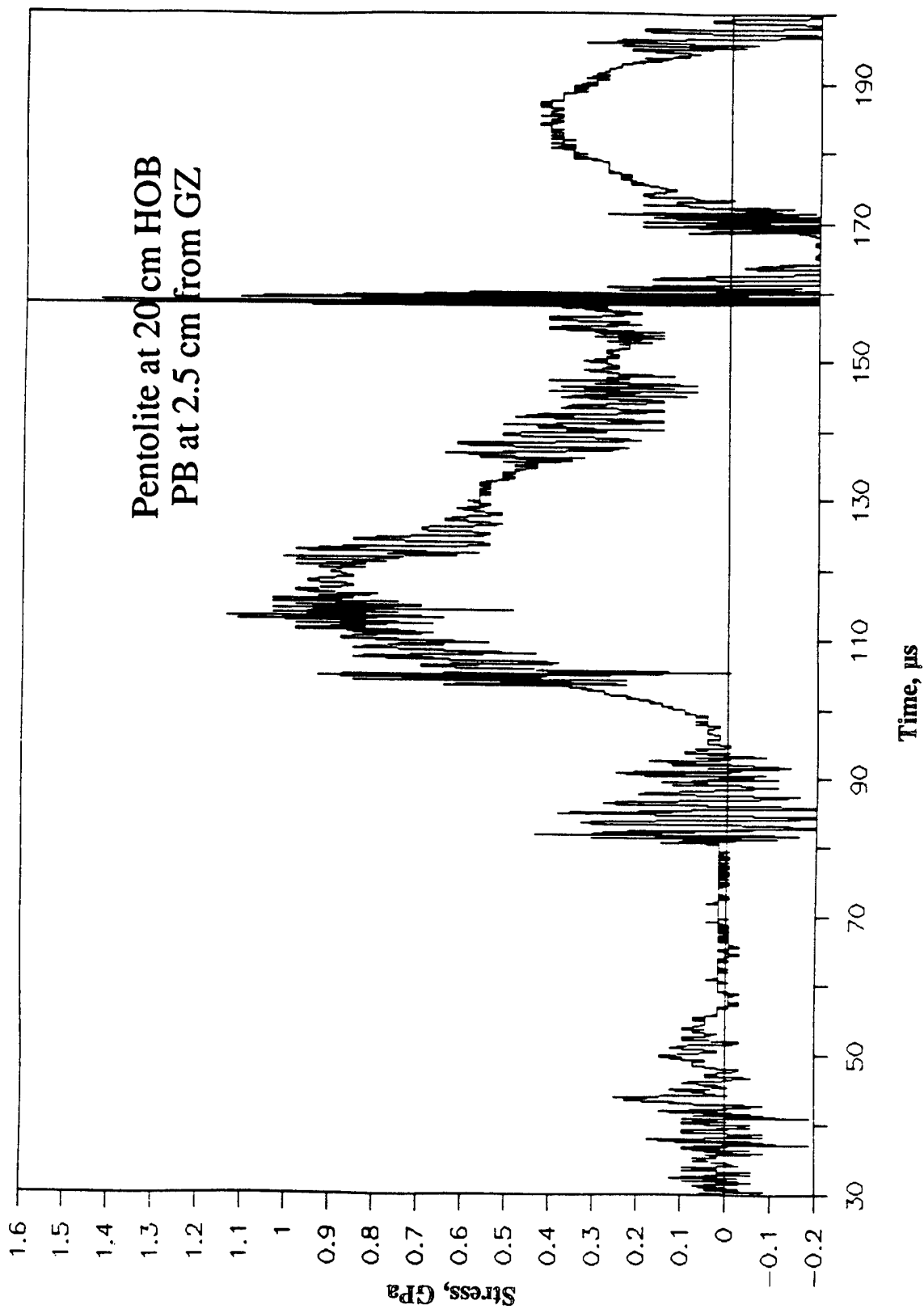


Figure B-35. Stress-Time Record From Bar Gage PB-6, 2.5 cm From Centerline, Baseplate Test 2A.12, Pentolite at 20-cm HOB.

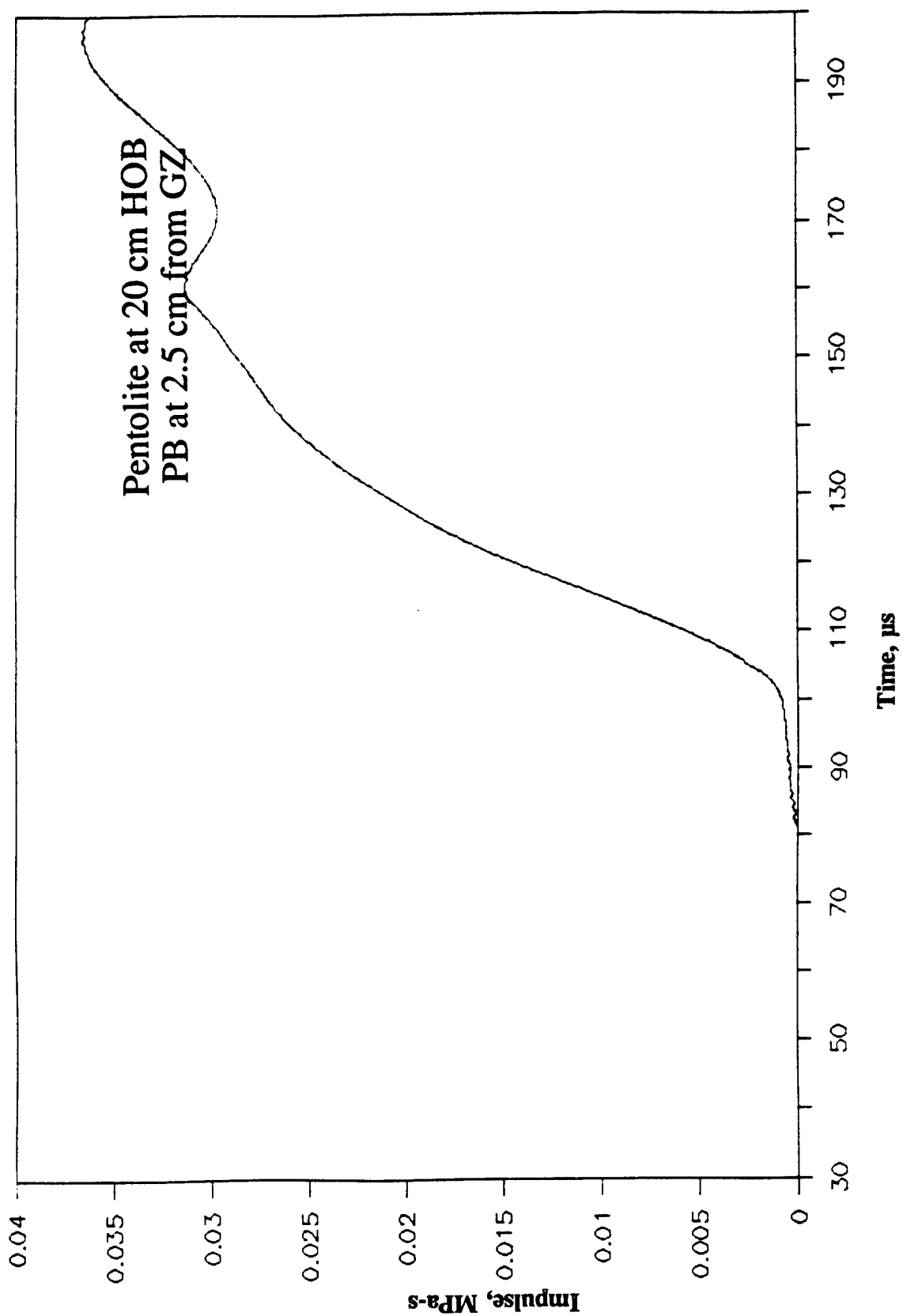


Figure B-36. Impulse-Time Record From Bar Gage PB-6, 2.5 cm From Centerline, Baseplate Test 2A.12, Pentolite at 20-cm HOB.

APPENDIX C:
COMPUTED STRESS HISTORIES
BASEPLATE TESTS 2A.1-2A.12

INTENTIONALLY LEFT BLANK.

Pressures for Close-In Blast
Case 009A, Comp B, 20cm HOB
Base Plate Gage Locations 0, 1, 2, 2.5, 3, 4 cm

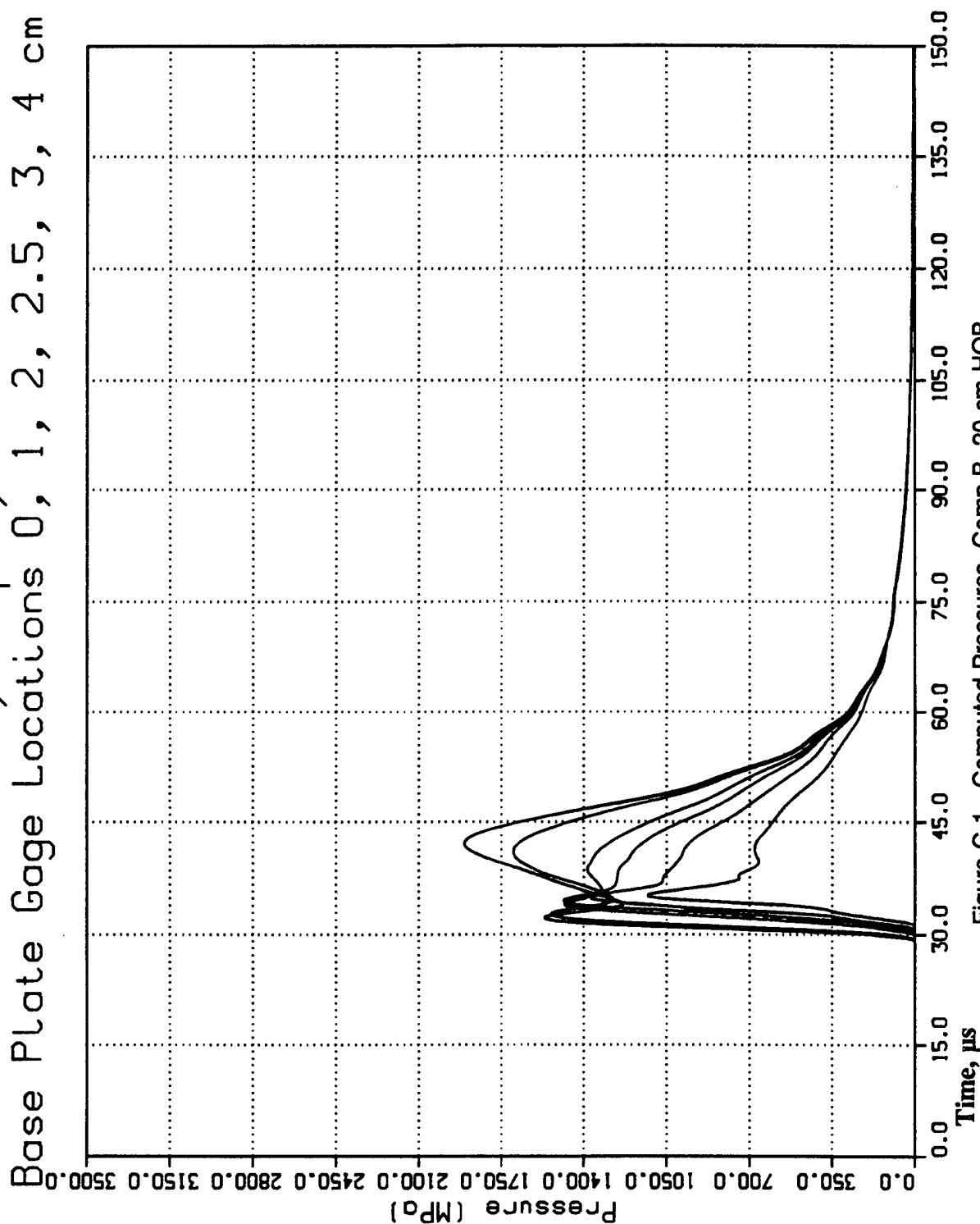


Figure C-1. Computed Pressures, Comp B, 20-cm HOB.

Pressures for Close-In Blast
Case 009A, Comp B, 20cm HOB
Base Plate Gage Locations 5, 6, 7, 10 cm

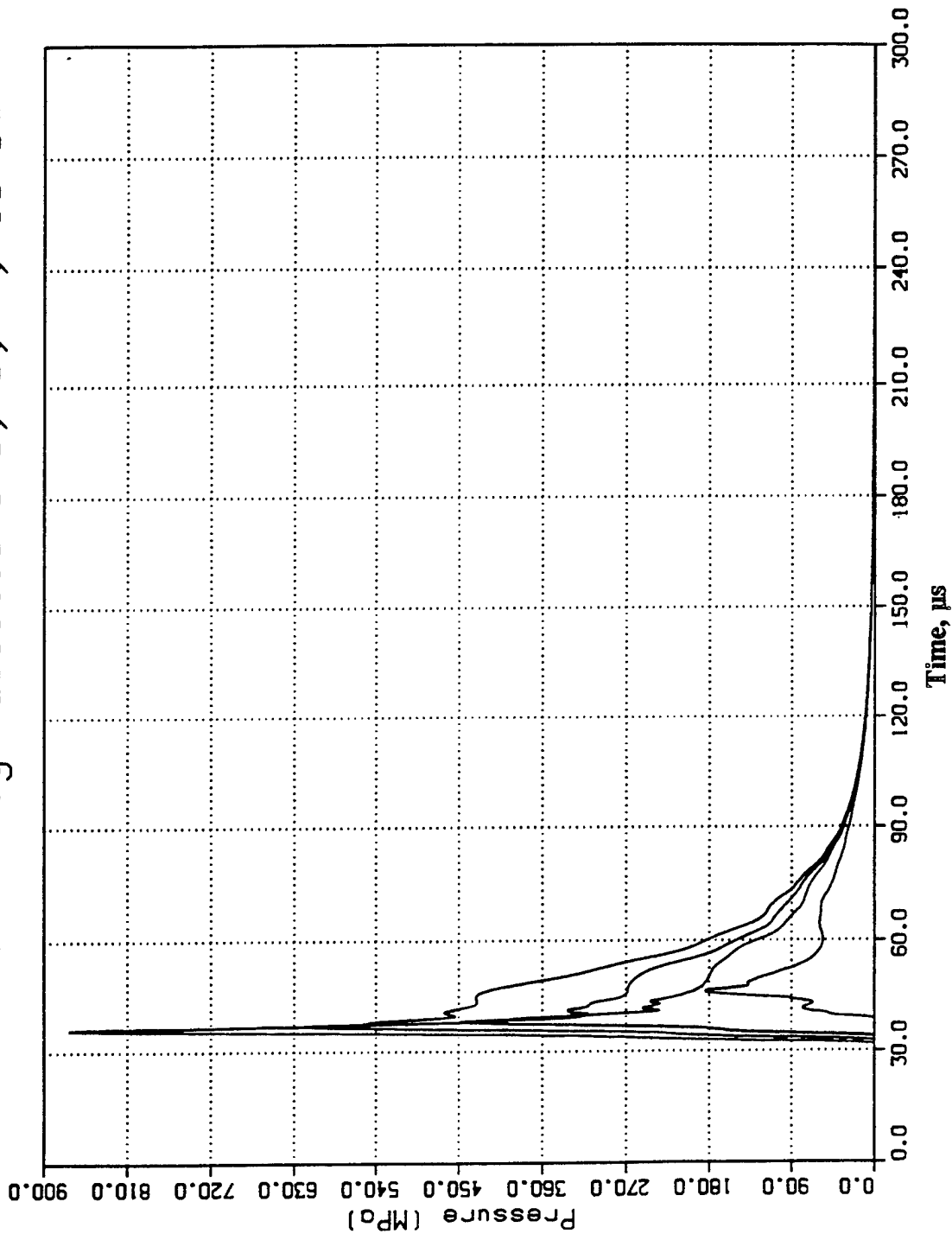


Figure C-2. Computed Pressures, Comp B, 20-cm HOB.

Pressures for Close-In Blast Case 009A, Comp B, 20cm HOB Base Plate Gage Locations 13, 16, 20, 30, 40, 45 cm

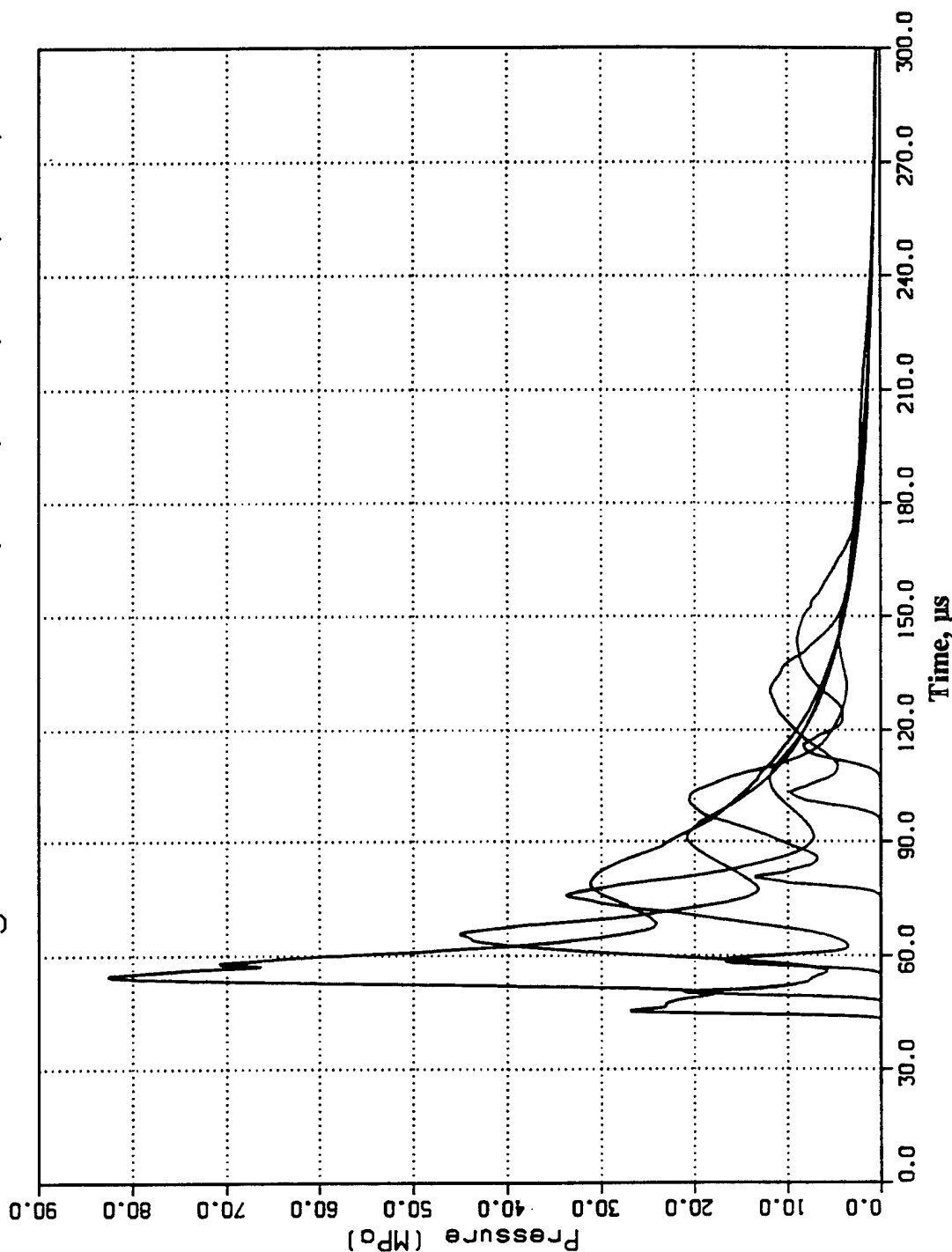


Figure C-3. Computed Pressures, Comp B, 20-cm HOB

Pressures for Close-In Blast
Case 009B, Comp B, 15cm HOB
Base Plate Gage Locations 0, 1, 2, 2.5, 3, 4 cm

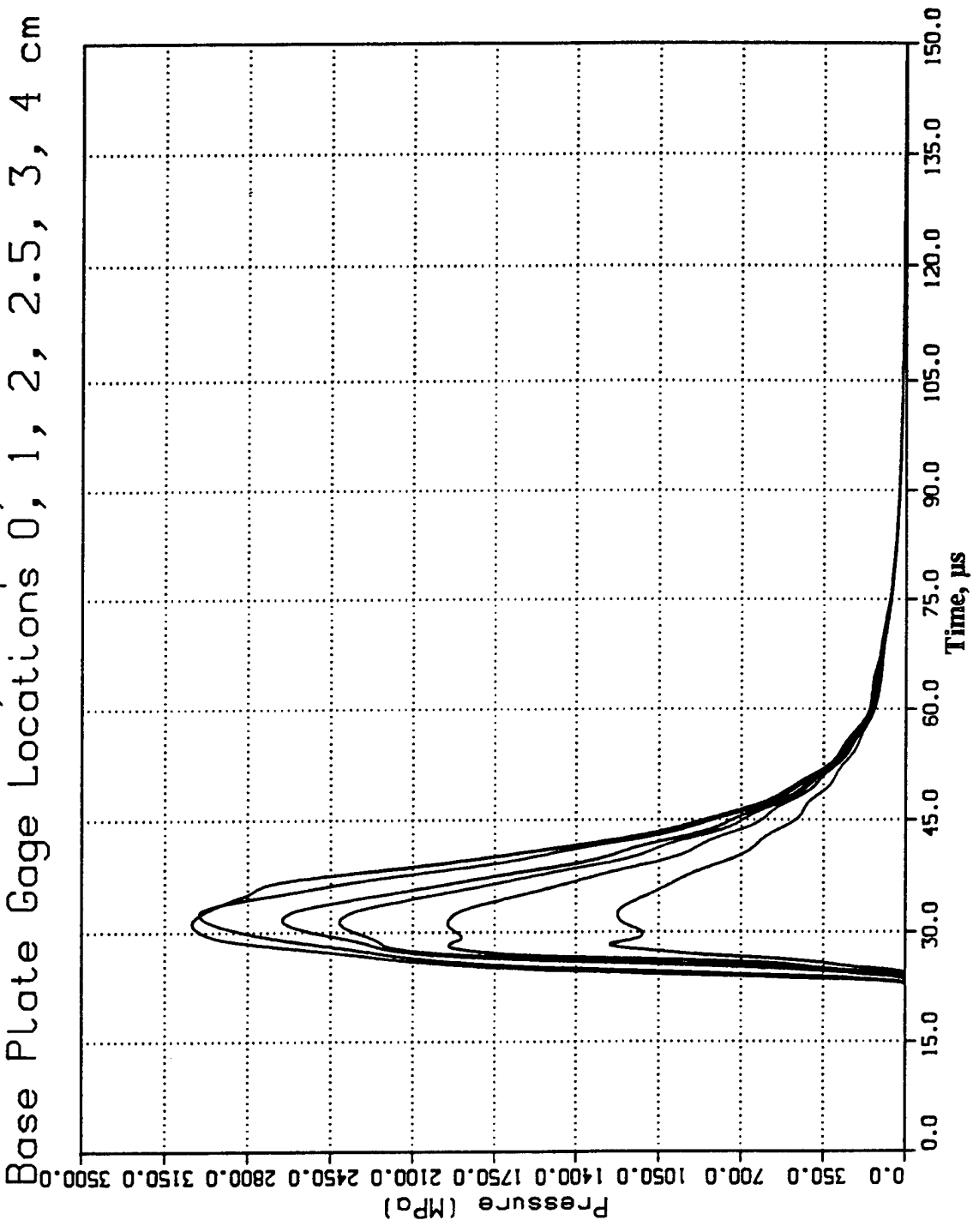


Figure C-4. Computed Pressures, Comp B, 15-cm HOB.

Pressures for Close-In Blast
Case 009B, Comp B, 15cm HOB
Base Plate Gage Locations 5, 6, 7, 10 cm

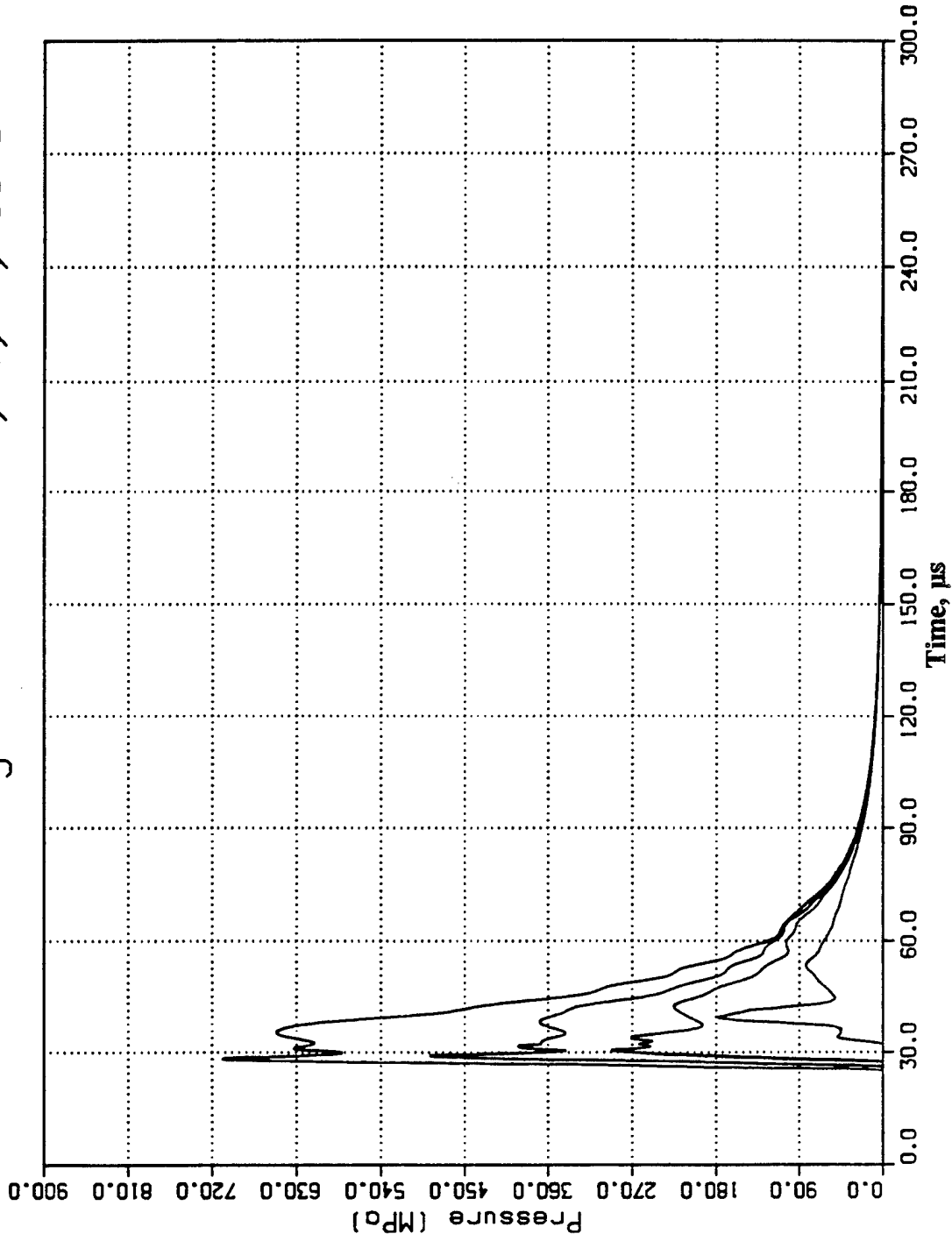


Figure C-5. Computed Pressures, Comp B, 15-cm HOB.

Pressures for Close-In Blast
 Case 009B, Comp B, 15cm HOB
 Base Plate Gage Locations 13, 16, 20, 30, 40, 45 cm

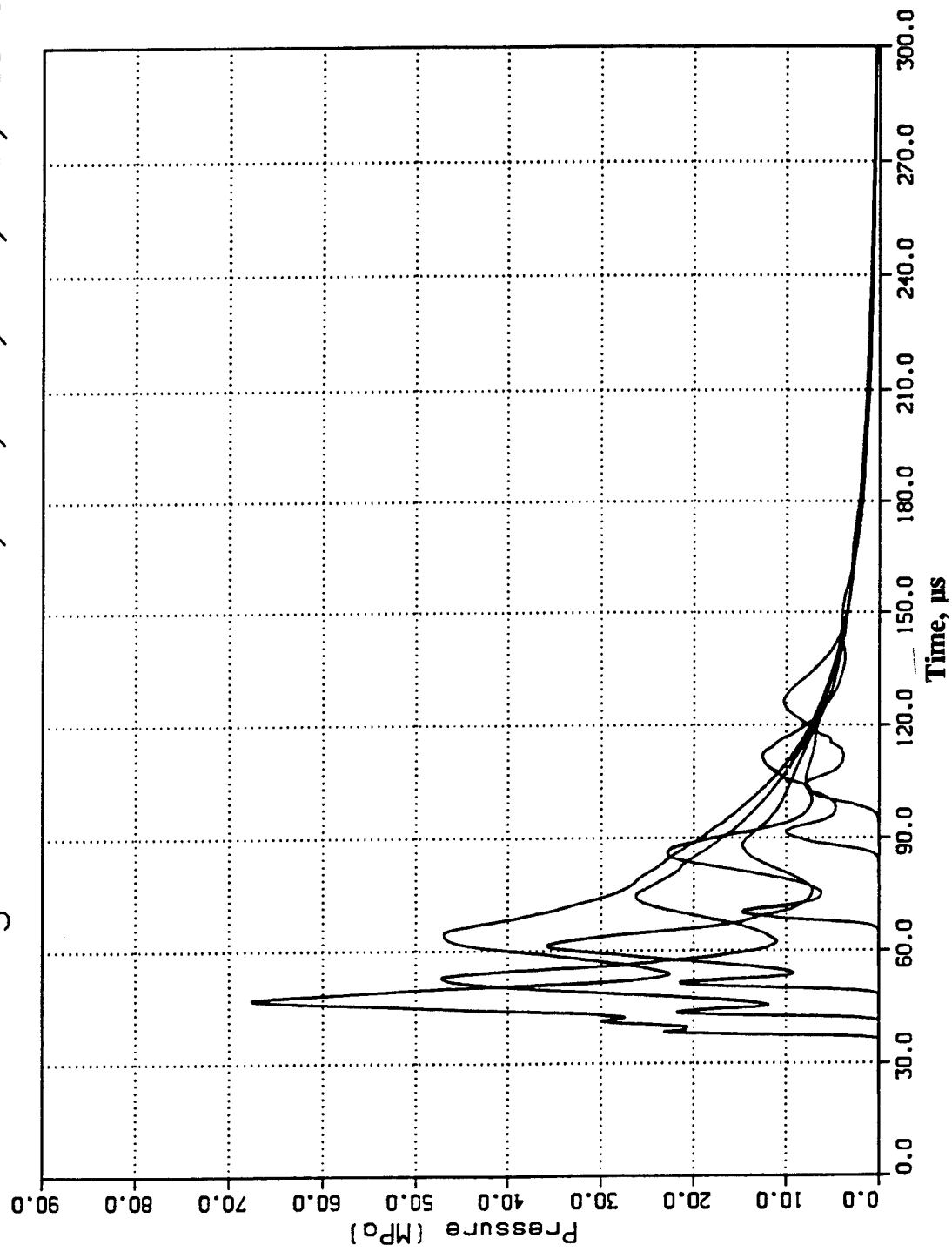


Figure C-6. Computed Pressures, Comp B, 15-cm HOB

Pressures For Close-In Blast
 Case 14A, Pentolite, 15cm HOB
 Base Plate Gage Locations 0, 1, 2, 2.5, 3, 4 cm

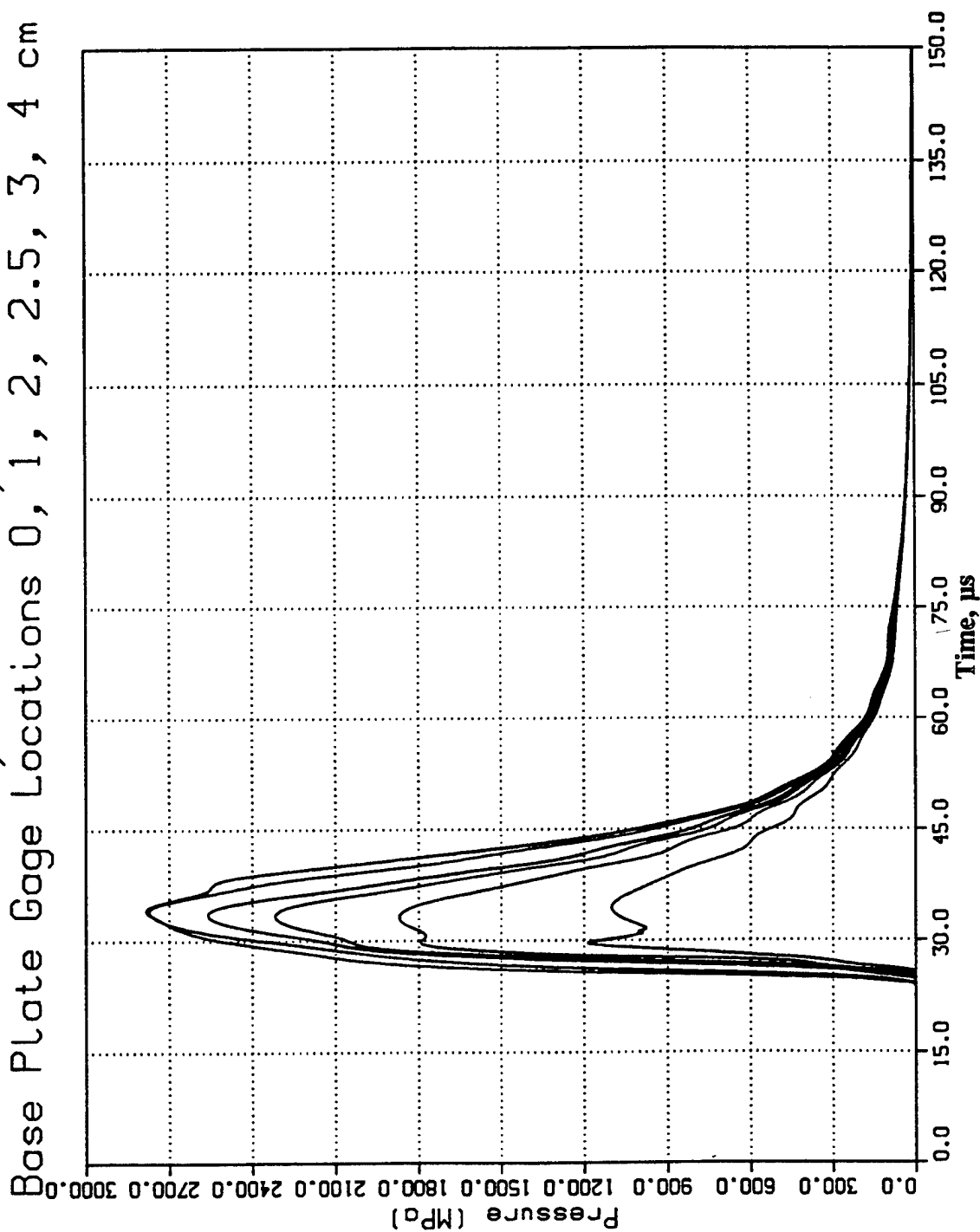


Figure C-7. Computed Pressures, Pentolite, 15-cm HOB.

Pressures For Close-In Blast
Case 14A, Pentolite, 15cm HOB
Base Plate Gage Locations 5, 6, 7, 10 cm

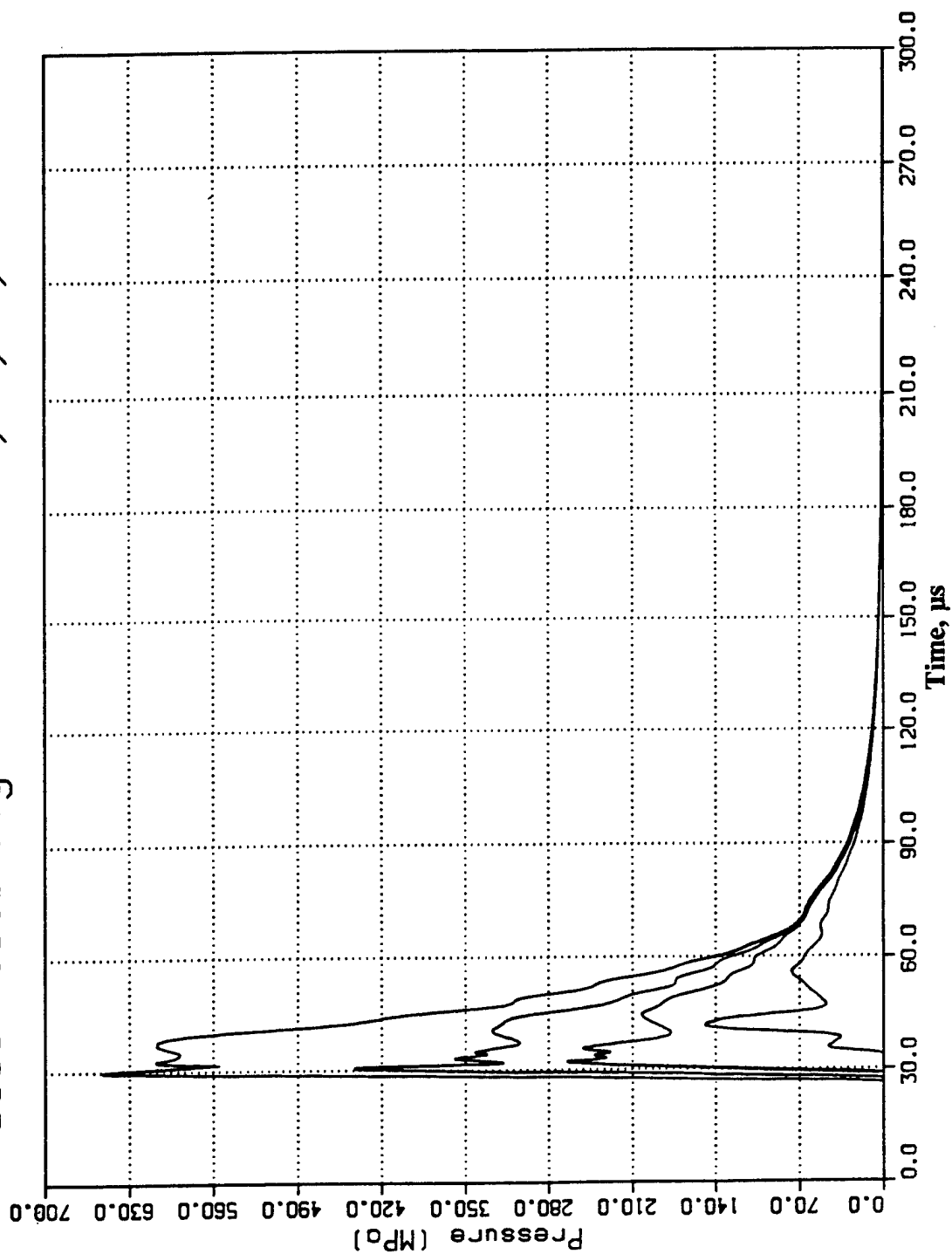


Figure C-8. Computed Pressures, Pentolite, 15-cm HOB.

Pressures For Close-In Blast
 Case 14A, Pentolite, 15cm HOB
 Free Field Gage Locations 25, 35, 45 cm

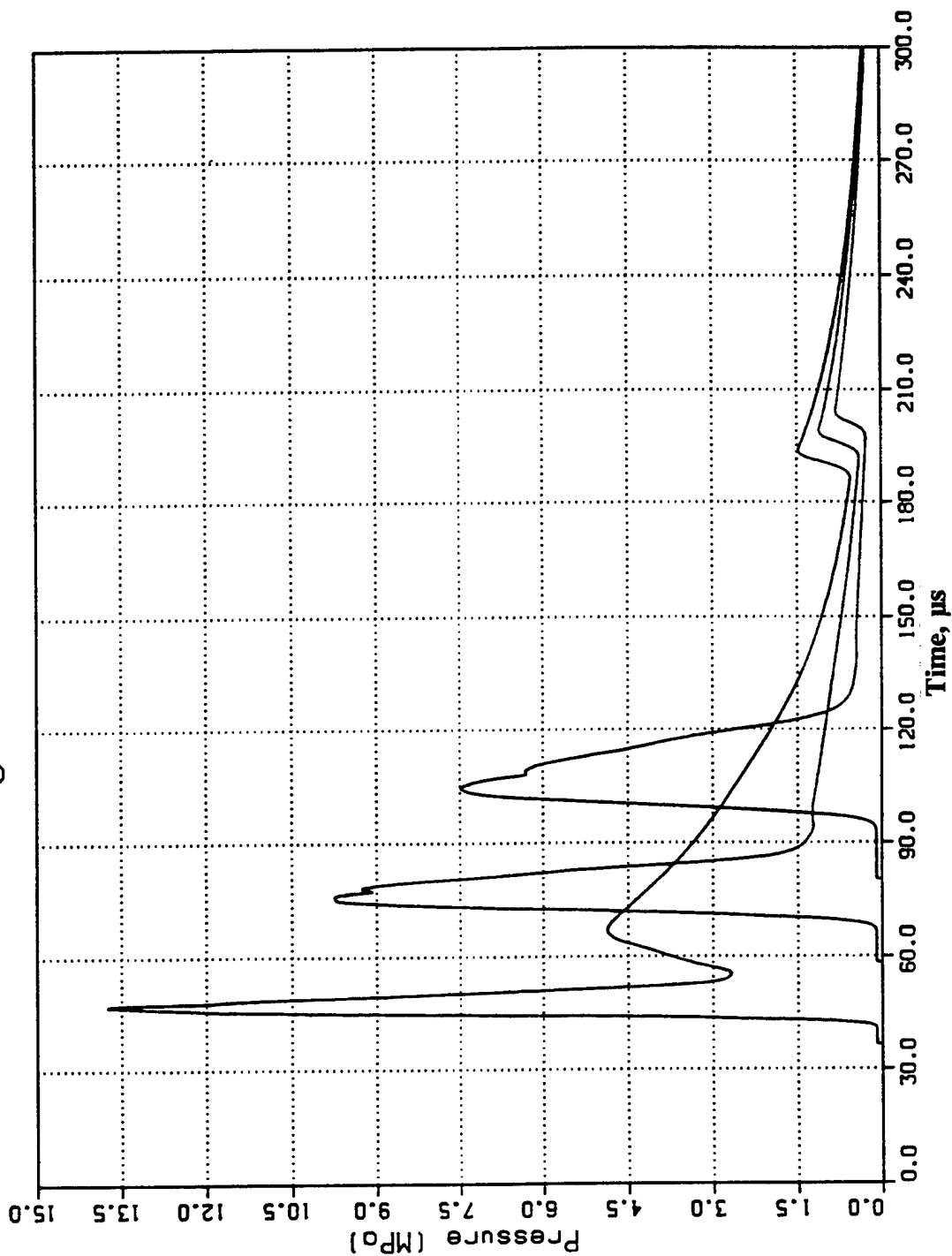


Figure C-9. Computed Pressures, Pentolite, 15-cm HOB.

Pressures For Close-In Blast
 Case 14B, Pentolite, 20cm HOB
 Base Plate Gage Locations 0, 1, 2, 2.5, 3, 4 cm

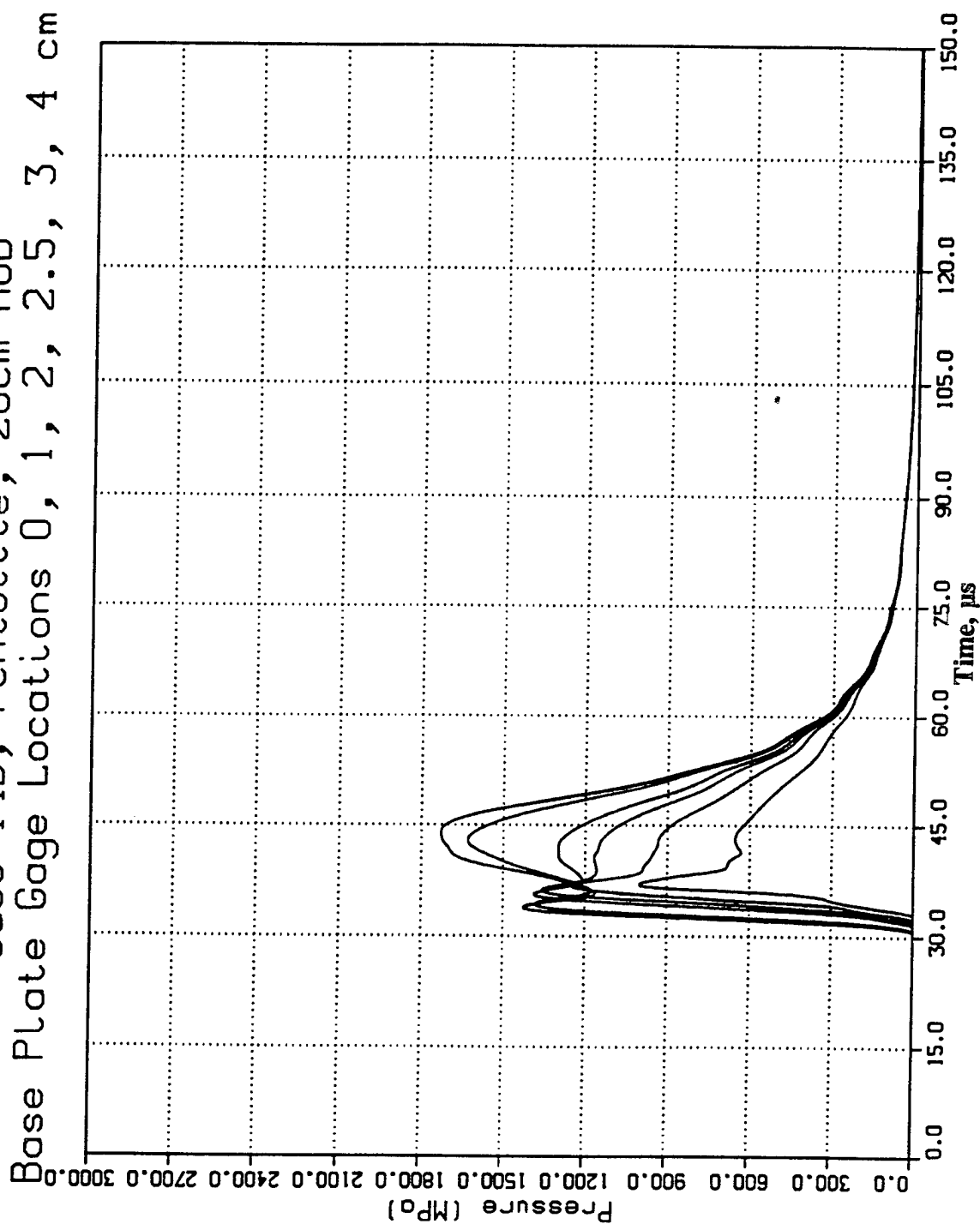


Figure C-10. Computed Pressures, Pentolite, 20-cm HOB.

Pressures For Close-In Blast
Case 14B, Pentolite, 20cm HOB
Base Plate Gage Locations 5, 6, 7, 10 cm

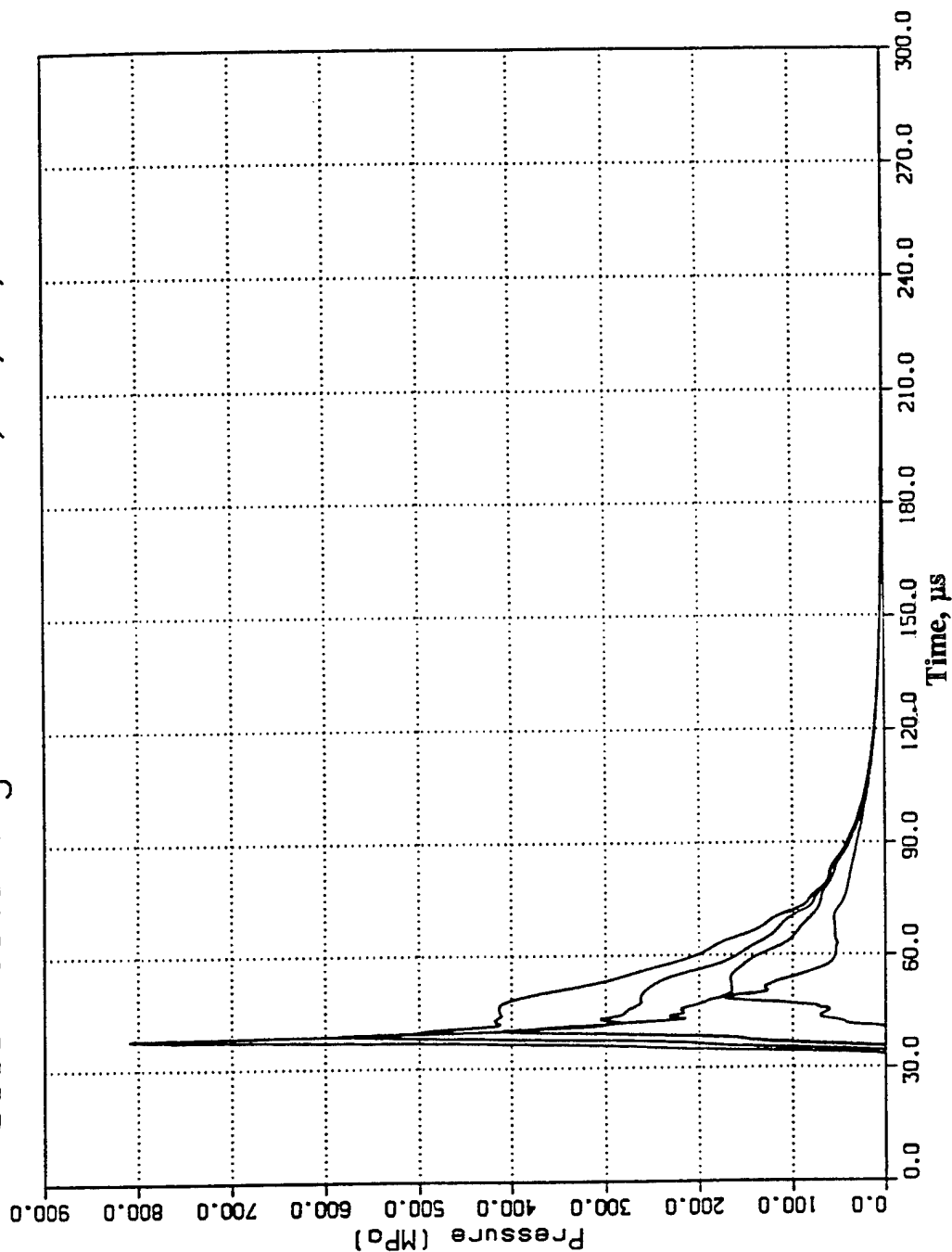


Figure C-11. Computed Pressures, Pentolite, 20-cm HOB.

Pressures For Close-In Blast Case 14B, Pentolite, 20cm HOB Free Field Gage Locations 25, 35, 45 cm

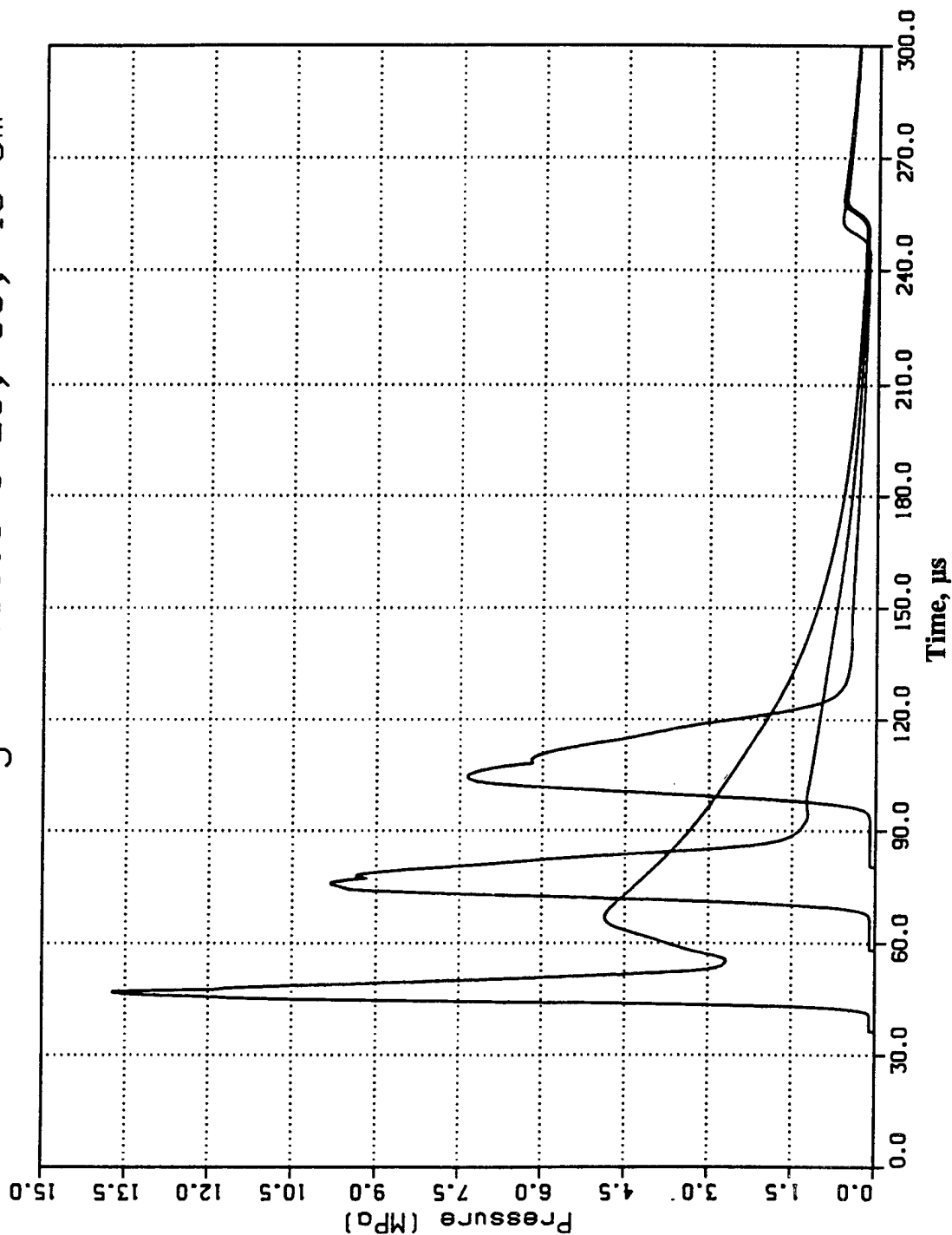


Figure C-12. Computed Pressures, Pentolite, 20-cm HOB.

APPENDIX D:
DATA REDUCTION PROCEDURES
FOR BASEPLATE INSTRUMENTATION

INTENTIONALLY LEFT BLANK.

Appendix D

Data Reduction Procedures for Baseplate Instrumentation

Signals from pressure transducers are first recorded as voltage, then "reduced" to provide stress histories. These stress histories are then integrated to provide specific impulse histories for each gage element (ytterbium or manganin).

Ytterbium and manganin gages are transducers based on the principle of piezoresistivity-- that is, the resistance (or resistivity) of the gage material changes under pressure. That change in resistance creates a change in voltage, which is recorded and compared (or calibrated) to a known change in voltage generated by a precision calibration resistor. The resistance histories are converted to stress using calibration curves obtained from laboratory experimentation.

For these experiments, we used a Wheatstone bridge circuit containing a calibration resistor in series with the gage resistance (Figure D-1). In its balanced state, the calibration resistor was contained in the circuit. After power was supplied to the bridge, the calibration resistor was taken out of the circuit so as to produce a change in voltage attributable to a known change in resistance. This calibration occurs about 2 msec before shock arrival (Figure D-2). For each record obtained, the calibration voltage and resistance were measured and a factor was applied to the recorded voltage to obtain a resistance history. This resistance was divided by the resistance of the gage element to obtain the relative resistance change used to convert to stress.

Ytterbium resistance histories were converted to stress in two parts, loading and unloading. During the loading cycle, the relative resistance changes were converted using the well-documented loading curve given below and plotted in Figure D-3 [11]:

$$\sigma = 1.082[1 - \exp(-2.08 \times dr/R_o)] + 0.9168 \times dR/R_o$$

Here, sigma is stress in gigapascals. This curve was first used by Ginsberg in 1973 [12] and has been refined over the years by Keough and others [11] using results obtained from laboratory gas gun experimentation.

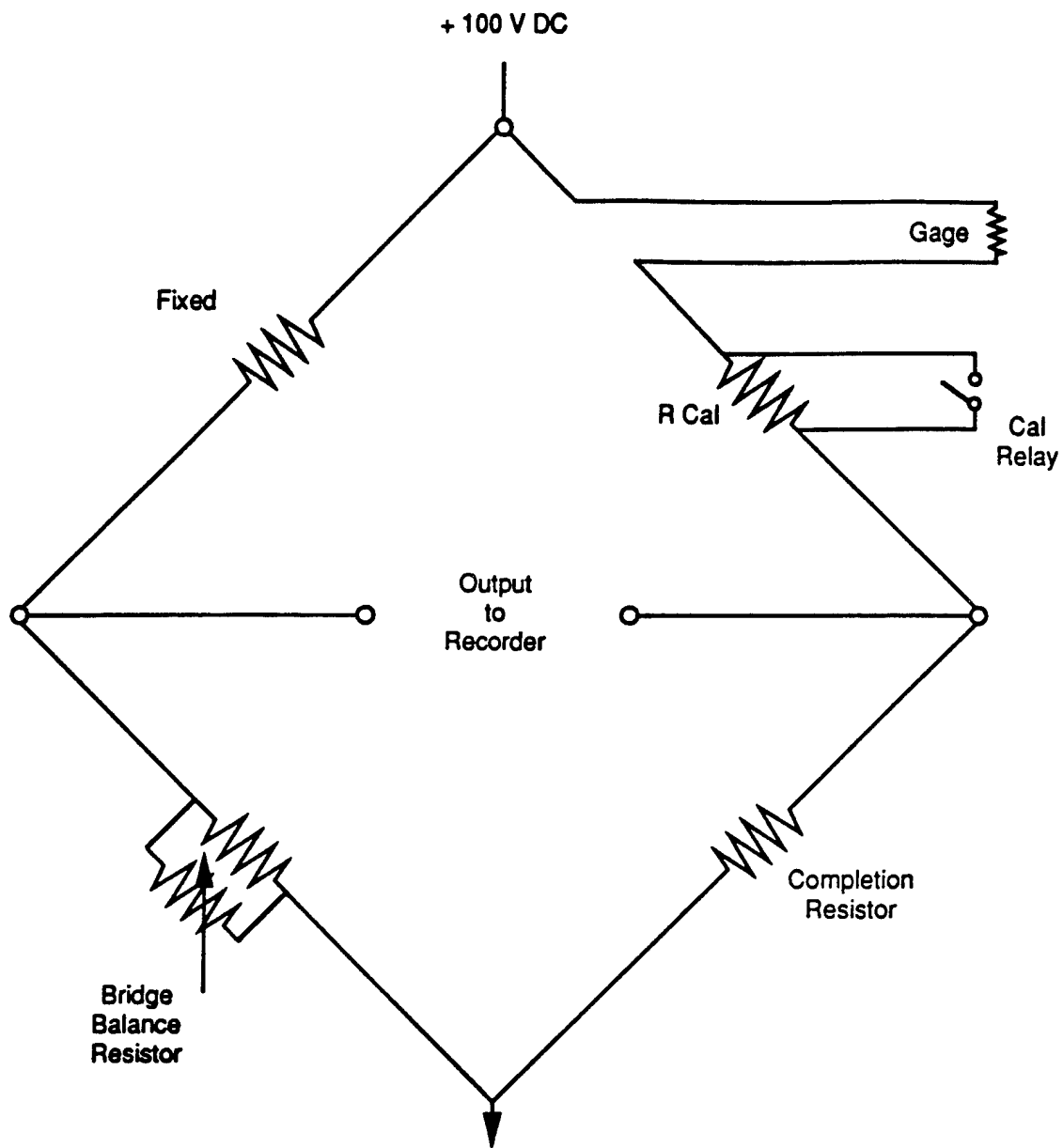


Figure D-1. Wheatstone Bridge Circuitry Used for Piezoresistant Elements.

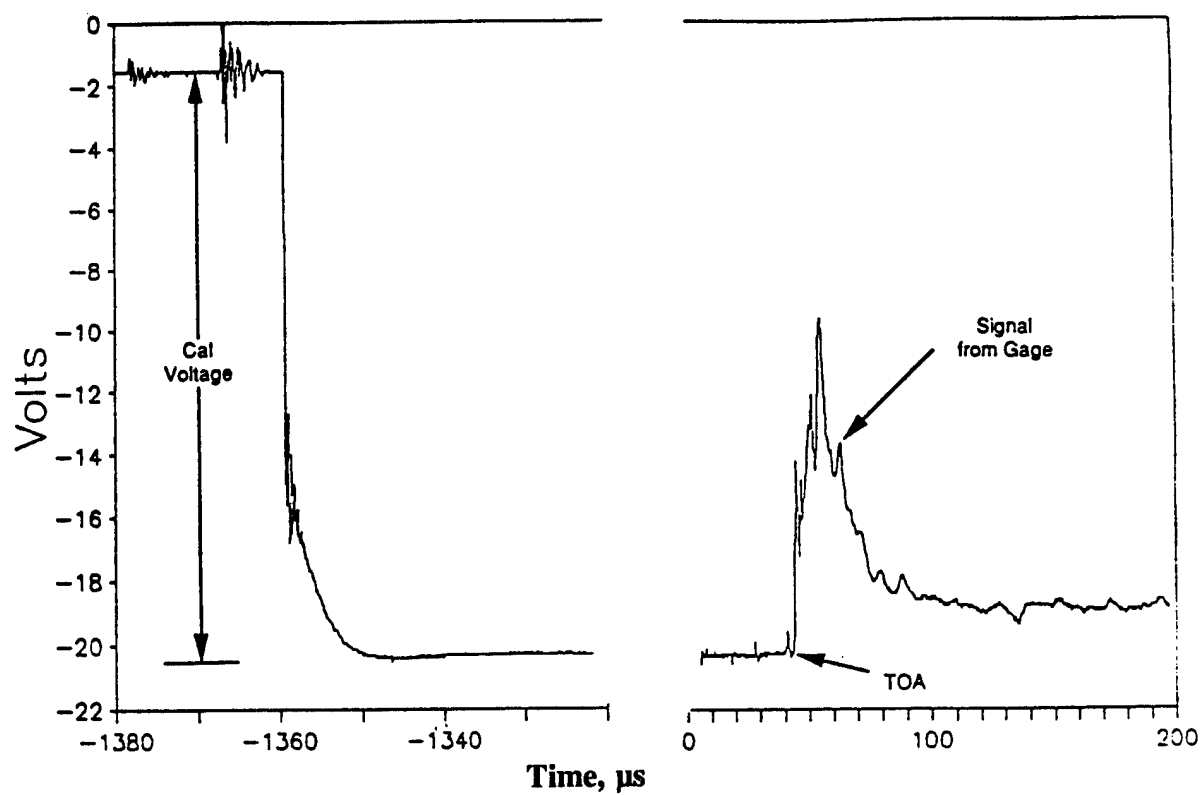


Figure D-2. Typical Long-Term Voltage Trace From Ytterbium Element.

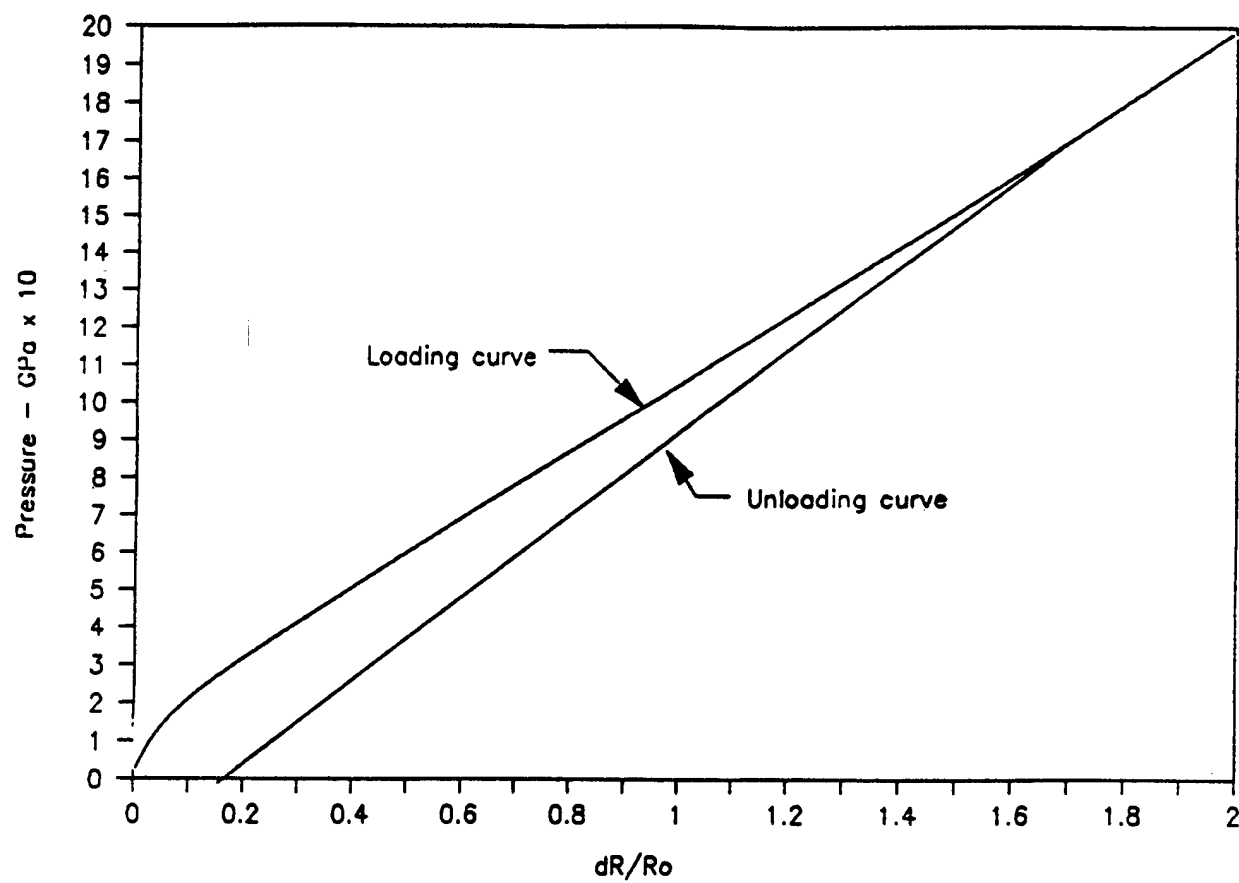


Figure D-3. Typical Loading and Unloading Curves Used for Conversion From dR/R_o to Stress for Ytterbium.

The unloading portion (assumed to be linear) follows the path shown in Figure D-3. The linear equation for unloading is solved using two points: (1) peak resistance and peak stress; and (2) residual resistance and zero stress.

The hysteretic unloading of ytterbium is not well characterized mathematically. Instead, each record must be carefully examined to determine the residual resistance, defined as the zero stress point. Thus, the gage must produce a record long enough for the stress to reach zero. Figure D-4 shows the complete resistance history from an ytterbium gage, along with the selected residual resistance.

Manganin (consisting of 84% copper, 12% manganese and 4% nickel) was first used as a pressure transducer in hydrostatic measurements by Bridgeman in 1911 [13]. It is insensitive to temperature variations, although other materials, such as ytterbium, have a larger piezoresistive coefficient.

In 1964 Bernstein and Keough [14] reported on their development of the manganin stress wave transducer. Since that time, manganin stress transducers have become generally used as in-material gages. Piezoresistance coefficients from 2.0%/GPa up to 2.9%/GPa have been reported. Keough and coworkers measured a coefficient of about 2.9%/GPa in various insulators. From their work it appears that in-material manganin measurements can be made with an accuracy of +/- 3% over the stress range of 2.0 to 20.0 GPa using a linear piezoresistive coefficient of 2.8%/GPa.

The manganin resistance histories obtained in this study were converted to stress by using the following linear loading and unloading curve

$$\sigma = (dR/R_o)/0.029$$

where sigma is stress in gigapascals. Because of the lower sensitivity of manganin, the records produced in this study had low signal-to-noise ratios and were not used after the first four tests.

Test 2A.1

Yb-3

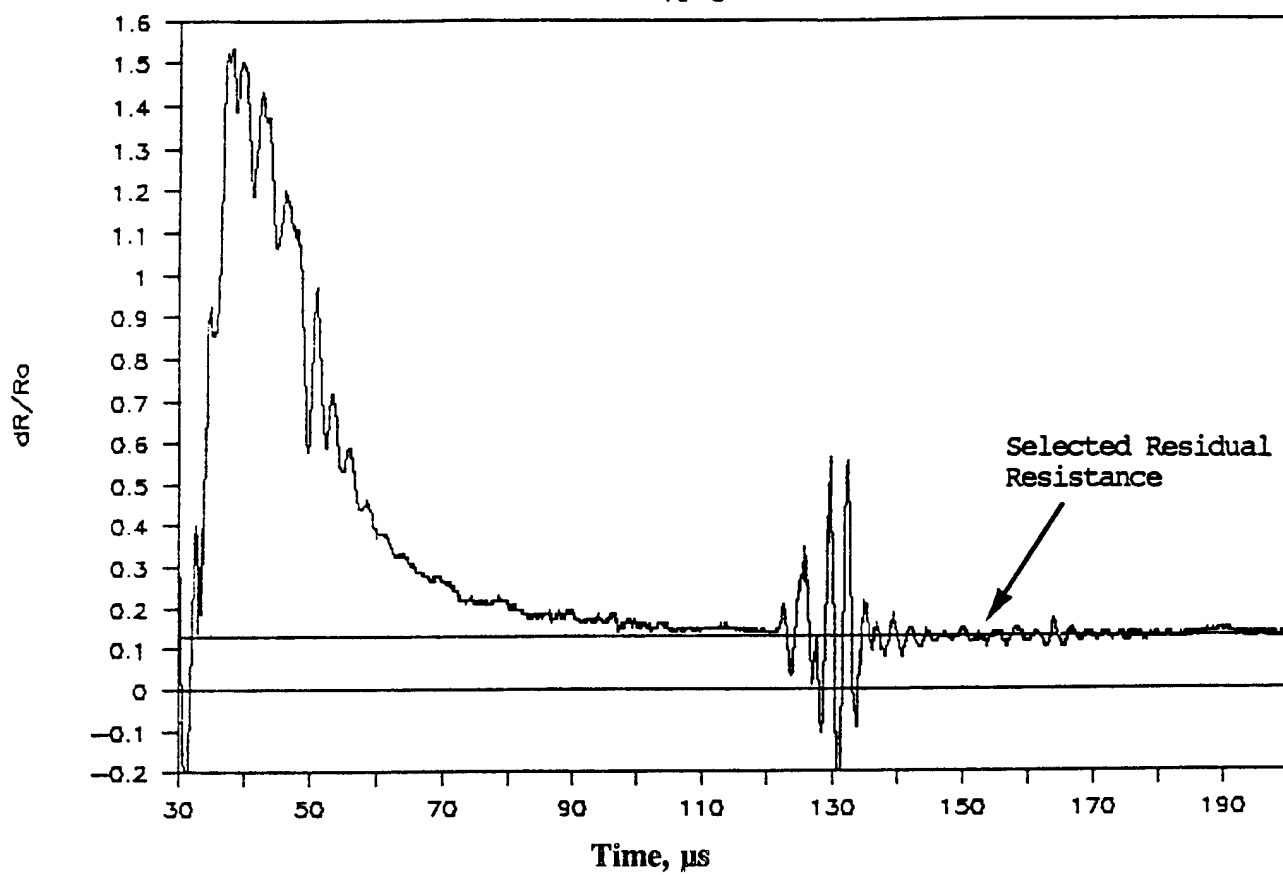


Figure D-4. Typical Ytterbium Resistance History.

<u>NO. OF COPIES</u>	<u>ORGANIZATION</u>
2	DEFENSE TECHNICAL INFO CTR ATTN DTIC DDA 8725 JOHN J KINGMAN RD STE 0944 FT BELVOIR VA 22060-6218

1	DIRECTOR US ARMY RESEARCH LAB ATTN AMSRL OP SD TA 2800 POWDER MILL RD ADELPHI MD 20783-1145
---	---

3	DIRECTOR US ARMY RESEARCH LAB ATTN AMSRL OP SD TL 2800 POWDER MILL RD ADELPHI MD 20783-1145
---	---

1	DIRECTOR US ARMY RESEARCH LAB ATTN AMSRL OP SD TP 2800 POWDER MILL RD ADELPHI MD 20783-1145
---	---

ABERDEEN PROVING GROUND

2	DIR USARL ATTN AMSRL OP AP L (305)
---	---------------------------------------

<u>NO. OF COPIES</u>	<u>ORGANIZATION</u>
2	HQDA ATTN SARD TR MS K KOMINOS DR R CHAIT PENTAGON WASHINGTON DC 20310-0103
2	HQDA ATTN SARD TT DR F MILTON C NASH PENTAGON WASHINGTON DC 20310-0103
2	FED EMERGENCY MGT AGCY ATTN PUBLIC RELATIONS OFC TECH LIB WASHINGTON DC 20472
1	CHAIRMAN DOD EXPLSVS SAFETY BD ROOM 856 C HOFFMAN BLDG 1 2461 EISENHOWER AVENUE ALEXANDRIA VA 22331-0600
1	DIR OF DEFNS RSRCH AND ENGRNG ATTN DD TWP WASHINGTON DC 20301
1	DEFNS INTELLIGENCE AGCY ATTN DT 2 WPNS & SYS DIV WASHINGTON DC 20301
1	ASSIST SECRETARY OF DEFNS ATOMIC ENERGY ATTN DOCUMENT CONTROL WASHINGTON DC 20301
5	DEFNS SPEC WEAPONS AGCY ATTN CSTI TECH LIB ESA W SUMMA E SEIDEN WEP T KENNEDY M FRANKEL 6801 TELEGRAPH RD ALEXANDRIA VA 22310-3398
1	CHAIRMAN JOINT CHIEFS OF STAFF ATTN J5 R&D DIVISION WASHINGTON DC 20301

<u>NO. OF COPIES</u>	<u>ORGANIZATION</u>
2	DA DCSOPS ATTN TECH LIB DIR OF CHEM & NUC OPS WASHINGTON DC 20310
4	COMMANDER FIELD COMMAND DSWA ATTN FCTTIS E L MARTINEZ FCTOSL F MOYNIHAN FCTIH H ROSS FCTIH W BRENNAN KIRTLAND AFB NM 87115
1	US ARMY RSRCH DEVELOPMENT & STANDARDIZATION GRP UK ATTN ROY E REICHENBACH PSC 802 BOX 15 FPO AE 09499-1500
10	CENTRAL INTEL AGENCY DIR DB STANDARD ATTN GE 47 HQ WASHINGTON DC 20505
1	DIRECTOR DARPA ATTN TECH LIB 3701 NORTH FAIRFAX DR ARLINGTON VA 22203-1714
2	COMMANDER US ARMY NRDEC ATTN AMSNA D D SIELING STRNC UE J CALLIGEROS NATICK MA 01762
2	COMMANDER US ARMY CECOM ATTN AMSEL RD AMSEL RO TPPO P FT MONMOUTH NJ 07703-5301
1	COMMANDER US ARMY CECOM R&D TECH LIB ATTN ASQNC ELC IS L R MYER CTR FT MONMOUTH NJ 07703-5000
1	MIT ATTN TECH LIB CAMBRIDGE MA 02139

NO. OF
COPIES ORGANIZATION

1 COMMANDER
US ARMY NGIC
ATTN RSRCH & DATA BR
220 7TH STREET NE
CHARLOTTESVILLE VA
22901-5396

1 COMMANDER
US ARMY ARDEC
ATTN AMSTA AR FSM W
MR BARBER BLDG 94
PICATINNY ARSENAL NJ
07806-5000

1 US ARMY TRAC FT LEE
ATTN ATRC L MR CAMERON
FORT LEE VA 23801-6140

1 US ARMY MISSILE & SPACE
INTELLIGENCE CTR
ATTN AIAMS YDL
REDSTONE ARSENAL AL
35898-5500

1 COMDG OFFICER CODE L51
NAVAL CIVIL ENGRNG LAB
ATTN J TANCRETO
PORT HUENEME CA 93043-5003

2 COMMANDER
US ARMY STRTGC DEFNS CMD
ATTN CSSD H MPL TECH LIB
CSSD H XM DR DAVIES
PO BOX 1500
HUNTSVILLE AL 35807

2 COMMANDER
US ARMY CORPS OF ENGNRS
WATERWAYS EXPRMNT STATION
ATTN CEWES SS R J WATT
CEWES TL TECH LIB
PO BOX 631
VICKSBURG MS 39180-0631

1 COMMANDER
US ARMY ENGINEER DIVISION
ATTN HNDED FD
PO BOX 1500
HUNTSVILLE AL 35807

NO. OF
COPIES ORGANIZATION

3 COMMANDER
US ARMY NUC & CHEML AGCY
7150 HELLER LOOP STE 101
SPRINGFIELD VA 22150-3198

1 COMMANDER
US ARMY CORPS OF ENGNRS
FT WORTH DISTRICT
ATTN CESWF PM J
PO BOX 17300
FT WORTH TX 76102-0300

1 TRAC FLVN
ATTN ATRC
FT LEAVENWORTH KS
66027-5200

1 COMMANDER
US ARMY RSRCH OFFICE
ATTN SLCRO D
PO BOX 12211
RSRCH TRIANGLE PARK NC
27709-2211

1 HQ TRAC RPD
ATTN ATRC RPR RADDA
FT MONROE VA 23651-5143

2 OFFICE OF NAVAL RSRCH
ATTN DR A FAULSTICK CODE 23
800 N QUINCY STREET
ARLINGTON VA 22217

1 TRAC WSMR
ATTN ATRC WC KIRBY
WSMR NM 88002-5502

2 COMMANDER
US ARMY WSMR
ATTN STEWS NED DR MEASON
STEWES DATTS O R L PENNY
WSMR NM 88002-5158

2 CHIEF OF NAVAL OPS
DEPARTMENT OF THE NAVY
ATTN OP 03EG
OP 985F
WASHINGTON DC 20350

<u>NO. OF COPIES</u>	<u>ORGANIZATION</u>
1	COMMANDER DAVID TAYLOR RSRCH CTR ATTN CODE 522 TECH INFO CTR BETHESDA MD 20084-5000
1	OFFCR IN CHARGE CODE L31 CIVIL ENGRNG LAB NAVAL CNSTRCTN BATTLN CTR ATTN TECH LIB PORT HUENEME CA 93041
1	COMMANDING OFFICER WHITE OAK WARFARE CTR ATTN CODE WA501 NNPO SILVER SPRING MD 20902-5000
1	COMMANDER CODE 533 NAVAL WEAPONS CTR ATTN TECH LIB CHINA LAKE CA 93555-6001
1	COMMANDER DAHLGREN DIVISION NAVAL SURFACE WARFARE CTR ATTN CODE E23 LIB DAHLGREN VA 22448-5000
1	COMMANDER NAVAL RSRCH LAB ATTN CODE 2027 TECH LIB WASHINGTON DC 20375
1	OFFICER IN CHARGE WHITE OAK WARFARE CTR DETACHMENT ATTN CODE E232 TECH LIB 10901 NEW HAMPSHIRE AVE SILVER SPRING MD 20903-5000
1	AL LSCF ATTN J LEVINE EDWARDS AFB CA 93523-5000
1	COMMANDER NAVAL WPNS EVALUATION FAC ATTN DOCUMENT CONTROL KIRTLAND AFB NM 87117

<u>NO. OF COPIES</u>	<u>ORGANIZATION</u>
2	COMMANDER US ARMY NRDEC ATTN SSCNC YSD J ROACH SSCNC WST A MURPHY KANSAS ST NATICK MA 10760-5018
1	RADC EMTLD DOCUMENT LIB GRIFFISS AFB NY 13441
1	AEDC ATTN R MCAMIS MAIL STOP 980 ARNOLD AFB TN 37389
1	OLAC PL TSTL ATTN D SHIPLETT EDWARDS AFB CA 93523-5000
1	AFIT ENY ATTN LTC HASEN PHD WP AFB OH 45433-6583
2	AIR FORCE ARMAMENT LAB ATTN AFATL DOIL AFATL DLYV EGLIN AFB FL 32542-5000
1	IDAHO NATL ENGRNG LAB ATTN SPEC PRGMS J PATTON 2151 NORTH BLVD MS 2802 IDAHO FALLS ID 83415
3	PHILLIPS LAB AFWL ATTN NTE NTED NTES KIRTLAND AFB NM 87117-6008
1	LAWRENCE LIVERMORE NATL LAB ATTN TECH INFO DEPT L 3 PO BOX 808 LIVERMORE CA 94550
1	AFIT ATTN TECH LIB BLDG 640 B WP AFB OH 45433

<u>NO. OF COPIES</u>	<u>ORGANIZATION</u>
1	NASA ATTN SCI & TECH INFO FAC PO BOX 8757 BWI AIRPORT BALTIMORE MD 21240
1	FTD NIIS WP AFB OH 45433
3	KAMAN SCIENCES CORP ATTN LIB P A ELLIS F H SHELTON PO BOX 7463 COLORADO SPRINGS CO 80933-7463
4	IDAHO NATL ENGRNG LAB EG&G IDAHO INC ATTN R GUENZLER MS 3505 R HOLMAN MS 3510 R A BERRY W C REED PO BOX 1625 IDAHO FALLS ID 83415
3	SANDIA NATL LABS ATTN DOC CONTROL 3141 D GARDNER DIV 1421 J MCGLAUN DIV 1541 PO BOX 5800 ALBUQUERQUE NM 87185-5800
1	LOS ALAMOS NATL LAB REPORT COLLECTION RESEARCH LIB MS P362 PO BOX 7113 LOS ALAMOS NM 87544-7113
1	SANDIA NATL LABS LIVERMORE LAB ATTN DOC CNTRL FOR TECH LIB PO BOX 969 LIVERMORE CA 94550
1	NASA AMES RSRCH CTR APPLIED COMPTNL AERO BR ATTN DR T HOLTZ MS 202 14 MOFFETT FIELD CA 94035

<u>NO. OF COPIES</u>	<u>ORGANIZATION</u>
1	NASA LANGLEY RSRCH CTR ATTN TECH LIB HAMPTON VA 23665
2	APPLIED RSRCH ASSOC INC ATTN J KEEFER N H ETHRIDGE PO BOX 548 ABERDEEN MD 21001
4	APPLIED RSRCH ASSOC INC ATTN C NEEDHAM J CREPEAU S HIKIKA R NEWELL 4300 SAN MATEO BLVD ALBUQUERQUE NM 87110
1	ADA TECHNOLOGIES INC ATTN JAMES R BUTZ HONEYWELL CTR STE 110 304 INVERNESS WAY SOUTH ENGLEWOOD CO 80112
1	CARPENTER RSRCH CORP ATTN H JERRY CARPENTER 27520 HAWTHORNE BLVD SUITE 263 ROLLING HILLS ESTATES CA 90274
1	AEROSPACE CORP ATTN TECH INFO SERVICES PO BOX 92957 LOS ANGELES CA 90009
1	THE BOEING COMPANY ATTN AEROSPACE LIB PO BOX 3707 SEATTLE WA 98124
2	FMC CORP ADVANCED SYSTEMS CTR ATTN J DROTLEFF C KREBS MDP 95 BOX 58123 2890 DE LA CRUZ BLVD SANTA CLARA CA 95052

<u>NO. OF COPIES</u>	<u>ORGANIZATION</u>
1	SVERDRUP TECHNOLOGY INC SVERDRUP CORP AEDC ATTN BD HEIKKINEN MS 900 ARNOLD AFB TN 37389-9998
2	DYNAMICS TECHNOLOGY INC ATTN D T HOVE G P MASON 21311 HAWTHORNE BLVD STE 300 TORRANCE CA 90503
1	KTECH CORP ATTN DR E GAFFNEY 901 PENNSYLVANIA AVE NE ALBUQUERQUE NM 87111
1	EATON CORP DEFNS VALVE & ACTUATOR DIV ATTN J WADA 2338 ALASKA AVE EL SEGUNDO CA 90245-4896
2	MCDONNELL DOUGLAS ASTRONAUTICS CORP ATTN ROBERT W HALPRIN K A HEINLY 5301 BOLSA AVENUE HUNTINGTON BEACH CA 92647
4	KAMAN AVIDYNE ATTN R RUETENIK S CRISCIONE R MILLIGAN T STAGLIANO 83 SECOND AVENUE NORTHWEST INDUSTRIAL PARK BURLINGTON MA 01830
1	MDA ENGRNG INC ATTN DR DALE ANDERSON 500 EAST BORDER STREET SUITE 401 ARLINGTON TX 07601
2	POINTWISE INC ATTN J CHAWNER J STEINBRENNER PO BOX 210698 BEDFORD TX 76095-7698

<u>NO. OF COPIES</u>	<u>ORGANIZATION</u>
2	PHYSICS INTRNTL CORP PO BOX 5010 SAN LEANDRO CA 94577-0599
2	KAMAN SCIENCES CORP ATTN DASAC 2 CP 816 STATE ST SANTA BARBARA CA 93102-1479
1	LOGICON RDA ATTN G P GANONG PO BOX 9377 ALBUQUERQUE NM 87119
1	LOGICON RDA ATTN B LEE 6053 W CENTURY BLVD LOS ANGELES CA 90045
1	LOCKHEED MIS & SPACE CO ATTN J J MURPHY DEPT 81 11 BLDG 154 PO BOX 504 SUNNYVALE CA 94086
2	SCIENCE CTR ROCKWELL INTRNTL CORP ATTN DR S CHAKRAVARTHY DR D OTA 1049 CAMINO DOS RIOS THOUSAND OAKS CA 91358
1	METACOMP TECHNOLOGIES INC ATTN S CHAKRAVARTHY 650 WESTLAKE BLVD SUITE 203 WESTLAKE VILLAGE CA 91362
1	ORLANDO TECHNOLOGY INC ATTN D MATUSKA 60 SECOND ST BLDG 5 SHALIMAR FL 32579
4	S CUBED DIV OF MAXWELL LABS INC ATTN TECH LIB R DUFF K PYATT J BARTHEL PO BOX 1620 LA JOLLA CA 92037-1620

<u>NO. OF COPIES</u>	<u>ORGANIZATION</u>
1	SAIC ATTN J GUEST 2301 YALE BLVD SE SUITE E ALBUQUERQUE NM 87106
1	SUNBURST RECOVERY INC ATTN DR C YOUNG PO BOX 2129 STEAMBOAT SPRINGS CO 80477
1	SVERDRUP TECHNOLOGY INC ATTN RF STARR PO BOX 884 TULLAHOMA TN 37388
1	S CUBED DIV OF MAXWELL LABS INC ATTN JAMES SEVIER 2501 YALE BLVD SE ALBUQUERQUE NM 87106
3	SRI INTERNATIONAL ATTN DR GR ABRAHAMSON DR J GRAN DR B HOLMES 333 RAVENWOOD AVE MENLO PARK CA 94025
1	TRW BALLISTIC MISSILE DIV ATTN H KORMAN MAIL STATION 526 614 PO BOX 1310 SAN BERNADINO CA 92402
1	BATTELLE TWSTIAC 505 KING AVENUE COLUMBUS OH 43201-2693
1	THERMAL SCIENCE INC ATTN R FELDMAN 2200 CASSENS DR ST LOUIS MO 63026
2	DENVER RSRCH INSTITUTE ATTN J WISOTSKI TECH LIB PO BOX 10758 DENVER CO 80210

<u>NO. OF COPIES</u>	<u>ORGANIZATION</u>
1	STATE UNIV OF NEW YORK MCHNCL & AEROSPACE ENGRNG ATTN DR PEYMAN GIVI BUFFALO NY 14260
2	UNIV OF MARYLAND INST FOR ADV COMP STUDIES ATTN L DAVIS G SOBIESKI COLLEGE PARK MD 20742
1	CALIFORNIA INSTITUTE OF TECHNOLOGY ATTN T J AHRENS 1201 E CALIFORNIA BLVD PASADENA CA 91109
1	STANFORD UNIV ATTN DR D BERSHADER DURAND LABORATORY STANFORD CA 94305
1	UNIV OF MINNESOTA AHCRC ATTN DR TAYFUN E TEZDUYAR 1100 WASHINGTON AVE SO MINNEAPOLIS MN 55415
3	SOUTHWEST RSRCH INSTITUTE ATTN DR C ANDERSON S MULLIN A B WENZEL PO DRAWER 28255 SAN ANTONIO TX 78228-0255

NO. OF
COPIES ORGANIZATION

ABERDEEN PROVING GROUND

1	CDR USATECOM ATTN: AMSTE-TE-F, L TELETSKI
1	CDR USATHAMA ATTN: AMSTH-TE APG-EA
1	CDR USATC ATTN: STEC-LI
27	DIR USARL ATTN: AMSRL-SC-C, C NIETUBICZ AMSRL-SC-CC, C ELLIS D HISLEY P COLLINS T KENDALL R SHEROKE AMSRL-SC-I, W STUREK AMSRL-SC-S, R PEARSON AMSRL-SL-CM, E FIORVANTE AMSRL-WT-TB, R FREY J STARKENBERG K BENJAMIN W LAWRENCE T DORSEY R LOTTERO J CONDON L FERGUSON C MERMAGEN A MIHALCIN P MULLER R LOUCKS S SCHRAML J SULLIVAN AMSRL-WT-PB, P PLOSTINS P WEIHNACHT B GUIDOS AMSRL-WT-TC, K KIMSEY

USER EVALUATION SHEET/CHANGE OF ADDRESS

This Laboratory undertakes a continuing effort to improve the quality of the reports it publishes. Your comments/answers to the items/questions below will aid us in our efforts.

1. ARL Report Number/Author Drotleff (POC: R. Lottero) Date of Report September 1996

2. Date Report Received _____

3. Does this report satisfy a need? (Comment on purpose, related project, or other area of interest for which the report will be used.) _____

4. Specifically, how is the report being used? (Information source, design data, procedure, source of ideas, etc.) _____

5. Has the information in this report led to any quantitative savings as far as man-hours or dollars saved, operating costs avoided, or efficiencies achieved, etc? If so, please elaborate. _____

6. General Comments. What do you think should be changed to improve future reports? (Indicate changes to organization, technical content, format, etc.) _____

CURRENT
ADDRESS

Organization

Name

Street or P.O. Box No.

City, State, Zip Code

7. If indicating a Change of Address or Address Correction, please provide the Current or Correct address above and the Old or Incorrect address below.

OLD
ADDRESS

Organization

Name

Street or P.O. Box No.

City, State, Zip Code

(Remove this sheet, fold as indicated, tape closed, and mail.)
(DO NOT STAPLE)

DEPARTMENT OF THE ARMY

OFFICIAL BUSINESS

BUSINESS REPLY MAIL
FIRST CLASS PERMIT NO 0001,APG,MD

POSTAGE WILL BE PAID BY ADDRESSEE

**DIRECTOR
US ARMY RESEARCH LABORATORY
ATTN AMSRLWT TB
ABERDEEN PROVING GROUND MD 21005-5066**



**NO POSTAGE
NECESSARY
IF MAILED
IN THE
UNITED STATES**

